Synthesis and Properties of Products of Radical Polymerisation of Multivinyl Monomers

Dissertation presented at Faculdade de Engenharia da Universidade do Porto to obtain the degree of Doctor in Chemical and Biological Engineering

by

Miguel Ângelo Diz Gonçalves

Supervisor: Prof. Mário Rui P.F.N. Costa
Co-supervisor: Prof. Rolando C.P.S. Dias

Laboratory of Separation and Reaction Engineering, Associate Laboratory LSRE/LCM
Department of Chemical Engineering, Faculty of Engineering, University of Porto

April 2014

Agradecimentos
Acknowledgements

Aos meus orientadores, Professor Rolando Dias e Professor Mário Rui Costa, pela oportunidade concedida, acompanhamento científico, dedicação, sabedoria e amizade demonstrada ao longo deste trabalho.

Ao LSRE (Laboratory of Separation Process and Engineering), nas pessoas do Professor Alírio Rodrigues e Professora Madalena Dias e à direcção da Escola Superior de Tecnologia e Gestão do Instituto Politécnico de Bragança, pelas condições técnicas disponibilizadas à realização deste trabalho.

Aos meus Pais, João e Irene, pelo Amor, força e encorajamento e principalmente por estarem sempre por mim. Agradeço à minha irmã Sandra, aos meus amigos e familiares, que estiveram sempre ao meu lado.

Aos meus colegas do LSRE pela amizade e espírito de camaradagem dados ao longo destes anos. Um agradecimento especial à Isabel Patrícia, ao Patrick, ao Marco, à Virgínia e à Patrícia.

À Maria João e à Paula, pela ajuda e apoio dados através dos laboratórios de química (LPQ e LQA) da Escola Superior de Tecnologia e Gestão, e pela amizade demonstrada.

À Fundação para a Ciência e Tecnologia (FCT) e ao FSE (Programa Operacional Potencial e Humano/POPH), pelo apoio financeiro através da bolsa de doutoramento SFRH/BD/76587/2011.

FCT, Ministry of Science and Technology of Portugal (Program COMPETE-QCAIII) and European Community through FEDER are gratefully acknowledged for supporting this research through the projects POCI/EQU/44784/2002, POCI-PPCDT/EQU/60483/2004 and POCI/EQU-EQU/098150/2008.

The financial support of BASF AG through the projects FEUP/IPB/BASF/2007 and FEUP/IPB/BASF/2008 is gratefully acknowledged.

EU is also gratefully acknowledged for supporting this research through the Marie Curie Initial Training Network “Nanopoly” ITN-GE-2009-238700.

À minha mulher Anabela

Ao meu filho André

Abstract

Many materials used in coating and adhesive industries (paints, glues), sanitary industries and agriculture (superabsorbent polymers), biomedicine and pharmaceutics (smart hydrogels for drug delivery) or separation processes in different industries or environment (such as ion exchange or chelating resins) are produced through the polymerisation of multivinyl monomers. The performance of these materials is dependent on their production process and therefore it is important to find the link between their synthesis conditions and properties.

The structure of the networks has a strong influence on their properties. The materials obtained by conventional radical polymerisation (FRP) lead to networks with high amounts of relatively short loops which contribute little to the elasticity modulus.

The aim of this work was to carry out a study on the synthesis and characterization of hyperbranched polymers, gels and hydrogels arising from the radical polymerisation of multivinyl monomers to provide data for testing current knowledge on chemical and process modelling. Here the synthesis and characterization of materials obtained by free radical polymerisation (FRP) and controlled radical polymerisation techniques (CRP), namely ATRP, NMRP and RAFT, using organic (styrenics, acrylates and methacrylates) and water soluble monomers (acrylic and methacrylic acids copolymers, acrylamides) in different reaction systems (solution/bulk, suspension and inverse-suspension) using semi-batch and batch reactors in atmospheric and pressurized operation is reported. Temperature, monomers concentration, crosslinker concentration and functionalization, initiation system and concentration/kind of polymerisation controlling agents were the parameters tested in these polymerisations.

A secondary goal of this work was to use these experimental results to test simulation tools for predicting molecular masses and radius of gyration before and after gelation in the absence/presence of intramolecular cyclizations.

Molecular architecture of the polymerisation products was experimentally measured using size exclusion chromatography with multiple detectors, namely refractive index, multi-angle laser light scattering, intrinsic viscosity and ultraviolet extinction. *In-line* and *off-line* FTIR-ATR measurements were also performed in order to obtain information concerning the kinetics of formation and final structures of gels. In batch mode, FTIR yielded information on the presence and amounts of pendant double bonds. Gel fractions and swelling ratios were quantified and the performance of the synthesized water compatible polymer networks

(hydrogels) was studied through drug delivery tests. The morphology of the gel beads was observed by scanning electron microscopy. The concentration of pendant double bonds was also measured by the iodine chloride addition method.

It was observed that the used polymerisation mechanisms have a huge effect on the network structure and this feature can be exploited to design tailored materials.

Hyperbranched polymers with different architectures result from stopping molecular growth before gel point and were obtained by changing the feed policy of the reactants, using semi-batch reactors and chain transfer agents.

Controlled radical polymerisation techniques (ATRP, NMRP and RAFT) were used along the experimental program. These polymerisation mechanisms allowed an improvement on the final properties of the polymers and networks, by decreasing the relative rate of intramolecular cyclizations.

Water compatible monomers were used to produce superabsorbent polymers and smart hydrogels. Such networks can be used in controlled drug delivery by exploiting the change of active substance retention with pH, temperature or other environmental variables.

Resumo

Muitos materiais usados nas indústrias de revestimentos e adesivos (tintas, colas), indústrias sanitárias e agricultura (polímeros superabsorventes), biomedicina e farmácia (hidrogéis inteligentes para libertação controlada de fármacos) ou em processos de separação industriais e ambientais (tais como resinas de permuta iónica ou resinas quelatantes) são produzidos através da polimerização de monómeros multivinílicos. O desempenho e a utilidade destes materiais dependem do processo de produção e portanto é importante encontrar a relação entre as condições de síntese e as suas propriedades.

A estrutura das redes poliméricas tem uma forte influência nas suas propriedades. Os materiais obtidos por polimerização radicalar convencional (FRP) são em geral redes de polímero contendo grandes quantidades de pequenos ciclos que contribuem pouco para a sua elasticidade.

O objectivo deste trabalho consistiu na realização de estudos de síntese e caracterização de polímeros híper-ramificados, géis e hidrogéis, obtidos através de polimerizações radicalares de monómeros multivinílicos, de forma a obter dados experimentais úteis para a avaliação do conhecimento actual sobre a química e modelização desses processos. É aqui relatada a síntese e a caracterização de materiais obtidos por polimerização radicalar "livre" (FRP) e técnicas de polimerização radicalar controladas (CRP), nomeadamente ATRP, NMRP e RAFT, usando monómeros orgânicos (estirenicos, acrilatos e metacrilatos) e solúveis em água (acrílicos, acrilamidas). Foram também experimentados diversos sistemas de reacção (solução/massa, suspensão e suspensão-inversa) e considerados diferentes reactores fechados ou semi-fechados, operando à pressão atmosférica ou sob pressurização. Nestas polimerizações, a temperatura, concentração de monómeros, concentração e funcionalidade dos reticulantes, sistema de iniciação e tipo/concentração de agentes controladores da polimerização foram testados como parâmetros de operação.

Um objectivo secundário deste trabalho foi a utilização destes resultados experimentais para teste de ferramentas de simulação úteis na previsão de massas moleculares e raios de giração antes e depois da gelificação e na presença (ou ausência) de ciclizações intramoleculares.

A arquitectura molecular dos produtos foi medida experimentalmente usando cromatografia por exclusão de tamanhos com detecção múltipla, nomeadamente índice de refracção, dispersão *de luz* multi-angular, índice de viscosidade e absorção no ultravioleta. Medições *in-*

line e *off-line* por FTIR-ATR foram também realizadas com o propósito de obter informação acerca da cinética de formação e das estruturas finais dos géis. Em modo fechado, a análise FTIR revelou informação sobre a presença e quantidades de ligações duplas pendentes. As fracções de gel e as razões de inchamento foram quantificadas e o desempenho das redes poliméricas compatíveis com água (hidrogéis) foram estudados através de testes de libertação controlada. A morfologia dos produtos foi observada por microscopia electrónica de varrimento e a concentração de ligações duplas pendentes foi também medida pelo método da adição de cloreto de iodo.

Foi observado que os mecanismos de polimerização usados têm um enorme efeito na estrutura das redes e este aspecto pode ser explorado para produzir materiais com propriedades por medida.

Polímeros hiper-ramificados com diferentes arquitecturas, resultando da paragem do crescimento molecular antes do ponto de gel, foram também obtidos mudando o modo da alimentação dos reagentes, usando reactores semi-fechados ou considerando agentes de transferência de cadeia na composição inicial do sistema químico.

Diferentes técnicas de polimerização radicalar controladas (nomeadamente ATRP, NMRP e RAFT) foram usadas ao longo do programa experimental. Estes mecanismos de polimerização permitiram o melhoramento das propriedades finais dos polímeros e das correspondentes redes, através da diminuição da velocidade relativa dos mecanismos cinéticos de ciclização intramolecular.

Monómeros compatíveis com a água foram usados na produção polímeros superabsorventes a hidrogéis *inteligentes* (sensíveis a estímulos resultantes de variações nas condições envolventes). Foi demonstrado que estas redes podem ser usadas na libertação controlada de fármacos, explorando mudanças na retenção da substância activa em função de alterações no pH, temperatura ou em outras variáveis das soluções aquosas circundantes (ex. força iónica).

Table of Contents

List of Figures

ATOM TRANSFER RADICAL POLYMERISATION OF ACRYLATES

NITROXIDE MEDIATED RADICAL POLYMERISATION OF STYRENE/DIVINYLBENZENE

REVERSIBLE ADDITION-FRAGMENTATION CHAIN-TRANSFER POLYMERISATION OF STYRENE AND COPOLYMERISATION OF STYRENE/DIVINYLBENZENE

INVERSE-SUSPENSION FREE-RADICAL POLYMERISATION LEADING TO HYDROGELS FORMATION

INVERSE-SUSPENSION REVERSIBLE ADDITION-FRAGMENTATION RADICAL POLYMERISATION LEADING TO HYDROGELS FORMATION

APPENDICES

List of Tables

CONVENTIONAL FREE-RADICAL COPOLYMERISATION OF MULTIVINYL MONOMERS

ATOM TRANSFER RADICAL POLYMERISATION OF ACRYLATES

NITROXIDE MEDIATED RADICAL POLYMERISATION OF STYRENE/DIVINYLBENZENE

REVERSIBLE ADDITION-FRAGMENTATION CHAIN-TRANSFER POLYMERISATION OF STYRENE AND COPOLYMERISATION OF STYRENE/DIVINYLBENZENE

INVERSE-SUSPENSION FREE-RADICAL POLYMERISATION LEADING TO HYDROGELS FORMATION

INVERSE-SUSPENSION REVERSIBLE ADDITION-FRAGMENTATION RADICAL POLYMERISATION LEADING TO HYDROGELS FORMATION

List of Symbols

A_i	Radical from monomer or PDB of kind *i*.
A_m	Length of Kuhn's statistical segment of polymer chain.
APn	Dormant polymer chain.
B	Parameter in Fixman (Eq. 3.25) and Kurata-Stockmayer-Roig (3.27) extrapolation.
b_0	Contribution of monomer units to the length of polymer chains.
C	Parameter in Stockmayer-Fixman (Eq. 3.26) extrapolation.
C_{CTA}	Reactivity ratio for chain transfer to chain transfer agent.
C_{DB}	Concentration of pendant double bonds.
C_{fpCH3}	Reactivity ratio for intermolecular chain transfer to CTP.
C_{fpH}	Reactivity ratio for intermolecular chain transfer to HTP.
C_i	Compound of kind *i*.
C_I	Reactivity ratio for chain transfer to initiator.
C_M	Reactivity ratio for chain transfer to monomer.
C_P	Reactivity ratio for global intermolecular chain transfer to polymer.
C_{PDB}	Reactivity ratio for the propagation of PDB.
C_{PDBm}	Reactivity ratio for the propagation of PDB of *m*-divinylbenzene.
C_{PDBp}	Reactivity ratio for the propagation of PDB of *p*-divinylbenzene.
C_R	Reactivity ratio for radical of PDB.
C_{RD}	Factors for calculating termination rate constants of acrylate monomers.
C_T	Reactivity ratio for chain transfer to solvent.
C_{TDB}	Reactivity ratio for global polymerisation of terminal double bonds.
C_{TDBD}	Reactivity ratio for global polymerisation of TDBD.
C_{TDBM}	Reactivity ratio for global polymerisation of TDBM.
C_{tit}	Concentration of titulant.

C_∞	Characteristic ratio.
C_η	Factors for calculating termination rate constants of acrylate monomers.
D	Dormant radical.
D_i	Dormant radical from species of kind *i*.
D_M	Molecular weight dispersity.
dn/dc	Refractive index increment.
DP	pressure across middle of bridge.
DY_i	Dormant primary radical of the type *i*.
E_p	Activation energy of propagation.
E_t	Activation energy of propagation.
f	Initiator decomposition efficiency.
f_{DVB}	Initial mole fraction of divinylbenzene in total monomer content.
f_{HEP}	Volumetric fraction of *n*-heptane in the diluent mixture (*n*-heptane+toluene).
F_i	Inactive fragment of kind *i* in polymer chains.
f_I	Initial mole ratio between initiator and total amount of monomers double bonds.
f_M	Initial volumetric fraction of monomers in the organic phase.
f_{OR}	Initial volumetric fraction of organic phase in the total liquid content.
g(α)	Function in Kurata-Stockmayer-Roig (Eq. 3.27) extrapolation.
G_x	Characteristics for calculation of chain length distribution using the extended method of moments.
H_{pc}	Peak height of C=C consumption.
H_{pt}	Peak height of the internal tracer.
I_x	Intensity of peak with wavelength *x*.
k_{ATRP}	Equilibrium constant for radical activation/deactivation.
k_{ax}	Rate coefficient of activation for the specie x.
k_{CTAi}	Rate coefficient of chain transfer to CTA with a polymer radical of kind *i*.

k_d	Rate coefficient of the thermal initiator decomposition.
k_{dax}	Rate coefficient of deactivation for the specie *x*.
k_{dec}	Rate coefficient of the decomposition of dormant monomeric radicals.
k_{dim}	Rate coefficient of the Mayo dimerization of styrene.
k_{dim}^{-1}	Rate coefficient of the dimer decomposition in polymerisation of styrene.
k_f	RAFT fragmentation rate coefficient.
k_{fx}	Rate coefficient of chain transfer to specie *x*.
K_G	Coefficient in the scaling law$\bar{R}_g$ *versus* $\bar{M}_w$.
k_h	Rate coefficient of the enhancement reaction of the dimer of styrene.
k_I	Rate coefficient of the initiation step.
k_{IA}	Rate coefficient of the thermal initiation of styrene.
k_{Ijk}	Rate coefficient of initiation of a monomer or PDB of kind *k* with a primary radical of kind *j*.
k_{Ix}	Rate coefficient of monomer initiation with a primary radical of the specie *x*.
k_p	Propagation rate coefficient.
k_p^*	Rate coefficient of the propagation of PDB.
k_p^{**}	Rate coefficient of the propagation of TDB.
k_{pij}	Propagation rate coefficient involving a radical of kind *i* with a monomer or PDB of kind *j*.
k_{pm}^*	Rate coefficient of propagation of PDB of *m*-DVB.
k_{pp}^*	Rate coefficient of propagation of PDB of *p*-DVB.
k_{ri}	Rate coefficient of retardation with a polymer radical of kind *i*.
k_{Si}	Rate coefficient of chain transfer to solvent with a polymer radical of kind *i*.
k_t	Rate coefficient of the global radical termination.
k_{tc}	Rate coefficient of radical termination by combination.
k_{tcij}	Rate coefficient of radical termination by combination of a polymer radical of kind *i* with a polymer radical with kind *j*.

k_{td}	Rate coefficient of radical termination by disproportionation.
k_{tdij}	Rate coefficient of radical termination by disproportionation of a polymer radical of kind *i* with a polymer radical with kind *j*.
k_{trx}	Rate coefficient of the irreversible chain transfer to specie *x*.
$k_{t,SD}$	Factor for calculating termination rate constants of acrylate monomers.
$k_{t,TD}$	Factor for calculating termination rate constants of acrylate monomers.
k_{ZPi}	Rate coefficient of a inhibitor Z with a primary radical of kind *i*.
k_{Zi}	Rate coefficient of a inhibitor Z with a polymer radical of kind *i*.
M_0	Initial mass fraction of monomer.
l	Bond length.
m_{equi}	Weight of the gel in equilibrium.
m_{gel}	Weight of gel.
M_i	Monomer, macromonomer or PDB of kind *i*.
m_{pol}	Weight of polymer.
$\overline{M}_n$	Number-average relative molecular mass.
m_S	weight of sample collected from the reactor.
Mw	Polymer chain molecular weight.
Mw_0	molecular weight of a repetitive unit.
$\overline{M}_z$	*z*-average relative molecular mass.
N	Number of skeletal bonds of the polymer chain.
n_x	Refractive index of the specie *x*.
P	Monomer conversion.
$P_{k,m,n}$	Polymer molecules bearing *k* radicals, *m* PDB and *n* repeating units.
r^*	Reactivity ratio of PDB as compared to the double bonds of the monovinyl monomer.
R_{AM}	Reactivity ratio for radicals derived from chain transfer to monomer.
r_f^2	Square of the random-flight end-to-end distance.

R_g	Root mean square radius of gyration.
$\bar{R}_g$	*z*-average mean square radius of gyration.
$R_{g\theta}$	Unperturbed root mean square radius of gyration.
$\bar{R}_{g\theta}$	Unperturbed root z-average mean square radius of gyration.
R_i	radical in polymer molecule of the kind *i*.
$r_{i,j}^{ap}$	Apparent values of reactivity ratio between a radical of kind *i* with a monomer or macromonomer of kind *j*.
r_{ij}	Polymerization reactivity ratio between a radical of kind *i* with a monomer or macromonomer of kind *j*.
R_{INT}	Reactivity ratio for internal radicals.
r_M	Initial mole ratio between monomer and initiator.
r_{PDB}	Reactivity ratio of PDB comparatively to the double bonds of the crosslinker monomer.
R_{PDB}	Reactivity ratio for pendant double bond radicals.
r_t	Rate of termination.
r_θ^2	Unperturbed polymer dimensions in the absence of long range interactions.
s_x	Characteristics for calculation of chain length distribution using the extended method of moments.
T	Temperature.
T	Time.
T_g	Glass transition temperature.
U_i	Repeating unit of kind *i* in polymer chains.
V_{AA}	Volume fraction of acrylic acid in the aqueous phase.
V_m	Volume fraction of vinyl monomer in the solution.
V_{titB}	volume of titrant spend in blank sample.
V_{titS}	volume of titrant spend in polymer sample.
w_{EGDMA}	Weight fraction of EGDMA in the total monomer content.
w_g	Weight fraction of gel.

W_{MAA}^{0}	Initial fraction of MAA weight.
X	Stable radical.
X_D	*X* coordinate in a Debye plot.
y_C	Initial mole fraction of crosslinker in the total monomer mixture.
Y_D	*Y* coordinate in a Debye plot.
y_D	Mole fraction of initial double bonds belonging to the crosslinker.
y_{DVB}	Initial mole fraction of divinylbenznene in the total monomer mixture.
Y_i	Primary radical of the kind *i.*
y_I	Initial mole ratio between initiator and total amount of monomers double bonds.
y_I^{RAFT}	Initial mole ratio between RAFT agent and initiator.
y_m	Initial mass fraction of monomers in the organic phase.
y_M	Initial volumetric fraction of monomers in the organic phase.
y_{OR}	Initial volumetric fraction of organic phase in the total liquid content (organic phase plus water).
y_{RAFT}^{M}	Initial mole ratio between monomer and RAFT agent.
y_{TEMPO}	Initial mole ratio between NMRP mediator (TEMPO) and initiator.

Greek Symbols

α	Functionality of the crosslinker (number of active double bonds).
α_{tc}	Relative rate of radical termination by combination.
α_{td}	Relative rate of radical termination by disproportionation.
$\delta_{[i-j]}^{k}$	Krönecker symbols.
$\delta_{i,j}^{k}$	Krönecker symbols.
η	Specific viscosity of the polymer in the solvent.

η_0	Specific viscosity of pure solvent.
η_{SP}	Specific viscosity of solution.
λ	Wavelength of the light.
λ_0	Vacuum Wavelength of the incident light in MALLS.
θ	Scattering angle in MALLS.
Θ	Good solvent conditions.
γ	Propagation probability.
ν	Exponent in the scaling law $\bar{R}_g$ *versus* $\bar{M}_w$.

List of Abbreviations

A	RAFT agent.
AA	Acrylic acid.
AAM	Acrylamide.
AIBN	2,2´-azobis(2-methylpropionitrile).
APS	Ammonium persulfate.
ATR	Attenuated total reflectance.
ATRP	Atom Transfer Radical Polymerisation.
BEDA	Bisphenol-A ethoxylate diacrylate.
BPO	Benzoyl peroxide.
BS	Branching site.
CDT	Cyanomethyl dodecyl trithiocarbonate.
CL	Cross-linker.
$[CL]_0$	Initial concentration of cross-linker.
CLD	Chain length distribution.
CM	Transition metal/ligand complex.
CPA	4-cyano-4-phenyl carbonothioylthio-pentanoic acid.
CRP	Controlled radical polymerisation.

CS	Crosslinking site.
CTA	Chain transfer agent.
CTP	CH_3 transfer to polymer center.
CX	Oxidized transition metal/deactivator.
D	Dimer.
DDMAT	2-(dodecylthiocarbonothioylthio)-2-methylpropionic acid.
DMA	N,N-dimethylacrylamide.
DMAEMA	2- (dimethylamino)ethyl methacrylate.
DMF	N,N-dimethylformamide.
DNA	Deoxyribonucleic acid.
DT	Degenerative chain transfer.
DTLRP	Degenerative chain living radical polymerisation.
DVB	Divinylbenzene.
$[DVB]_0$	Initial concentration of divinylbenzene.
EBrP	Ethyl 2-bromopropionate.
EGDMA	Ethylene glycol dimethacrylate.
$[EGDMA]_0$	Initial concentration of ethylene glycol dimethacrylate.
EPR	Electron paramagnetic resonance.
FRP	Free-radical polymerisation.
FTIR	Fourier transform infra-red.
5Fu	5-fluorouracil.
GPC	Gel Permeation chromatography.
HDDA	1,6-hexanediol diacrylate.
HHU	Head-head units from termination by combination.
HMTETA	1,1,4,7,10,10-hexamethyltriethylenetetramine.
HTP	Chain transfer to polymer center (methine group).
I	Initiator.
$[I]_0$	Initial concentration of initiator.
IDB	Non-reactive internal double bond.
IP	Inlet pressure through the bridge top to bottom.
IPDB	Index of pendant double bonds.
IPN	Interpenetrating polymer networks.

ITP	Iodine transfer polymerisation.
IUPAC	International union of pure and applied chemistry.
IVDP	Intrinsic viscosity differential pressure.
LCB	Long chain branching.
LCST	Lower critical solubility temperature.
LS	Light scattering.
M	Monomer.
$[M]_0$	Initial concentration of monomer.
MAA	Methacrylic acid.
$[MAA]_0$	Initial concentration of methacrylic acid.
MALLS	Multi angle laser light scattering.
MBAm	N,N´-methylenebisacrylamide.
MBPA	Methyl α-bromophenylacetate.
$[MBPA]_0$	initial concentration of methyl α-bromophenylacetate.
MCT	Mercury cadmium telluride.
m-DVB	*meta*-divinylbenzene.
MEQH	Monomethyl ether hydroquinone.
MIPs	Molecular imprinted polymers.
MMA	Methyl methacrylate.
MW	Molecular weight.
MWD	Molecular weight distribution.
*n*BuA	*n*-butyl acrylate.
NIPA	N-isopropylacrylamide.
NMR	Nuclear magnetic resonance.
NMRP	Nitroxide Mediated Radical Polymerisation.
PAA	Poly(acrylic acid).
PBAA	Poly(butyl acrylic acid).
PDB	Pendant double bonds.
PDI	Polydispersity index.
PDMA	Poly(dimethyl acrylamide).
PDMAEMA	Poly (2-(dimethylamino)ethyl methacrylate).
PDVB	Poly(divinylbenzene).

p-DVB	*para*-divinylbenzene.
PEAA	Poly(ethyl acrylic acid).
PLP	Pulsed laser polymerisation.
PMAA	Poly(methacrylic acid).
PMDETA	N,N,N´,N´´,N´´,-pentamethyldiethylenetriamine.
PMMA	Poly(methyl methacrylate).
P*nBuA*	Poly(*n*-butyl acrylate).
PNIPA	Poly(N-isopropylacrylamide).
PPAA	Poly(propyl acrylic acid).
PS	Polystyrene.
PVA	Poly(vinyl alcohol).
PVC	Poly(vinyl chloride).
[R]	Concentration of radicals.
RAFT	Reversible addition-fragmentation chain transfer polymerisation.
RALS	Right angle light scattering.
RI	Refractive index.
RX	ATRP initiator.
STY	Styrene.
$[STY]_0$	Initial concentration of styrene.
SAP	Superabsorbent polymers.
SCB	Short chain branching.
SEC	Size Exclusion Chromatography.
SEM	Scanning Electron Microscopy.
SET	Outer sphere single electron transfer.
SG	Saturated end group in polymer chains.
SM	Dormant radical from the monomer.
SP	Single pulse.
Span 60	Sorbitan monostearate.
SRa	Swelling ratio.
SR	Dormant radical from the initiator.
T	Solvent.
$[T]_0$	Initial concentration of solvent.

TAM	Transfer to acrylate monomer reaction.
TAO	Tetrallyloxyethane.
TBP	Theory of branching process.
TDBD	Terminal double bond from termination by disproportionation.
TDBM	Terminal double bond from chain transfer to monomer.
TDM	Transfer to diacrylate monomer reaction.
TEMED	N,N,N’,N’-tetramethylethylenediamine.
TEMPO	2,2,6,6-tetramethylpiperidinyl-1-oxy.
THF	Tetrahydrofuran.
TMPTA	Trimethylolpropane triacrylate.
TPBVP	Two point boundary value problems.
TS	Saturated nitroxyl radicals.
UCST	Upper critical solubility temperature.
UV	Ultra violet.
V50	2,2´-azobis(2-methylpropionamidine) dihydrochloride.
Vac	Vinyl acetate.
VC	Vinyl chloride.

CHAPTER 1

INTRODUCTION

1.1 Introduction

1.1.1 Free-Radical (Radical) Polymerisation

Here, a short discussion on chemical terminology will be introduced on how to cope with IUPAC recommendations. Thus, the terms "radical" or "free-radical" are restricted to those radicals which do not form parts of radical pairs. In the past the term "radical" was used to designate a substituent group bound to a molecular entity, as opposed to "free-radical", which nowadays is simply called radical. The bound entities should no longer be called radicals (McNaughton and Wilkinson, 2012).

The different kinds of polymers can be classified by their molecular architecture, namely whether they can be linear, branched or crosslinked polymers. The molecular structure of a linear polymer (Figure 1.1(a)) is a continuous chain of multiple repeating units. These units are added to the main chain following continuously without any side chain, besides the ones that are part of monomer structure. A branched polymer (Figure 1.1(b)) is composed by polymeric segments joint to the main chain. These segments are called branches, lateral chains or pending chains. At last, a crosslinked polymer (Figure 1.1(c)) is the result of the bond of polymer chains, forming a network of interconnected chains. The formation of multiple interconnections could lead to a single giant molecule consisting of all polymer chains of the system connected by at list one link. Thus, a polymer network can be considered as one or many polymer chains of extremely high molecular mass or infinite (Carothers, 1936).

The radical polymerisation reaction involving a monomer with a double bond with another monomer with two double bonds is a typical example of a copolymerisation with simultaneous occurrence of branching/crosslinking. The divinyl monomer besides its function as a co-monomer is also a branching agent. With the polymerisation process advancement it is formed a tridimensional network. In this system can be found at the same time linear chains, branched chains or main chains connected by crosslinking points.

In recent years the synthesis and characterization of branched/crosslinked polymers has been a subject with growing research activity. Indeed, there is much room for improving several properties of these materials as compared with their linear counterparts. Higher functional group densities and appropriated solubility and viscosity ranges can be exploited by producing hyperbranched polymers with different applications fields, such as drug or gene

delivery in biomedicine, as rheology modifiers or coatings. Moreover, with these polymerisation systems it is also possible to obtain insoluble polymer networks with important applications in a broad range of separation processes of pharmaceutical or bioengineering industries, in the production of microelectronic devices or as superabsorbents hydrogels. The synthesis of hyperbranched polymers is a well established subject for step-growth polymerisation systems but less developed when vinyl monomers are involved. Some works concerning the production of hyperbranched materials involving multi-functional vinyl monomers and using classical (Gretton-Watson *et al*., 2006; Saunders *et al*., 2005; O'Brien *et al*., 2000) or living (Bannister *et al*,. 2006) radical polymerisation have been published. A major problem of these polymerisation systems is the occurrence of gelation for low monomer conversion even when a small amount of crosslinker is used. In the aforementioned works (Gretton-Watson *et al*., 2006; Saunders *et al*., 2005; O'Brien *et al*., 2000; Bannister *et al*., 2006) some strategies have been put forward (such as the introduction of chain transfer agent) to minimize this problem and make possible the production of soluble branched polymers at high monomer conversion. Thus, radical copolymerisation of mono and multivinyl monomers offers the possibility of synthesizing polymers with a combination of high average molecular weight with a low viscosity. In addition, with these polymerisation systems it is also possible to obtain insoluble copolymers networks by intentionally promote the gelation of these kind of vinyl (and divinyl) monomers specially styrene+divinylbenzene (Okay, 2000). In this case, macroporous gel as insoluble swollen particles are formed and have important applications in a broad range of separation processes in biotechnology, pharmaceutical industry (Bayramoglu *et al.*, 2007) and the well known application in polymer molecular size fractionation by size exclusion chromatography or as superabsorbent hydrogels. Therefore, it was inevitable the start-up of a growing research activity related with the polymer reaction engineering of vinyl/divinyl copolymerisation. Landin and Macosko (1988) and Hamielec and co-workers (Li *et al*., 1989a and 1989b), using different modelling approaches carried out two decades ago two of the most important kinetic studies in this subject and paved the way for the more recent studies.

Polymer networks are among the most ancient and well known synthetic materials. Indeed, the branching/crosslinking reactions had been deeply analysed since the pioneer study of macromolecular compounds from Staudinger and co-workers (Staudinger *et al*., 1936; Staudinger and Husemann, 1935). Linear and crosslinked polymers with the same chemical composition exhibit completely different properties. The linear polymers are thermoplastics

and thus can be molten and afterwards extruded, calendered or injection moulded, while crosslinked polymers are insoluble material and thermo stables (cannot be melted by heat). In the last years, polymer networks had been subject of increasing research activity trying to achieve molecular architectures, structures and morphology of a model polymer network. With this purpose, studies had been made related with the synthesis of polymer networks by free-radical polymerisation (Moad and Solomon, 2006).

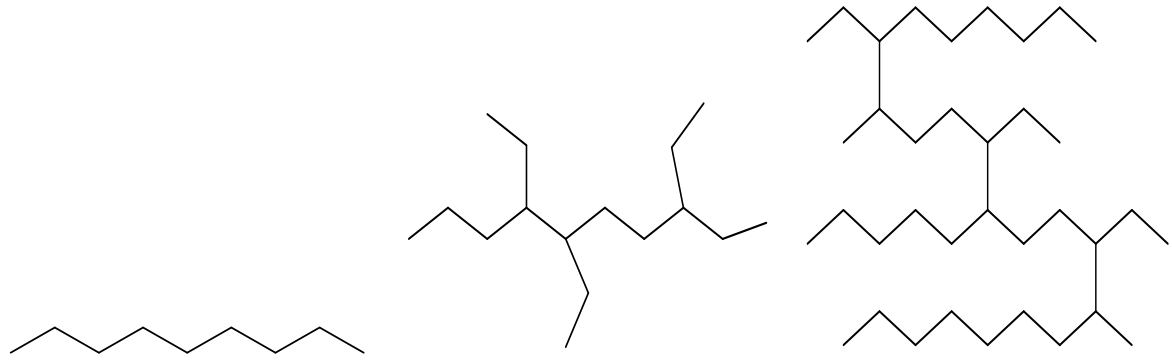

(a) (b) (c)

Figure 1.1. Schematic representation of (a) linear polymer chain (b) branched polymer chain and (c) crosslinked polymer chain.

Some polymer networks can be used as advanced materials due to the sensitivity of their microscopic properties to external inputs. These polymers are often classified as stimuli responsive or smart polymers. Applications of these kinds of materials in biomedicine or bionanotechnology are nowadays a subject attracting considerable research efforts. Huge swelling ratios are also observed in many gels which are explored to produce superabsorbent materials. Formation of macroporous structures in polymer networks also makes possible their use as particles and membranes for many separation processes.

The synthesis and characterization of these materials has received great attention by the investigation groups in recent times with special attention to insoluble networks compatible with water (hydrogels) sensible to temperature and/or pH changes with applications in biomedicine and biotechnology (Galaev and Mattiasson, 2008; Bajpai *et al*., 2010). Hyperbranched polymers (soluble non-linear polymers) allow the improvement of specific properties of some materials when compared with their linear counterparts. Functional group densities, solubility and viscosity ranges can be obtained through hyper-branched polymers. These kinds of materials are applied in various fields including biomaterials and nanotechnology (Gao and Yan, 2004; Gretton-Watson *et al*., 2006; Bannister *et al*., 2006).

The production of polymer networks and hyperbranched polymers is conventionally made through Free-Radical Polymerisation (FRP) of multivinyl monomers. The project of new synthesis conditions to improve these materials is an important line of investigation in this field due to their final structure heterogeneity. In recent years different techniques of controlled radical polymerisation had been tested aiming the increasing of polymer homogeneity and thus allowing the synthesis of new advanced materials with improved properties (Galaev and Mattiasson, 2008; Bajpai *et al*., 2010, Gao and Yan, 2004; Gretton-Watson *et al*., 2006; Bannister *et al*., 2006).

1.1.2 Reversible Deactivated ("controlled") Radical Polymerisation

Again, some considerations are made for polymer terminology accordingly to IUPAC recommendations. Thus, in radical polymerisations in which certain additives react reversibly with the radicals, thus enabling the reactions to take on much of the character of living polymerisations have been subject of various terminology. These reactions have often been referred to "controlled/living" or "living" polymerisations. The IUPAC recommendation (Jenkins *et al.*, 2010) for this kind of radical polymerisation states that the full name is "reversible-deactivation radical polymerisation". The term controlled is only permitted as long as the type of control is defined at its first occurrence. As the terms "controlled" and "living" are well established use among scientific community, they will be used along this work.

Living anionic polymerisation discovered by Szwarc more than fifty years ago (Szwarc, 1956) is generally considered to be one of the foundations of modern nanotechnologies. Ionic living polymerisations may lead to well-defined polymer architectures such as block copolymers, stars, combs or hyperbranched polymers. However, these processes require stringent conditions and only a limited number of monomers can be used. Most of those difficulties have been removed thanks to the emergence of reversible deactivated or controlled radical polymerisation techniques in the early nineties (Georges *et al*., 1993; Solomon *et al*., 1986). CRP makes possible the synthesis of materials with tailored molecular weight, low polydispersities and different kinds of well-defined molecular architectures, instead of the random polymers obtained by conventional free-radical polymerisation. In contrast to ionic living polymerisation, CRP can be performed in amenable conditions, e.g., temperatures in the range 20–140 °C, with minimal requirements concerning the presence of impurities in the polymerisation system and are also applicable to a broad set of monomers. These advantages

justify the huge research effort followed in the last years concerning the improvement and development of CRP techniques for use in the synthesis of advanced polymers (Destarac, 2010).

Three main variants of CRP have been used in the last few years, i.e., stable free-radical polymerisation (SFRP) with nitroxide- mediated radical polymerisation (NMRP) as a particular case, atom-transfer radical polymerisation (ATRP) and reversible addition-fragmentation chain transfer polymerisation (RAFT). A common feature of these techniques is the establishment of equilibrium between radicals and dormant species allowing the concentration of radicals to be kept at a low enough level to almost suppress termination reactions. Indeed, considering FRP, the expected lifetime of a radical, t_1, is very short (of the order of 1 s) owing to the termination reaction according to Eq. 1.1:

$$t_1 = [R]/r_t \backsimeq 1/(2k_t\,[R]) \tag{1.1}$$

In Eq. (1.1), [R] represents the concentration of radicals, r_t is the rate of termination and k_t is the related rate coefficient. However, with CRP, the expected lifetime of a radical can reach several hours, since it is determined by the dynamic equilibrium between activated and deactivated states.

A process with a similar effect (reduced radical concentration), but involving reversible chain transfer, is the distinguished feature of RAFT. In all cases, these intermittent exchanges reduce the concentration of growing radicals, and therefore, minimize the termination reactions: usually less than 5 % of the total polymer chains undergo termination in CRP techniques.

Since their inception, the almost living character of CRP techniques has been exploited for the synthesis narrow mass distribution, linear homo-polymers and block copolymers of different architectures. Moreover a few research works in the last years have shown that CRP techniques can also be useful for the controlled production of well-defined hyperbranched polymers. Based on the analysis of the kinetic mechanisms involved in the formation of crosslinked polymers, it is possible to speculate that CRP of vinyl/divinyl monomers leads to the formation of more homogeneous non-linear molecular architectures than the correspondent FRP of the same monomers. More homogeneous structures seen to be a consequence of the lower extent of intramolecular cyclizations formed mostly at a low monomer conversion due to the propagation of pendant double bonds with radicals belonging to the same molecule. These cycles are undesirable because of the waste of crosslinking sites

and reduction of the network elasticity modulus. Indeed, known drawbacks of FRP are slow initiation, fast propagation and strong incidence of termination reactions. This means that, during a FRP process, molecules with very different time scales of formation/termination coexist within the polymer population. This age heterogeneity of the polymer population increases the probability of intramolecular reactions due to the concomitant space heterogeneity of species concentrations. CRP processes with fast initiation and reduced impact of termination reactions are a possible route to improve the homogeneity of these products due to the almost uniform age of the polymer population. These aspects were investigated is the last few years in order to synthesize networks with improved homogeneous structure (Gao *et al*., 2007, 2008 and 2009; Hernández-Ortiz *et al.,* 2009; Ide and Fukuda, 1997 and 1999). An extensive list of works concerning the polymer network formation through different kinds of CRP processes is presented by Hernández-Ortiz *et al.,* 2009, and indirect evidence for the formation of more homogeneous polymer networks through CRP compared to those produced by FRP are also discussed. It should be noted that in both cases (CRP and FRP), the monomer concentration plays an important role in the minimization of intramolecular cyclizations. At low monomer concentration (high dilution), the probability that a radical reacts inside the same molecule increases since few monomer units or polymer molecules are found in the surroundings.

1.1.2.1 Atom Transfer Radical Polymerisation

The first reports of ATRP appeared in 1995 from the groups of Sawamoto (Kato *et al*., 1995), Matyjzaszewski (Wang and Matyjaszewski, 1995) and Percec (Percec and Barboiu, 1995). These works had clearly displayed the characteristics of living polymerisation. In recent years, a number of reviews on ATRP have appeared being the most informative on the scope of the process those made by Matyjaszewsky (Matyjaszewski and Xia, 2001 and 2002) and Sawamoto (Kamigaito *et al*., 2001 and 2004). The kinetics of ATRP is discussed in reviews by Fischer (Fischer and Radom, 2001) and Goto and Fukuda (2004). The generic representation of the deactivation/activation process of radicals occurring in ATRP is given by Eq. (1.2). In the deactivation process, propagating radicals are trapped by atom or group transfer (usually a halogen (Cl, Br, I)) from a metal complex in its higher oxidation state. The activation process involves a redox reaction between the polymer end group and the metal complex in its reduced form.

$$R + CX \underset{k_a}{\overset{k_{da}}{\Leftrightarrow}} D + CM \quad (1.2)$$

Where R represents a radical in a polymer molecule, CM is a transition metal complex, CX is the correspondent oxidized metal complex and D is a dormant radical.

Ideally, the metal complex is a catalyst and is only required in very small quantities. The most commonly used catalysts are metal complexes based on Cu (cooper) and Ru (ruthenium). Most of monomers that are polymerised by a radical mechanism can be used in ATRP.

A successful experiment in ATRP will yield a polymer with potentially labile halogen end groups which can harm polymer stability. Moreover, corrosive by-products (hydrogen halide acids) can be formed by thermal elimination. However, it is possible to transform such end groups into inert or even useful other functionalities, such as precursors to block, star comb and more complex architectures (Moad and Solomon, 2006).

1.1.2.2 Nitroxide Mediated Radical Polymerisation

Prior to the development of NMRP, nitroxides were known as inhibitors and stabilizers of polymerisation (they still are used in that way). Both applications are based on the property of nitroxides to efficiently scavenge carbon-centered radicals by combining with them at near diffusion-controlled rates for alkoxyamines. These assets also saw nitroxides exploited as trapping agents for defining initiations mechanisms (Moad and Solomon, 2006).

The exploitation of alkoxyamines as polymerisation initiators and the use of NMRP for producing block and end-functional polymers were first described by Solomon (Solomon *et al.*, 1986). In this patent NMRP was described as a method of living radical polymerisation, but only in 1993 with the demonstration by Georges *et al*., that NMRP could be used to prepare PS with narrow molecular weight distribution. Nowadays the literature on NMRP has expanded and is now one of the most cited methods for living radical polymerisation (Moad and Solomon, 2006). In NMRP, the dynamic equilibrium is described by Eq. (1.3), where *R* represents an active polymer radical, X a stable radical (e.g. TEMPO) and *D* a dormant radical (alkoxyamine):

$$R + X \underset{k_a}{\overset{k_{da}}{\Leftrightarrow}} D \quad (1.3)$$

1.1.2.3 Reversible Addition-Fragmentation Polymerisation

Radical polymerisations involving a reversible chain transfer step for chain equilibration and also displaying the characteristics of living polymerisations were first reported in 1995 (Krstina *et al*. and Matyjaszewsky *et al*.). The mechanism of the reversible chain transfer step may involve homolytic substitution or addition-fragmentation. An essential feature is that the product of chain transfer is also a chain transfer agent with similar activity to the precursor transfer agent. The process has also been termed degenerate or degenerative chain transfer since the polymeric starting materials and products have equivalent properties and differ only in molecular weight (Moad and Solomon, 2006). Depiction of the main polymer core-equilibration step in RAFT polymerisation is carried out in Figure 1.2.

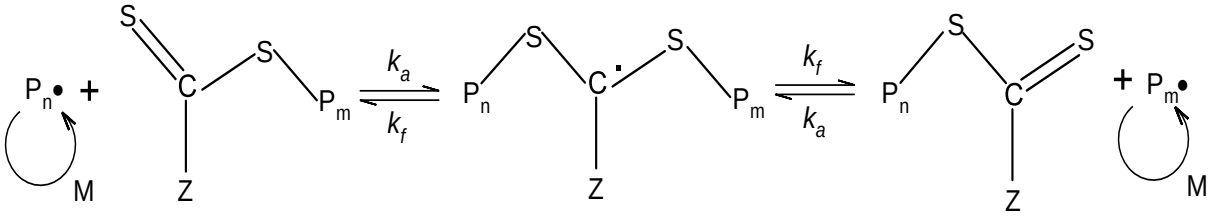

Figure 1.2. Depiction of main polymer equilibration step in a RAFT polymerisation.

1.1.2.4 Other Controlled Polymerisation Techniques

There are other controlled/living polymerisation techniques with scientific and industrial importance, namely, a combination of competitive outer sphere single electron transfer (SET) and degenerative chain transfer mechanisms (DT). Iodine-transfer, telluride-mediated and stibine-mediated polymerisations are the degenerative chain transfer most used. Here, will be only reported iodine transfer polymerisation (ITP) as illustration as none of this techniques as been performed in this work.

Iodine transfer polymerisation as a method of living radical polymerisation was reported firstly by Tatemoto in 1992. The process involves conducting a polymerisation with a conventional initiator (e.g. AIBN) in the presence of an activated alkyl iodide. This controlled technique has been used for styrene (Gaynor *et al*., 1995; Goto *et al*., 1998), acrylates (Gaynor *et al*., 1995) and fluoro-olefins (Ameduri and Boutevin 1999; Tatemoto, 1992) polymerisations. The occurring of various side reactions in polymerisation of vinyl acetate like head addition during propagation and the formation of an aldehyde end group by acid catalyzed decomposition of end group (Iovu and Matyjaszewski, 2003) are drawbacks of

Iodine-transfer polymerisation. Despite this side reactions, relatively low dispersities <1.4 are observed for molecular weights less than 20000 (Moad and Solomon, 2006).

Outer sphere single electron transfer has a significant role in organic chemistry. This process provides an intermediate radical anion or cation. The living polymerisation of vinyl chloride (VC) with alkyl iodide initiators and nascent Cu(0) catalyst is considered to involve an SET process (Percec *et al*., 2002 and 2003). SET does not require a metal catalyst and can involve other single electron reducing agents as dithionite (Percec *et al*., 2005). The Percec group developed for the first time, a polymerisation process able to produce PVC with controlled features (Percec *et al*., 2002 and 2003). The further discovery of the single electron transfer-degenerative chain living radical polymerisation (SET-DTLRP) (Percec *et al*., 2004a), made possible the use in synthesis of activated (Coelho *et al*., 2008 and 2009) and non-activated monomers (Percec *et al*, 2004a and 2004b), using a method which should hopefully be possible to implement at industrial scale (Coelho *et al*., 2011a and 2011b).

The main interest of SET-DTLRP is the production of poly(vinyl chloride) block copolymers. By controlling the composition and the molecular weight of this block copolymer it is possible to produce a material with similar mechanical and thermal properties to conventional plasticized poly(vinyl chloride) (Coelho *et al*., 2006a, 2006b and 2006c) without requiring the use of extractable and possibly toxic external plasticizers.

1.2 Intramolecular Cyclization Reactions

The issue of intramolecular cyclization reactions was revealed with the first studies about copolymerisation with crosslinking and gel formation. The cyclizations reactions occur between a radical site and a pendant double bond in the same polymer molecule and may be classified in two types: primary cyclization (Figure 1.3), which occurs in primary molecules (without branching or crosslinking) and secondary cyclization (Figure 1.4), which occurs in molecules containing two or more primary chains. These intramolecular reactions have a huge influence on the homogeneity of the network and gel formation. Thus, the understanding of these reactions is of great importance to ensure the product quality and to improve the polymer properties. The effect of cyclization is more pronounced in FRP with more diluted systems (Gonçalves *et al*., 2007; Trigo *et al*., 2008). Some significant improvements are achieved with controlled systems, ATRP (Gonçalves *et al*., 2010a, 2010b, 2010c and 2010d), NMRP (Gonçalves *et al*., 2013a) and especially with RAFT, where the Luo group has

achieved some important results on particle size by decreasing the level of the amphiphilic RAFT agent (Ye *et al*., 2011).

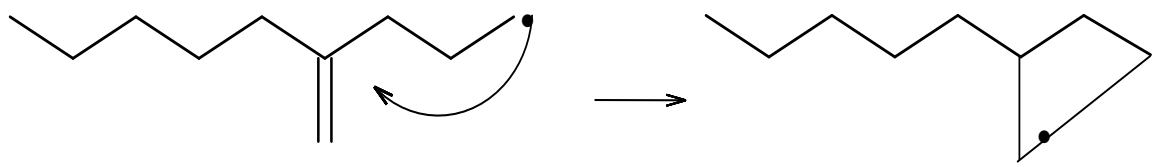

Figure 1.3. Schematic of a general primary cyclization reaction.

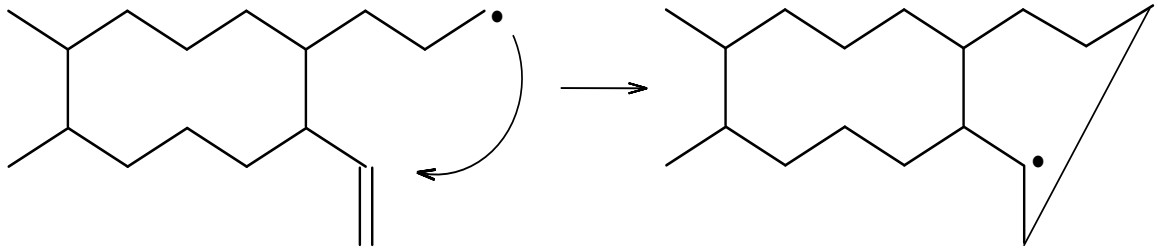

Figure 1.4. Schematic of a general secondary cyclization reaction.

1.3 Relevance and Motivation

The free-radical polymerisation of vinyl monomers is responsible for more than 50 % of the industrial production of synthetic polymers. The economic impact of product and process engineering in this area is obviously very important even arising from small improvements. Besides commodity polymers, new materials for special technology applications are also produced through this class of chemical processes. Development of tools allowing the design of polymers with tailored properties is especially important in this context owing to the strong relation between the molecular architecture and the end-use properties of such advanced materials.

The synthesis of hyperbranched polymers through step-growth polymerisation is a well studied subject. However, some materials are produced by free-radical polymerisation. One of the major characteristics of this method is the gel formation at relatively low monomer conversion, which can harm the properties of the final product. Thus, to avoid the gelation at low conversion is necessary to implement new synthesis techniques such as the use of a chain transfer agent, semi-batch reactor (Gonçalves *et al.*, 2007). In the last decades, many synthetic polymers have been produced by free-radical polymerisation. The most used synthesis

techniques are bulk, solution, emulsion and suspension. In the last years, new technologies have been employed like miniemulsion and supercritical carbon dioxide. This work will focus on the "living" controlled radical polymerisation which allows the production of polymers with high homogeneity comparatively to free-radical polymerisation technique. There are various kinds of controlled techniques being ATRP, NMRP and RAFT the most used. The ATRP technique is very versatile, and may be used in several chemical systems but has the inconvenience of generate huge quantities of metals in the final product. The NMRP technique it is based on nitroxide radicals which are very easy to handle but are almost restricted to styrenic monomers. The RAFT technique can be used with a wide range of monomers and in different chemical systems but the RAFT transfer agents are not easy to obtain.

In the industrial area, the advances in the polymer production occur in a rapid way. This material have a lot of properties to be analysed which are modified in function of the process variables (feed concentration, temperature, etc.). Many polymers are commercialized without knowing all the reactions involving on its production. Indeed, CRP techniques have the need for a definition of the mechanism that is responsible for the controlled copolymerisation process, with presence of secondary reactions; with effects of the controlling agent on the gel point and the formation of intramolecular cyclizations with effects on properties of the final product. The present work also includes the issues above described. The experimental data obtained associated with the modeling tool used allow the improvement of the molecular architecture of the produced materials and its future implementation at industrial level. Besides that, the results obtained in this work can be used to obtain useful tools in the project of hyperbranched and polymer networks with tailored properties.

1.4 Objectives and Outline

The scope of the present is the synthesis and properties of the products from Free-Radical Polymerisation (FRP) and Controlled Radical Polymerisation (CRP) of multivinyl monomers. Therefore, it is experimentally assessed the impact of the synthesis conditions on the formation mechanism and on the properties of hyperbranched polymers, gels and hydrogels. Namely, the following parameters were changed along the experimental program:

- Different synthesis techniques are used (FRP, ATRP, NMRP and RAFT) with various types of mediator agents, initiators, solvents, degree of neutralization (in acrylic and methacrylic acids) and temperatures.

- Different types of monomers families (acrylates, methacrylates, styrenics and acrylamides).
- Solution, suspension and inverse-suspension are used as polymerisation systems.
- Two bench polymerisation reactors are used, one atmospheric with a semi-industrial capacity of 2.5 L and a pressurized reactor with capacity of 1 L to allow the performance of aqueous reactions near and above 100 °C.
- The partial and the final products are characterized through a set of techniques to assess their properties and the molecular architecture. Namely are evaluated the following properties:
    - Dynamic of conversion is performed by gravimetry, size exclusion chromatography with refractive index detection and in some case by *in-line* FTIR-ATR.
    - Dynamic of product formation through the determination of average molecular weights, *z*-average radius of gyration and absolute molecular weight distribution by gel permeation chromatography with different detectors (light scattering, refractive index, intrinsic viscosity and ultra violet (both in the aqueous case)).
    - Also by gravimetry is determined the swelling ratio capacity, gel and sol fractions.
    - Iodine chloride derivatization method is used to determine the concentration of pendant double bonds of the networks. This variable is also estimated less accurately by FTIR in *off-line* mode.
    - Using the ultraviolet and refractive index detection is determined the dynamics of drug releasing by the hydrogels produced (aqueous system).

With “smart polymers” it is assessed the response of these hydrogels to environmental changes on pH or/and temperature

As a complement to this work, these experimental studies are supported by the development of kinetic models with the capacity to describe these non-linear polymerisations systems (Costa and Dias, 1994, 2003, 2005, 2006 and 2007; Dias and Costa, 2003, 2005a, 2005b, 2006, 2007 and 2010). It is used a computational package that allows the automatic inclusion into the kinetic schemes of different kinds of branching and crosslinking phenomena. Thus, using the experimental runs performed in this work has leaded to the improvement of a tool that could help in the inception of synthesis conditions to obtain materials with tailored properties.

Chapter 2 deals with conventional free-radical copolymerisation of multivinyl monomers.

Chapter 3 is focused on the study of atom transfer radical copolymerisation of acrylates.

Chapter 4 shows the results obtained with nitroxide mediated radical copolymerisation of STY/DVB.

Chapter 5 presents the reversible addition-fragmentation polymerisation of styrene and copolymerisation of styrene/divinylbenzene.

In Chapter 6 it is assessed the conventional free-radical copolymerisation synthesis of hydrogels from water compatible monomers.

Chapter 7 shows the importance of RAFT to the production of water compatible polymers.

Chapter 8 describes the conclusions and suggests some recommendations for future work.

CHAPTER 2

CONVENTIONAL FREE-RADICAL COPOLYMERISATION OF MULTIVINYL MONOMERS

Abstract. In the present chapter the impact of the synthesis conditions on the formation mechanism and on the properties of hyperbranched polymers is assessed through experiments on styrene/divinylbenzenes and of methyl methacrylate/ethylene glycol dimethacrylate polymerisations. Gel formation and some gel properties were also studied with the former chemical system. More specifically, the experimental program has carried out measurements on:

- Solution polymerisation at batch and semi-batch operation. Suspension polymerisation at batch operation.
- Dynamics of conversion using gravimetry, size exclusion chromatography (SEC) with refractive index (RI) detection and in some cases exploiting *in-line* FTIR-ATR.
- The molecular architecture of the products through the determination of average molecular weights, *z*-average radius of gyration and absolute molecular weight distribution by size exclusion chromatography coupled with light scattering and refractive index detectors.
- The influence of key polymerisation parameters on the dynamics of gelation, namely the initial relative amount of crosslinker on gel formation through the determination of gel and sol fraction along polymerisation time and the assessment of the influence of initial proportions between monomers and inert diluents.
- The morphology of the produced gel beads of STY/DVB by SEM with different kinds and amounts of the diluent.

Intramolecular cyclization was mostly neglected in the complementary studies on modelling using the experimental data obtained below cited.

This chapter is based on the following publications:

M.A.D. Gonçalves, R.C.S. Dias, M.R.P.F.N. Costa, *Macromol Symp.* 259 (2007) 124-134.

I.M.R Trigo, M.A.D. Gonçalves, R.C.S. Dias, M.R.P.F.N. Costa, *Macromol. Symp.* 271 (2008) 107-119.

M.A.D. Gonçalves, V.D. Pinto, R.C.S. Dias, M.R.P.F.N. Costa, *Macromol Symp.* 302 (2011) 179-190.

2.1 Introduction

In recent years the synthesis and characterization of branched/crosslinked polymers has been a subject with increasing research activity. Indeed, there is much room for improving some properties of these materials as compared with their linear counterparts. Higher functional group densities as well as suitable solubility and viscosity ranges can be exploited by producing hyperbranched polymers. Thus, new research lines have been explored in order to control the synthesis of soluble branched polymers from vinyl and divinyl monomers, namely by trying to achieve higher monomer conversions without gelation through the use of a chain transfer agent (Gretton-Watson *et al.*, 2006; O'Brien *et al.*, 2000). Other important experimental works have dealt with the characterization of the molecular architecture of these materials (O'Brien *et al*., 2000; Saunders *et al*., 2005). In another application field, copolymer networks are intentionally prepared by promoting the gelation of mono and divinyl monomers such as styrene with divinylbenzene (Okay, 2000). In this case, formation of macroporous structures in polymer networks also makes possible their use as particles and membranes for many separation processes. Styrene/divinylbenzene gels are well known for that purpose, usually after chemical derivatizing, such as with ion-exchange resins. The formation of insoluble networks based on these monomers was studied by Staudinger and Husemann (1935) at the very beginning of polymer science (Okay, 2000)

In this chapter, three different systems are studied. At first the polymerisation/copolymerisation of styrene/divinylbenzene in a semi-batch reactor is discussed. An experimental confirmation of the theoretical work of Dias and Costa (2005a) concerning the control of the crosslinked structure of the copolymer by adjusting the feed policy of the reagents has been achieved. The results here presented show that is possible to usefully modify the current production process of branched/crosslinked polymers, namely with the purpose of obtaining soluble branched polymers at higher conversions than the conventional batch operation. A further benefit of this research was the possibility of having a better insight on the kinetics of these polymerisation systems. In the second system, the general kinetic approach is applied to the conventional radical polymerisation of MMA with EGDMA in a batch reactor. It is shown that besides the prediction of the dynamics of molecular weights it is also possible to explore the dynamics of the mean square radius of gyration of the polymers. These predictions are compared with measurements by SEC/RI/MALLS for the whole set of different experiments performed. It was shown that the same fitting parameters calculated from the measured molecular weights and monomer

conversions yield also good predictions of the mean square radius of gyration whenever intramolecular reactions are negligible. This consolidated knowledge about the molecular architecture of these materials shows the possibility of carrying out the prediction of physical properties relevant for their uses. The third part is focused in the dynamics of formation of such gel beds in a batch reactor, with the goal of obtaining new insights in the polymer reaction engineering of such processes. The experimental program has covered the synthesis and characterization of polymer networks, both in the pre- and post-gelation periods. Final materials were also characterized by Scanning Electronic Microscopy (SEM). These experiments are complemented with kinetic modelling studies in the frame-work of a general theory which can be used regardless of gelation (Costa and Dias, 1994, 2005, 2006 and 2007; Dias and Costa, 2003, 2005a, 2005b, 2006 and 2007).

2.2 Experimental Details

2.2.1 Materials

In this work on the model system for the radical polymerisation of STY/DVB in solution medium were used toluene at 99.7 % purity, AIBN at 98 % purity, styrene stabilized with 0.005 % w/w 4-tert-butylcatcehol (to avoid room temperature polymerisation) at 99 % purity and commercial grade divinylbenzene stabilized with 0.1 % w/w 4-tert-butylcatcehol at 80 % purity. All of them have been purchased from Sigma Aldrich and used as received. The commercial DVB is a mixture of isomers, 56.2 % *m*-divinylbenzene and 24.3 % *p*-divinylbenzene, plus 19.6 % of ethylvinylbenzene.

For the model system of radical polymerisation of MMA/EGDMA in solution medium were used toluene at 99.7 % purity, AIBN at 98 % purity, benzoyl peroxide (BPO) moistened with 25 % water at 97 % purity (calculate on the dry substance, methyl methacrylate stabilized with 10 to 100 ppm monomethyl ether hydroquinone at 99 % purity and ethylene glycol dimethacrylate stabilized with 100 ppm of monomethyl ether hydroquinone at 98 % purity have been purchased form Sigma-Aldrich and used as received.

In suspension polymerisation runs of radical polymerisation of STY/DVB were used the same reactants as in the solution process now including *n*-heptane with 99 % purity and poly (vinyl alcohol) with $\bar{M}_w$ of 85000-124000, 87-89 % hydrolyzed purchased from Sigma-Aldrich. As continuous phase ultra pure water was used.

2.2.2 Polymerisation Set-up

Figure 2.1 depicts the experimental set-up used to carry out all the experiments in atmospheric pressure. The stainless steel reaction vessel with 2.5 dm^3 capacity is equipped with a refrigerator jacket for maintaining reaction temperature at the desired set-point. A thermocouple is used for on-line measurement of temperature of the reaction medium. The computer control of temperature is executed by acting on the refrigeration bath. The time programmed feed of the monomer, solvent, initiator and chain transfer agent is possible thanks to the two metering pumps which are also computer controlled. A third pump can operate at a constant flow rate. The reactants to be fed into the reactor using the semi-batch mode are stored into three stainless steel reservoirs kept at the same temperature as the reactor using a heating/cooling bath. An argon stream is used to purge the contents of the reactor and is continuously bubbled through the polymerisation medium during the reaction. The reactor is equipped with a condenser in order to prevent monomer or solvent losses due to the bubbling process. A mechanical stirrer with four blades is used to keep the reaction medium homogeneous and is also controlled by computer.

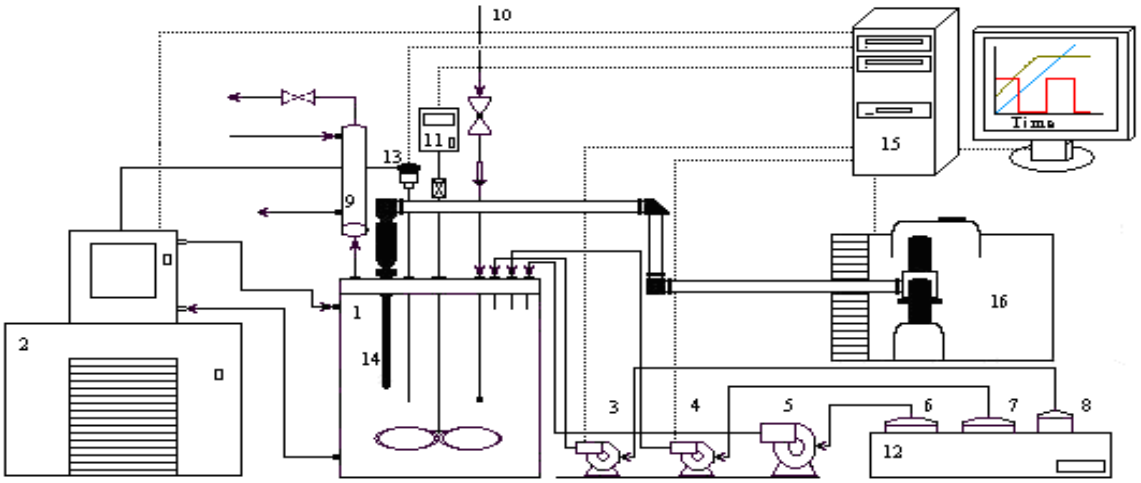

1 – Reaction Vessel (2.5 L)	2 – Thermostatic Bath	3,4 – Peristaltic Pumps
5 – Manual Pump	6,7 – Reservoirs (1 L)	8 – Reservoir (200 mL)
9 – Condenser	10 – Argon Inlet	11 – Mechanical Stirrer
12 – Heating Bath	13 - Thermocouple	14 – ATR Immersion Probe
15 – Computer	16 - FTIR instrument with MCT detector	

Figure 2.1. Experimental set-up used in the reaction polymerisations.

In all the solution polymerisations runs the desired initial amounts of monomers and solvent were charged to the reaction vessel and brought up to the desired reaction temperature. The feeding reservoirs were charged at the same time when semi-batch mode was used and also brought up to the desired reaction temperature. Argon was bubbled in the reaction vessel at flow rate 40 cm^3/min during one hour, before the start of the polymerisation in order to deoxygenate the reaction medium, and that same flow rate was kept during the whole polymerisation process.

The solution polymerisations of STY/DVB were started by adding the initiator (AIBN) to the reactor (see Table 2.1) and the feeding system was turned on. At prescribed polymerisation times, samples of the reaction medium were withdrawn from the reactor. For each sample, a portion was diluted in tetrahydrofuran and analysed in the SEC/RI/MALLS system, the remaining amount was precipitated in methanol in order to determine monomer conversion by gravimetry. The final dry polymer was later analysed also by SEC/RI/MALLS.

Table 2.1. Description of the set of experiments performed in the study of the radical copolymerisation of STY with DVB in toluene solution at 60 °C in a semi-batch reactor. Concentrations are in mol/L.

Run	$[STY]_0$	$[DVB]_0$	$[I]_0$	$[T]_0$	Feed Conditions
1	4.350	0.000	0.081	4.694	Batch
2	4.312	0.061	0.081	4.654	Batch with $f_{DVB} = 0.01395$
3	4.312	0.061	0.081	4.654	Batch with $f_{DVB} = 0.01395$ and mole ratio CTA/DVB=0.08168
4	4.350	0.000	0.081	4.694	Constant feed rate 0.73 ml/min during 2 h. (final $f_{DVB} = 0.01358$)
5	4.350	0.000	0.081	4.694	Constant feed rate 0.40 ml/min during 6 h. (final $f_{DVB} = 0.01371$)
6	4.350	0.000	0.050	4.694	Constant feed rate 0.65 ml/min during 5.5 h. (final $f_{DVB} = 0.01390$)

In the MMA/EGDMA solution polymerisation runs the desired quantities of reactants were charged to the reactor (see Table 2.2) and brought to the prescribed temperature of 60 °C. Polymerisations were started by defining the instant $t = 0$ when the initiator was added to the reactor. Samples of reaction mixture were withdrawn from the reactor at prescribed polymerisation times and analysed in the SEC/RI/MALLS system to measure molecular weights, monomer conversion and average molecular radius of gyration. Monomer conversion was also measured by gravimetry.

Table 2.2. Set of experiments performed in the radical copolymerisation of MMA with EGDMA in toluene solution at 60 °C.

Run	$[MMA]_0$(mol/L)	$[EGDMA]_0$(mol/L)	$[I]_0$(mol/L)	$[T]_0$(mol/L)
1	3.269	5.170×10^{-3}	1.56×10^{-2}AIBN	6.097
2	3.267	7.692×10^{-3}	1.57×10^{-2}AIBN	6.094
3	3.272	0.000	1.55×10^{-2}BPO	6.103
4	3.271	1.697×10^{-3}	1.55×10^{-2}BPO	6.101
5	3.270	3.037×10^{-3}	1.57×10^{-2}BPO	6.099
6	3.267	7.585×10^{-3}	1.55×10^{-2}BPO	6.094

In the suspension radical polymerisations of STY/DVB an excess of aqueous phase was used. A known amount of PVA was dissolved in ultra-pure water, at room temperature, using a magnetic stirrer. The concentration of PVA in aqueous phase was set using the total monomer weight as reference. In all experiments 0.09 % of PVA by total monomer weight was used, similarly to the reported in related works (Kiatkamjornwong *et al*., 2001). The desired amount of aqueous phase (around 913 ml) was charged to the reactor and brought to the polymerisation temperature of 60 °C with the mechanical stirrer working at 400 rpm. The polymerisation medium was purged with argon at a flow rate of 40 ml/min before and during the operation. The organic phase was prepared by forming a solution involving the required amounts of chemicals, namely: STY, DVB, AIBN and solvents as detailed in Table 2.3. This solution was prepared immediately before the start of the reaction, at room temperature, in order to minimize the premature thermal decomposition of AIBN. When the temperature set point for the aqueous phase was reached, the organic phase (around 287 ml) was charged to the reactor defining the start of the polymerisation. Product samples were collected at prescribed polymerisation times. All polymerisations were stopped after six hours of reaction.

Table 2.3. Description of the set of experiments performed in the study of the suspension copolymerisation of styrene/divinylbenzene at 60 °C.

Run	V_T(L)	f_{OR}	f_M	f_{DVB}	$100\times f_I$	f_{HEP}
1	1.2	0.24	0.5	0.2	1.24	0.00
2	1.2	0.24	0.5	0.2	1.25	0.25
3	1.2	0.24	0.5	0.2	1.25	0.50
4	1.2	0.24	0.5	0.2	1.24	0.75
5	1.2	0.24	0.5	0.2	1.25	1.00
6	1.2	0.24	0.5	0.1	1.25	0.50

2.2.3 SEC/RI/MALLS Products Analysis

Molecular weights, average molecular radius of gyration and monomer conversion of the products were measured using THF as solvent with a Polymer Laboratories PL-GPC-50 integrated SEC system with differential refractometer working at 950 ± 30 nm attached to a Wyatt technology Dawn8+ HELEOS 658 nm Multi Angle Laser Light Scattering detector. The polymer samples were fractionated by molecular size (hydrodynamic radius) using a train of three GPC columns PL gel (300×7.5 mm) with nominal particle size of 10 μm and pore type MIXED B-LS, maintained at constant temperature of 30 °C and using THF as the eluent at a flow rate of 1 ml/min. For the suspension runs samples were collected from the reactor at different polymerisation times, including aqueous and organic phases. Then they were poured in a decanting ampoule containing a large quantity of cold water in order to stop the reaction. After decanting, most of the organic phase was diluted in a large amount of methanol in order to precipitate the polymer (soluble and insoluble fractions). For samples collected before gelation, a small amount of organic phase was directly diluted in THF and analysed by SEC/RI/MALLS. With samples containing gel, the soluble fraction analysed by SEC/RI/MALLS was obtained after the immersion of the global material in THF during one day (a detailed procedure can be found in appendix A).

2.2.4 Gravimetric Measurements

The remaining mixture resulting from the above described sampling process was weighed and precipitated into a large excess of methanol in order to isolate the polymer. After vacuum drying at 40 °C during 24 hours, monomer conversion could also be estimated by recording the weight loss (the full procedure is described in appendix A).

2.2.5 Refractive Index Increment Measurement

For the measurement of the refractive index increment (*dn/dc*) of the polymers, solvents and monomers was used a Wyatt Technology OPTILAB DSP 633 nm interferometric refractometer. The results obtained for polystyrene, toluene, styrene, poly(methyl methacrylate), MMA and EGDMA in THF were 0.189, 0.110, 0.170, 0.0912, 0.0077 and 0.0475 ml/g, respectively, and are required by the ASTRA software for the determination of the averages molecular weights and for estimating the overall conversion from the values of the differential refractometer (RI) peak areas of monomer and polymer in the

chromatographic traces of the SEC analysis (the full procedure to obtain these results is described in appendix A).

2.2.6 *In-line* FTIR-ATR Monitoring

These polymerisations were monitored *in-line* using an Attenuated Total Reflection immersion probe coupled to a Fourier Transform Infra-Red spectrophotometer. The following instruments were used: Axiom analytical immersion probe model DPR 207 (ZnSe element with spectral cut-off at 600 cm^{-1}, maximum pressure and temperature operation 60 bar and 280 °C, respectively) and an ABB Bomem Fourier Transform Infra-Red spectrophotometer, model FTLA2000-104. The probe and the spectrophotometer are connected by a three arms light guide and an ABB Bomem Mercury-Cadmium-Telluride (MCT) detector (model D10B), cooled with liquid nitrogen. The spectrometer is equipped with this kind of the detector in order to increase the sensitivity of the analysis. These FTIR-ATR measurements were performed using the spectrum of air taken at room temperature as the reference background being the optical system continuously flushed with argon. A resolution of 4 cm^{-1} was used for the spectra that were taken over the full MIR range from 600 cm^{-1} to 4000 cm^{-1}. Each spectrum was calculated from 128 interferograms (the full procedure is described in appendix A).

2.2.7 Measurement of the Weight Fraction of Gel

Polymer samples (soluble and insoluble fractions) obtained by precipitation in methanol were filtrated and dried in vacuum overnight. Afterwards, they were washed several times, during one week, in large amounts of THF in order to collect the insoluble network. The time evolution of the insoluble weight fraction of polymer during the polymerisation was thus measured (the full procedure is described in appendix A).

2.2.8 Swelling Ratio Measurements

For each run, the final suspension, correspondent to six hours polymerisation reaction time, was processed as above described in order to isolate the produced gel beads (section 2.4.1.5). The swelling ratio of the dried gel beads was estimated by weighing around 1 g of material which was afterwards immersed in a large amount of THF. After 24 hours the swollen gel beds were weighed again and the ratio between swollen and dried weights was used to estimate the swelling ration of these materials (the full procedure is described in appendix A).

2.2.9 Scanning Electron Microscopy

The dried gel beads above described were also analysed by Scanning Electron Microscopy (SEM) in the Centro de Microscopia da Universidade do Porto (CEMUP). The influence of the synthesis conditions in the structure (macroporous formation) of the produced materials could thus be assessed.

2.3 Solution copolymerisation of Styrene with Divinylbenzene

2.3.1 Kinetic Modelling

The modelling of the present case study was carried out using the general kinetic approach allowing the prediction of molecular weight as well as *z*-average molecular radius of gyration for non-linear irreversible polymerisations system (Costa and Dias, 2005 and 2007; Dias and Costa, 2005a and 2006).

2.3.1.1 Chemical Species

Twenty nine chemical species are considered in the kinetic modelling for the copolymerisation of styrene with divinylbenzene initiated by AIBN (Table 2.4). In Figures 2.2 and 2.3 are represented the monomers and the pendant double bonds present in this system: styrene monomer, divinylbenzene monomers consisting of two isomers (*meta*- and *para*-) with different reactivities. Hence, the two pendant double bonds arising from DVB isomers are treated as two additional monomers. Some other chemical groups such as initiator, solvent and chain transfer agent as well as their primary radicals are represented in Figures 2.4 and 2.5.

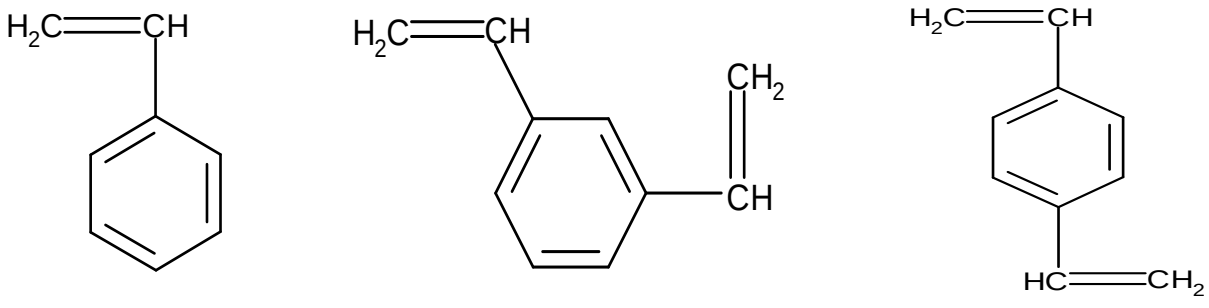

(a) (b) (c)

Figure 2.2. Schematic representations of (a) styrene (b) *m*-divinylbenzene and (c) *p*-divinylbenzene.

Table 2.4. Chemical groups for the modelling of radical copolymerisation of styrene/ divinylbenzene.

Group description	Alias
Styrene (STY)	M_1
m-Divinylbenzene (*m*-DVB)	M_2
p-Divinylbenzene (*p*-DVB)	M_3
Initiator (I)	C_1
Solvent (T)	C_2
Chain transfer Agent (CTA)	C_3
Inhibitor (Z)	C_4
Retarder (R)	C_5
Primary Radical from initiator (PRI)	R_1
Primary radical from solvent (PRS)	R_2
Primary radical from chain transfer agent (PRCTA)	R_3
Radical from styrene (RS)	A_1
Radical from *m*-divinylbenzene (R*m*DVB)	A_2
Radical from *p*-divinylbenzene (R*p*DVB)	A_3
Radical from *m*-pendant double bonds (R*m*PDB)	A_4
Radical from *p*-pendant double bonds (R*p*PDB)	A_5
Radical from retarder (RR)	A_6
m-pendant double bonds (*m*-PDB)	M_4
p-pendant double bonds (*p*-PDB)	M_5
Polymerised Styrene	U_1
Polymerised *m*-Divinylbenzene	U_2
Polymerised *p*-Divinylbenzene	U_3
Crosslinking site from *m*-divinylbenzene	U_4
Crosslinking site from *p*-divinylbenzene	U_5
Fragments from initiator, solvent, chain transfer agent, inhibitor and retarder	F_1-F_5

Five different kinds of polymer radicals are shown in Figures 2.6-2.8 since they present different structures and therefore different reactivities are also expected (Okay, 2000; Moad and Solomon, 2006; Nyhus *et al*., 1999; Hecker, 2000). Pendant double bonds (PDB) arising from commercial divinylbenzene, which are akin of two additional monomers in the present analysis, are also mutually distinguished as well as from the double bonds in the monomers as they are known to show different reactivities (Hecker, 2000).

(a) (b)

Figure 2.3. Schematic representations of (a) *p*-pendant double bond and (b) *m*-pendant double bond.

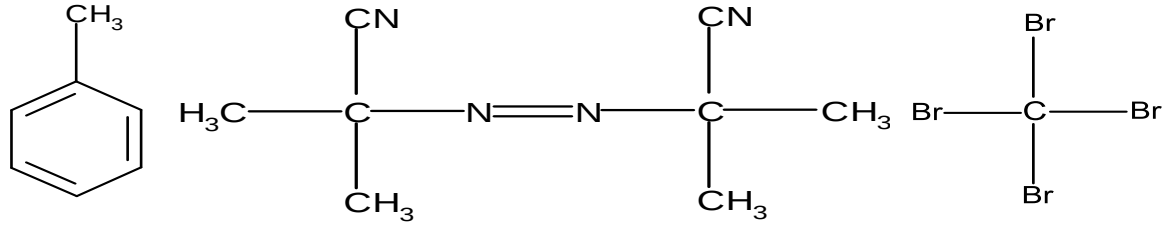

(a) (b) (c)

Figure 2.4. Schematic representation of (a) toluene (b) AIBN and (c) carbon tetrabromide.

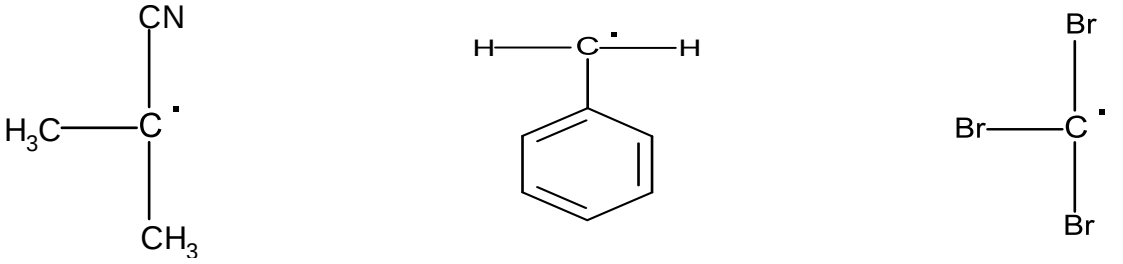

(a) (b) (c)

Figure 2.5. Schematic representations of primary radicals from (a) initiator (b) solvent and (c) chain transfer agent.

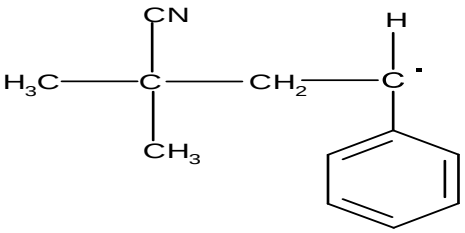

Figure 2.6. Schematic representation of the radical from styrene.

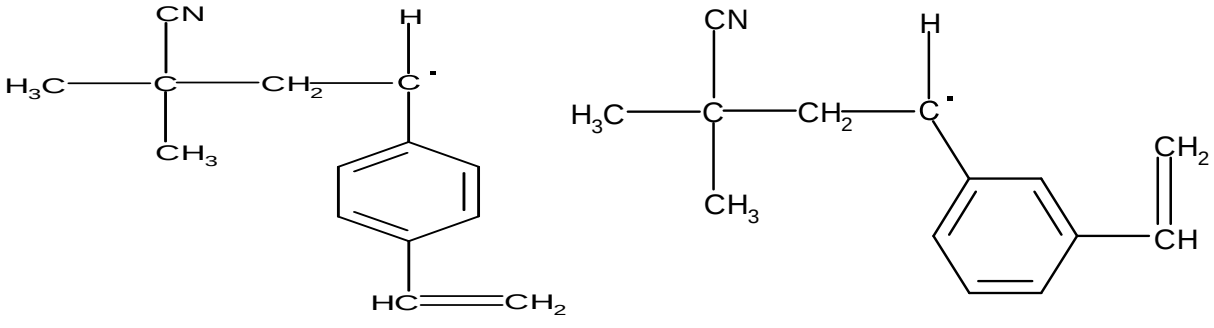

(a) (b)

Figure 2.7. Schematic representations of radical from (a) *p*-divinylbenzene and (b) radical from *m*-divinylbenzene.

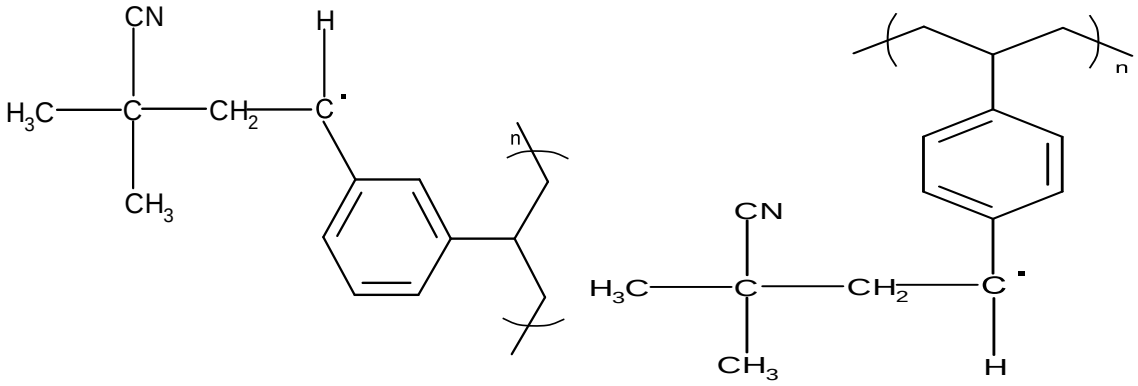

(a) (b)

Figure 2.8. Schematic representation of the radicals arising from (a) *m*-PDB and (b) *p*-PDB.

2.2.1.2 Chemical Reactions

The kinetic mechanism considered in the polymerisation/copolymerisation of a monovinyl monomer (styrene) with a divinyl monomer (divinylbenzene) initiated by a thermal initiator (AIBN) will be now discussed. In this case, as previously stated, one must take into account the two isomers of divinylbenzene, *meta*- and *para*-, as they show different reactivities. In Table 2.5 the kinetic scheme considered for this polymerisation system is presented. A total count of 114 chemical reactions is supposed to exist: initiator decomposition (1), initiation of monomers and pendant double bonds from primary radicals (15), propagation of monomers and pendant double bonds with different kinds of polymer radicals (30), chain transfers to solvent (6), chain transfer to chain transfer agent (6), inhibition of polymer and primary radicals (9), retardation of polymer centered radicals (21), termination by disproportionation of polymer radicals (21), termination by combination of polymer radicals (21). Despite the often difficult distinction between inhibitors (such as 4-tert-butylcatechol) and retarders (deactivation of primary radicals- deactivation/slowing of polymer radicals), the kinetic steps here considered involving these two species take into account the deactivation of all kinds of radicals and the existence of a polymer radical site with a lower reactivity coming from propagation with a retarder (such as oxygen). This radical is supposed to polymerise with monomers, as commonly accepted for oxygen centered radicals in styrene polymerisation (Moad and Solomon, 2006). The leading chemical reactions present in this system are below described.

As in nearly every free-radical polymerisations, it is convenient to consider the initiator decomposition as its first step. In Figure 2.9 it is represented that process leading here to the

formation of two primary radicals and nitrogen, where f represents the initiator efficiency factor.

Table 2.5. Kinetic scheme of radical copolymerisation of styrene/divinylbenzene.

Kinetic Step	Chemical Equation
Initiator Decomposition	$C_1 \xrightarrow{k_d} 2fR_1$
Initiation of monomers and PDBs	$R_j + M_k \xrightarrow{k_{Ijk}} A_k + U_k + F_j$
Styrene Propagation	$A_i + M_1 \xrightarrow{k_{pi1}} A_1 + U_1$
m-DVB and *p*-DVB propagations	$A_i + M_j \xrightarrow{k_{pij}} A_j + M_{2+j} + U_j$
m-PDB and *p*-PDB propagations	$A_i + M_j \xrightarrow{k_{pij}} A_j + U_j$
Chain transfer to solvent	$A_i + C_2 \xrightarrow{k_{Si}} dead\ chain + R_2$
Chain transfer to agent	$A_i + C_3 \xrightarrow{k_{CTAi}} dead\ chain + R_3$
Inhibition of polymer radicals	$A_i + C_4 \xrightarrow{k_{Zi}} dead\ chain + F_4$
Inhibition of primary radicals	$R_i + C_4 \xrightarrow{k_{ZPi}} inactive\ products$
Retardation of polymer radicals	$A_i + C_5 \xrightarrow{k_{ri}} A_6 + F_5$
Termination by combination	$A_i + A_j \xrightarrow{k_{tcij}}$Head-Head Unit
Termination by disproportionation	$A_i + A_j \xrightarrow{k_{tdij}}$Saturated + Unsat. Units

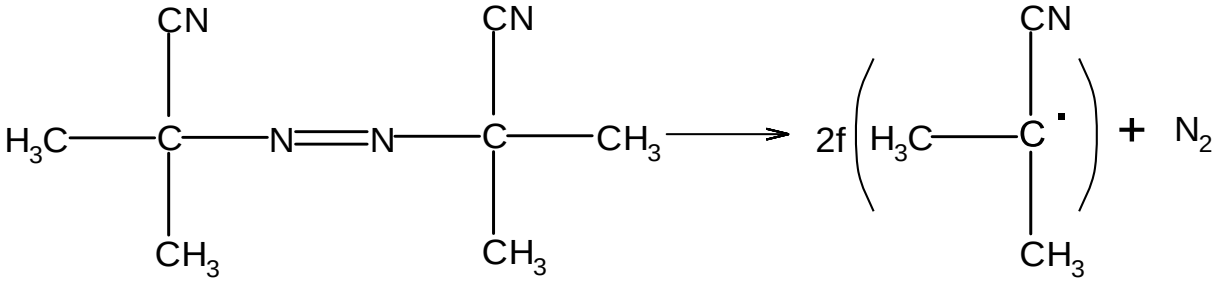

Figure 2.9. AIBN decomposition leading to primary radicals.

The initiation stage consists in the set of chemical reactions of primary radicals, arising from the initiator decomposition with the carbon-carbon double bonds present in the system. The reactivities of the double bonds depend on the monomer where they belong and therefore the initiation reactions present different kinetic constants. In Figures 2.10-2.12 are presented the initiation reaction by primary radicals of styrene monomer and divinylbenzene isomers.

The reactivity of the double bonds of the same monomer varies when one of them has been converted in a macromolecular chain. This fact is an example of a substitution effect and thus, as we have seen above, is necessary to distinguish the pendant double bonds from both DVB isomers. In Figures 2.13 and 2.14 are depicted the initiation reactions of the pendant double bonds from *m*-DVB and *p*-DVB, respectively.

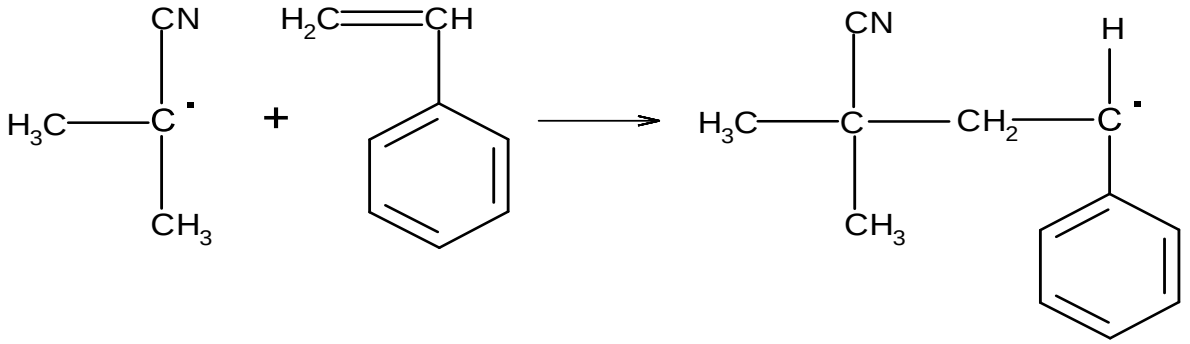

Figure 2.10. Initiation reaction of the styrene monomer by primary radicals.

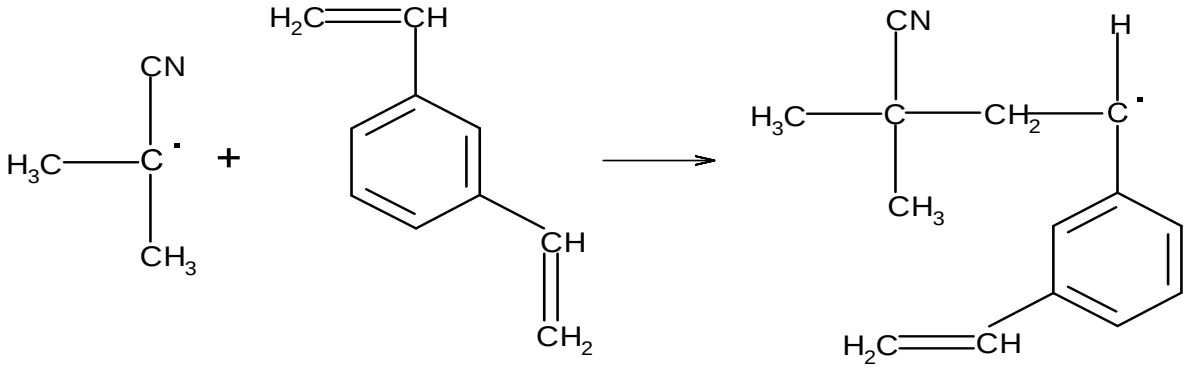

Figure 2.11. Initiation reaction of the *m*-divinylbenzene monomer by primary radicals.

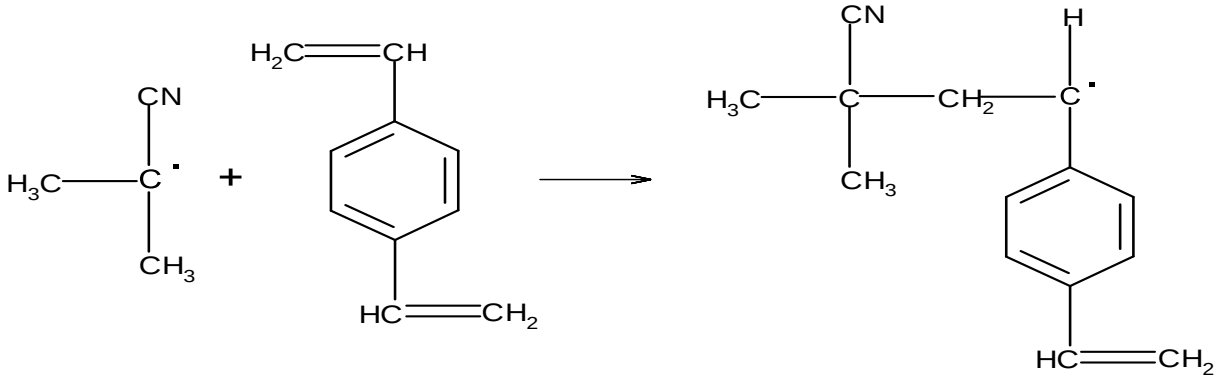

Figure 2.12. Initiation reaction of the *p*-divinylbenzene monomer by primary radicals.

The reactivities of double bonds depend on the monomer type and by the effect of substitution inside the divinyl monomer; also the macromolecular radicals present different reactivities depending on the parent monomer and their chain position. Thus, the reactivity of the free-radical depends on the substituent of the carbon atom where the radical is located. Thus, is

necessary to distinguish the propagation reactions according to the nature of monomer, kinds of double bonds and macromolecular radicals involved. It was already stated that it is necessary to consider five different kinds of double bonds and it will be also necessary to consider five kinds of macromolecular radicals. Therefore in the propagation reaction stage it is required to describe twenty five different processes.

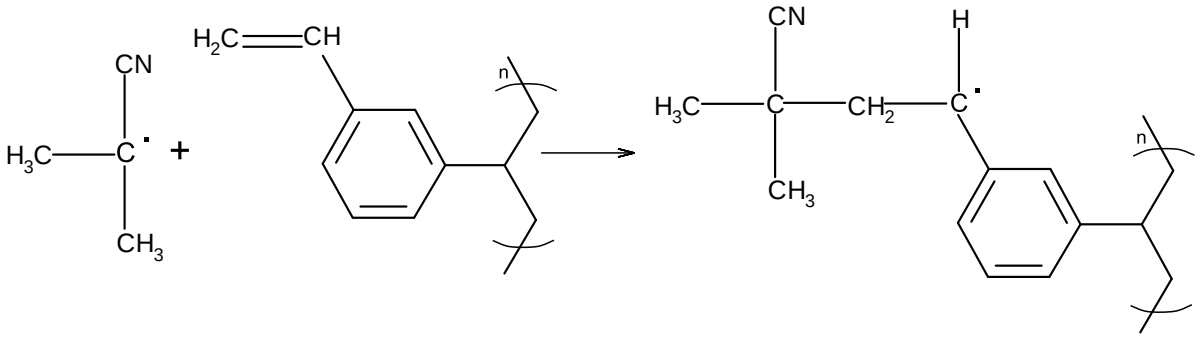

Figure 2.13. Initiation reaction of the *m*-divinylbenzene pendant double bond by primary radicals.

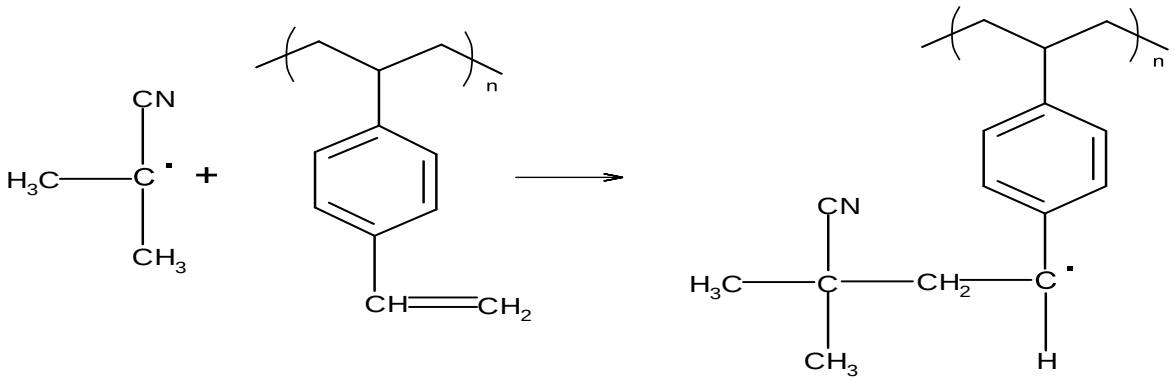

Figure 2.14. Initiation reaction of the *p*-divinylbenzene pendant double bond by primary radicals.

In Figure 2.15 it is represented the propagation stage of the styrene monomer with a macromolecular radical of the same monomer (homopropagation). The new formed radical is derived from the styrene monomer.

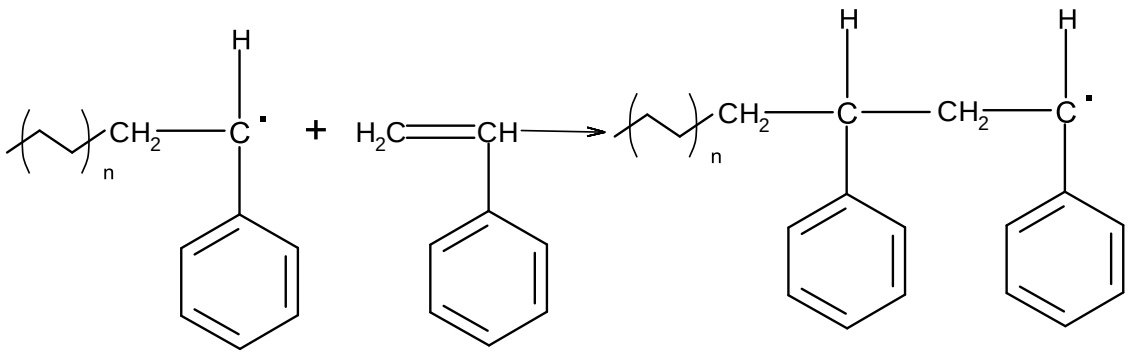

Figure 2.15. Propagation of styrene monomer with a radical formed by styrene monomer.

A radical formed by styrene can also react with one of the double bonds of the *meta*- or *para*-divinylbenzene being formed by this process a radical derived from *meta*- or *para*-divinylbenzene as shown in Figures 2.16 and 2.17, respectively. At last, a radical from styrene reacts with a pendant double bond of *meta*- or *para*- divinylbenzene by the process shown on Figures 2.18 and 2.19, respectively. The macromolecular radical resulting from this process is different from the previous because it belongs to the internal structure of the macromolecule. Hence it is called internal radical or radical from the pendant double bond. Furthermore, this process creates a tetrafunctional branched (crosslinking) point of the polymer and therefore leads to the formation of a branched structure.

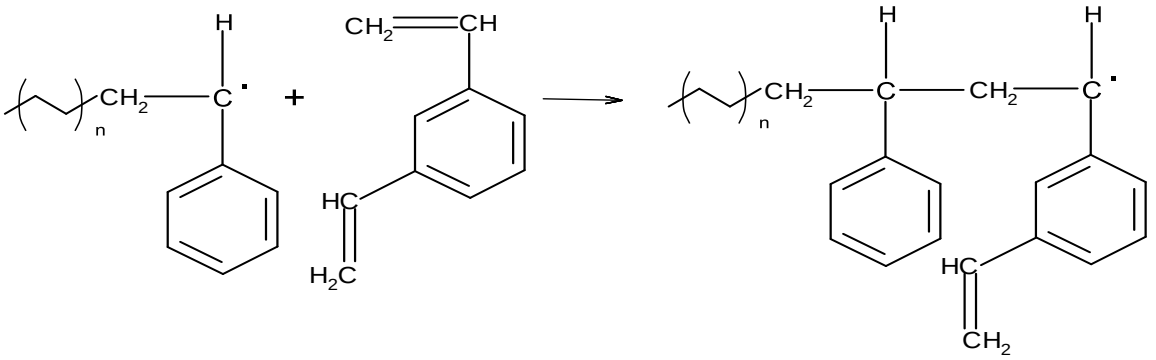

Figure 2.16. Propagation of *m*-DVB monomer with a radical formed by styrene monomer.

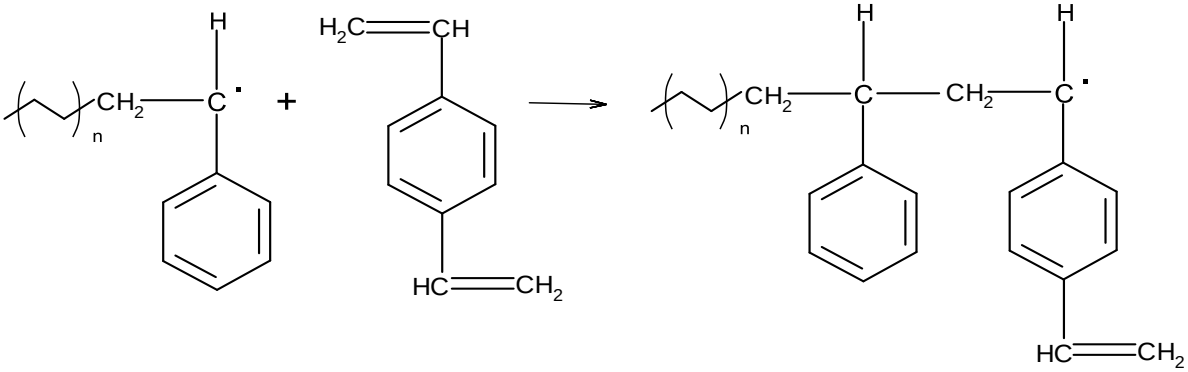

Figure 2.17. Propagation of *p*-DVB monomer with a radical formed by styrene monomer.

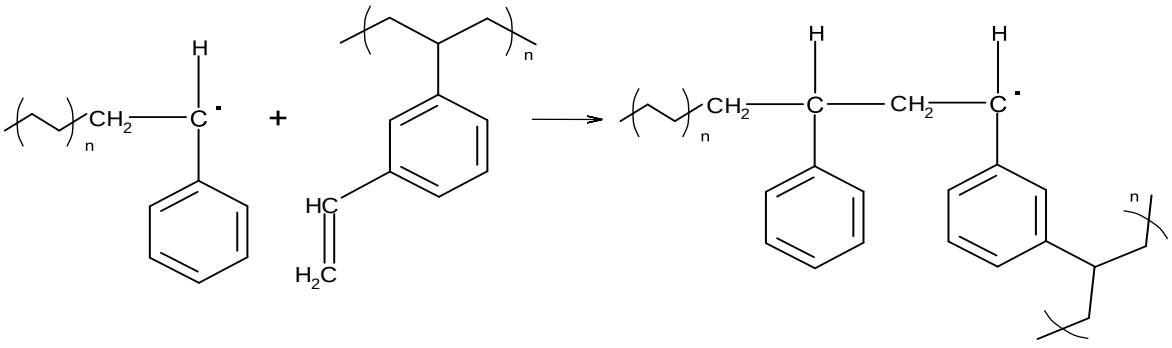

Figure 2.18. Propagation of *m*-DVB pendant double bond with a radical formed by styrene monomer.

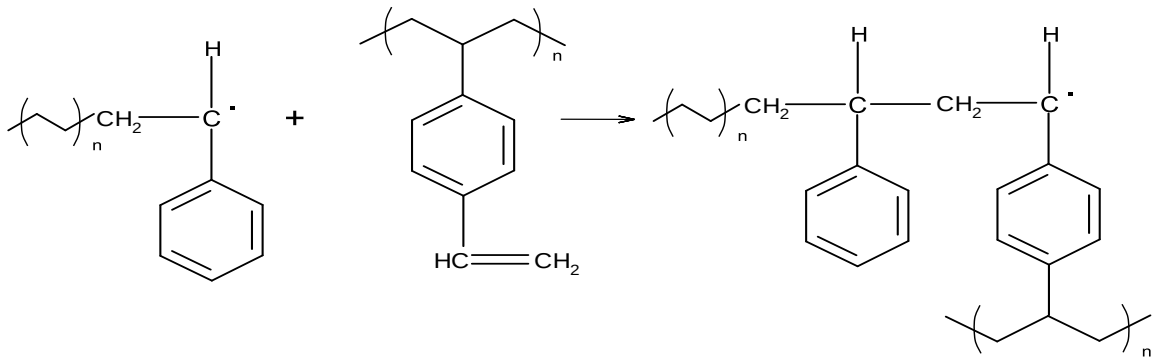

Figure 2.19. Propagation of *p*-DVB pendant double bond with a radical formed by styrene monomer.

When a radical derived from *meta*- or *para*- divinylbenzene propagates with a styrene unit as shown in Figures 2.20 and 2.21 a radical of styrene and a pendant double bond (with position depending on the DVB isomer) are formed. This is called a cross-propagation.

The propagation of a *meta*- or *para*- divinylbenzene with a radical formed by *meta*- or *para*- divinylbenzene monomer is represented in Figures 2.22-2.25. From this reaction is obtained a new radical of *meta*- or *para*- divinylbenzene and also a pendant double bond.

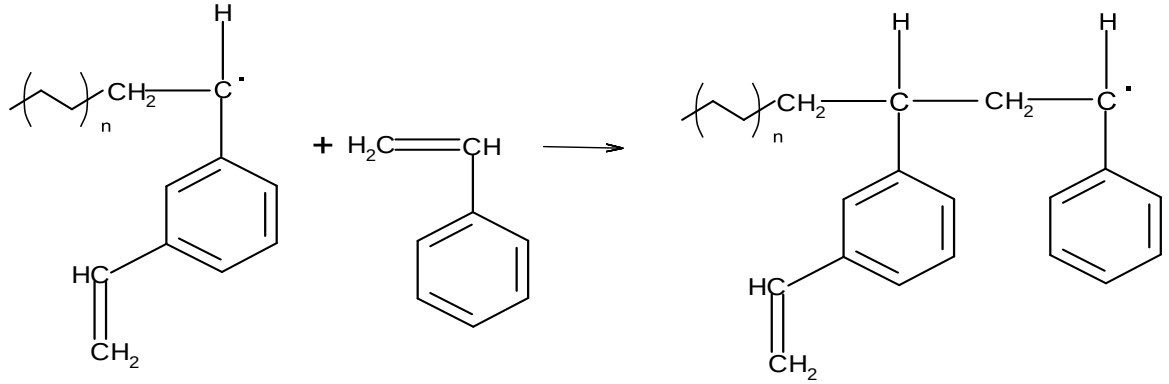

Figure 2.20. Propagation of styrene monomer with a radical formed by *m*-DVB monomer.

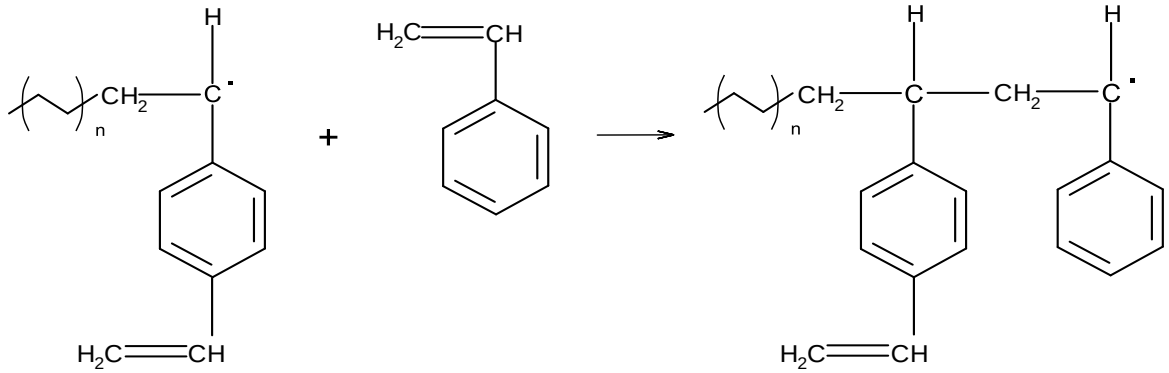

Figure 2.21. Propagation of styrene monomer with a radical formed by *p*-DVB monomer.

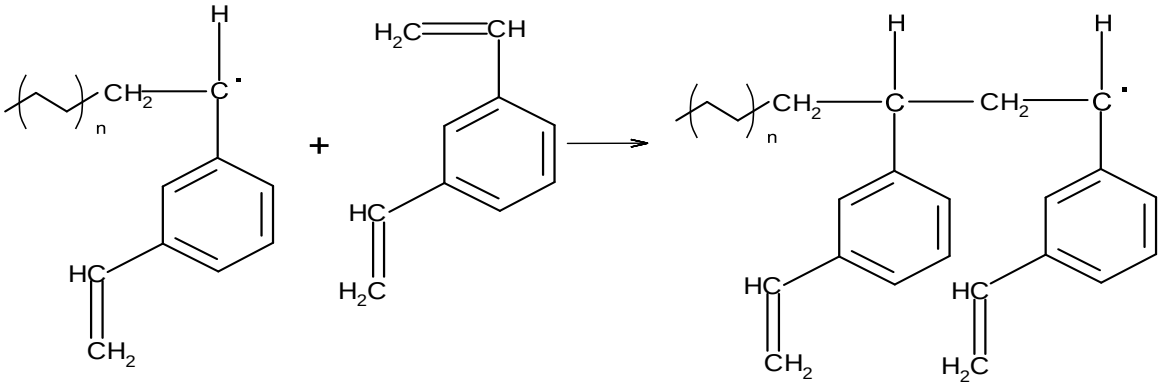

Figure 2.22. Propagation of *m*-DVB monomer with a radical formed by *m*-DVB monomer.

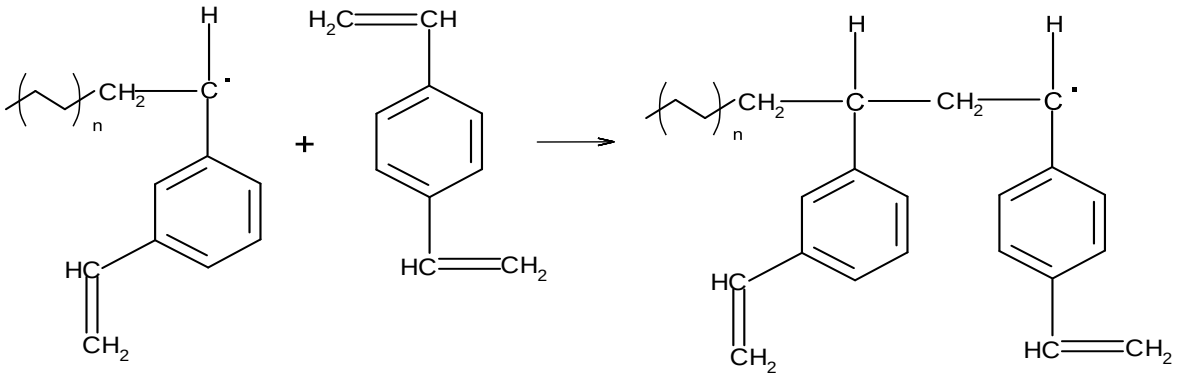

Figure 2.23. Propagation of *p*-DVB monomer with a radical formed by *m*-DVB monomer.

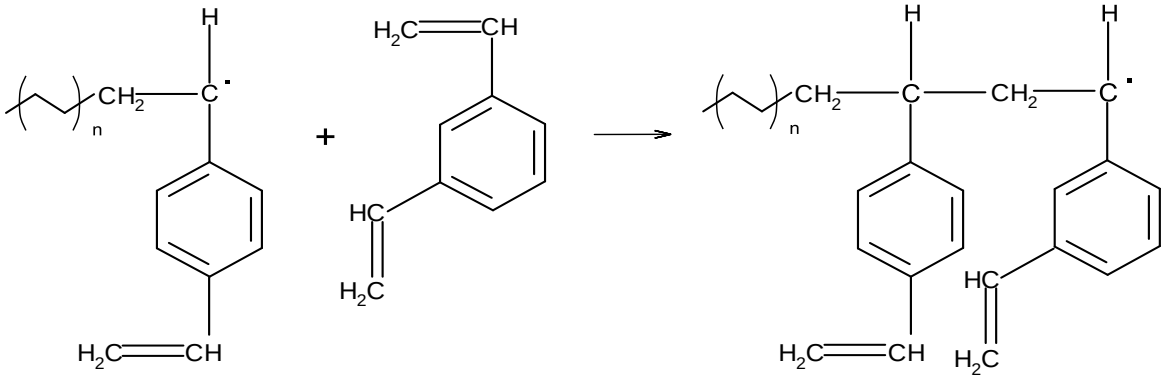

Figure 2.24. Propagation of *m*-DVB with a radical formed by *p*-DVB monomer.

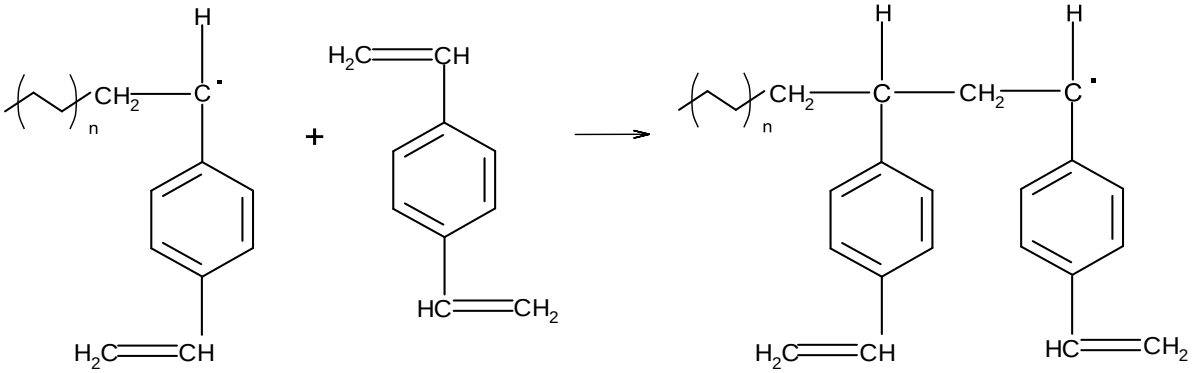

Figure 2.25. Propagation of *p*-DVB with a radical formed by *p*-DVB monomer.

It results from the propagation of a radical from *meta*- or *para*- divinylbenzene with a pendant double bond derived from *meta*- or *para*- divinylbenzene the formation of a radical from *meta*- or *para*- DVB pendant double bond, a pendant double bond and a crosslinking site. These reactions are represented by Figures 2.26-2.29.

The radicals from the pendant double bonds have also the possibility of participate on three different kinds of propagation reactions. When they react with a styrene unit it is formed a radical from styrene and a branching point (Figures 2.30 and 2.31).

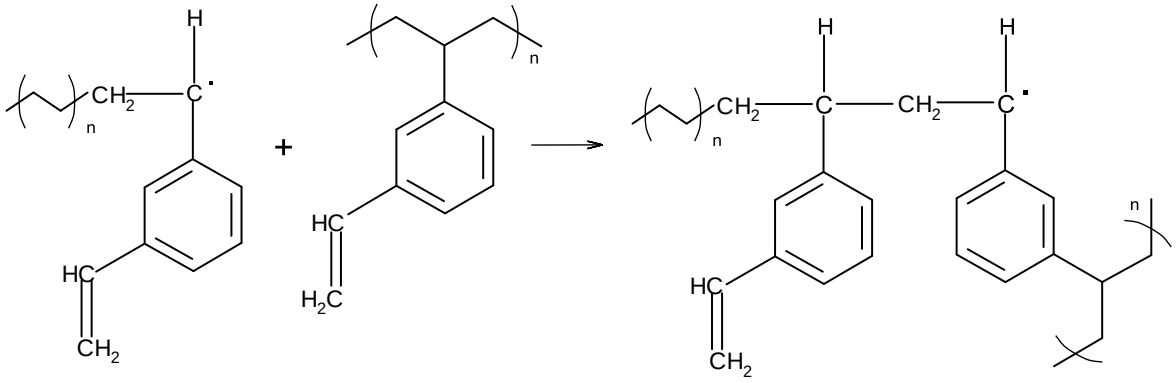

Figure 2.26. Propagation of *m*-DVB pendant double bond with a radical formed by *m*-DVB monomer.

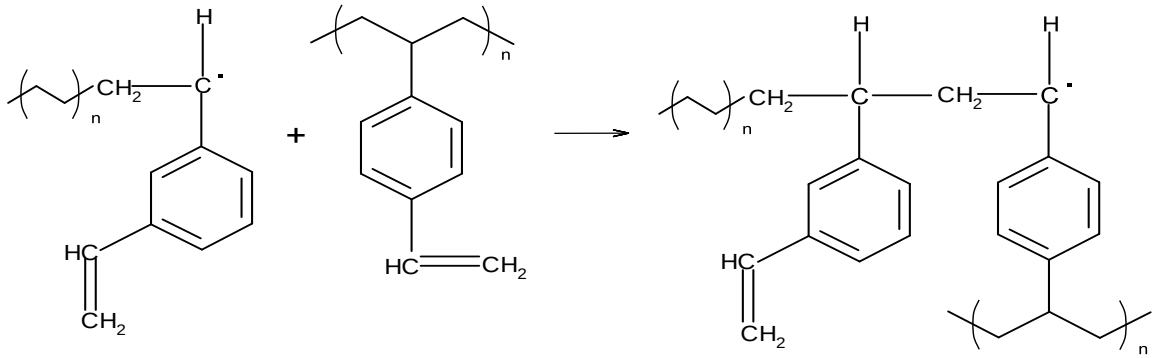

Figure 2.27. Propagation of *p*-DVB pendant double bond with a radical formed by *m*-DVB monomer.

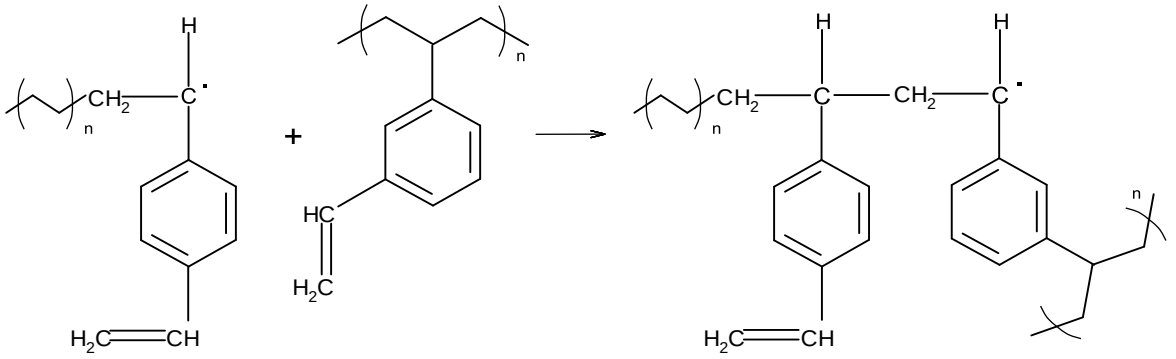

Figure 2.28. Propagation of *m*-DVB pendant double bond with a radical formed by *p*-DVB monomer.

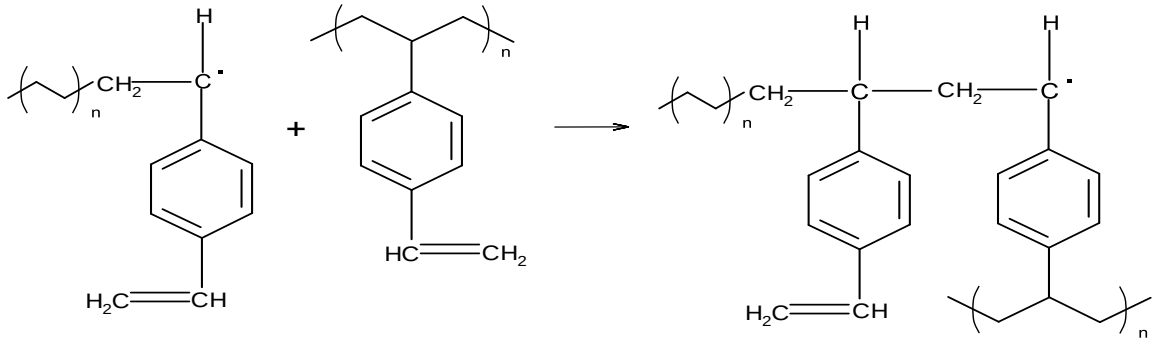

Figure 2.29. Propagation of *p*-DVB pendant double bond with a radical formed by *p*-DVB monomer.

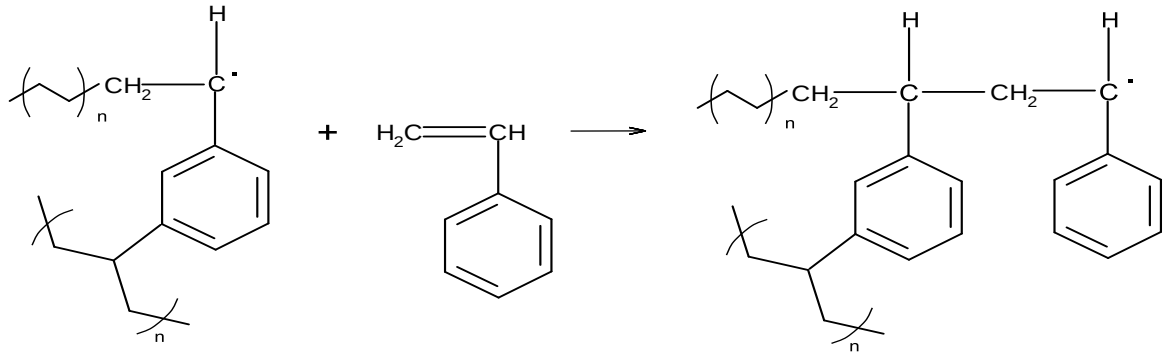

Figure 2.30. Propagation of styrene monomer with a radical formed by *m*-DVB pendant double bond.

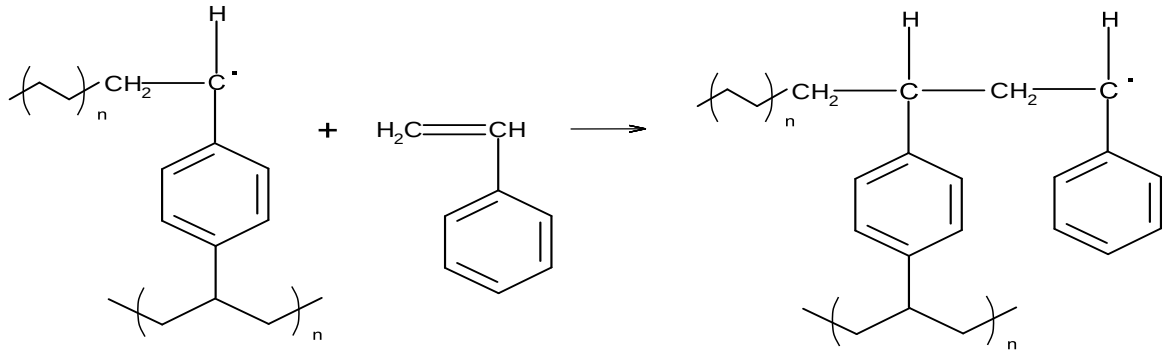

Figure 2.31. Propagation of styrene monomer with a radical formed by *p*-DVB pendant double bond.

From the propagation of a radical from the pendant double bond (*meta* or *para*) with a isomer of DVB results the formation of a radical from *meta*- or *para*- divinylbenzene (Figures 2.32-2.35).

In the process of the propagation of a pendant double bond with a radical from a pendant double bond it is formed a radical from the pendant double bond and a branching point (Figures 2.36-2.39).

In the termination stage of free-radicals the processes of termination by combination and disproportionation can both take place. As already stated, in this system it is necessary to distinguish 5 different kinds of macromolecular radicals. Accordingly it is possible to find 25

termination reactions between radicals from each process. However, by symmetry reasons only 15 reactions are actually distinguishable. The relative proportion of the terminations by combination and disproportionation is a key aspect to describe free-radical polymerisations. In the particular case of polymerisation of monomers with multiple double bonds the problem is amplified due to the higher number of termination reactions that is possible to distinguish. Termination in styrene polymerisation is known to occur nearly always through radical combination (Moad and Solomon, 2006), but disproportionation was included in the modelling for sensitivity analysis purposes.

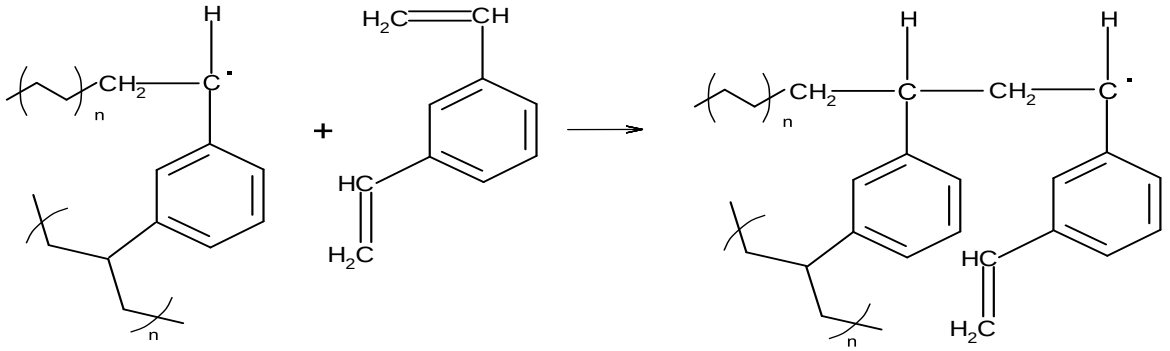

Figure 2.32. Propagation of *m*-DVB monomer with a radical formed by *m*-DVB pendant double bond.

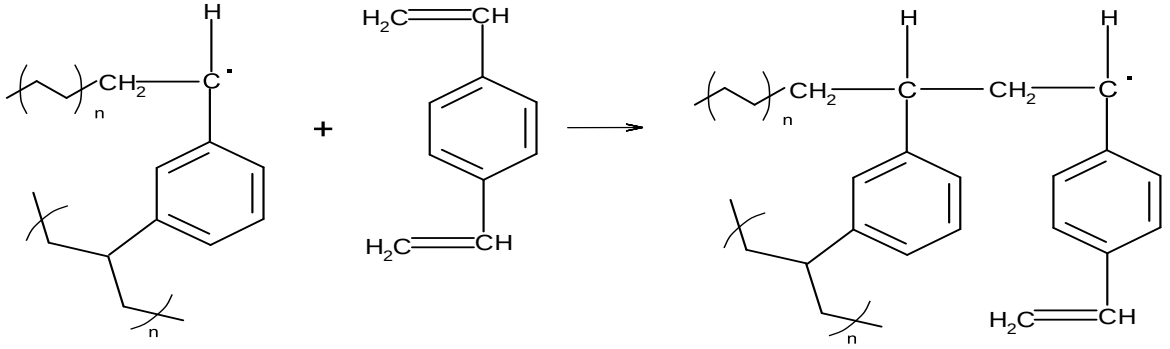

Figure 2.33. Propagation of *p*-DVB monomer with a radical formed by *m*-DVB pendant double bond.

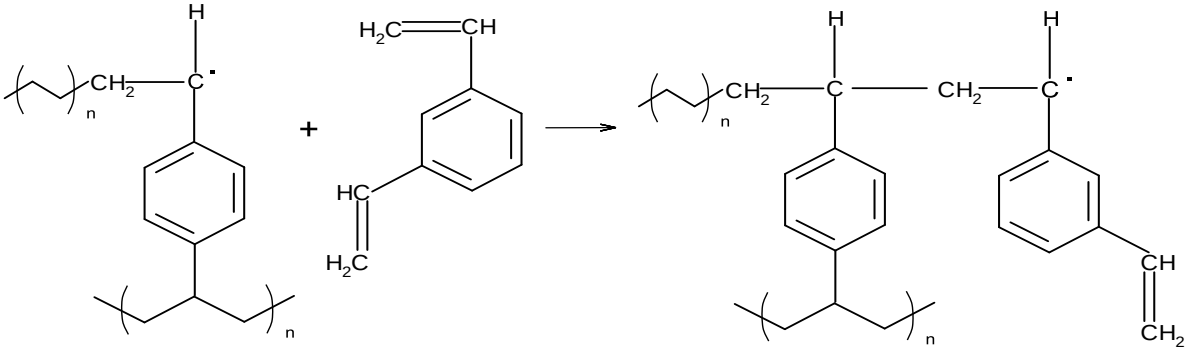

Figure 2.34. Propagation of *m*-DVB monomer with a radical formed by *p*-DVB pendant double bond.

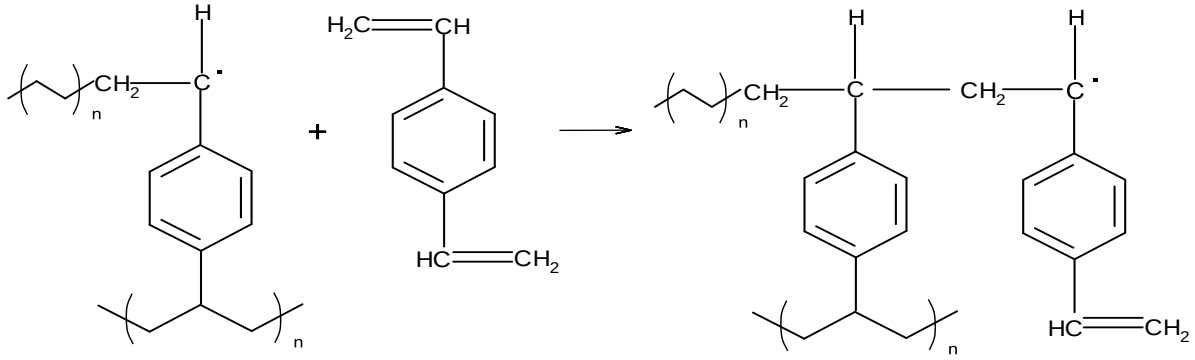

Figure 2.35. Propagation of *p*-DVB monomer with a radical formed by *p*-DVB pendant double bond.

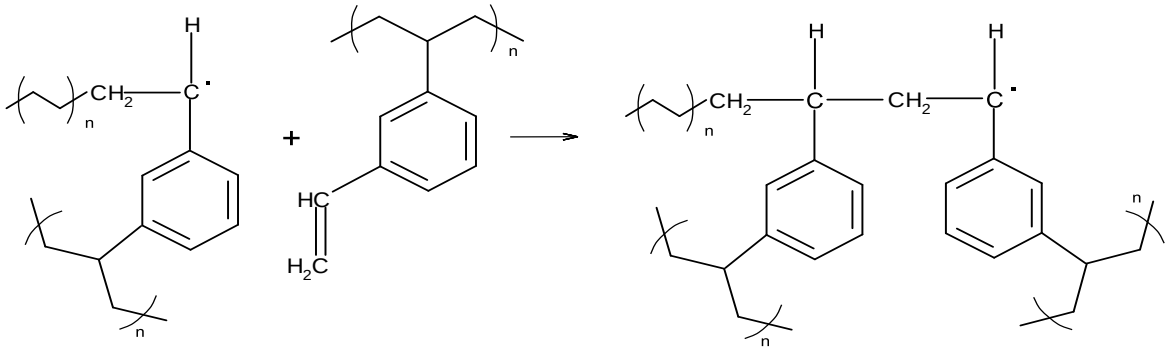

Figure 2.36. Propagation of *m*-DVB pendant double bond with a radical formed by *m*-DVB pendant double bond.

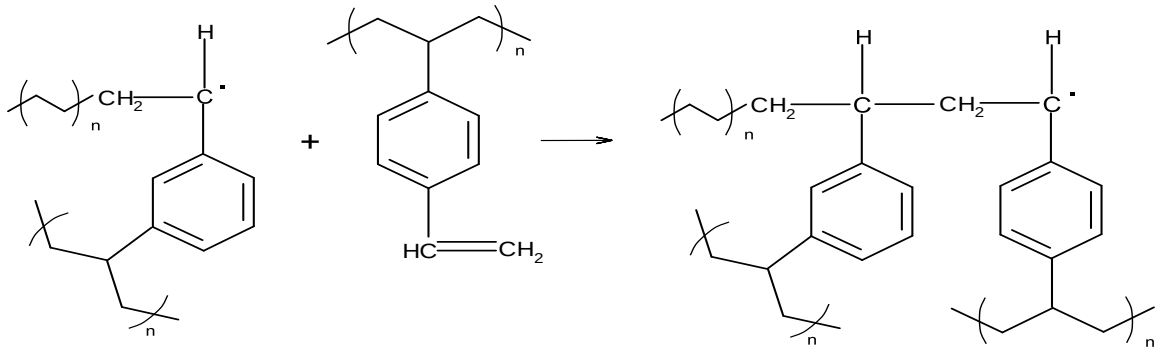

Figure 2.37. Propagation of *p*-DVB pendant double bond with a radical formed by *m*-DVB pendant double bond.

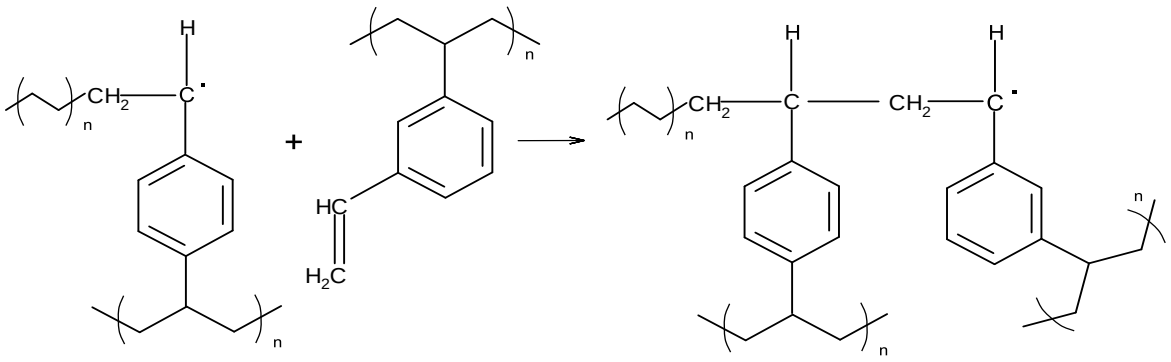

Figure 2.38. Propagation of *m*-DVB pendant double bond with a radical formed by *p*-DVB pendant double bond.

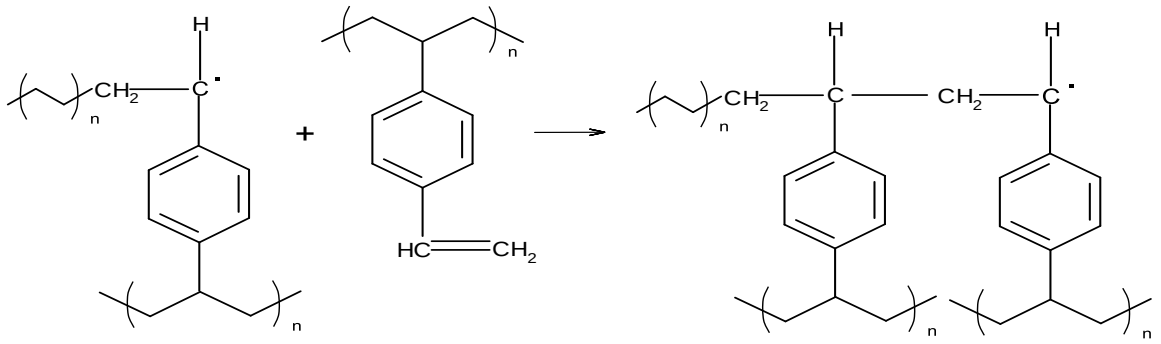

Figure 2.39. Propagation of *p*-DVB pendant double bond with a radical formed by *p*-DVB pendant double bond.

In the next Figures are represented some termination by combination reaction examples involving two radicals from styrene (Figure 2.40), two radicals of *p*-DVB (Figure 2.41) and two radicals from *m*-DVB pendant double bond (Figure 2.42). All the other termination reactions by combination can be described by a similar way.

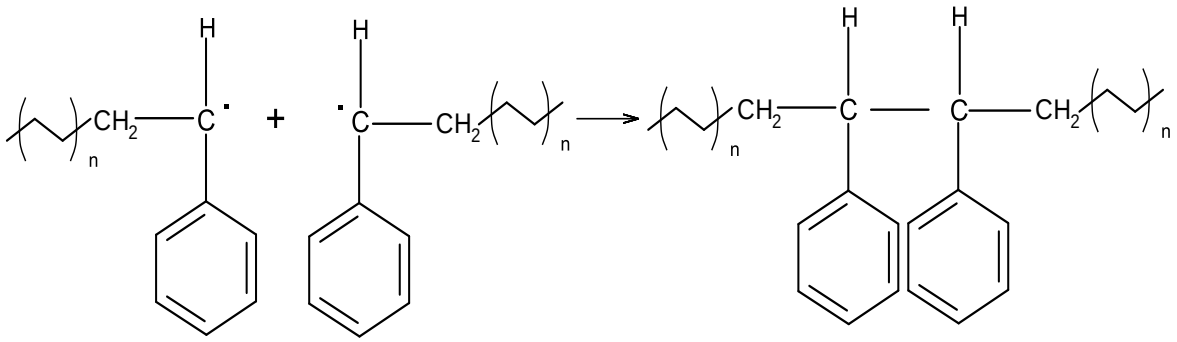

Figure 2.40. Termination by combination of two radicals derived from styrene monomer.

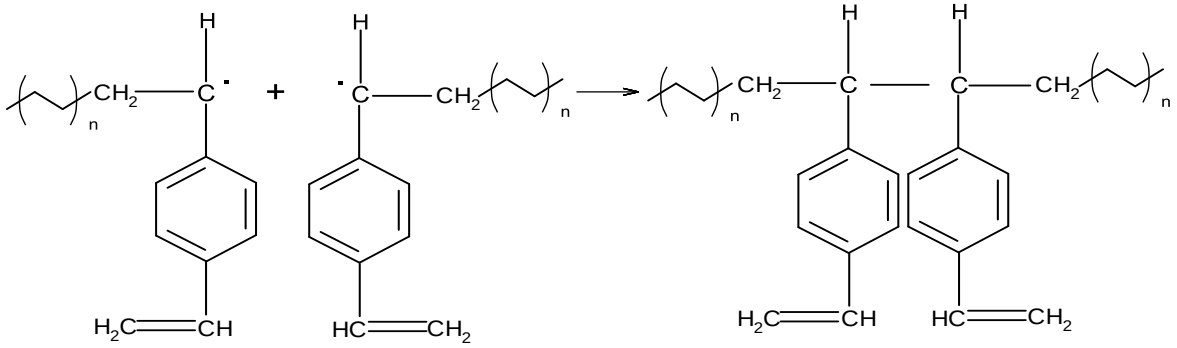

Figure 2.41. Termination by combination of two radicals derived from *p*-divinylbenzene monomer.

Chain transfer is the reaction of a propagating radical with a non-radical substrate to produce a dead polymer chain and a new radical capable of initiating a polymer chain. The transfer agent may be deliberately added or it may be the initiator, monomer, polymer, solvent or even an impurity. A transfer without further initiation is called inhibition. When the reaction

produces a dead polymer chain and a radical that is less reactive than the propagating radical but still capable of reinitiating the polymerisation is called retardation or degradative chain transfer.

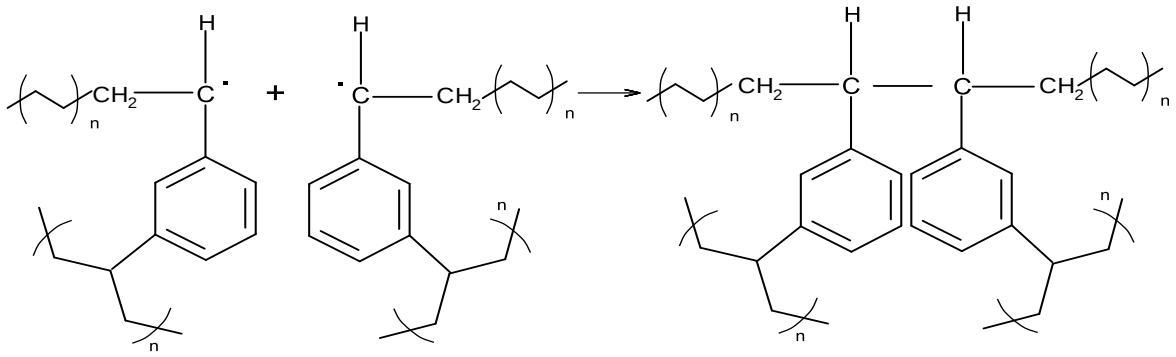

Figure 2.42. Termination by combination of two radicals derived from *m*-divinylbenzene pendant double bonds.

In Figure 2.43 the formation of a primary radical of toluene (solvent used in this system) with a radical derived from styrene is depicted. In Figure 2.44 it is shown the formation of a primary radical of the chain transfer agent (CBr_4) with a radical derived from styrene. Each macromolecular radical is capable of forming a primary radical of toluene and CBr_4 resulting on eight more chemical reactions due to chain transfer reactions. The transfer agents can be used industrially in a radicalar polymerisation with the purpose of controlling the molecular mass of the polymer, the polymerisation rate or the nature of the end groups in the polymer.

Intramolecular cyclization reactions occur when a radical site reacts with a pendant double bond in the same polymer molecule. When that reaction takes place in a primary chain of the polymer molecule it is called a primary cyclization and is depicted in Figure 2.45, with the copolymerisation of styrene with divinylbenzene as an example. If the intramolecular reaction occurs between a radical located in a different chain from the pendant double bond it is called a secondary cyclization. For the sake of a good comprehension of the scheme, it is used now a less detailed representation in Figure 2.46.

Table 2.6 and 2.7 present the numerical values of the 115 kinetic parameters used in the simulations. Past experimental works concerning the homopolymerisation of styrene (Moad and Solomon, 2006), pure *m*-divinylbenzene or pure *p*-divinylbenzene (Nyhus *et al*., 1999) and the crosslinking of styrene with both pure DVB isomers and their mixture (Hecker, 2000) were used for estimating most of the needed parameters.

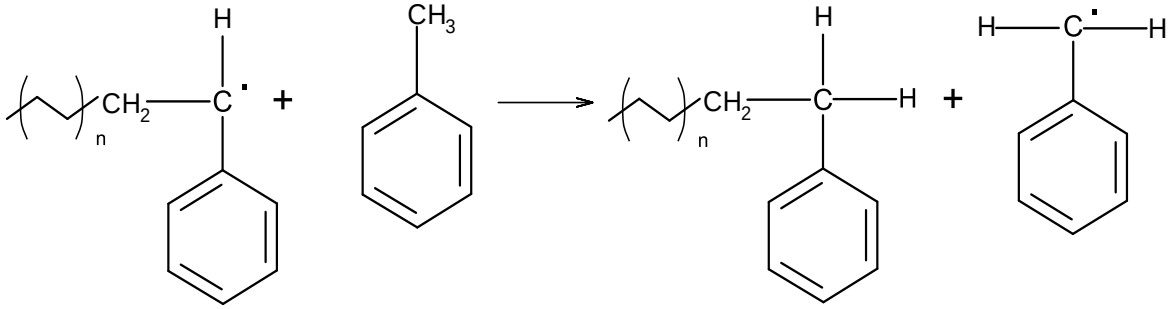

Figure 2.43. Transfer to solvent reaction between a radical from styrene and toluene.

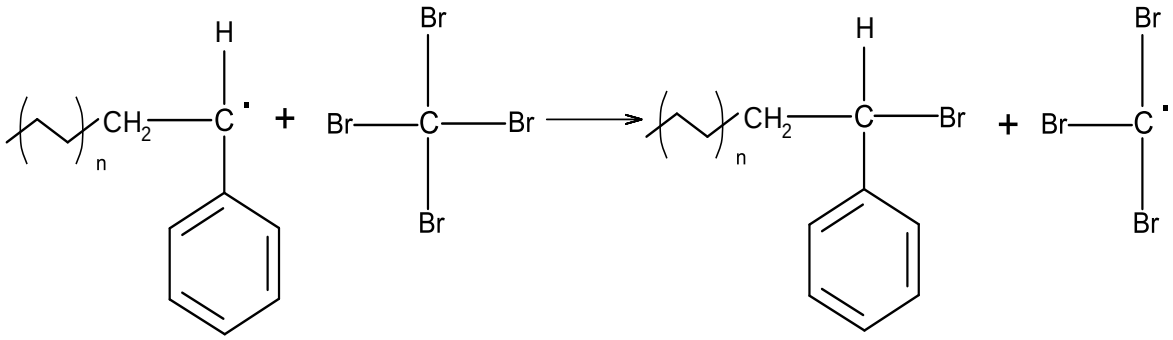

Figure 2.44. Transfer to chain transfer agent reaction between a radical from styrene and CBr_4.

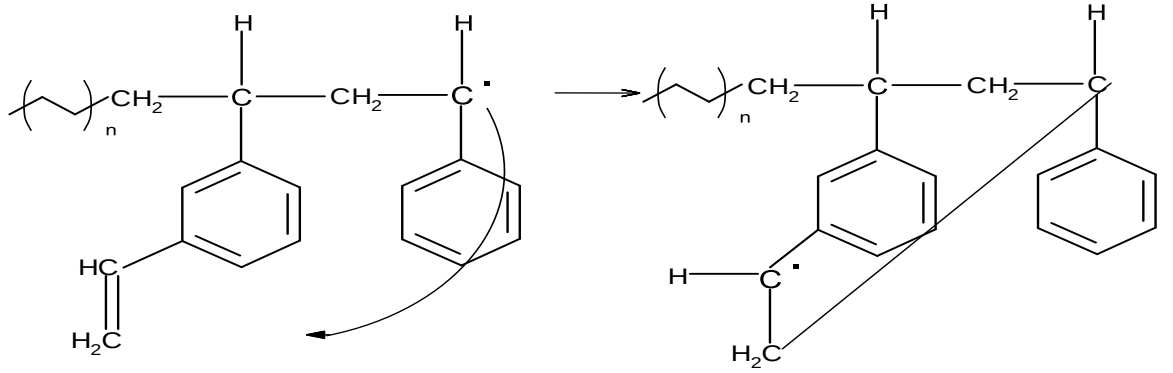

Figure 2.45. Schematic representation of a primary intramolecular cyclization reaction in the copolymerisation of styrene and divinylbenzene.

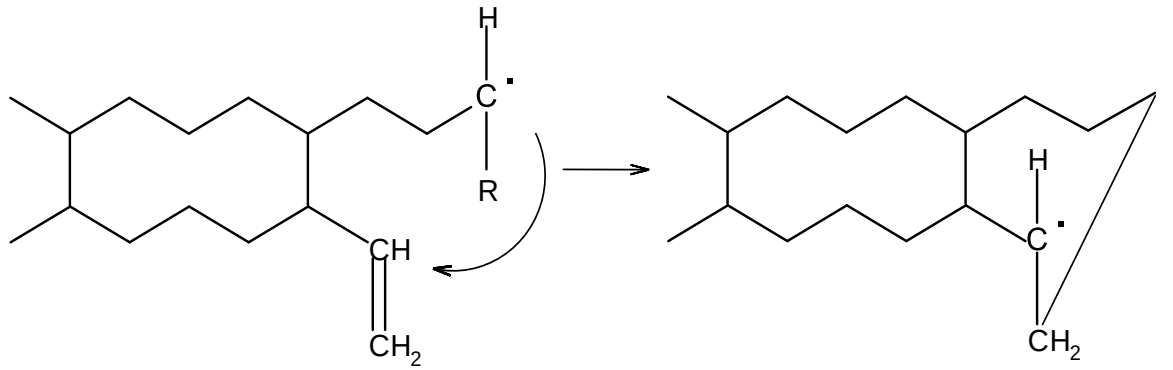

Figure 2.46. Schematic representation of a secondary intramolecular cyclization reaction.

Table 2.6. Basic set of kinetic parameters considered in the modelling of the radical copolymerisation of styrene with divinylbenzene at 60 °C.

Kinetic Step	Kinetic parameter involved [a)]
AIBN decomposition [b)]	$k_d = 9.6 \times 10^{-6}(\mathrm{s}^{-1}), f = 0.6(-)$
Styrene homopropagation [c)]	$k_{p11} = 340$
Styrene/*m*-and *p*-DVB propagations [d)]	$r_{12} = \frac{k_{p11}}{k_{p12}} = 0.43, k_{p12} = 790.70$
	$r_{13} = \frac{k_{p11}}{k_{p13}} = 0.24, k_{p13} = 1416.67$
Styrene/*m*-and *p*-PDB propagations [d)]	$r_{14} = \frac{k_{p11}}{k_{p14}} = 0.92, k_{p14} = 369.57$
	$r_{15} = \frac{k_{p11}}{k_{p15}} = 0.50, k_{p15} = 680$
m- and *p*-DVB homopropagations [e)]	$k_{p22} = 607.55, k_{p33} = 403.90$
Polymer radicals termination [f)]	$\frac{k_{p11}}{\sqrt{k_t}} = 0.035, k_t = 9.44 \times 10^7$
	$k_{tc} = \alpha_{tc} k_t, k_{td} = \alpha_{td} k_t$
Chain transfer to solvent [g)]	$C_S = \frac{k_{S1}}{k_{p11}} = 0.12 \times 10^{-4}$
Chain transfer to agent [h)]	$C_{CTA} = \frac{k_{CTA1}}{k_{p11}} = 1$
Inhibition [i)]	$C_Z = \frac{k_{Z1}}{k_{p11}} = 520$
Reaction radical/retarder [j)]	$k_{R1} = 10^9$

[a)] All the kinetic parameters are expressed in $\mathrm{dm^3 mol^{-1} s^{-1}}$, unless otherwise stated. [b)] Collected from Moad and Solomon, (2006) (p.71) and f from Bevington (1955). [c)] IUPAC benchmark value (Moad and Solomon, 2006) collected from Buback *et al*., (1995). [d)] Reactivity ratios r_{12}, $r_{13,}$ r_{14} and r_{15} were collected from Hecker (2000). [e)] Propagation constants k_{p22} and k_{p33} are based on the experimental evaluation of the parameter $k_p/\sqrt{k_t}$ for the homopolymerisation of *m*-divinylbenzene and *p*-divinylbenzene (Nyhus *et al*., 1999) at 70 °C. Activation energies of propagation ($E_p = 32.5$ $\mathrm{kJmol^{-1}}$) Moad and Solomon (2006) and for termination ($E_t = 7.03$ $\mathrm{kJmol^{-1}}$) (Brandrup *et al*., 1999) were used to estimate this parameter at 60 °C. An overall average termination constant (k_t) was considered in these calculations. [f)] k_t is an average termination constant in the framework of the classical kinetics. Scattered values in the range 0.01 to 0.04 for the parameter $k_p/\sqrt{k_t}$ can be found on the literature (Okay, 2000; Brandrup *et al*., 1999; Odian, 2004; Matheson *et al*., 1951; Beuermann and Buback, 2002). The value $\frac{k_p}{\sqrt{k_t}} = 0.035$ $\mathrm{dm^3/(mol\,s)^{1/2}}$ was estimated from time/conversion data (prior to noticeable Norrish-Trommsdorff effect) as measured in the present work. Termination of styrene is generally accepted to occur by combination ($\alpha_{tc} = 1$). Nevertheless, values of $k_{td}/k_{tc} = 0.2$ are also mentioned in the literature (Moad and Solomon, 2006). Experimental data of the present work are also consistent with $\alpha_{tc} = 1$. [g)] Correspondent to the pair styrene/toluene (Moad and Solomon, 2006). [h)] Scattered values for the pair styrene/CBr_4 (C_{CTA}) are reported in Brandrup *et al*., (1999): the experimental results of the present system are consistent with transfer constant close to ideality ($C_{CTA} = 1$) as also reported in the literature (Moad and Solomon, 2006). [i)] Correspondent to the pair styrene/*p*-benzoquinone (Moad and Solomon, 2006). [j)] In the range of known rate constants for reaction of carbon-centered radicals with oxygen (Moad and Solomon, 2006).

Table 2.7. Assumptions used in the present system for some kinetic parameters considered in the radical copolymerisation of styrene with divinylbenzene at 60 °C.

Kinetic Step	Kinetic parameter involved
Propagation of STY, DVB and PDB with radicals [a] A_2 to A_5	Geometric decay
Propagations with radicals RR [b]	$\frac{k_{p6j}}{k_{p1j}} = 0.01(j = 1,\dots,5)$
Initiations [c]	$k_{Ikj} = k_{p1j}(k = 1,\dots,3, j = 1,\dots.5)$
Chain transfer to agent and to solvent [d]	$k_{CTAi} = C_{CTA}k_{pi1}, k_{Si} = C_S k_{pi1}$
Inhibition [d][e]	$k_{Zi} = C_Z k_{pi1}(i = 1,\dots,6)$
	$k_{ZPi} = C_Z k_{p11}(i = 1,\dots,3)$
Reaction of radicals with retarder [d]	$\frac{k_{Ri}}{k_{R1}} = \frac{k_{pi1}}{k_{p11}}(i = 1,\dots,5)$
Termination [f]	$k_{tcij} = k_{tc}, k_{tdij} = k_{td}(i,j = 1,\dots,6)$

[a] It is considered that a decrease of reactivity of R*m*DVB relatively to RS occurs as inferred from experimental data leading to $k_{p22}/k_{p11} = 0.77$. In the same conditions a lower reactivity ratio for R*p*DVB ($k_{p33}/k_{p13} = 0.29$) is estimated. It is postulated that R*m*PDB and R*p*PDB present a reactivity drop in a geometric sequence relatively to R*m*DVB and R*p*DVB ($0.77^2 = 0.59$ and $0.29^2 = 0.08$, respectively). These reactivity drops are plausible owing to steric factors. It has been previously shown (Costa and Dias, 2003) that only with a strong deviation from ideality a noticeable influence of these parameters in the gelation of the system is expected. [b] The propagation for the monomers with non-carbon centered radicals (oxygen centered) is considered to be much slower than with the correspondent normal propagation (Moad and Solomon, 2006). [c] The rate constant for the initiation of the different monomers (*j*=1,...,5) with different kinds of primary radicals (*k*=1,...,3) are considered to take the same values as in the corresponding propagations with RS. [d] The different propagating radical sites are considered to have similar reactivity decays for reactions with CTA, solvent, inhibitor and retarder. [e] The inhibition of the primary radicals is supposed to occur with RS at the same relative extent. [f] It is considered that the kinetic constants for all termination reactions take the same values as the average termination rate constant.

2.3.2 Results and Discussion

Table 2.1 describes the set of experiments on the radical copolymerisation of STY with DVB in toluene solution at 60 °C. Linear polystyrene (run 1) and STY/DVB without (run 2) and with CTA (run 3) have been produced in a batch reactor. Semi-batch runs using different feeding policies of DVB are described in experiments 4, 5 and 6. A more or less constant global mole fraction of DVB was used in all batch and semi-batch experiments. In Figure 2.47 are presented the experimentally measured and predicted values of global monomer conversion. Those data were used to estimate the parameter $\frac{K_p}{\sqrt{K_t}} = 0.035\ \mathrm{dm}^{3/2}(\mathrm{mol\ s})^{-1/2}$

considering kinetic controlled polymerisation (Okay *et al*., 1999) for STY/DVB copolymerisation prior to gelation.

In Figure 2.48 are compared the experimental measurements of $\bar{M}_w$ for the non-linear polymerisations of STY/DVB in batch reactor (run 2) with the predictions obtained considering the set of kinetic parameters presented in Table 2.6 and 2.7. It can be observed that in these conditions ($r_{14} = 0.92, r_{15} = 0.50$) a huge discrepancy between predictions and experimentally values of $\bar{M}_w$ (and gelation time) occurs. Some of this discrepancy can be explained by the influence of the reaction medium, namely the effect of the solvent (Nyhus *et al*., 1999) on the kinetics of these polymerisation systems (toluene in this case versus nearly bulk polymerisation in (Hecker, 2000)). However, the most important cause of the delay of the gelation is likely to be the occurrence of cyclization (intramolecular) reactions (Okay, 2000; Dias and Costa, 2005).

For the sake of simplicity, in the present work, these combined effects are taken into account by fitting apparent values of the reactivity of pendant double bonds, as they are the major parameters controlling the crosslinking process. It is also considered that the reactivity of *m*- and *p*- pendant double bonds is affected in the same proportion by these phenomena. Apparent values of reactivity ratios $r_{14}^{ap} = 2.72$ and $r_{15}^{ap} = 1.48$ were therefore estimated using the experimental information in run 2 (see Figure 2.48). Note that these apparent reactivity ratios are consistent with a decrease of reactivity of PDB ($C_{PDB} = 2r_{12}/r_{14}^{ap} = 2r_{13}/r_{15}^{ap} = 0.32$) as reported in other works in this field (Okay, 2000). This modified set of kinetic parameters was used in the remaining predictions here presented.

In this system, the priority was the description of semi-batch operation, with a main goal being the prediction of the polymerisation behaviour using the same set of kinetic parameters as for batch operation and this was achieved, as shown in Figure 2.49. Figure 2.50 shows the comparison of measured and predicted values of, $\bar{M}_n$, $\bar{M}_w$ and $\bar{M}_z$ for a semi-batch run. A good agreement is obtained for $\bar{M}_w$ (which is the molecular mass directly measured by MALLS) but significant deviations are observed for $\bar{M}_n$ and $\bar{M}_z$ close to gel point when a high dispersion of molecular sizes occurs. This is a consequence of the approximations involved in the indirect estimation of $\bar{M}_n$ e $\bar{M}_z$ which considers a homogeneous polymer population inside each SEC slice. Inaccurate measurements for $\bar{M}_n$ and $\bar{M}_z$ are thus obtained using SEC/RI/MALLS for highly polydispersed polymers.

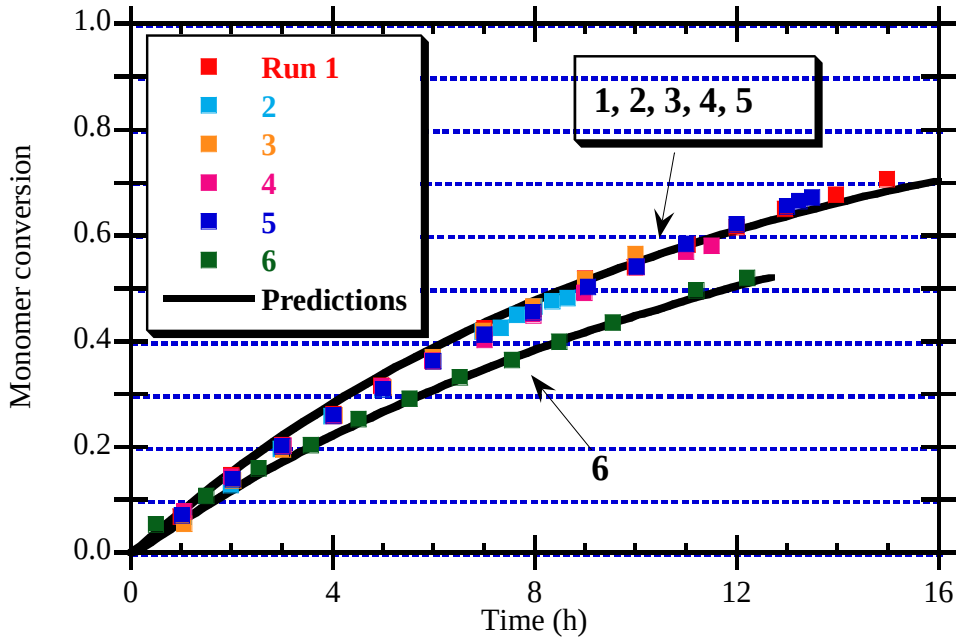

Figure 2.47. Time evolution of the measured overall conversion for linear and non-linear polymerisation systems also considering different operation conditions.

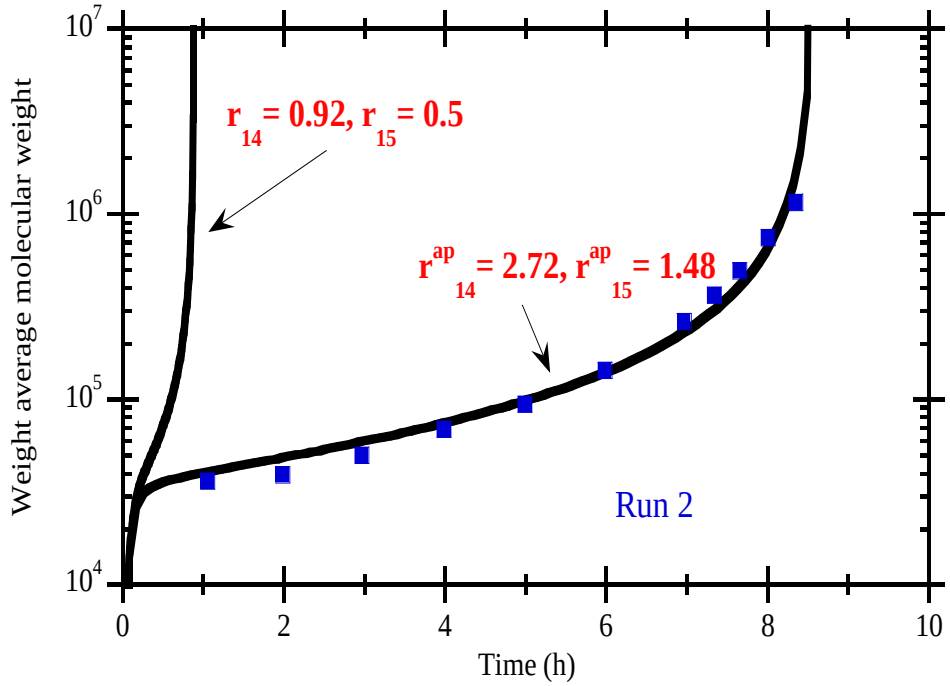

Figure 2.48. The influence of the reactivity of the pendant double bonds on the predicted $\bar{M}_w$ (run 2) and its comparison with the correspondent measured values.

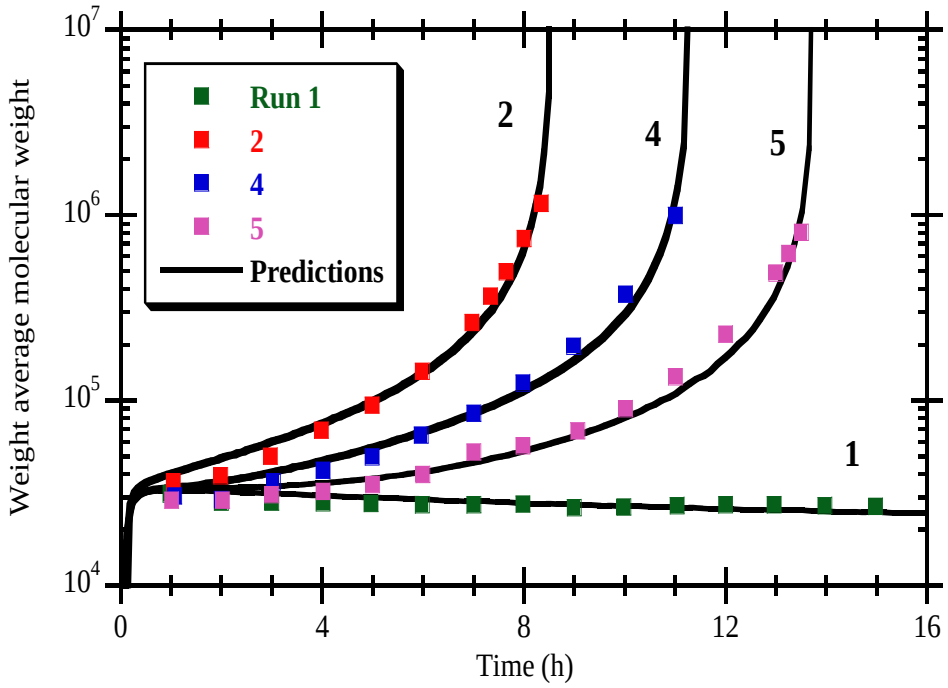

Figure 2.49. Predicted and measured $\bar{M}_w$ for linear and non-linear polymerisation systems in batch and semi-batch reactor.

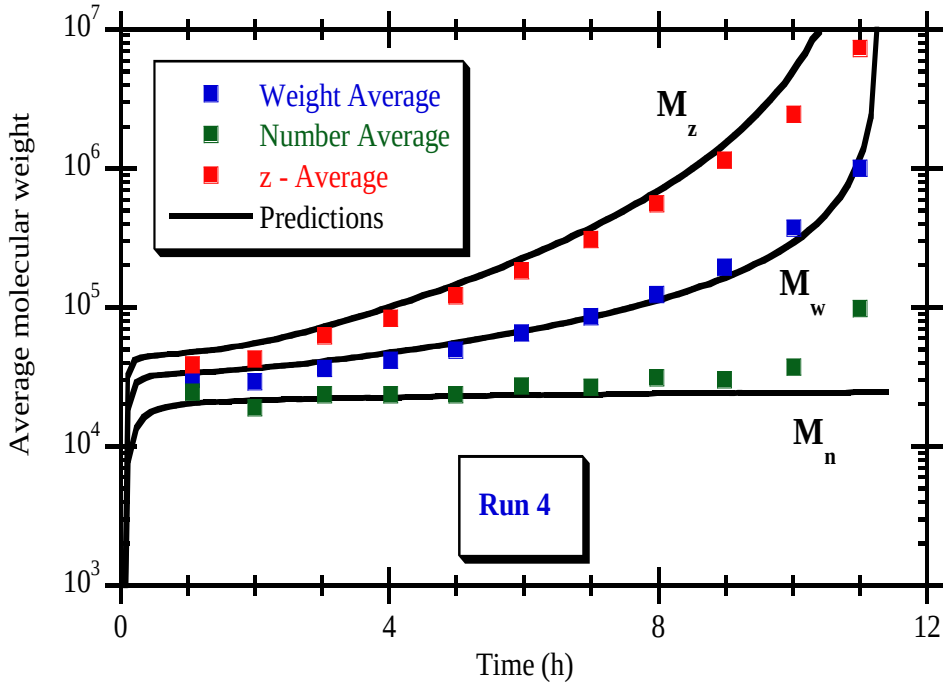

Figure 2.50. Time evolution of $\bar{M}_n$, $\bar{M}_w$ and $\bar{M}_z$ during the radical copolymerisation of STY/DVB in semi-batch reactor using different feed policies.

Figure 2.51 shows the comparison of batch operation including a CTA and different feed policies of DVB to a semi-batch reactor. These results show that operation in semi-batch reactor can be used as an alternative to the inclusion of CTA in batch operation, namely for producing soluble branched polymers at higher monomer conversions. The time evolution of the experimental *z*-average mean square radius of gyration ($\bar{R}_g$) in THF solution as obtained by MALLS is presented in Figure 2.52. For the smaller molecular dimensions approaching 10 nm, higher experimental errors are observed as the lower limit of the instrument detections is attained.

The theoretical predictions of $\bar{R}_g$ are only valid for Gaussian chains, described as a set of beads connected separated by length b=0.692 nm from the experimental $\bar{R}_{g,lin_\Theta} = 0.0277M^{0.5}$ nm with a theta solvent (trans-decaline at 22 °C from Terao and Mays (2004)). For polystyrene in THF, $\bar{R}_{g,lin} = 0.0118M^{0.6}$ nm at 25 °C (Terao and Mays, 2004). Neglecting the small temperature differences, we estimate an expansion factor of the gyration radius for linear polydispersed polystyrene in THF at 30 °C as $\frac{\bar{R}_{g,lin}}{\bar{R}_{g,lin_\Theta}} = 0.426M_z^{0.1}$.

Since an extension of this method for taking into account the presence of the excluded volume effect has not yet been developed (Costa and Dias, 2007) it was assumed the equality of the expansion factors for branched and linear polymer molecules for obtaining the predictions in Figure 2.52. This assumption has been previously used by several researchers (Dobkowski, 1985) and has not been questioned in more recent works with similar goals. Note that Monte Carlo simulation and molecular dynamics have gone a long way to describe real chains and even branched ones (Steinhauser, 2005), but the complexity of kinetic schemes such as the one here discussed precludes the direct use of the approaches which have successfully tackled simpler structures such as comb and star polymers.

A polymer population with large dimensions but at a low concentration is detected by SEC/RI/MALLS close to gel point, as presented in Figures 2.53 and 2.54. Figure 2.55 shows the chromatogram of an STY/DVB sample collected close to gel point. A molecular fraction with strong light scattering signal but weak refractive index response is easily indentified. Figure 2.56 compares chromatograms of samples synthesized at different conditions. In the presence of CTA (run 3) a high polydispersity of molecular sizes is observed. In both case, an inversion in the relation of MW versus elution volume is observed, confirming the erroneous interpretation of chromatograms of branched polymers which would be caused from using a

calibration with linear polymers, as seen in Figure 2.57. Similar observations have been reported in the literature (Bannister *et al*., 2006).

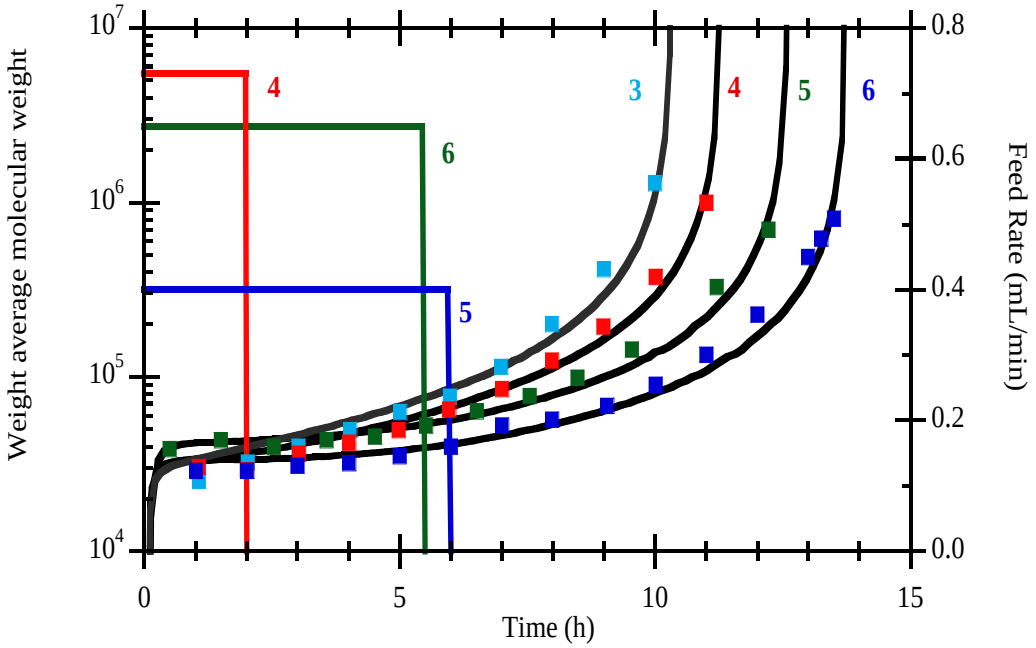

Figure 2.51. Time evolution of $\bar{M}_w$ in the presence of CTA or using different feed policies in semi-batch reactor.

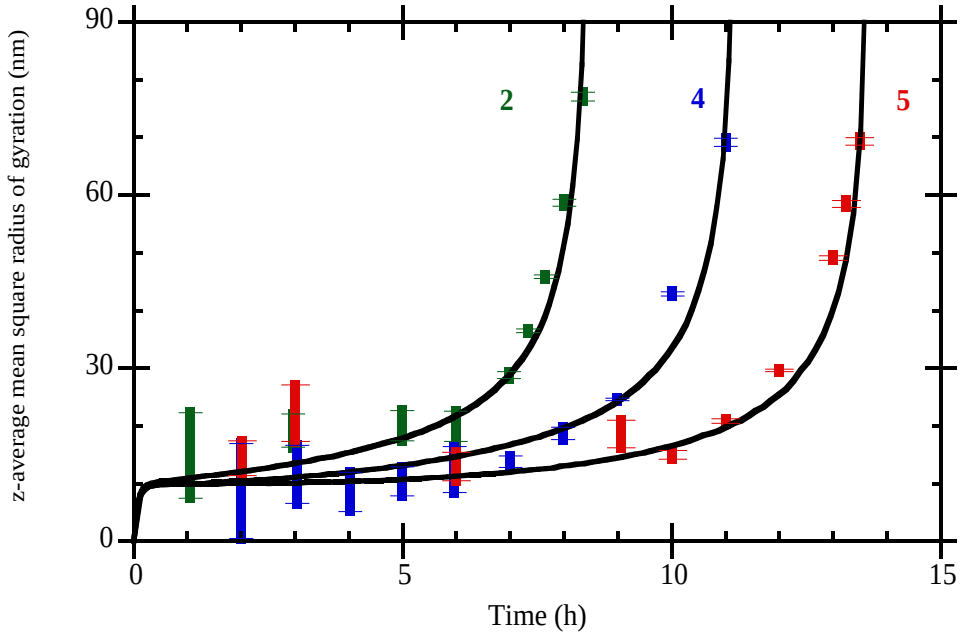

Figure 2.52. Time evolution of $\bar{R}_g$ in THF solution during the radical copolymerisation of STY/DVB in batch or semi-batch reactor.

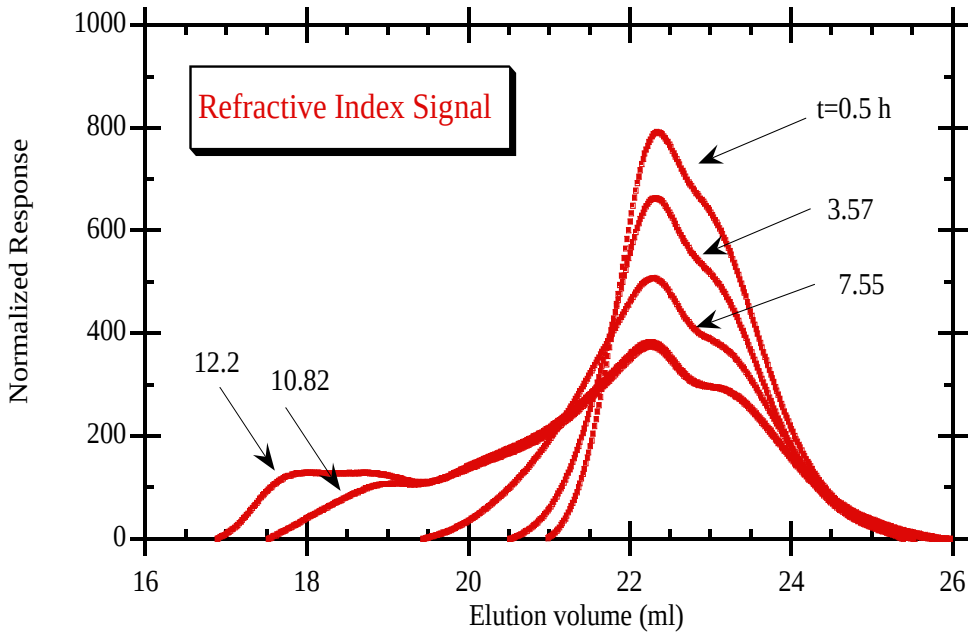

Figure 2.53. Measured refractive index signal in the SEC chromatograms of samples of STY/DVB corresponding to different polymerisation times in a semi-batch reactor.

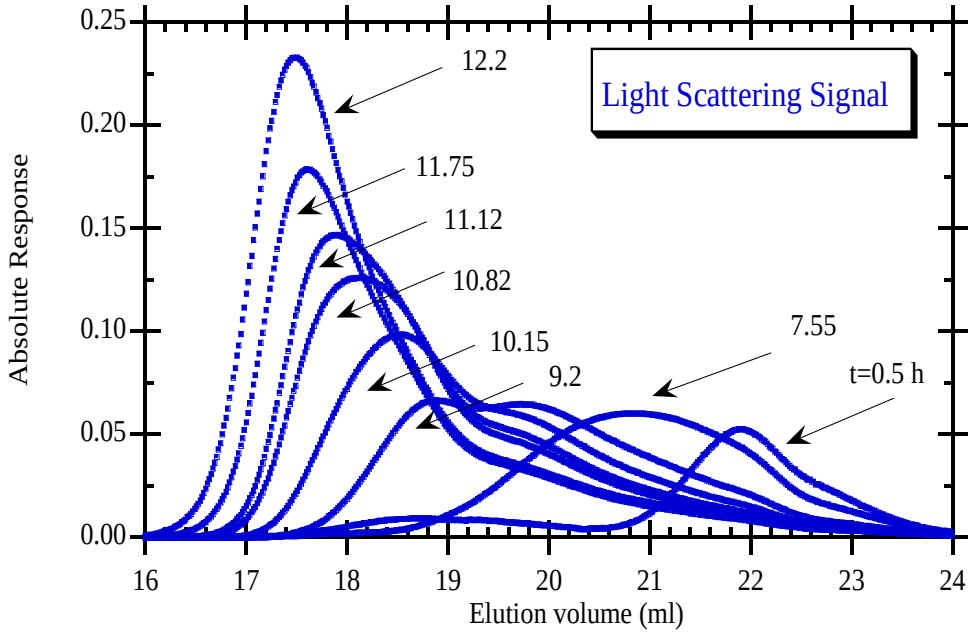

Figure 2.54. Measured 90° light scattering signal in the SEC chromatograms of samples of STY/DVB corresponding to different polymerisation times in a semi-batch reactor.

Note that in the interpretations of chromatograms such as the one presented in Figure 2.55 the lower limit of light scattering detection must be accounted for and a small region at the right

side cannot be quantitatively analysed. Figure 2.58 shows the time evolution of the molecular weight distribution of branched STY/DVB: the formation of a long end tail as gelation is approached agrees with theoretical results (Dias and Costa, 2005b).

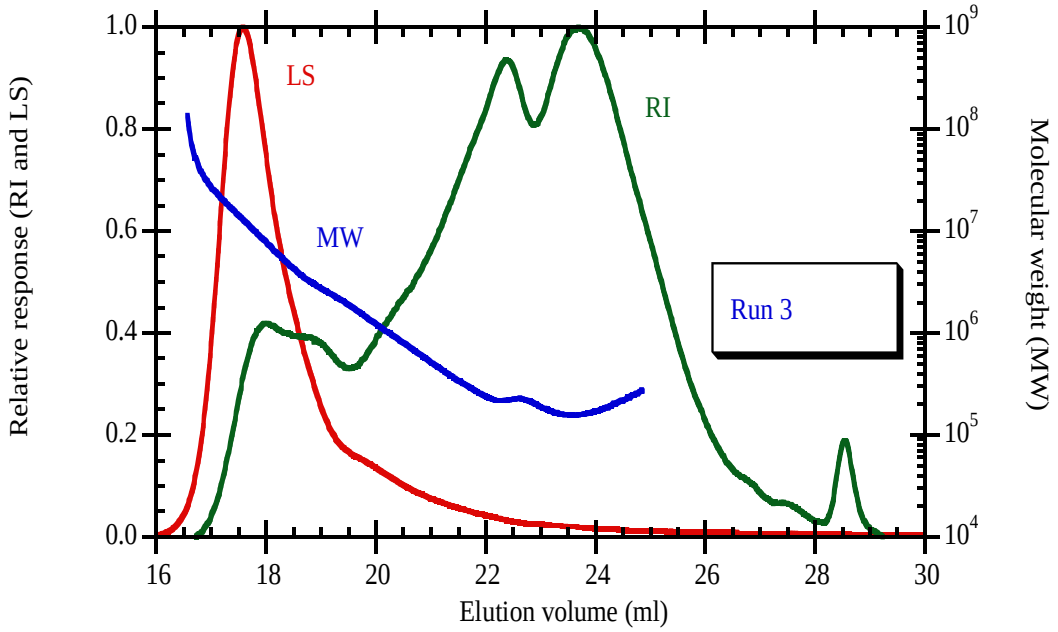

Figure 2.55. Molecular weight along the SEC chromatogram for samples of STY/DVB synthesized using different operation conditions in polymerisation times very near to gel point.

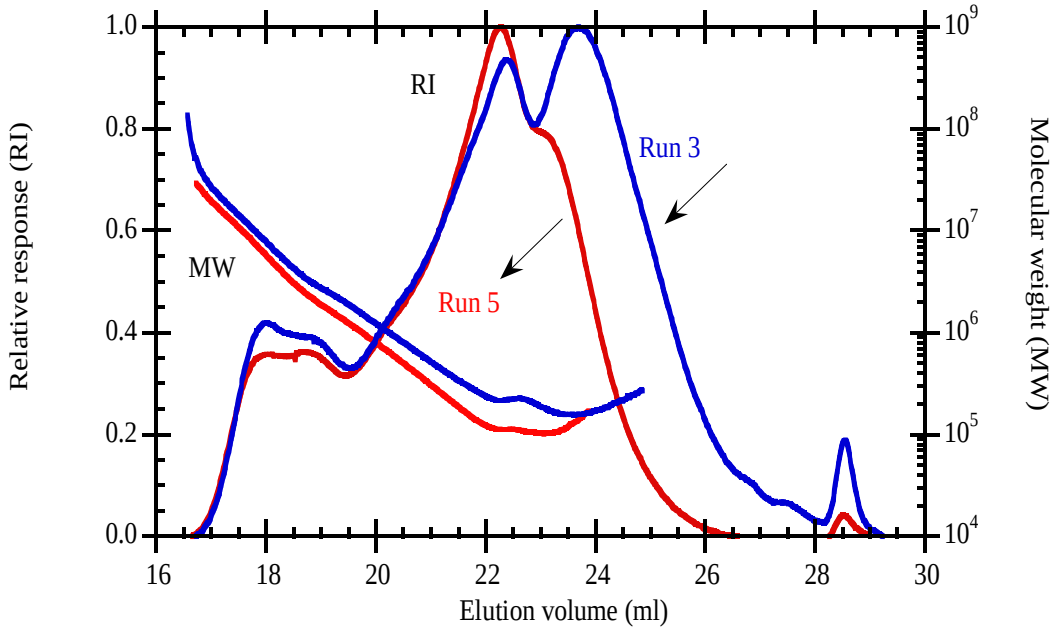

Figure 2.56. Molecular weight along the SEC chromatogram for samples of STY/DVB synthesized using different operation conditions in polymerisations times very near to gel point.

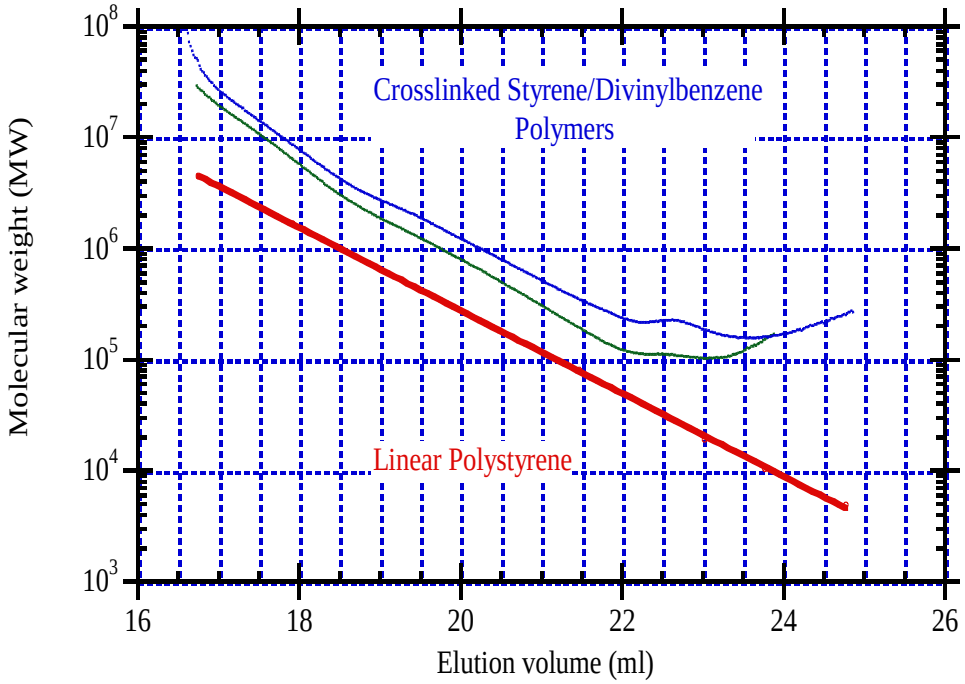

Figure 2.57. Observed relations molecular weight versus elution volume for STY/DVB.

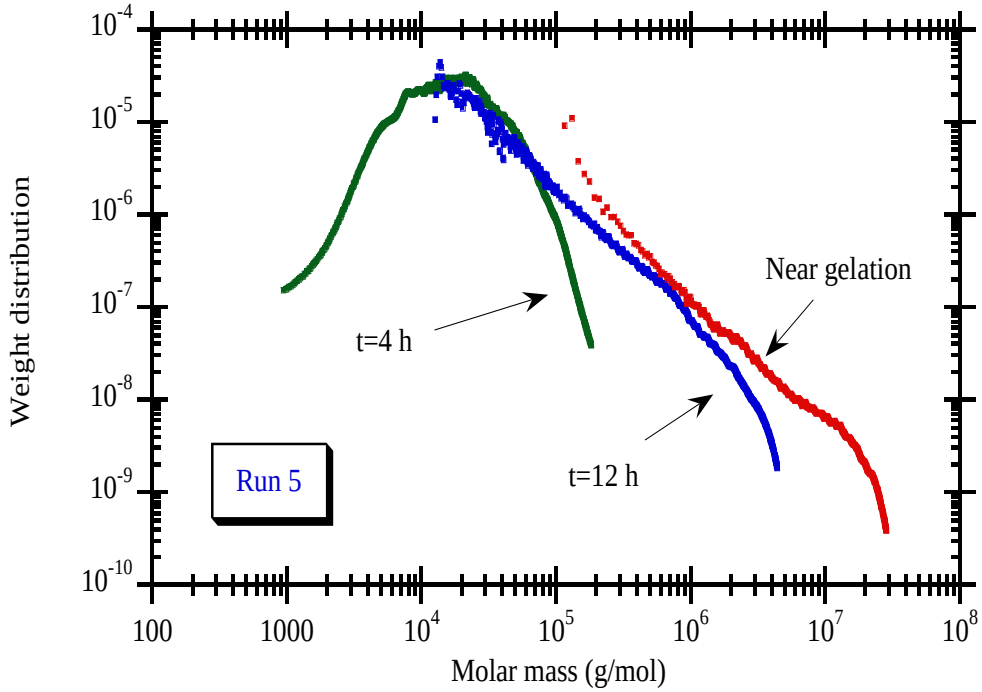

Figure 2.58. Time evolution of the molecular weight distribution of STY/DVB synthesized in semi-batch reactor showing a formation of a long end tail as gelation is approached.

2.4 Solution Copolymerisation of MMA/EGDMA

2.4.1 Kinetic Modelling

2.4.1.1 Chemical Species

For this chemical system twenty three different chemical species are considered as shown in Table 2.8. The copolymerisation of MMA with EGDMA, eventually in the presence of an inhibitor and/or retarder (besides initiator, solvent and chain transfer agent) is discussed. Two different kinds of polymer radicals are distinguished since they present different structures and therefore different reactivities are also plausible. Pendant double bonds arising from EGDMA, which are akin of one additional monomer, are also distinguished for the double bonds in the monomers as they are known to show different reactivities (Landin *et al*., 1988; Li *et al*., 1989a and 1989b). In Figures 2.59 and 2.60 are represented the structures of MMA, EGDMA and BPO.

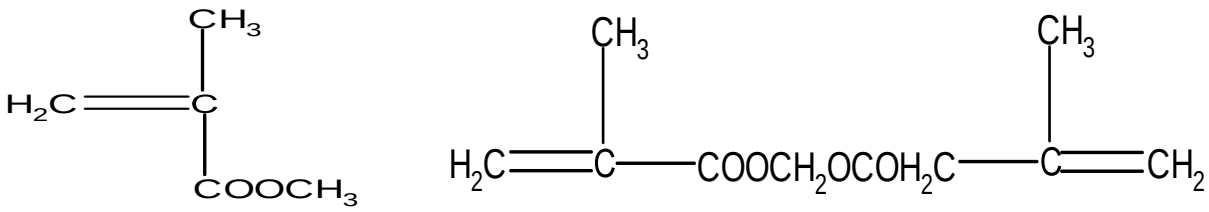

(a) (b)

Figure 2.59. Schematic representation of (a) methyl methacrylate and (b) ethylene glycol dimethacrylate.

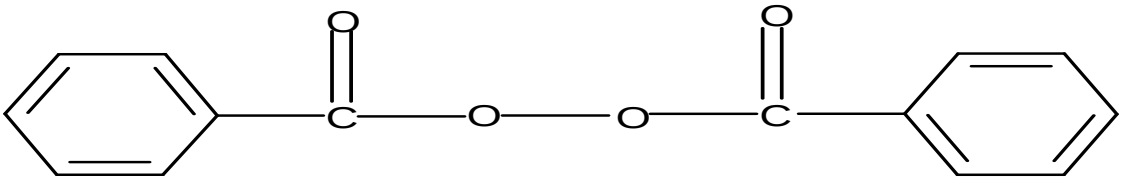

Figure 2.60. Schematic representation of benzoyl peroxide (BPO) thermal initiator.

2.4.1.2 Chemical Reactions

Table 2.9 shows the kinetic scheme describing this polymerisation system. A total count of 76 chemical reactions is assumed to exist: initiator decomposition, initiation of monomers and PDB by primary radicals, propagations of monomers and PDB with the different kinds of polymer radicals, chain transfer to solvent, chain transfer to CTA, inhibition of polymer and primary radicals, retardation of centered polymer radicals, terminations by combination and

by disproportionation of polymer radicals. For the sake of generality, transfers to monomers and to initiator are also considered in this analysis.

Table 2.8. Chemical groups for the radical copolymerisation of MMA with EGDMA.

Group description	Alias
Methyl methacrylate (MMA)	M_1
Ethylene glycol dimethacrylate (EGDMA)	M_2
Initiator (I)	C_1
Solvent (T)	C_2
Chain transfer Agent (CTA)	C_3
Inhibitor (Z)	C_4
Retarder (R)	C_5
Primary Radical from initiator (PRI)	R_1
Primary radical from solvent (PRS)	R_2
Primary radical from chain transfer agent (PRCTA)	R_3
Radical from methyl methacrylate (RMMA)	A_1
Radical from ethylene glycol dimethacrylate (REGDMA)	A_2
Radical from pendant double bonds (RPDB)	A_3
Radical from retarder (RR)	A_4
Pendant double bonds (PDB)	M_3
Polymerised methyl methacrylate	U_1
Polymerised ethylene glycol dimethacrylate	U_2
Crosslinking site	U_3
Fragments from initiator, solvent, chain transfer agent, inhibitor and retarder	F_1-F_5

The leading chemical reactions here considered follow the same principle as the vinyl/divinyl reactions of STY/DVB in section 2.222, only the structure around the vinyl group is changed. For the system MMA/EGDMA initiated by BPO we must include chain transfer to monomer and chain transfer to initiator. With the chain transfer to monomer reaction a propagating chain reacts with MMA and it forms a saturated chain and a radical from the monomer (see Figure 2.61). Transfer to initiator introduces a new end group into the polymer, lowers the molecular weight of the polymer, reduces the apparent initiator efficiency and increases the rate of initiator disappearance. In Figure 2.62 is presented an example of chain transfer to initiator reaction.

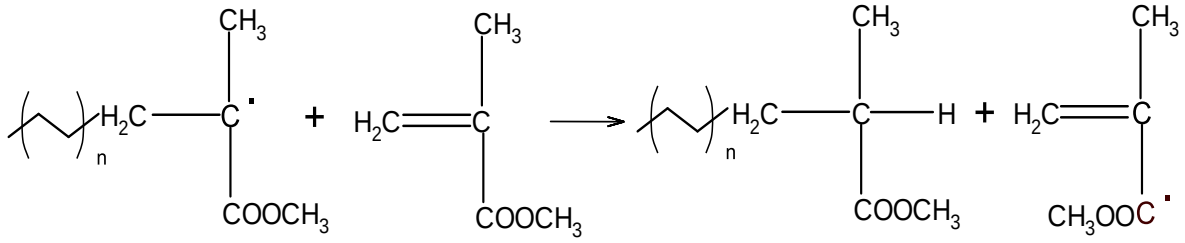

Figure 2.61. Transfer to monomer reaction between a radical from MMA and MMA.

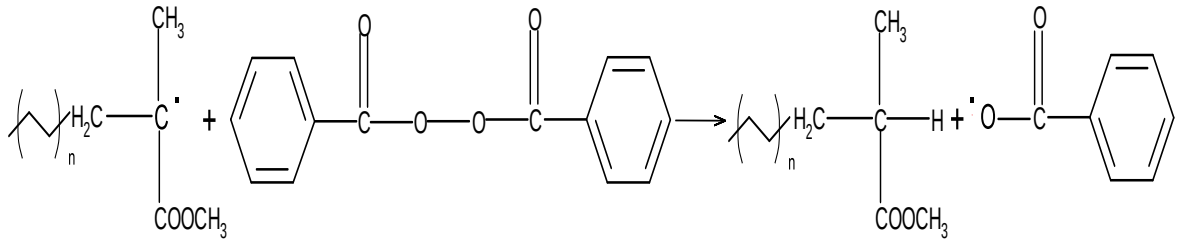

Figure 2.62. Transfer to initiator reaction of a radical from MMA with BPO.

Table 2.9. Kinetic scheme considered in the radical copolymerisation of MMA/EGDMA at 60 °C.

Kinetic Step	Chemical Equation
Initiator Decomposition	$C_1 \xrightarrow{k_d} 2fR_1$
Initiation of monomers and PDBs	$R_j + M_k \xrightarrow{k_{Ijk}} A_k + U_k + F_j(+M_3 if\ k = 2)$
Methyl methacrylate propagation	$A_i + M_1 \xrightarrow{k_{pi1}} A_1 + U_1$
EGDMA propagation	$A_i + M_2 \xrightarrow{k_{pi2}} A_2 + M_3 + U_2$
PDB propagations	$A_i + M_3 \xrightarrow{k_{pi3}} A_3 + U_3$
Chain transfer to initiator	$A_i + C_1 \xrightarrow{k_{Ii}} dead\ chain + R_1$
Chain transfer to solvent	$A_i + C_2 \xrightarrow{k_{Si}} dead\ chain + R_2$
Chain transfer to agent	$A_i + C_3 \xrightarrow{k_{CTAi}} dead\ chain + R_3$
Chain transfer to MMA	$A_i + M_1 \xrightarrow{k_{M1i}} dead\ chain + A_1 + U_1$
Chain transfer to EGDMA	$A_i + M_2 \xrightarrow{k_{M2i}} dead\ chain + A_2 + M_3 + U_2$
Inhibition of polymer radicals	$A_i + C_4 \xrightarrow{k_{Zi}} dead\ chain + F_4$
Inhibition of primary radicals	$R_i + C_4 \xrightarrow{k_{ZPi}} inactive\ products$
Retardation of primary radicals	$A_i + C_5 \xrightarrow{k_{ri}} A_4 + F_5$
Termination by combination	$A_i + A_j \xrightarrow{k_{tcij}}$ Head-Head Unit
Termination by disproportionation	$A_i + A_j \xrightarrow{k_{tdij}}$ Sat.+ Unsat. Units

Tables 2.10 and 2.11 present the numerical values of some of the 77 kinetic parameters used in the modelling. In Table 2.12 are depicted the values considered for the propagation rate coefficients which are the major parameters governing the crosslinking process. Past experimental works concerning the copolymerisation of MMA with EGDMA have been used for estimating most of the needed kinetic parameters (Li *et al.*, 1989a and 1989b) involved in this crosslinking polymerisation. Nevertheless, here are distinguished the radicals from PDB and therefore other assumptions concerning the reactivity of these species must be used. In the present work a sensitivity analysis with respect to the prediction of the reactivities of these radicals is also presented. Other assumptions are described in the footnotes of the aforementioned Tables 2.10-2.12.

Table 2.10. Assumptions used for some kinetic parameters considered in the modelling of radical copolymerisation of MMA with EGDMA at 60 °C.

Kinetic Step	Kinetic parameter involved
Propagations with radicals RR [a)]	$\frac{k_{p4j}}{k_{p1j}} = 0.01(j = 1, \dots, 3)$
Initiations [b)]	$k_{Ikj} = k_{p1j}(k = 1, \dots, 3, j = 1, \dots 3)$
Chain transfer to agent and to solvent [c)]	$k_{CTAj} = C_{CTA}k_{pj1}, \quad k_{Sj} = C_S k_{pj1}$
Chain transfer to monomers and to initiators [d)]	$k_{Mij} = C_M k_{pij}, \quad k_{Ij} = C_I k_{pj1}$
Inhibition [b)e)]	$k_{Zi} = C_Z k_{pi1} \quad (i = 1, \dots, 4)$
	$k_{ZPi} = C_Z k_{p11} \quad (i = 1, \dots, 3)$
Reaction of radicals with retarder [b)]	$\frac{k_{Ri}}{k_{R1}} = \frac{k_{pi1}}{k_{p11}} \quad (i = 1, \dots, 3)$
Termination [f)]	$k_{tcij} = k_{tc}, k_{tdij} = k_{td} \quad (i, j = 1, \dots, 4)$

[a)] The propagation of the monomers with non-carbon centered radicals (e.g. oxygen centered) is considered to be much slower than with the related normal propagation (Moad and Solomon, 2006). **[b)]** The rate constants for the initiation of the different monomers (j=1,…,3) with different kinds of primary radicals (k=1,…,3) are considered to take the same values in the related propagations with RMMA. **[c)]** The rate constants of the reactions between the various propagating radicals with, CTA, solvent, inhibitor and retarder are assumed to be proportional to the propagation constant with MMA. [d)] The rate constant of transfer to monomers are proportional to the similar propagation reactions using the transfer to MMA as reference. The same assumption is used for the reactions of transfer to initiator. [e)] The inhibition of the primary radicals is supposed to occur with MMA at the same extent. [f)] It is considered that the kinetic constants for all termination reactions take the same values as the average termination rate constant.

Table 2.11. Basic set of kinetic parameters considered in the modelling of radical copolymerisation of MMA with EGDMA at 60 °C.

Kinetic Step	Kinetic parameter involved [a)]
Initiator decomposition [b)c)]	$k_d = 9.6 \times 10^{-6}(\mathrm{s}^{-1}), f = 0.6(-)$(AIBN)
	$k_d = 2.8 \times 10^{-6}(\mathrm{s}^{-1}), f = 1(-)$(BPO)
Methyl methacrylate homopropagation [d)]	$k_{p11} = 820$
Polymer radicals termination [e)]	$\frac{k_{p11}}{\sqrt{k_{t_0}}} = 0.15 dm^{3/2}(mol\ s)^{-1/2}$
	$k_{tc} = \alpha_{tc} k_t, k_{td} = \alpha_{td} k_t$
	$k_t = \begin{cases} k_{t_0} if\ X < X_C = 0.3 \\ k_{t_0} exp[-Z(X - X_C)]\ if\ X > X_C \end{cases}; Z = 2$
Chain transfer to solvent [f)]	$C_S = \frac{k_{S1}}{k_{p11}} = 0.2 \times 10^{-4}$
Chain transfer to agent [g)]	$C_{CTA} = \frac{k_{CTA1}}{k_{p11}} = 0.25$
Inhibition [h)]	$C_Z = \frac{k_{Z1}}{k_{p11}} = 10^4$
Reaction radical/retarder [i)]	$k_{R1} = 10^9$
Chain transfer to monomer [j)]	$C_M = \frac{k_{M1}}{k_{p11}} = 0.2 \times 10^{-4}$
Chain transfer to initiator [k)]	$C_I = \frac{k_{I1}}{k_{p11}} = 0.02$ (BPO);=0 (AIBN)

[a)] All the kinetic parameters are expressed in $\mathrm{dm^3 mol^{-1} s^{-1}}$, unless otherwise stated. [b)] For AIBN, k_d was collected from Moad and Solomon, (2006) at p.71 and f from Bevington (1955). [c)] For BPO, k_d was taken to be the value for a benzene solution measured by inhibition with DPPH (Bevington *et al*., 2003) which should be more accurate than the previously reported (Barson and Bevington, 1997) and f is known to be above 0.9 (Moad *et al*., 1982). [d)] k_{p11} is a IUPAC benchmark value (Moad and Solomon, 2006) collected from Beuermann *et al*., 1997. [e)] k_t is an average termination constant in the framework of classical kinetics. Scattered values in the range 0.12 to 0.27 for the parameter $k_p/\sqrt{k_{t_0}}$ can be found in the literature (Matheson *et al*., 1949; Fernández-Garcia *et al*., 1998; Hutchinson, 2005; Brandrup *et al*., 2009). $k_p/\sqrt{k_{t_0}} = 0.15\ \mathrm{dm^{3/2}(mol\ s)^{-1/2}}$ was estimated from time versus conversion data (prior to noticeable Norrish-Trommsdorff effect) as measured in the present work. Termination of MMA occurs predominantly by disproportionation ($\alpha_{td} = 0.6$) but note that values of α_{td} from 0.16 to 0.7 are also mentioned in the literature (Moad and Solomon, 2006). [f)] The C_S parameter was collected from Hutchinson, 2005 at p.168. [g)] The C_{CTA} parameter was collected from Li *et al*., (1989a) and Li *et al*., (1989b). [h)] C_Z parameter in the range of the inhibition reactions by some quinones (Moad and Solomon, 2006). [i)] k_{R1} in the range of the rate constant for the reaction of carbon centered radicals with oxygen. [j)] The C_M parameter was collected form Hutchinson (2005) at p.169. [k)] The C_I parameter from Brandrup *et al*., (1999).

Table 2.12. Propagation rate coefficients (k_{pij}) considered in the radical copolymerisation of MMA with EGDMA at 60 °C.

Radical/monomer	M_1	M_2	M_3
A_1	820.0 [a)]	1223.9 [b)]	237.7 [c)]
A_2	1122.7 [b)]	1672.8 [b)]	324.9 [c)]
A_3	598.9 [d)]	895.5 [d)]	173.9 [d)]

[a)] IUPAC benchmark value and can be found in Moad and Solomon, 2006 at p.219. [b)] The rate coefficients k_{p21}, k_{p12} and k_{p22} are based on the reactivity ratios $r_1 = 0.67$, $r_2 = 1.49$ and $\frac{k_{p22}}{k_{p11}} = 2.04$ and were collected from Li *et al*., (1989a) and Li *et al*., (1989b). [c)] The rate coefficients k_{p13} and k_{p23} are based on the reactivity ratio $r_{13} = \frac{k_{p11}}{k_{p13}} = 3.45$ obtained in this work from experimental data and on the ratios $\frac{k_{p13}}{k_{23}} = \frac{k_{12}}{k_{p22}}$ as suggested in Li *et al*., (1989a and 1989b). [d)] It is considered in this work that a geometric decay relation holds for the reactivity of radical A_3 with the different kind of monomers: $k_{p3j} = \frac{(k_{p1j})^2}{k_{p2j}}$. These reactivity drops are plausible owing to steric factors. The effect of this assumption is also discussed in the current work.

2.4.2 Results and Discussion

In Figure 2.63 are presented the experimentally measured and predicted values of the overall monomer conversion. Those data were used to estimate the parameter $\frac{k_p}{\sqrt{k_{t_0}}} = 0.15\ \mathrm{dm}^{3/2}(\mathrm{mol\ s})^{-1/2}$ considering valid the classical polymerisation kinetics, which was estimated to hold up to monomer conversion $p = 0.3$. A decrease of k_t owing to a different regimen of diffusion control was observed for higher monomer conversions and this effect was quantified using an empirical correlation of the decrease of the termination rate constant as proposed by Tobita and Hamielec (1989). These solution data do not show the slight influence of the presence of EGDMA on k_t which is nevertheless known to occur at bulk polymerisation when w_{EGDMA} is increased from 0 to 0.01 (Li *et al*., 1989b).

In Figures 2.64 and 2.65 are compared the experimental measurements and theoretical predictions for $\bar{M}_w$ in the non-linear polymerisation of MMA+EGDMA initiated by AIBN and BPO. Error bars presented in those two Figures for the experimental measurements of this work are those directly indicated by the software (ASTRA) of the SEC/RI/MALLS system. The experimental data on $\bar{M}_w$ lead to an estimation of the reactivity ratio of PDB, which is $r_{13} = k_{p11}/k_{p13} = 3.45$. With this apparent reactivity ratio, good agreement between measurements and predictions for runs carried out with different amounts of EGDMA was achieved except when the reaction conditions are favourable to the occurrence of

intramolecular reactions (high monomer conversion with non-linear systems). Is important to note that this reactivity ratio is consistent with a decrease of reactivity of PDB ($C_P = 2\,k_{p13}/k_{p12} = 0.39$), as reported in other works on this subject (Landin *et al*., 1988; Li *et al*., 1989a and 1989b). Further studies in order to clarify the values of PDB reactivities (which actually should be higher than these apparent values) should include experiments at higher dilutions in order to assess the intramolecular cyclization effects (Landin *et al.*, 1988; Dias and Costa, 2005a).

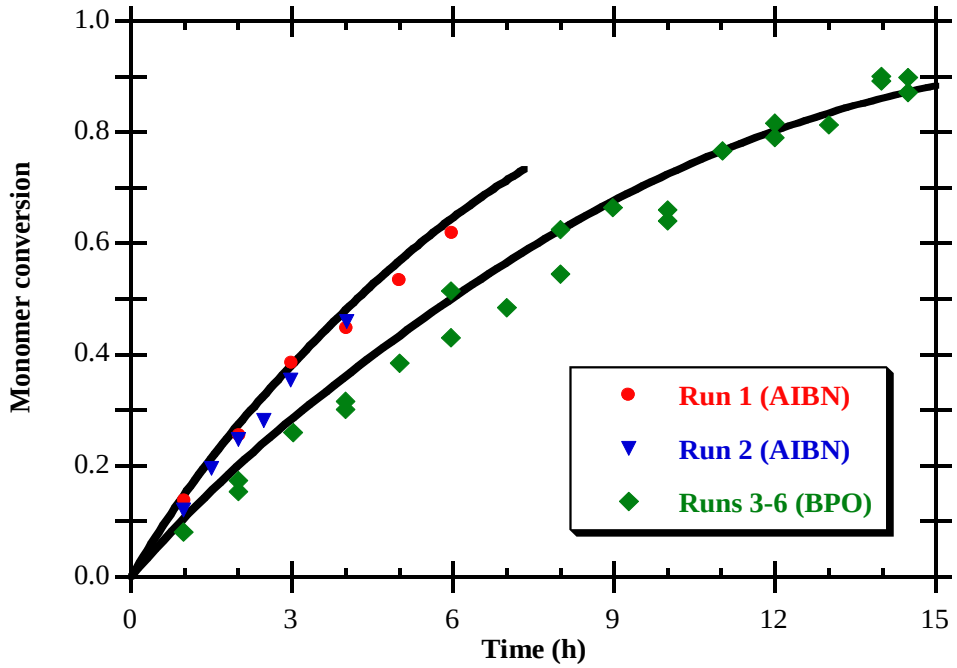

Figure 2.63. Time evolution of the measured and predicted overall monomer conversion for different polymerisation runs performed with AIBN and BPO as initiators.

Note that the kinetic approach used lumps all isomers with same counts of groups into the same conventional chemical species. Therefore, an accurate consideration of intramolecular reactions is possible only for the smallest sized loops (Dias and Costa, 2005a). It is nevertheless conceivable that models using empirical pseudo-rate constants of cyclization might prove to be useful. They present some mathematical difficulties in their implementation namely when generating functions are introduced and this has delayed their development.

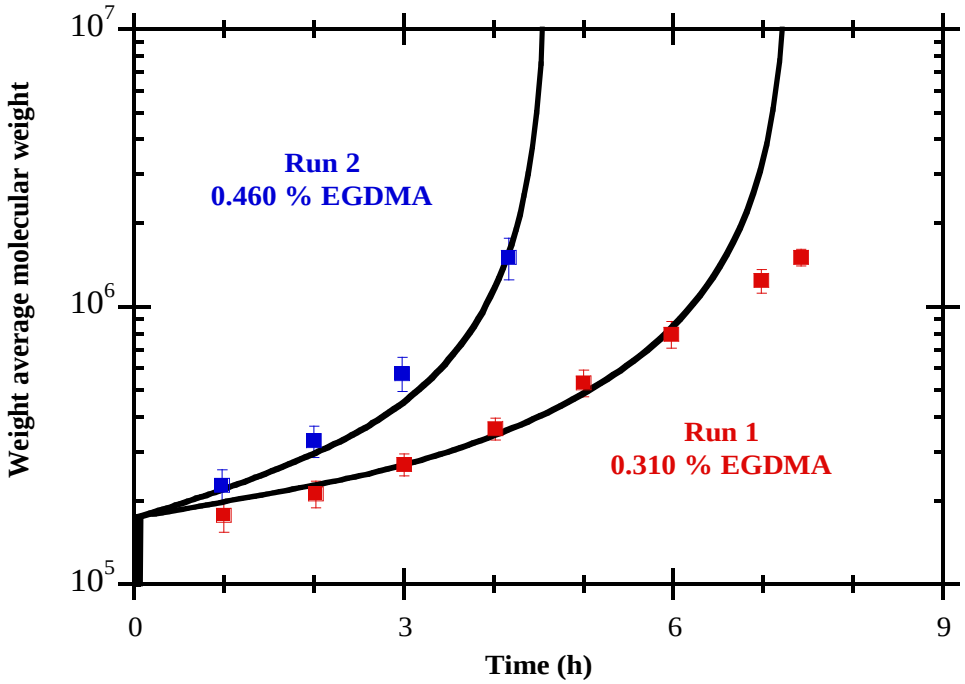

Figure 2.64. Time evolution of the measured and predicted $\bar{M}_w$ for polymerisations runs performed with AIBN.

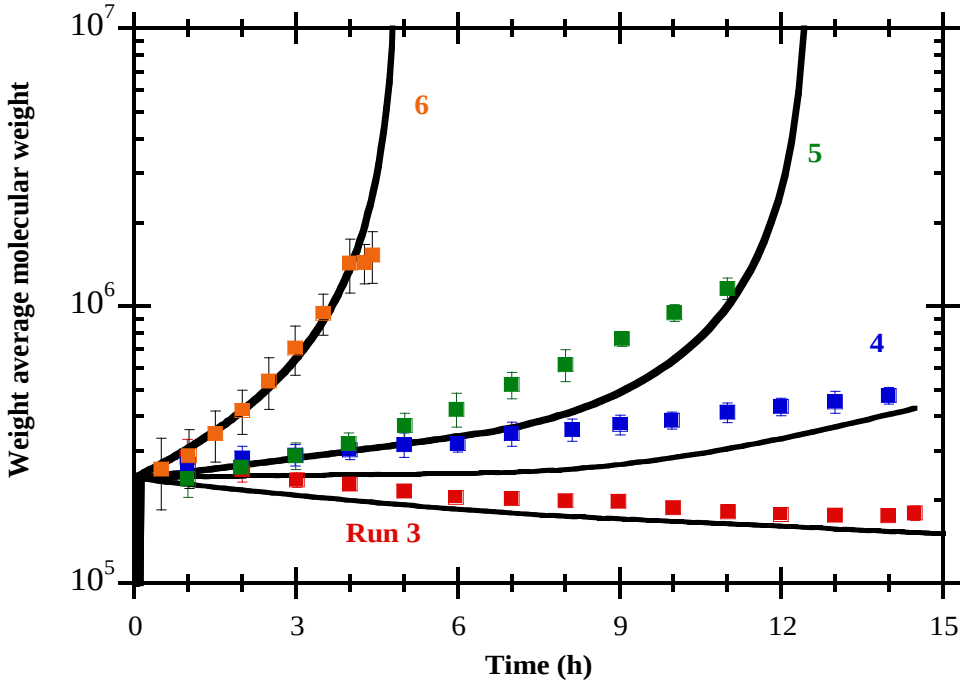

Figure 2.65. Time evolution of the measured and predicted $\bar{M}_w$ for polymerisations runs performed with BPO.

The most innovative results of this work are presented in Figures 2.66 and 2.67, where experimental *z*-average mean-square molecular radius of gyration ($\bar{R}_g$) of the synthesised copolymers are compared with the predictions of the present kinetic approach (Costa and Dias, 2007). This method is valid for tree-like polymers with Gaussian chains considered as a set of beads connected by massless freely rotating rods. These predictions are therefore valid at Θ conditions. Molecular expansion in good solvents (the excluded volume effect) should be taken into account because the experimental measurements were performed in THF at 30 °C. The length of the Kuhn segment connecting centers of mass repeating units $b = 0.615$ nm was estimated using the relation $\bar{R}_{g,lin_\Theta} = 0.0251M^{0.5}$ valid for poly(methyl methacrylate) in a in Θ solvent (Ioan *et al.*, 1995; Búrdalo *et al*., 2000). Using the published value for poly(methyl methacrylate) in THF, $\bar{R}_{g,lin} = 0.011M^{0.596}$ at 30 °C (Búrdalo *et al*., 2000) we estimate that also in THF at 30 °C for linear polydispersed poly(methyl methacrylate) $\frac{\bar{R}_{g,lin}}{\bar{R}_{g,lin_\Theta}} = 0.438M_z^{0.096}$. An extension of this method for taking into account the presence of the excluded volume effect has not yet been developed (Costa and Dias, 2007) and in this system we have assumed equality of the expansion factors for branched and linear polymer molecules. Several other researchers (Dobkowvski, 1985) have also considered this assumption in more recent works with similar goals, but a more exact estimation of $g = \frac{\bar{R}_{gbra}}{\bar{R}_{glin}}$ is needed.

In spite of these assumptions, a good agreement is often observed between the predictions and the experimental measurements of $\bar{R}_g$ when intramolecular reactions are less important and therefore some reliable information concerning the molecular architecture of these polymers can be obtained using this approach. The exceptions are, as it could be expected, the high discrepancies between predictions and measurements with runs 1 and 5 where higher monomer conversions at gel point are observed.

The complexity of kinetic schemes such as the one here discussed precludes the direct use of other approaches (such as Monte Carlo simulation or molecular dynamics) which should be improved order to efficiently describe real linear or branched chains (Steinhauser, 2005). A major advantage of this general kinetic approach is the possibility of considering more complex kinetic schemes whenever desired. In the present case study, radicals from pendant double bonds (A_3) were distinguished from radicals of MMA or EGDMA because it is plausible that they present different reactivities (see Table 2.10). Figure 2.68 shows the

predicted effect of the reactivity of RPDB on the time evolution of $\bar{M}_w$, using run 2 as an example.

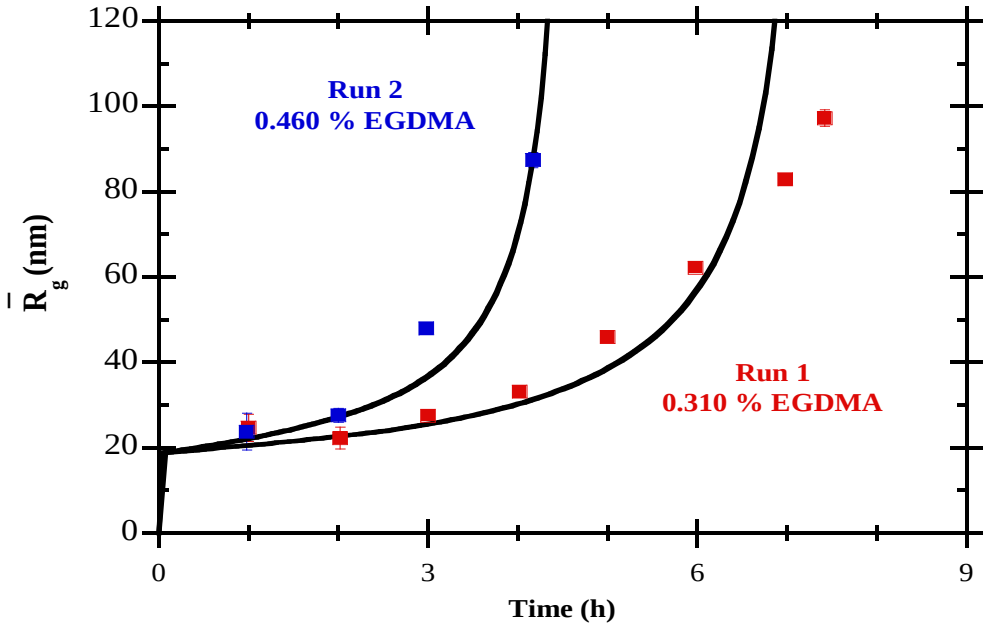

Figure 2.66. Predicted and measured time evolution of $\bar{R}_g$ in the copolymerisation system MMA/EGDMA initiated by AIBN.

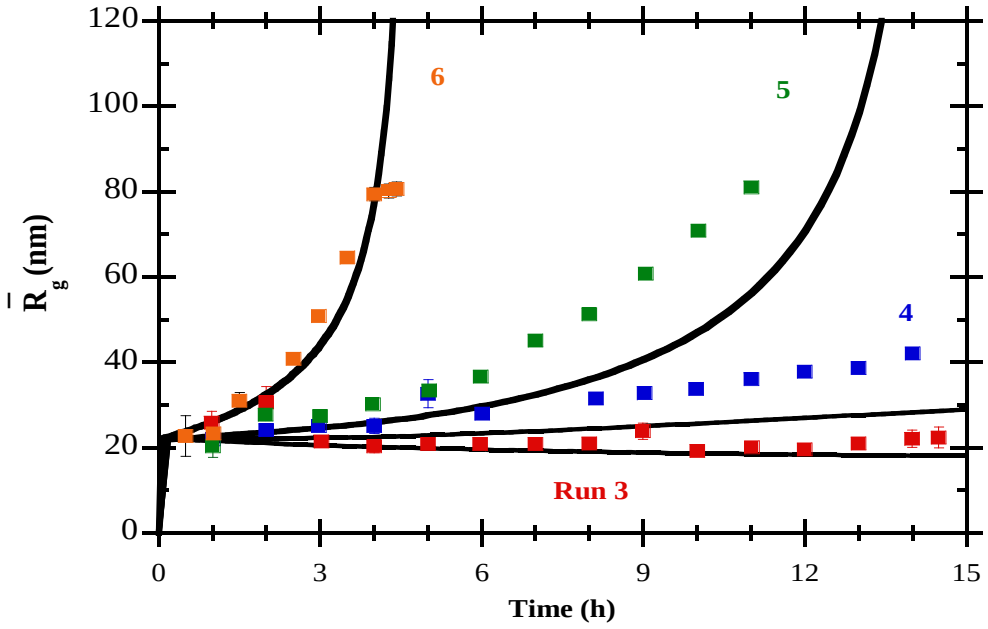

Figure 2.67. Predicted and measured time evolution of $\bar{R}_g$ in the copolymerisation system MMA/EGDMA initiated by BPO.

Different values of the reactivities of RPDB $k_{p3j}^{*} = C_R k_{p3j}$ were considered in the simulations using the values (k_{p3j}) present in Table 2.11 as a reference. It can be observed that these parameters can have a major effect on the predictions only when these radicals are reacting much more slowly ($C_R < 0.01$) than the reference situation we have considered. However, this is a plausible situation due to lower mobility of these radicals and therefore the estimation apparent reactivity ratios of PDB can also be affected by this phenomenon. The reliability of the predictions of the present kinetic approach was also assessed using experimental data previously obtained for bulk polymerisation of MMA/EGDMA (Li *et al.*, 1989a and 1989b). Considering the polymerisation conditions and the kinetic parameters used in these works, our predictions of the monomer conversion at gel point were compared with the experimental values observed in the presence of CBr_4 as CTA. This comparison is presented in Figure 2.69 and the good agreement between the predictions and measurements confirms the correctness of the foundations of this method.

Figure 2.70 shows the relation between measured average radius of gyration and average molecular weight for linear MMA and different non-linear samples of MMA/EGDMA synthesized in this case. The well known decrease of the size of non-linear polymers when compared with the linear analogous is here confirmed. Nevertheless, it is important to recall that these polymer samples are highly dispersed in molecular mass and the correct comparison is made using $\bar{M}_z$ as a reference instead of $\bar{M}_w$. Indeed, for a population of linear polymer molecules a power relation (with exponent 0.5 for Gaussian chains) between $\bar{R}_g$ and $\bar{M}_z$ should be observed (Dias and Costa, 2007). Note in the same Figure the high estimated errors in the measurements of $\bar{M}_z$ by SEC/RI/MALLS (only $\bar{M}_w$ can be directly measured) when highly dispersed polymer samples are analysed, as previously presented in the system styrene/divinylbenzene (Gonçalves *et al*., 2007). Figure 2.71 shows the build-up of a polymer population with large dimensions but at low concentration (forming a kind of cluster) as the gel point is approached.

The chromatogram presented in Figure 2.72 of a MMA/EGDMA sample collected close to gel point shows in detail a molecular fraction with a strong light scattering signal but a weak refractive index. Figure 2.73 shows an inversion in the relation molecular mass versus elution volume of two highly crosslinked samples of MMA/EGDMA confirming again the existence in the samples of polymer species with same molecular weight but very different molecular sizes. Similar observations have also been recently reported in the literature (Bannister *et al*., 2006). Figure 2.74 presents the time evolution of the chromatograms of MMA/EGDMA

samples showing the formation of a long end tail as the gel point is approached, in agreement with previously theoretical results (Dias and Costa, 2005b).

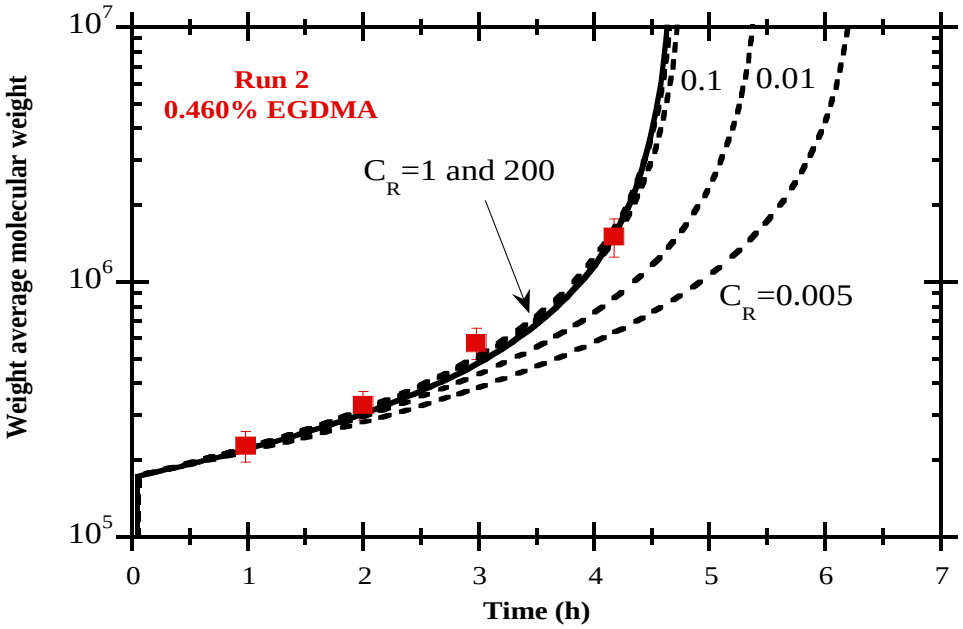

Figure 2.68. The predicted effect of the reactivity of radicals of pendant double bonds on the time evolution of $\overline{M}_w$.

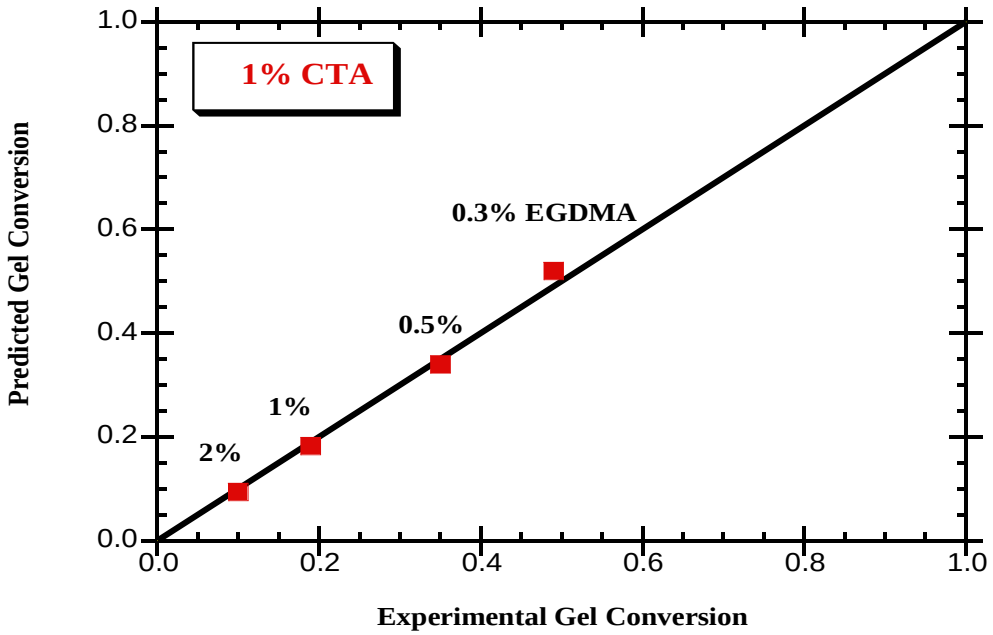

Figure 2.69. Predicted and measured gel conversion for the system MMA/EGDMA in the presence of CTA. Experimental data collect from Li *et al*. (1989a and 1989b) and predictions from the present kinetic model.

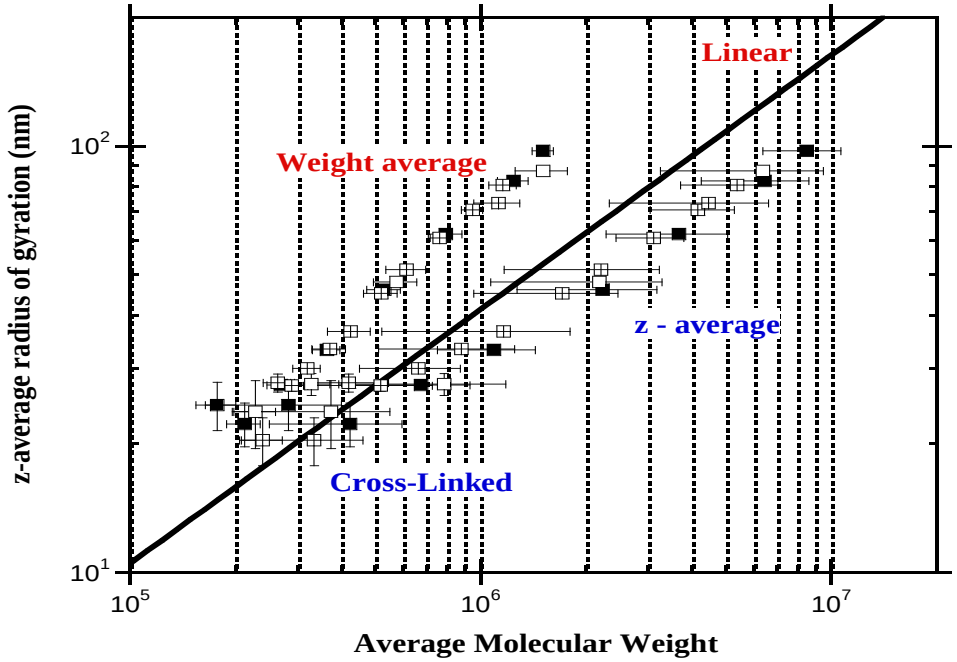

Figure 2.70. Relation between average radius of gyration and average molecular weight for linear MMA and several non-linear samples of MMA/EGDMA.

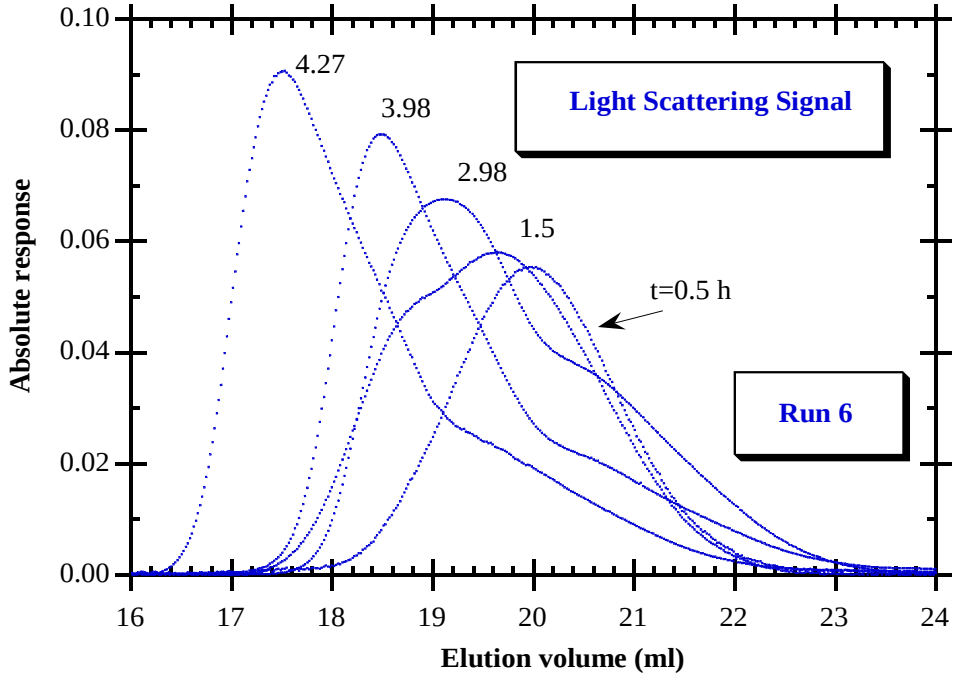

Figure 2.71. Observed 90° light scattering signal in the SEC chromatograms of samples of MMA/EGDMA corresponding to different polymerisation times.

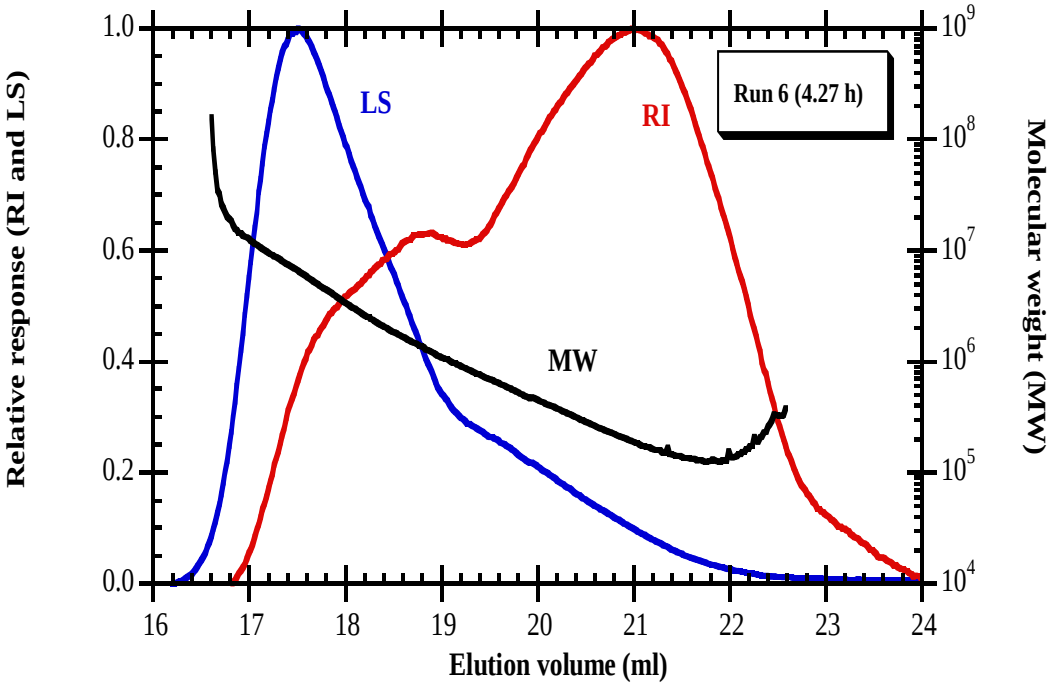

Figure 2.72. Molecular weight along the SEC chromatogram for a sample of MMA/EGDMA.

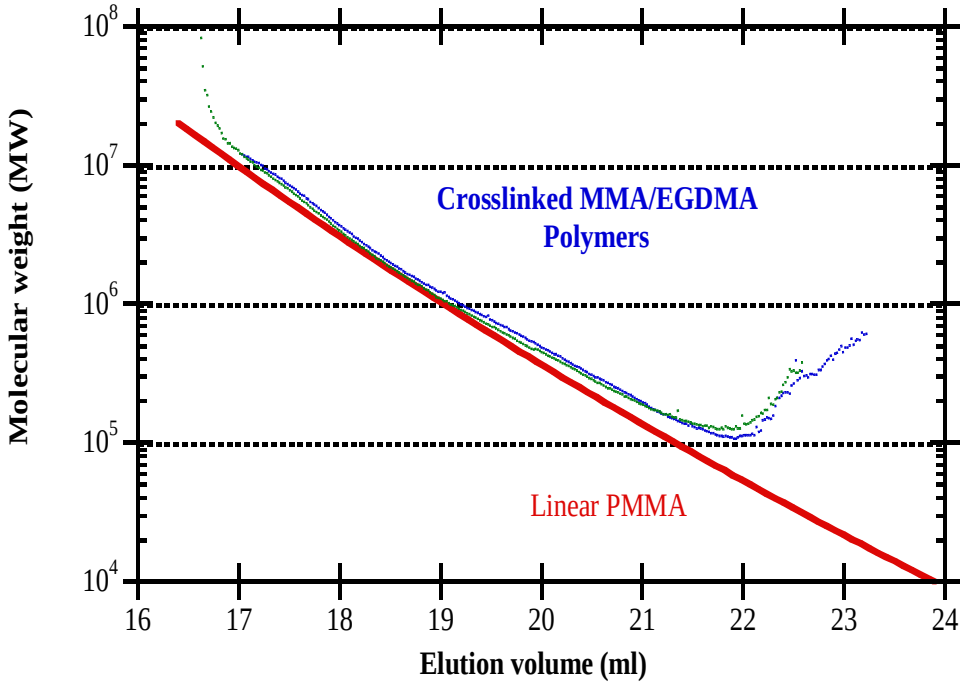

Figure 2.73. Observed relations molecular weight versus elution volume for MMA/EGDMA copolymers.

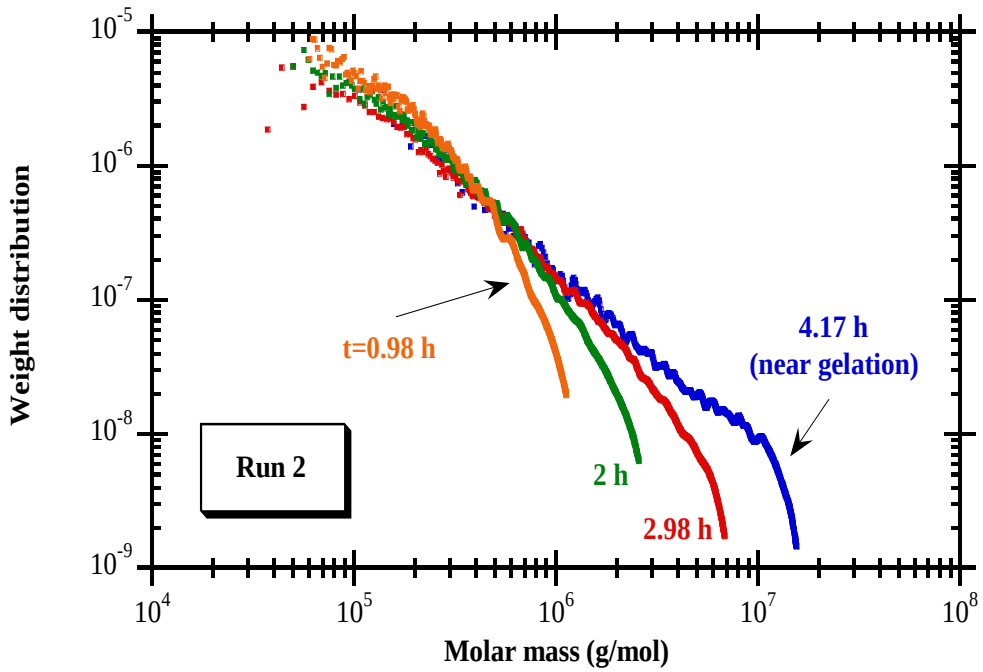

Figure 2.74. Time evolution of the molecular weight distribution of MMA/EGDMA copolymerisation showing the formation of a long end tail as gelation is approached.

2.5 Suspension Polymerisation of STY/DVB Leading to Gel Formation

2.5.1 Kinetic Scheme

The kinetics schemes, chemical species and chemical reactions involved in the suspension polymerisation of STY/DVB is the same as the solution polymerisation of STY/DVB presented in section 2.3.1 in this chapter.

2.5.2 Results and Discussion

Figure 2.75 show the predicted and observed time evolution of the weight average molecular weight ($\overline{M}_w$) during the suspension copolymerisation of STY/DVB at 60 °C (see Table 2.3). Experimental values were measured before and after gelation by SEC/RI/MALLS, as above described. The effect of the mole fraction of DVB in the initial monomer mixture ($f_{DVB} = 10$ and 20 %) on the dynamics of $\overline{M}_w$ in batch reactor is clearly put into evidence, namely for what concerns the delay in gelation time. This dynamics was also predicted before and after gelation using the aforementioned calculation techniques. A good agreement between measurements and predictions can be obtained if the reactivity of PDB is used as a fitting

parameter. In this context the following reactivity ratios of PDB comparatively with styrene were estimated: $C_{PDB} = \frac{k_{p4}}{k_{p1}} = 0.055$ for $f_{DVB} = 20\ \%$ and $C_{PDB} = 0.07$ for $f_{DVB} = 10\ \%$. These unrealistic low values obtained by the fitting procedure are a consequence of neglecting intramolecular cyclizations, which are a competitive kinetic mechanism decreasing crosslinking efficiency, as previously shown (Gonçalves *et al*., 2007; Trigo *et al*., 2008). The slightly different values of the reactivity ratios of PDB estimated for $f_{DVB} = 20\ \%$ and $f_{DVB} = 10\ \%$. are also probably a result of the different impact of intramolecular cyclizations which, for the same dilution, should increase with the initial mole fraction of DVB. Simple attempts to include intramolecular cyclizations in the framework of the present kinetic approach have already been performed (Dias and Costa, 2005a) but a lot more additional theoretical developments are needed in this context. Despite this limitation, results presented in Figure 2.75 show that some important features of gel formation can be captured by the simple kinetic scheme here considered.

Figure 2.76 shows a comparison between the predicted and measured time evolution of the weight fraction of gel (w_g) during the suspension copolymerisation of STY/DVB. In this case, high deviations between the measured values and predictions are observed for both initial compositions. The same kinetic parameters resulting from the fitting studies described in Figure 2.75 were used in the calculation of w_g considering a non-ideal crosslinking process ($C_{PDB} < 1$). The ideal behaviour corresponded to $C_{PDB} = 1$ (ideal crosslinking in the absence of intramolecular cyclizations) is also presented in Figure 2.76. Experimental measurements are confined between the predictions corresponded to these two simulation systems, confirming the modelling limitations before described (intramolecular cyclizations not included). In fact, the produced gels were several times washed in THF and only small amounts of sol are expected to be entrapped in the final products given their not so large molecular weight. Therefore, deficient gel washing cannot explain the huge differences observed. Formation of microgel and inhomogeneous gel structures along polymerisation can be at the source of such discrepancies, with intramolecular cyclizations playing a major role. These phenomena were not taken into account in the present modelling studies (complex developments are needed) and the predicted gel fraction is underestimated for the non-ideal system and overestimated for the ideal crosslinking behaviour. In the presence of very high contents of DVB (10 and 20 %) and due to relative small length of primary chains (namely when compared with non-linear acrylic system), intramolecular cyclizations phenomena are likely to occur in the formation of STY/DVB networks.

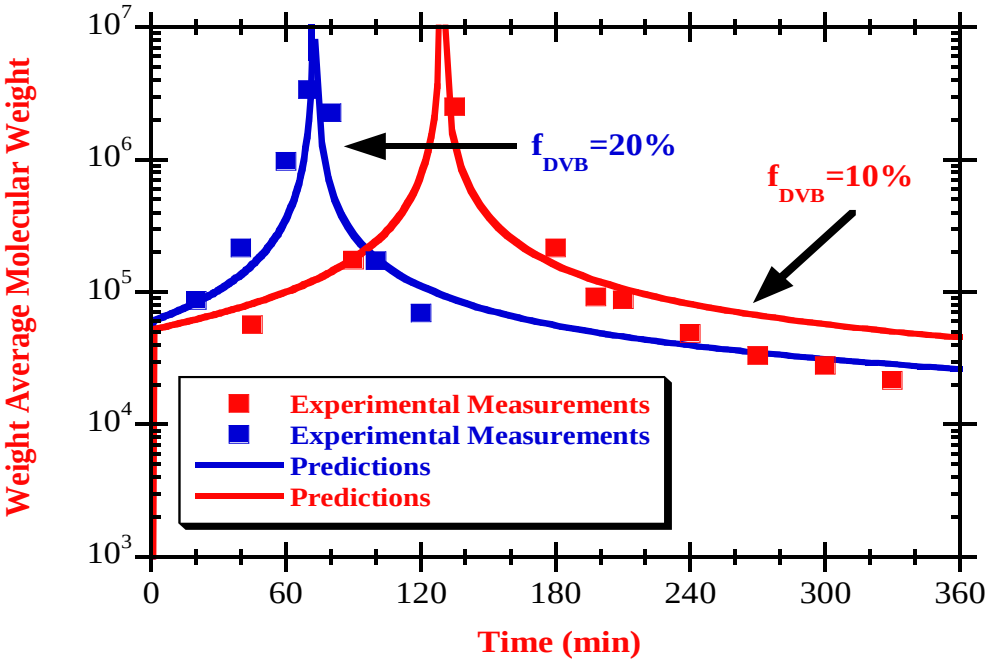

Figure 2.75. Predicted and measured time evolution of the weight average molecular weight $\bar{M}_w$. The effect of the mole fraction of DVB in the initial monomer mixture over the dynamics of $\bar{M}_w$ in batch reactor is observed.

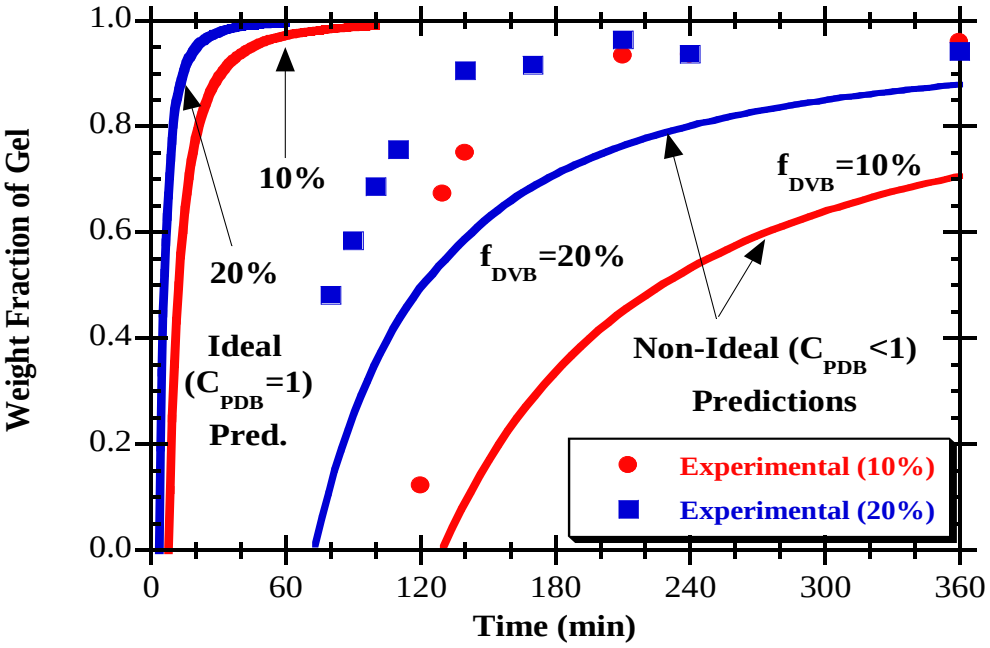

Figure 2.76. Predicted and measured time evolution of the weight fraction of gel w_g. The effect of the mole fraction of DVB in the initial monomer mixture over the dynamics of w_g is observed.

It is a relevant result from this case study the finding that a simplistic model assuming reduced PDB reactivity is unable to predict both sol average molecular weight and radius of gyration and also sol and gel fraction. The influence of the synthesis conditions in the end-use properties of STY/DVB gel beads was extensively studied in the last decades (Kiatkamjornwong *et al*., 2001; Coutinho and Rabelo, 1992; Wieczorek *et al*., 1982; Wojaczyańska *et al*., 2005). Experimental studies concerning the effects of initiator concentration, temperature, stirring speed, concentration of crosslinking agent, diluents concentration, and thermodynamic affinity are reported in these works. The influence of these parameters in the gel beads appearance, namely concerning fusion and coalescence has also been studied (Kiatkamjornwong *et al.,* 2001).

The morphology of the products obtained in the present research was also studied using Scanning Electron Microscopy (SEM) as shown in Figure 2.77 where the micrographs of STY/DVB gel beads synthesized in different conditions (see Table 2.3) are presented. Comparison of Figures 2.77(a) and 2.77(b) puts into evidence the effect of the DVB content in bead formation. Higher DVB amounts seem to promote the formation of such structures, avoiding the synthesis of clustered and fused products (Kiatkamjornwong *et al*., 2001). The effect of the thermodynamic affinity of the diluent (Coutinho and Rabelo, 1992) with the copolymer can be observed by comparison of Figures 2.77(c) and 2.77(d) where runs with very different *n*-heptane/toluene ratios are analysed. Gel beads prepared with a large fraction of bad solvent in the diluent (*n*-heptane in the present work) show very rough surfaces as observed in Figure 2.77(d). When the thermodynamic affinity of the diluents increases (higher proportion of toluene) gel beads produced have a smoother surface, characteristic of non-porous materials, as observed in Figure 2.77(c). Other details of the morphology of such materials can be observed in Figures 2.77(e) and 2.77(f) where a cavity and a macroporous structures are showed by SEM.

Figure 2.78 depicts the measured swelling ratio for STY/DVB gel beads synthesized using different proportions of *n*-heptane/toluene in the organic phase and different initial mole fractions of DVB in the monomer mixture, as detailed in Table 2.3. Note that the amount of DVB in the initial mixture and the diluent composition plays an important role in this end-use property of the gel beads. With the materials synthesised with the present system, a maximum swelling ratio around 11 was measured for gel beads produced with $f_{DVB} = 10\,\%$ and $f_{HEP} = 0.5$. The dependency of the swelling ratio of STY/DVB gel beads on diluent, styrene

and DVB concentrations used in the synthesis process has also been previously reported in other research works (Kiatkamjornwong *et al.*, 2001).

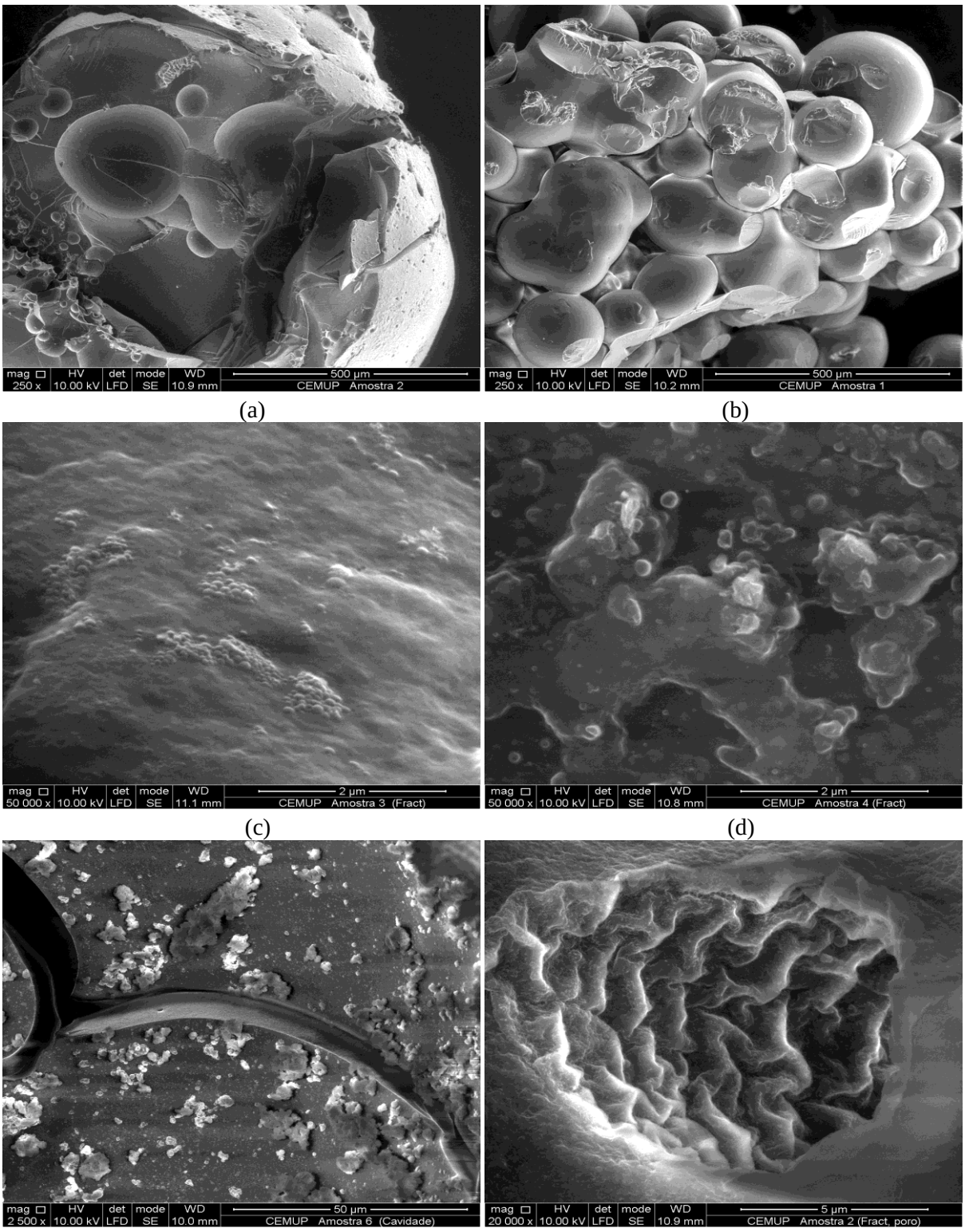

(a) (b)

(c) (d)

(e) (f)

Figure 2.77. (a) SEM of STY/DVB gel beds obtained in run 3 with magnification of 250 ×. (b) Gel beads for run 6 with magnification of 250 ×. (c) Run 1 with magnification of 50000 ×. (d) Run 5 with magnification of 50000 ×. (e) Run 2 with magnification of 2500 ×. (f) Run 3 with magnification of 20000 ×.

In-line FTIR-ATR monitoring of vinyl monomer polymerisation has been investigated in the last years driven by the need for improvement of product quality. The establishment of feed policies of monomers in semi-batch co-terpolymerisations, with an expected impact on the molecular architecture of linear polymers is such an application of *in-line* FTIR-ARTR monitoring. The determination of the reactivity ratios for different groups of vinyl monomers is also an important application of this technique.

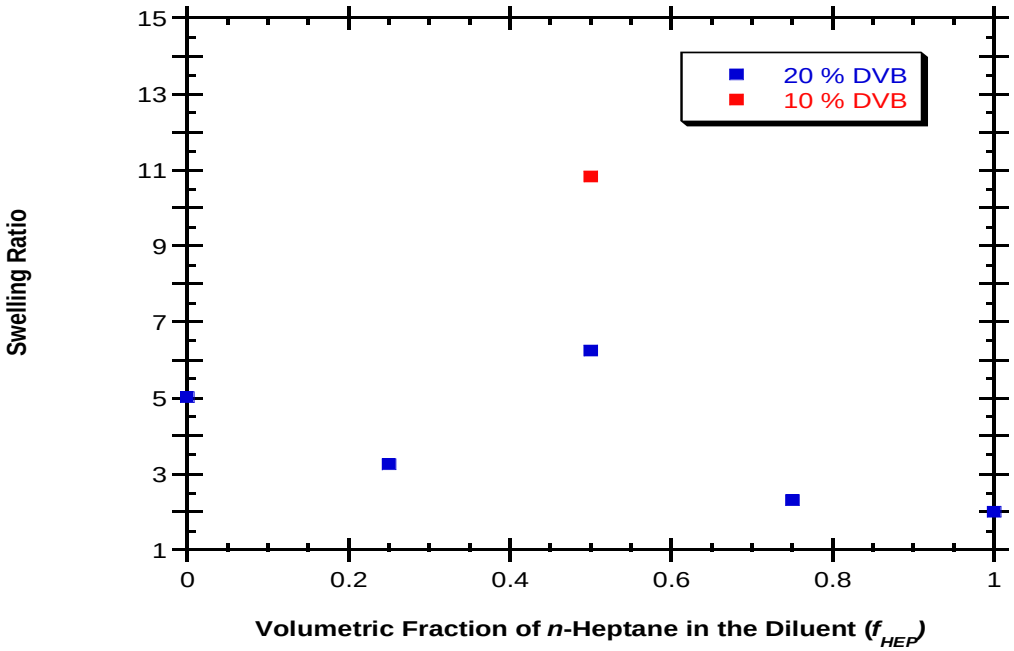

Figure 2.78. Measured swelling ratio for STY/DVB gel beads synthesized using different proportions of *n*-heptane/toluene.

Several works reporting the *in-line* FTIR-ATR of homo-, co-, terpolymerisations using different operational conditions, namely emulsion and solution processes, can be found in the literature (Chatzi *et al*., 1997; Storey *et al*., 1998; Hua and Dubé, 2001; Jovanović and Dubé, 2001 and 2003; Hua and Dubé, 2002; Ouzineb *et al*., 2003; Hua *et al*., 2004; Roberge and Dubé, 2007). Suspension crosslinking copolymerisations performed in the present chapter were also monitored by *in-line* FTIR-ATR, as previously described. Typical results obtained with that technique are presented in Figure 2.79. The goal with such *in-line* monitoring is to obtain real time information concerning the building process of the synthesised non-linear materials. The reactivity ratios of the involved vinyl monomers, divinyl monomers and PDBs are valuable information in such context, as above discussed. Results present in Figure 2.79 show the occurrence of a phenomenon similar to the "*catastrophic coagulation"* reported for

instance in the *in-line* monitoring of butyl acrylates/vinyl acetate emulsion copolymerisation (Jovanović and Dubé, 2003). With emulsion processes, this phenomenon is due to unstable polymerisation conditions which seem also to occur at the gel point for the suspension crosslinking polymerisation performed in the present chapter. For the operation conditions used in the present chapter, gelation occurs at low monomer conversion (around 10 % with $f_{DVB} = 10\,\%$ as estimated by SEC/RI/MALLS) and by consequence "*catastrophic coagulation"* precluded the obtainment by *in-line* FTIR-ATR of reliable quantitative information concerning the reactivity of the different monomers/pendant double bonds involved. Besides this clogging phenomenon, it is possible that the spectra observed with *in-line* FTIR-ATR can also be a result of coating of the ATR crystal during the polymerisations. Further experiments with different operating conditions (e.g changing the kind of stabilizer, its concentration and agitation speed) must be performed to elucidate this issue with suspension polymerisation. On other hand, *in-line* FTIR-ATR monitoring of emulsion polymerisation of vinyl monomers is reported is previous research works without apparent occurrence of coating of ATR crystal (Chatzi *et al*., 1997; Storey *et al*., 1998; Hua and Dubé, 2001; Jovanović and Dubé, 2001; Hua and Dubé, 2002; Ouzineb *et al*., 2003; Jovanović and Dubé, 2003).

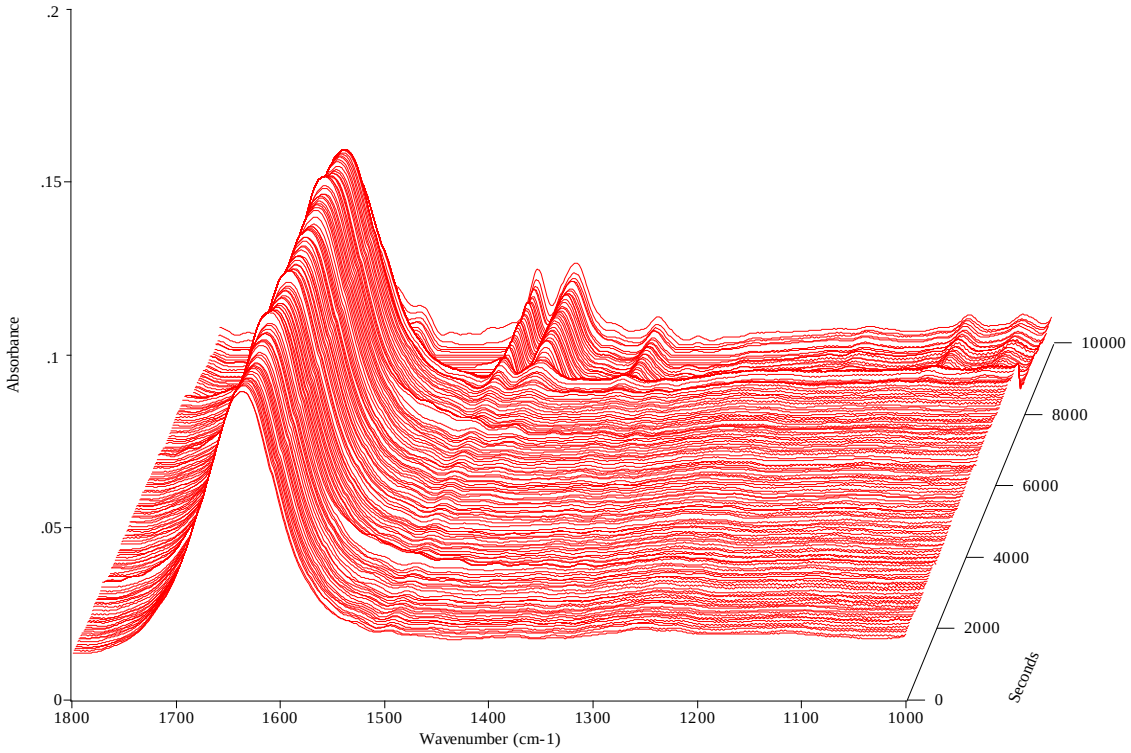

Figure 2.79. FTIR-ATR spectra observed in the *in-line* monitoring of the suspension copolymerisation of STY/DVB using *n*-heptane and toluene as diluents of the organic phase.

However, given its different initiation mechanism and likely occurrence of space separation of radicals, emulsion polymerisation is completely different from the suspension polymerisation operation here studied and major modelling changes would have to be discussed. Use of confocal Raman spectroscopy (with a higher penetration depth) should overcome the coating of ATR crystal in both circumstances (suspension/emulsion), but this requires major changes on the experimental set-up here used.

2.6 Conclusions

The conventional radical copolymerisation (FRP) of mono- and divinyl monomers has been experimentally studied in batch and semi-batch reactors using STY/DVB as model system. It was shown that the production of hyperbranched polymers with an improved control of molecular architecture can be carried out by adjusting the feed policy of the divinyl monomer (semi-batch operation). These results can be especially useful to obtain soluble branched polymers at higher conversions than with a batch operation.

Experimental results here presented concerning the semi-batch solution polymerisation of styrene and divinylbenzene showed the possibility of control of gelation through the design of appropriated feeding policies. Nevertheless, some shortcomings of this approach should be here stressed. Lack of reproducibility of the polymerisations was found during this research. This problem is probably a consequence of non-constant feeding rates due to the peristaltic pumps used. Note that even a small error in the feeding flow rates has a high effect on crosslinking process, especially when divinyl monomer is to be feed to the polymerisation mixture. In principle, this shortcoming can be avoided using higher precision pumps (e.g. syringe pumps/GPC pumps). Semi-batch STY/DVB here studied cannot also be extended to the production of polymer particles in a process similar to suspension polymerisation (process later on explored in this research).

Emulsion semi-batch polymerisation of vinyl/multivinyl monomers is an alternative to the production of these kinds of particles but much more complex mechanistic issues are expected in the framework of such heterogeneous processes. Inter-phase transport of both monomers (vinyl/multivinyl) and radical compartmentalization are some phenomenon leading to the need of development of a much more complex analysis when emulsion semi-batch crosslinking polymerisation is considered.

For the produced STY/DVB and MMA/EGDMA hyperbranched copolymers their molecular architecture was also assessed through the used SEC/RI/MALLS system. It was shown that a complicated interpretation of SEC chromatograms of branched polymers arises due to the possible change in the relation between molecular weight and elution time (or hydrodynamic radius), owing to the existence of copolymer chains with the same molecular weight but quite different molecular sizes (elution volumes).

Suspension copolymerisation of styrene/divinylbenzene with gel formation was also experimentally studied by performing a set of different runs in a batch reactor. The dynamics of product molecular properties was measured by SEC/RI/MALLS. These reactions were *in-line* monitored by FTIR-ATR. The produced gel beads were analysed by scanning electron microscopy (SEM) and the impact on the morphology of these materials of parameters such as the proportion of thermodynamically "bad/good" solvents in the diluent was studied. The dynamics of the gel fraction in batch reactor was followed and the swelling ratio of the resulting gel beads was also quantified. SEM characterization of these gel beads confirmed the formation of macroporous structures if appropriated synthesis conditions are used, namely concerning the thermodynamic affinity of the diluent mixture. In the present work, different proportions of *n*-heptane/toluene (bad/good solvents) were considered for this purpose. Measured swelling ratios of these gel beads are also in agreement with previous works and a maximum swelling ratio of 11 was here observed. *In-line* FTIR-ATR monitoring of the crosslinking process here performed has shown the occurrence of *"catastrophic coagulation"* at the gel point thus precluding the intended *in-line* measurement of the building parameters of the polymer networks. A new design of operating conditions should be carried out in order to avoid this phenomenon so that this spectroscopic technique can be fully exploited. Further experimental studies with more emphasis on describing cyclization effects should be undertaken in order to clarify these issues.

CHAPTER 3

ATOM TRANSFER RADICAL POLYMERISATION OF ACRYLATES

Abstract. This chapter reports experimental and modelling studies concerning the conventional (FRP) and atom transfer radical polymerisation (ATRP) of hyperbranched acrylates and methacrylates. A set of experiments was performed in solution polymerisation in a batch reactor using *n*-butyl acrylate, methyl acrylate and methyl methacrylate as monomers, 1,6- hexanediol diacrylate, bisphenol A ethoxylate diacrylate and ethylene glycol dimethacrylate as crosslinkers. Some variables have been changed and their effect is assessed along the experimental program:

- Parameters changed:
    - Polymerisation temperature.
    - Monomer dilution.
    - Kind/amount of crosslinker used.
    - ATRP mediation system.
- Products characterization in terms of:
    - Monomer conversion through GPC and gravimetry.
    - Molecular architecture of the products through SEC/RI/MALLS allowing the determination of average molecular weights, *z*-average radius of gyration and absolute molecular weight distribution.
    - *In-line* FTIR-ATR to observe polymer formation and quantitatively analyse the reactivity of PDB and the formation of intramolecular cyclizations.
- This experimental analysis is complemented with modelling studies including branching and crosslinking in the absence of cyclization.

This chapter is based on the following publications:

M.A.D. Gonçalves, R.C.S. Dias, M.R.P.F.N. Costa, *Macromol. Symp*. 289 (2010) 1-17.

M.A.D. Gonçalves, V.D. Pinto, R.C.S. Dias, M.R.P.F.N. Costa, *Macromol. Symp*. 296 (2010) 210-228.

M.A.D. Gonçalves, I.V.R Trigo, R.C.S. Dias, M.R.P.F.N. Costa, *Macromol. Symp*. 291-292 (2010) 239-250

M.A.D. Gonçalves, R.C.S. Dias, M.R.P.F.N. Costa, *Chem. Eng. Technol*. 33 (2010) 1797-1813

3.1 Introduction

Non-linear radical polymerisations are used to produce soluble and insoluble crosslinked materials with important applications in several domains, such as biomedicine, pharmaceutics, biotechnology, environment and microelectronics. Conventional free radical polymerisation (FRP) leads to microgels (very high molecular weight soluble non-linear polymers) and gels (insoluble materials) with inhomogeneous structures due to the combination of slow initiation, fast propagation and termination. Formation of loops due to intramolecular cyclization reactions is another mechanism with negative impact in the properties of FRP synthesized non-linear polymers (Matsumoto, 1995). Controlled radical polymerisation (CRP) has been recently exploited to increase the homogeneity and therefore to obtain products with higher performances in their end-use applications. The use of Atom Transfer Radical Polymerisation (ATRP) to obtain acrylate/diacrylate copolymers is an example of such efforts (Yu *et al*., 2007; Gao *et al.*, 2007 and 2008). In Figure 3.1 is depicted the ATRP main equilibrium reaction of a polymer radical from *n*-butyl acrylate mediated by CuBr using PMDETA or HMTETA as ligand.

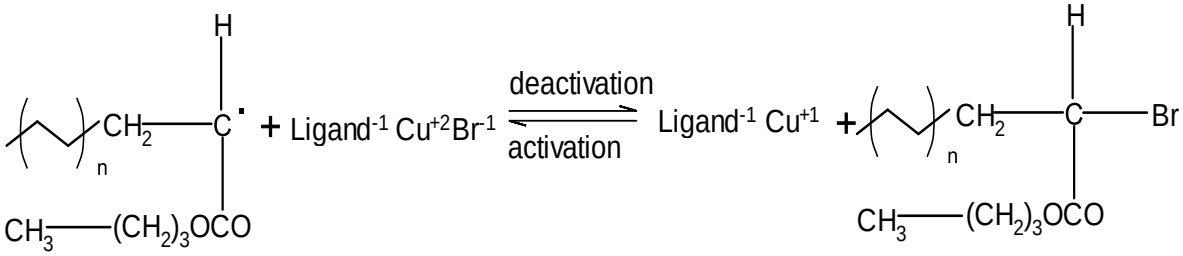

Figure 3.1. Schematic of an ATRP equilibrium reaction of a polymer radical from *n*-butyl acrylate.

Nowadays, there are still some important open issues in this field, namely concerning the impact of intramolecular cyclizations/unequal functional group reactivity in the structure of these materials. The design of new operation conditions to manipulate the molecular architecture (e.g. operation in semi-batch reactor (Gonçalves *et al*., 2007)) or the control of gelation and/or post gel properties are other important aspects concerning the polymer reaction engineering of these kinds of polymerisation systems.

This work reports experimental and theoretical studies concerning the FRP and ATRP production of acrylate/diacrylate microgels. Some important features of the molecular architecture of these materials are investigated and differences between the two kinds of polymerisation systems are studied. The impact of the synthesis conditions on the structure of the products is assessed in order to develop tools for the design of materials with improved end use properties. Hyperbranched polyacrylates (only soluble polymers will be here

discussed) were synthesized in a laboratory batch reactor and the products were characterized by size exclusion chromatography with detection of refractive index and multi-angle laser light scattering (SEC/RI/MALLS) signals. Chemical properties describing the molecular architecture of these materials were measured, namely molecular weights and *z*-average radius of gyration. The influence of the synthesis technique (ATRP *versus* FRP) on the structure of these materials was also investigated. The FTIR-ATR *in-line* monitoring of these non-linear copolymerisations was also performed in order to assess the ability of this technique to provide information about specific features of the formation mechanisms and structure of hyperbranched polyacrylates (e.g. reactivity of pendent double bonds and cyclizations). FTIR-ATR *in-line* monitoring also has an important potential use for the specification of feed programs with semi-batch reactors which have impact on the molecular architecture of the produced hyperbranched polymers, as recently shown for the system styrene/divinylbenzene (Gonçalves *et al*., 2007).

3.2 Experimental Details

3.2.1 Materials

In ATRP experiments of acrylates/diacrylates and MMA/EGDMA, *N*,*N*-dimethylformamide (DMF) of 99.8 % purity, ethyl 2-bromopropionate (EBrP) of 99 % purity, Cu(I)Br of 98 % purity, *N,N,N′,N″,N″*-pentamethyldiethylenetriamine (PMDETA) of 99 % purity, *n*-butyl acrylate (*n*BuA) of 99 % purity stabilized with 10 to 55 ppm monomethyl ether hydroquinone (MEHQ), methyl acrylate (MA) of 99 % purity stabilized with 100 ppm MEHQ, 1,6-Hexanediol diacrylate (HDDA) of 80 % purity stabilized with 100 ppm MEHQ, bisphenol A ethoxylate diacrylate (BEDA) with $\bar{M}_n = 688$ and 99 % purity stabilized with 250 ppm MEHQ, anisole of 99 % purity, methyl α-bromophenylacetate (MBPA) of 97 % purity, 1,1,4,7,10,10-hexamethyltriethylenetetramine (HMTETA) of 97 % purity methyl methacrylate of 99 % purity stabilized with 10 to 100 ppm monomethyl ether hydroquinone and ethylene glycol dimethacrylate (EGDMA) of 98 % purity stabilized with 100 ppm monomethyl ether hydroquinone were purchased from Sigma Aldrich and used as received. In FRP experiments the same monomers and crosslinkers were used and AIBN of 98 % purity and toluene of 99.7 % purity were also purchased from Sigma Aldrich and used as received. Monomers were used as received to mimic the industrial practice, and the presence of inhibition/retardation of polymerisation is taken into account in kinetic modelling.

3.2.2 Polymerisation Set-up

All experiments were carried out using the experimental set-up described in chapter 2.

In ATRP experiments with acrylates/diacrylates (see Table 3.1), DMF, acrylate monomer, diacrylate monomer, PMDETA and CuBr were premixed at 60 °C for at least 30 min in a volumetric flask. Good solubility of CuBr in the polymerisation system was observed. That mixture was afterwards charged to the reactor, which had previously been purged with argon at a flow rate 40 cm^3/min, and brought up to the polymerisation temperature (60 °C). When the temperature set-point was attained, the bubbling process was maintained for one hour before initiation (as well as for the whole polymerisation). Then, the initiator (EBrP) was added to the system defining $t = 0$. At prescribed polymerisation times, samples of polymer were withdrawn from the reactor and analysed by SEC/RI/MALLS. In these set of experiments the monomer concentration is expressed in mol/dm^3. Similar procedures were performed in FRP experiments (see Table 3.2) with exception of the pre-mixing period which is absent. In these experiments the monomer and initiator concentrations are expressed in mol/dm^3.

Table 3.1. Description of a set of experiments performed in the study of the ATRP copolymerisation of acrylate/diacrylate monomers at 60 °C.

Run	M	$[M]_0$(mol/L)	CL	$\mathbf{y_C}$(%)	M/EBrP/CuBr/PMDETA	V_M(%)
1	MA	2.44		0	50/1/0.45/0.5	22
2	*n*BuA	2.44		0	50/1/0.45/0.5	35
3	*n*BuA	2.41	HDDA	2	50/1/0.45/0.5	35
4	*n*BuA	2.28	HDDA	10	50/1/0.45/0.5	35
5	*n*BuA	2.18	HDDA	16.8	50/1/0.45/0.5	35
6	*n*BuA	2.24	BEDA	5	50/1/0.45/0.5	35
7	*n*BuA	1.64	BEDA	5	50/1/0.45/0.5	25
8	*n*BuA	1.04	BEDA	5	50/1/0.45/0.5	15
9	*n*BuA	2.26	BEDA	5	200/1/0.45/0.5	35

In ATRP experiments (see Table 3.3) with MMA/EGDMA, the solvents, monomers, CuBr and HMTETA were premixed at 60 °C for at least 30 min in a volumetric flask. Solubility problems with copper specie were avoided by using anisole (Xia and Matyjaszewski, 1997) plus DMF (only a small amount is needed) as a co-solvent (Pascual *et al*., 1999). That mixture was afterwards charged to the reactor, which had previously been purged with argon at a flow

rate of 40 ml/min, and brought up to the desired temperature. This heating period is at most 80 min for runs between 60 and 90 °C. When the temperature set-point was attained, the bubbling process was maintained for one hour before initiation, as well as for the whole polymerisation. Then, the initiator (MBPA) was added to the system defining *t*=0. The polymerisations were carried out in solution of anisole + DMF with MMA/(anisole + DMF)= 1/1(v/v), and % DMF is the volume fraction of DMF in the solvent. In all of the three sets of experiments y_C is the mole fraction of diacrylate in the monomers mixture $=\frac{[CL]}{[CL]+[M]}$ and V_M represents the volume fraction of acrylate monomer in the solution.

Table 3.2. Description of a set of experiments performed in the study of the FRP copolymerisation of acrylate/diacrylate monomers at 60 °C.

Run	M	$[M]_0$ (mol/L)	CL	y_C(%)	$[I]_0$(mol/L)	V_M(%)
1	*n*BuA	1.05		0	2.75×10^{-3}	15
2	*n*BuA	1.05		0.02	2.75×10^{-3}	15
3	*n*BuA	1.05	HDDA	0.5	2.76×10^{-3}	15
4	*n*BuA	1.04	HDDA	2.1	2.74×10^{-3}	15
5	*n*BuA	1.04	HDDA	4.1	2.75×10^{-3}	15
6	*n*BuA	2.44		0.0	2.74×10^{-3}	35
7	*n*BuA	2.43	HDDA	0.5	2.73×10^{-3}	35
8	*n*BuA	2.41	HDDA	2	2.71×10^{-3}	35

Table 3.3. Description of the set of experiments performed in the study of the ATRP of MMA/EGDMA.

Run	*T* (°C)	$[MMA]_0$	$[CL]_0$	$[I]_0$	y_C(%)	DMF (%)
1	90	4.610	0	9.193×10^{-3}	0	2
2	80	4.656	0	9.337×10^{-3}	0	7
3	70	4.656	0	9.335×10^{-3}	0	7
4	90	4.545	2.304×10^{-2}	9.113×10^{-3}	0.5	4
5	80	4.635	2.360×10^{-2}	9.301×10^{-3}	0.5	7
6	70	4.635	2.356×10^{-2}	9.281×10^{-3}	0.5	7
7	90	4.555	1.153×10^{-2}	9.142×10^{-3}	0.25	4
8	90	4.558	0.843×10^{-2}	9.122×10^{-3}	0.18	4
9	90	4.561	0.470×10^{-2}	8.945×10^{-3}	0.1	4

Concentrations are expressed in mol/dm^3 and the ratio between MBPA/CuBr/HMTETA was 1/1/1 in all runs.

3.2.3. Gravimetric Measurements

The gravimetric procedure here used was the same as described in chapter 2.

3.2.4 SEC/RI/MALLS Products Analysis

Molecular weights and average molecular radius of gyration were measured in THF with a Polymer Laboratories PL-GPC-50 integrated SEC system with a differential refractometer working at 950 ± 30 nm attached to a Wyatt Technology DAWN8^{+}HELEOS 658 nm Multi Angle Laser Light Scattering (MALLS) detector. The polymer samples were fractioned by molecular size using a train of 3 GPC columns PL gel (300×7.5 mm) with nominal particle size 10 μm and pore type MIXED-B-LS, maintained at constant temperature of 30 °C and using THF as the eluent at 1 mL/min flow rate.

3.2.5 Refractive Index Increment Measurement

A Wyatt Technology OPTILAB DSP 633 nm interferometric refractometer was used to measure the refractive index increment (*dn*/*dc*) for the polymers, solvents and monomers in THF, required for analysing the MALLS results and for estimating the conversion from the values of the differential refractometer (RI) peak areas of monomers and polymer in the chromatographic traces of the SEC analysis. In Table 3.4 are presented the *dn*/*dc* values for monomers, polymers and solvents obtained with THF as eluent using the procedure described in appendix A.

Table 3.4. List of measured values of *dn/dc* for monomers, polymers and solvents.

Compound	*dn/dc* (cm^3/g)
Poly(butyl acrylate)	0.0634
Poly(methyl methacrylate)	0.0830
Anisole	0.0958
Dimethylformamide	0.0281
Methyl methacrylate	0.0077
Ethylene glycol dimethacrylate	0.0475
HDDA	0.0592
BEDA	0.1110
Methyl acrylate	-0.0059
n-butyl acrylate	0.0131

3.2.6 *In-line* FTIR-ATR Monitoring

An Axiom Analytical Attenuated Total Reflection (ATR) immersion probe, model DRR207, with ZnSe element, spectral cut-off at $600\,cm^{-1}$, maximum pressure and temperature operation 60 bar and 280 °C, was used to carry out the *in-line* monitoring of the polymerisation reactions. A three arms light guide connects the immersion probe to an ABB Bomem Fourier Transform Infra-Red (FTIR) spectrophotometer, model FTLA2000-104. The spectrophotometer is equipped with an ABB Bomem, Mercury-Cadmium Telluride (MCT) detector (model D10B) which is cooled with liquid nitrogen. The optical system is continuously flushed with argon. Most of ATR-FTIR measurements were performed using the spectrum of air taken at room temperature as the reference background. The use of backgrounds other than air was also tested in this work. The spectra were taken over the full MIR range from $600\,cm^{-1}$ to $4000\,cm^{-1}$ with resolution of $4\,cm^{-1}$. Each spectrum was calculated from 64 or 128 interferograms.

3.3 Kinetic Modelling

3.3.1 ATRP of *n*BuA/Diacrylates

3.3.1.1 Chemical Species and Chemical Reactions

In modelling studies of ATRP with *n*BuA/diacrylate a kinetic scheme involving a total of 40 different chemical groups is considered: 9 different kinds of growing polymer radicals, 9 different kinds of dormant polymer radicals, 5 different kinds of macromonomers, namely, pendant double bonds (from diacrylate monomer), terminal double bonds (from termination by disproportionation and chain transfer to monomer) and H and CH_3 chain transfer to polymer centres. In Tables 3.5-3.7 is presented the set of chemical groups considered in the mathematical modelling of the ATRP of acrylate/diacrylate monomers performed in the framework of the general kinetic analysis of non-linear irreversible polymerisations previously developed (Costa and Dias, 1994, 2003, 2005, 2006 and 2007; Dias and Costa, 2003, 2005a, 2005b, 2006 and 2007). Nine different kinds of growing radicals are considered (R_1 to R_9) and the correspondent nine different kinds of dormant radicals (D_1 to D_9) are also distinguished due to the ATRP dynamic equilibrium of activation/deactivation. Seven kinds of monomers (M_1 to M_7) are considered: two real monomers (acrylate/diacrylate monomers) and five macromonomers correspondent to pendent double bonds, two kinds of terminal double bonds and also two kinds of intermolecular chain transfer to polymer centres. All these

chemical groups (except M_1 and M_2) are reactive and belong to polymer chains. The most general situation with these groups having different reactivities is here considered.

The groups M_1, M_2, RX, CM, R, T, R_{11} and D_{11} are also reactive but do not belong to polymer chains. Other species such as the deactivator (CX) and different kinds of primary active/dormant radicals (R, R_{11} and D_{11}) are formed/consumed during the polymerisation.

Table 3.5. Description of the active groups belonging to the polymer chains considered in the modelling studies of the ATRP copolymerisation of *n*BuA/diacrylates monomers.

Group description	Alias
Growing radical from acrylate monomer	R_1
Growing radical from diacrylate monomer	R_2
Growing radical from PDB	R_3
Growing radical from TDBM	R_4
Growing radical from TDBD	R_5
Growing radical from HTP	R_6
Growing radical from CTP	R_7
Growing radical from transfer to acrylate monomer (TAM) reaction	Y_1, R_8
Growing radical from transfer to diacrylate monomer (TDM) reaction	Y_2, R_9
Dormant radical from acrylate monomer	D_1
Dormant radical from diacrylate monomer	D_2
Dormant radical from PDB	D_3
Dormant radical from TBDM	D_4
Dormant radical from TDBD	D_5
Dormant radical from HTP	D_6
Dormant radical from CTP	D_7
Dormant radical from transfer to acrylate monomer (TAM) reaction	DY_1, D_8
Dormant radical from transfer to diacrylate monomer (TDM) reaction	DY_2, D_9
Pendant double bond	M_3
Terminal double bond from transfer to acrylate monomer (TDBM)	M_4
Terminal double bond from transfer to diacrylate monomer (TDBM)	M_5
H transfer to polymer centre (HTP)	M_6
CH_3 transfer to polymer centre (CTP)	M_7

Groups that belong to polymer chains but are inactive: U_1, U_2, F_1, F_2, CS, BS, SG and IDB are presented in Table 3.7. These chemical groups are needed for the calculation of structural

properties of the polymer such as MWD, radius of gyration or crosslinking/branching densities.

In equations (3.1) to (3.14) is presented the kinetic scheme considered for ATRP *n*BuA/diacrylate modelling studies. These modelling studies were performed by considering a kinetic scheme with 196 different chemical reactions which comprises the following main classes: 2 reactions of reversible activation/deactivation of initiator, 20 initiations, 35 propagations of different kinds of macromonomers, 14 intermolecular chain transfers to polymer, 21 chain transfers to monomers and solvent, 84 terminations by combination and disproportionation, 20 reversible activation/deactivation radicals.

Table 3.6. Description of the active groups not belonging to the polymer chains considered in the modelling studies of the ATRP copolymerisation of *n*BuA/diacrylates monomers.

Group description	Alias
Acrylate monomer	M_1
Diacrylate monomer	M_2
Initiator	RX (D_{10})
Transition metal/ligand complex	CM
Deactivator	CX
Radical from initiator	R (R_{10})
Solvent	T
Primary radical from solvent	Y_3, R_{11}
Dormant primary radical from solvent	DY_3, D_{11}

Table 3.7. Description of the inactive groups considered in the modelling studies of the ATRP copolymerisation of *n*BuA/diacrylates monomers.

Group description	Alias
Polymerised acrylate monomer unit	U_1
Polymerised diacrylate monomer unit	U_2
Fragments from initiator and solvent	F_1,F_2
Crosslinking site	CS
Branching site	BS
Non-reactive saturated group	SG
Internal double bond	IDB

In these equations, RX represents the ATRP initiator, COM the complex transition metal/ligand and CX the correspondent oxidized form. For the present polymerisation system,

RX represents the EBrP initiator and COM the complex CuBr/PMDETA. Bromine ligands are transferred in the ATRP mechanism. The primary radicals generated by the initiator decomposition are represented by R, as described by Eq. (3.1). In batch operation, this copolymerisation starts with *n*BuA monomer (M_1), diacrylate monomer (M_2), solvent (T), initiator and transition metal/ligand present in the reactor. Three kinds of chain growth sites in polymer molecules are included in this study, i.e., pendant double bonds (M_3), terminal double bonds created by chain transfer to monomer reactions (M_4) and terminal double bonds originating from termination by disproportionation (M_5). These monomers and macromonomers containing the above double bonds are initiated by primary radicals of the initiator as described by Eq. (3.2). Various kinetic steps were condensed into a single equation through the use of Krönecker symbols, i.e., $\delta_{1,2}^{k} = 1$ if $k = 1$ or $k = 2$ and $\delta_{1,2}^{k} = 0$ otherwise, $\delta_{2}^{k} = 1$ if $k = 2$ and $\delta_{2}^{k} = 0$ otherwise. In the same way, $\delta_{[1-5]}^{k} = 1$ if $k \in [1-5]$ and $\delta_{[1-5]}^{k} = 0$ otherwise. The polymerisation of each kind of monomer (M_i) generates also a different kind of growing radical (R_i). Therefore, the model can accommodate different reactivities of the several different polymer radicals. in Eq. (3.2), F_1 represents the inactive fragment that is introduced in the polymer chains by the initiator radicals and U_1, U_2 the repeating units stemming from vinyl and divinyl monomers, respectively. Pendant double bonds (M_3) are created due to initiation and propagation of the diacrylate monomer (M_2).

Besides primary radicals produced from the initiator, three other kinds of such radicals exist due to chain transfer to monomers and chain transfer to solvent reactions (see Eqs. (3.10-3.12)). These kinds of primary radicals are named Y_i with i = 1,…,3. Initiation of monomers and macromonomers by these primary radicals is depicted by Eq. (3.3) with F_2 representing the inactive fragment that is introduced in the polymer chains by the solvent radicals.

Propagation of monomers/macromonomers, PDB and TDB with the correspondent set of growing radicals is described by Eq. (3.4). Propagation of PDB generates crosslinking sites (CS) in the polymer structure and propagation of TDB leads to the formation of branching sites (BS) in the molecular architecture of the chains. Crosslinking sites are tetra-functional, i.e., growing in 4 directions, whereas branching sites are three-functional, i.e., chains with 3 distinct directions. In order to take into account intermolecular chain transfer to polymer mechanisms, the characteristic of acrylates, methane groups (-CH(R)-) and methyl groups ($-CH_3$), which are the potential chain transfer to polymer centres (through H-atom abstraction), are also distinguished in the present analysis. These groups are generically named M_6 and M_7, respectively. Propagation of all kind of monomers and macromonomers leads to the formation

of (-CH(R)-) groups (HTP) while (-CH_3) groups (CTP) are introduced in the polymer chains only via the propagation of *n*BuA. Radicals derived from HTP and CTP are also distinguished due to their expected different reactivity and named R_6 and R7, respectively. These radicals can also undergo propagation reactions with monomers/macromonomers as depicted in Eq. (3.5). The main distinctive features of ATRP compared to conventional radical polymerisation are due to activation (R_i)/deactivation(D_i) equilibrium of all kinds of polymer radicals described by Eq. (3.6). The same activation/deactivation equilibrium is considered to hold for the primary radicals, as described by Eq. (3.7). Although they transport polymer structures such as terminal double bonds or polymerisation repeating units, radicals derived by chain transfer to monomers are here named primary radicals due to their small size.

The formation of three-dimensional branched architectures (BS) is possible due to reactions consisting of the intermolecular chain transfer to polymers involving the 7 different kinds of polymer radicals and the 2 kinds of chain transfer to polymer sites (HTP and CTP), as represented in Eqs. (3.8) and (3.9). Saturated chains ends (SG) are formed when monomer/macromonomer derived growing radicals are involved and HTP and CTP are reformed with the correspondent growing radicals undergo such process.

Chain transfer to monomers and chain transfer to solvent reactions are described by Eqs. (3.10-3.12). Besides the formation of the aforementioned kinds of primary radicals, saturation of chain ends (SG) results when monomer/macromonomers polymer radicals are involved while reformation of HTP and CTP is expected when R_6 and R_7 undergo chain transfer. Terminal double bonds (M_4) are formed in mechanism involving chain transfer to monomers.

Termination by combination reactions described by Eq. (3.13) promotes the formation of HTP centres when monomer/macromonomers polymer radicals are involved or else they merely connect 2 polymer molecules. Termination by disproportionation, depicted by Eq. (3.14), leads to the saturation (SG) or the formation of HTP/CTP centres in one chain end. Conversely, in the other chain end, reactive terminal double bonds (M_5) or non-reactive internal double bonds (IDB) are formed.

Reversible activation/deactivation of initiator:

$$RX + CM \underset{k_{da}}{\overset{k_a}{\rightleftharpoons}} R + CX \tag{3.1}$$

Initiation of monomers, PDBs and TDBs by primary radicals of initiator:

$$R + M_k \xrightarrow{k_{IRk}} R_k + U_k\delta_{1,2}^k + F_1 + M_{k+1}\delta_2^k \quad k = 1, \dots, 5 \tag{3.2}$$

Initiation of monomers, PDBs and TDBs by primary radicals derived by transfer to monomers and to solvent:

$$Y_j + M_k \xrightarrow{k_{IPjk}} R_k + U_k\delta_{1,2}^k + F_2\delta_3^j + M_{k+1}\delta_2^k \quad k = 1, \dots, 5;\ j = 1, \dots, 3 \tag{3.3}$$

Propagations involving growing radicals of monomers, PDBs and TDBs:

$$\mathrm{R}_j + M_k \xrightarrow{k_{pjk}} R_k + U_k\delta_{1,2}^k + M_6 + M_7\delta_1^k + M_{k+1}\delta_2^k + CS\delta_3^k + BS\delta_{4,5}^k \quad k = 1, \dots, 5;\ j = 1, \dots, 5 \tag{3.4}$$

Propagations involving radicals of HTP and CTP:

$$\mathrm{R}_j + M_k \xrightarrow{k_{pjk}} R_k + U_k\delta_{1,2}^k + M_7\delta_1^k + M_{k+1}\delta_2^k + CS\delta_3^k + BS\delta_{4,5}^k \quad k = 1, \dots, 5\ ;\ j = 6, 7 \tag{3.5}$$

Reversible activation/deactivation of growing radicals:

$$D_k + CM \underset{k_{dak}}{\overset{k_{ak}}{\rightleftharpoons}} R_k + CX \quad k = 1, \dots, 7 \tag{3.6}$$

Reversible activation/deactivation of primary radicals:

$$DY_j + CM \underset{k_{dPj}}{\overset{k_{aPj}}{\rightleftharpoons}} Y_j + CX \quad j = 1, \dots, 3 \tag{3.7}$$

Chain transfer to HTP polymer centre:

$$\mathrm{R}_k + M_6 \xrightarrow{k_{fPHk}} R_6 + SG\delta_{[1-5]}^k + M_k\delta_{6,7}^k + BS \quad k = 1, \dots, 7 \tag{3.8}$$

Chain transfer to CTP polymer centre:

$$\mathrm{R}_k + M_7 \xrightarrow{k_{fPCk}} R_7 + SG\delta_{[1-5]}^k + M_k\delta_{6,7}^k + BS \quad k = 1, \dots, 7 \tag{3.9}$$

Chain transfer to an acrylate monomer:

$$\mathrm{R}_k + M_1 \xrightarrow{k_{fMk1}} Y_1 + SG\delta_{[1-5]}^k + M_k\delta_{6,7}^k + M_4 + U_1 \quad k = 1, \dots, 7 \tag{3.10}$$

Chain transfer to a diacrylate monomer:

$$\mathrm{R}_k + M_2 \xrightarrow{k_{fMk2}} Y_2 + SG\delta^k_{[1-5]} + M_k\delta^k_{6,7} + 2M_4 + U_2 \qquad k = 1,\dots,7 \tag{3.11}$$

Chain transfer to solvent:

$$\mathrm{R}_k + T \xrightarrow{k_{fTk}} Y_3 + SG\delta^k_{[1-5]} + M_k\delta^k_{6,7} \qquad k = 1,\dots,7 \tag{3.12}$$

Termination by combination:

$$R_i + R_j \xrightarrow{k_{tdij}} \delta^i_{[1-5]}M_6 + \delta^j_{[1-5]}M_6 \qquad i = 1,\dots,7;\ j = i,\dots,7 \tag{3.13}$$

Termination by disproportionation:

$$\begin{matrix} R_i+R_j \xrightarrow{\frac{k_{tdij}}{2}} SG\delta^i_{[1-5]}+M_i\delta^i_{[1-5]}+M_5\delta^j_{1,2}+IDB\delta^j_{[3-7]} \\ R_i+R_j \xrightarrow{\frac{k_{tdij}}{2}} M_5\delta^i_{1,2}+M_j\delta^j_{6,7}+IDB\delta^j_{[3-7]}SG\delta^j_{[1-5]} \end{matrix} \quad i = 1,\dots,7;\ \ j = i,\dots,7 \tag{3.14}$$

Modelling studies of FRP and ATRP acrylate/diacrylate were carried out considering basic sets of rate coefficients collected from previous works (see also Table 3.8)), namely for initiator thermal decomposition (Moad and Solomon, 2006), *n*BuA propagation (Asúa *et al*., 2004), chain transfer to monomer (Maeder and Gilbert, 1998), chain transfer to solvent (Moad and Solomon, 2006; McKenna *et al.*, 1999), intramolecular chain transfer to polymer (Brandrup *et al*., 1999), termination (McKenna *et al.*, 1999; Fernández-Garcia *et al*., 2004). Rate coefficients for reversible kinetic steps of ATRP, namely, radical activation, radical deactivation or equilibrium constant activation/deactivation, measured/estimated in previous works (Tang and Matyjaszewsky, 2007; Matyjaszewski *et al*., 2001; Tang *et al*., 2006), were also here considered. Sensitivity analysis of the branching and crosslinking processes to kinetic parameters was performed by considering perturbations of the rate coefficients governing different reaction steps, namely: propagation of pendent double bonds, propagation of the different kinds of terminal double bonds, intermolecular chain transfer to different polymer centres, reactivity of the different kinds of polymer radicals and probabilities of radical termination by combination/disproportionation. Under the experimental conditions here used, simulation results show a particular sensitivity to the reactivity of pendent double bonds of diacrylate monomer and therefore only this parameter was used in the fitting of experimental results, as discussed below.

Table 3.8. Basic set of rate coefficients considered in the modelling studies of the FRP and ATRP copolymerisation of acrylate/diacrylate monomers.

Kinetic Step	Rate Coefficient Expression [a)]
Initiator thermal decomposition	$k_d = 4.31 \times 10^{15} \exp(-131.7 \times 10^3/RT)$ $(s^{-1}), f = 0.6$
*n*BuA propagation	$k_p = 2.21 \times 10^7 \exp(-17.9 \times 10^3/RT)$
Initiation by primary radicals [b)]	$k_I = k_p$
Chain transfer to monomer	$k_{fM} = 2.9 \times 10^5 \exp(-32.6 \times 10^3/RT)$
Chain transfer to solvent	$C_T = \frac{k_{fT}}{k_p} = 2.7 \times 10^{-4}$
Intermolecular chain transfer to polymer	$10^{-5} < C_P = \frac{k_{fP}}{k_p} < 10^{-3}$
Radical termination	$\frac{k_p}{\sqrt{k_t}} = 0.15 + 0.4[M]$
Combination/disproportionation	$\alpha_{td} = \frac{k_{td}}{k_t} = 0.05, \alpha_{tc} = \frac{k_{tc}}{k_t} = 0.95$
ATRP equilibrium constant	$K_{ATRP} = \frac{k_a}{k_{da}} = 3.27 \times 10^{-8}$
Radical deactivation	$k_{da} = 6.1 \times 10^6$
Propagation of terminal double bonds [b)]	$0.01 \leq C_{TDB} = \frac{k_p^{**}}{k_p} \leq 1$
Propagation of pendent double bonds [b)]	$0.01 \leq C_{PDB} = \frac{k_p^{*}}{k_p} \leq 1$

[a)] Kinetic parameters expressed in $dm^3\ mol^{-1}s^{-1}$, unless otherwise stated.
R= 8.314 $Jmol^{-1}K^{-1}$.
[b)] This work.

Intramolecular chain transfer to polymer (backbiting) is also an important source of short chain branching (SCB) in acrylates polymerisation. It has been studied in several recent works, namely by Nikitin, Hutchinson and co-workers (Nikitin and Hutchinson, 2005 and 2006; Nikitin *et al.*, 2009) aiming to obtain kinetic data and theoretical models of this phenomenon (Plessis *et al.*, 2000a; Nikitin *et al.*, 2007; Wang and Hutchinson, 2008; Willemse *et al.*, 2005; Barner-Kowollik *et al.*, 2008, Buback *et al.*, 2008a). This mechanism involves the formation of a mid-chain radical due to the intramolecular abstraction of an H-atom from a neighbour methine group.

Additional propagation of this radical leads to the occurrence of SCB in the main polymer chain. These mid-chain radicals can also undergo β-scission reactions which either reform terminal radicals belonging to short polymer chains or generate terminal double bonds later

producing LCB. Propagation, termination and chain transfer reactions involving these species were theoretically and experimentally analysed and evidence for branching in *n*BuA polymerisation up to high conversions, due to intramolecular chain transfer to polymer, were thus obtained (Nikitin *et al*., 2009). Nowadays it is consensual in the scientific community that mid-chain radicals formed in acrylates polymerisation strongly differ from terminal radicals, namely due to their slow propagation rate. A more complex kinetics is therefore expected with polymerisation conditions where these effects are dominant. Branching mechanisms (intramolecular/intermolecular) in acrylates polymerisation should be especially important at high temperatures (e.g. in the range 75 to 100 °C) and at high polymer concentration (e.g. emulsion/suspension polymerisation at high monomer conversion) leading eventually to gelation (Plessis *et al*., 2000b; González *et al*., 2006). Simulations here performed, considering the experimentally used polymerisation conditions show that the contribution of intermolecular chain transfer to polymer to the formation of non-linear connections is negligible as compared with the main crosslinking process. Therefore, it is plausible that intramolecular chain transfer to polymer can be neglected under the experimental conditions (rather low temperature) considered in the present research and thus this mechanism was not included in the modelling studies.

Past experimental/theoretical works using the same simulation method (Gonçalves *et al*., 2007; Trigo *et al*., 2008) considered the effect of inhibition/retardation reactions in FRP and CRP polymerisation process. Kinetic models accounting for the presence of an inhibitor and/or a retarder in the polymerisation system were developed and it was concluded that, for those experimental conditions, the effect of inhibition on average molecular weights should only be noticeable above around 500 ppm. Results thus obtained showed that this possible issue was avoided with the monomers and experimental set-up used. Transient behaviour studies (before and after AIBN addition) due to thermal initiation of acrylates concerning the importance of the induction period were obtained with the present chemical system. Note that the high proportion initiator/monomer used (namely in ATRP experiments) and relatively low polymerisation temperature makes this issue negligible. However, this issue is relevant in the case of FRP and NMRP of styrene at high temperatures (130 °C) as we will see in chapter 4.

3.3.2 ATRP of MMA/EGDMA

3.3.2.1 Chemical Species and Chemical Reactions

In the ATRP of MMA/EGDMA modelling studies are used 22 chemical groups. 15 active species and 7 non-active groups are taking into account in order to refine the description of the non-linear copolymer structure in the present analysis.

The equations (3.15) to (3.23) describe the kinetic scheme considered in the ATRP of MMA/EGMA comprising a total of 44 chemical reactions. Once more, each reversible process contributes two different elementary steps. In these equations, M_1 and M_2 represent the two monomers (MMA and EGDMA), RX the initiator (MBPA), R the radical from the initiator, CX the deactivator ($CuBr_2$/HMTETA) and CM the complex transition metal/ligand (CuBr/HMTETA). On the other hand, T represents the solvent and RT the radical from the solvent. In this instance, only one macromonomer is considered, which corresponds to the PDB resulting from EGDMA initiation/propagation (M_3). Three different growing radicals (R_k) resulting from the polymerisation of monomers/macromonomers are distinguished and the correspondent deactivated chain ends are named D_k. therefore this are the 15 active species presents in this system. The seven inactive species included in the present analysis are MMA and EGDMA repeating units (U_1 and U_2, respectively), crosslinking sites resulting from the polymerisation of PDB (CS), polymerized fragments from initiator and solvent (F_1 and F_2, respectively), saturated terminal units (SG) and head-head units from termination by combination reactions (HHU). In this set of 44 chemical reactions depicted in Eqs. (3.15-3.23), the following main classes are present: 2 reactions of activation/deactivation of initiator, 6 of initiations, 9 propagations, 6 activation/deactivation of polymer radicals, 9 chain transfers and 12 terminations.

Reversible activation/deactivation of initiator:

$$RX + CM \underset{k_{da}}{\overset{k_a}{\rightleftharpoons}} R + CX \tag{3.15}$$

Initiation of monomers and PDBs by primary radicals of initiator:

$$R + M_k \xrightarrow{k_{IRk}} R_k + U_k\delta_{1,2}^k + F_1 + M_{k+1}\delta_2^k \quad k = 1, \dots, 3 \tag{3.16}$$

Initiation of monomers and PDBs by primary radicals of solvent:

$$RT + M_k \xrightarrow{k_{ITk}} R_k + U_k\delta_{1,2}^k + F_2 + M_{k+1}\delta_2^k \quad k = 1,\dots,3 \tag{3.17}$$

Propagations involving growing radicals of monomers and PDBs:

$$\mathrm{R}_j + M_k \xrightarrow{k_{pjk}} R_k + U_k\delta_{1,2}^k + M_{k+1}\delta_2^k + CS \quad k = 1,\dots,3;\ j = 1,\dots,3 \tag{3.18}$$

Reversible activation/deactivation of growing radicals:

$$D_k + CM \underset{k_{dak}}{\overset{k_{ak}}{\rightleftharpoons}} R_k + CX \quad k = 1,\dots,3 \tag{3.19}$$

Chain transfer to monomers:

$$\mathrm{R}_k + M_j \xrightarrow{k_{fMkj}} SG + R_j + U_j \quad k = 1,\dots,3;\ j = 1,\dots,2 \tag{3.20}$$

Chain transfer to solvent:

$$\mathrm{R}_k + T \xrightarrow{k_{fTk}} SG + RT \quad k = 1,\dots,3 \tag{3.21}$$

Termination by combination:

$$R_k + R_j \xrightarrow{k_{tcij}} HHU \quad k = 1,\dots,3;\ j = k,\dots,3 \tag{3.22}$$

Termination by disproportionation:

$$R_k + R_j \xrightarrow{k_{tdij}} SG + SG \quad k = 1,\dots,3;\ j = k,\dots,3 \tag{3.23}$$

Table 3.9 presents a basic set of rate parameters considered in the modelling of the ATRP of MMA/EGDMA. All these parameters have been collected from previous works concerning mostly the linear FRP and ATRP of methacrylate monomers. Initiator and radical activation/deactivation and initiation of MMA with primary radicals were collected from Ohno *et al.* (1998); Tang *et al*. (2008); Shipp and Matyjaszewski, (2000). The propagation constant of MMA have been taken from Beuermann *et al*., (1997). Rate coefficients for chain transfer to monomer and to solvent were collected from Hutchinson, (2005). Radical termination constants were retired from (Fernández-Garcia *et al*., (1998); Moad and Solomon (2006). The extension to the non-linear case studies here considered is not straightforward because of the large number of kinetic parameters involved (notice the number of radicals and double bonds with different reactivities) and little information can be found in the literature concerning the kinetic of the ATRP of similar systems. The calculations presented here are

based on some postulated reactivity ratios of the different kinds of radicals and double bonds which have been previously discussed in the framework of FRP of MMA/EGDMA (Trigo *et al.*, 2008 and references therein). Nevertheless, it should be pointed out that the major parameters governing the crosslinking process are the reactivities of the pendant double bonds and these parameters will be estimated here using the available experimental data. These estimates have been obtained by neglecting intramolecular cyclizations. However, this can be an important issue even at 50 % dilution, as it will be discussed below. Particularities of the activation/deactivation equilibrium are also addressed in this chapter.

Table 3.9. Basic set of rate parameters considered in the modelling studies of the ATRP of MMA/EGDMA.

Kinetic Step	Rate Coefficient Expression [a)]
Initiator and radicals activation	$k_a = 140$ (EBPA at 22 °C in Acetonitrile)
	$k_a = 0.45$ (PS-Br at 110 °C in BPH)
Initiator and radicals deactivation	$k_{da} = 1.1 \times 10^7$
MMA propagation	$k_{p11} = 2.67 \times 10^6 \exp\left(-22.36 \times \frac{10^3}{RT}\right)$
Initiator of MMA by primary radicals	$k_{iR1} = 10k_{p11}, k_{iS1} = 10k_{p11}$
Chain transfer to monomer	$C_M = \frac{k_{fM11}}{k_{p11}} = 0.2 \times 10^{-4}$
Chain transfer to solvent	$C_T = \frac{k_{fT1}}{k_{p11}} = 0.2 \times 10^{-4}$
Radical termination	$\frac{k_{p11}}{\sqrt{k_t}} = 17.8 \exp\left(-13.7 \times \frac{10^3}{RT}\right)$
	$\alpha_{td} = \frac{k_{td11}}{k_t} = 0.56, \alpha_{tc} = \frac{k_{tc11}}{k_t} = 0.4$

[a)] Kinetic parameters expressed in $dm^3\ mol^{-1}s^{-1}$, unless otherwise stated.
R= 8.314 $Jmol^{-1}K^{-1}$.

3.3.2.2 Mathematical Modelling Including Branching and Crosslinking

It is known (Hutchinson and Penlidis, 2007) that acrylate monomers (among others) are susceptible to undergo chain transfer to monomer reactions because they contain aliphatic tertiary hydrogens which can be involved in an H-atom abstraction, as presented in Figure 3.2. A new polymer chain created by the resulting radical will contain an unsaturated end group (terminal double bond) capable of undergoing a further reaction with concomitant formation of non-linear structures via Long Chain Branching (LCB). Other sources of LCB in acrylates polymerisation are intermolecular chain transfer to polymer mechanisms. These

reactions usually involve the H-atom abstraction of a methine group (-CH(R)-) with formation of a mid-chain radical as presented in Figure 3.3 and/or the H-atom abstraction in a -CH_3- group, as depicted in Figure 3.4. Intermolecular chain transfer to polymer centres (-CH(R)- and-CH_3-) are created via the incorporation of monomer units in polymer chains (propagation reactions). LCB in acrylates via intermolecular chain transfer to polymer is usually considered to be result of H-atom abstraction of a methine group (Figure 3.3). For the sake of generality, here both mechanisms will be considered. Termination by combination and termination by disproportionation are also a source of chain transfer to polymer centres (methine groups) and terminal double bonds, respectively. This means that termination mechanisms can also have an indirect contribution for LCB. NMR spectroscopy has been applied to quantify the incidence of the different long chain branching mechanisms (Britton *et al*., 1998; Ahmad *et al*., 1998) in different polymerisation systems, namely involving *n*BuA and vinyl acetate. Gelation due to simultaneous intermolecular chain transfer to polymer and termination by combination was also experimentally observed and theoretically studied in a several works, namely concerning emulsion polymerisation of *n*BuA (Arzamendi *et al*., 1994; Plessis *et al*., 2000a and 2001; González *et al*., 2006 and 2007). The importance of intermolecular chain transfer to polymer was also recently shown through the synthesis of Z-RAFT star acrylate polymers (Boschmann and Vana, 2007).

Besides LCB, non-linear structures are formed in acrylate/diacrylate copolymerisation due to the polymerisation of pendent double bonds, as depicted in Figure 3.5. This crosslinking process is intentionally promoted through the addition of the diacrylate monomer to the polymerisation system. The amount of divinyl monomer is used in practice to manipulate the extent of the crosslinking process. Reactivity of pendent double bonds and/or incidence of intramolecular cyclization reactions are parameters with a strong influence in the efficiency of crosslinking polymerisations.

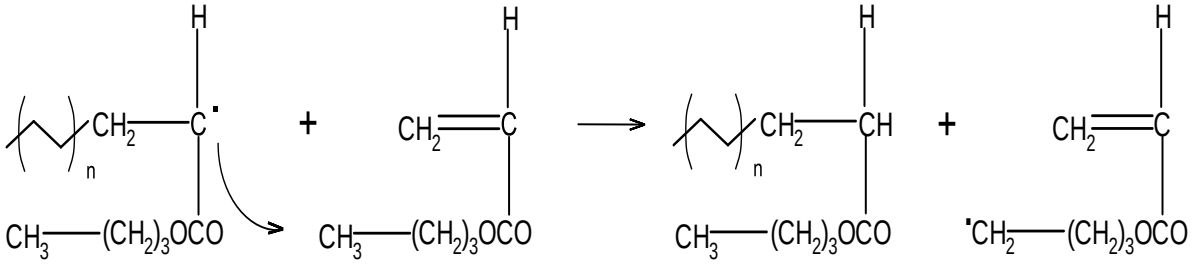

Figure 3.2. Depiction of a chain transfer reaction involving an acrylate monomer (*n*-butyl acrylate used for illustration) with creation of a terminal double bond that can lead to long chain branching.

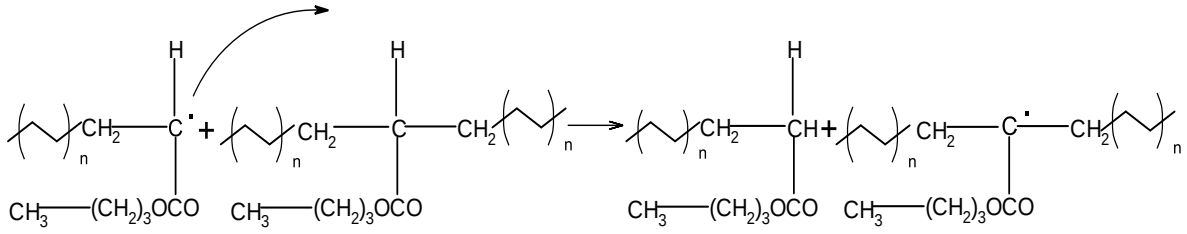

Figure 3.3. Depiction of intermolecular chain transfer to polymer in acrylates due to the H-atom abstraction of methine hydrogen.

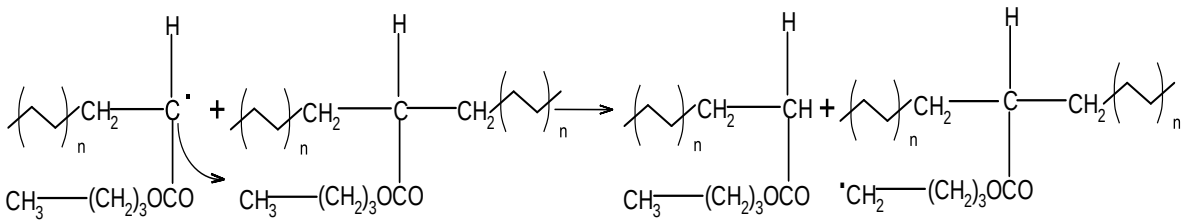

Figure 3.4. Depiction of intermolecular chain transfer to polymer in acrylates due to the H-atom abstraction of a $–CH_3$ group.

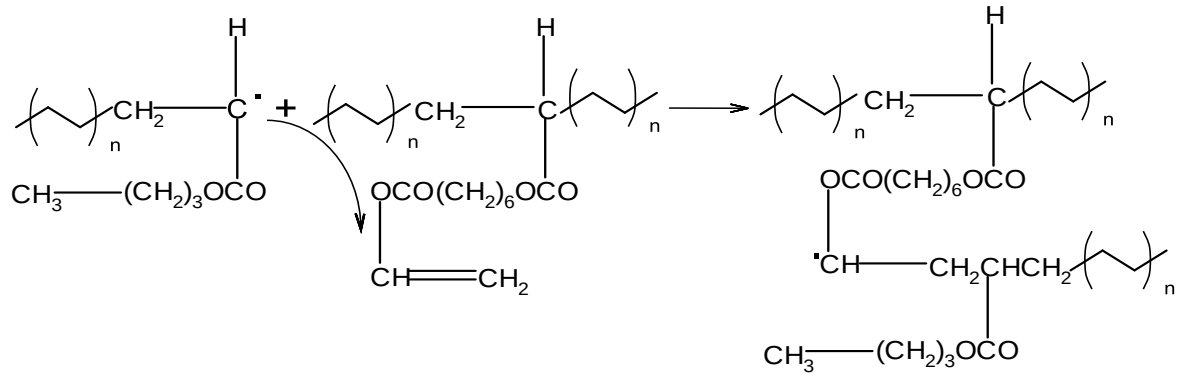

Figure 3.5. Depiction of pendant double bonds propagation (crosslinking) in acrylate/diacrylate copolymerisation.

Note that even if it is desirable that as many as possible of these kinetic parameters can be measured from experimental data, or indirectly estimated by more or less fundamental models of chemical reactions (an area which is expected to yield more and more accurate predictions in the not so distant future), only a few of them need be accurately known for the range of initial compositions and temperatures in our experiments and the actual number of fitted parameters is very small as discussed in the next section.

The present modelling approach is able to accommodate mechanisms such as intramolecular chain transfer to polymer (backbiting) leading to SCB. Much more complex kinetic schemes must be considered in these circumstances, as previously shown for a case study including primary cyclizations (Dias and Costa, 2005a). Results of the present work show that, under the polymerisation conditions here considered (diluted solution polymerisation at relatively low monomer conversion), crosslinking is dominant in comparison to intermolecular chain

transfer to polymer leading to LCB and that this mechanism can be neglected in the formation of non-linear architectures. Moreover, is known that SCB is unable to lead to gelation, in contrast to LCB at some particular conditions. The impact of SCB in the development of hyperbranched polyacrylates is even lower than that of LCB and therefore will be not considered in the present analysis.

Chain-length dependence of propagation and termination are important effects in several radical polymerisation systems. A recent analysis of these issues (Heuts *et al*., 2007) conclude that chain-length dependence of propagation cannot be neglected in living systems with low average degree of polymerisation (e.g. < 10) and that it should also be considered in conventional radical polymerisations with average degree of polymerisation lower than 100. It was pointed out that this effect should be negligible for higher values of DPn (Heuts *et al*., 2007). Scaling laws reflecting the decrease of termination coefficient with DPn were also presented in recent works (Heuts *et al*., 2007; Smith and Russell, 2007). These issues are probably even more complex in non-linear radical systems such as those considered in the present work. Due to the high values of DPn involved in most polymerisations here considered, it is plausible that chain-length dependence of propagation can be neglected. The opposite can be anticipated for the change of termination coefficient with chain length but, as far is of our knowledge there is no published development of this theory to non-linear radical systems. The general kinetic modelling approach here used is able to deal with chain-length dependence of propagation and termination. However, the need for estimating the full CLD and not simply its moments will increase the associated computing time by 2 or 3 powers of ten.

3.4 Results and Discussion

3.4.1 Acrylate/diacrylate Copolymerisations

3.4.1.1 Unperturbed Dimensions and Prediction of the *z*-Average Radius of Gyration in a Good Solvent

Several effects are involved in the short-range interactions leading to increased molecular size of linear random-coil polymers. The restriction to fixed bond angles expands the polymer chains. Molecular dimensions are further increased due to restricted rotations resulting from steric hindrances or due to rigid planar conformations (e.g. presence of aromatic rings in the main chain). Conformations which would place too close pairs of atoms in neighbour repeating units along the polymer chain are also forbidden. The mean square distance between

chain ends including short-range interactions (r_θ^2- unperturbed dimensions in the absence of long-range interactions) divided by the square of the random-flight end-to-end distance (r_f^2) defines the characteristic ratio C_∞:

$$C_\infty = \lim_{n\to\infty}\left(\frac{r_\theta^2}{r_f^2}\right) = \lim_{n\to\infty}\left(\frac{6R_{g\theta}^2}{nl^2}\right) = \lim_{n\to\infty}\left(\frac{6M}{nl^2}\frac{R_{g\theta}^2}{M}\right) = \frac{6M_0}{2l^2}\frac{R_{g\theta}^2}{Mw} \qquad (3.24)$$

In above relation *n* represents the number of (equal) skeletal bonds of the polymer chain of molecular weight *Mw*, M_0 being the molecular weight of the repetitive unit bearing two C-C bonds of length $l = 0.154$ nm. For random coil chains the unperturbed value of the mean square end to end distance (r_θ^2) is related with the unperturbed (Θ conditions) value of the mean square radius of gyration through $r_\theta^2 = 6R_{g\theta}^2$.

The Θ dimensions of linear polymers can be estimated from experimental measurements performed in a good solvent using a SEC/RI/MALLS system (Búrdalo *et al*., 2000; Tarazona *et al*., 2003). For polymer chains in a good solvent with dimensions greater than $\lambda/20$, with λ being the wavelength of the incident light, the mean square radius of gyration can be measured for each slice of elution volume (considered as monodispersed samples) in a SEC/RI/MALLS apparatus. With the instrument used in this work and operating with THF, the lower detection limit is around $\frac{\lambda}{20} \cong \frac{\lambda_0}{(20\times n_{THF})} = \frac{658}{(20\times 1.4)} = 23.5$ nm. Measurements below this limit are possible (e.g. 10 nm) but with high associated uncertainty (e.g. errors in the order of 50 %). Typical SEC traces of ATRP synthesized acrylate/diacrylate copolymers corresponding to different polymerisation times (monomer conversion) showing the consumption of monomers and the evolution of the crosslinking process is presented in Figure 3.6 (only refractive index signal). Figure 3.7 shows the measured refractive index and light scattering (90°) signals in the SEC trace of an ATRP synthesized acrylate/diacrylate copolymer showing the formation of a cluster of high molecular weight at a low concentration. Figures 3.8 and 3.9 show measured variations of apparent weight-average molecular weight (M_w) (can slightly differ from the true one owing to variable refractive index increment, not an issue here) and of root mean square radius of gyration (R_g) along the SEC trace of a P*n*BuA sample synthesized in this work. Observed light scattering (90°) and RI signals are also shown in these Figures. In this analysis, the head and tail regions of the chromatograms were eliminated due to their very low LS and RI signals, which would also cause high errors in the estimation of M_w and R_g.

The following average properties of this sample were measured:

$\bar{M}_n \times 10^{-5} = 2.0 \pm 0.1$,

$\bar{M}_w \times 10^{-5} = 3.0 \pm 0.1$,

$\bar{M}_z \times 10^{-5} = 4.2 \pm 0.7$,

$\bar{R}_g = 32 \pm 1$ nm.

Measured values of M_w and $\bar{R}_g$ along the chromatogram of the P*n*BuA sample were used to establish a relation $\bar{R}_g$ *versus* M_w which is known to follow a scaling law $R_g = QM_w^q$. Figure 3.10 shows the scaling law $R_g = 0.0146M_w^{0.593}$that was estimated in this work for P*n*BuA in THF at 30 °C. This result is consistent with measurements reported in other research works using other polymers, namely $R_g = 0.011M_w^{0.596}$ for PMMA (Jackson *et al.*, 1996) in THF at 30 °C and $R_g = 0.0118M^{0.6}$ for PS (Terao *et al.*, 2004) in THF at 25 °C that are also presented in Figure 3.10.

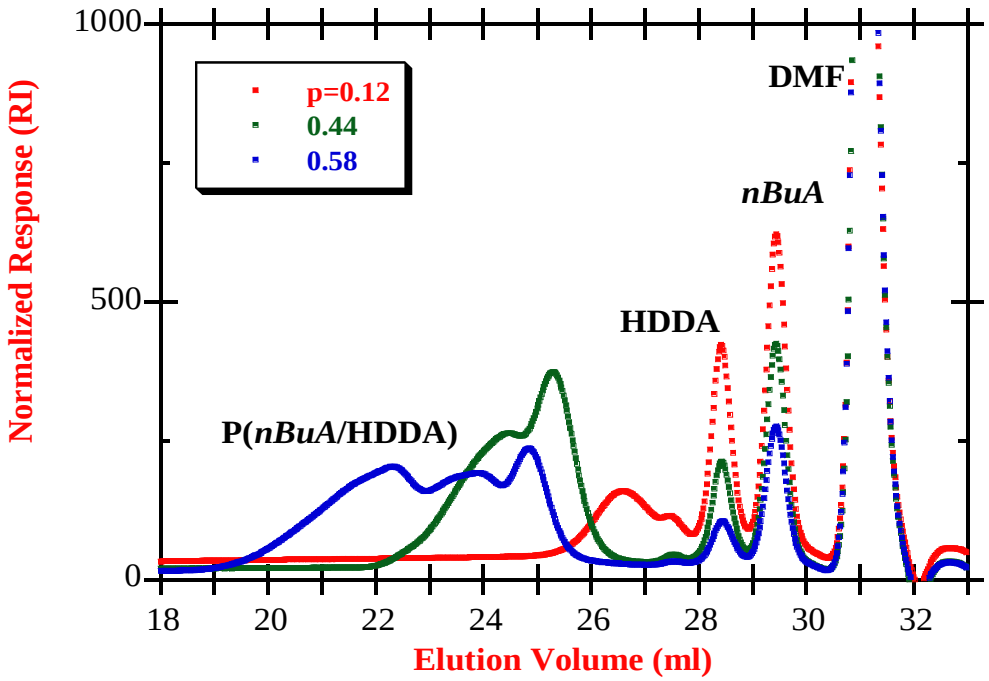

Figure 3.6. Observed refractive index signal in the SEC traces of ATRP synthesized acrylate/diacrylate copolymers corresponding to different polymerisation times (monomer conversion).

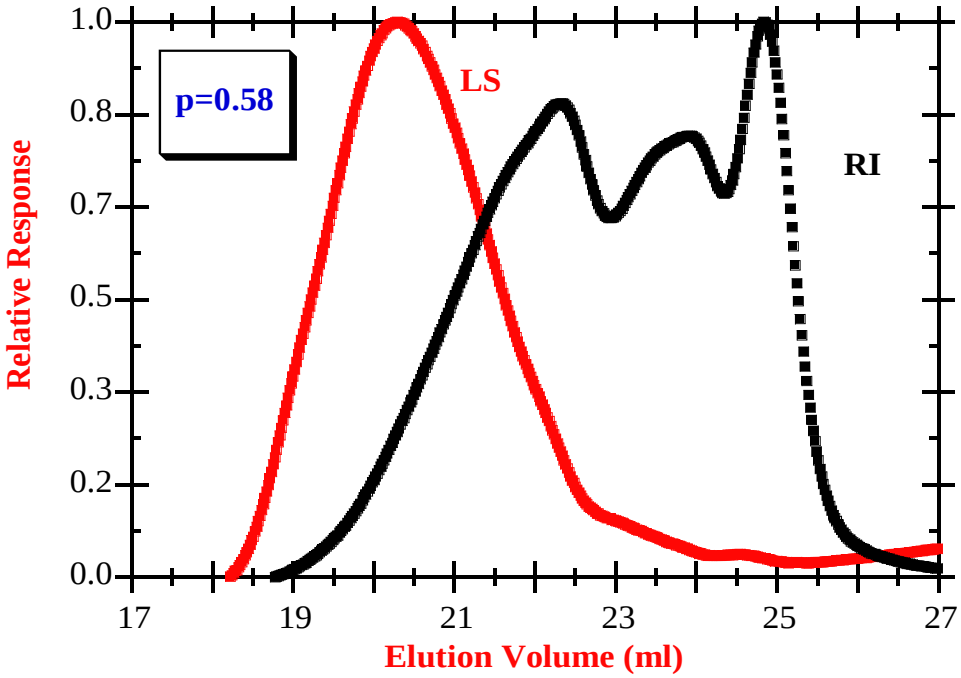

Figure 3.7. Measured refractive index and light scattering (90°) signals in the SEC trace of ATRP synthesized acrylate/diacrylate copolymer.

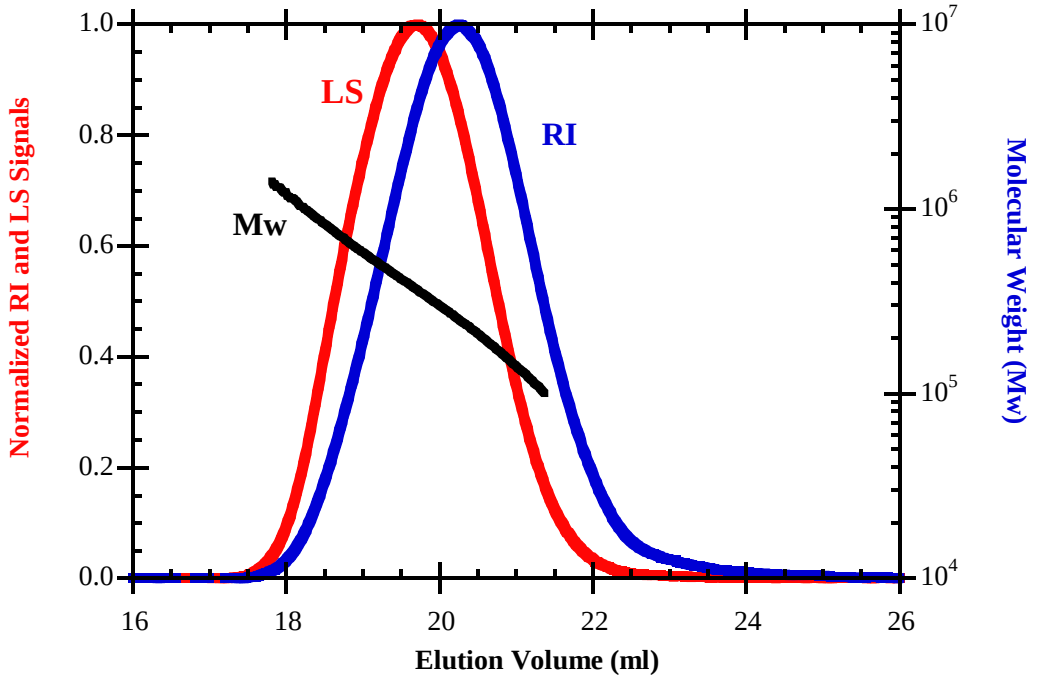

Figure 3.8. Measured relation of molecular weight *versus* elution volume in the SEC trace of a FRP synthesized P*n*BuA sample.

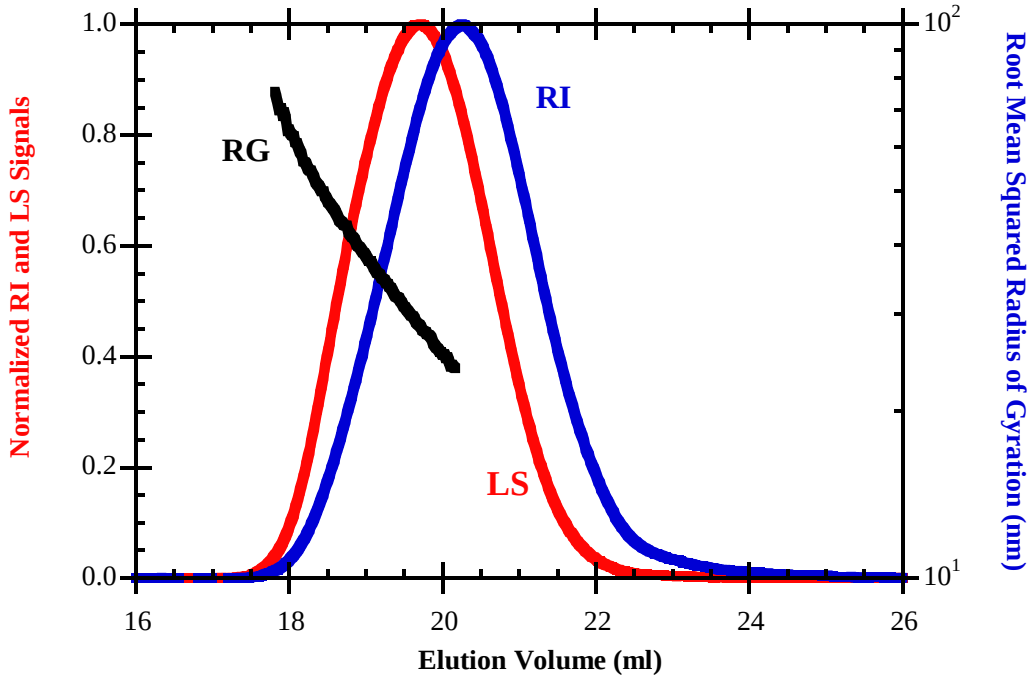

Figure 3.9. Measured relation of root mean square radius of gyration *versus* elution volume for the same sample of Figure 3.8.

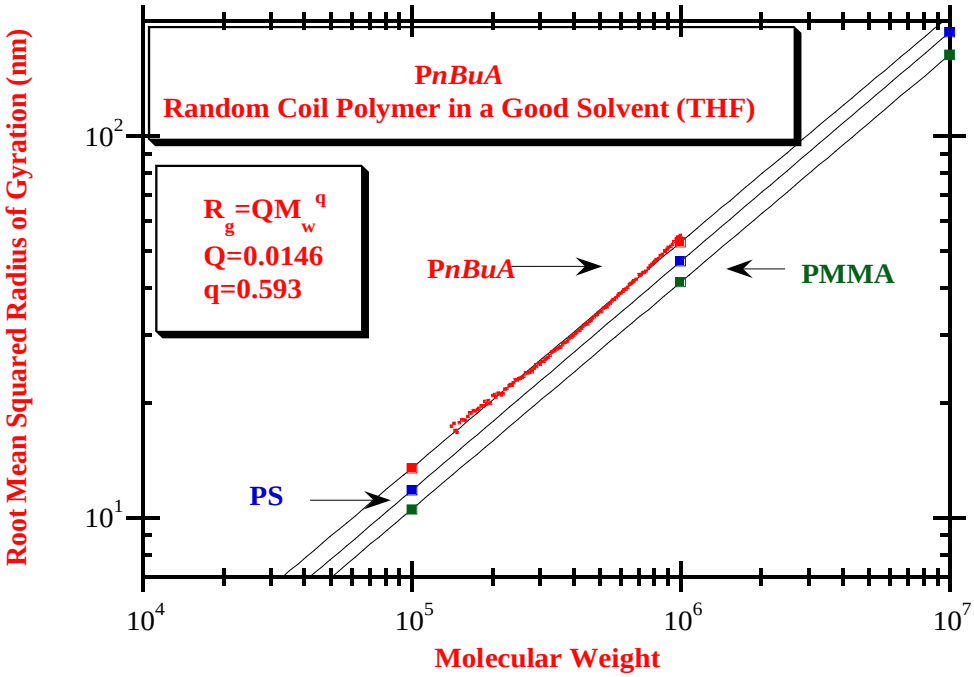

Figure 3.10. Scaling law for the radius of gyration versus molecular weight observed for P*n*BuA in a good solvent and its comparison with scaling laws measured for the dimensions of other polymers.

Experimental values expressing the dependence of the dimensions of P*n*BuA in THF on molecular weight were used to estimate the unperturbed dimensions of this polymer. Different extrapolation procedures were used for this purpose:

Fixman (Fixman, 1955) extrapolation:

$$\frac{R_g^2}{M_w} = \frac{R_{g\theta}^2}{M_w} + 0.0299B\left(\frac{R_{g\theta}^2}{M_w}\right)^{-1/2} {M_w}^{1/2} \tag{3.25}$$

Stockmayer-Fixman (Stockmayer and Fixman, 1963) extrapolation:

$$\left(\frac{R_g^2}{M_w}\right)^{3/2} = \left(\frac{R_{g\theta}^2}{M_w}\right)^{3/2}\left(1 + C{M_w}^{1/2}\right) \tag{3.26}$$

Kurata-Stockmayer-Roig (Kurata *et al*., 1960) extrapolation:

$$\frac{R_g^2}{M_w} = \frac{R_{g\theta}^2}{M_w} + 0.0286Bg(\alpha)\left(\frac{M_w}{R_g}\right) \tag{3.27}$$

The application of these extrapolation procedures to the synthesized P*n*BuA sample is shown in Figures (3.11)-(3.13). Good agreement between experimental values and theoretical predictions are obtained with the three different methods. Extrapolated unperturbed dimensions of P*n*BuA are closer when Stockmayer-Fixman or Kurata-Stockmayer-Roig extrapolations are used and higher dimensions are estimated with Fixman extrapolation. Characteristic ratios $C_\infty = \frac{3\times128\times0.0208^2}{0.154^2} = 7.0$, $C_\infty = 9.5$ and $C_\infty = 16.2$ are estimated when Kurata-Stockmayer-Roig, Stockmayer-Fixman and Fixman extrapolation results are considered, respectively. The length of a C-C bond, $l = 0.154$ nm was here considered.

Experimental studies concerning the polymer chain flexibility of polyacrylic esters (Penzel and Goetz, 1990a and 1990b); report (among others) the length of the Kuhn segment for P*n*BuA: $A_m = 6\frac{R_{g\theta}^2}{M_w}\frac{M_{w0}}{b_0} = 3.54$ nm, with b_0 representing the contribution of each monomeric unit to the length of the polymer chain ($b_0 = 0.211$ nm was considered in these works (Penzel and Goetz, 1990a and 1990b) for polyacrylates). This definition is generically consistent with Eq. (3.24) if the relation $b_0^2 = 2l^2$ is considered. These experimental results can be used to estimate the characteristic ratio of P*n*BuA because its relation with Kuhn's statistical segment is expressed by $C_\infty = \frac{\sqrt{2}A_m}{2l}$ and therefore $C_\infty = 16.3$ results for P*n*BuA. Based on these same works, $C_\infty = 9.3$ ($A_m = 2.02$ nm) can be estimated for PMA.

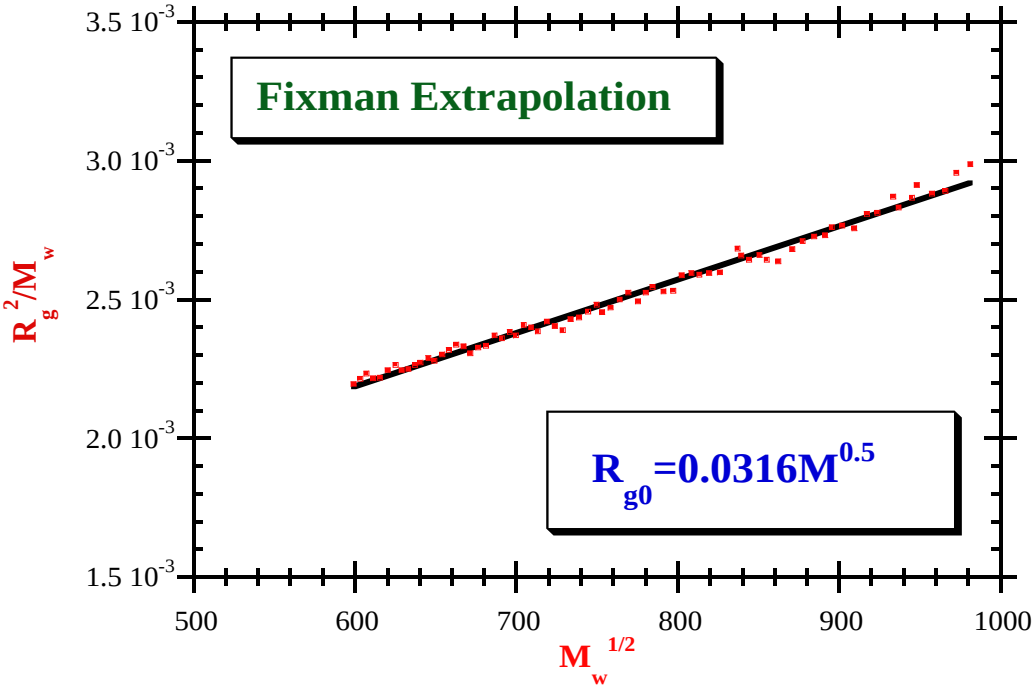

Figure 3.11. Estimated unperturbed dimensions of P*n*BuA considering Fixman extrapolation.

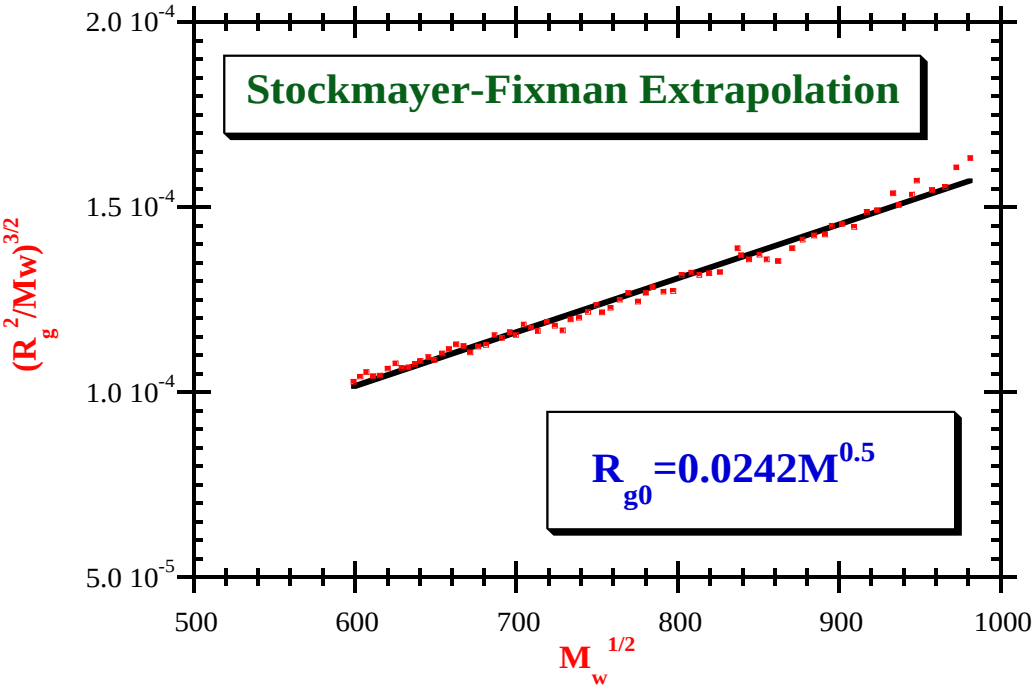

Figure 3.12. Estimated Θ dimensions of P*n*BuA with Stockmayer-Fixman extrapolation.

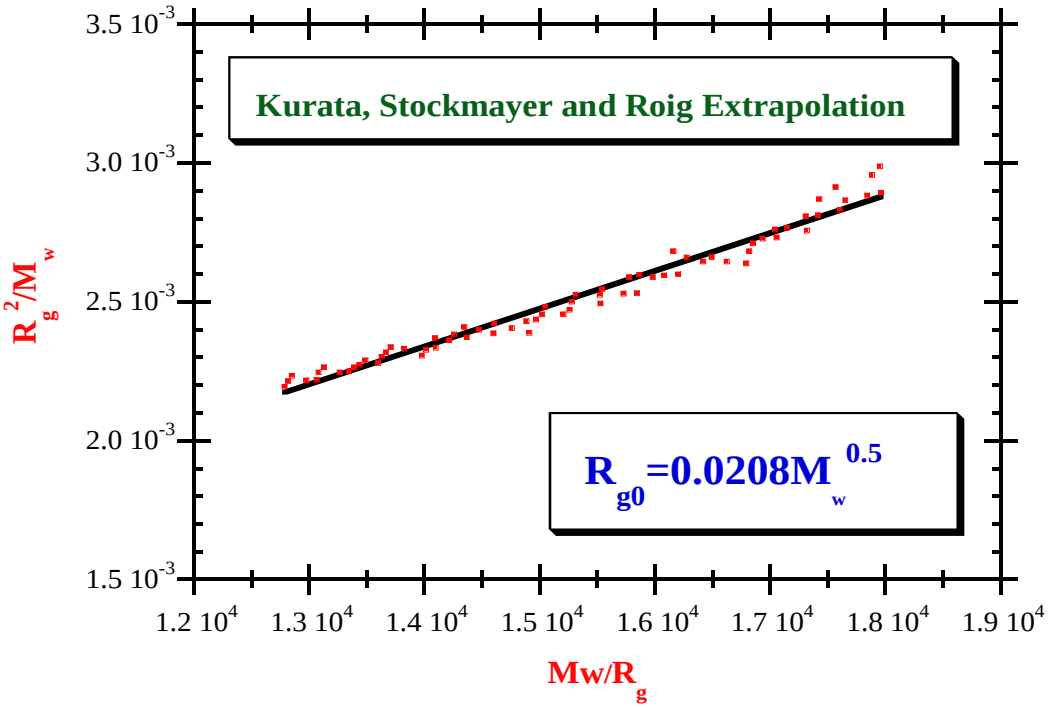

Figure 3.13. Estimated Θ dimensions of P*n*BuA with Kurata-Stockmayer-Roig extrapolation.

Other experimental/theoretical studies (Yoon *et al*., 1975) estimate $C_\infty = 8.4$ for PMA. It is well known that the structure of polymer chains plays a strong influence on the polymer chain flexibility. For polymethacrylates the effect of the substituent on the chain flexibility was thoroughly studied and values of C_∞ are reported (Xu *et al*., 1995) to lie between 7.3 (methyl methacrylate) and 26.4 (pentachlorophenyl methacrylate). For *n*-butyl methacrylate (P*n*BuMA) the characteristic ratio was experimentally evaluated and theoretically predicted (Xu *et al*., 1995; Karyappa and Natarajan, 2008) to be in the range 8.6 to 9.6. Chain flexibility of polymethacrylates has been extensively studied but for polyacrylates only few research works are available. Characteristic ratios of poly(tetrahydrofurfuryl acrylate) and poly(2-ethylbutyl acrylate) were more recently measured and $C_\infty = 8.6$ and 9.2, respectively, have been reported (Zioga *et al*., 1997). Based on the available range values of the characteristic ratio of PMMA, PMA and P*n*BuMA as well as on the effect of substitution groups, a value around 10 is expected for P*n*BuA. The measurement of C_∞ around 16 before reported for P*n*BuA (Penzel and Goetz, 1990a and 1990b), and also obtained in the present work when Fixman extrapolation is considered, seems to be overestimated.

Similarly to other works dealing with estimation of unperturbed dimensions of polymer chains considering different extrapolation methods (Búrdalo *et al*., 2000; Tarazona *et al*.,

2003; Penzel and Goetz, 1990b), in the present work, the mean of the three extrapolations for the unperturbed dimensions of P*n*BuA will be used: $R_{g\theta} = 0.0255M^{0.5}$. This estimate leads to a characteristic ratio $C_\infty = 10.5$ and a Kuhn segment of length $A_m = 2.29$ nm. Note that an imaginary bond length (b) connecting a set of beads (repeating units) in the context of the freely rotating model can be calculated because the following relation holds: $b^2 = A_m b_0 = \sqrt{2}A_m l$. Therefore, in the predictions of the *z*-average radius of gyration performed in the present work, a bond length of $b = 0.706$ nm was considered to link *n*BuA repeating units.

Using the experimentally observed relation $R_g = 0.0146M^{0.593}$ for P*n*BuA in THF at 30 °C and the extrapolation $R_{g\theta} = 0.0255M^{0.5}$ estimated for a Θ solvent, it was estimated that also in THF at 30 °C, for polydispersed P*n*BuA, the following expansion relation holds: $\frac{\bar{R}_g}{\bar{R}_{g\theta}} = 0.573\bar{M}_z^{0.093}$. The simulation method is able to estimate the *z*-average radius of gyration in the Θ state ($\bar{R}_{g\theta}$) but experimental measurements were performed in THF at 30 °C (good solvent regimen). Predictions of R_g are therefore needed and this expansion relation was used with this purpose in the present work. This same expansion relation was considered in the linear and non-linear polymerisation systems, as described below.

3.4.1.2 *In-line* FTIR-ATR Monitoring Results

FTIR-ATR real-time monitoring of vinyl monomers polymerisation was reported more than one decade ago (Chatzi *et al.*, 1997; Storey *et al.*, 1998). In more recent years, further research works were performed with the goal of studying the potentialities of this technique in the solution homo-, co- and terpolymerisation of different monomers (Hua and Dubé, 2001; Jovanović and Dubé, 2001; Hua *et al.*, 2004). Owing to its industrial importance, *in-line* FTIR-ATR monitoring of emulsion/miniemulsion polymerisation processes is also a subject with growing research activity (Roberge and Dubé, 2007; Hua and Dubé, 2002; Ouzineb *et al.*, 2003; Jovanović and Dubé, 2003). Indeed, *in-line* FTIR-ATR spectroscopy is a suitable technique to monitor vinyl polymerisations because several difficulties associated with alternative techniques are eliminated; negligible time lags and absence of sampling difficulties are important issues allowing the use of *in-line* FTIR-ATR monitoring to implement feedback control policies. Production of more homogeneous materials is therefore possible using for instance semi-batch reactors. Use in kinetic studies (e.g. quantification of copolymer reactivity ratios) is another important application of this technique. One goal of the present work was the assessment of *in-line* FTIR-ATR spectroscopy in the monitoring of

vinyl/divinyl copolymerisations using acrylate/diacrylate model chemical systems. *In-line* FTIR-ATR simultaneous monitoring of vinyl and divinyl monomers can be used to the real time specification of feed policies in semi-batch reactor, which is a possible strategy to design non-linear polymers with tailored properties as recently shown with the system styrene/divinylbenzene (Gonçalves *et al*., 2007).

The spectra of the various components have enough differences allowing their simultaneous quantitative estimation. Figure 3.14 shows the *off-line* FTIR-ATR spectra observed for some monomers used in this work, namely *n*BuA, HDDA and BEDA. Vibrational assignments of these acrylate monomers are confirmed and different characteristic absorbance bands can (in principle) be used for the quantitative analysis of these polymerisation processes, namely $=CH_2$ twist at $810.6\,cm^{-1}$ and $=CH_2$ deformation at $1409\,cm^{-1}$ (Hua and Dubé, 2001; Jovanović and Dubé, 2001). Notice that additional vibrational assignments are identified for BEDA due to the presence of aromatic rings in the chemical structure. In Figure 3.15 are presented the FTIR-ATR spectra observed for *in-line* monitoring the *n*BuA homopolymerisation with $V_M = 35\ \%$ confirming the usefulness of this technique to carry out the real-time monitoring of the formation of vinyl polymers.

Nevertheless, real-time monitoring of vinyl/divinyl copolymerisation is a challenging task because diluted solution polymerisation is required in order to avoid the auto-acceleration effect as non-isothermal temperature profiles make very difficult the quantitative analysis. Moreover, when producing hyperbranched polymers, a low content of divinyl monomer should be used to avoid gelation. Consequently, the intensity of the characteristic bands of divinyl monomer is very low in these copolymerisations; the consequence is a low sensitivity in the monitoring of this component.

It is therefore not unexpected that difficulties arise when the formation of hyperbranched acrylate/diacrylate copolymers is monitored, as presented in Figure 3.16 for the *n*BuA/HDDA copolymerisation (run 7 in Table 3.2) with these operational conditions, the specific sensitivity to the presence of crosslinker is too low, thus precluding the quantitative analysis of important parameters such as the reactivity of pendent double bonds or the formation of intramolecular cyclizations. Similar conclusions are obtained by observation of the spectra in the region 3400 to $4000\,cm^{-1}$ where the polymer formation is detected due to the creation of aliphatic C-H bonds, as represented in Figures 3.17 and 3.18 for the FTIR-ATR monitoring of *n*BuA and *n*BuA/HDDA copolymerisations, respectively.

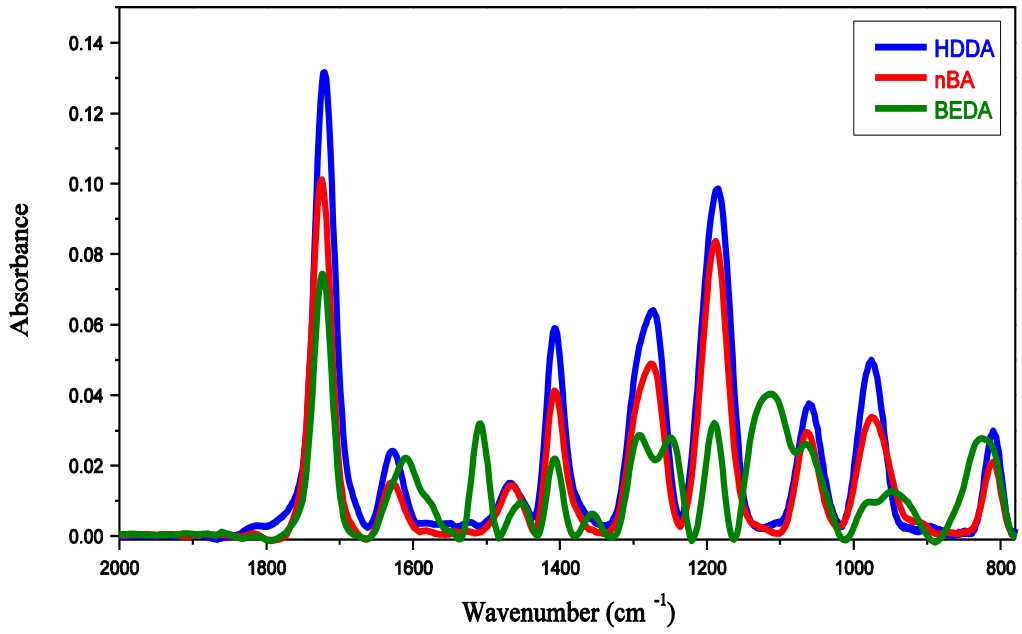

Figure 3.14. *Off-line* FTIR-ATR spectra observed for *n*BuA, HDDA and BEDA monomers.

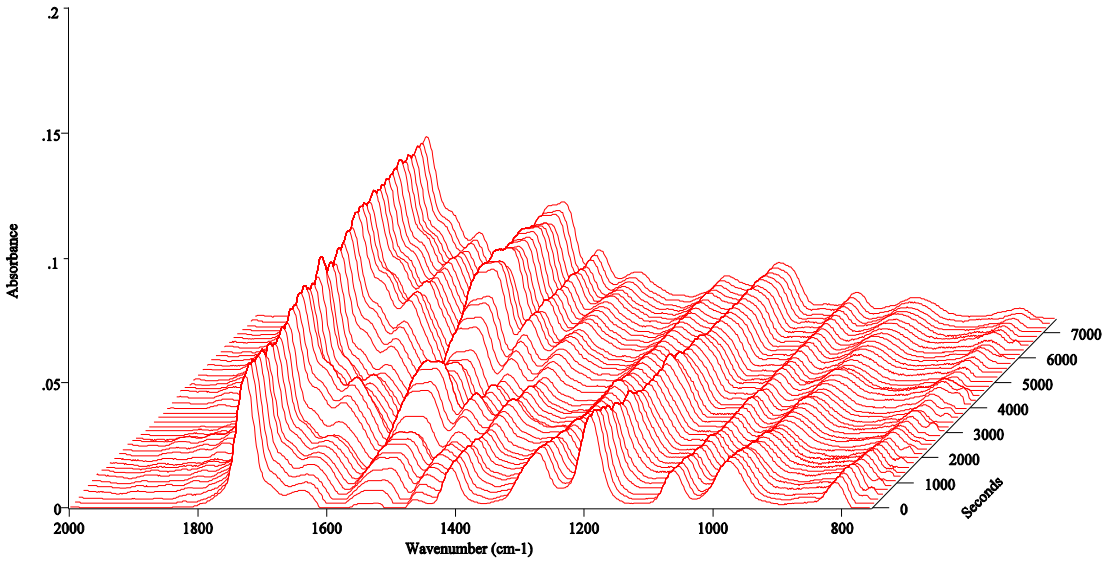

Figure 3.15. FTIR-ATR spectra observed in the *in-line* monitoring of the *n*BuA polymerisation (Run 6 of Table 3.2).

Figure 3.19 shows the FTIR-ATR spectra obtained in the *in-line* monitoring of the MA homopolymerisation (run 1 in Table 3.2) but using the reference background of the initial mixture. In this case, only the polymer formation is also monitored. Notice that the use of reference backgrounds other than the air can be useful in water polymerisation media (suspension/emulsion) or when trying to monitor small amounts of divinyl monomers. Indeed, the results here presented show that in the solution production of hyperbranched polymers resulting from vinyl/divinyl copolymerisation only the vinyl monomer can be *in-line* monitored with reliability.

However, suspension polymerisation is a promising way to overcome these difficulties. It should allow work at higher monomer concentrations and extend the polymerisation beyond gelation if desired. Higher monomer conversions should also be easier to observe in suspension polymerisation therefore yielding higher variations of the intensity of characteristic absorbance bands. These improvements should go in parallel with developments of suspension ATRP which is nowadays a less explored subject than solution ATRP.

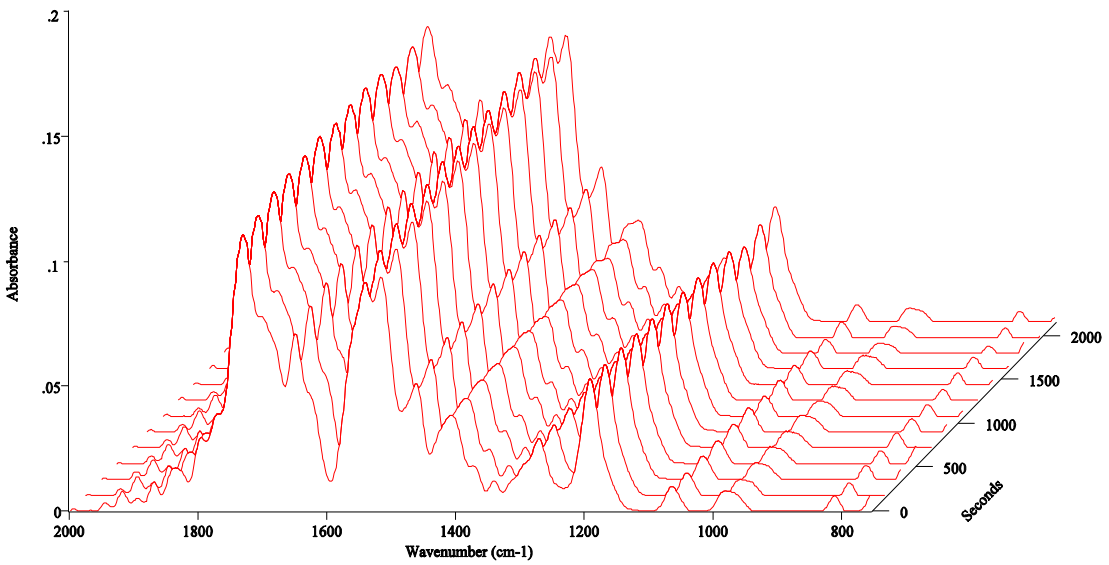

Figure 3.16. FTIR-ATR spectra observed in the *in-line* monitoring of *n*BuA/HDDA copolymerisation (Run 7 in Table 3.2).

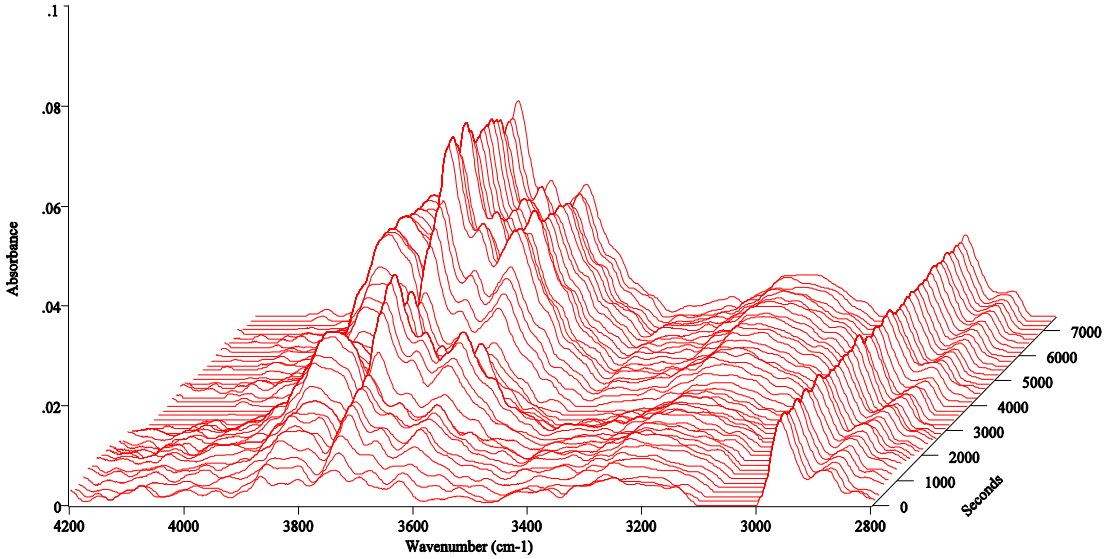

Figure 3.17. Polymer formation (Run 6 in Table 3.2) detected by FTIR-ATR monitoring of the region with wave numbers in the range of 3400 to 4000 cm^{-1} (aliphatic C-H bonds).

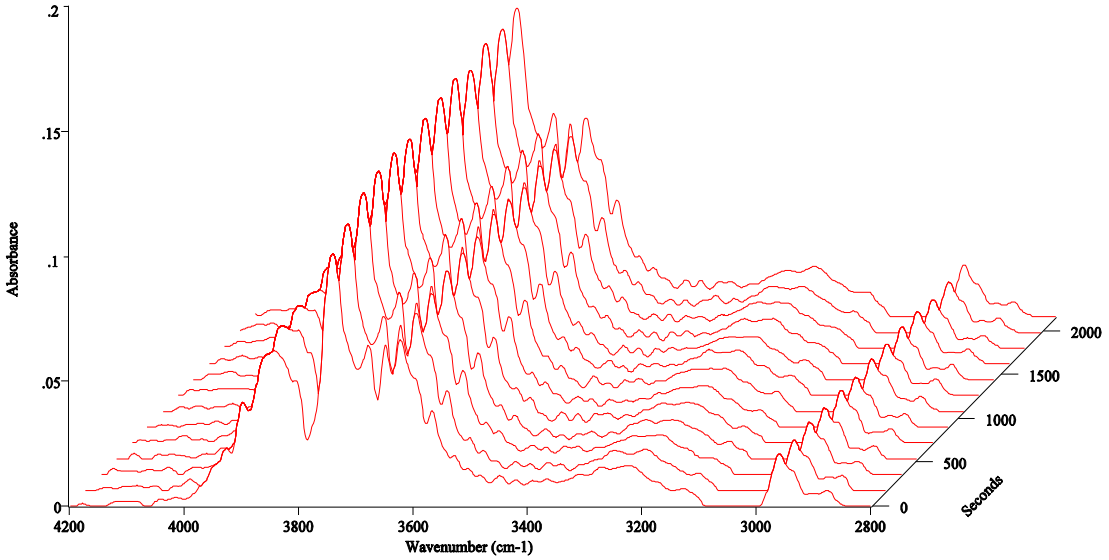

Figure 3.18. Similar analysis as in Figure 3.17 for the copolymerisation of *n*BuA/HDDA (Run 7 in Table 3.2).

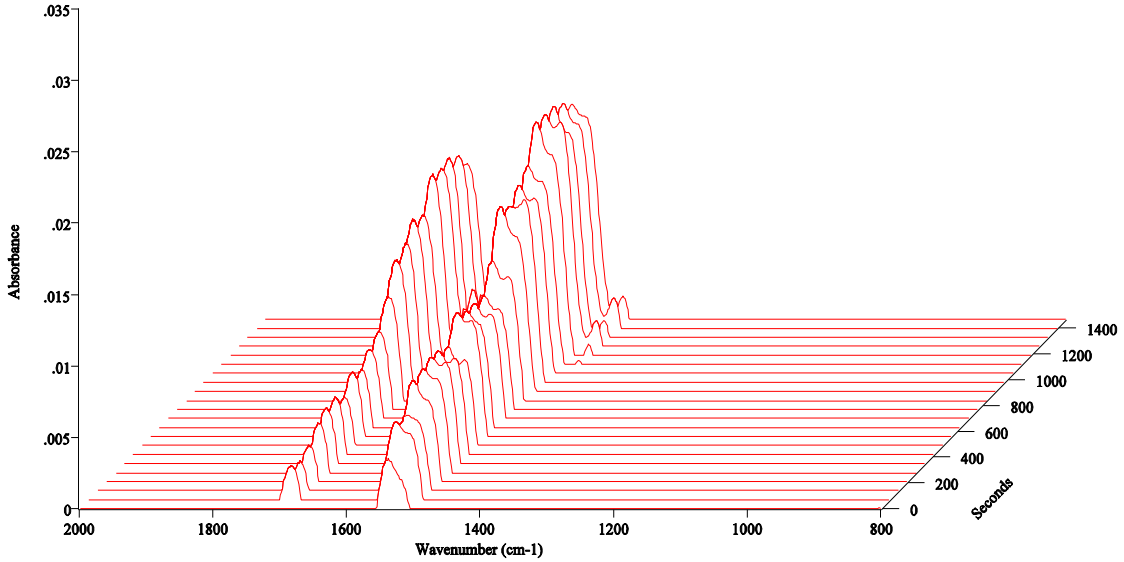

Figure 3.19. FTIR-ATR *in-line* monitoring of MA homopolymerisation (run 1 in Table 3.2) using the reference background of the initial mixture.

3.4.1.3 Acrylate/Diacrylate FRP and ATRP Copolymerisation

The general mathematical tool above described and experimental results obtained through the characterization by SEC/RI/MALLS of samples of the produced polymers are here used to carry out the kinetic modelling of acrylate/diacrylate copolymerisation. The task will be the isolation of the most influential kinetic parameters in the branching and crosslinking processes. The effect of dilution will also be put into evidence and a brief comparison between FRP and ATRP of acrylate/diacrylate monomers is also presented.

Figure 3.20 shows measured and predicted monomer conversion evolutions of $\overline{M}_w$ in FRP *n*BuA/HDDA copolymerisations, at 15 % initial volume fraction of monomer ($V_M = 15$ %), with different mole fractions of crosslinker, showing the strong influence of the initial amount of HDDA in the dynamics of polymer properties. These experiments were simulated using the reactivity of PDBs as fitting parameters. It was estimated that PDBs present a lower reactivity as compared to *n*BuA, with a ratio of relative propagation rate constant $C_{PDB} = k_p^*/k_p = 0.06$. Simulation results have shown a low sensitivity to changes in other kinetic parameters besides the reactivity of PDB. Reactivities of the different kinds of polymer radicals have a

small effect on the branching/crosslinking process only if they are very low as compared with the reactivity of the radical correspondent to the acrylate monomer (e.g. below 1/1000). Simulations also have shown that, under the polymerisation conditions here considered, the branching process due to intermolecular chain transfer to polymer (H and CH_3 chain transfer centres were considered) have a negligible contribution to the formation of non-linear architectures, namely when compared with the crosslinking phenomena.

Reactivity ratios for intermolecular chain transfer to polymer in the range $10^{-5} < C_P = \frac{k_{fP}}{k_P} < 10^{-3}$ are reported in the literature (Brandrup *et al.*, 1999) and simulations have shown a very small impact of this mechanism on the polymer properties only when the upper limit of this interval is approached and the mole fraction of diacrylate monomer is very small (e.g.$y_C <$ 0.5 %). Note that chain transfer to solvent ($C_S = \frac{k_{fS}}{k_S} = 2.7 \times 10^{-4}$) is here an important competitive mechanism as compared with chain transfer to polymer (Dias and Costa, 2003, 2005b). Similar conclusions were obtained with respect to the impact of polymerisation of terminal double bonds. Simulations were performed considering that the fraction of termination by combination is 95 %.

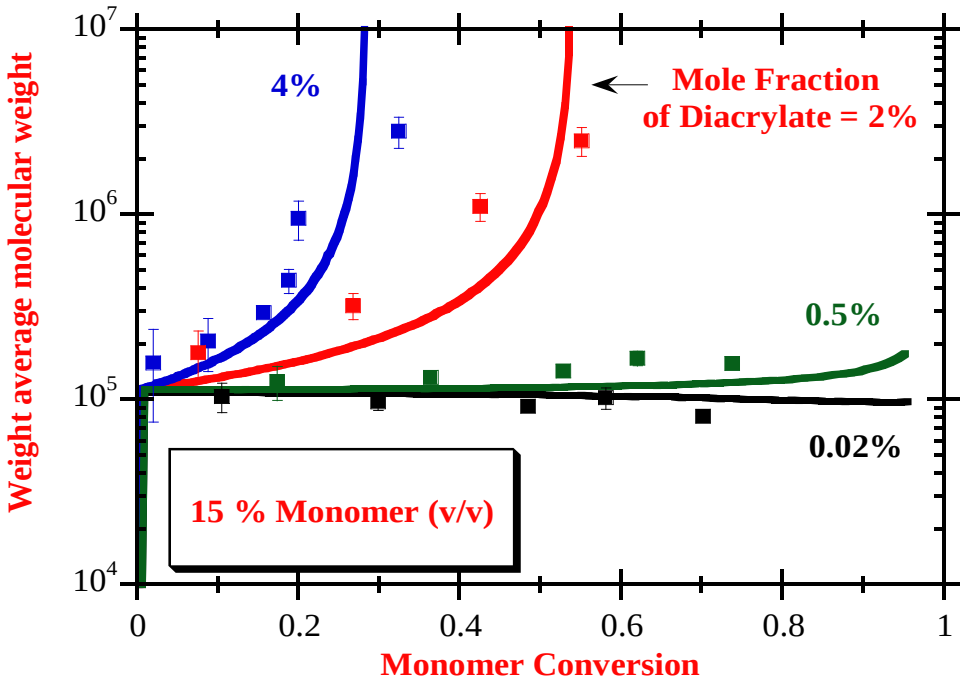

Figure 3.20. Measured and predicted evolution of $\bar{M}_w$ in *n*BuA/HDDA FRP copolymerisation with different initial amounts of diacrylate (V_M = 15 %).

In Figure 3.21 is presented the effect of the monomer dilution (experiments with $V_M = 15$ % and $V_M = 35$ %) in the evolution of $\bar{M}_w$ for *n*BuA/HDDA FRP copolymerisations with the same initial mole fraction of diacrylate ($y_C = 0.5$ %). Completely distinct evolutions of $\bar{M}_w$ with monomer conversion were experimentally measured and different values for the reactivity of PDBs were fitted from these two experiments: $C_{PDB} = 0.16$ for $V_M = 35\%$ and $C_{PDB} = 0.06$ for $V_M = 15$ %. It is plausible that these reactivity ratios are only apparent values due to the influence of intramolecular cyclization reactions which had been neglected in these modelling studies. Increased deviation from the ideal case $C_{PDB} = 1$ with dilution seems to confirm this issue. Figure 3.22 shows the effect of the reactivity of PDB on $\bar{M}_w$ for FRP synthesized polyacrylates using $T = 60$ °C, $V_M = 35$ %, $\frac{[I]_0}{[M]_0} = 0.1\%$ and $y_C = 5$ %. Besides crosslinking, simulations also take into account LCB with help of the following parameters: $C_P = C_{fpH} = C_{fpCH_3} = 10^{-4}$, $C_{TDBM} = C_{TDBD} = 1$, $R_{INT} = 10^{-2}$, $R_{AM} = 1$, $\alpha_{td} = 5$ %. It can be noticed the strong impact of the reactivity of PDB on the polymer properties, showing that this mechanism is the dominating phenomenon in these kind of polymerisation systems.

Comparison of experimental results with predictions allows the fitting of this parameter, as shown in Figures 3.21 and 3.22. It is plausible that this reactivity ratio of PDB is much lower than one mostly owing to the effect of intramolecular cyclizations which had not been considered in the modelling studies. Intramolecular cyclizations consume PDB and consequently decrease the crosslinking efficiency which is also reflected by delaying gelation. These effects are especially important at higher dilution, as more deeply discussed elsewhere (Gonçalves *et al*., 2007, 2010a and 2010b; Trigo *et al*., 2008) for different kinds of polymerisation systems.

The effect of the initial amount of crosslinker in the evolution of $\bar{M}_w$ for ATRP *n*BuA/HDDA copolymerisation at constant initial dilution ($V_M = 35$ %) is presented in Figure 3.23. A similar fitting procedure as in Figure 3.22 is presented in Figure 3.24 for ATRP synthesized polyacrylates using $T = 60$ °C, $V_M = 35\%$, r_M/CuBr/PMDETA= 50/0.45/0.5 and $y_C = 10$ %. LCB was also taken into account in the calculations considering: $C_P = C_{fpH} = C_{fpCH_3} = 10^{-4}$, $C_{TDBM} = C_{TDBD} = 1$, $R_{INT} = 10^{-1}$, $R_{AM} = 1$,. $\alpha_{td} = 5$ %.

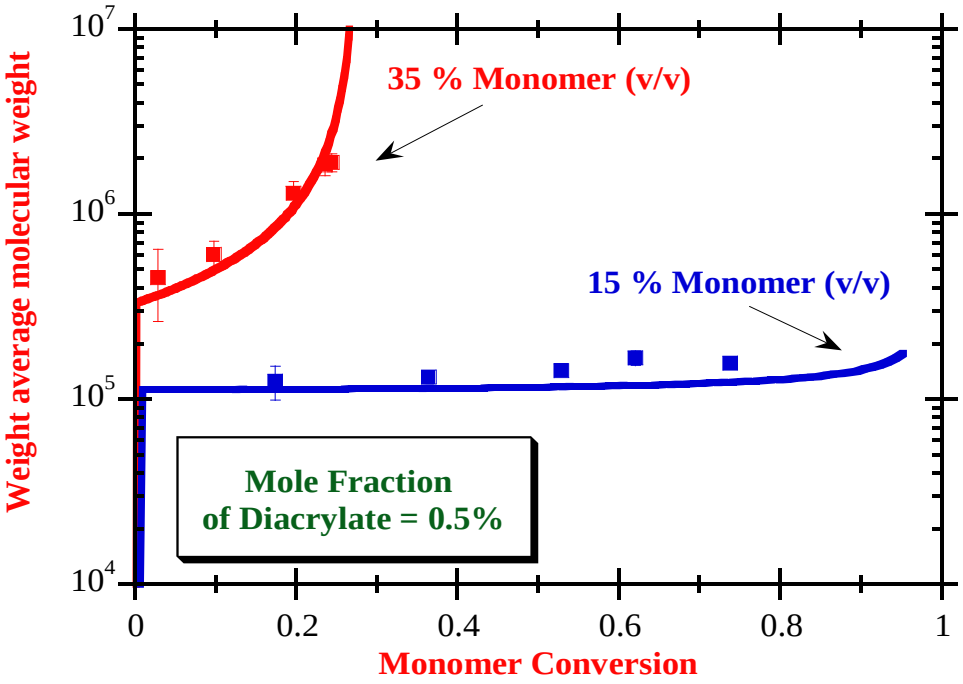

Figure 3.21. Effect of the dilution in the evolution of $\bar{M}_w$ for FRP copolymerisation of *n*BuA/HDDA.

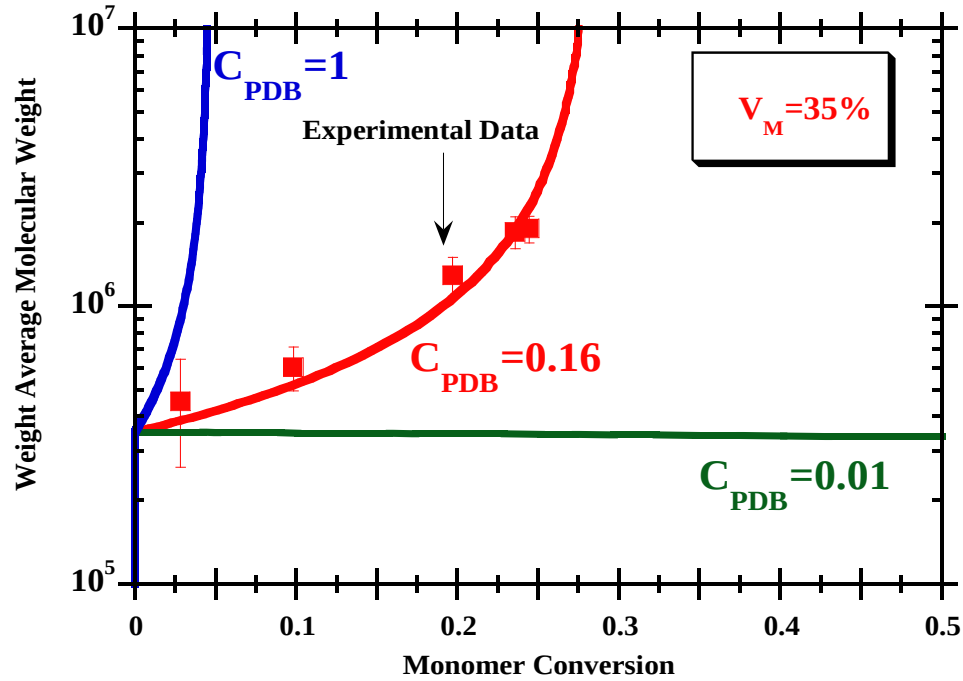

Figure 3.22. Predicted effect of the reactivity of PDB on $\bar{M}_w$ for FRP of *n*BuA/HDDA (run 7 in Table 3.2.

Also for ATRP, polymerisation of PDB is the major factor governing the crosslinking process and therefore the formation of hyperbranched structures. A higher value for the apparent reactivity of PDB (C_{PDB} = 0.3) was here obtained (Figures 3.23 and 3.24) indicating that intramolecular cyclizations are also present in ATRP but with a much lesser extent that in FRP. Note that simulations with the ATRP case study also have confirmed the negligible impact (at least with the operation conditions here considered) of intermolecular chain transfer to polymer and polymerisation of terminal double bonds, when compared with the crosslinking process. Estimated values of the reactivity ratios of PDB for ATRP process are also apparent due to the effect of intramolecular cyclizations. Figure 3.25 shows the effect of the monomer dilution in the ATRP of *n*BuA/BEDA copolymerisations at constant initial mole fraction of diacrylate (y_C = 5 %). These results confirm the importance of the intramolecular cyclizations reactions, even in ATRP. Estimated reactivity ratios of C_{PDB}= 0.3, 0.2 and 0.17 at V_M = 35, 25 and 15 %, respectively, show the increasing importance of this mechanism at higher dilutions.

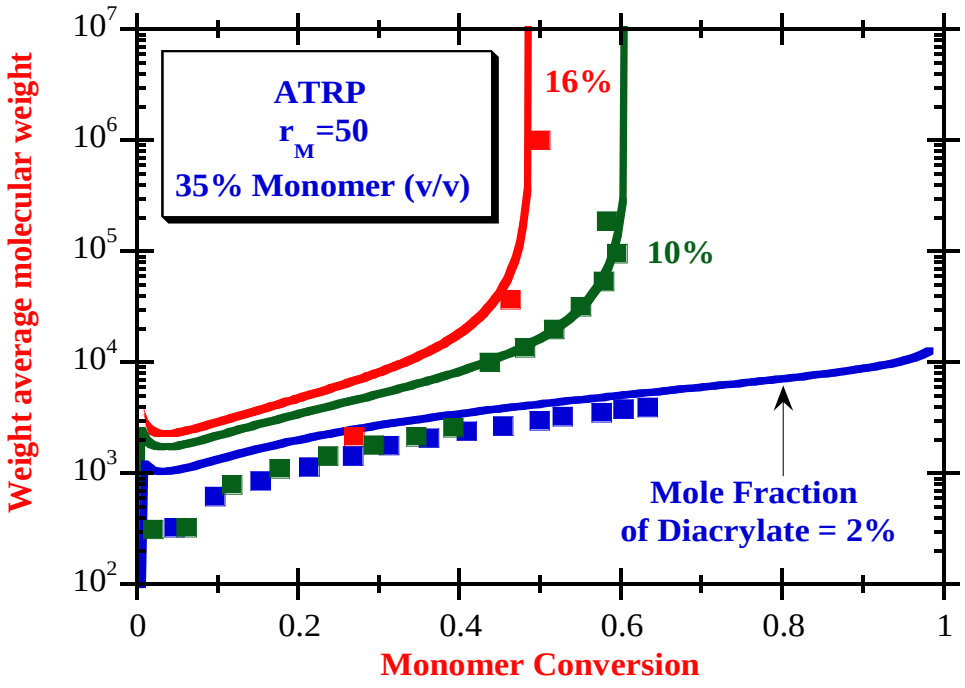

Figure 3.23. Effect of the initial amount of crosslinker in the evolution of $\bar{M}_w$ for ATRP copolymerisation of *n*BuA/HDDA.

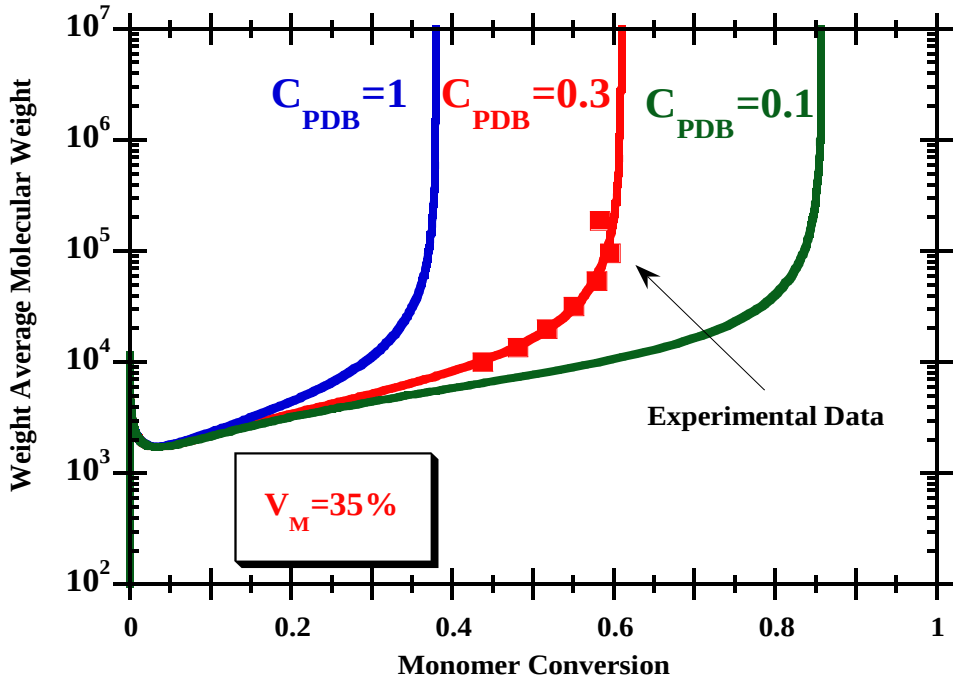

Figure 3.24. Predicted effect of the reactivity of pendant double bonds on $\bar{M}_w$ for ATRP of *n*BuA/HDDA (run 4 in Table 3.1).

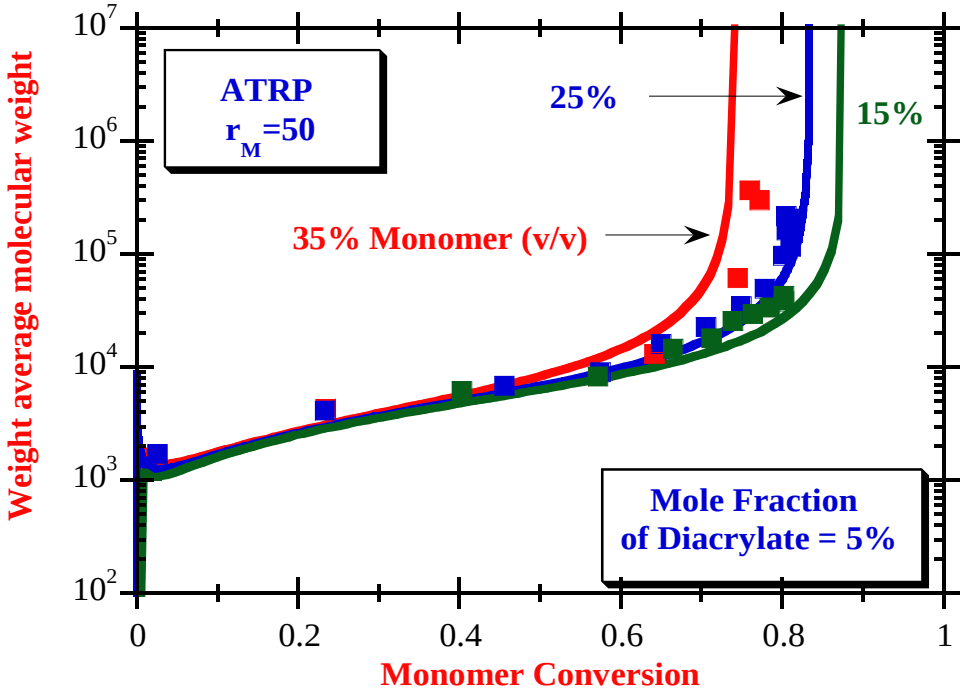

Figure 3.25. Effect of the dilution in ATRP copolymerisation of *n*BuA/BEDA.

In Figure 3.26 are compared FRP and ATRP *n*BuA/HDDA copolymerisations with the same initial dilution ($V_M = 35$ %) and the same amount of crosslinker ($y_C = 2$ %). Experimental results and simulations show the distinct behaviour of the crosslinking process when FRP and ATRP synthesis techniques are used. In fact, ATRP can be used at least to have a better control on the dynamics of gelation of acrylate/diacrylate polymerisation systems. Operation at higher contents of crosslinker without gelation is possible with ATRP when compared with FRP and this is an important issue in the production of hyperbranched polymers.

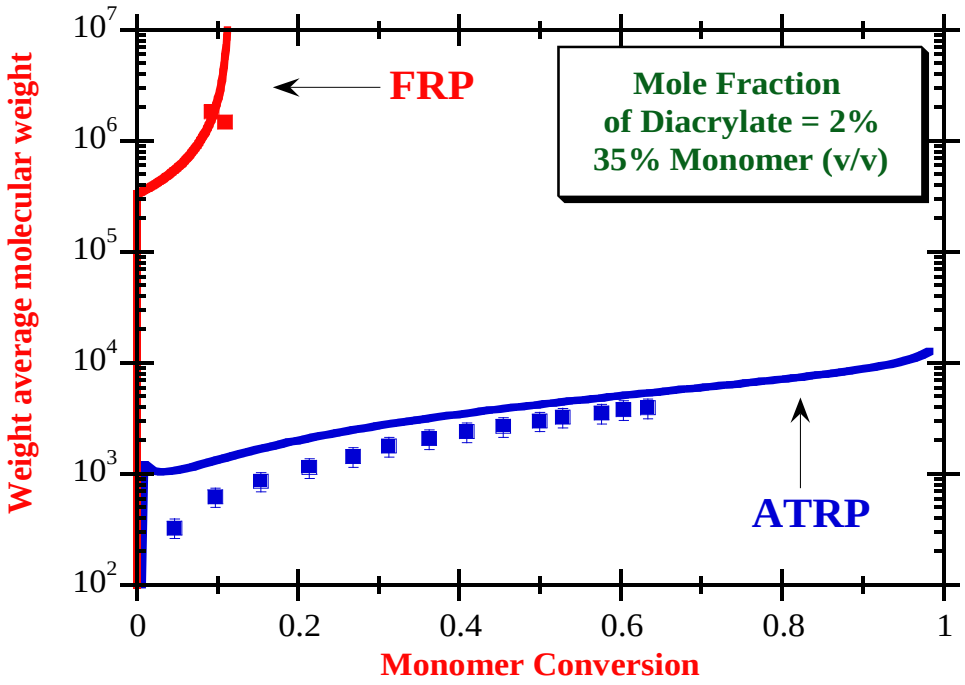

Figure 3.26. Comparison of FRP and ATRP copolymerisations of *n*BuA/HDDA with the same initial dilution and amount of crosslinker.

Figure 3.27 present the prediction of the dynamics of $\bar{M}_w$ for different values of the reactivity of the pendant double bonds of diacrylate monomer compared to *n*BuA. It should be noted that if, for instance, equal reactivity of PDB ($C_{PDB} = 1$) prevails, a substantial growth of $\bar{M}_w$ with monomer conversion is predicted, which was not confirmed experimentally, as can be observed in Figure 3.32. Experimental measurements can be explained if a decrease of the reactivity of PDB is considered, as also performed in the simulations presented in Figure 3.28 for polymerisations systems with higher diacrylate content ($y_C = 5$ % and $y_C = 16$ %), where the correspondent observed values of $\bar{M}_w$ are also presented in Figure 3.28.

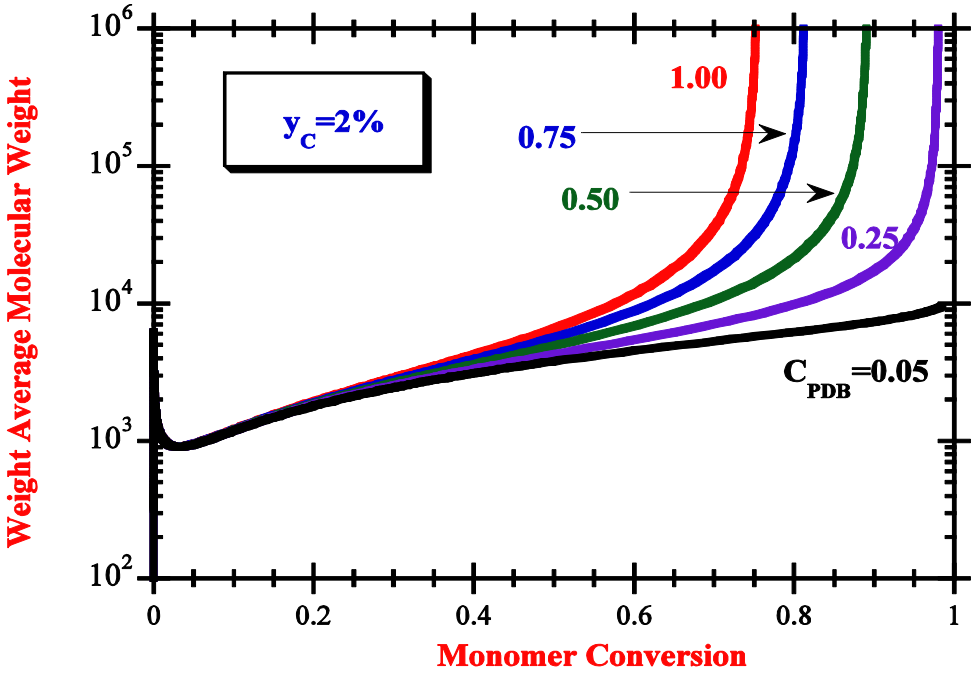

Figure 3.27. Predicted effect of the reactivity of the pendant double bonds (C_{PDB}) on the time evolution of $\bar{M}_w$ in the ATRP of *n*BuA/HDDA copolymerisation (run 3 in Table 3.1).

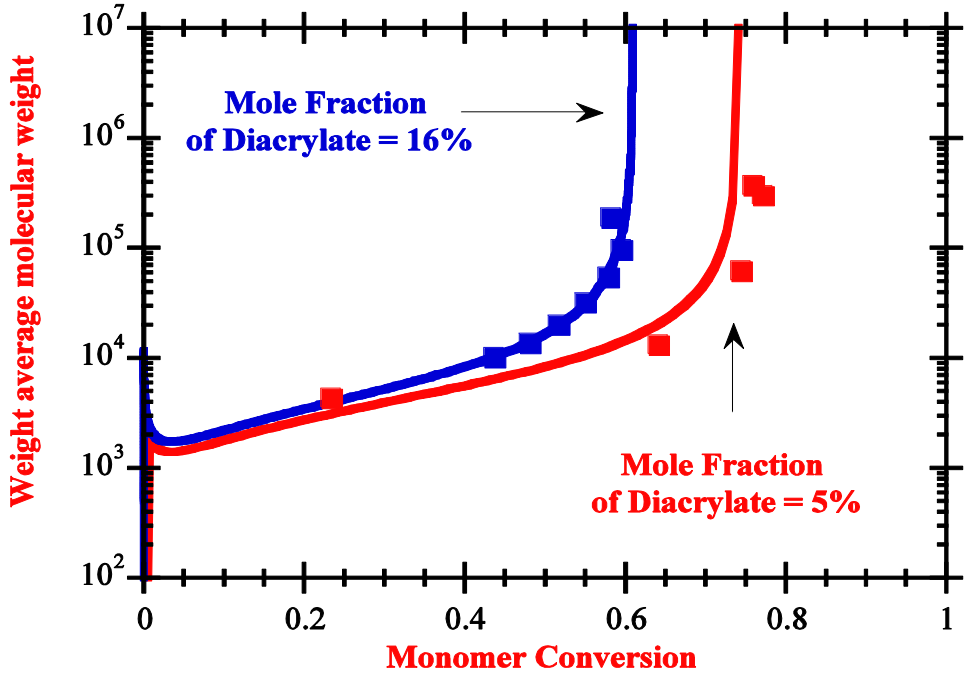

Figure 3.28. Predicted and observed evolution of $\bar{M}_w$ during the ATRP of *n*BuA/diacrylate considering different initial mole of crosslinker (runs 5 and 6 in Table 3.1).

Distinctive features of the used kinetic approach concerning the prediction of the dynamics of the *z*-average radius of gyration at Θ temperature are illustrated in Figure 3.29 and 3.30. The effect of the reactivity of pendant double bonds and of the initial mole fraction of crosslinker on the time evolution of this physical property is predicted for operation in batch reactor. These predictions can be compared with measurements of $\bar{R}_g$ performed in a good solvent.

The measured relation $\ln\left(\frac{[M]_0}{[M]}\right) = -\ln(1-p)$ *versus* time, for polymerisation of different ATRP experiments with *n*BuA is presented in Figure 3.31. The impact on the polymerisation rate of the use of two different initial mole ratios monomer/initiator can be assessed. The observed linear relations between these two quantities are consistent with the expected living character of these ATRP experiments and are also a major distinctive feature of this polymerisation technique compared to the conventional radical polymerisation (FRP) of the same monomers. The measured linear relations between weight average molecular weight ($\bar{M}_w$) and monomer conversion presented in Figure 3.32 underline the difference between the ATRP and FRP techniques.

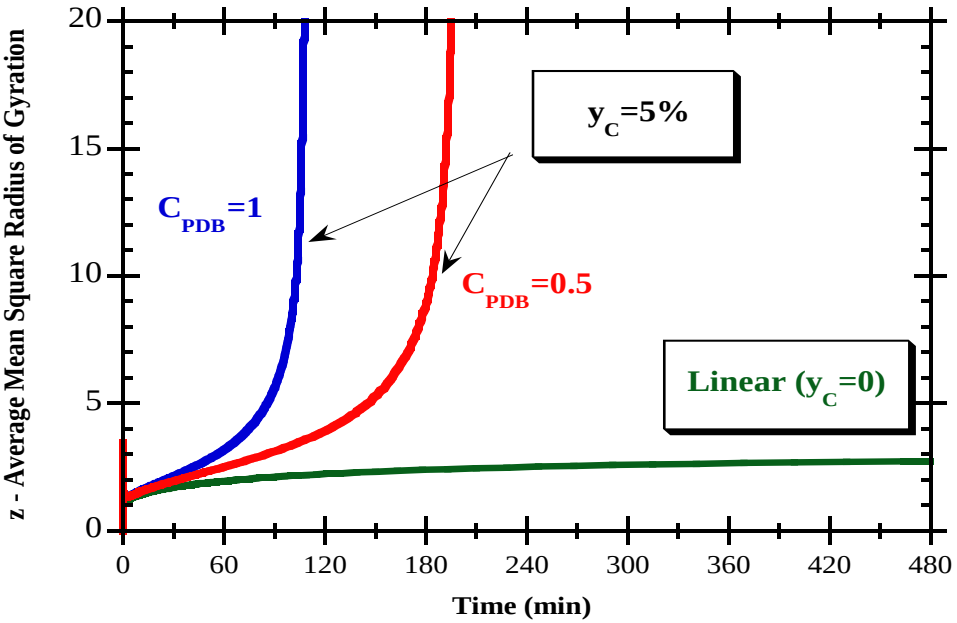

Figure 3.29. Predicted effect of the reactivity of PDBs on the dynamics of the $\bar{R}_g$ (Θ state and normalized by the bond length, $\bar{R}_g\,/b$) of ATRP synthesized polyacrylates. (Operating conditions: $T = 60$ °C, $V_M = 35$ %, $y_C = 0$ %, r_M/CuBr/PMDETA=50/0.45/0.5. Kinetic parameters: $C_{fpH} = 10^{-4}, C_{fpCH_3} = 10^{-5}$, $C_{TDBM} = C_{TDBD} = 1$, $R_{INT} = R_{PDB} = 0.1$, $R_{AM} = 1, \alpha_{td} = 5$ %, $k_{ATRP} = 1.25 \times 10^{-10}, C_I = 1$).

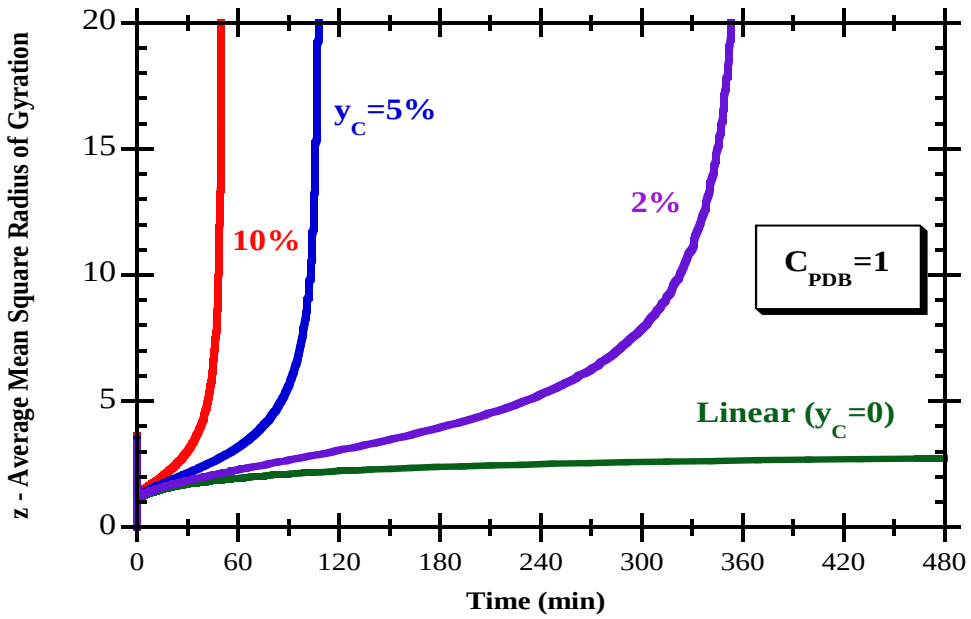

Figure 3.30. Predicted effect of the initial mole fraction of crosslinker on the dynamics of the $\bar{R}_g$ of ATRP synthesized polyacrylates (same conditions of Figure 3.29).

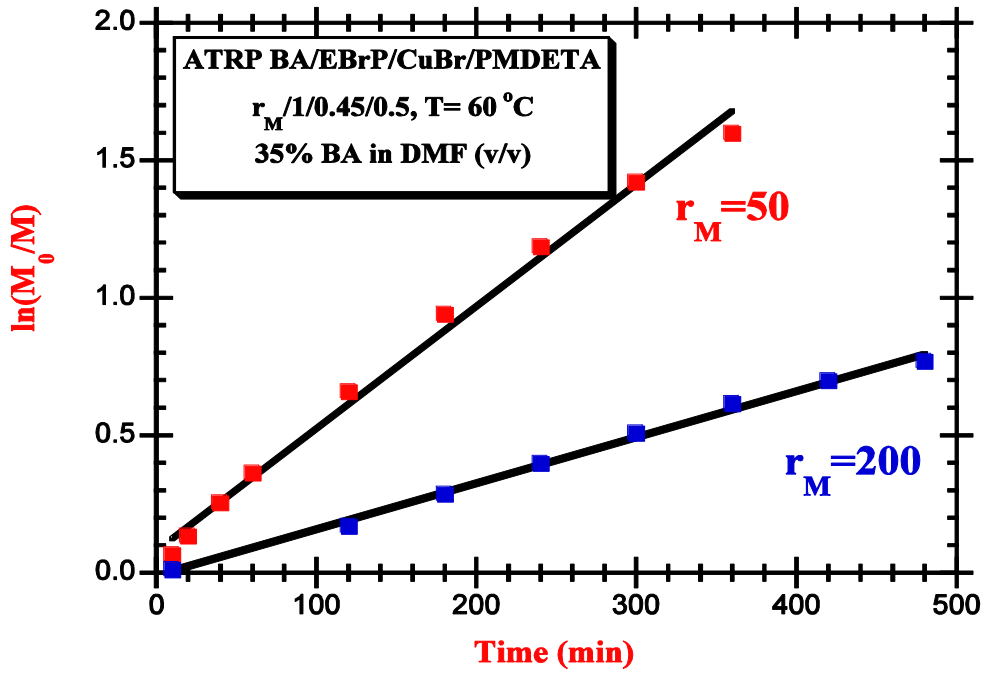

Figure 3.31. Measured relation $\ln\left(\frac{[M]_0}{[M]}\right) = -\ln(1-p)$ *versus* time of polymerisation in different ATRP experiments of *n*BuA.

Non-linear ATRP experiment included in Figure 3.32 with $y_C = 2\,\%$ also shows important advantages of ATRP relative to FRP for the production of hyperbranched polymers, i.e., the ability to operate with higher crosslinker mole fraction without gel formation. It should be noted that similar FRP operation leads to gelation when the monomer conversion is around 0.1. In Figure 3.33 is shown that the initial molar ratio between monomer and initiator (r_{M}) can also be used, through the manipulation of the length of the primary chain, to control the crosslinking process and therefore to help in the production of tailored hyperbranched polymers. Measured and predicted evolution of the *z*-average radius of gyration ($\bar{R}_g$) for FRP acrylate/diacrylate copolymerisations performed with different amounts of diacrylate are presented in Figure 3.34.

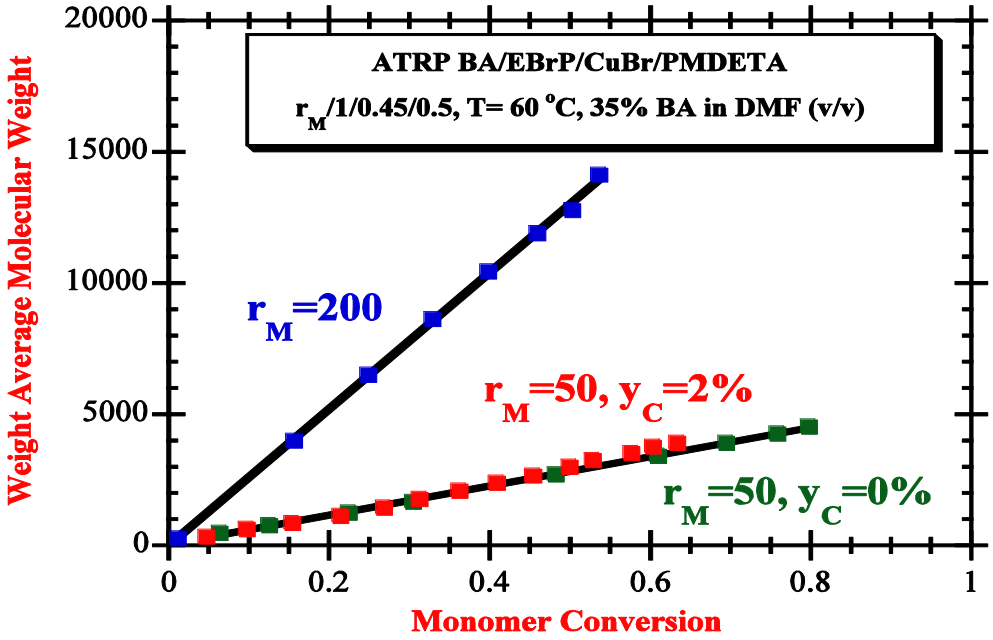

Figure 3.32. Observed relation of $\bar{M}_w$ versus monomer conversion in linear (*n*BuA) and non-linear (*n*BuA/HDDA) experiments considering different initial mole ratios monomer/initiator (r_{M}).

Calculations of $\bar{R}_g$ have been carried out using the same set of kinetic parameters as in the calculations of molecular weights. Despite the huge simplifications above discussed which were used in the prediction of $\bar{R}_g$, a good agreement between experimental observations and predictions is obtained with different conditions. Figure 3.35 shows predicted and observed monomer conversion evolution of $\bar{R}_g$ and $\bar{M}_w$ in *n*BuA/BEDA ATRP copolymerisation with initial mole fraction of diacrylate $y_C = 5\,\%$ and $r_{\mathrm{M}} = 200$. A simultaneous good agreement

between measurements and predictions of average molecular weights and *z*-average radius of gyration is observed, confirming this general kinetic approach as a valuable tool to predict and design some important features of the molecular architecture of such complex materials.

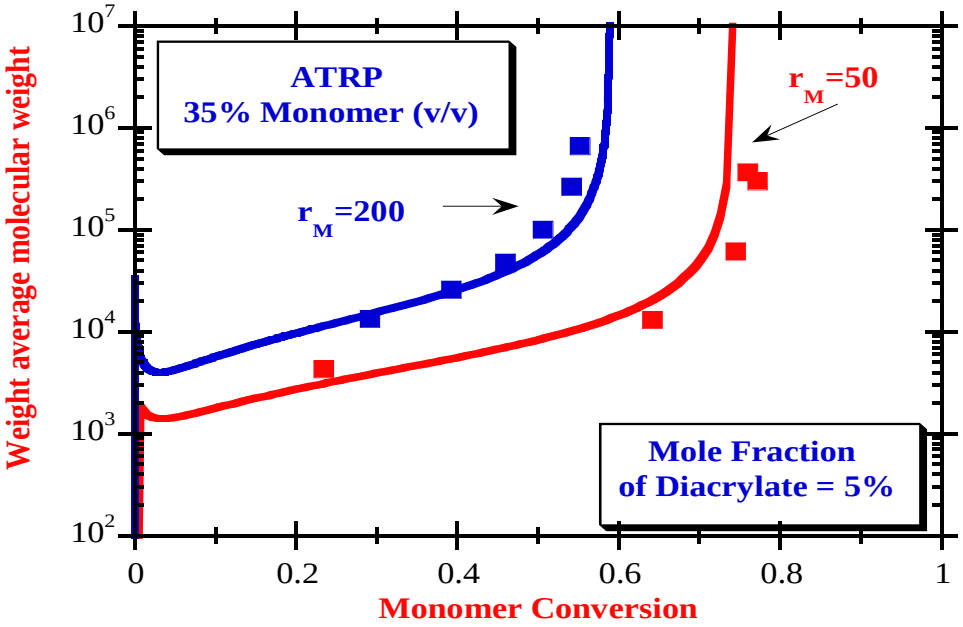

Figure 3.33. Effect of the initial ratio monomer/initiator in ATRP copolymerisation of *n*BuA/BEDA.

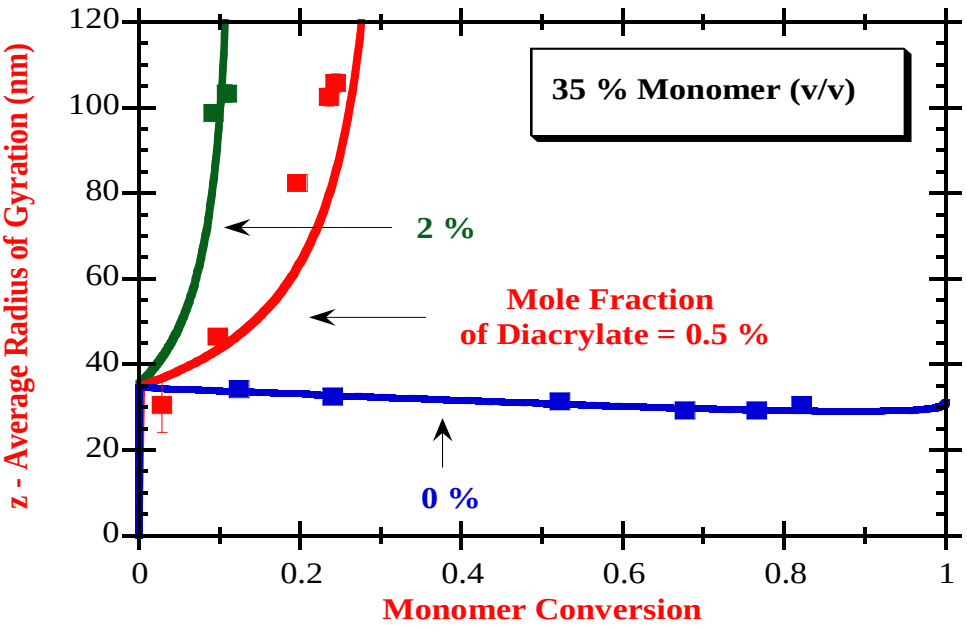

Figure 3.34. Measured and predicted evolution of $\bar{R}_g$ in FRP homopolymerisation on *n*BuA and *n*BuA/HDDA copolymerisation with different amounts of diacrylate.

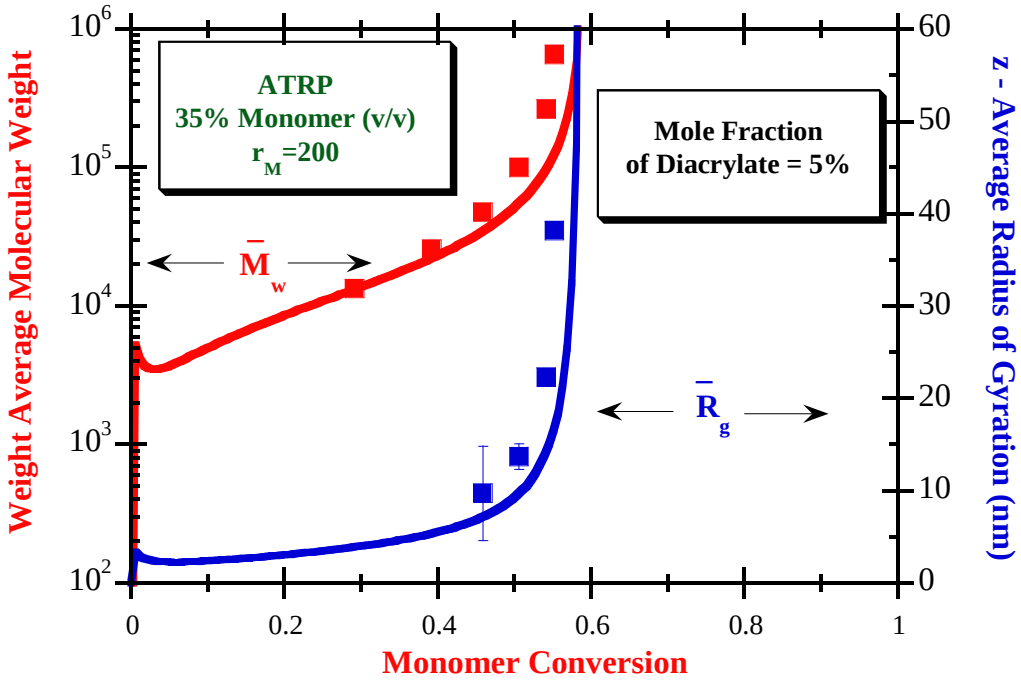

Figure 3.35. Measured and predicted evolution of $\bar{R}_g$ and $\bar{M}_w$ in *n*BuA/BEDA ATRP copolymerisation (run 9 in Table 3.1).

Typical SEC traces observed by SEC/RI/MALLS of ATRP synthesized polymer samples are presented in Figure 3.36. It should be noted that only the RI signal is presented here. The analysis by SEC/RI/MALLS of samples collected at different polymerisation times allows the estimation of the dynamics of monomer conversion, molecular weights and *z*-average radius of gyration ($\bar{R}_g$).

Figure 3.37 shows the predicted influence of intermolecular chain transfer to polymer on $\bar{M}_w$ for the solution FRP of *n*BuA at $T = 60$ °C, $V_M = 35$ %, $\frac{[I]_0}{[M]_0} = 0.1$ and $y_C = 0$ %. (without crosslinker). In these simulations, a basic set of kinetic parameters presented in Table 3.8 was considered and the magnitude of intermolecular chain transfer to polymer was changed through the parameter $C_P = C_{fpH} = 10 \times C_{fpCH_3}$. Other parameters were fixed in the simulations, namely those related to polymerisation of terminal double bonds ($C_{TDB} = C_{TDBM} = C_{TDBD} = 0$), reactivity of internal polymer radicals ($R_{INT} = 10^{-2}$), reactivity of radicals derived from chain transfer to monomer ($R_{AM} = 1$) and fraction of termination by disproportionation $\alpha_{td} = 5$ %. Simulations are compared with experimental observations for $\bar{M}_w$ obtained in the solution (toluene) polymerisation of *n*BuA in the same operation

conditions. These results are consistent with a reactivity ratio for intermolecular chain transfer to polymer at most about $C_P = 10^{-4}$. Gelation (not observed) is predicted only for much higher values of C_P (e.g. 10^{-3}). Note that chain transfer to solvent is a very important competitive mechanism with chain transfer to polymer which explains the modest incidence of the latter in diluted solution.

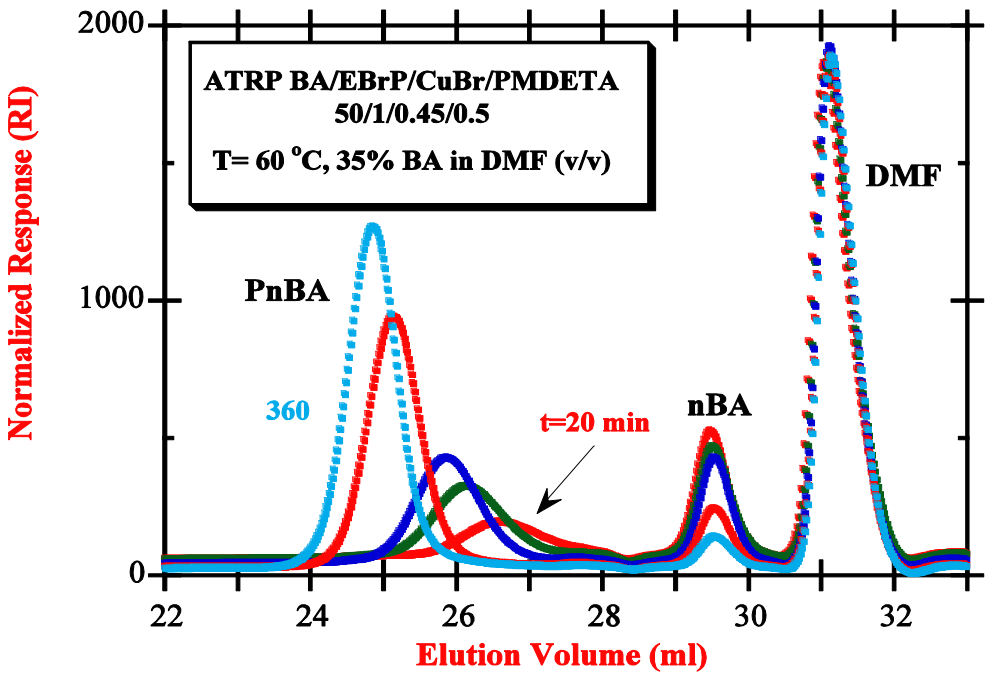

Figure 3.36. Typical SEC traces observed in the characterization by SEC/RI/MALLS of ATRP synthesized polymer samples (only RI signal is shown).

Figure 3.38 shows the predicted effect (through changes in the parameter C_{TDBM}) on $\overline{M}_w$ of the polymerisation of terminal double bonds created by chain transfer to monomer. Two initial dilutions were considered ($V_M = 35\ \%$ and $V_M = 100\%$), and the remaining parameters were considered: $T = 60$ °C, $\frac{[I]_0}{[M]_0} = 0.1\ \%$, $y_C = 0\ \%$ and $C_P = C_{fpH} = C_{fpCH_3} = 0$, $C_{TDBD} = 1$, $R_{INT} = 10^{-2}$, $R_{AM} = 1$, $\alpha_{td} = 5\ \%$. Hence, this comparison confirms the almost negligible effect of LCB, now via polymerisation of terminal double bonds, at higher dilutions. LCB should be more important at nearly bulk polymerisation and/or very high monomer conversions.

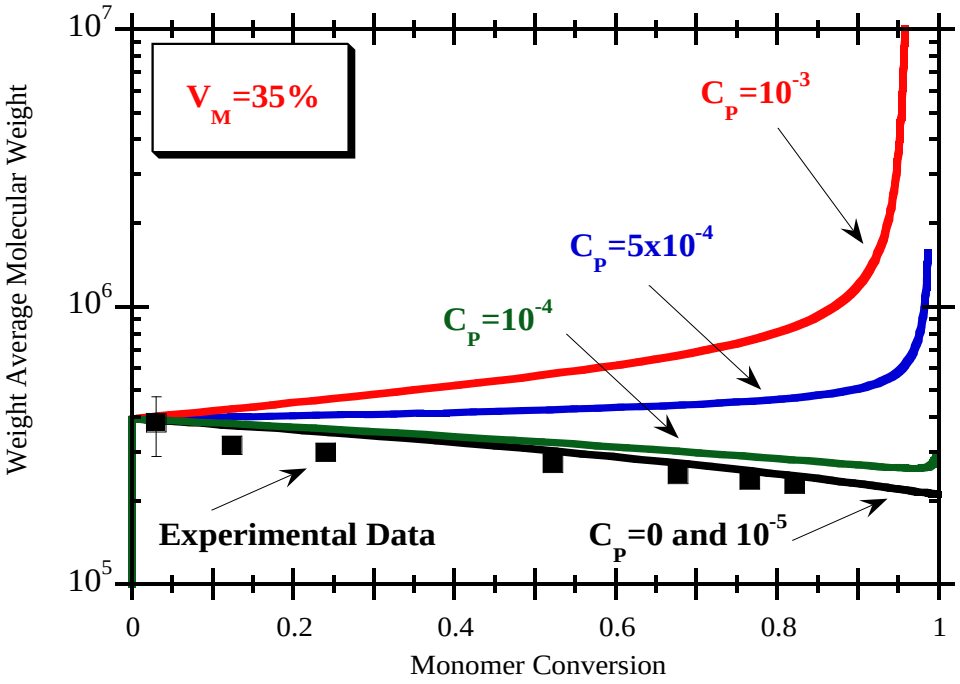

Figure 3.37. Predicted influence of intermolecular chain transfer to polymer on $\bar{M}_w$ for FRP of *n*BuA (run 6 in Table 3.2).

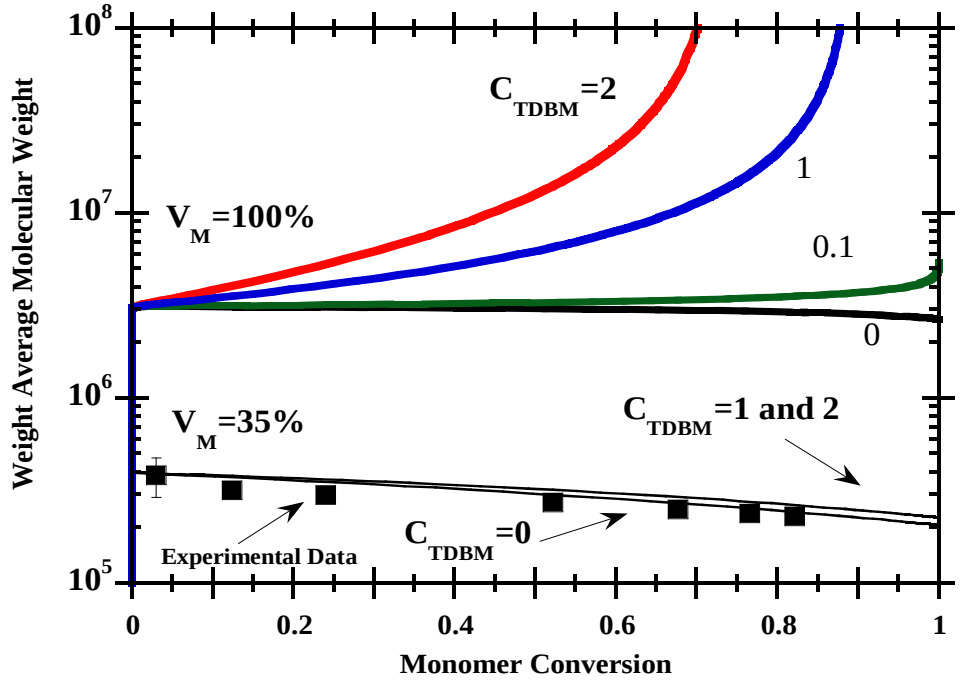

Figure 3.38. Predicted influence of terminal double bonds on $\bar{M}_w$ for FRP on *n*BuA at different dilutions (runs 1 and 5 in Table 3.2).

The predicted influence of intermolecular chain transfer to polymer on $\bar{M}_w$ for the solution ATRP of *n*BuA at $T = 60$ °C, $V_M = 35$ %, r_M/CuBr/PMDETA= 50/0.45/0.5 and $y_C = 0$ % is put into evidence in Figure 3.39. Chain transfers to polymer centres were distinguished ($C_P = C_{fpH} = 10 \times C_{fpCH_3}$) and the following simulation parameters were also considered: $C_{TDB} = C_{TDBM} = C_{TDBD} = 1$, $R_{INT} = 10^{-1}$, $R_{AM} = 1$ and $\alpha_{td} = 5$ %. Comparison with experimental results shows that, at higher dilutions, the influence of LCB in ATRP should also be very low. Note that the incidence of termination reactions, namely termination by combination, is much more pronounced in FRP than in ATRP. Termination by combination plays a special role in LCB development, namely in gel formation due to this mechanism. Even increasing the primary chain length (increasing the initial ratio $\frac{[M]_0}{[I]_0}$), under the experimental conditions here used, LCB has a tiny contribution for the formation of non-linear structures in ATRP. In Figure 3.40 it is shown the relation $\bar{R}_g$ *versus* $\bar{M}_w$ for FRP (*n*BuA/HDDA, $y_C = 0.5$ %, and ATRP (*n*BuA/BEDA, $y_C = 5$ %, $[M]_0/[I]_0 = 200$) synthesized hyperbranched polyacrylates. Good agreement between experimental measurements and predictions is observed for both systems, confirming the good predictive power of the theoretical approach (Costa and Dias, 2007) used in the simulations despite the remaining uncertainty concerning the magnitude of the expansion factor for branched polymers.

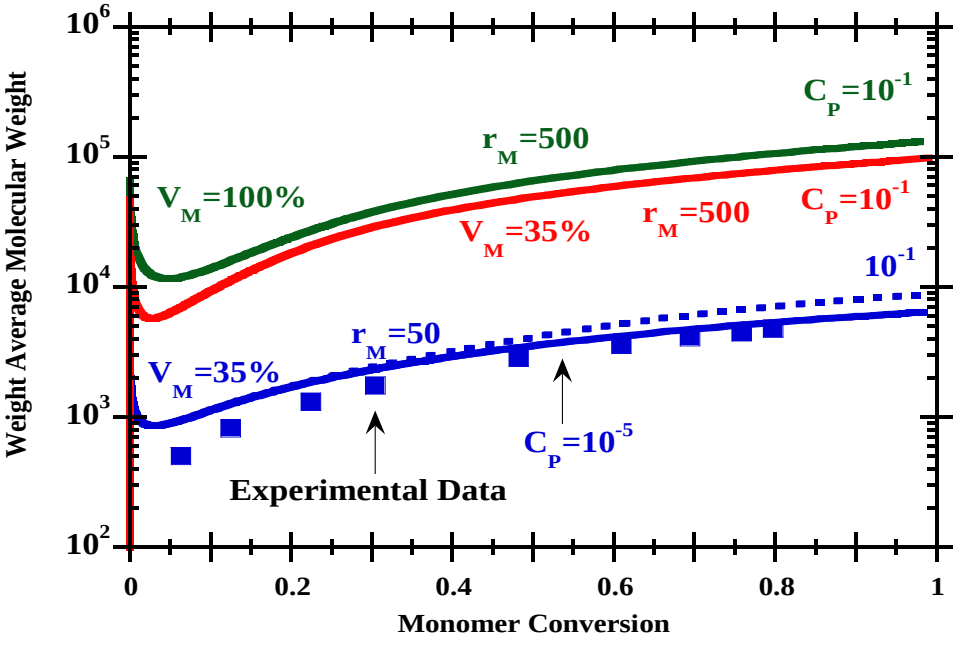

Figure 3.39. Predicted influence of long chain branching for the ATRP of *n*BuA (run 2 in Table 3.1).

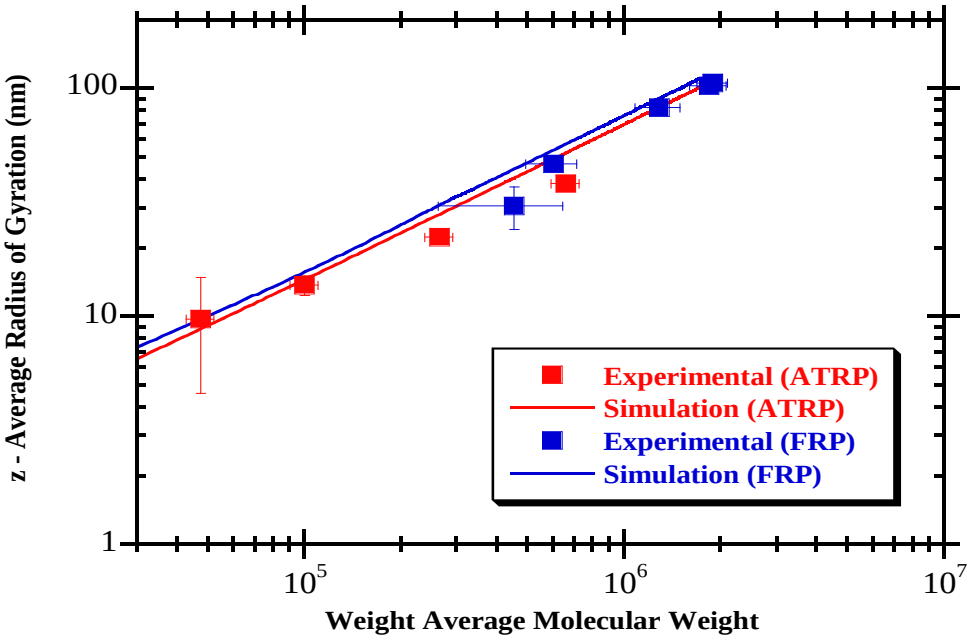

Figure 3.40. Relation $\bar{R}_g$ *versus* $\bar{M}_w$ for FRP (run 7 in Table 3.2) and ATRP (run 9 in Table 3.1) hyperbranched polyacrylates.

Interestingly, with all these branched polymers a nearly identical relation $\bar{R}_g$ *versus* $\bar{M}_w$ is observed despite the expected structural dissimilarities between their formation by FRP and ATRP. For the results presented in Figure 3.40, a scaling law $\bar{R}_g = K_G \bar{M}_w^{\nu}$ is observed and the estimated exponent is $\nu = 0.65$ which deviates from the value $\nu = 0.5 - 0.6$ expected for linear random coils. Polymer physics of branched/crosslinking polymers is a complex subject with important observed deviations from a power law behaviour, as reported recently for branched polysaccharides (Rolland-Sabaté *et al.*, 2008). A more rigorous theory for the prediction of physical properties of non-linear polymers should more correctly calculate the effect of excluded volume expansion and take into account the presence of intramolecular loops.

The predictive value of the developed kinetic model is hampered by the high number of kinetic parameters to be known. This problem has been often alleviated by performing a sensitivity analysis of the predictions leaving only a restricted set of kinetic parameters to fit. Indeed, for these systems this approach shows that LCB is a minor effect as compared to crosslinking. Other uses of this strategy are illustrated in Figure 3.41 where additional results concerning the sensitivity analysis of the kinetic parameters are shown, namely concerning the influence of the reactivity of the radicals from transfer to monomer. These simulations

show that, if the radicals from transfer to monomer are reactive enough, under bulk polymerisation, gelation can occur due to LCB originated by chain transfer to monomer. A different combination of kinetic parameters was considered in the simulations presented in Figure 3.42 (where the dynamics of crosslinking/branching density (average number of crosslinking/branching sites per polymer molecule). Here crosslinking and LCB are both considered and different reactivities are assumed for different kinds of polymer radicals. Note the much higher contribution of crosslinking to the non-linear density, comparatively to LCB.

The interpretation of SEC/RI/MALLS with branched/crosslinked polymer samples is a particularly difficult task because two different values in the relation molecular mass versus elution volume are possible as reported in some recent works (Bannister *et al.*, 2006). These observations are a consequence of the existence in non-linear polymers of populations with the same molecular weight but very different molecular sizes. Important advances concerning the theory of multiple-detection by SEC of non-linear polymers were recently obtained showing that some current commercial software used in the calculation of average molecular weights are affected by significant errors (Gaborieau, *et al.*, 2007).

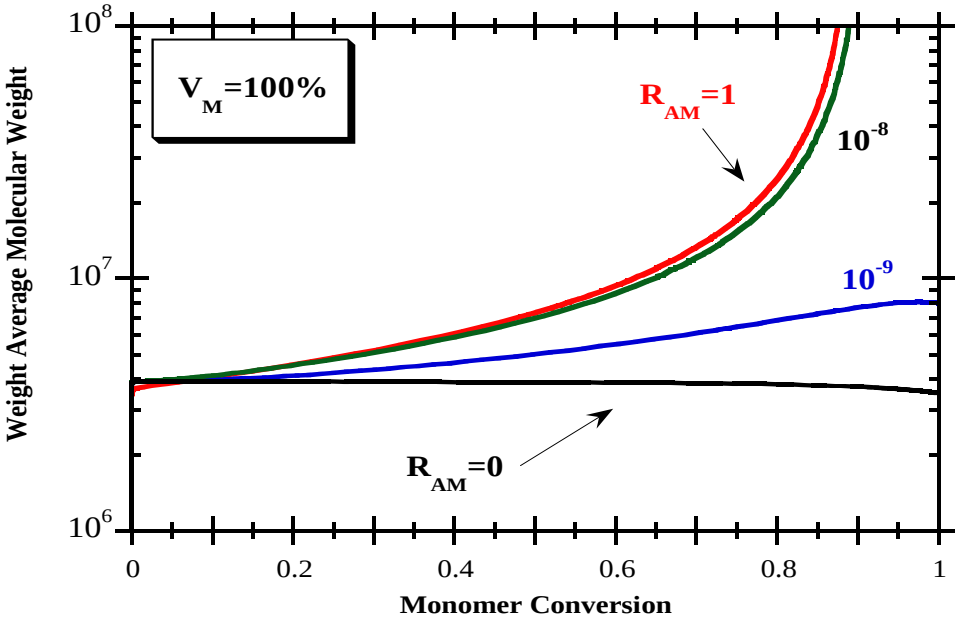

Figure 3.41. Predict effect of the reactivity of radicals from transfer to monomer on $\bar{M}_w$ of FRP synthesized polyacrylates (operating conditions: $T = 60$ °C, $V_M = 100$ %, $[I]_0/[M]_0 = 0.1$ %, $y_C = 0$ %. Kinetic parameters: $C_P = C_{fpH} = C_{fpCH_3} = 0$, $C_{TDBM} = C_{TDBD} = 1$, $R_{INT} = 10^{-2}$, $\alpha_{td} = 5$ %).

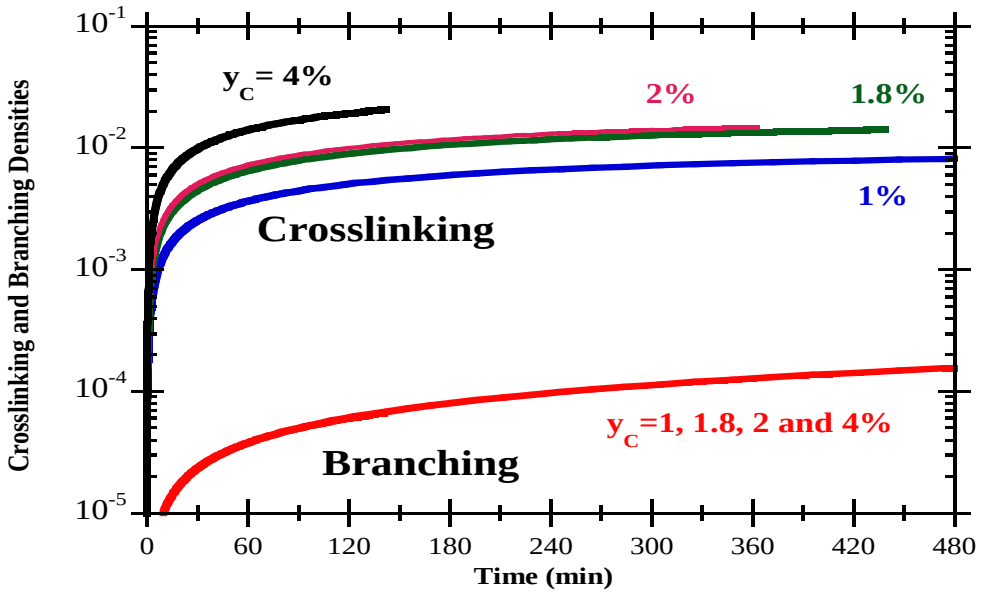

Figure 3.42. Predicted effect of the initial amount of crosslinker on the dynamics of crosslinking and branching densities of ATRP synthesized polyacrylates (operating conditions: $T = 60$ °C, $V_M = 35$ %, r_M/CuBr/PMDETA=50/0.45/0.5. kinetic parameters: $C_{fpH} = 10^{-4}, C_{fpCH_3} = 10^{-5}, C_{PDB} = C_{TDBM} = C_{TDBD} = 1, R_{INT} = R_{PDB} = 0.1,\ R_{AM} = 1, \alpha_{td} = 5$ %).

A rigorous interpretation of the SEC traces of non-linear should take into account these reported limitations and also the difficulties associated with the existence in these polymer populations of position isomers leading to molecules with the same molecular weight but different molecular size. As far as it is of our knowledge this is an open issue.

In Figure 3.43 are presented the measured refractive index and light scattering (90°) signals in the SEC trace of an ATRP synthesized acrylate/diacrylate sample. The detection by SEC/RI/MALLS of a polymer cluster with high molecular weight but with very low concentration is detected when gelation is approached. In the same figure, the change of the molar mass with the elution volume is also presented. Molar mass and radius of gyration of each slice in a SEC/RI/MALLS system are often calculated using a Debye plot, as exemplified in Figure 3.44 with $X_D = \sin^2\left(\frac{\Theta}{2}\right)$ and $Y_D = K^* \frac{c}{R(\Theta)}$. The intercept with the Y axis yields the molar mass and the slope of the fitted straight line yields the radius of gyration. Using this information and considering that each slice is monodispersed, it is possible to obtain estimates of the differential weight fractions of the molar mass and radius of gyration distributions, as exemplified in Figures 3.45 and 3.46 for branched polyacrylates. In this case, multimodal distributions seem to occur. Multimodal CLD in controlled living polymerisation

of vinyl/divinyl monomers were recently predicted using the present kinetic approach (Dias and Costa, 2010).

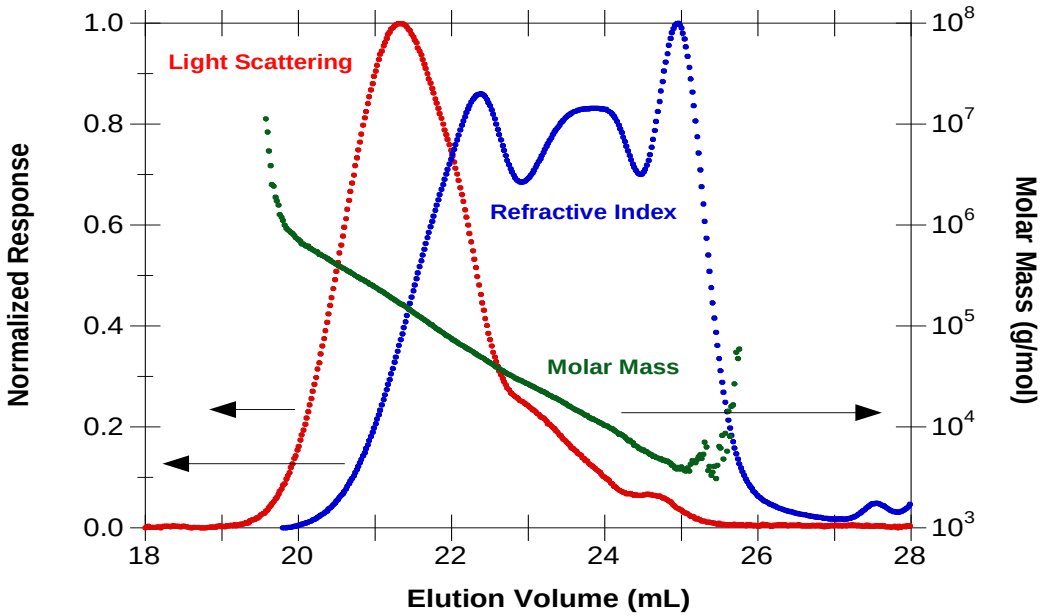

Figure 3.43. Measured refractive index and light scattering (90°) signals in the SEC trace of ATRP synthesized acrylate/diacrylate sample. Change of absolute molecular weight along the elution volume is also shown.

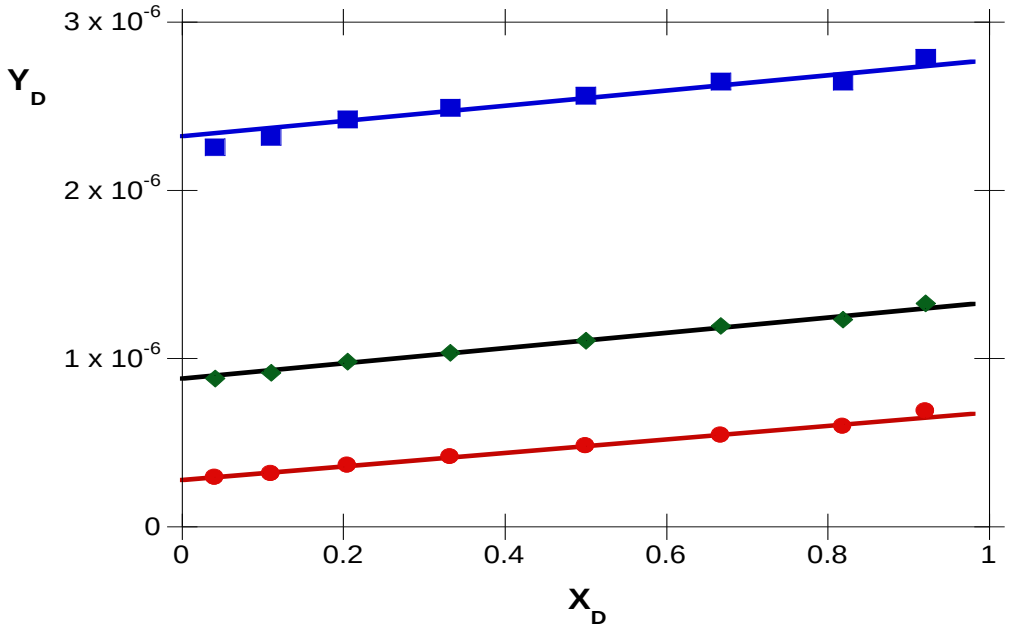

Figure 3.44. Examples of Debye plots along the SEC trace of a branched polyacrylate sample. Three different elution volumes were considered and the measured signals with the eight MALLS detectors are shown.

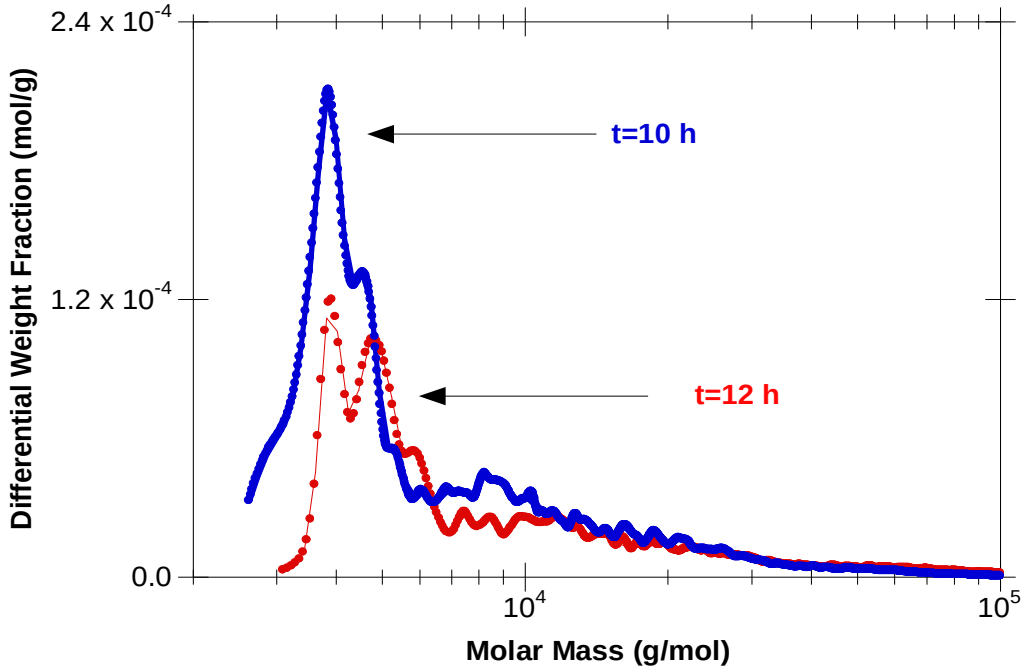

Figure 3.45. Typical differential weight fraction of the molar mass distributions measured for branched polyacrylate samples. Time evolution of the crosslink process can be observed.

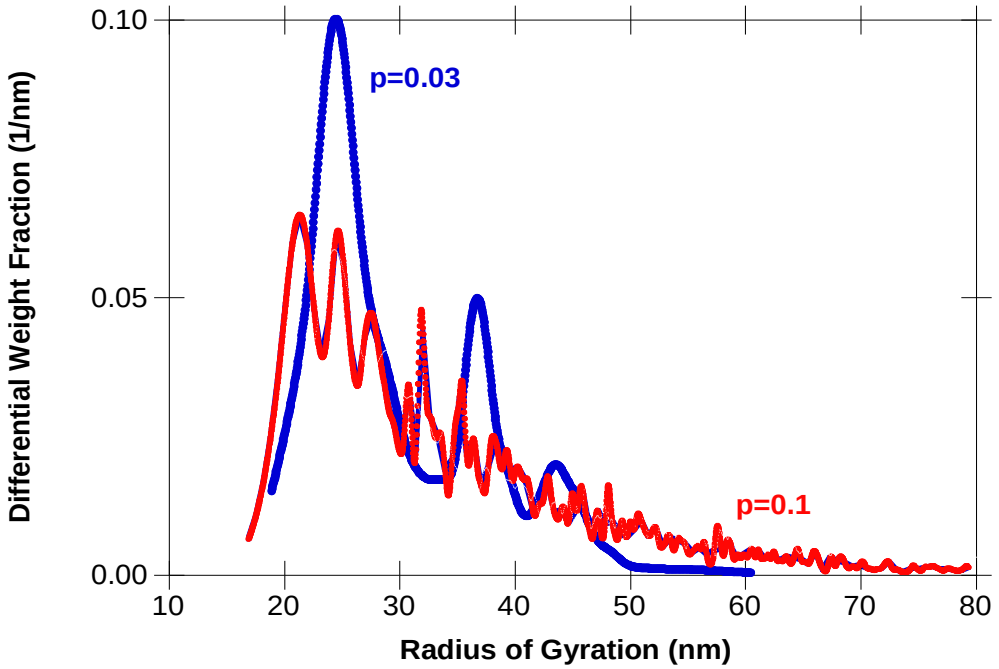

Figure 3.46. Typical differential weight fraction of the radius of gyration distributions measured for branched polyacrylate samples. Change of the distribution with monomer conversion is depicted.

Thus, this set of experimental (Tables 3.1 and 3.2) and theoretical studies performed with the ATRP and FRP of *n*BuA/diacrylate monomers shows the important impact of intramolecular cyclizations in the production of hyperbranched polymers. This phenomenon increases as expected when the monomer concentration decreases and improved homogeneity (minimization of intramolecular cyclizations formed at low conversions) is expected at bulk polymerisations. A further important outcome of this research is the confirmation that at the same monomer concentration, the impact of cyclization is much reduced in ATRP as compared to FRP. Kinetic modelling studies also shown that, under the experimental conditions considered, branching mechanisms by chain transfer to polymer and polymerisation of terminal double bonds are negligible in comparison with the governing crosslinking process, which is the polymerisation of PDBs. This set of conclusions shows the usefulness of the detailed kinetic model presented here for this complex polymerisation system.

3.4.2 ATRP of MMA/EGDMA

The observed SEC/RI/MALLS traces of ATRP MMA/EGDMA polymer samples collected at different polymerisation times are shown in Figure 3.47. It should be noted that only the RI signal is shown here. These SEC traces correspond to the non-linear copolymer samples synthesized using a mixture of anisole and DMF as solvent (50 % volume of MMA) at $T =$ 80 °C and with an initial mole fraction of EGDMA in monomer mixture $y_C = 0.5$ The initial mole ratio between MMA and ATRP initiator was MMA/MBPA = 500 and the remaining reactants content verify the proportions MBPA/CuBr/HMTETA = 1/1/1. Experimental observations such as those presented in Figure 3.47 are especially important in the synthesis of hyperbranched, or generically non-linear, polymers since the time evolution of the crosslinking process can be measured. For instance, from Figure 3.47 it is possible to conclude that for t = 1 h, the polymer population is dominated by linear chains (primary). The formation of non-linear structures is observed as the reaction time proceeds and a large cluster with low concentration can also be detected as gelation is approach at t = 5.6 hours. Figure 3.48 shows the measured light scattering signal (90°) in the SEC traces for the same sample in Figure 3.47 with samples corresponding to different polymerisation times. Here the closeness to the gel point can be detected by the gradual formation of a cluster of high molecular weight albeit at very low concentration. Note that the RI signal corresponding to the high molecular weight region is very weak, as depicted in Figure 3.49. In this figure it is also shown the

molecular weight along the SEC trace for an ATRP synthesized sample of MMA/EGDMA corresponding to a polymerisation time close to the gel point. Note that a huge deviation from the linear case is here identified. Figure 3.49 also shows that erroneous interpretations of chromatograms of non-linear polymers will result from using molecular weight calibration with linear polymers.

An important distinctive feature of the general kinetic approach used here is the ability to predict the *z*-average radius of gyration of non-linear polymers when Θ conditions prevail ($\bar{R}_{g\Theta}$) (Costa and Dias, 2007). Generally, experimental measurements are performed with good solvents (THF at 30 °C in the present work), and therefore, the molecular expansion (excluded volume effect) must be taken into account when predictions are compared with the observed values ($\bar{R}_g$), and a good estimation of the excluded volume effect taking into account the full complexity of molecular structure within the framework of the current kinetic approach as still to be developed. For the time being, the expansion factor of linear chains to a scaling power has been used. Despite these difficulties, a good agreement between measurements and predictions is observed for the description of the dynamics of $\bar{R}_g$ in batch/semi-batch reactors of FRP and CRP processes (Trigo *et al*, 2008; Gonçalves *et al*., 2007). The kinetic model presented above for the ATRP of acrylates was used to predict $\bar{R}_g$ and simulations of the dynamics of such properties in a batch reactor for polymerisations systems with different initial amounts of EGDMA are presented in Figure 3.50. The measured values of $\bar{R}_g$ for the corresponding set of experiments (Table 3.3) are also presented and important deviations between predictions and measurements are observed for long polymerisation times. It should be noted that a loss of accuracy in the measurements is expected for $\bar{R}_g$in the range of 10-20 nm as the lower detection limit of the MALLS detector is approached. Conversely, a good agreement between measurements and predictions is observed for run 4. Lack of control of ATRP at higher temperatures (90 °C) and the effect of intramolecular cyclizations are plausible sources of the discrepancies observed. Indeed, for this polymerisation system, the reactivity ratio of PDB was estimated to be $C_{PDB} = 0.45$, which, in the same way as the value for *n*BuA/diacrylates system, is probably underestimated. Figure 3.51 shows the predicted and observed time evolution of $\bar{M}_w$ in copolymers produced by ATRP MMA/EGDMA using different mole fractions of EGDMA at 90 °C. Here important deviations between measurements and predictions are observed at low EGDMA contents. This can be a consequence of the aforementioned lack of control of ATRP at high temperatures.

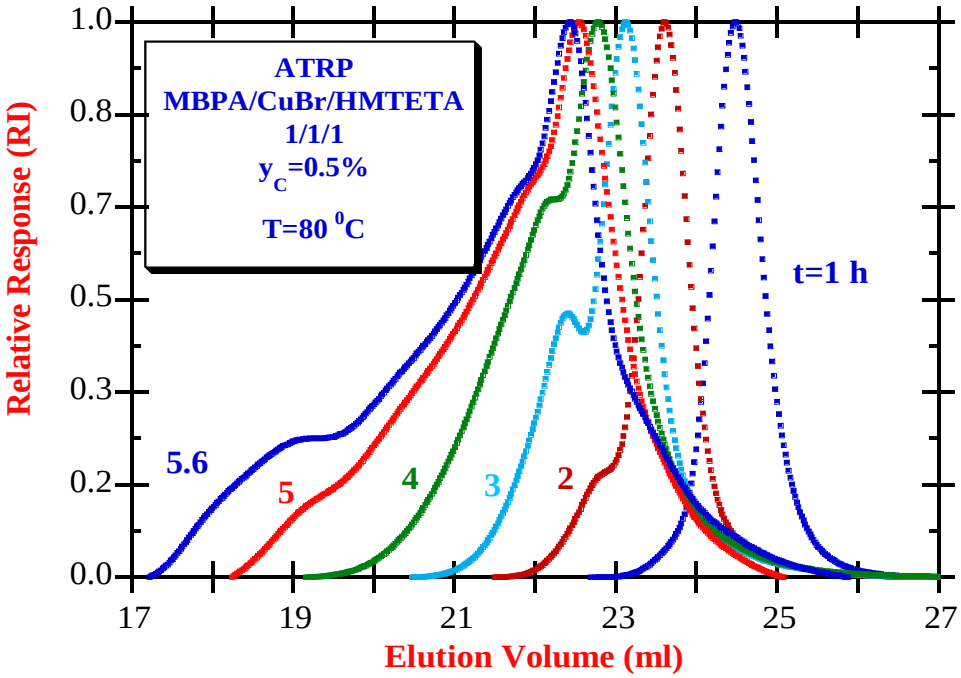

Figure 3.47. Observed SEC/RI/MALLS traces (only RI signal) of ATRP MMA/EGDMA (run 5 in Table 3.3) polymer samples collected at different polymerisation times.

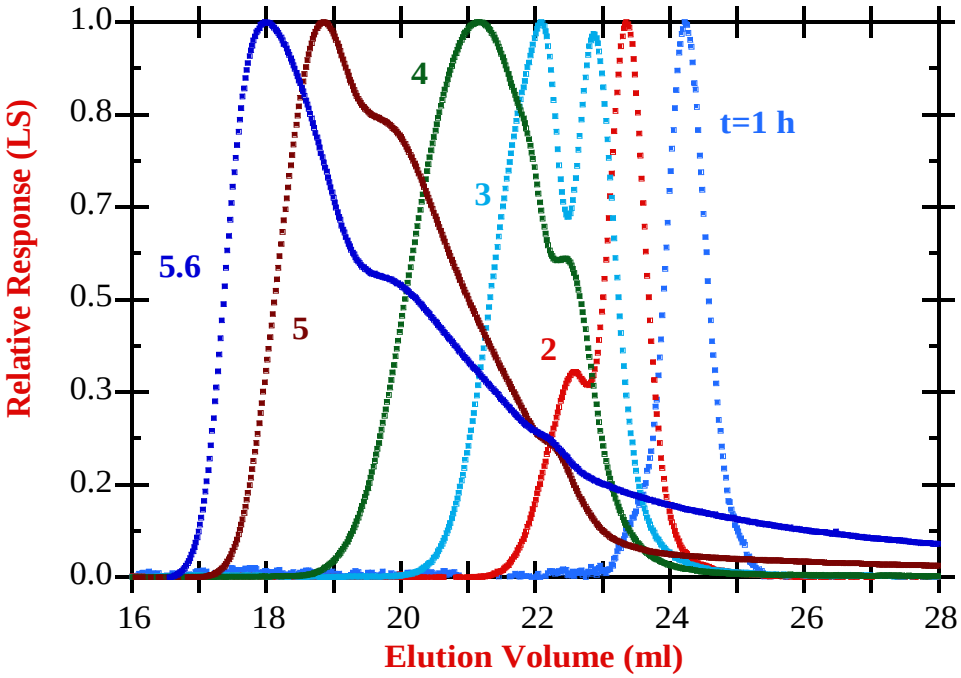

Figure 3.48. Observed SEC/RI/MALLS traces (only LS signal) of ATRP MMA/EGDMA (run 5 in Table 3.3) polymer samples collected at different polymerisation times.

Figure 3.52 depicts a kinetic plot showing the living character of ATRP runs at different temperatures. It is well known that the variable $\ln\left(\frac{[M]_0}{[M]}\right) = -\ln(1-p)$ should ideally follow a linear relation with polymerisation time and this is confirmed by the experimental observations presented in Figure 3.52. The effects of ligand and initiator structures on the equilibrium constants for ATRP were recently studied (Tang *et al.*, 2008) and for EBPA (ethyl α-bromophenylacetate) an activation rate constant $k_a = 140\ \mathrm{dm^3 mol^{-1} s^{-1}}$ is reported at 22 °C in acetonitrile and using the pair CuBr/HMTETA. In the same work, the correspondent equilibrium constant is estimated to be $K_{ATRP} = \frac{k_a}{k_{da}} = 1.1 \times 10^{-4}$. Similar rate coefficients should be valid for MBPA. Nevertheless, our kinetic measurements are consistent with much lower equilibrium constant values, namely of the order 10^{-8}.

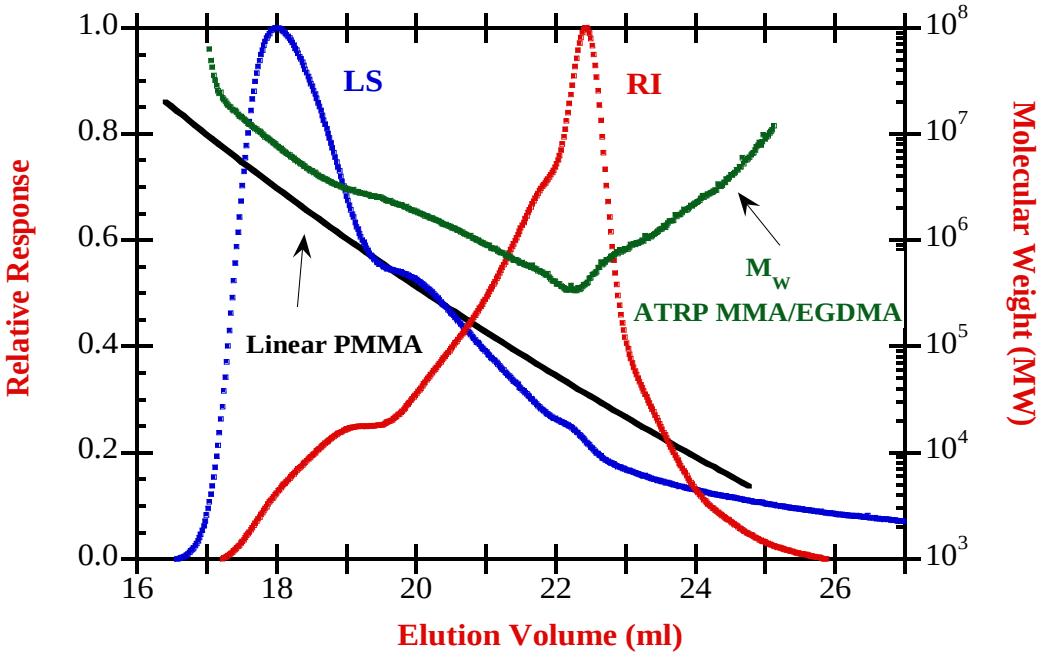

Figure 3.49. Molecular weight along the SEC trace for an ATRP synthesized sample of MMA/EGDMA with a polymerisation time close to gel point.

A drop of polymerisation rate in the presence of DMF is reported in the literature due to possible competitive complexation or ligand exchange of the copper species by DMF (Pascual *et al.*, 1999). Other complexities related with the apparent external orders of the reactants, heterogeneity of the reaction medium or use of very reactive initiators can also contribute to modify the expected rate of polymerisation (Shipp and Matyjaszewski, 2000). Major deviations between measurements and predictions are also here observed at higher

temperatures (90 °C), probably due to the increasing importance of side reactions and loss of the termination control characteristics of ATRP at high temperatures. Despite these discrepancies, once again, the reactivity of the PDB of EGDMA has an almost negligible impact on monomer conversion.

The predicted and experimentally observed influence of temperature on $\bar{M}_w$ in ATRP MMA/EGDMA with a constant mole fraction of crosslinker ($y_C = 0.5\,\%$) is presented in Figure 3.53. These predictions were obtained using the reactivity of PDB of EGDMA which fits the experimental data. A reactivity ratio of PDB relative to the MMA double bonds $C_{PDB} = \frac{k_p^*}{k_{p11}} = 0.45$ was estimated. Nevertheless, probably the value of the reactivity ratio is underestimated due to the influence of intramolecular cyclizations which have been neglected in our calculations. For ATRP synthesized polyacrylate networks (Gao *et al.*, 2007 and 2008) equal reactivity of vinyl groups is reported ($C_{PDB} = 1$) as well as evidence for the increase of intramolecular cyclizations with dilution. The effect of cyclization causing the underestimation of reactivity ratio of PDB was also identified in other works involving the FRP of dimethacrylates (Trigo *et al.*, 2008).

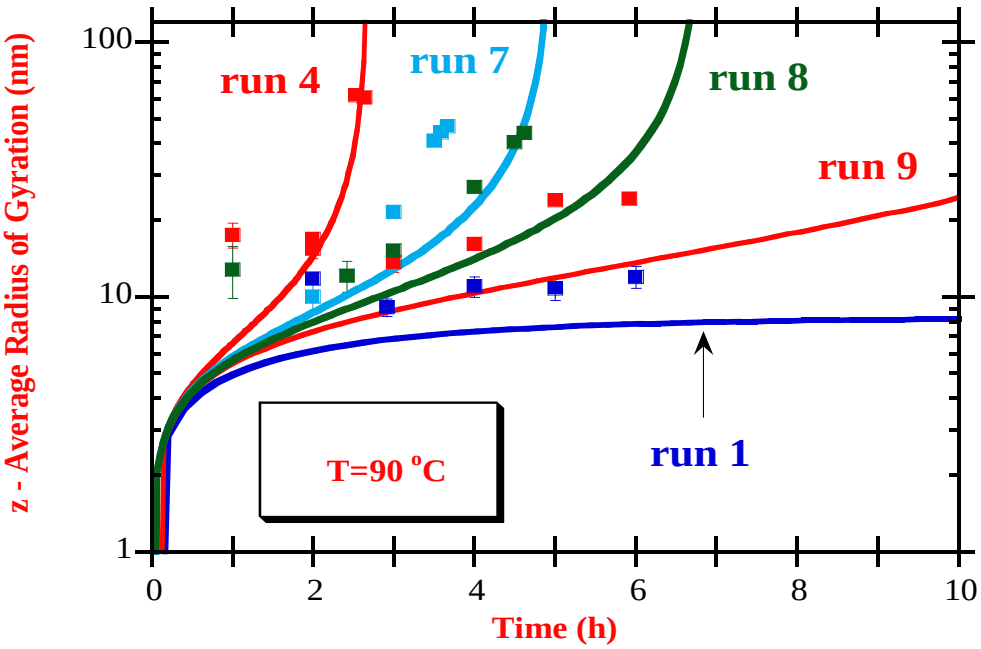

Figure 3.50. Predicted and observed evolution of $\bar{R}_g$ during the ATRP of MMA/EGDMA considering different initial mole fraction of crosslinker (see runs in Table 3.3).

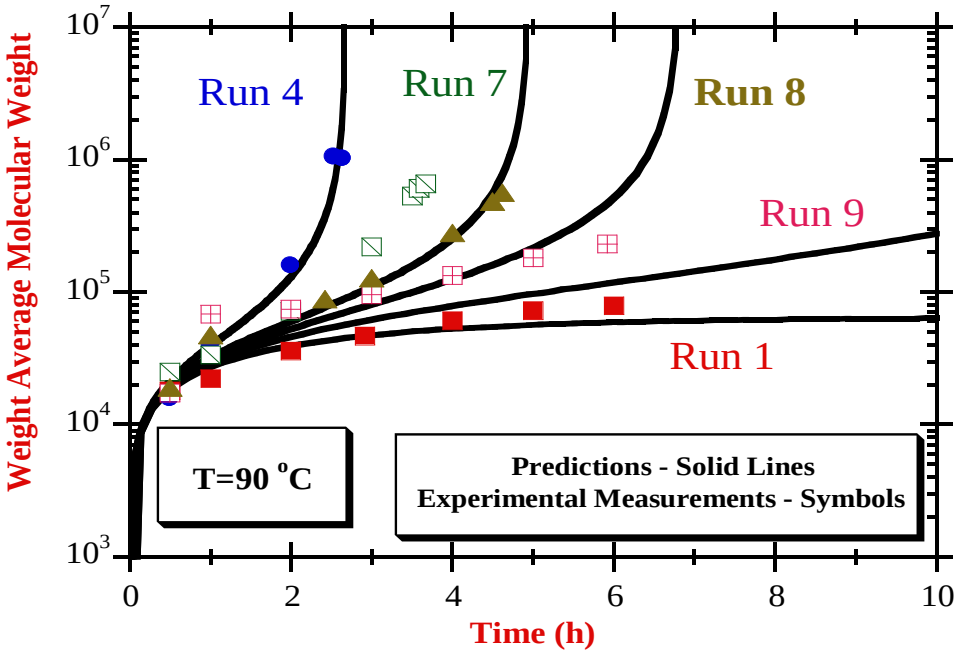

Figure 3.51. Predicted and observed evolution of $\bar{M}_w$ during the ATRP of MMA/EGDMA considering different initial mole fraction of crosslinker (see runs in Table 3.3).

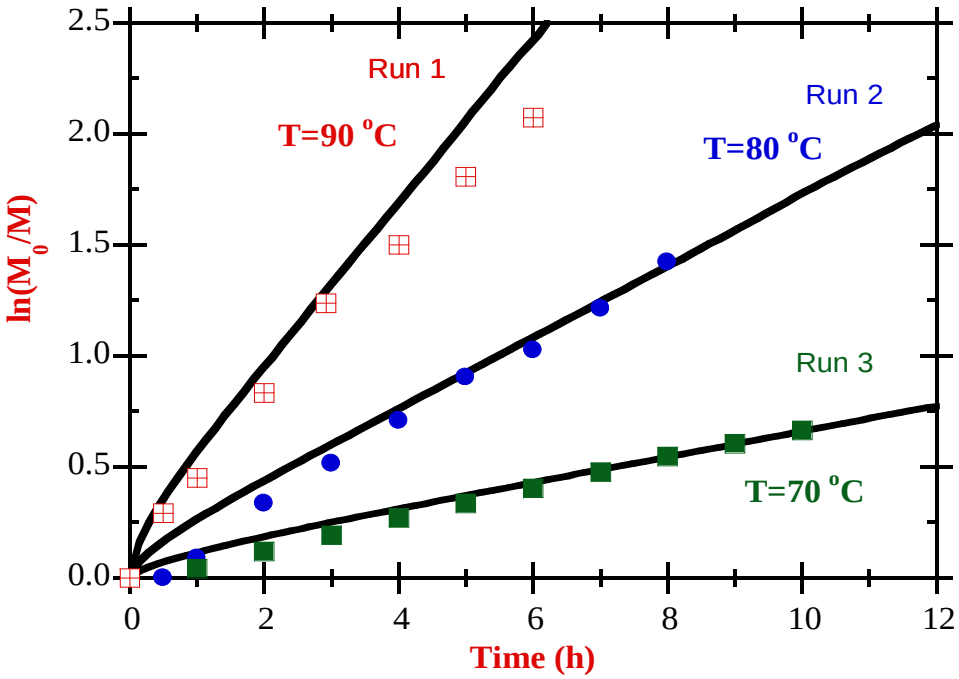

Figure 3.52. Predictions and experimental observations for monomer conversion in the ATRP of MMA/EGDMA at different temperatures. Initial mole ratio MBPA/CuBr/HMTETA=1/1/1.

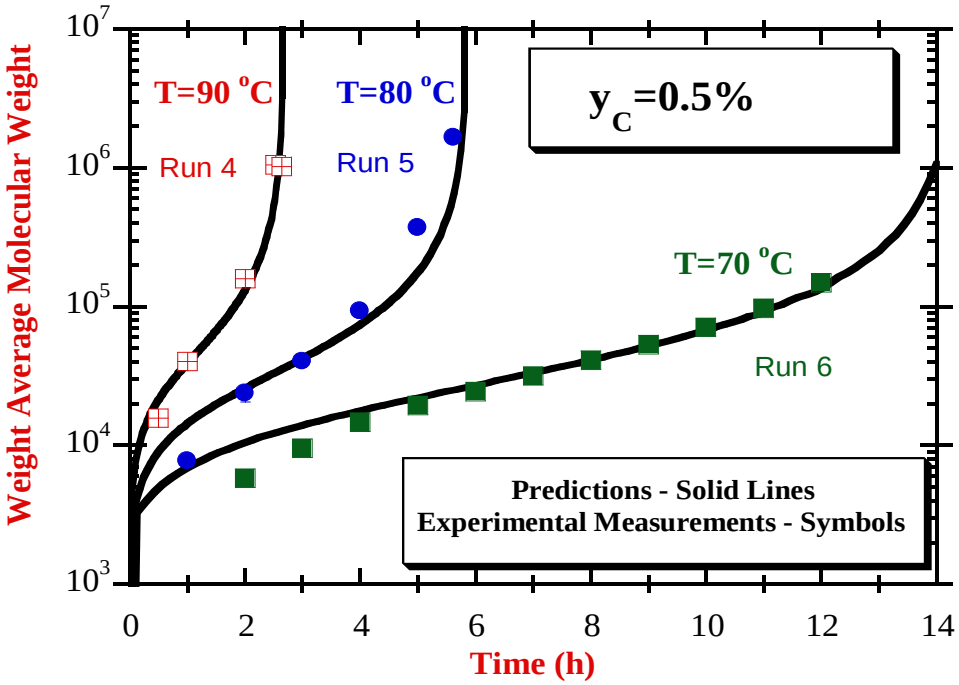

Figure 3.53. Predicted and experimentally observed influence of the temperature on $\bar{M}_w$ in ATRP copolymerisations of MMA/EGDMA with constant initial mole fraction of crosslinker.

Figure 3.54 shows predicted and observed time evolution of $\bar{M}_n$, $\bar{M}_w$, $\bar{M}_z$ and $\bar{R}_g$ in the ATRP of MMA/EGDMA at 70 °C with $y_C = 0.5$ %. A simultaneous good agreement between measurements and predictions of the average molecular weights and *z*-average radius of gyration is observed, confirming the good foundations of the present kinetic approach in the computation of some details of the molecular architecture of these complex materials. The $\bar{R}_{g\Theta}$ predicted by this method was transposed to a good solvent (THF) assuming the equality of the expansion factors of branched and linear polymer molecules, $\frac{\bar{R}_g}{\bar{R}_{g\Theta}} = 0.438\bar{M}_z^{0.096}$ (see Trigo *et al*. (2008) and references therein for the MMA/EGDMA system).

Besides its simplicity (comparatively to *n*BuA/diacrylate system), the kinetic model developed for ATRP of MMA/EGDMA monomers can also be used to identify the key parameters in the production of hyperbranched polymers based on these monomers, as for instance the expected improvement of the homogeneity (less intramolecular cyclizations) of the resulting materials when monomer concentrated polymerisation media are used, e.g., suspension/emulsion polymerisation. Improved materials are also expected using ATRP of MMA/EGDMA instead of FRP of the same monomers (Trigo *et al.*, 2008).

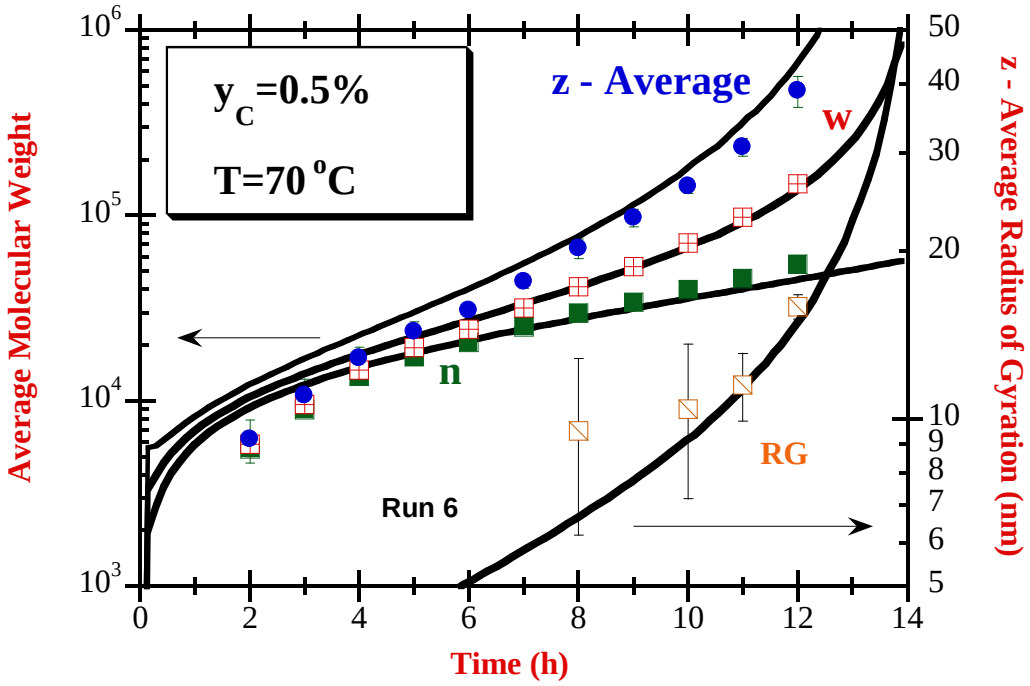

Figure 3.54. Predicted and observed time evolution of $\bar{M}_n$, $\bar{M}_w$, $\bar{M}_z$ and $\bar{R}_g$ in the ATRP of MMA/EGDMA.

3.5 Conclusions

In this chapter, the molecular architecture of FRP and ATRP synthesized polyacrylate hyperbranched polymers and networks were experimentally and theoretically studied. Such non-linear polymers were synthesized at 1 dm^3 scale and the dynamics of formation of products was characterized by SEC/RI/MALLS. In the framework of a general kinetic approach, for both polymerisation systems, models were developed taking into account the polymerisation of different kind of macromonomers (pendent double bonds, terminal double bonds and chain transfer to polymer centres) and the existence of different kinds of polymer radicals.

Under the experimental/theoretical conditions here considered, namely low temperature (60 °C) and low monomer concentration (e.g. 35 % v/v), the impact of branching processes (intermolecular chain transfer to polymer, polymerisation of terminal double bonds) in the molecular architecture of acrylate/diacrylate copolymers is very low as compared with the main crosslinking process (polymerisation of pendent double bonds).

Experimental results at different monomer dilutions have put into evidence the important effect of intramolecular reactions (cyclizations) on the molecular architecture of these microgels. The influence of these reactions has been detected at 50 % dilution, showing that at best only in bulk conditions (Ide and Fukuda, 1997) networks with small extent of cyclizations can be produced. The experimental results of this work agree with those reported for polyacrylate networks with ATRP (Gao *et al*., 2007 and 2008) which have also provided evidence for intramolecular cyclizations at similar dilutions ratios.

These solution polymerisation reactions were also *in-line* monitored using a FTIR-ATR immersion probe and products were characterized by SEC/RI/MALLS. Dynamics of molecular weights and of *z*-average radius of gyration were measured in batch reactor.

A general kinetic approach allowing the prediction of important details of the molecular architecture of non-linear polymers was applied to those hyperbranched polyacrylates with crosslinking and branching mechanisms simultaneously considered. Comparison of simulations with experimental results obtained by SEC/RI/MALLS leads to conclude that, under the experimental conditions used in this study, crosslinking is the dominant mechanism in the formation of non-linear architectures and that long chain branching can be neglected.

It was concluded that *in-line* FTIR-ATR is a reliable technique to monitor the acrylate monomer in solution acrylate/diacrylate copolymerisation but the *in-line* monitoring of diacrylate monomer is a challenging task. The use of diluted polymerisation systems with the goal of obtaining isothermal profiles and a low content of diacrylate monomer to avoid gelation are drawbacks for the monitoring of diacrylate monomers by this technique.

Improved results are expected with suspension polymerisation concerning, not only the production of hyperbranched polymers with a higher homogeneity (minimization of cyclizations), but also better performing the *in-line* monitoring of divinyl monomers by FTIR. With an operation at a much higher content of divinyl monomer it is possible to keep isothermal profiles and the polymerisation can be extended to the post gelation period if desired.

CHAPTER 4

NITROXIDE MEDIATED RADICAL POLYMERISATION OF STYRENE/DIVINYLBENZENE

Abstract. The model chemical system styrene/divinylbenzene (STY/DVB) is experimentally investigated in solution (hyperbranched polymers) and aqueous suspension (gel formation) NMRP polymerisation. The range of temperatures used was between 90 and 130 °C respectively in an atmospheric reactor and in a pressurized reactor (for aqueous suspensions). Comparison with FRP of the same system was also performed. Thus, the following variables were changed:

- Parameters changed:
    - Polymerisation technique (FRP and NMRP).
    - Monomer dilution, amount of crosslinker and mediator (TEMPO) in NMRP polymerisations.
- Product characterization:
    - Dynamics of conversion using gravimetry and size exclusion chromatography (SEC) with refractive index (RI) detection using THF as eluent.
    - The molecular architecture of the products through the determination of average molecular weights, *z*-average radius of gyration and absolute molecular weight distribution using the SEC/RI/MALLS system.
    - *Off-line* FTIR-ATR for qualitatively assess pendant double bonds.
    - Concentration of pendant double bonds was also quantified by means of ICl titration.
    - The morphology of the produced gel beads of STY/DVB by SEM with different kinds and amounts of diluent.
- Modelling with intramolecular cyclization was included in the complementary studies using the experimental data obtained below cited.

This chapter is based on the following publications:

M.A.D. Gonçalves, I.V.R Trigo, R.C.S. Dias, M.R.P.F.N. Costa, *Macromol. Symp.* 291-292 (2010) 239-250.

M.A.D. Gonçalves, R.C.S. Dias, M.R.P.F.N. Costa, *Chem. Eng. Technol.* 33 (2010) 1797-1813.

M.A.D. Gonçalves, V.D. Pinto, R.C.S. Dias, M.R.P.F.N. Costa, L.G. Aguiar, R. Giudici, *Macromol. React. Eng. 7* (2013) 155-175.

L.G. Aguiar, M.A.D. Gonçalves, V.D. Pinto, R.C.S. Dias, M.R.P.F.N. Costa, R. Giudici, *Macromol. React. Eng.* (2013) DOI: 10.1002/mren.201300105.

L.G. Aguiar, M.A.D. Gonçalves, V.D. Pinto, R.C.S. Dias, M.R.P.F.N. Costa, R. Giudici, *Macromol. React. Eng.* (2013) DOI: 10.1002/mren.201300171.

4.1 Introduction

Nitroxide Mediated Radical Polymerisation of vinyl/divinyl styrenic monomers using stable radical TEMPO with the goal of avoiding lack of structural control characteristics of the FRP of the same monomers has been studied by several groups (Ide and Fukuda, 1997 and 1999; Abrol *et al*., 1997and 2001; Tuinman *et al.*, 2006).

Copolymers of styrene (STY) and divinylbenzene (DVB) find an important use as stationary phases for liquid chromatography. Their comparatively easier chemical analysis makes this system a good choice for fundamental studies, despite the presence of the substitution effects of the several vinyl groups attached to the same aromatic ring. Gel particles produced by FRP can be inherently heterogeneous as they form through the association of microgels with very different crosslinking histories (Hernández-Ortiz *et al*., 2009 and 2012). Hence, in spite of the maturity of the research on STY/DVB network formation, room for improvement of materials properties and/or the corresponding production process still exists as testified by the works concerning their synthesis in supercritical carbon dioxide using a modified anionic polymerisation procedure (Cooper *et al*., 1998 and 1999) or FRP (García-Morán *et al.*, 2009).

In contrast to FRP, controlled radical polymerisation (CRP) is characterized by slow rates and the production of shorter polymer chains with almost constant and comparatively higher concentration of end groups. Under these circumstances, intermolecular crosslinking of radical/PDBs is enhanced because the activation and deactivation mechanisms provide enough time for chain relaxation and diffusion (Hernández-Ortiz *et al*., 2012; Wang *et al*., 2012).

These features make the CRP techniques advantageous, comparatively to FRP, to synthesize hyperbranched polymers (soluble) and gels (insoluble) with an improved control of the molecular architecture. Expected differences between CRP and FRP crosslinking systems include (among others) the delay in the onset of gelation, a steady increase of gel fraction, and higher swelling ratios of the synthesized gels (Jaramillo-Soto and Vivaldo-Lima, 2012). These issues were studied in past works dealing with NMRP crosslinking using different synthesis approaches: 4,4´-divinylphnyl/Sty bulk copolymerisation (in sealed tubes) mediated by TEMPO adduct at 125 °C (Ide and Fukuda, 1997 and 1999), *t*-butylstyrene/DVB microgels preparation in benzene solution (sealed tubes) at 130 °C (Abrol *et al*., 1997 and 2001), production of STY/DVB monoliths directly in stainless columns (sonicated monomer/porogen mixture) at 130 °C considering different TEMPO-based mediators (Peters

et al., 1999; Viklund *et al.*, 2001), miniemulsion/micro-suspension of TEMPO mediated STY/DVB copolymerisation in shake ampoules at 125 °C (Zetterlund *et al*., 2005; Alam *et al*., 2006; Tanaka *et al*., 2007; Saka *et al.*, 2007) and bulk STY/DVB copolymerisation at 120 °C mediated by TEMPO in sealed ampoules (Tuinman *et al.*, 2006).

This chapter reports experimental and modelling studies for the NMRP of STY/DVB. The synthesis of hyperbranched polymers (using solution polymerisation) and networks formation (using aqueous suspension) was assessed. The hyperbranched polymers were experimentally characterized by SEC/RI/MALLS using different operation conditions, e.g., crosslinker amount, the dynamics of monomer conversion, molecular weights and z-average radius of gyration. A different synthesis approach was considered for the NMRP aqueous suspension copolymerisation of STY/DVB when compared with the above described works (Ide and Fukuda, 1997 and 1999; Abrol *et al*., 1997 and 2001; Peters *et al*., 1999; Viklund *et al.*, 2001; Zetterlund *et al*., 2005; Alam *et al*., 2006; Tanaka *et al*., 2007; Saka *et al.*, 2007; Tuinman *et al.*, 2006). The experiments were performed using a one-pot stirred reactor, allowing the direct measurement of the dynamics of gelation. The molecular architecture of the products (sol fraction) was probed using SEC/RI/MALLS. Quantification of PDB concentration and weight fraction of gel were also performed. Nano and micro-structures of the materials were also observed using scanning electron microscopy (SEM). The influence of production conditions (temperature, composition, dilution) on the structure of the networks was thus sought. Comparison with similar products synthesized by FRP was performed in order to try to elucidate the influence of the polymerisation technique on the materials morphology.

4.2 Experimental part

4.2.1 Materials

In experiments presented in Table 4.1 and 4.2 xylene of 98.5 % purity, AIBN of 98 % purity, TEMPO of 98 % purity, styrene of 99 % purity stabilised with 0.005 % w/w 4-tert-butylcatechol and commercial grade divinylbenzene of 80 % purity stabilized with 0.1 % w/w 4-tert-butylcatechol were purchased from Sigma-Aldrich and used as received. Commercial DVB is a mixture of isomers, 56.2 % *m*-divinylbenzene and 24.2 % *p*-divinylbenzene, plus 19.6 % of ethylvinylbenzene. Xylene solvent is also a mixture of xylenes plus ethylbenzene (≤ 25 % in the latter component). For aqueous suspension polymerisations have been added deionized water as the continuous phase and PVOH as the suspending agent.

4.2.2 Polymerisation Set-up

All experiments were carried out using the experimental set-up which has a detailed description in Chapter 2. For these experiments the reactor was operated in batch mode and without the FTIR-ATR instrument.

Typically, NMRP and FRP STY/DVD solution copolymerisations (see Table 4.1) were carried out as follows: the empty reactor was purged with an argon stream (40 cm^3/min) and the heating process was set to reach 130 °C. After 15 min, the desired quantities of styrene, xylene, divinylbenzene and TEMPO (in NMRP experiments) were charged to the reactor.

Table 4.1. Description of the set of experiments performed in the study of the TEMPO-mediated copolymerisation of STY/DVB at 130 °C. All concentrations are in mol/dm^3.

Run	$[STY]_0$	$[DVB]_0$	$[AIBN]_0$	$[TEMPO]_0$	$\mathbf{y_C}$(%)	TEMPO/ AIBN
1	4.364	0.0	8.606×10^{-3}	0.0	0	0
2	4.351	2.157×10^{-2}	8.533×10^{-3}	0.0	0.5	0
3	4.364	0.0	8.649×10^{-3}	9.617×10^{-3}	0	1.1
4	4.350	2.211×10^{-2}	8.726×10^{-3}	9.607×10^{-3}	05	1.1
5	4.343	3.296×10^{-2}	8.540×10^{-3}	9.668×10^{-3}	0.75	1.1
6	4.331	5.360×10^{-2}	8.520×10^{-3}	9.534×10^{-3}	1.22	1.1
7	4.307	9.108×10^{-2}	8.457×10^{-3}	9.521×10^{-3}	2.07	1.1
8	4.247	1.874×10^{-1}	8.349×10^{-3}	9.377×10^{-3}	4.23	1.1
9	4.247	1.872×10^{-1}	8.352×10^{-3}	1.125×10^{-2}	4.23	1.3
10	4.247	1.869×10^{-1}	8.309×10^{-3}	1.687×10^{-2}	4.23	2.0

Throughout the whole heating process the polymerisation system was bubbled with the same argon flow-rate 40 cm^3/min. Owing to the heat losses, time delays between 100 and 120 min were needed to reach the set-point temperature of 130 °C in the FRP and NMRP experiments, respectively. This difference is explained by the heat generated by the auto-initiation of styrene in the conventional runs during the heating period. When the set-point was reached, samples of the reaction mixture were withdrawn from the reactor to be analysed by SEC/RI/MALLS (details of this technique are presented in appendix A) and immediately afterwards AIBN was added to the system, defining the initial time $t = 0$ of the polymerisation. The analysis of these samples confirmed the existence of thermal initiation of

styrene during the heating process (monomer conversion of around 4 % was experimentally measured) in conventional runs and also that this phenomena is negligible in the NMRP experiments. Later, samples of the reaction mixture were withdrawn from the reactor at prescribed polymerisation times and analysed by SEC/RI/MALLS. During the polymerisation process the argon flow rate used to bubble the system was reduced to 20 cm^3/min in order to decrease mass losses by evaporation. Note that the polymerisation temperature is close to the xylene boiling point (around 140 °C) and that the reactor is operated at atmospheric pressure.

Table 4.2 describes the set of experiments performed in aqueous suspension of NMRP STY/DVB. Polymerisations were carried out at two different temperatures (90 and 130 °C) and the following parameters were also changed along the experimental program: volumetric fraction of the global monomer mixture in the organic phase (y_M) using toluene and xylene as solvents, initial mole fraction of commercial DVB in monomer mixture (y_C), initial mole ratio between initiator (AIBN or BPO) and total number of monomers double bonds (y_I), initial mole ratio between NMRP mediator (TEMPO) and initiator (y_{TEMPO}).

Table 4.2. Set of experiments performed with NMRP aqueous suspension copolymerisation of STY/DVB.

Run	y_M(%)	y_C(%)	y_I(%)	y_{TEMPO}(%)	T (°C)
1	50	3	0.5	1.1	90
2	60	28	0.5	1.1	90
3	60	100	0.4	1.1	90
4	60	100	0.4	1.2	90
5	100	100	0.4	1.1	90
6	100	0	0.5	1.1	90
7	50	1	0.05	0.0	90
8	50	100	0.9	0.75	130
9	50	50	0.2	1.0	130
10	50	5	0.2	1.0	130
11	20	50	0.2	1.0	130
12	50	0	0.2	1.0	130
13	100	0	0.05	0.0	90
14	50	0	0.5	1.1	90

These aqueous suspension experiments were performed using typically a volumetric ratio of 9 between continuous and dispersed phase. Polyvinyl alcohol (PVA) was chosen as the suspending agent with a typical concentration in aqueous phase of 0.1 % w/w. Considering the used volumetric ratio between aqueous/organic phases (reactor sampling becomes difficult at higher solid content) and the monomer dilution in the organic phase, the ratio PVA/monomer ranges between 0.15 and 2 % w/w and the correspondent ratios PVA/(monomer + solvent) between 0.08 and 1 % w/w. these values are reasonable for a typical suspension polymerisation in which concentration of suspending agent relative to the organic phase is in the range 0.01-1 % w/w. Concentrations of PVA of 0.06-0.12 % (by monomer weight) are reported in previous works concerning the FRP suspension polymerisation of STY/DVB (Kiatkamjornwong, *et al.*, 2001). Here, higher PVA concentrations were chosen in order to improve reactor sampling by decreasing average particle size. An atmospheric reactor (described in chapter 2) with maximum capacity of 2.5 L was used to perform the polymerisations at 90 °C. It was used a Parr 5100 pressurized glass reactor with 1 L capacity to perform aqueous suspension experiments at 130 °C. The reactor is equipped with a magnetic drive internal stirrer including double turbine type six-blade impellers at 45°. The reactor was initially pressurized with argon at 2 bar and a final pressure (when temperature set-point is at 130 °C) of around 4.6 bar was observed. A total polymerisation of 850 mL volume was normally considered in these experiments. Polymerisations were performed with a stirring speed of 400 rpm (this relatively high stirring speed was also used to decrease the average particle diameter). In order to observe the dynamics of products formation, polymer samples were taken at prescribed reaction times. This procedure can also be carried out even after gelation has occurred.

Different processes for synthesis of STY/DVB particles are described in the literature using, for example, FRP aqueous suspension polymerisation in reaction flasks (at 60-80 °C) (Kiatkamjornwong, *et al.*, 2001), precipitation polymerisation in shake vials at 70 °C (Shim *et al.*, 2004) or in supercritical carbon dioxide using high-pressure cells ($P = 172$ bar, $T = 65$ °C) (Garcín-Morán, *et al.*, 2009). In the last few years, many other studies have explored CRP in dispersed systems (Zetterlund *et al*., 2008) aiming to combine the synthesis of particles with different morphologies and the control of polymer molecular architecture. Suspension, emulsion, miniemulsion, microemulsion, precipitation and dispersion polymerisation were thus combined with different CRP techniques namely ATRP, RAFT and NMRP (Zetterlund *et al*., 2008). In this work, the dynamics of production of STY/DVB networks using NMRP

aqueous suspension copolymerisation is studied. Synthesis in one-pot stirred chemical reactor at relatively high mass scale and considering also higher temperatures (requiring pressurization) are distinctive features of this chapter.

4.2.3 SEC/RI/MALLS Products Analysis

Molecular weights and average molecular radius of gyration in THF were measured with a Polymer Laboratories PL-GPC-50 integrated SEC system with a differential refractometer working at 950 ± 30 nm attached to a Wyatt Technology DAWN8^{+}HELEOS 658 nm Multi Angle Laser Light Scattering (MALLS) detector. The polymer samples were fractioned by molecular size using a train of 3 GPC columns PL gel (300×7.5 mm) with nominal particle size 10 μm and pore type MIXED-B-LS, maintained at constant temperature of 30 °C and using THF as the eluent at 1 mL/min flow rate.

For the solution polymerisation system samples were collected from the reactor at different polymerisation times directly to THF and injected into the SEC/RI/MALLS. In aqueous polymerisation reaction samples (containing both organic and aqueous phases) were collected into previously cooled 20 ml glass vials that were immediately poured in the refrigerator at -14 °C to stop the reaction. At least 24 hours later, samples were allowed to reach room temperature, the two phases were separated and a small amount of the organic phase was diluted in THF and filtered to be injected in the SEC/RI/MALLS system. The detailed procedure and apparatus description of SEC/RI/MALLS is presented in appendix A.

4.2.4 Gravimetric Measurements

The remaining organic phase resulting from the above described sampling process was weighed and precipitated into a large excess of methanol in order to isolate the polymer. After vacuum drying, monomer conversion could also be estimated by recording the weight loss. Thereafter, a portion of the dried polymer was weighed and poured in a large excess of THF to extract the soluble phase. After several cycles of filtration and washing with THF, the insoluble material (when present) was dried under vacuum and weighed, thus yielding the weight fraction of gel. Soxhlet extraction was not used in this polymerisation system owing to the low amount of polymer usually sampled from the reactor (especially at intermediate reaction times).

4.2.5 Refractive Index Increment Measurement

A Wyatt Technology OPTILAB DSP 633 nm interferometric refractometer was used to measure the refractive index increment (*dn*/*dc*) for the polymers, solvents and monomers in THF, required for analysing the MALLS results and for estimating the conversion from the values of the differential refractometer (RI) peak areas of monomers and polymer in the chromatographic traces of the SEC analysis.

4.2.6 Pendant Double Bonds Concentration Measurements

Quantification of PDBs concentration in the polymer (soluble and insoluble phases) was performed using chemical analysis, as reported in the literature (Hecker, 2000; Cheyney and Kelley, 1942; Kemp and Peters, 1943; Lee *et al.*, 1948 and 1950; Crompton and Reid, 1963; Knothe, 2002). Around 0.5 g of dried polymer was kept in contact with 20 ml of carbon tetrachloride during 15 hours for samples collected before gelation and during 90 hours for materials containing gel (in order to promote swelling). Afterward, 25 ml of Wijs reagent were added to the mixture and content was kept in dark during 30 h (before gel) and 75 h (when gel was present). Reaction between iodine monochloride (ICl) and carbon-carbon PDBs present in polymer structure was thus promoted. At the end of these periods, 25 ml of potassium iodide and 100 ml of water were added to the mixture. In this step, KCl and I_2 (iodine) are formed due to the reaction of free ICl and the KI present in excess. The resulting solution was titrated with 0.1 N solution of sodium thiosulfate, in a first step until the partial disappearance of the dark yellow colour. Afterward, 2 ml of 1 % starch solution were added to the mixture and the titration continued until the new colour change from blue to white was observed. Comparison of observed titration volume with that from a blank run (without polymer sample) allows the estimation of the amount of PDBs present in the material.

4.3 Kinetic Laws considered in the modelling studies for NMRP of STY/DVB

4.3.1 Chemical Species and Chemical Reactions

In this chemical system of NMRP STY/DVB a kinetic scheme comprising a total of 36 chemical groups was considered as summarized in Tables 4.3, 4.4 and 4.5. The propagations, initiations, chain transfer, terminations and cyclizations reactions are analogous to the ones presented in Chapter 2. Here, are depicted the main activation/deactivation reaction of

NMRP, the Mayo dimerization of styrene and the thermal initiation of styrene. Thus, in Figure 4.1 is represented the main activation/deactivation mechanism in a polymerisation mediated by TEMPO of a polymer radical formed by styrene monomer. In Figures 4.2 and 4.3 are represented the reactions of Mayo dimerization and thermal initiation of styrene that occur at high temperature (> 100 °C).

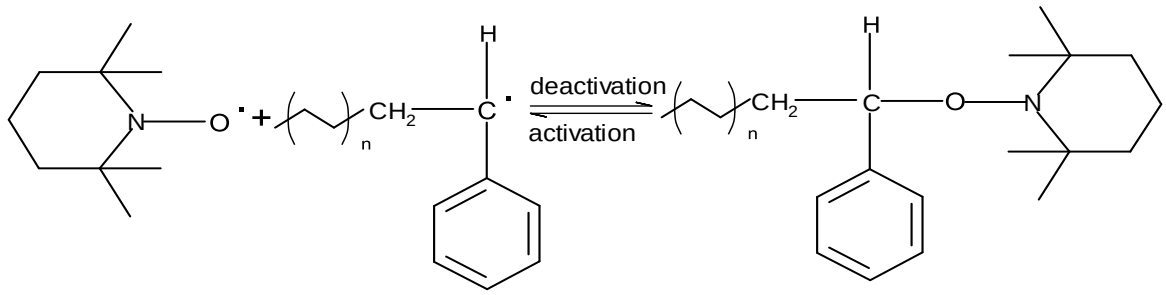

Figure 4.1. Mechanism of activation/deactivation involving a polymer radical formed by styrene and the mediator nitroxide (TEMPO).

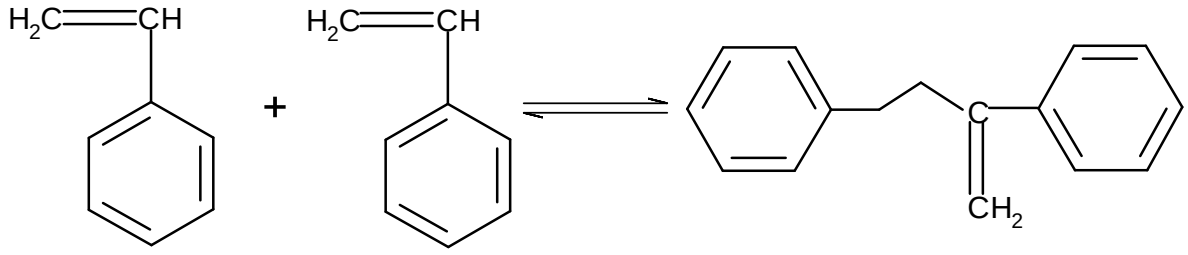

Figure 4.2. Schematic representation of the Mayo dimerization.

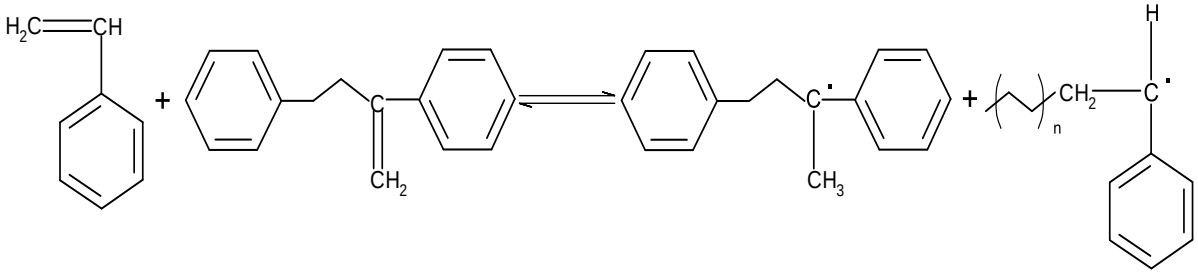

Figure 4.3. Mechanism showing the reaction of auto-initiation of styrene.

The full kinetic scheme considered in the simulations of the NMRP of STY/DVB is presented in Eqs. (4.1)-(4.19), comprising a total of 125 different chemical reactions. Termination comprises 30 different reactions that are condensed in Eqs. (4.18) and (4.19). Again, two different elementary steps describe each reversible process. In these equations M_1, M_2 and M_3 represent the three monomers (styrene, *m*-divinylbenzene and *p*-divinylbenzene), I the

initiator (AIBN), TEMPO the stable radical and T the solvent (xylene). These are the reactants initially fed to the reactor.

Table 4.3. Description of the active groups belonging to the polymer chains considered in the modelling studies of the NMRP copolymerisation of STY/DVB monomers.

Group description	Alias
Growing radical from styrene	R_1
Growing radical from *m*-divinylbenzene	R_2
Growing radical from *p*-divinylbenzene	R_3
Growing radical from *m*-pendant double bond	R_4
Growing radical from *p*-pendant double bond	R_5
Dormant radical from styrene monomer	D_1
Dormant radical from *m*-divinylbenzene monomer	D_2
Dormant radical from *p*-divinylbenzene monomer	D_3
Dormant radical from *m*-pendant double bond	D_4
Dormant radical from *p*-pendant double bond	D_5
Pendant double bond from *m*-divinylbenzene	M_4
Pendant double bond from *p*-divinylbenzene	M_5

As a consequence of thermal decomposition of the initiator, primary radicals (R) are formed and due to high polymerisation temperature, thermal auto-initiation of styrene must be accounted through the formation of a dimer (D) and radicals from the monomeric styrene (RM) and from the dimer (RD). Primary radicals from the initiator and monomer are exposed to the reaction with TEMPO resulting in the consequent formation of the related dormant radicals (SR and SM, respectively). The formation of saturated nitroxyl radicals (TS) is possible due to the rate enhancement reaction (represented by Eq. (4.7)) and primary radicals from the solvent (RT) can be formed as a result of the correspondent chain transfer process (depicted by Eq. (4.13)).

Five different kinds of polymer radicals are considered according to the monomer or macromonomer involved in their formation, i.e., STY, *m*-DVB, *p*-DVB, *m*-PDB and *p*-PDB. Here, *m*-PDB and *p*-PDB are pendant double bonds present in polymer molecules that are the chemical species promoting the crosslinking process. These five kinds of growing radicals also lead to the formation of five different kinds of dormant radicals (D_k), as a consequence of the exchange process promoted by TEMPO, as represented by Eq. (4.17). Various kinetic

steps were condensed into a single equation through the use of Krönecker symbols, i.e., $\delta^k_{1,2} = 1$ if $k = 1$ or $k = 2$ and $\delta^k_{1,2} = 0$ otherwise, $\delta^k_2 = 1$ if $k = 2$ and $\delta^k_2 = 0$ otherwise. In the same way, $\delta^k_{[1-5]} = 1$ if $k \in [1-5]$ and $\delta^k_{[1-5]} = 0$ otherwise.

Table 4.4. Description of the active groups not belonging to the polymer chains considered in the modelling studies of the NMRP copolymerisation of STY/DVB monomers.

Group description	Alias
Styrene monomer	M_1
m-divinylbenzene monomer	M_2
p-divinylbenzene monomer	M_3
Initiator (AIBN)	I
Nitroxide radical (TEMPO)	TEMPO
Radical from initiator (primary radical)	R
Radical from styrene (monomeric radical)	RM
Solvent	T
Radical from solvent	RT
Dormant primary radical	SR
Dormant monomeric radical	SM
Dimer of styrene	D
Radical from dimer	RD
Saturated nitroxyl radical	TS

Table 4.5. Description of the inactive groups considered in the modelling studies of the NMRP copolymerisation of STY/DVB monomers

Group description	Alias
Polymerised styrene monomer unit	U_1
Polymerised *m*-divinylbenzene monomer unit	U_2
Polymerised *p*-divinylbenzene monomer unit	U_3
Fragments from initiator, solvent and dimer	F_1,F_2,F_3
Crosslinking site from *m*- and *p*- pendant double bond	CS
Non-reactive saturated group	SG
Head-to-Head units from termination by combination	HHU

The set of 125 different chemical reactions represented by Eqs. (4.1)-(4.19) can be summarized as follows: 1 initiation decomposition, 2 Mayo dimerization of styrene, 1 thermal initiation of styrene, 20 initiations, 25 propagations, 14 living/dormant exchanges of radicals,

30 chain transfers, 30 terminations and 2 rate enhancements. These equations are depicted below:

Initiation thermal decomposition:

$$I \overset{k_d}{\rightarrow} 2fR \tag{4.1}$$

Living/dormant exchange of primary radicals:

$$R + TEMPO \underset{k_{aR}}{\overset{k_{daR}}{\rightleftharpoons}} SR \tag{4.2}$$

Mayo dimerization of styrene:

$$M_1 + M_1 \underset{k_{dim}^{-1}}{\overset{k_{dim}}{\rightleftharpoons}} D \tag{4.3}$$

Thermal initiation of styrene:

$$M_1 + D \overset{k_{IA}}{\longrightarrow} RM + RD \tag{4.4}$$

Living/dormant exchange of monomeric radicals:

$$RM + TEMPO \underset{k_{aM}}{\overset{k_{daM}}{\rightleftharpoons}} SM \tag{4.5}$$

Decomposition of dormant monomeric radicals:

$$SM \overset{k_{dec}}{\longrightarrow} M_1 + TS \tag{4.6}$$

Rate enhancement reaction:

$$D + TEMPO \overset{k_h}{\rightarrow} RD + TS \tag{4.7}$$

Initiation of monomers and PDBs by primary radicals of initiator:

$$R + M_k \overset{k_{IRk}}{\longrightarrow} R_k + U_k\delta_{[1-3]}^k + F_1 + M_{k+1}\delta_{2,3}^k \quad k = 1, \dots, 5 \tag{4.8}$$

Initiations by radicals from dimer:

$$RD + M_k \overset{k_{IRDk}}{\longrightarrow} R_k + 2U_1 + U_k\delta_{[1-3]}^k + M_{k+1}\delta_{2,3}^k \quad k = 1, \dots, 5 \tag{4.9}$$

Initiations by monomeric radicals:

$$RM + M_k \xrightarrow{k_{IRMk}} R_k + U_1 + U_k\delta^k_{[1-3]} + M_{k+1}\delta^k_{2,3} \quad k = 1, \dots, 5 \tag{4.10}$$

Initiations by radicals from the solvent:

$$RT + M_k \xrightarrow{k_{IRTk}} R_k + F_2 + U_k\delta^k_{[1-3]} + M_{k+1}\delta^k_{2,3} \quad k = 1, \dots, 5 \tag{4.11}$$

Chain transfers to monomers:

$$\mathrm{R}_k + M_j \xrightarrow{k_{fMkj}} SG + R_M\delta^j_1 + R_j\delta^j_{2,3} + M_{j+2}\delta^j_{2,3} \quad k = 1, \dots, 5 \text{ and } j = 1, \dots, 3 \tag{4.12}$$

Chain transfer to solvent:

$$\mathrm{R}_k + T \xrightarrow{k_{fTk}} SG + RT \quad k = 1, \dots, 5 \tag{4.13}$$

Chain transfer to dimer:

$$\mathrm{R}_k + D \xrightarrow{k_{fDk}} SG + RD \quad k = 1, \dots, 5 \tag{4.14}$$

Chain transfer to initiator:

$$\mathrm{R}_k + I \xrightarrow{k_{fIk}} SG + R \quad k = 1, \dots, 5 \tag{4.15}$$

Propagations involving growing radicals of monomers and PDBs:

$$\mathrm{R}_k + M_j \xrightarrow{k_{pkj}} R_j + U_j\delta^j_{[1-3]} + M_{j+2}\delta^j_{2,3} + CS\delta^j_{4,5} \quad k = 1, \dots, 5 \text{ and } j = 1, \dots, 5 \tag{4.16}$$

Reversible activation/deactivation of growing radicals:

$$D_k \underset{k_{dak}}{\overset{k_{ak}}{\rightleftharpoons}} R_k + TEMPO \quad k = 1, \dots, 5 \tag{4.17}$$

Termination by combination

$$R_k + R_j \xrightarrow{k_{tckj}} HHU \quad k = 1, \dots, 5 \text{ and } j = k, \dots, 5 \tag{4.18}$$

Termination by disproportionation

$$R_k + R_j \xrightarrow{k_{tdkj}} SG + SG \quad k = 1, \dots, 5 \text{ and } j = k, \dots, 5 \tag{4.19}$$

Table 4.6 presents a basic set of rate coefficients considered in the modelling studies of the NMRP of STY/DVB. All these parameters have been collected from previous works concerning mostly the linear FRP and/or CRP of styrenic monomers.

Table 4.6. Basic set of rate parameters considered in the modelling studies of the NMRP copolymerisation of STY/DVB monomers.

Kinetic Step	Rate coefficient expression [a)]
Initiator thermal decomposition [b)]	$k_d = 4.31 \times 10^{15} \exp(-131.7 \times 10^3/RT)$ $(s^{-1}), f = 0.6$
STY propagation [g)]	$k_p = 4.27 \times 10^7 \exp(-32.5 \times 10^3/RT)$
Initiation of STY primary radicals [e),h)]	$k_{IR} = k_{ID} = k_{IM} = k_{IT} = k_P$
Chain transfer to monomer [d),e),i),j)]	$C_M = \frac{k_{fM}}{k_P} = 0.2128 \exp(-23.5 \times 10^3/RT)$
Chain transfer to solvent [h)]	$k_{fT} = 1.8$
Chain transfer to dimer [e)]	$k_{fD} = 50$
Mayo dimerization of STY [e)]	$k_{dim} = 188.97 \exp(-67.7 \times 10^3/RT)$
Dimer decomposition [e),h)]	$k_{dim}^{-1} = 5.49 \times 10^9 \exp(-106.1 \times 10^3/RT)$
Thermal initiation of STY [e)]	$k_{IA} = 6.539 \times 10^{12} \exp(-153.1 \times 10^3/RT)$
Decomposition of dormant monomeric radicals [e)]	$k_{dec} = 5.7 \times 10^{14} \exp(-153.3 \times 10^3/RT)$
Rate enhancement reaction [e)]	$k_h = 10^{-3}$
Radical deactivation [c),d),e)]	$k_{da} = 5.03 \times 10^9 \exp(-15.57 \times 10^3/RT)$
Radical activation [d),e),f)]	$k_a = 2 \times 10^{13} \exp(-124.2 \times 10^3/RT)$
Radical termination [b),d),e),i),j)]	$k_p/\sqrt{k_t} = 426.4 \exp(-26 \times 10^3/RT)$ $\alpha_{td} = \frac{k_{td}}{k_t} = 0, \alpha_{tc} = \frac{k_{tc}}{k_t} = 1$

[a)] Kinetic parameters expressed in $dm^3 mol^{-1} s^{-1}$, unless otherwise stated. [b)] Moad and Solomon, 2006; [c)] Beckwith *et al*., 1992; [d)] Zhang and Ray, 2002; [e)] Belincanta-Jimenez *et al*., 2007; [f)] Fukuda *et al*., 1996; [g)] Buback *et al*., 1995; [h)] Fu *et al*., 2007a and 2007b; [i)] Hui and Hamielec, 1976; [j)] Greszta and Matyjaszewski, 1996.

4.4 Hyperbranched Polymers Formed by Solution Polymerisation

4.4.1 Results and Discussion

Comparisons between measured and predicted monomer conversions for FRP and NMRP copolymerisations are presented in Figure 4.4. Note that these simulations are almost insensitive to the reactivities of the pendant double bonds (the major factor influencing the crosslinking process) due to the low concentration of these species in the reaction media. This means that with the basic set of kinetic parameters presented above it is possible to have a good description of the system in terms of polymerisation rate. Predictions and experimental

observations for $\bar{M}_n$ and $\bar{M}_w$ in FRP and NMRP linear runs ($y_C = 0$) are presented in Figure 4.5. A good agreement between experiments and theory is also observed. The ability of the present modelling studies to take into account the thermal initiation of styrene during the heating period (before introduction of AIBN) is clear: simulations in Figure 4.5 shows that self-polymerisation of styrene during the heating process is negligible in NMRP (but not in FRP) due to the TEMPO stable radicals present in the polymerisation system. This fact was experimentally confirmed in this work by measuring the monomer conversion before the addition of AIBN.

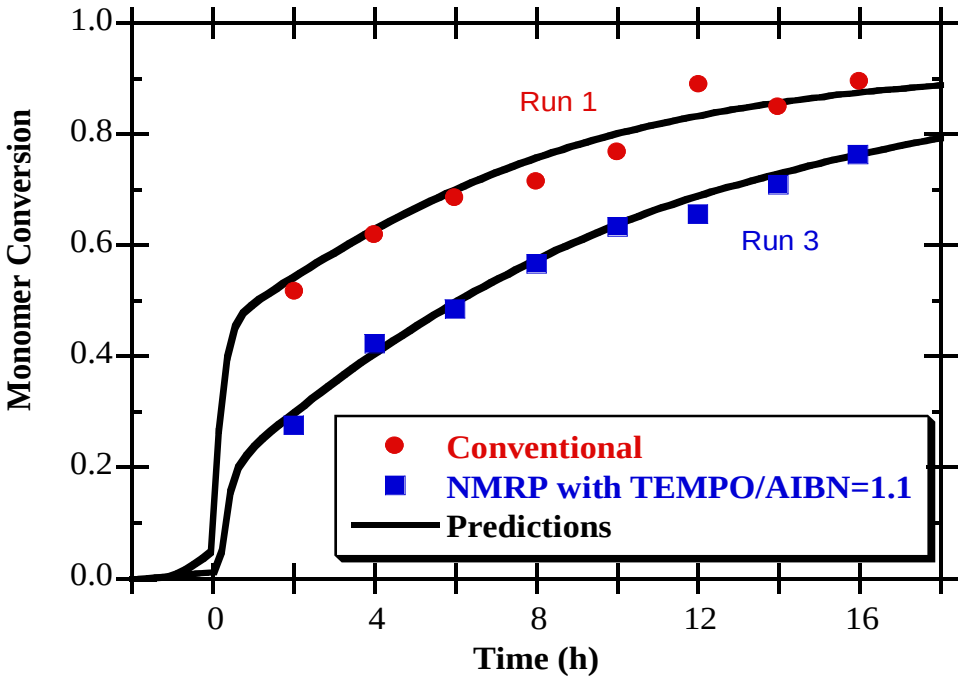

Figure 4.4. Predictions and experimental observations for monomer conversion in conventional and NMRP runs.

Figure 4.6 compares FRP and NMRP STY/DVB runs with the same initial mole fractions of DVB ($y_{DVB} = 0.5$ %). These experiments and theoretical predictions confirm that NMRP can be used at least to have a better control on the dynamics of such polymerisation systems. Figure 4.7 shows measured and predicted time evolutions of $\bar{M}_w$ in NMRP STY/DVB runs with different mole fractions of crosslinker, stressing the influence of the initial amount of DVB in the dynamics of polymer properties. These experiments were simulated using the reactivity of PDBs as fitting parameters. It was estimated that PDBs present a lower reactivity as compared to styrene, with a ratio of propagation constant $C_{PDB} = k_p^*/k_p = 0.35$. Other

details concerning the postulated relation between the reactivity of other species with minor impact on the crosslinking process can be found elsewhere (Gonçalves *et al.*, 2007). Once again, this lower reactivity ratios of PDBs here estimated should be only apparent values since the effect of neglected intramolecular cyclizations reactions should be more important at the 50 % dilution, which was used in the experiments, as compared with bulk polymerisations used in related works (Ide and Fukuda, 1997) which have found an equal reactivity of PDB ($C_{PDB} = 1$). An apparent decrease in the reactivity of PDB for diluted conditions has also been previously estimated in the framework of FRP of STY/DVB (Gonçalves *et al.*, 2007). Indeed, NMRP of STY/DVB as compared to FRP allows an improved control over the crosslinking process and gelation, which is an important advantage in the production of hyperbranched polymers.

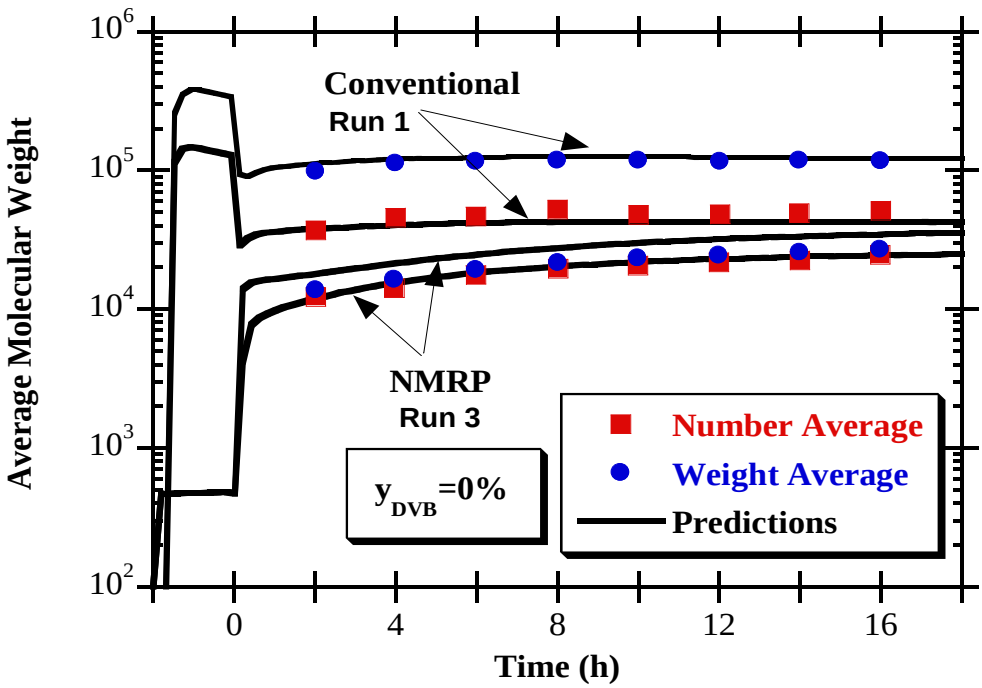

Figure 4.5. Predictions and experimental observations of $\bar{M}_n$ and $\bar{M}_w$ in FRP and NMRP linear runs. Simulations include the thermal initiation of styrene during the heating period.

Figure 4.8 shows the measured and predicted time evolution of *z*-average radius of gyration ($\bar{R}_g$) of NMRP of STY/DVB samples synthesized with different initial amounts of DVB. A good agreement between measurements and simulations can be observed and it should be noticed that calculations of $\bar{R}_g$ have been carried out using the same set of kinetic parameters as in the calculations of molecular weights. The measurements of $\bar{R}_g$ were performed in THF

solution using SEC/RI/MALLS system and our theoretical predictions of $\bar{R}_g$ are only valid for Gaussian chains (Costa and Dias, 2007) in a Θ solvent. To obtain the predictions presented here was assumed equality of the expansion factors of branched and linear polymer molecules $\bar{R}_g/\bar{R}_{g,\theta} = 0.426\bar{M}_z^{0.1}$ (see Gonçalves *et al.*, 2007 and references therein). The influence of the initial mole ratio of TEMPO/AIBN in the time evolution of $\bar{R}_g$ of STY/DVB copolymers is presented in Figure 4.9. Again, despite the simplifications used in the computational of $\bar{R}_g$, a good agreement with measurements is observed. These results also show the possibility of using the ration TEMPO/AIBN to control the dynamics of crosslinking of these products.

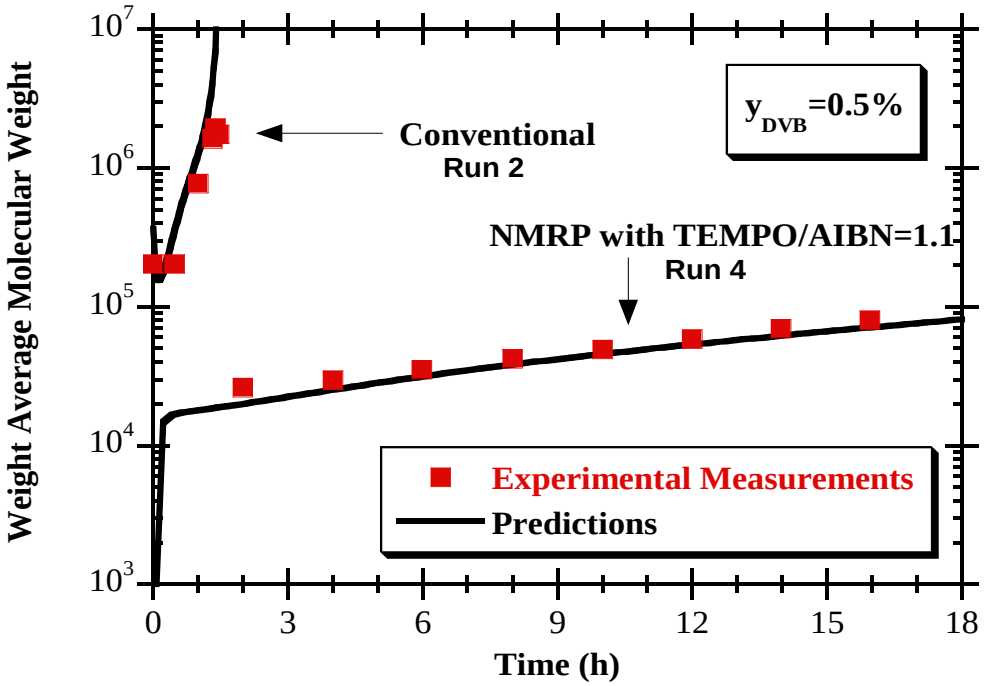

Figure 4.6. Measured and predicted time evolution of $\bar{M}_w$ in FRP and NMRP STY/DVB runs.

Figure 4.10 shows the measured dependencies of molecular weight (MW) on elution volume for NMRP synthesized samples of STY/DVB corresponding to different polymerisation times. One can observe the progressive shift of the molecular architecture of the products from the linear case and an inversion in the relation of MW versus elution volume (hydrodynamic radius) owing to the existence of polymer chains with the same molecular weight but different molecular sizes (elution volume), as observed for other non-linear polymerisation systems (Bannister *et al.*, 2006). Figure 4.11 confirms the presence of important differences in the molecular architecture of FRP and NMRP STY/DVB samples

collected near the corresponding gelation points. For the same molecular size, NMRP products have higher molecular weight than the FRP materials.

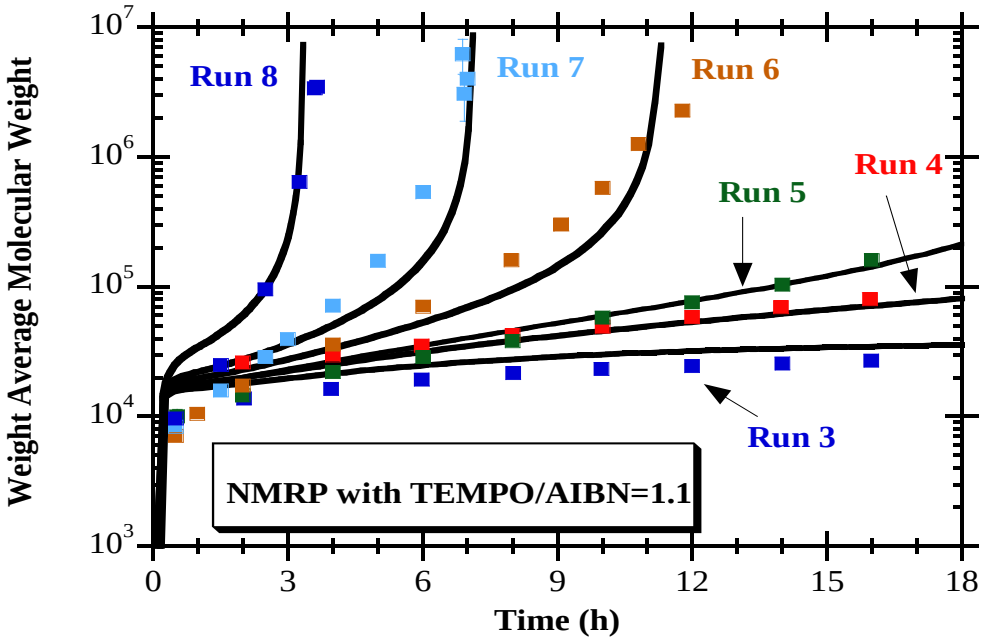

Figure 4.7. Measured and predicted time evolution of $\bar{M}_w$ in FRP and NMRP STY/DVB runs with different amounts of crosslinker.

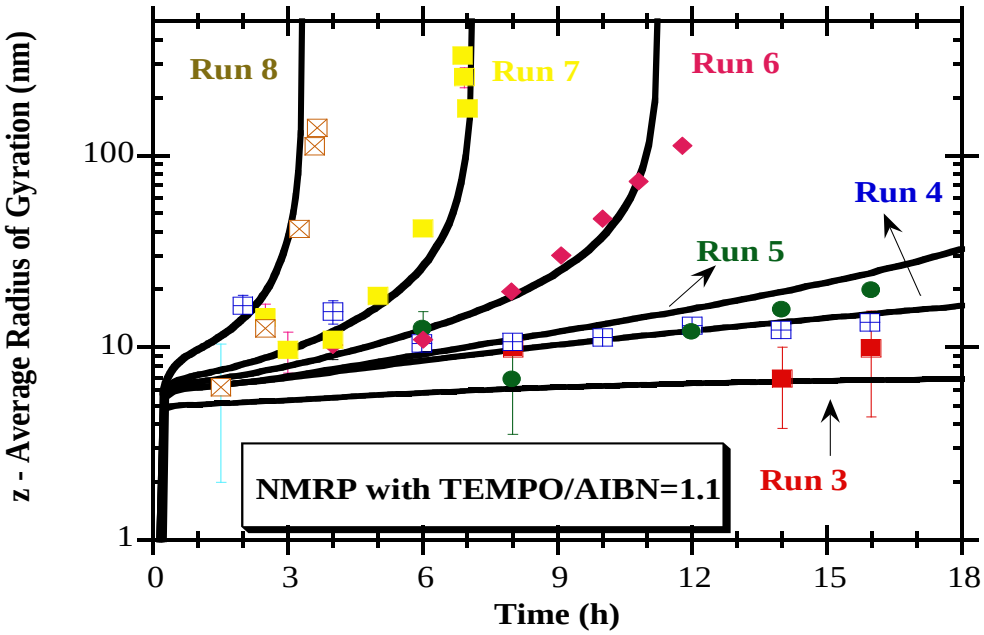

Figure 4.8. Measured and predicted time evolution of $\bar{\bar{R}}_g$ in FRP and NMRP STY/DVB runs with different amounts of crosslinker.

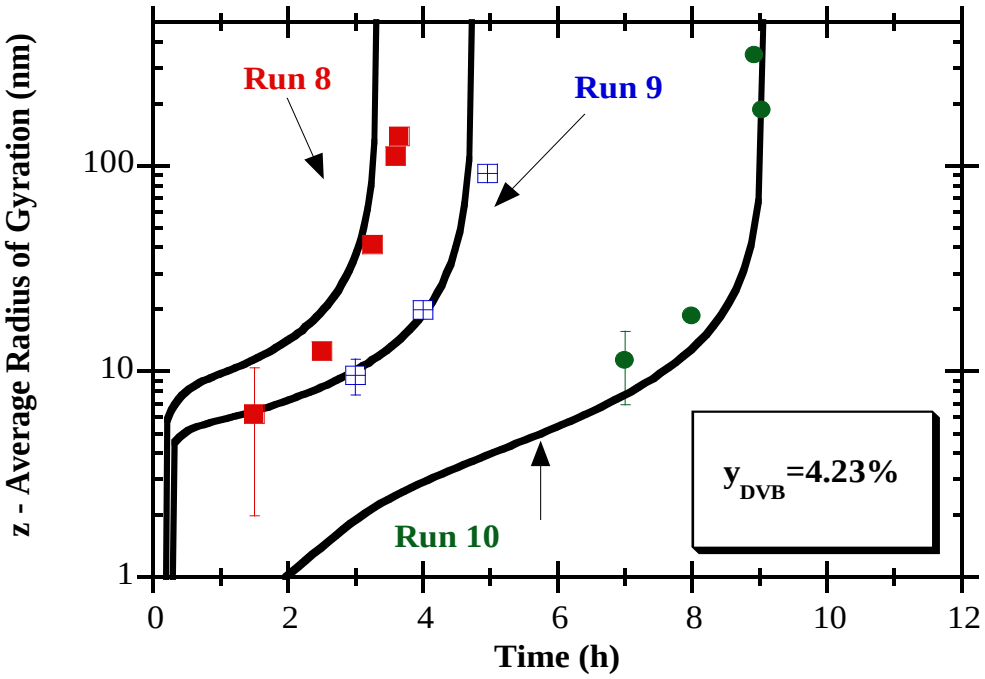

Figure 4.9. Comparison of experimentally observed and predicted influence of the initial molar ratio TEMPO/AIBN on the time evolution of $\bar{R}_g$ in NMRP STY/DVB runs.

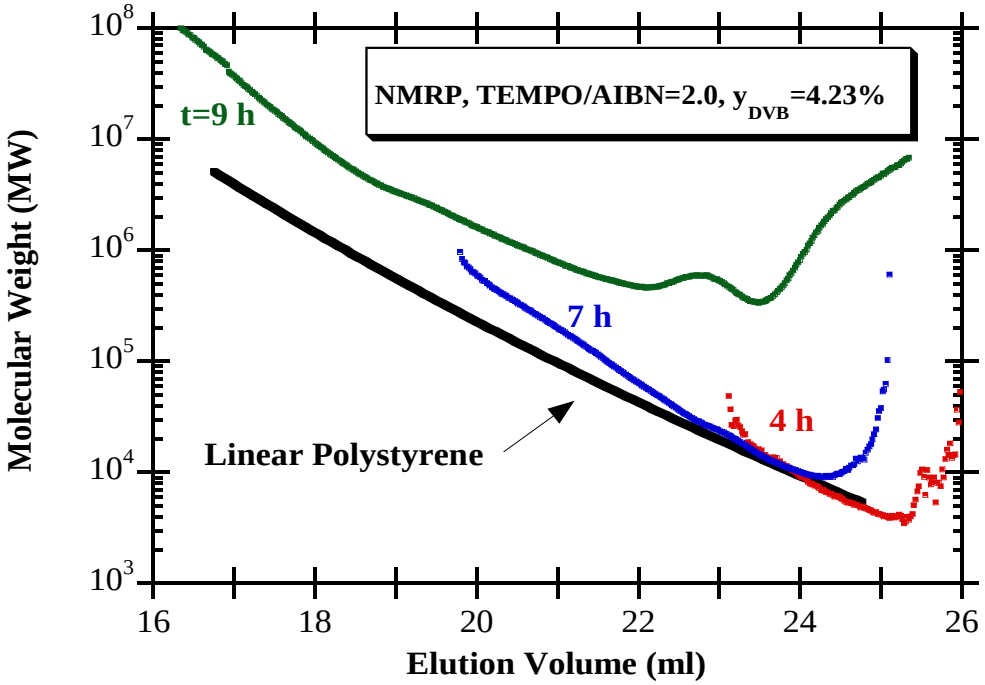

Figure 4.10. Observed relations of molecular weight *versus* elution volume in SEC traces of run 10 in Table 4.1 corresponding to different polymerisation times.

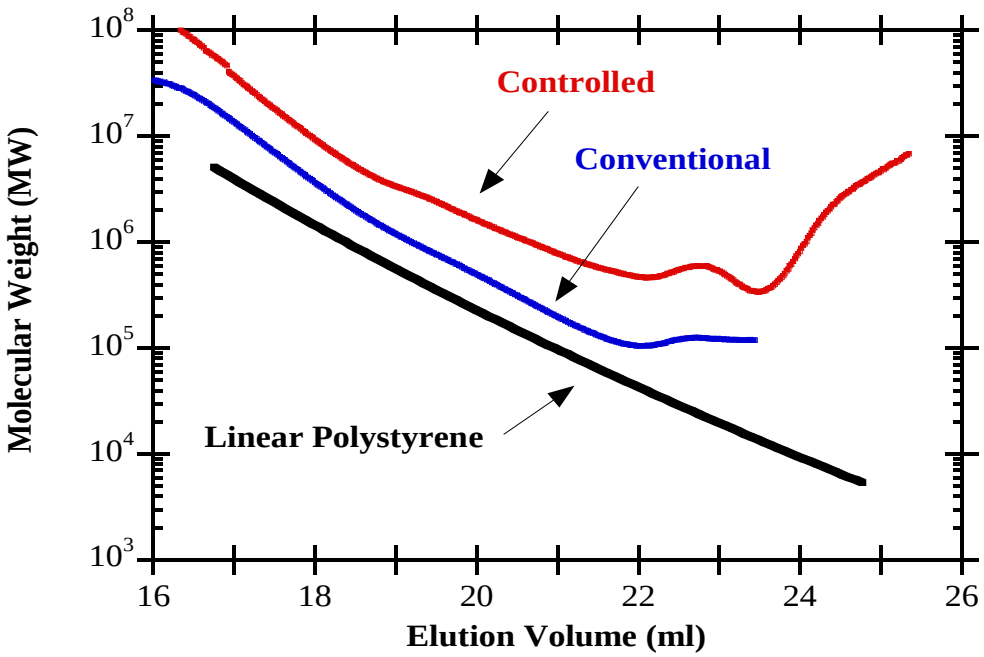

Figure 4.11. Observed relations of molecular weight *versus* elution volume in SEC traces of conventional and NMRP synthesized samples of STY/DVB corresponding to polymerisation times near the gel point.

The measured relation $\ln([M]_0/[M]) = -\ln(1-p)$ versus polymerisation time in two NMRP experiments with different initial mole ratios TEMPO/AIBN (1.1 and 2.0) is shown in Figure 4.12. These polymerisations were performed in xylene solution (50 vol. % monomer) at *T*=130 °C. It should be noted that TEMPO was fed to the reactor in the initial mixture being submitted to the warming-up process, which is depicted in Figure 4.13 for a typical run. It can be concluded that NMRP is useful not only for manipulating the dynamics of crosslinking of these materials but also for modifying the structure of the products, with a likely impact on their end uses. In these experiments, polymerisation was initiated by the addition of AIBN ($t = 0$), as also shown in Figures 4.13 and 4.14. The linear relations observed in Figure 4.12 point to a living character of the NMRP runs performed but a non-ideal behaviour of such process is identified for low polymerisation times (near $t = 0$). This is probably a consequence of side reactions involving the AIBN decomposition, which should start at $t = 0$. These effects have a lower impact for higher initial proportion TEMPO/AIBN, which is consistent with an increasing control of the polymerisation. Nevertheless, the decrease of the reaction rate is a drawback associated with the use of a high initial mole ration of TEMPO/AIBN.

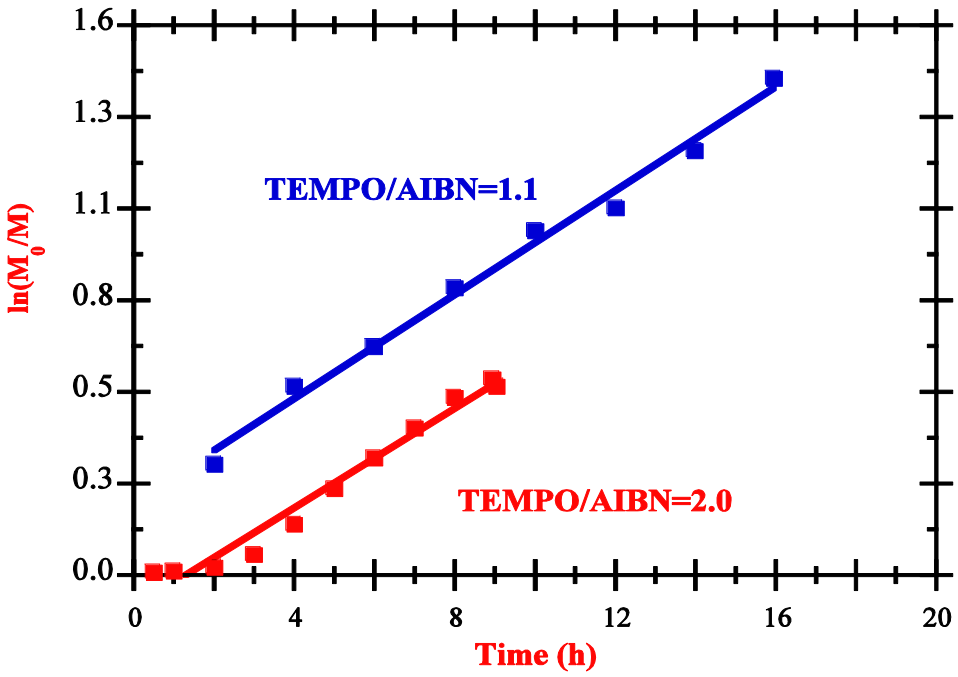

Figure 4.12. Measured relation $\ln([M]_0/[M]) = -\ln(1-p)$ versus polymerisation time in NMRP experiments with different initial mole ratios TEMPO/AIBN.

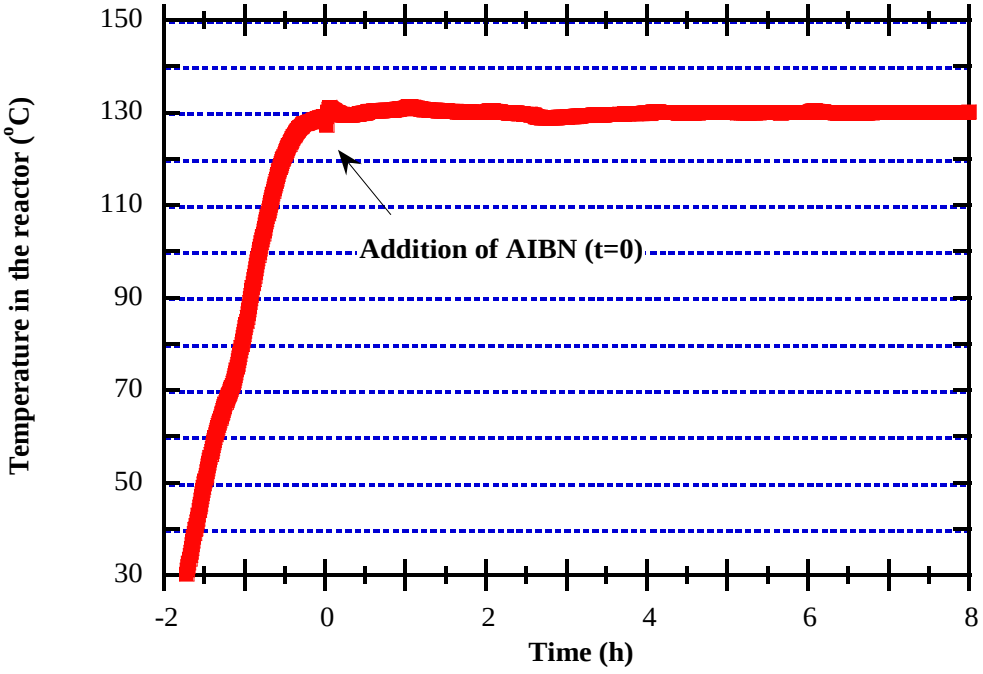

Figure 4.13. Observed dynamics of reactor temperature during the warming-up of NMRP process.

The usefulness of the kinetic modelling presented here for the NMRP of STY/DVB becomes clear in Figure 4.14, where the predicted and observed time evolution of $\bar{M}_w$ during the NMRP of STY/DVB with $y_C = 2\,\%$ and TEMPO/AIBN = 1.1, are presented. Indeed, it is possible to include in the simulations the warming-up period before the addition of AIBN, where the kinetic mechanisms involving the thermal polymerisation of styrene could have an important role. Simulations show that, due to the presence of TEMPO in the mixture, auto-polymerisation is practically avoided during this period. This prediction is confirmed by experimental measurements concerning samples collected before the addition of AIBN, as also presented in Figure 4.14. Evolution of the crosslinking process after addition of AIBN was also predicted and experimentally measured. It should be noted that in many vinyl/divinyl CRP experiments reported in the present work, i.e., those presented in Figure 4.14, gelation was experimentally observed.

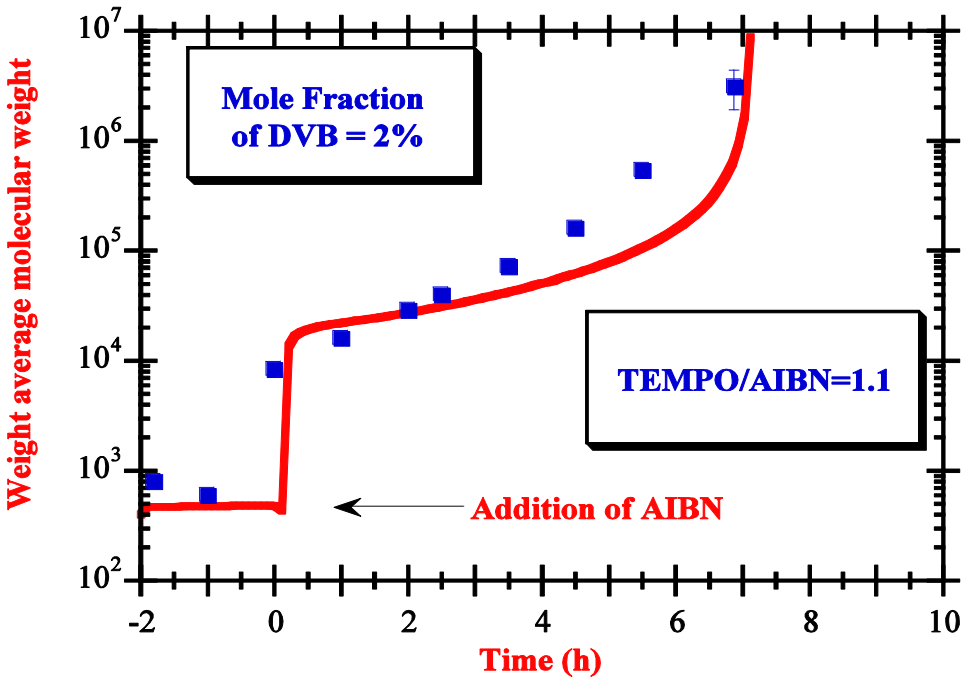

Figure 4.14. Predicted and observed time evolution of $\bar{M}_w$ during the NMRP of STY/DVB with $y_C = 2\,\%$ and TEMPO/AIBN = 1.1. Simulations and experimental studies include the warming-up period before the addition of AIBN.

It should be noted that the living characteristic of linear NMRP systems is identified through the linearity of the evolution of the molecular weight (degree of polymerisation) with reaction time and also due to the associated very low polydispersity index (PDI). Nevertheless, this

chapter is mostly concerned with non-linear NMRP systems, and therefore, linearity of molecular weight or very low PDI cannot be observed in general. Such non-linear evolution of molecular weight with polymerisation time is illustrated in Figure 4.14 with regard to the NMRP of STY/DVB. This issue becomes even more clear in Figure 4.15, where the predicted and the experimentally measured time evolution of PDI in the linear NMRP of STY and non-linear STY/DVB ($y_C = 1.22\ \%$), are compared. In both cases, the initial mole ratio between TEMPO and AIBN is 1.1. A very low (and constant) PDI is observed and predicted in the linear case, which results from the living character of the polymerisation. In the non-linear case (STY/DVB with $y_C = 1.22\ \%$), a living polymerisation is also promoted but PDI grows substantially with polymerisation time due to the crosslinking process. Gelation can be attained with the associated infinite PDI.

Important works dealing with theoretical and experimental studies concerning the NMRP of STY/DVB have been reported in the last few years (Hernández-Ortiz *et al*., 2009; García-Morán, *et al*., 2009; Quintero-Ortega *et al*., 2009; Saldívar-Guerra *et al*., 2009; Nogueira *et al*., 2010). The NMRP of STY/DVB in supercritical carbon dioxide has been described and that analysis is also extended to the post gelation period. Significant modelling efforts (Hernández-Ortiz *et al*., 2009) were also performed using the *pseudo-kinetic* method approach and the post gelation period is analysed by means of the Flory-Stockmayer theory of gelation (Flory, 1941a, 1941b and 1941c; Stockmayer, 1943 and 1944).

An extensive comparison between the present general kinetic approach and alternative methods used to describe non-linear polymerisation has been presented in (Costa and Dias, 1994, 2005, 2006 and 2007; Dias and Costa, 2006 and 2007). These comparisons show the often important deleterious effect of approximations such as the pseudo-steady state for radical concentrations and neglecting the existence of polymer molecules with more than one radical (monoradical assumption), neglecting the existence of polymer molecules with more than one terminal/pendant double bond. In the context of CRP systems, it is also often considered that dormant polymer molecules contain only one capping unit (monofunctionality assumption). These and other approximations are avoided with the present approach, as shown in (Costa and Dias, 1994, 2005, 2006 and 2007; Dias and Costa, 2006 and 2007). It should be noted that this theory is also applicable after gelation and will be discussed further in this chapter.

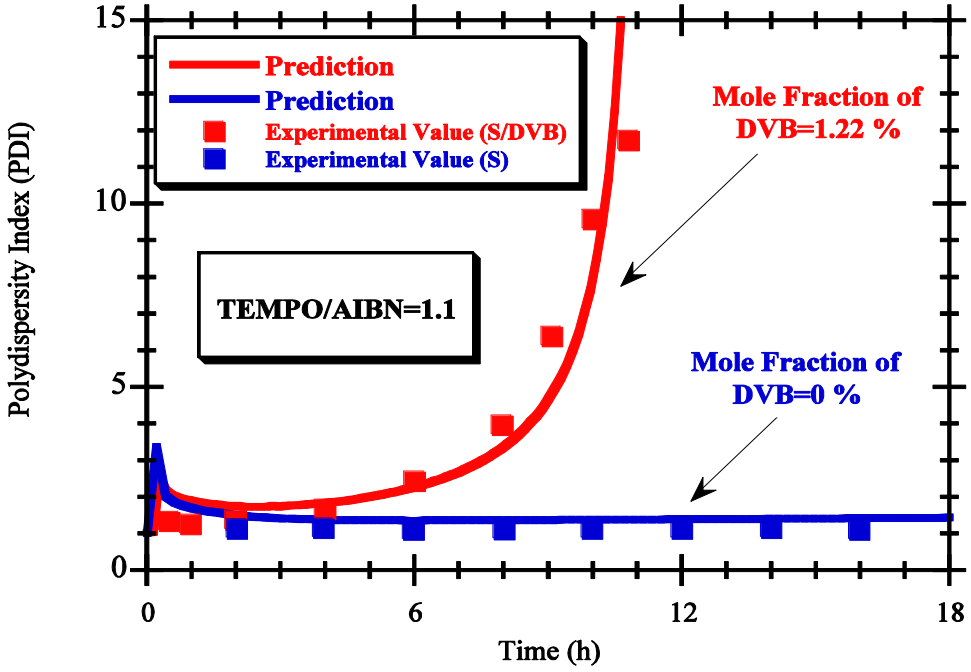

Figure 4.15. Predicted and experimentally measured time evolution of PDI in linear NMRP of styrene and non-linear NMRP of STY/DVB.

Another source of complexity in the analysis of STY/DVB copolymerisations is found if the DVB contains a mixture of *m*- and *p*-DVB isomers, which in the case of the commercial DVB used in the present experimental studies. Different reactivities of the two isomers and correspondent PDBs have been reported in several works but scattered values of these parameters have also been reported (see Hernández-Ortiz *et al.*, 2009; Hecker, 2000 and references therein). In this context, the detailed kinetic model presented here for the NMRP of STY/DVB is especially useful because such complexities can be considered in the simulations. This issue is illustrated in Figure 4.16, depicting the predicted effect of the reactivities of the pendant double bonds of *m*- and *p*-DVB (C_{PDBm} and C_{PDBp}, respectively) in time evolution of PDI in NMRP of STY/DVB ($y_C = 4.2\ \%$). In all of the simulations, the same initial mole ratio TEMPO/AIBN = 1.1 was considered. The strong influence of these parameters on the time evolution of polymer properties and even the importance of the distinction between the two isomers should be noted.

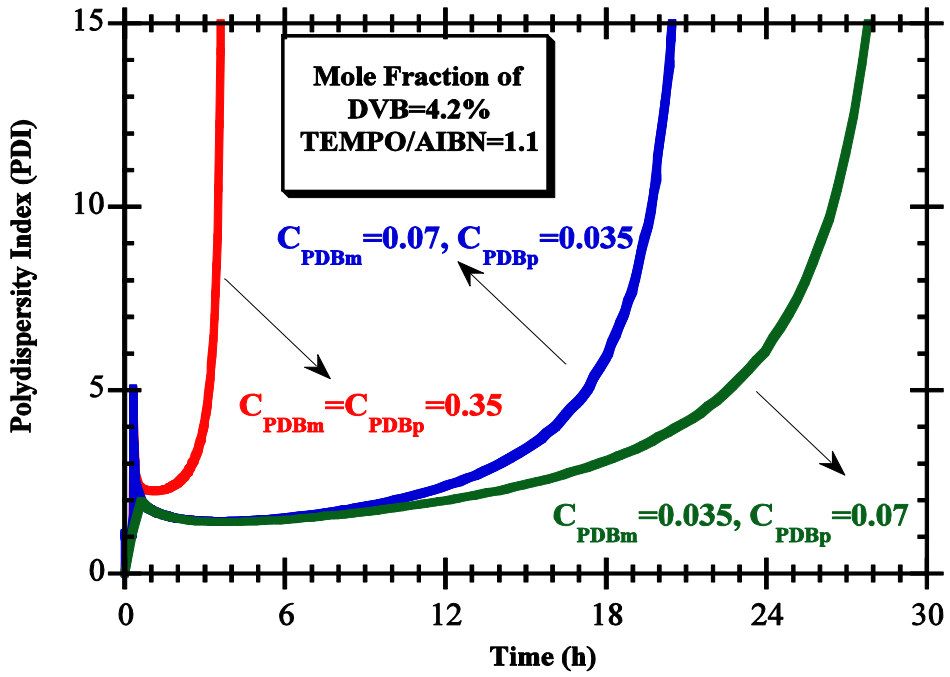

Figure 4.16. Predicted effect of the reactivity of the pendant double bonds of *m*- and *p*-divinylbenzene in the time evolution of PDI for the NMRP of STY/DVB.

4.5 Suspension Copolymerisation of NMRP of STY/DVB Leading to Gel Formation

4.5.1 Results and Discussion

4.5.1.1 NMRP Homopolymerisation of Styrene

An assessment of the efficiency of controlled polymerisation (NMRP) under the particular experimental conditions here considered (with special emphasis to the effect of operating at an aqueous suspension) was performed by taking the STY homopolymerisation as a reference. Typical results thus obtained are presented in Figures 4.17 to 4.20. Figure 4.17 depicts the measured time evolution of monomer conversion for NMRP of STY aqueous suspension polymerisation at 130 °C, with operation conditions from run 12 in Table 4.2. When these values are used to generate a plot of $-\ln(1-p)$ versus reaction time, as presented in Figure 4.18, a nearly relation after the inhibition delay is observed, confirming the controlled character of the polymerisation. Another usual feature of controlled polymerisation is illustrated in Figure 4.19 (linear growth of molecular weights with

monomer conversion) and Figure 4.20 where a polymer population of low (around 1.1) molecular weight dispersity is shown to be formed along the polymerisation.

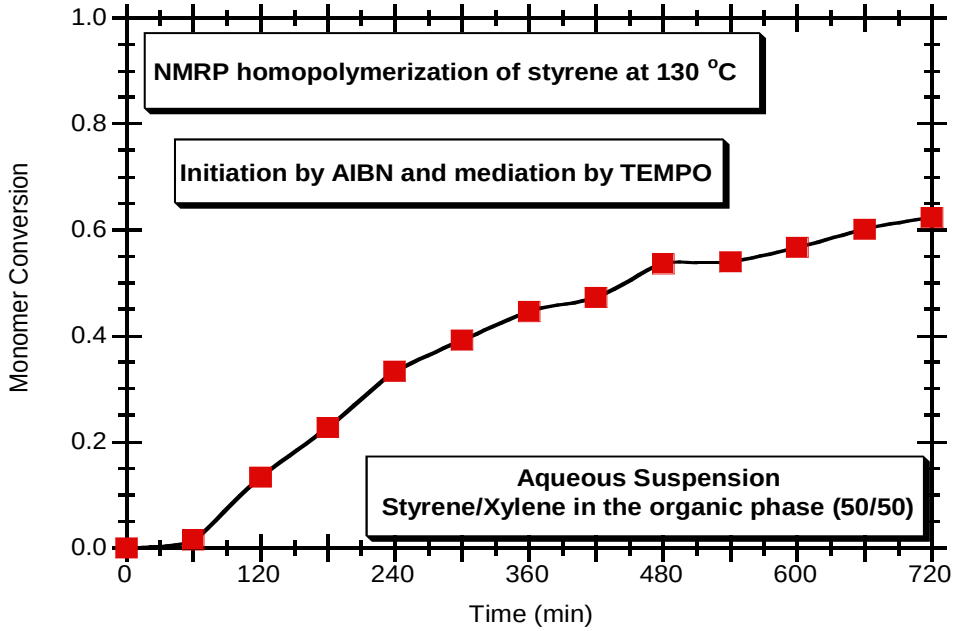

Figure 4.17. Measured reaction time evolution of monomer conversion for the NMRP aqueous suspension of STY at 130 °C. Solid lines connecting experimental measurements are only visual aids.

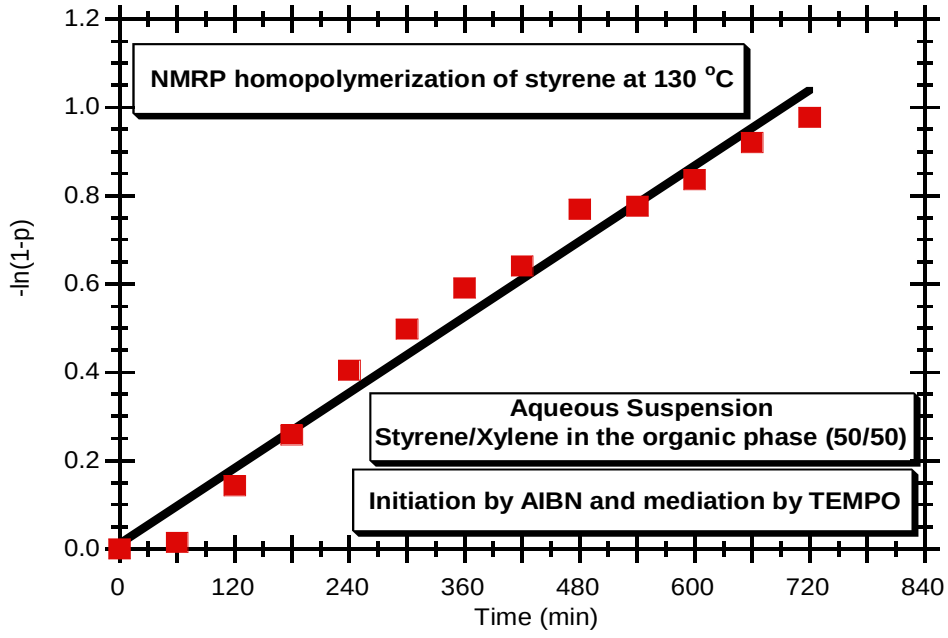

Figure 4.18. Plot of $-\ln(1-p)$ *versus* time for the same data of Figure 4.17.

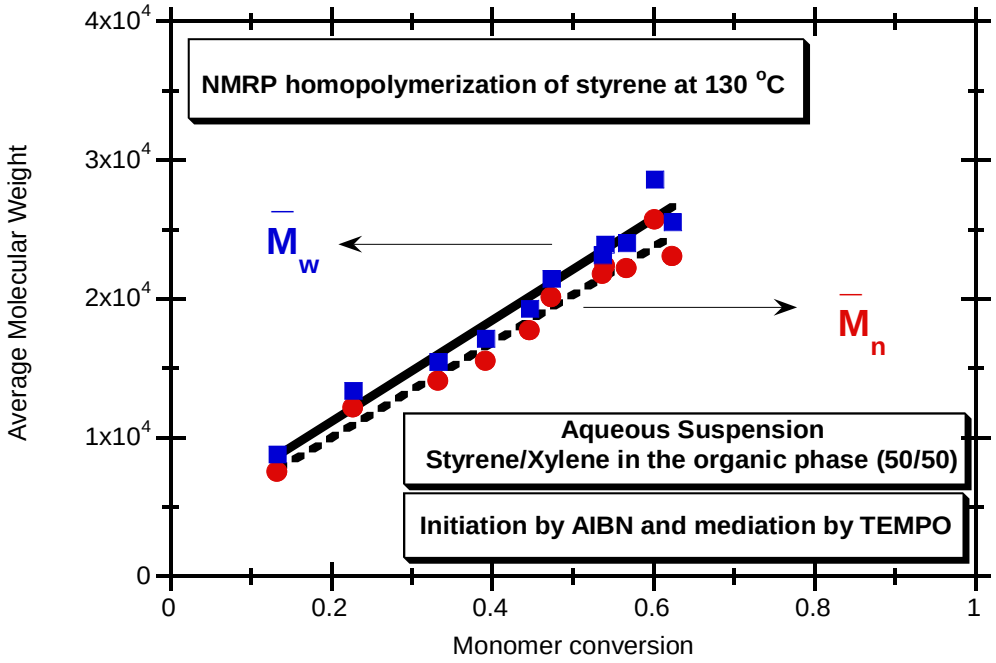

Figure 4.19. Measured dependence with monomer conversion of $\bar{M}_n$ and $\bar{M}_w$ for the NMRP aqueous suspension of STY at 130 °C.

These observations were supported by SEC/RI/MALLS analysis of samples collected at different polymerisation times, as above described. Typical SEC traces observed are shown in Figure 4.21 (RI signal with normalization by the peak maximum arising from the monomer/solvent elution) and Figure 4.22 (MALLS signal with normalization by the peak maximum arising from the polymer elution). Growth with reaction time of polymer concentration can be observed in Figure 4.21, whereas Figure 4.22 shows the progressive growth of the molecular size of these polymer populations.

4.5.1.2 Comparison Between NMRP/STY and NMRP STY/DVB

A huge change in the molecular architecture of NMRP products is observed when even a small amount of DVB is added to the reaction mixture. Owing to the crosslinking process, a very broad distribution of non-linear species is formed and gelation (formation of macroscopic insoluble network) is possible. With FRP of vinyl/divinyl monomers, this crosslinking mechanism was extensively theoretically characterized in past works (Gonçalves *et al.*, 2007 and 2011a; Trigo *et al.*, 2008 and references therein) and these issues are here investigated for NMRP of STY/DVB with gel formation. Figure 4.23 shows the RI signal of

samples with different polymerisation time from NMRP of STY/DVB with conditions of run 10 in Table 4.2 (5 mol % of DVB in the monomer mixture).

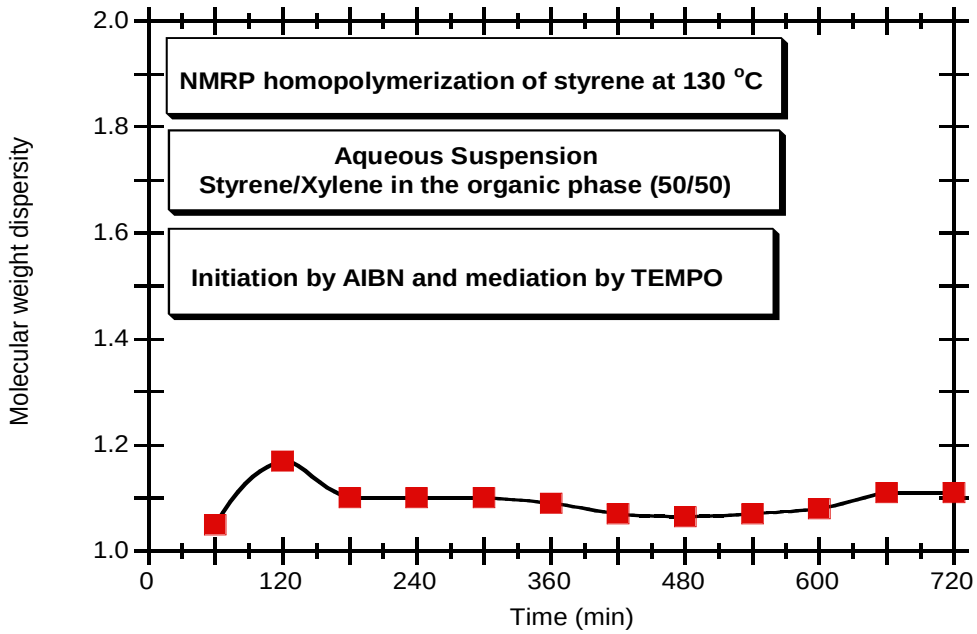

Figure 4.20. Measured reaction time evolution of molecular weight dispersity of the products of NMRP aqueous suspension of STY at 130 °C.

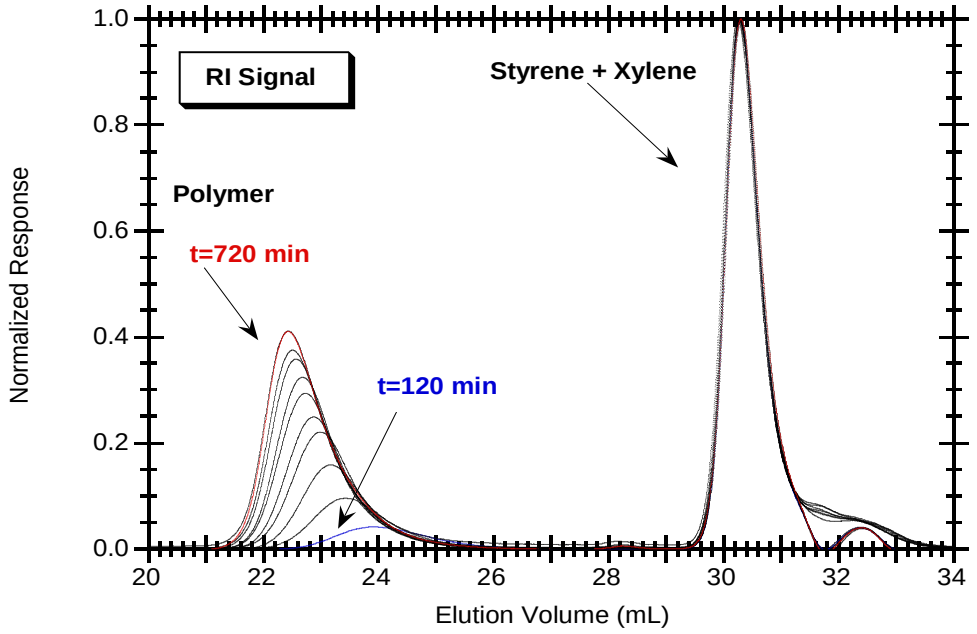

Figure 4.21. RI signal observed for samples of NMRP synthesized polystyrene with different reaction time (run 12 in Table 4.2).

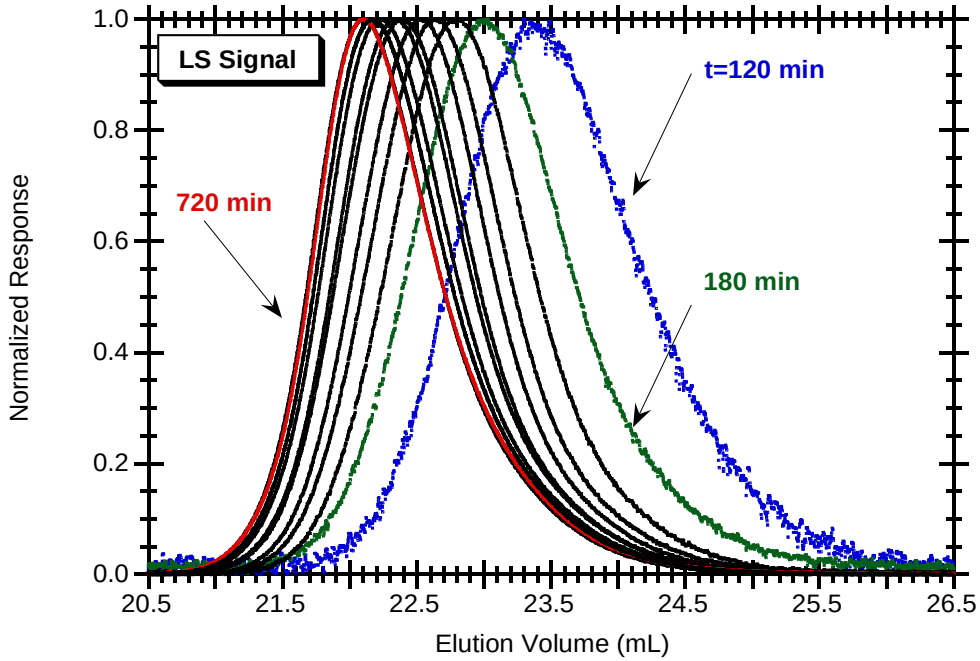

Figure 4.22. LS signal observed (only the 90° is presented) for samples of NMRP synthesized polystyrene with different reaction time (run 12 in Table 4.2).

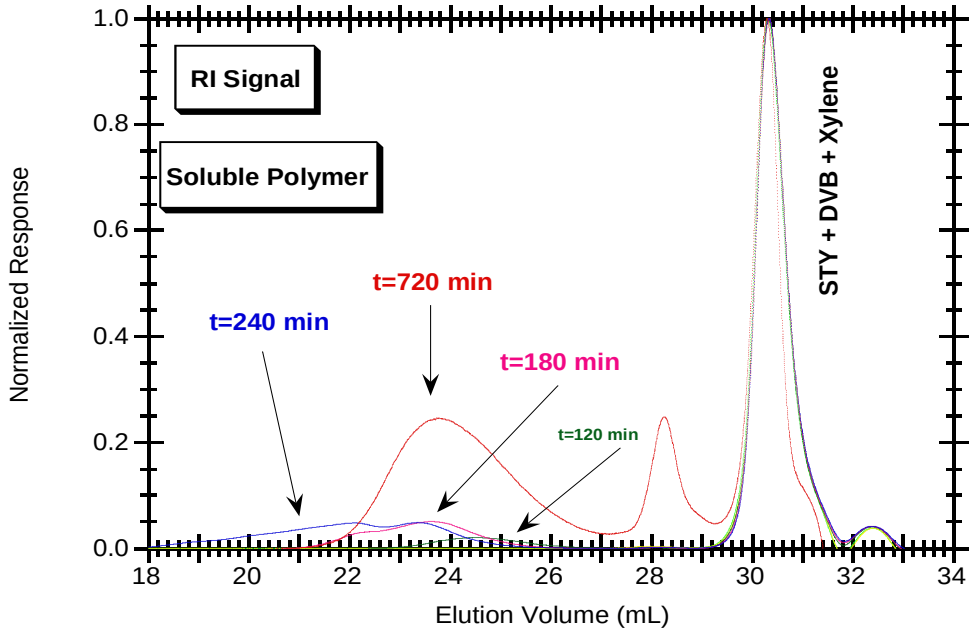

Figure 4.23. RI signal of samples collected at different polymerisation times from NMRP of STY/DVB (run 10 in Table 4.2).

Similar measurements from the MALLS signal (90°) are presented in Figure 4.24. Dissimilitudes between linear and non-linear NMRP become clear when Figures 4.21 and 4.22 are compared with Figures 4.23 and 4.24. Formation of a polymer population with broad size distribution, formation of a low amount of polymer cluster of very high size near gelation (see also Figure 4.25), and the shift of the size distribution to lower values after gelation are general features associated with crosslinking processes, which are also observed with FRP mechanisms (Gonçalves *et al.*, 2007 and 2011a; Trigo *et al.*, 2008). In contrast to the linear case, no significant differences between CRP and FRP are observed concerning this aspect.

Differences between molecular architecture of linear and non-linear are also highlighted in Figure 4.26, where the RI and MALLS signals of samples resulting from NMRP/STY and NMRP/STY/DVB (5 % DVB) are compared. Both samples were formed at the same polymerisation time and were synthesized with similar initial conditions, namely concerning the global monomer concentration, initiator and mediator (runs 10 and 12 in Table 4.2). The overall monomer conversion has similar values in both cases, but the highly dispersed/high size crosslinked polymer population presents a huge contrast with the almost homogeneous population arising from the linear case. Bimodality is observed for the RI signal of the crosslinked samples and the first peak should represent the low (or non-) crosslinked chains in these populations (see comparison with the RI signal of the linear sample).

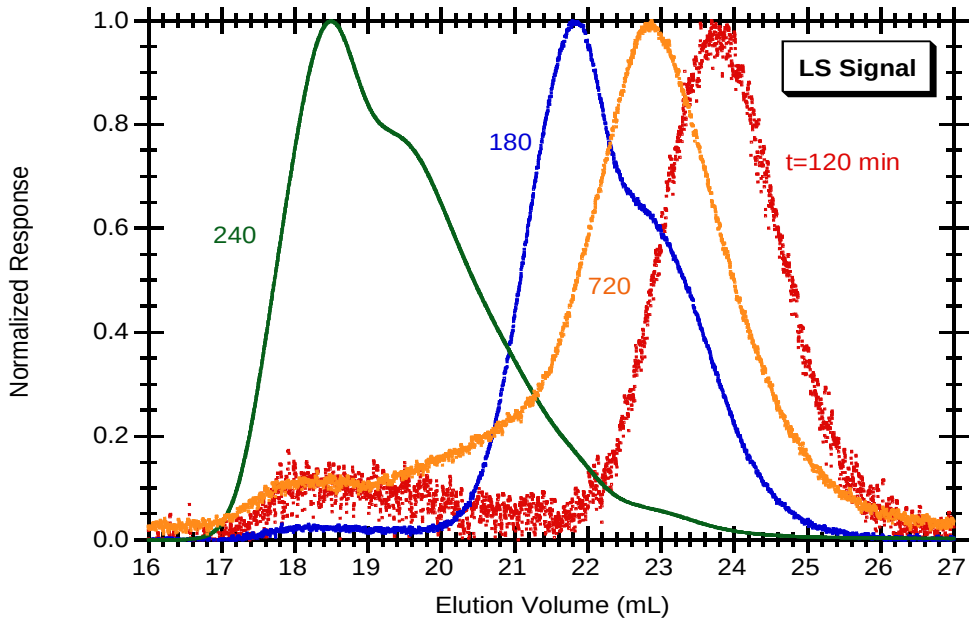

Figure 4.24. LS signal of samples collected at different polymerisation times from NMRP of STY/DVB (run 10 in Table 4.2).

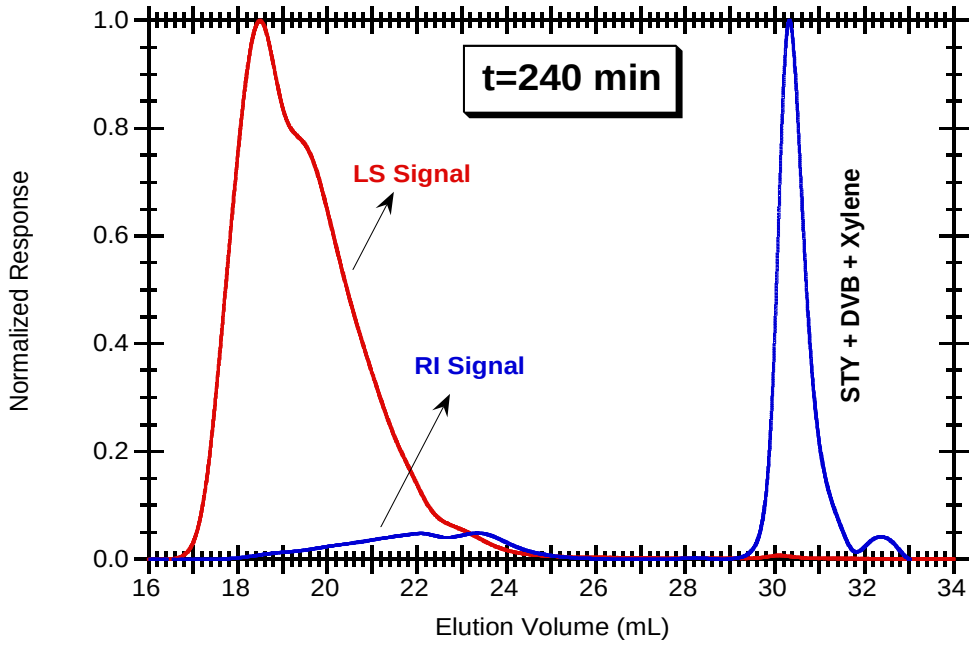

Figure 4.25. Normalized RI and LS signals of a sample with polymerisation time $t = 240$ min synthesized using NMRP of STY/DVB (Run 10 in Table 4.2).

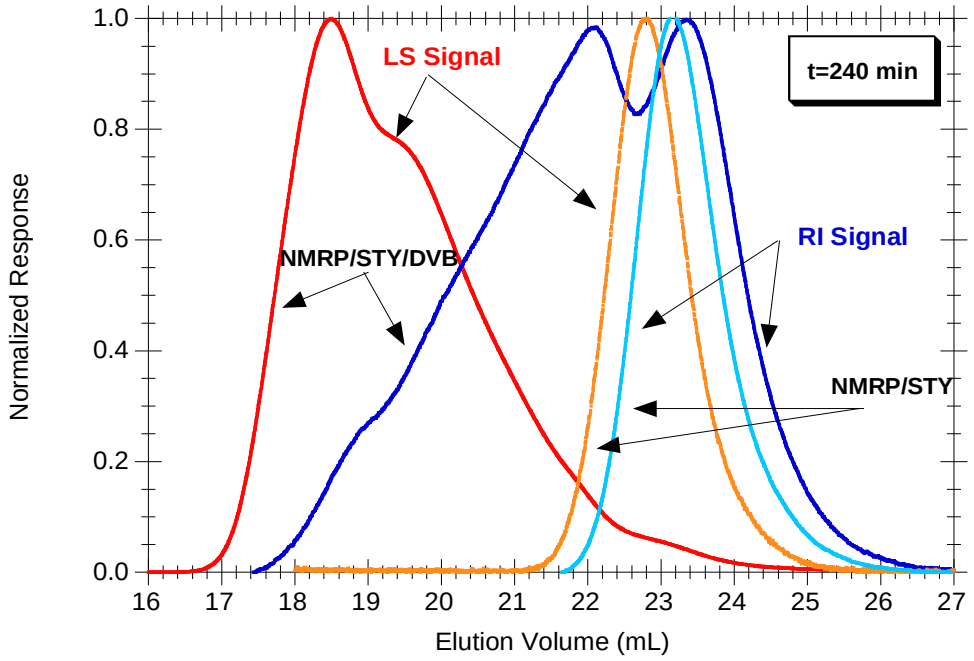

Figure 4.26. Comparison of the normalized RI and LS signals for samples with the same polymerisation time (240 min) in NMRP/STY (run 12 in Table 4.2) and NMRP/STY/DVB (run 10 in Table 4.2).

4.5.1.3 Effect of DVB Content

Gels based on STY/DVB and related crosslinked materials resulting from vinyl/divinyl copolymerisation were extensively studied in the past decades due to the applications as advanced materials. Manipulation of the gel swelling ratio through the adjustment of the DVB content, formation of macroporous materials by induced phase separation (presence of solvent with low thermodynamic affinity) and minimization of elastically ineffective chains due to non-ideal crosslinking are some important issues in this field. Most of the studies carried out on this subject were, however, based on the use of FRP synthesis, as described in the review by Okay (2000). Especially important in this field were the developments obtained by Dušek (1996 and 2007). Experimentally researches have been accompanied by the development of different theories aiming at the description of the crosslinking process and gel formation (Costa and Dias, 1994 2005 and 2007; Dias and Costa, 2003, 2005, 2006 and 2007).

With the advent of CRP in the early nineties (Georges *et al.,* 1993, Solomon *et al*., 1986) the synthesis of linear polymers and copolymers with a prescribed molecular architecture became possible, as above depicted for the NMRP of STY. Therefore, it is worth knowing whether a high degree of control on the structure of non-linear products is also possible when FRP is replaced by CRP techniques. This issue was addressed in recent works considering different CRP techniques namely ATRP (Yu *et al*., 2007; Gao *et al*., 2007 and 2008; Gonçalves *et al.,* 2010a, 2010b, 2010c and 2010d), RAFT (Wang *et al*., 2012; Krasia and Patrickios, 2006; Achilleos *et al.*, 2007; Poly *et al*., 2008; Yu *et al*., 2008; Roa-Luna *et al*., 2010; Jaramillo-Soto and Vivaldo-Lima, 2012) and NMRP (Hernández-Ortiz *et al*., 2008; Gonçalves *et al*., 2010c and 2010d; Ide and Fukuda, 1997 and 1999; Abrol *et al*., 1997 and 2001; Peters *et al*., 1999; Viklund *et al.*, 2001; Zetterlund *et al*., 2005; Alam *et al*., 2006; Tanaka *et al*., 2007; Saka *et al.*, 2007; Tuinman *et al.*, 2006). In the present work, these studies are extended to the NMRP aqueous suspension copolymerisation of STY/DVB and new insights concerning gel particles formation in stirred reactors are presented, as below described.

Transition from the linear case ($y_C = 0$) to crosslinked systems with different initial amount of DVB is illustrated in Figure 4.27. NMRP aqueous suspension at 130 °C was considered and three runs with the same initial monomer concentration (runs, 9, 10 and 12 in Table 4.2) are compared in terms of the observed resection time evolution of $\overline{M}_w$. It was possible to carry out the measurement of product properties before and also after gelation for each single run due to the operation at aqueous suspension, which is a key distinctive feature of this section.

Results presented in Figure 4.27 qualitatively resemble FRP of the same monomers in terms of gelation. A huge difference is observed between the linear case and the crosslinked system since gel formation is observed in the latter case (see Gonçalves *et al*., 2010c and 2010d) for additional comparisons of FRP/NMRP of STY/DVB with solution polymerisation). Increasing the initial DVB content leads, as expected, to a lower gelation reaction time also with NMRP.

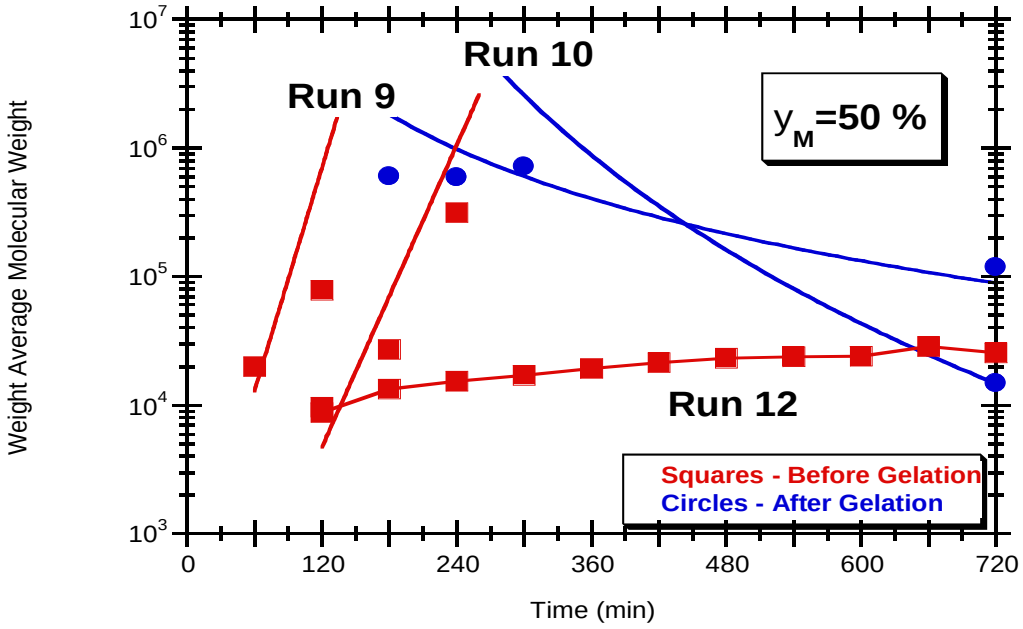

Figure 4.27. Measured effect of initial DVB content on reaction time evolution of $\bar{M}_w$ for NMRP aqueous suspension at 130 °C. Three runs are compared (runs 9, 10 and 12 in Table 4.2). Solid lines connecting experimental measurements are only visual aids.

The influence of initial amount of DVB on the molecular architecture of NMRP STY/DVB products is depicted in Figures 4.28 and 4.29. Samples with the same reaction time, for three different initial DVB compositions, are compared in terms of the observed RI and MALLS signals. Comparison with a linear sample ($y_C = 0$) highlights the effect of the amount of DVB on the dynamics of the products molecular structure. Under the conditions specified in Figure 4.28 and 4.29, the RI signal of sample with 5 % of DVB shows a polymer population close to the linear product with the development of a shoulder of small concentration products which should mark the beginning of the crosslinking process. Conversely, with $y_C = 50$ % the polymer population is shifted to upper molecular sizes due to the higher crosslinking degree of the sample. Note that t = 180 min is very close to the gel point for $y_C = 50$ % as

presented in Figure 4.27. A shoulder from a linear/low crosslinked population is also observed in the RI signal of this sample. Similar features are depicted in Figure 4.29 arising from the observed MALLS signal of the same samples. A very high molecular size cluster is identified in the $y_C = 50\,\%$ sample and mixed size polymer populations (linear and crosslinked) are observed with $y_C = 5\,\%$.

For an ideal crosslinking process the size distribution should consist of narrow peaks corresponding to polymer populations with different numbers of crosslinking points (Dias and Costa, 2010). As such distributions were not observed, important deviations from the ideal behaviour must be inherent to NMRP of STY/DVB. Therefore, NMRP, comparatively to FRP, allows only some (limited) control on the crosslinking process. By contrast, observation of multimodal distributions in the living anionic polymerisation of 1,4-DVB (at −78 °C) was recently reported in the literature (Hirao *et al*., 2011).

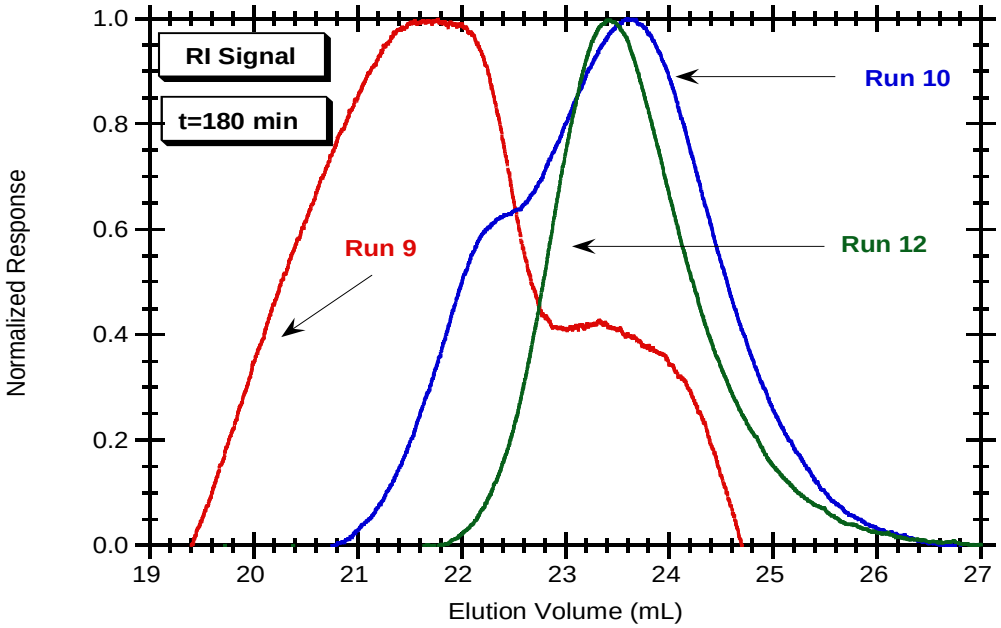

Figure 4.28. Effect of the initial DVB content on the observed RI signal of STY/DVB samples synthesized using NMRP aqueous suspension at 130 °C.

The effects of the initial amount of DVB on the dynamics of other important polymer properties in gel production are illustrated in Figures 4.30 and 4.31. The time evolution of the concentration of polymer PDBs is depicted in Figure 4.30 for NMRP polymerisation runs at 130 °C with 5, 50, and 100 % DVB (runs 8, 9, and 10). As expected, under conditions specified in Figures 4.30 and 4.31, the concentration of PDB in polymer decreases consistently with the initial amount of DVB. This information is critical for the production of

functionalized materials. Observation of the dynamics of PDB concentration during polymerisation is also a crucial issue to elucidate the impact of intramolecular cyclizations.

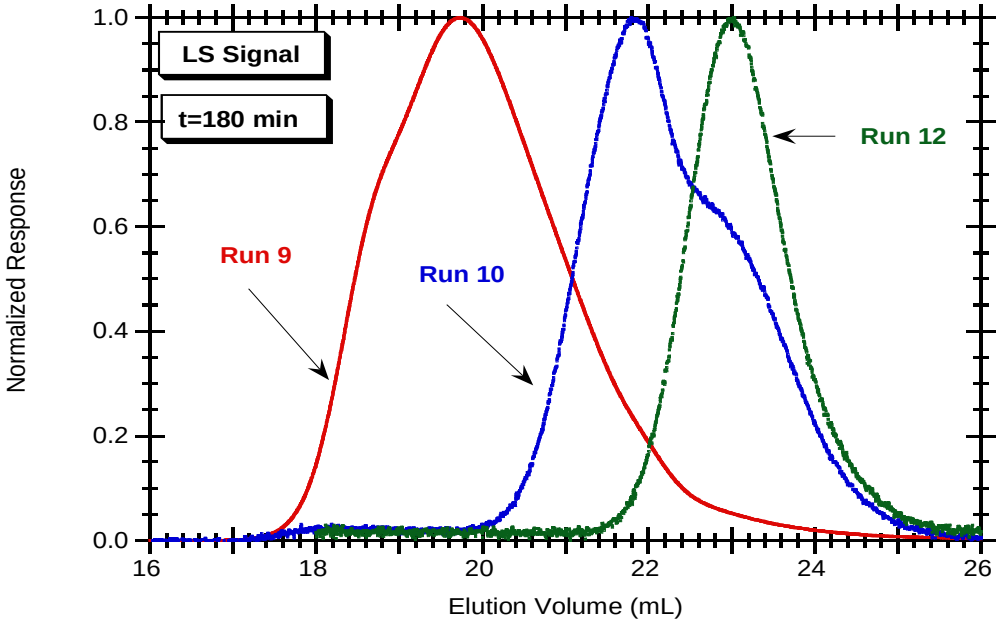

Figure 4.29. Effect of the initial DVB content on the observed LS signal of STY/DVB samples synthesized using NMRP aqueous suspension at 130 °C.

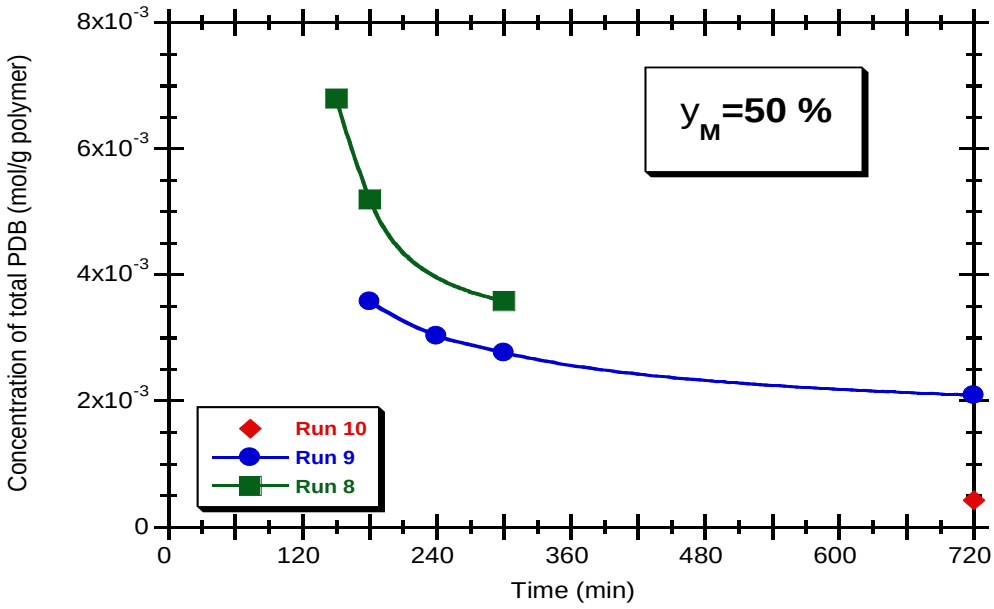

Figure 4.30. Measured effect of the initial DVB content on reaction time evolution of concentration of PDB. Three initial compositions are compared (100, 50 and 5 %) with NMRP aqueous suspension at 130 °C.

Dependence of the dynamics of gel formation on the initial amount of DVB is depicted in Figure 4.31. A final weight fraction of gel close to one is observed with very different initial compositions thus highlighting the ability of the insoluble network, also in NMRP, to incorporate the soluble polymer which is being produced along the polymerisation.

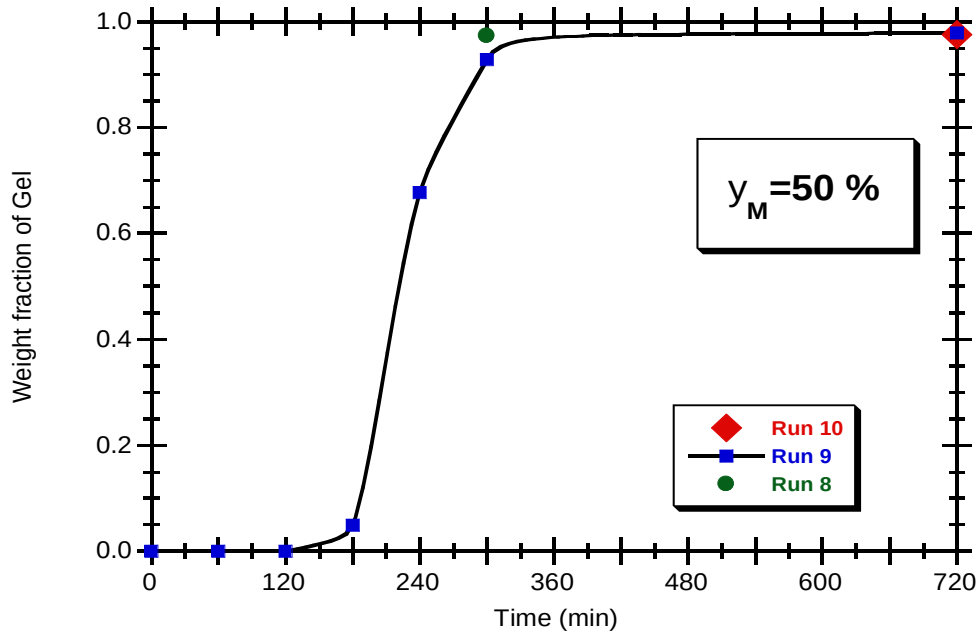

Figure 4.31. Measured effect of the initial DVB content on reaction time evolution of concentration of weight fraction of gel. Three initial compositions are compared (100, 50 and 5 %) with NMRP aqueous suspension at 130 °C.

4.5.1.4 Effect of Dilution

A major issue in the synthesis of polymer networks is the control of intramolecular reactions leading to formation of finite loops (cyclization) within the polymer structure. The crosslinking efficiency is reduced by these processes with a concomitant negative impact on the mechanical properties of the final materials. The reduced reactivity of PDBs (previously discussed for solution NMRP and ATRP crosslinking processes (Gonçalves *et al.*, 2010a, 2010b, 2010c and 2010d) is another issue leading to unexpected deviations from uniform random networks. The two mechanisms (loop formation/reduced reactivity of PDB) have similar effects on network properties related to elastically active concentrations of chains and junctions and are difficult to separate through a comparison with theoretical predictions of swelling. Additional information from kinetic modelling would certainly help.

Incidence of intramolecular cyclization is enhanced in diluted reaction media (as above described for the initial polymerisation stages) and comparison of polymerisation runs with the same amount of crosslinker at different monomer concentration should provide some clues to this problem. In particular, it is worth knowing whether, comparatively to FRP, the incidence of cyclizations decreases when NMRP is used.

The initial monomer concentration has an important effect on NMRP rate, as shown in Figure 4.32. Aqueous suspension NMRP runs at 130 °C with $y_M = 50$ and 20 % are compared in this plot. An obvious decrease in polymerisation rate was measured when initial monomer concentration changes from $y_M = 50$ to 20 %. After 12 h reaction time, a monomer conversion close to 60 % was measured with $y_M = 50$ % (Run 12 was used as reference for monomer conversion with $y_M = 50$ %), whereas the correspondent monomer conversion with $y_M = 20$ % is around 30 %.

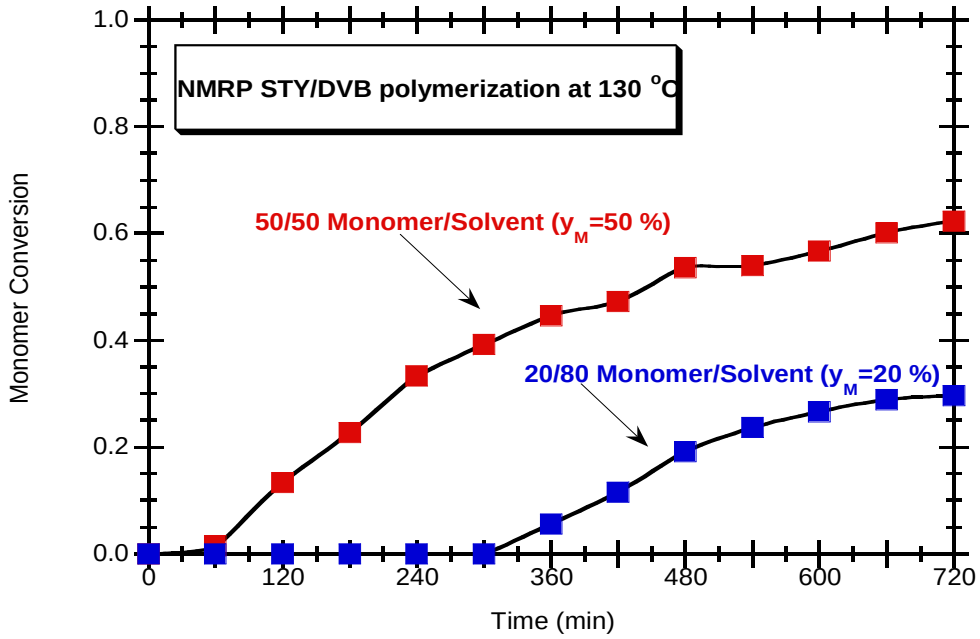

Figure 4.32. Measured effect of the initial monomer dilution on reaction time evolution of conversion for NMRP aqueous suspension at 130 °C. Solid lines connecting experimental measurements are only visual aids.

A comparison of the measured dependence of the weight fraction of gel (w_g) on reaction time is presented in Figure 4.33 considering two NMRP runs at 130 °C with the same initial DVB content ($y_C =$ 50 %), but at different initial monomer concentration ($y_M = 50$ and 20 %). It is interesting to note that with much diluted conditions the final weight fraction of gel ($t = 12$ h)

is close to zero, whereas for $y_M = 50$ % the correspondent weight fraction of gel is around one. This is also a consequence of the lower monomer conversion with $y_M = 20$ % delaying gel point. However, when a comparison of the dynamics of gelation is performed using the monomer conversion as the independent variable, as depicted in Figure 4.34, it seems that a delay in gelation does occur. This phenomenon should be the consequence of a higher incidence of intramolecular cyclization in the diluted system with a consequent waste of PDB along the crosslinking process.

The measured dynamics of weight-average molecular weight $\bar{M}_w$ for the same two runs is presented in Figures 4.35 and 4.36. Reaction time evolution of $\bar{M}_w$ with $y_M = 50$ % shows the occurrence of gelation at around $t = 180$ min, whereas a steady increase of $\bar{M}_w$ without the observation of a critical phenomenon is shown for $y_M = 20$ % (see Figure 4.35). With a plot where monomer conversion is the independent variable (see Figure 4.36) a critical conversion for gelation of around 20 % is identified with $y_M = 50$ % whereas the critical conversion for gelation with $y_M = 20$ % seems to be close to 30 %. These data confirm the expected increase of cyclizations with NMRP of STY/DVB when initial monomer dilution is higher.

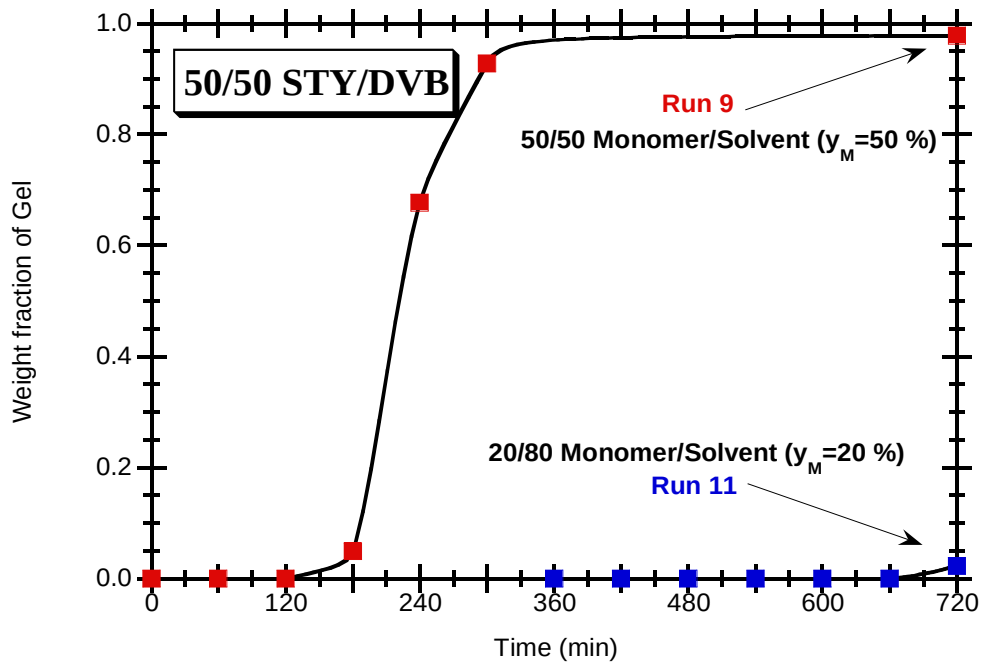

Figure 4.33. Measured effect of initial monomer dilution on reaction time evolution of weight fraction of gel for NMRP aqueous suspension at 130 °C. Solid lines connecting experimental measurements are only visual aids.

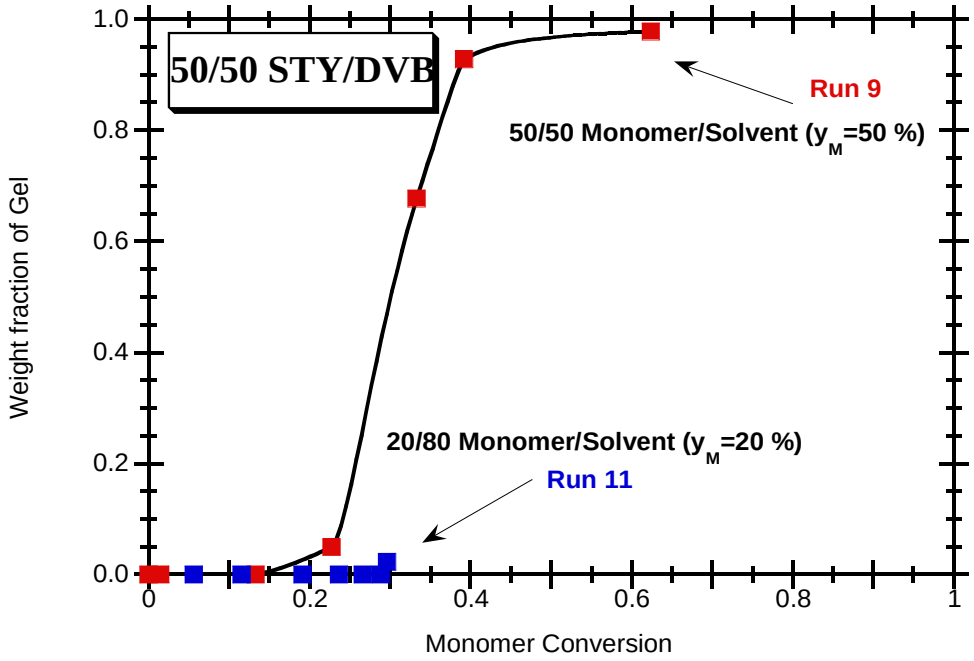

Figure 4.34. Measured effect of initial monomer dilution on monomer conversion of weight fraction of gel for NMRP aqueous suspension at 130 °C. Solid lines connecting experimental measurements are only visual aids.

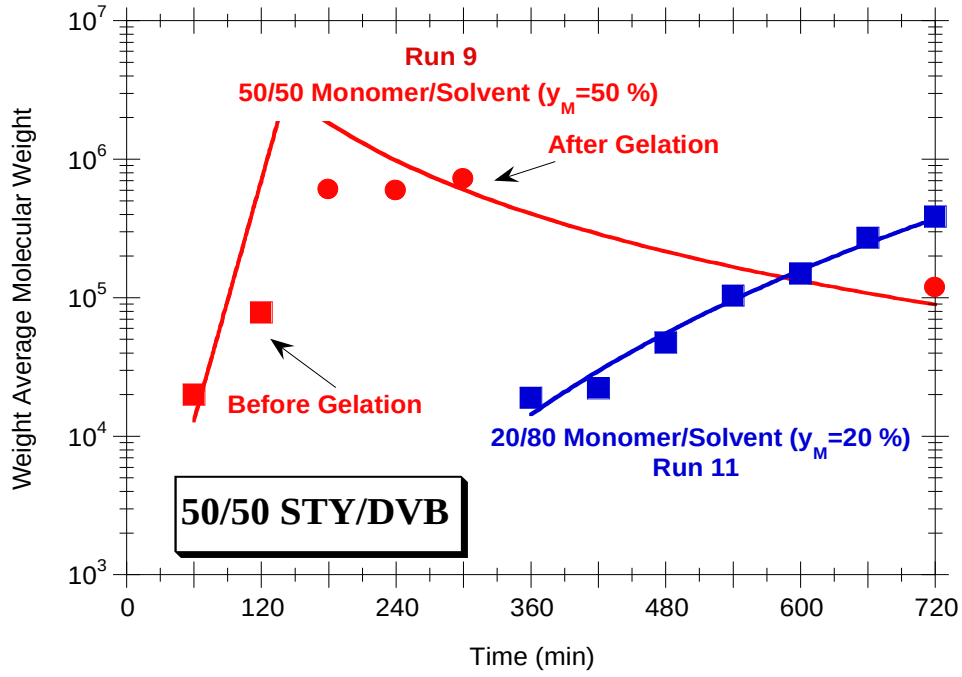

Figure 4.35. Measured effect of initial monomer dilution on reaction time evolution of $\bar{M}_w$ for NMRP aqueous suspension at 130 °C. Solid lines connecting experimental measurements are only visual aids.

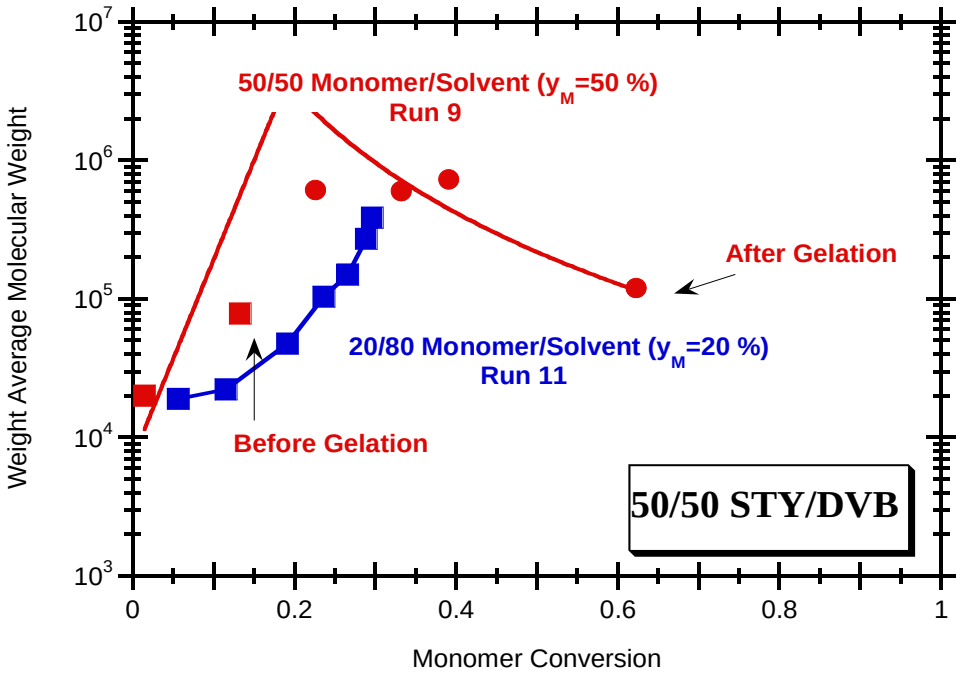

Figure 4.36. Measured effect of initial monomer dilution on monomer conversion evolution of $\bar{M}_w$ for NMRP aqueous suspension at 130 °C. Solid lines connecting experimental measurements are only visual aids.

Figure 4.37 depicts the LS signal observed for STY/DVB samples obtained considering the two above described polymerisation runs (monomer concentrations $y_M = 50$ and 20 %, both with $y_C = 50$ %). These chromatographic traces are from samples with nearly the same monomer conversion ($p \approx 0.23$). For comparison purposes, the LS of a linear sample ($y_C = 0$) was also included in this plot. Dissimilitudes in the molecular architecture of the three samples are an additional evidence for the dependence of particular kinetic mechanisms (namely intramolecular reactions) on monomer concentration. Note that the monomer conversion is the same for these samples and the population molecular size from $y_M = 20$ % looks like a mixture between the linear case and the STY/DVB at $y_M = 50$ %. Differences in the molecular architectures of these samples are also highlighted in Figure 4.38 where the RI signal of the related chromatography traces is shown. Besides the differences between the two samples with $y_C = 50$ % caused by distinct monomer dilution, a right side shoulder is observed in both crosslinked systems arising from the population of linear chains.

A final effect of initial monomer concentration on network features is shown with Figures 4.39 and 4.40. The dynamics of PDB concentration change is shown for the two

polymerisation runs with different monomer dilution above discussed. Reaction time and monomer conversion dependences of concentration of PDBs are shown in Figure 4.39 and 4.40, respectively. A lower concentration of polymer PDBs, observed at same monomer conversion, when dilution is increased is another evidence of additional reactions consuming PDBs. A likely cause is intramolecular propagation (despite NMRP use) at these diluted conditions.

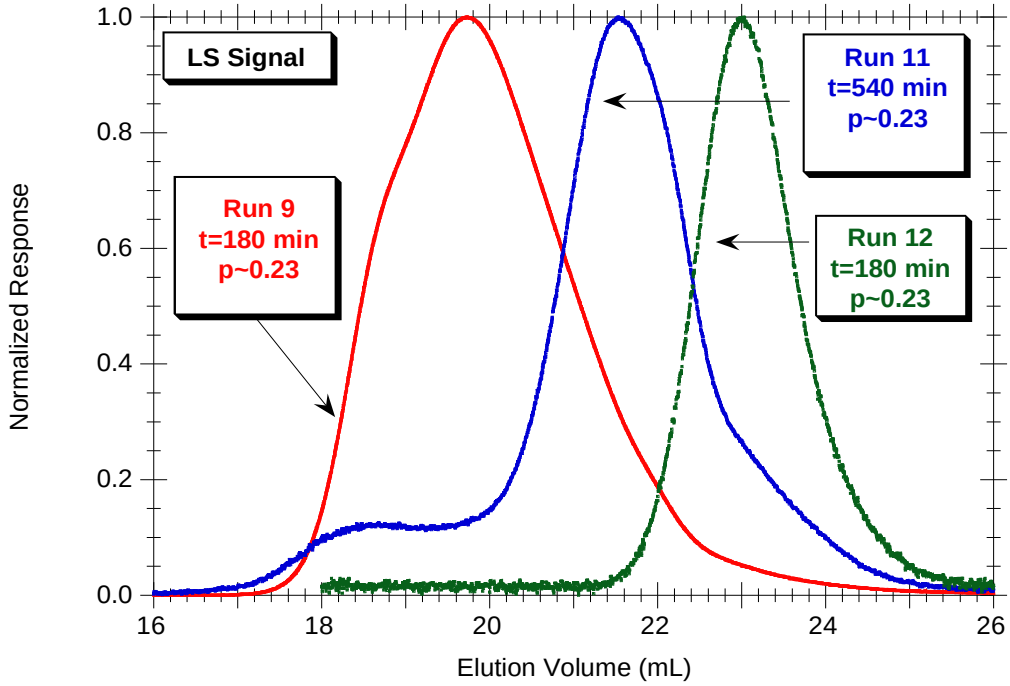

Figure 4.37. LS signal observed for STY/DVB samples obtained considering two different initial monomer concentrations (run 9 and 11 in Table 4.2) but the same mole fraction of DVB (50 %). For comparison purposes, the LS of a linear sample (run 12 in Table 4.2) was also included.

4.5.1.5 Effect of Polymerisation Mechanism on Gelation

A few research works after 2000 have explored CRP techniques to obtain hyperbranched polymers and gels with tailored molecular structure. Production of linear polymers with well-defined architectures has become widespread since the discovery of CRP techniques, (Georges *et al*., 1993; Solomon *et al*., 1986) but the subject remains elusive when non-linear polymerisations are considered. Past works on the use of CRP with branching and crosslinking (Hernández-Ortiz *et al*., 2012; Yu *et al*., 2007, 2008 and 2009; Gao *et al*., 2007 and 2008; Gonçalves *et al*., 2010a, 2010b, 2010c and 2010d; Wang *et al*., 2012; Krasia and Patrickios, 2006; Achilleos *et al*., 2007; Poly *et al*., 2008; Roa-Luna *et al*., 2010; Jaramillo-

Soto and Vivaldo-Lima, 2012; Ide and Fukuda, 1997 and 1999; Abrol *et al*., 1997and 2001; Tuinman *et al.,* 2006; Peters *et al*., 1999; Viklund *et al.*, 2001; Zetterlund *et al*., 2005; Alam *et al*., 2006; Tanaka *et al*., 2007; Saka *et al.*, 2007) were performed, considering mostly solution polymerisation and trying to avoid gelation in order to obtain hyperbranched materials. In fact, it was concluded in these works that CRP allows the operation with higher contents of multivinyl monomers avoiding gelation. This is an important issue when functionalized or hyperbranched materials are sought. A decrease of intramolecular cyclizations with CRP was postulated, but their incidence remains an important issue, as recently shown with RAFT of vinyl/divinyl monomers (Wang *et al*., 2012). In some of the aforementioned works, studies were also extended beyond the gel point when carrying out: bulk polymerisation in sealed ampoules, (Roa-Luna *et al*., 2010; Ide and Fukuda, 1999; Tuinman *et al.,* 2006) miniemulsions in shaken sealed ampoules, (Saka *et al*., 2007) or high-pressure cells running with supercritical carbon dioxide (Jaramillo-Soto and Vivaldo-Lima, 2012). Dynamics of gelation is here studied considering a different synthesis approach consisting on the one-pot NMRP aqueous suspension copolymerisation of STY/DVB. SEC/RI/MALLS analysis of samples collected at different reaction times provides some new insights on the molecular architecture of CRP crosslinked products, as described below.

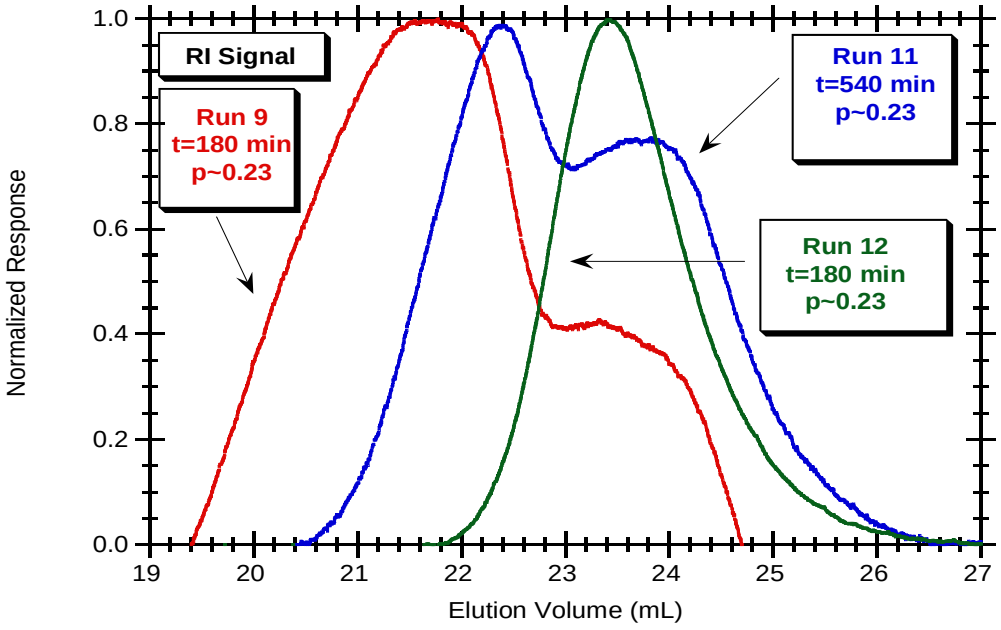

Figure 4.38. RI signal observed for STY/DVB samples obtained considering two different initial monomer concentrations (run 9 and 11 in Table 4.2) but same mole fraction of DVB (50 %). For comparison purposes, the LS of a linear sample (run 12 in Table 4.2) was also included.

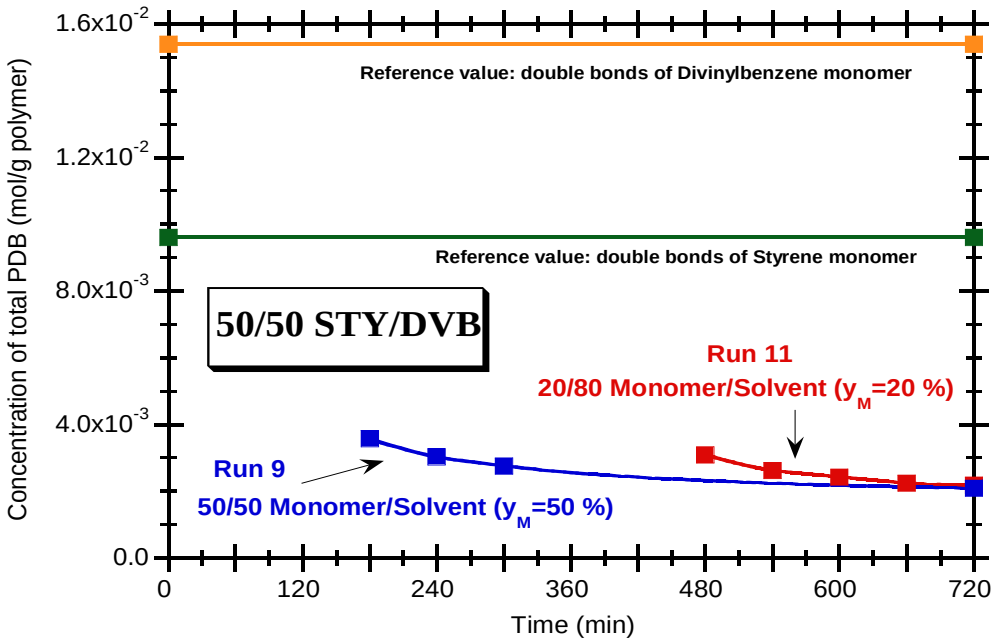

Figure 4.39. Measured effect of initial monomer dilution on reaction time evolution of polymer PDBs concentration for NMRP aqueous suspension at 130 °C. Solid lines connecting experimental measurements are only visual aids.

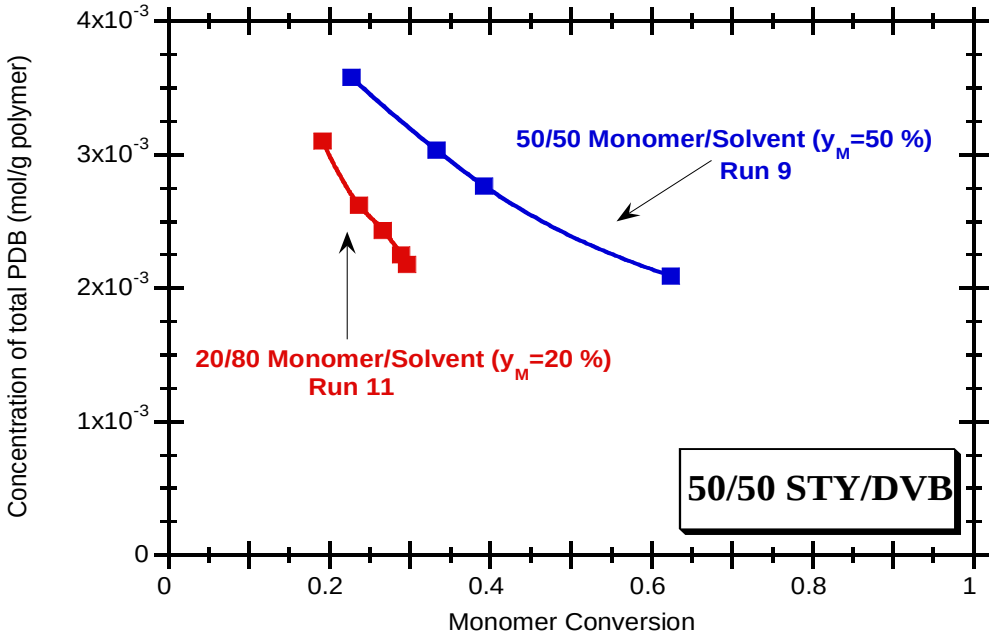

Figure 4.40. Measured effect of initial monomer dilution on monomer conversion evolution of polymer PDBs concentration for NMRP aqueous suspension at 130 °C. Solid lines connecting experimental measurements are only visual aids.

Dissimilitudes in the molecular architecture of FRP and CRP hyperbranched products were experimentally found in past works (Gonçalves *et al.*, 2010a, 2010b, 2010c and 2010d) using SEC/RI/MALLS analysis. In the present chapter, these differences are highlighted by considering gel formation in aqueous suspension processes. In Figure 4.41 is presented the dynamics of monomer conversion and weight fraction of gel during FRP of STY/DVB ($y_C = 1$ %, $y_M = 50$ %) at 90 °C (run 7 in Table 4.2). Dynamics of $\bar{M}_w$ or the same run is presented in Figure 4.42. These data show the higher polymerisation rate of FRP comparatively to NMRP and, moreover, the fast gelation process (around 45 min, 20 % monomer conversion, with 1 % DVB under conditions specified in Figures 4.41 and 4.42) observed with FRP considering only small amounts of crosslinker. Note that, as presented in the previous section, monomer conversions at gel point of 20 and 30 % were measured for NMRP of STY/DVB with $y_C = 50$ % at 130 °C and considering $y_M = 50$ and 20 %, respectively. Such huge differences highlight the mechanistic differences between FRP and NMRP crosslinking process and show a way to the incorporation of high amounts of multifunctional monomers in polymer chains without gelation.

In Figure 4.43 the comparison between FRP and NMRP of STY/DVB in aqueous suspension is reinforced considering three different runs at 90 °C (runs 1, 4, and 7 in Table 4.2). Measured reaction time dependence of $\bar{M}_w$ shows the occurrence of gelation in the FRP run despite the small amount of DVB in the monomer mixture. Conversely, for NMRP experiments (runs 1 and 4 in Table 4.2) gelation was not detected and a smooth evolution of $\bar{M}_w$ was found. Note that comparatively to the FRP run, a much higher amount of DVB was used in the NMRP runs (3 and 100 %). This means that NMRP allows a better control of the dynamics of gelation even when quite high amounts of crosslinker are chosen.

However, the above described advantages of NMRP should be placed within the context of the low reaction rates/monomer conversions observed in NMRP as compared to FRP. This issue is put into evidence in Figure 4.44 where the dynamics of $\bar{M}_w$ is presented in terms of monomer conversion dependence. Note that the achieved maximum monomer conversions in runs 1 and 4 are very small (30 and 20 %, respectively) and the critical onset for gelation was probably not attained. In Figure 4.44 the dynamics of molecular weight for run 3 was also included, highlighting the effect of the initial mole ratio between mediator (TEMPO) and initiator. Indeed, use of a smaller amount of TEMPO in run 3 ($y_{TEMPO} = 1.1$) leads to higher monomer conversion and in this case the onset for gelation (around 20 % monomer conversion with 100 % DVB) was exceeded. These results also show the importance of

kinetics on the description of branching/crosslinking process. With NMRP, low reaction rates are generally observed and polymerisation temperature plays an important role in this context.

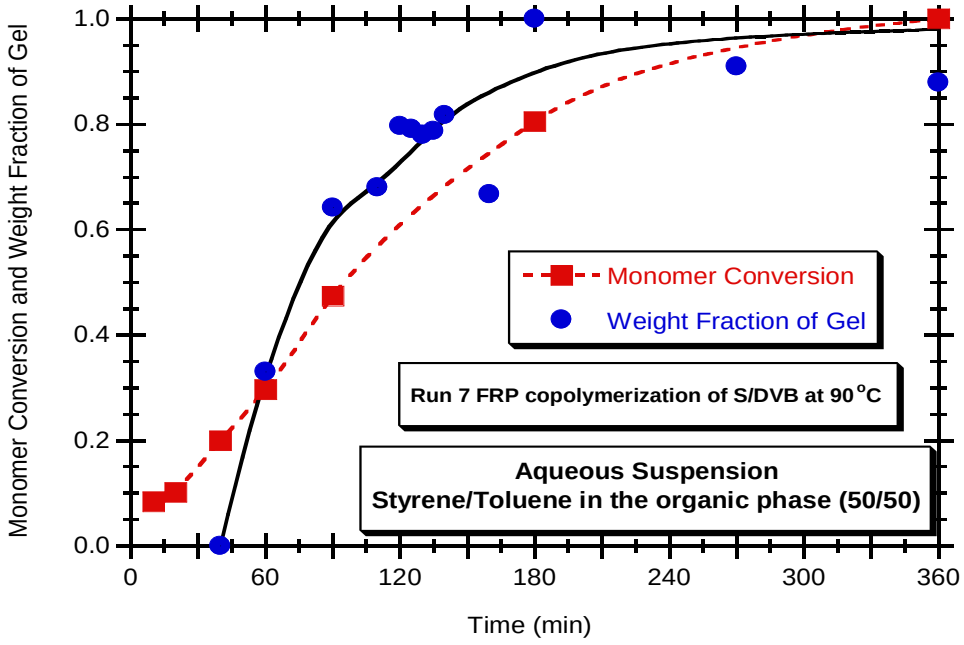

Figure 4.41. Reaction time evolution of monomer conversion and weight fraction of gel for FRP of STY/DVB in aqueous suspension at 90 °C. Solid lines connecting experimental measurements are only visual aids.

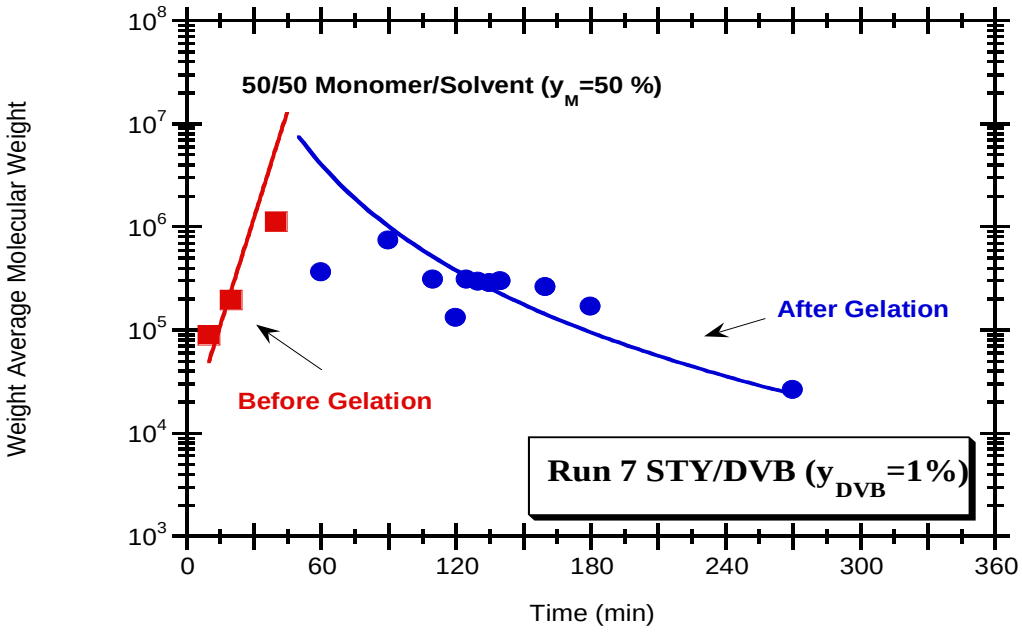

Figure 4.42. Reaction time evolution of weight average molecular weight for FRP of STY/DVB in aqueous suspension at 90 °C. Solid lines connecting experimental measurements are only visual aids.

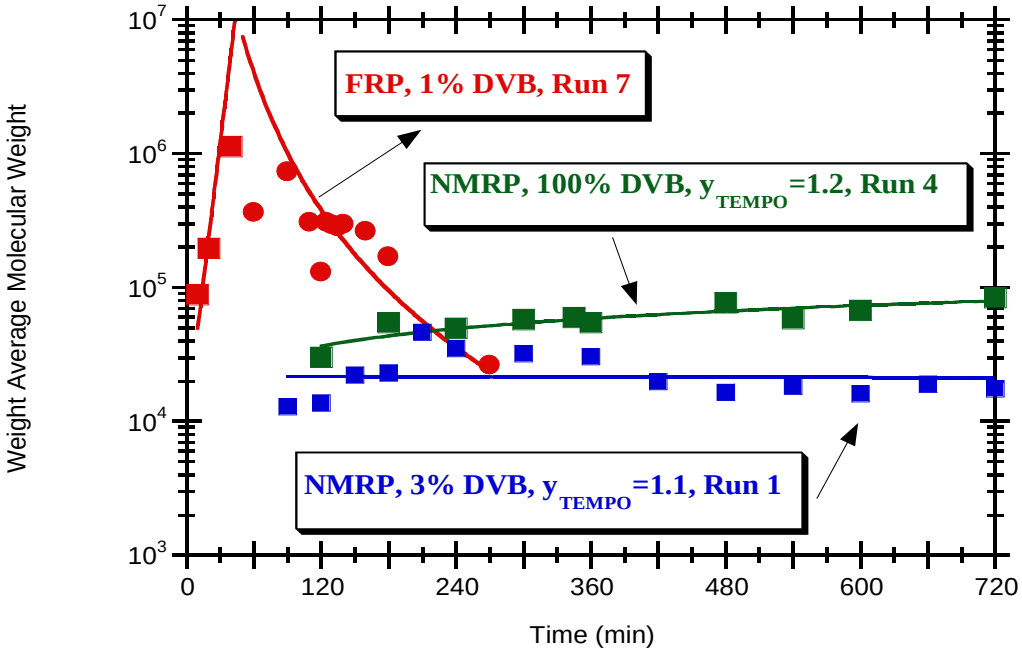

Figure 4.43. Measured reaction time evolution of $\bar{M}_w$ for FRP and NMRP of STY/DVB of aqueous suspension at 90 °C. Solid lines connecting experimental measurements are only visual aids.

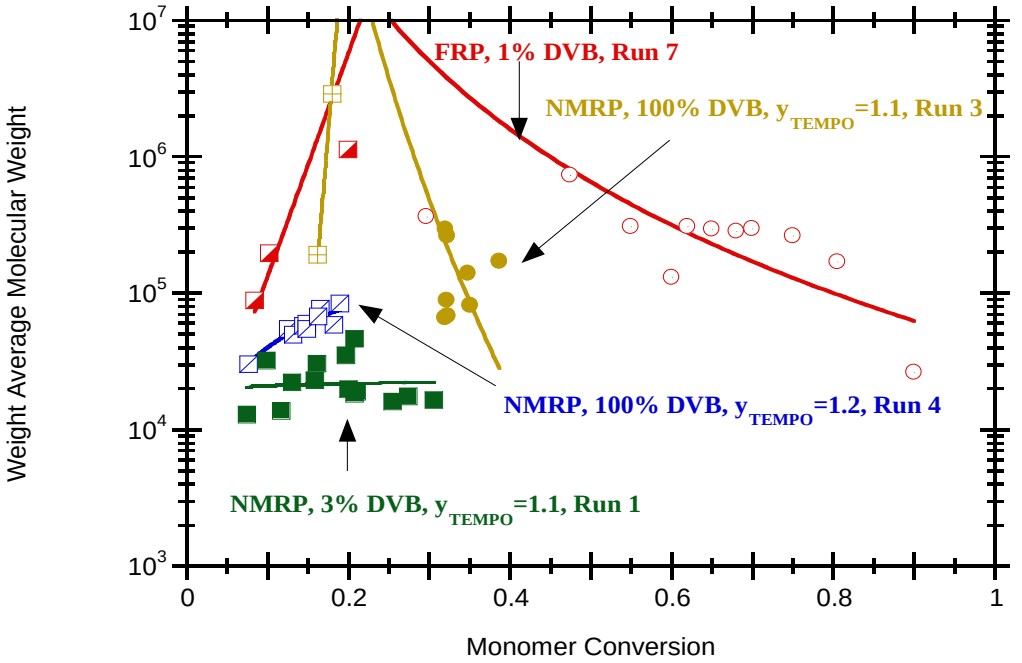

Figure 4.44. Measured monomer conversion evolution of $\bar{M}_w$ for FRP and NMRP of STY/DVB of aqueous suspension at 90 °C. Solid lines connecting experimental measurements are only visual aids.

4.5.1.6 Effect of Polymerisation Temperature

Kinetics of NMRP is strongly dependent on polymerisation temperature. Reasonable reaction rates can only be obtained with effectively controlled NMRP if the temperature is high enough. A decrease of initial ratio mediator/initiator (y_{TEMPO}) in the present work) leads to a higher reaction rate at some fixed temperature but the character of "living polymerisation" is negatively affected. Therefore, it is important to understand the impact of polymerisation temperature on the kinetics of aqueous suspension NMRP of STY/DVB and specifically on the crosslinking process and eventual gel formation.

In the present work polymerisation runs were performed at two different temperatures, 90 and 130 °C. Since reactors were operated with an aqueous suspension, polymerisation runs at 90 °C could be performed at atmospheric pressure (with a condenser included in the set-up) whereas the synthesis at 130 °C had to be performed in a pressurized reactor with an observed steady-state total pressure around 4.6 bar. Other previous studies on xylene solution NMRP of STY/DVB (up to the gel point) were performed at 130 °C in an atmospheric reactor (Gonçalves *et al*., 2010c and 2010d).

In Figure 4.45 the measured reaction time evolutions of monomer conversion for NMRP runs in aqueous suspension at 90 and 130 °C are compared (runs 3, 4, 5, and 6 at 90 °C and run 12 at 130 °C were considered for comparison purposes). As expected, higher reaction rates are observed at 130 °C with monomer conversion around 60 % for $t = 12$ h and $y_{TEMPO} = 1.1$. Lower conversion profiles are observed at 90 °C and peculiar time-evolution trajectories were measured for different runs at the same temperature, as presented in Figure 4.45. This particular behaviour at 90 °C is also reported in Figure 4.46 where a plot of $-\ln(1-p)$ *versus* polymerisation time is presented. A non-ideal CRP process seems to occur with NMRP at 90 °C. Probably this temperature is too low and the activation/deactivation steps are too much shifted toward the deactivated state with concomitant near- inhibition of the polymerisation. An additional kinetic study of NMRP at lower temperatures seems to be needed in order to elucidate these issues. Theoretical kinetic modelling studies should also provide useful insights on this subject.

Peculiarities of the dependence of NMRP process on temperature have an important impact on the crosslinking process and eventual gel formation, as exemplified in Figures 4.47 and 4.48. When gel production is sought with NMRP, higher temperatures (e.g., 130 °C) are advisable in order to obtain high polymerisation rates and to achieve the onset of gelation.

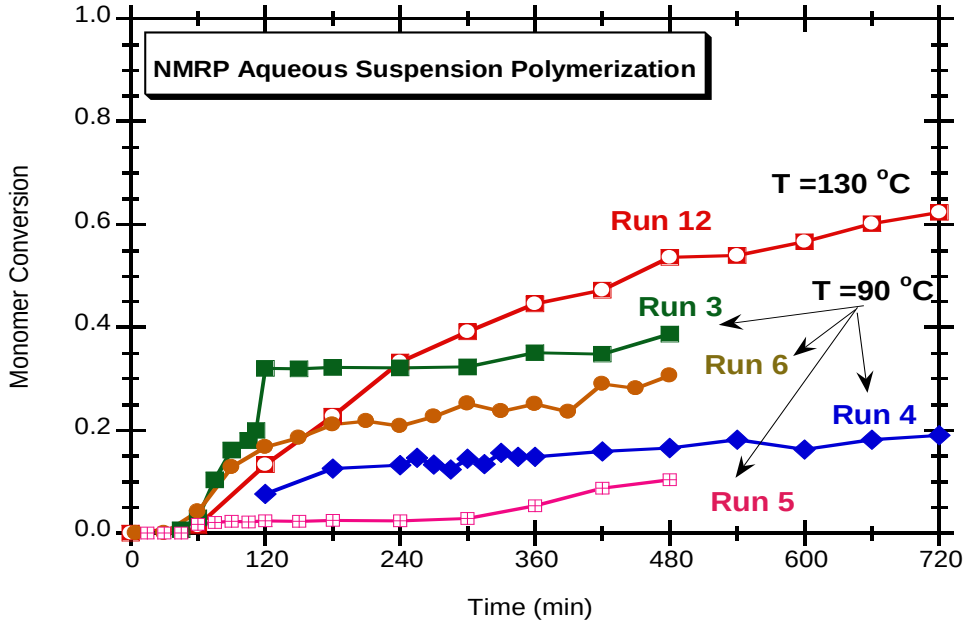

Figure 4.45. Comparison of the measured reaction time evolution of monomer conversion for NMRP runs in aqueous suspension at 90 and 130 °C.

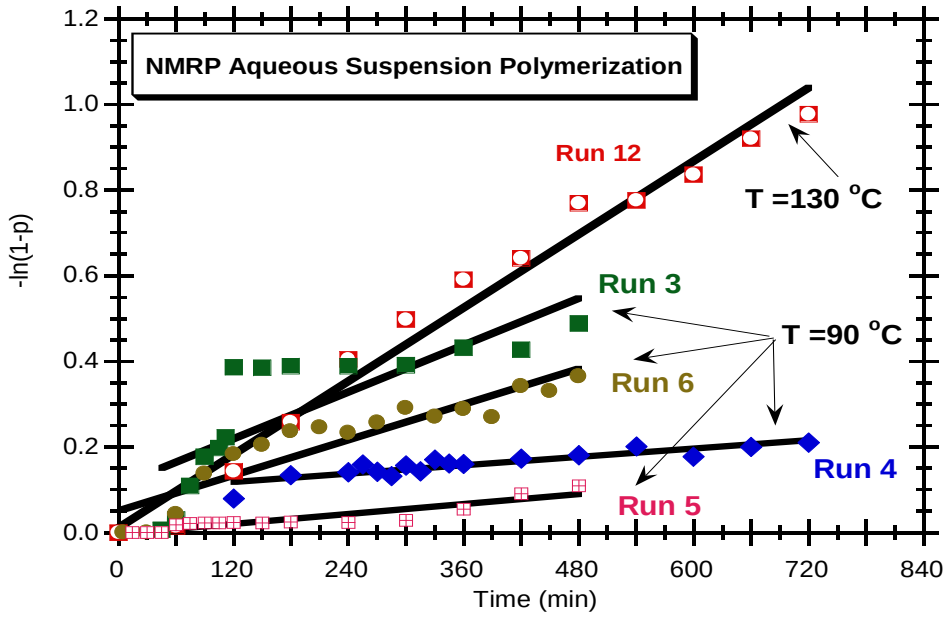

Figure 4.46. Plot of $-\ln(1-p)$ *versus* reaction time for NMRP runs in aqueous suspension at 90 and 130 °C.

A too low temperature (e.g., 90 °C) can prevent gelation even with high amounts of crosslinker; synthesis of hyperbranched polymers and highly functionalized materials are then

possible. However, the glass transition temperature of the materials(T_g) can be largely exceeded if a too high polymerisation temperature is used. This is a shortcoming when operating with aqueous suspension because too soft polymer particles can be formed with eventual aggregation phenomenon. Eventually, some optimum operating temperature could exist in the range 90-130 °C.

4.5.1.7 Effect of Intramolecular Cyclization Reactions

Results obtained in this research are especially useful in the study of the effect of intramolecular cyclization reactions on the crosslinking process. Experimental data obtained (Gonçalves *et al*., 2013a) were explored to develop mathematical models including the effect of primary cyclization based on the development of balance of sequences connecting radical centers and pendant double bonds present in the same polymer chain (Aguiar *et al*., 2013a). The rate constant for cyclization was considered a function of the sequence length. Studies included the pre- and post-gelation periods and comparisons between experimental measurements and model predictions for pendant double bond concentration, average molecular weights and weight fraction of gel were thus performed (Aguiar *et al*., 2013b). It was possible the estimation of the rate constant of cyclization for the smallest ring (3 monomeric units). A value in the order of 500 s^{-1} was estimated for this parameter at 90 °C rather high when compared with the intermolecular propagation (as k_p[M+PDB] lies between 1000 and 10000 s^{-1}). Jacobsen-Stockmayer theory predicts that pairs of radical site + PDB in the same molecule with longer distances between them show a decreasing rate of cyclization, but their impact stays strong even at bulk conditions and is a major factor in all multivinyl radical polymerisations. Influence of key polymerisation parameters (e.g. crosslinker content, monomer dilution, reaction temperature) on cyclization was also identified through the comparison of experimental data with different kinds of mathematical models (Gonçalves *et al*., 2013a; Aguiar *et al.*, 2013a and 2013b). In these studies, much higher relative crosslinking reactivity was observed at 130 °C as compared to 90 °C, likely an effect of the chain mobility (Aguiar *et al*., 2013b). In the spite of the efforts here reported for the clarification of these kinds of crosslinking processes, this is an open issue in the scientific community, as testified by other very recent publications on this field (Scott *et al*., 2014; Nikitin *et al*., 2013; Hamzehlou *et al*., 2013). Impact of the use of different kinds of polymerisation mechanisms (e.g. FRP/NMRP) on crosslinking (trying avoid/decrease cyclizations) and development of

mechanistic models able to describe such complex polymerisations are some research lines also explored in these publications which will be probably enhanced in future works.

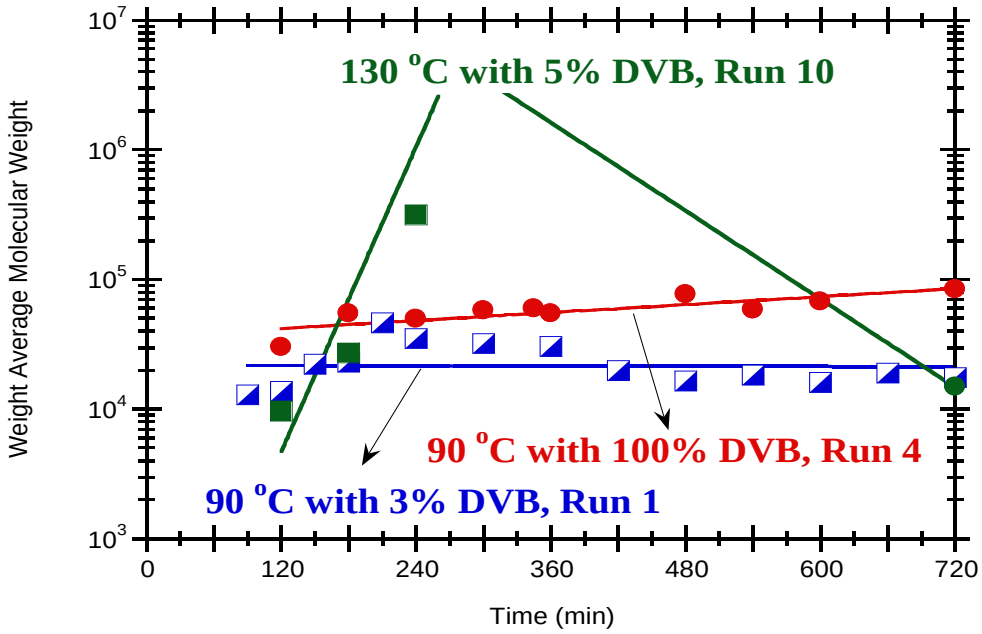

Figure 4.47. Measured reaction time evolution of $\bar{M}_w$ for NMRP of STY/DVB of aqueous suspension at 90 and 130 °C. Solid lines connecting experimental measurements are only visual aids.

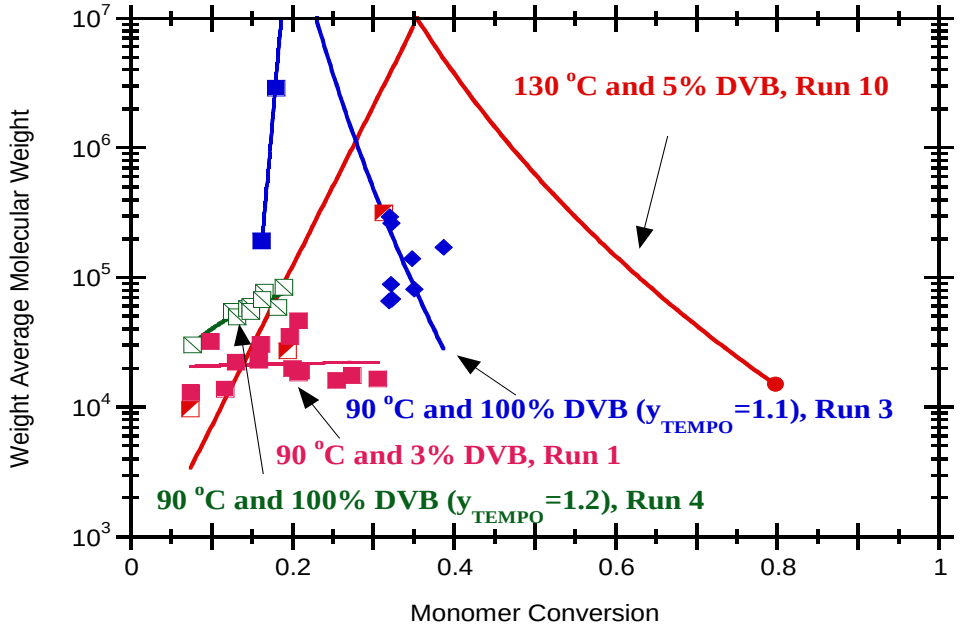

Figure 4.48. Measured monomer conversion evolution of $\bar{M}_w$ for NMRP of STY/DVB of aqueous suspension at 90 and 130 °C. Solid lines connecting experimental measurements are only visual aids.

4.5.1.8 Gel analysis by SEM

After precipitation in methanol and vacuum drying as above described, the final products of the runs described in Table 4.2 were analysed by SEM. The goal was to elucidate the connection between the synthesis conditions and the product morphology. In particular the formation of nano- and micro-structures due to the occurrence of spatially non-uniform gelation during STY/DVB gels synthesis was sought.

Representative results are presented in Figure 4.49 to 4.54. SEM micrographs of STY/DVB samples from polymerisation runs at 90 °C at different DVB content are compared in Figures 4.49(a) to (d). Smooth featureless surfaces were observed in products of NMRP runs (runs 1, 2, and 3) within a very broad range of DVB content (3–100 %). However, nanometer-sized spherical particles can be observed in products of run 7 (FRP with only 1 % of DVB). Even if this is a single example, it confirms previous works (Dušek, 1996) showing that FRP leads to phase separation due to nano-gelation and here we observe that this phenomenon is avoided by NMRP. Such nano-structures are not observed either in the products of runs 4 (NMRP with 100 % DVB) or run 6 (NMRP of STY), both polymerisations also at 90 °C (see Figure 4.50). These results seem also to deny phase segregation (due to nanogel formation) which could eventually occur with NMRP.

Nevertheless, such nano-structures are also observed in products of run 13 coming from FRP of STY, as presented in Figure 4.51(a). Therefore, hypothetical phase segregation can not be the result of nano-gelation. Particle populations with different sizes (e.g., 20 μm and around ten times smaller) can be identified in Figure 4.51(b) resulting from products of NMRP of STY (run 14 in Table 4.2).

SEM micrographs from products of other two NMRP STY/DVB runs are presented in Figure 4.52. Two magnifications are considered for the products of run 8 (100 % DVB at 130 °C) and run 9 (50 % DVB at 130 °C). In both cases, with 150× magnification agglomerates of particles with very different sizes are discernible. With higher magnifications (Figures 4.52(b) and (d)), particle populations with broad range sizes (from 100 μm to less than 1 μm) are observed. However, in both cases, domains of fused material are also visible. It is possible that this fused material appears due to the relatively high temperature of the polymerisation. These runs were carried out at 130 °C (in order to have higher NMRP rates) which is well above the glass transition temperature (T_g) of polystyrene (and likely of copolymers with divinylbenzenes).

It is plausible that, with these polymerisation conditions, softening of suspension particles can lead to agglomeration of polymeric material. Post-treatment of polymerisation products (precipitation in methanol and drying under vacuum at 70 °C) could also contribute to this agglomeration process.

Formation of fused material domains can also be detected in Figure 4.53 where besides the smooth surfaces arising from the softened regions (see also Figure 4.49(a) and (c) for products of run 1 and 3), micro- and nano-sized particles are also observed.

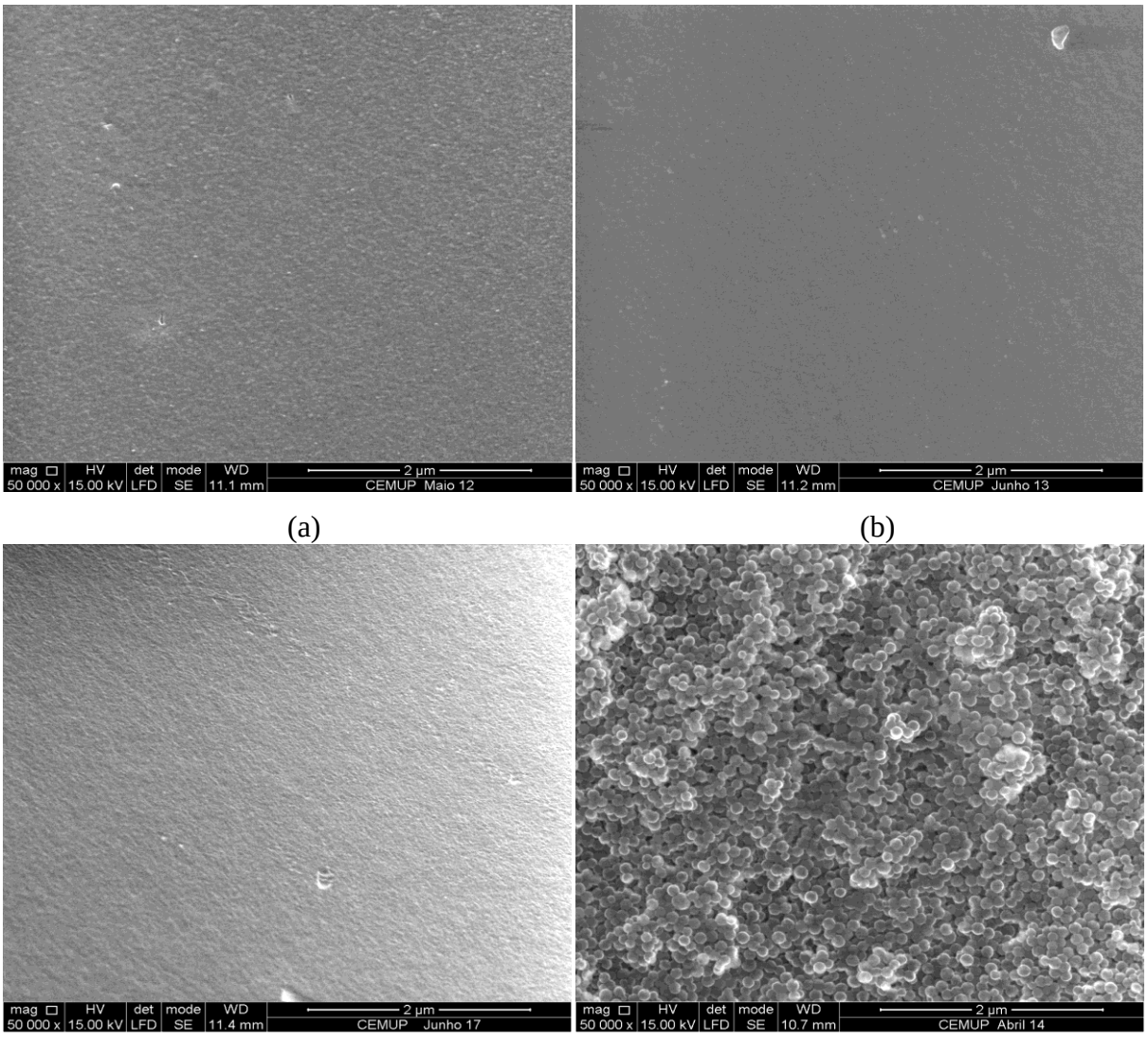

Figure 4.49. SEM micrographs of STY/DVB samples from polymerisation runs with different DVB content. All images with magnification 50000 ×. (a) Run 1 (3 % DVB). (b) Run 2 (28 % DVB). (c) Run 3 (100 % DVB). (d) Run 7 (1 % DVB-FRP). All polymerisations at 90 °C.

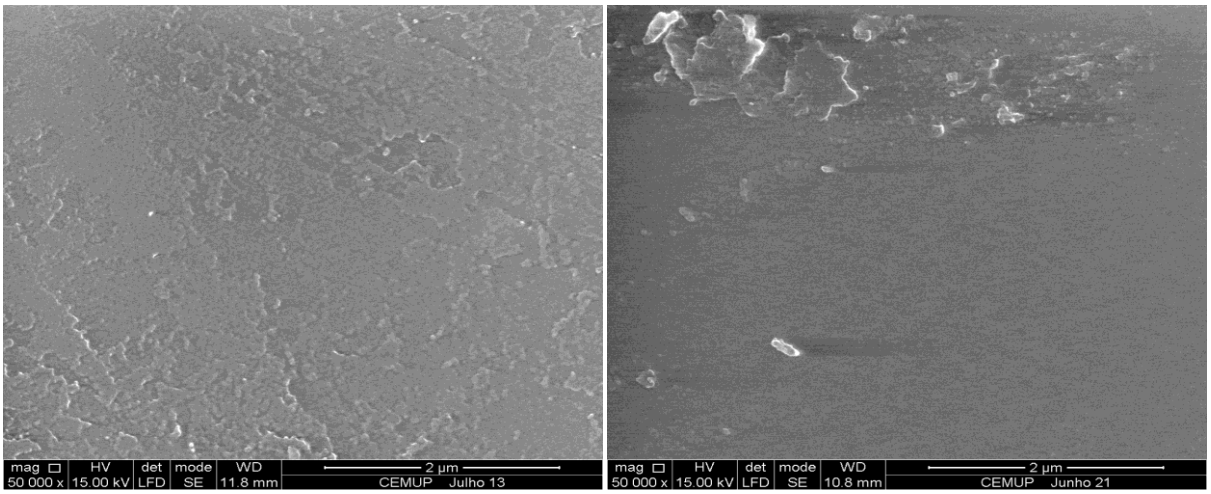

(a) (b)

Figure 4.50. SEM micrographs of samples from NMRP runs with 0 and 100 % DVB. Images with magnification 50000 ×. (a) Run 6 (0 % DVB). (b) Run 4 (100 % DVB).

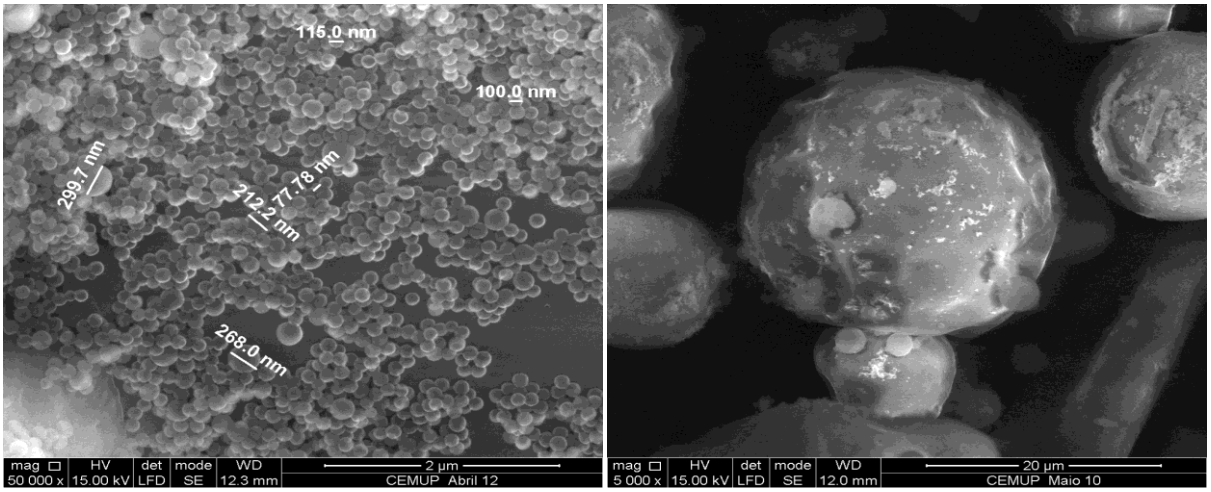

(a) (b)

Figure 4.51. SEM micrographs of polystyrene samples (0 % DVB) synthesized by FRP and NMRP. (a) Run 13 (FRP) with magnification 50000 ×. (b) Run 14 (NMRP) with magnification 5000 ×. Both runs at 90 °C.

For comparison purposes, Figure 4.54 depicts SEM analysis of products of FRP aqueous suspension of STY/DVB at 60 °C (Gonçalves *et al*., 2011a). Suspension gel beads with sizes up to 0.5 mm or lower can be observed in Figure 4.54(a). Micro- and nano-particles can also be observed in FRP STY/DVB products synthesized at 60 °C, as shown in Figure 4.54b). Note that with materials illustrated in Figure 4.54, the synthesis process includes a mixture of bad/good solvents (*n*-heptane/toluene) in order to promote the formation of macropores in the gel beads; macroporous structures with diameter size in the range of 5 µm were thus identified (Gonçalves *et al*., 2011a). In the present research, only solvents with a good thermodynamic

affinity with polymer (toluene and xylene) were used because the focus of this study is the effect of NMRP on the structural homogeneity of STY/DVB products.

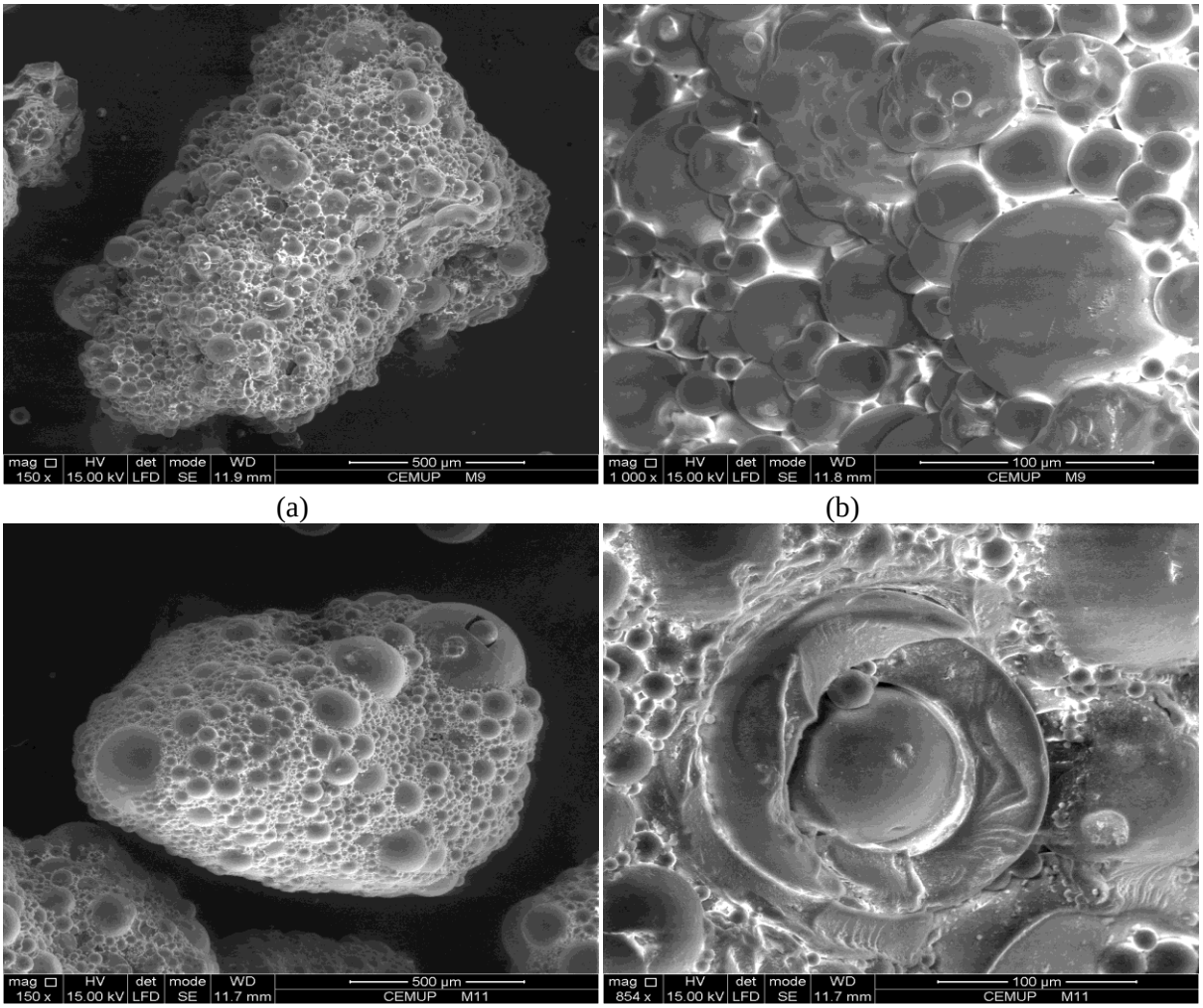

(a) (b)

(c) (d)

Figure 4.52. SEM micrographs of STY/DVB samples synthesized by NMRP. (a) Run 8 with magnification of 150 ×. (b) Run 8 with magnification of 1000 ×. (c) Run 9 with magnification of 150 ×. (d) Run 9 with magnification of 854 ×. Both runs at 130 °C.

The above described results of SEM analysis show that milli-, micro-, and nano-meter scale spherical structures are formed in suspension polymerisation of STY/DVB using different conditions (FRP, NMRP, different polymerisation temperatures). Such nano-structures were even identified with STY homopolymerisation. Therefore, it is difficult to conclude using SEM characterization whether those micro- and nano-structures are a result of phase segregation due to micro and nano-gelation in STY/DVB copolymerisation. Further experimental studies with a microchannel reactor can eventually elucidate this issue and allow a clear interpretation of SEM results. On the other hand, STY/DVB particles were observed by SEM after the above described manipulation of the reaction products, namely with their

precipitation in methanol. It is possible to interpret the observed particle fusion also as a consequence of this treatment. The direct observation of the suspended gel particles is another possibility (e.g., after centrifugal washing (Tanaka *et al.*, 2007)) eventually leading to a clear conclusion on this issue.

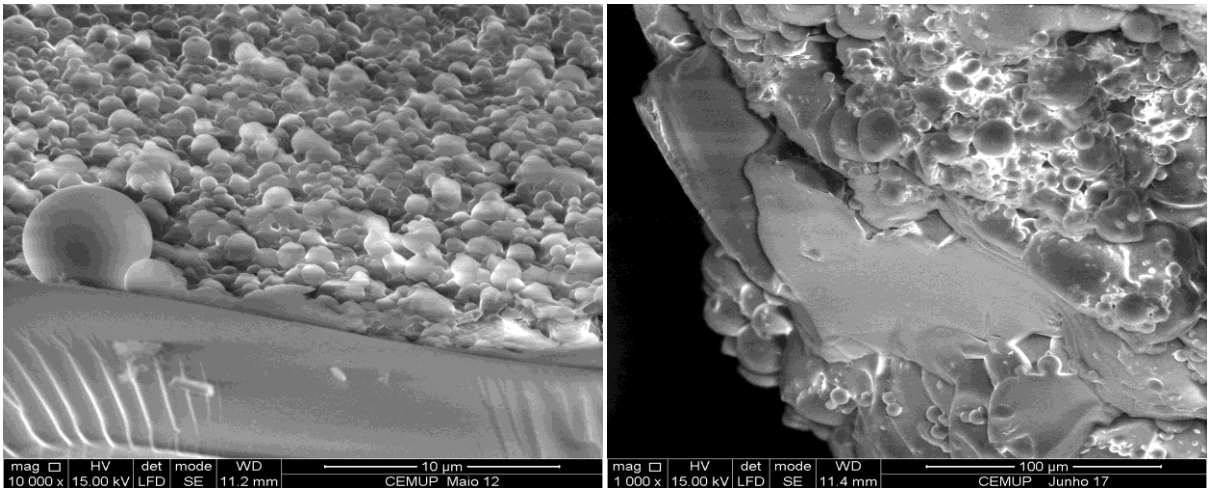

(a) (b)

Figure 4.53. SEM micrographs of STY/DVB samples synthesized by NMRP. (a) Run 1 with magnification of 10000 ×. (b) Run 3 with magnification 1000 ×. Both runs at 130 °C.

In fact, in recent works dealing with NMRP of STY/DVB in micro-suspension, (Tanaka *et al.*, 2007) a different manipulation of the gel particles is proposed: isolation of the polymer particles from the aqueous dispersion was performed by partial evaporation of water and unreacted monomer under vacuum at room temperature (not to complete dryness) (Tanaka *et al.*, 2007).

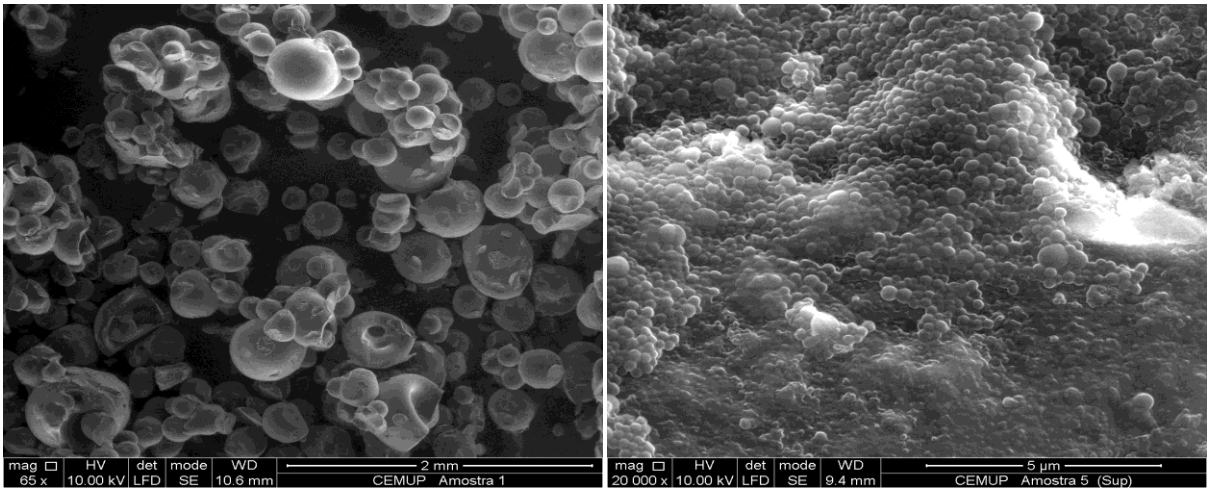

(a) (b)

Figure 4.54. SEM micrographs of STY/DVB samples synthesized by FRP at 60°C. (a) Run with: $y_M = 50$ %, $y_{DVB} = 10$ %, $y_I = 1.25$ % (in this run, a 50:50 v/v mixture of toluene/*n*-heptane was used as diluent in the organic phase). (b) Run with: $y_M = 50$ %, $y_{DVB} = 20$ %, $y_I = 1.25$ % (in this run, a 25:75 v/v mixture of toluene/*n*-heptane was used as diluent in the organic phase).

To avoid coagulation, an aqueous solution of PVA was afterwards added to the concentrated dispersion and the mixture was evaporated once again. Three similar cleaning cycles were performed. Particles corresponding to a secondary nucleation (problem tackled in Yuyama *et al*., 2000; Ma *et al*., 2001 and 2003) occurred during the polymerisation (observed with FRP but not with NMRP) were also removed by centrifugation and decantation and, after cycle washing with water, final particles were isolated using also precipitation in methanol (Tanaka *et al*., 2000). Well-defined gel particles in the range of 5 μm were thus observed. Although the concentration of PVA used in the present work (in the range 0.15–2 % by monomer weight, as above described) is rather higher than in related suspension STY/DVB polymerisation works (e.g., 0.06–0.12 in Kiatkamjornwong, *et al.*, 2001), a much higher value was considered with recent micro-suspension studies (e.g., 10 % in Tanaka *et al*., 2007). Thus, PVA concentration is another parameter with an important impact on the particles morphology and a further increase of the concentration used here should eventually avoid agglomeration of particles. Particle agglomeration into larger clusters is also reported in other recent works concerning STY/DVB polymerisation (García-Morán *et al*., 2009) due to poor non-homogeneous mixing provided by magnetic stirring bars. Nevertheless, due to the geometric characteristics of the stirrer and high-rotation speed used, it is unlikely that this problem has influenced the present work.

4.5.1.9 Analysis by FTIR

FTIR analysis of the isolated products can also be used to provide information concerning the presence of PDBs in the networks, as explored in previous works concerning the FRP of styrene and divinylbenzene (Hecker, 2000). This technique was also considered in the present research and some representative spectra are presented in Figures 4.55 to 4.58. FTIR analyses of the NMRP products synthesized in this work were performed after isolation of the polymer samples (washing by precipitation in methanol and drying). The powdered products were then mixed with KBr and pressed into pellets in order to collect the corresponding IR spectra.

Figure 4.55 shows the IR spectra of the two monomers used in this work. Especially important for following the kinetics of polymerisation are the assignments corresponding to C=C bonds that can be identified at around 992, 1019, 1410, 1452 and 1630 cm^{-1} (Hecker, 2000 and Colthup *et al.*, 1990). Particularly strong intensities of this functional group are observed at 992 and 1630 cm^{-1} (see Figure 4.55). The influence of other chemical groups in these regions of the IR spectra is very low and, therefore, these two assignments are specially

appropriate for obtaining information concerning the consumption of C=C bonds and the presence of pendant double bonds in the networks. Note that the commercial crosslinker used in this research contains two isomers (*m*- and *p*- divinylbenzene), and also ethylvinylbenzene. The IR spectrum corresponding to this mixture is much more difficult to analyse, particularly when compared with the spectrum of the purified isomers. In fact, for fundamental studies, the use of purified isomers of the divinylbenzene crosslinker would be advantageous, as reported before for the FRP of styrene/divinylbenzene (Hecker, 2000).

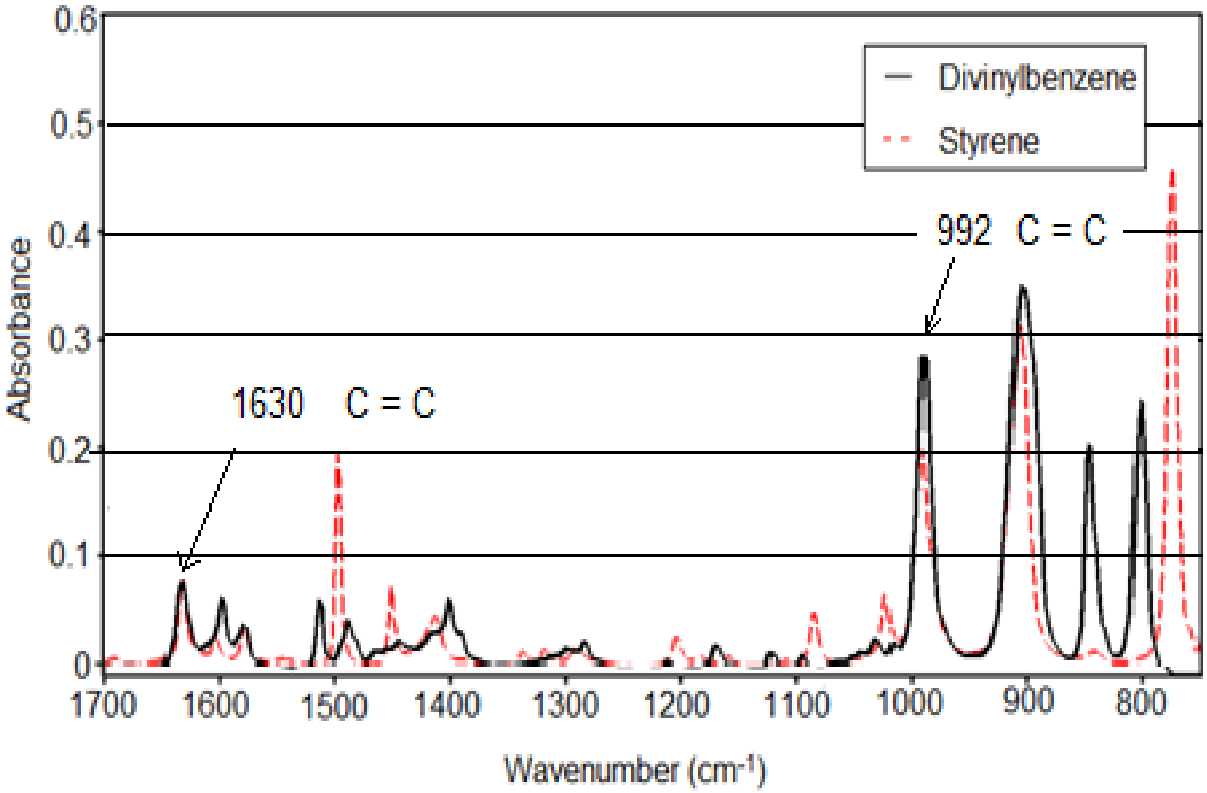

Figure 4.55. FTIR spectra of the styrene and divinylbenzene monomers. Assignments corresponding to C=C bonds in the monomers cab ne identified at around 992, 1019, 1410, 1452 and 1630 cm^{-1}. Peaks at 992 and 1630 cm^{-1} are especially useful in this context due to their strong intensities and the low interference of other chemical groups in this region of the spectra.

Figure 4.56 shows the FTIR spectrum observed for the isolated NMRP networks produced in run 9 where 50 % DVB was present in the initial monomer mixture. The peaks at 992 and 1630 cm^{-1} can be clearly observed in the spectrum of these products, showing the effective C=C functionalization (high concentration of pendant double bonds in the network) of the final materials obtained in this run. Figures 4.57 and 4.58 present the FTIR spectra observed for the isolated NMRP networks produced in runs 8 and 10, respectively. Note that in run 8 only DVB was used, whereas in run 10 the initial monomer mixture composition was 95/5 styrene/divinylbenzene. Strong IR absorbances can be observed at 992 and 1630 cm^{-1} for the

products of run 8 (see Figure 4.57), identifying a high concentration of pendant double bonds in these networks. Conversely, weak signals of these functional groups are observed in the spectrum corresponding to the products of run 10 (see Figure 4.58), showing (as expected) a lower presence of PDB in these networks. The comparison of results presented in Figures 4.56, 4.57 and 4.58 illustrates the usefulness of FTIR analysis of the isolated networks in order to obtain information concerning the presence of PDB in the synthesized materials. The qualitative effect of the synthesis conditions (initial composition, temperature, etc.) on the process of double bond incorporation in the networks is thus readily obtained through the comparison of the IR spectra of the different products.

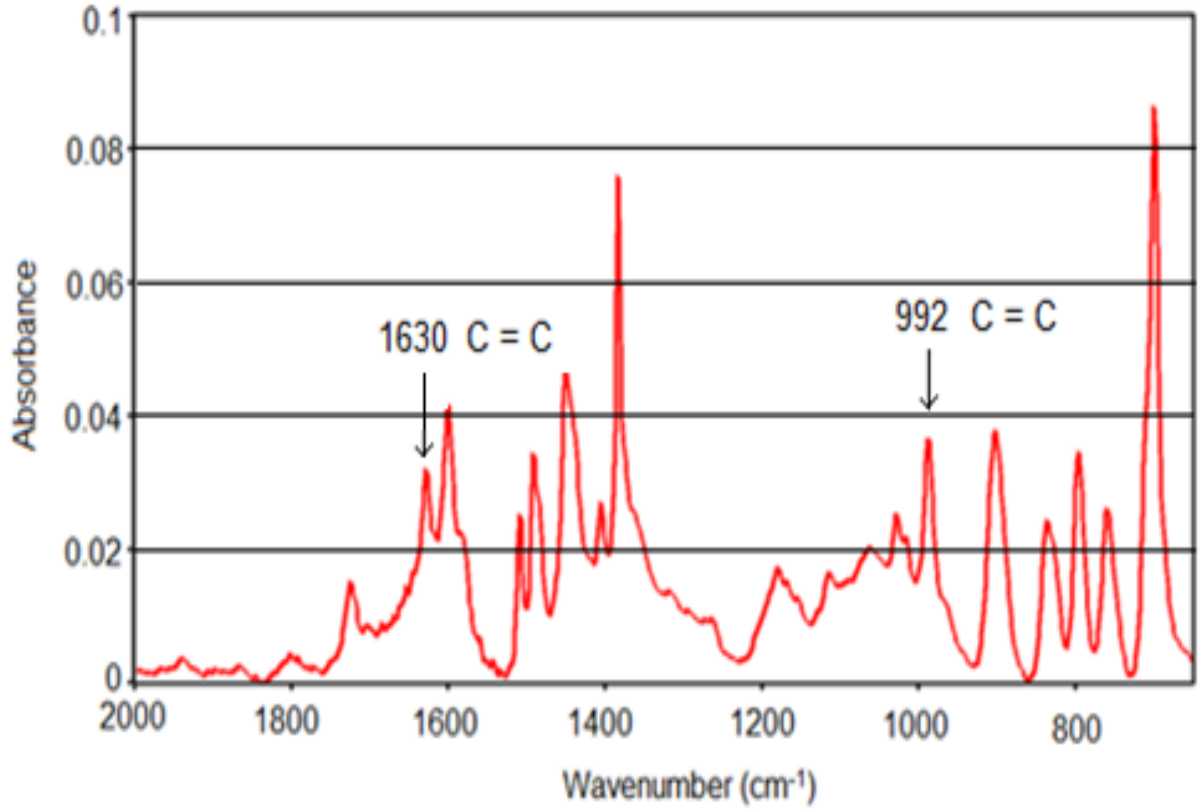

Figure 4.56. FTIR spectrum observed for the isolated NMRP network produced in run 9 (50 % DVB in the initial monomer mixture). Peaks at 992 and 1630 cm^{-1} can be clearly observed in the spectrum of the product, showing the C=C functionalization of the materials.

In principle, FTIR analysis can also be used to quantify the concentration of PDBs in the synthesized products (Hecker, 2000). Nevertheless, the reliability of the results requires the identification of an internal reference peak in the IR spectra with a constant proportion in the monomer and polymer. Alternatively, the use of model molecules to perform a group response calibration (e.g., based on 4-isopropyl styrene) seems to be a possibility to increase the reliability of the quantitative results in the IR-spectroscopy of PDBs (Hecker, 2000).

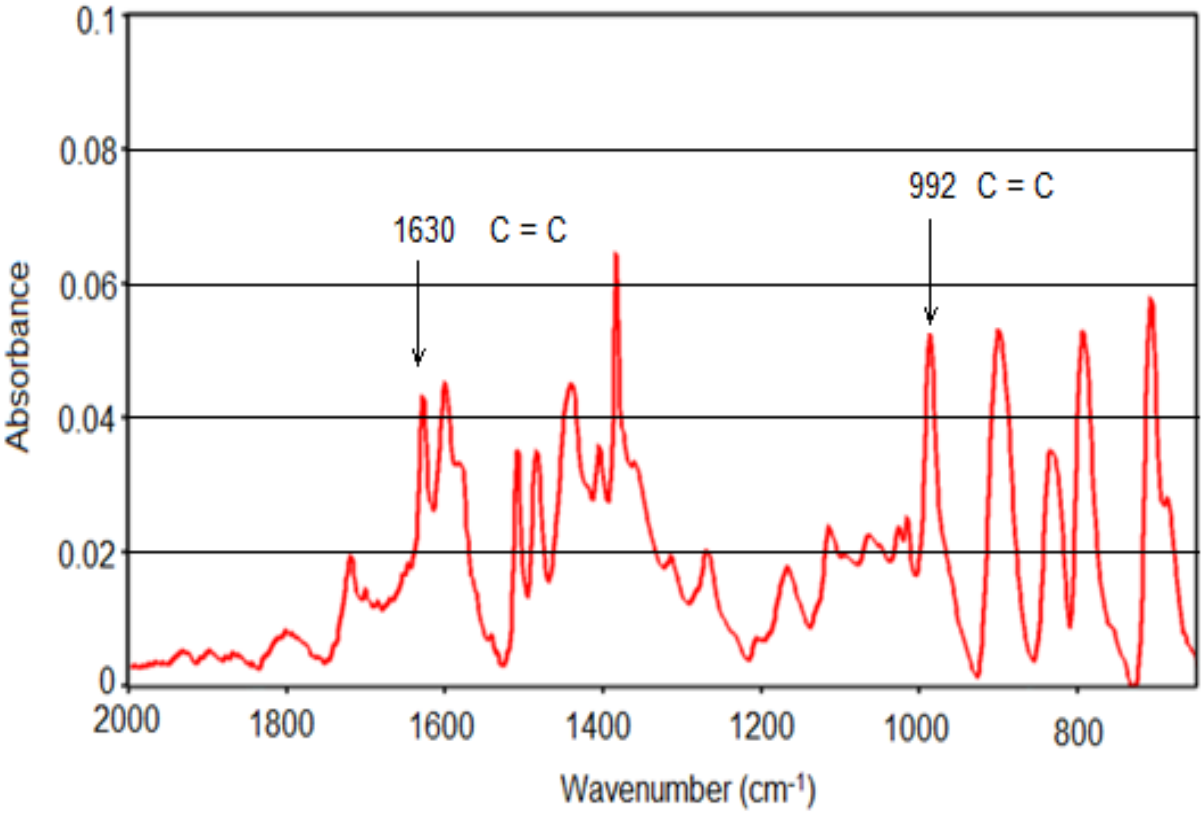

Figure 4.57. FTIR spectrum observed for the isolated NMRP network produced in run 8 (100 % DVB in the initial monomer mixture). Strong IR absorbances observed at 992 and 1630 cm^{-1} identify a high concentration of pendant double bonds in the network.

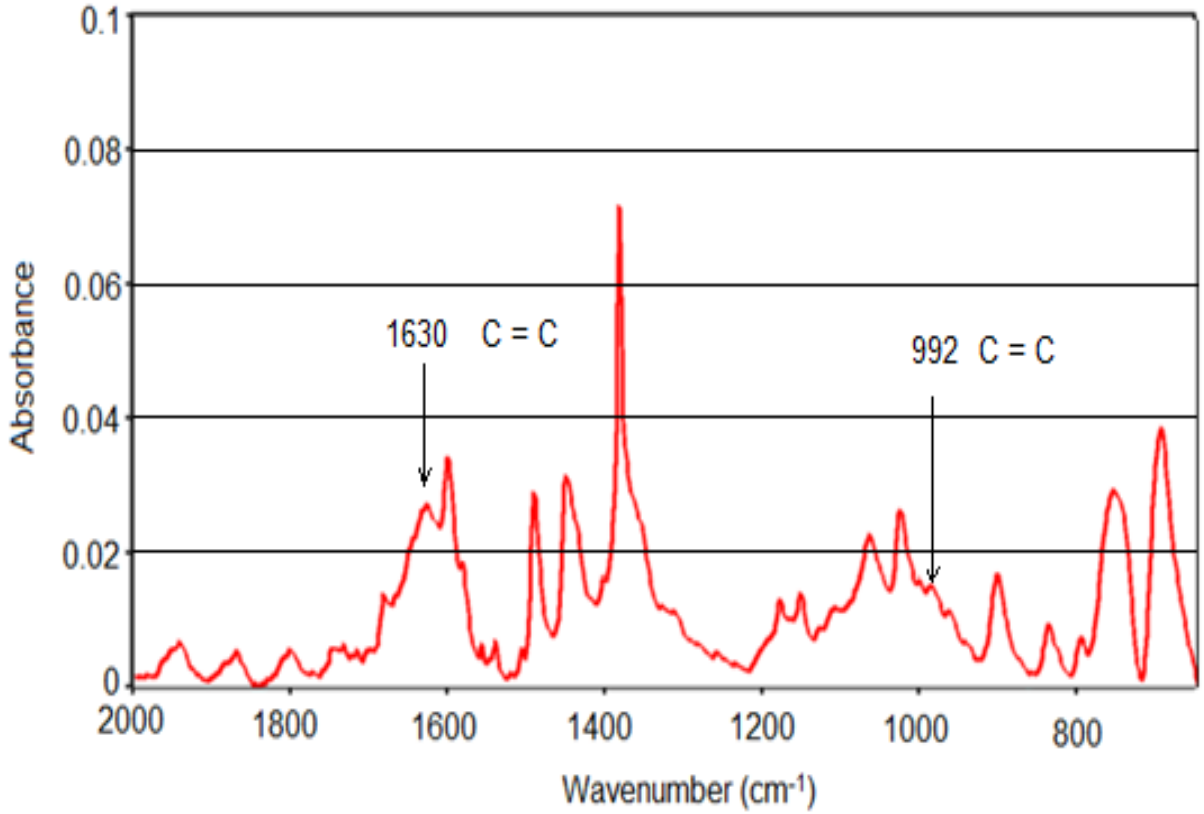

Figure 4.58. FTIR spectrum observed for the isolated NMRP network produced in run 10 (5 % DVB in the initial monomer mixture).

Another shortcoming associated with the use of this technique for PDB quantification occurs when the concentration of these functional groups in the material is low. Specific peaks corresponding to the C=C bonds present a weak intensity, particularly when compared with the responses of other chemical groups (see Figure 4.58), which hinders their rigorous quantification. Chemical titration, extensively used in this research, is a technique with a broader range of applicability concerning the observed concentration of PDBs in the networks.

4.6 Conclusions

The solution polymerisation system was experimentally studied through the synthesis and characterization by SEC/RI/MALLS of these non-linear copolymers. Model predictions were compared with the measured dynamics in a batch reactor of key polymer properties such as monomer conversion, molecular weights and *z*-average radius of gyration.

Different experimental methods were used to obtain insight on the molecular architecture of the networks, such as: the analysis by SEC/RI/MALLS proved to be especially useful in this research: reaction time evolution of the crosslinking process was, therefore, studied and the effect of the different polymerisation conditions on the molecular structure of products was compared. This technique showed that, when compared with FRP, NMRP allows only limited control over the crosslinking process. NMRP non-linear polymerisation proceeds in a similar way to a random FRP process and, therefore, a very broad polymer population is formed. And the analysis by SEM of the different products synthesized did not yield clear conclusions on the effect of operation conditions on materials morphology. Nano- and micro-sized structures were identified in linear/non-linear products obtained by FRP and also by NMRP. These structures seem to be a consequence of the synthesis process (e.g., operation at reaction temperature above the glass transition temperature and/or secondary nucleation (Yuyama *et al*., 2000; Ma *et al*., 2001 and 2003) and post-polymerisation treatment of products (precipitation/drying). Design of new operation conditions is needed (e.g., operation of a micro-channel suspension reactor) in order to elucidate the actual effect of nano- and micro-gelation on products morphology. Manipulation (isolation) of the produced gel beads (Tanaka *et al*., 2007) and minimization of secondary nucleation during polymerisation (Yuyama *et al*., 2000; Ma *et al*., 2001 and 2003) are also important issues on this subject.

This work has confirmed that NMRP technique allows the synthesis of hyperbranched polymers with improved homogeneity, owing to less intramolecular cyclizations as compared

to conventional radical polymerisations. Moreover, it was also shown that NMRP allows operation with higher divinyl monomer content without gelation, which is an important issue in the production of hyperbranched polymers. In addition, this work has allowed the assessment of NMRP capabilities for synthesizing networks and gel with controlled molecular architecture. An ideal crosslinking process has been predicted to lead to polymer populations with different numbers of crosslinking points and narrow size distributions (Dias and Costa, 2010). However, the results here presented show high deviations from this behaviour with NMRP of STY/DVB, in contrast with the recent observation for living anionic polymerisation of 1,4-divinylbenzene (Hirao *et al*., 2011). Compared with FRP, NMRP does indeed allow some control on the crosslinking process, but intramolecular cyclizations cannot be suppressed and remain a major feature. The design of operation conditions combining CRP with variable concentration of crosslinker along the reaction time (e.g. in a semi-batch process) can eventually lead to an even higher degree of control of network formation. The results presented here can also be used to carry out kinetic modelling studieSty/model development on NMRP crosslinking of STY/DVB, which should be useful in the design of such operation conditions. Recent modelling studies based on the use of the method of moments and the Flory-Stockmayer theory of gelation (Hernández-Ortiz *et al*., 2009 and 2012) showed that NMRP seems to lead to more homogeneous polymer networks, but this effect is less important when the initial content of crosslinker is increased. Combination of the new experimental results presented here with a general kinetic modelling approach based on generating functions (Costa and Dias, 1994, 2005, 2006 and 2007; Dias and Costa, 2003, 2005, 2006, 2007 and 2010) will hopefully improve this discussion.

Detailed kinetic models were developed for the NMRP of STY/DVB including intramolecular cyclization reactions, as a complement to this work. A comprehensive experimental program concerning the solution and suspension NMRP of STY/DVB was carried out. For comparison purposes, some FRP experiments with the same polymerisations systems were also performed.

CHAPTER 5

REVERSIBLE ADDITION-FRAGMENTATION CHAIN-TRANSFER POLYMERISATION OF STYRENE AND COPOLYMERISATION OF STYRENE/DIVINYLBENZENE

Abstract. Experimental studies concerning RAFT homopolymerisation of styrene (linear) and copolymerisation (non-linear) of styrene and commercial divinylbenzene were performed in aqueous suspension (leading to gel formation) to assess the use of controlled radical polymerisation for the production of non-conventional polymer networks. The experiments were carried out in stirred batch reactor and changes of a few operation parameters were tried in order to assess their effect in key properties:

- Kind of polymerisation reactor:
  - 2.5 L atmospheric reactor.
  - 1 L pressurized reactor.
- Explored parameters:
  - Temperature and monomer dilution.
  - Amount of crosslinker (DVB).
  - Kind of RAFT agent and the initial ratio of RAFT agent with monomer and initiator.
- Products characterization:
  - Monomer conversion determined by GPC and gravimetry.
  - Molecular architecture of the products, namely:
    - Average molecular weights.
    - Average radius of gyration.
  - *In-line* and *off-line* FTIR-ATR.
  - Iodine chloride titration for determine PDBs concentration.
  - Gel fraction
  - SEM for observation of polymer particle morphology.
  - Comparison between FRP/NMRP/RAFT of the chemical system STY/DVB.

This chapter is based on the following publication:

M.A.D. Gonçalves, V.D. Pinto, R.C.S. Dias, J.C. Hernández-Ortiz, M.R.P.F.N. Costa, *Macromol. Symp.* 333 (2013) 273-285.

5.1 Introduction

Among controlled radical polymerisation techniques, reversible addition-fragmentation Chain-Transfer (RAFT) polymerisation presents some advantages comparatively with other CRP techniques. It is especially versatile because it can be used with different classes of monomers (e.g. with organic and water compatible monomers) and considering a wide range of operation conditions (e.g. using a broad range of polymerisation temperatures) (Moad *et al*., 2012; Braunecker and Matyjaszewski, 2007). Due to these features, RAFT presents promising industrial applicability (Zhang e Ray, 2011; Russum *et al*., 2005 and 2006; Rivera *et al*., 2005; Smulders et al., 2005; Moad *et al*., 2005, 2009 and 2012) and its use with dispersed systems was recently assessed in many important works (Cunningham, 2008; Zetterlund *et al*., 2008). In fact, the "green" polymerisation offered by aqueous dispersed systems also provides high heat dissipation rates and low viscosity products that are easily handled when compared with solution or bulk polymers. It was stated that polymerisation techniques that do not change the number of radicals per particle (such RAFT) should be considered (Butté *et al*, 2000 and 2001). Also, minemulsion is preferable because monomer droplets become the main loci of particle nucleation when an oil-soluble initiator is used, and in these conditions particles behave as bulk reactors with large productivity due to radical compartmentalization. Typical RAFT agents are quite water insoluble and therefore, when operating with emulsion polymerisation, there is no efficient transport between droplets and particles as it would be needed to achieve a controlled polymerisation. Conversely, with water mobile RAFT agents, kinetics of emulsion polymerisation is strongly affected (lowering of reaction rates) because the aqueous phase radicals involved with particle formation become also deactivated (Russum *et al*., 2005). As above described, these difficulties can be circumvented on considering the operation with RAFT in miniemulsion, a combination offering two additional advantages: radical segregation leading to the decrease of bimolecular termination and improved retention of the control agent into the polymer particles due to permanent bounding polymer/RAFT CTA across the polymerisation (Russum *et al*., 2005; Butté *et al*, 2000 and 2001).

Avoiding a large excess of metal complexes in final product (characteristic of ATRP) and high reaction temperatures to achieve a fairly high polymerisation rates (usually higher than 100 °C with NMRP) are other key advantages of RAFT when industrial implementation is considered. Undesirable higher incidence of termination mechanisms associated with RAFT (which can be minimized by increasing the initial mole ratio between RAFT agent and

initiator- at the expense of decreasing the polymerisation rate), occurrence of retardation with some RAFT agents and possible need of end group removal from RAFT-synthesized polymers (Hornung *et al*., 2012) are shortcomings of this CRP technique.

Distinctive features of RAFT polymerisation have been explored to synthesise linear polymers with well-defined topologies and also advanced materials based on non-linear polymerisation, such as networks (Yu *et al.*, 2008 and 2009), amphiphilic networks which are networks containing hydrophilic and hydrophobic moieties (Krasia and Patrickios, 2006; Achilleos *et al*., 2007), nanoparticles/nanocapsules (Lu *et al.*, 2010; Liu *et al.*, 2010), nanogels (Poly *et al*., 2008) and to control branching/hyperbranching considering organic (Pinto *et al*., 2008) as well as aqueous polymerisation systems (Wang *et al*., 2012 and 2013).

RAFT production of styrene/divinylbenzene networks was also reported in a few recent works considering bulk polymerisation in sealed ampoules (Roa-Luna *et al*., 2010) and in supercritical carbon dioxide (Jaramillo-Soto and Vivaldo-Lima, 2012). The ultimate goal of these researches (see Roa-Luna *et al*., 2010; Jaramillo-Soto and Vivaldo-Lima, 2012 and references therein) is the assessment of the use of CRP techniques aiming at the production of networks with improved structural homogeneity. Results here presented are a contribution to this research line considering the aqueous suspension RAFT polymerisation of STY/DVB as case study. Operation with aqueous suspension is explored to perform single-pot reactions, eventually with gel formation, maintaining good stirring and heat dissipation conditions, as recently showed with NMRP for the same chemical system (Gonçalves *et al*., 2013a).

Considering suspension polymerisation, an environmentally friendly operation with low organic solvent content is also possible and higher monomer conversions can be achieved while maintaining the low process viscosities. Polymerisation takes place in droplets resembling batch reactors and problems concerning aqueous-phase transport and reaction, particularly important in emulsion polymerisation, are also in principle circumvented. Thus, the combination between aqueous suspension operation and RAFT polymerisation can also be used to improve processes and products in vinyl polymers industry. Some of these ideas were explored in the very few published works concerning aqueous suspension RAFT polymerisation (Biasutti *et al.*, 2005). Good control of RAFT polymerisation in aqueous suspension was reported for methyl methacrylate at 70 °C. The concentration of the RAFT agent (2-cyanoprop-2-yl dithiobenzoate- CPDB) was found to affect the initial molecular weights (higher than expected due to the low chain-transfer constant of CPDB) and also the

particle size who decreases when increasing CPDB due to early breakup of droplets (Biasutti *et al.*, 2005).

Dynamics of RAFT crosslinking has been here studied through the analysis by SEC/RI/MALLS and *off-line* FTIR of reaction samples collected at different polymerisations times. Chemical analysis has also been used to measure the dynamics of the pendant double bond concentration (PDB) and the usefulness of *in-line* FTIR-ATR to obtain information concerning the RAFT building-up of the networks is assessed. Influence of some operation parameters (e.g. polymerisation temperature, initial composition, RAFT agent used) on the kinetics of polymerisation and crosslinking was studied by changing these parameters along the experimental program.

5.2 Experimental Part

5.2.1 Materials

In these experiments, styrene of 99 % purity stabilised with 0.005 % w/w 4-tert-butylcatechol, commercial grade divinylbenzene of 80 % purity stabilized with 0.1 % w/w 4-tert-butylcatechol, xylene of 98.5 % purity, AIBN of 98 % purity and toluene 99.7 % purity were purchased from Sigma-Aldrich and used as received. Xylene solvent is also a mixture of xylenes plus ethylbenzene ($\leq 25\%$ in the latter component). Commercial divinylbenzene with mixture isomers, 56.2% *m*-divinylbenzene and 24.2 % *p*-divinylbenzene, plus 19.6 % of ethylvinylbenzene was used in the RAFT copolymerisations. The following three commercially available RAFT agents were also purchased from Sigma Aldrich and used as received: 2-(dodecylthiocarbonothioylthio)-2-methylpropionic acid (DDMAT) of 98 % of purity, S-(thiobenzoyl)thioglycolic acid (TBTGA) of 99 % purity and cyanomethyl dodecyl trithiocarbonate (CDT) of 98 % purity. Chemical structures of the RAFT agents used are depicted in Figure 5.1 and their particularities will be bellow useful to discuss the different degree of polymerisation control that is possible to achieve with each compound.

5.2.2 Polymerisation Set-up

A set of polymerisation and copolymerisations runs performed in this research are described in Tables 5.1 and 5.2. Along the experimental program some main parameters were changed, such as polymerisation temperature, volumetric fraction of the monomer in the organic phase (y_M), initial mole ratio between initiator (AIBN) and monomer (y_I), initial mole ratio between

RAFT agent and initiator (y_I^{RAFT}), initial mole ration between monomer and RAFT agent (y_{RAFT}^{M}), initial mole fraction of crosslinker in the monomer mixture (y_C) (in the copolymerisations runs) and three different RAFT agents (DDMAT, CDT and TBTGA) were alternatively used in the experimental program.

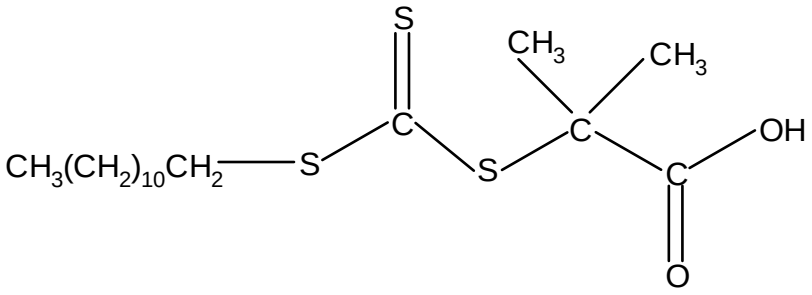

(a)

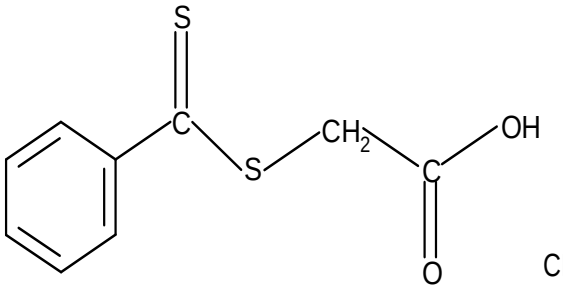

(b)

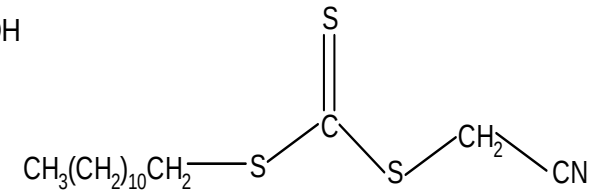

(c)

Figure 5.1. Chemical structures of the RAFT agents used in this chapter: (a) 2-dodecylthiocarbonothioylthio)-2-methylpropionic acid (DDMAT) (b) S-(thiobenzoyl)thioglycolic acid (TBTGA) (c) cyanomethyl dodecyl trithiocarbonate (CDT).

An atmospheric reactor with maximum capacity of 2.5 L was used to perform the polymerisations at lower temperatures (described in Chapter 2). A Parr 5100 pressurised glass reactor with 1 L maximum capacity was used to perform aqueous suspension experiments at higher temperature. The reactor is equipped with a magnetic drive internal stirrer including double turbine type six-blade impellers at 45°. The reactor was initially pressurized with argon at 2 bars: final pressures of 2.7, 3.5, 4.6 and 7.0 bars were observed when the temperature set-points of 90, 110, 130 and 150 °C, respectively, were approached. Technical description of both apparatus can be found in Gonçalves *et al.*, (2007, 2010b and 2013a). Typically these aqueous suspension RAFT polymerisation experiments were performed with 10 % volume of dispersed phase comparatively to the global volume (continuous + dispersed phase) polyvinyl alcohol (PVA was chosen as the suspending agent with a typical concentration in the aqueous phase of 0.1 % (w/w). Considering the used volumetric ratio

between aqueous/organic phases (reactor sampling becomes difficult at higher solid content) and the monomer dilution in the organic phase, the ratio PVA/monomer ranges between 0.15 and 2 % (w/w) and the correspondent ratios PVA/(monomer+solvent) between 0.08 and 1 % (w/w). These values are reasonable for a typical suspension polymerisation in which the concentration of suspending agent relative to the organic phase is the range 0.01 to 1 % (w/w). Concentrations of PVA of 0.06 to 0.12 % (by monomer weight) are reported in previous works concerning the FRP suspension polymerisation of styrene and divinylbenzene. Here, higher concentrations of PVA were chosen in order to improve reactor sampling by decreasing average particle size.

Table 5.1. A set of homopolymerisation runs performed in the suspension RAFT of styrene.

Run	T (°C)	y_M(%)	y_I(%)	y_I^{RAFT}	y_{RAFT}^{M}	RAFT Agent
1	70	50	0.208	1.841	261.0	TBTGA
2	70	50	0.216	1.869	47.8	DDMAT
3	70	50	0.213	1.884	249.5	CDT
4	70	100	0.105	1.991	498.4	CDT
5	90	50	0.210	1.828	260.2	DDMAT
6	110	50	0.218	1.796	255.9	DDMAT
7	130	50	0.214	1.882	248.3	DDMAT
8	130	50	0.202	3.931	125.9	DDMAT
9	150	50	0.215	1.890	246.4	DDMAT

5.2.3 SEC/RI/MALLS Products Analysis

Reaction samples were collected into previous cooled 20 ml glass vials and immediately stored in the refrigerator at -14 °C to stop the reaction. At least 24 hours later, samples were allowed to reach room temperature and aqueous/organic phases were separated. A small amount of the latter phase was diluted in THF (final concentration around 0.1% w/w) and filtered to be injected in the SEC/RI/MALLS system. The SEC/RI/MALLS apparatus is composed of a Polymer Laboratories PL-GPC-50 integrated SEC system with differential refractometer working at 950±30 nm, attached to a Wyatt Technology DAWN8+ HELEOS 658 nm Multi Angle Laser Light Scattering (MALLS) detector. The polymer samples were fractionated by molecular size using a train of 3 GPC columns PL gel (300×7.5 mm) with nominal particle size 10 μm and pore type MIXEDB-LS, maintained at constant temperature of 30 °C and using THF as the eluent at a flow rate of 1 mL/min. Molecular weight averages

and size distribution as well as *z* -average radius of gyration of the soluble polymer phase was thus measured. Monomer conversion was also estimated through the measurement of the monomers peak areas in these chromatograms. Typical chromatographic traces thus obtained by SEC/RI/MALLS are presented in Figure 5.2 where the normalized RI signal (using a peak maximum as reference) observed for samples of RAFT synthesized polystyrene is here showed. The aqueous suspension at 150 °C with conditions of run 9 in Table 5.1 is considered for illustration purposes. Increase of the concentration and molecular weight of the polymer population and monomer depletion along the reaction time are here observed.

Table 5.2. A set of copolymerisation runs performed in the suspension RAFT of styrene with divinylbenzene.

Run	T (°C)	y_C(%)	y_M(%)	y_I(%)	y_I^{RAFT}	y_{RAFT}^M	RAFT Agent	w_g
1	70	5.15	35	0.205	2.006	261.0	DDMAT	0.81
2	70	100	100	0.107	1.855	503.8	DDMAT	1.0
3	70	100	50	0.107	1.876	498.2	DDMAT	1.0
4	70	5.27	35	0.210	1.965	242.3	DDMAT	0.78
5	90	20.13	100	0.110	1.936	469.6	CDT	1.0
6	110	20.13	100	0.110	5.987	151.8	TBTGA	0.94
7	130	20.92	100	0.108	6.009	154.1	TBTGA	1.0

5.2.4 Gravimetric Measurements

The remaining organic phase resulting from the above described sampling process was weighed and precipitated into a large excess of methanol in order to isolate the polymer. After vacuum drying, monomer conversion could also be estimated by recording the weight loss.

5.2.5 *In-line* and *off-line* FTIR-ATR Measurements

In-line monitoring of some polymerisation runs was performed using an attenuated total reflection (ATR) immersion probe coupled with a Fourier-Transform Infra-Red (FTIR) instrument. Technical details of this apparatus were presented in Gonçalves *et al*., 2010b. Isolated polymer samples, after drying, were also *off-line* characterised by FTIR using the powered products mixed with KBr and pressed into pellets. This procedure is detailed in appendix A.

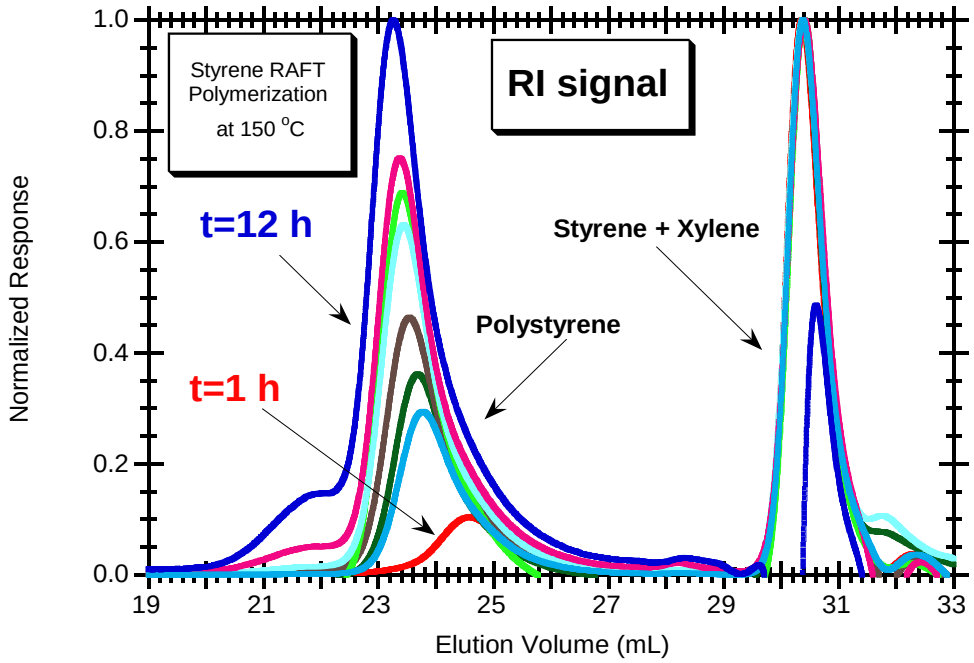

Figure 5.2. Typical chromatographic traces observed by SEC/RI/MALLS from reaction samples collected at different polymerisation times. Run 9 in Table 5.1 is used for illustration.

5.2.6 PDB Concentration Measurement

Quantification of pendant double bonds (PDB) concentration into the RAFT STY/DVB polymer networks was performed using chemical analysis (ICl titration), as recently reported for NMRP STY/DVB networks (Gonçalves *et al*., 2013a). Dynamics of PDB concentration was thus estimated, which is an important issue in the crosslinking process. This chemical method is an alternative/complementary approach to the FTIR analysis above described.

5.2.7 Product Morphology Characterization by SEM

The above described dried products were also analysed by scanning electron microscopy in the Centro de Microscopia da Universidade do Porto (CEMUP). The influence of the synthesis conditions on the morphology of the produced materials could thus be observed.

5.3 RAFT Homopolymerisation of Styrene

5.3.1 Chemical Species and Chemical Reactions

Different possibilities for kinetic schemes describing the RAFT polymerisation of styrene are traduced by Equations (5.1) to (5.25) complemented by Tables 5.3 and 5.4 where are represented the set of chemical species and the basic set of rate coefficients considered in the modelling studies of the RAFT polymerisation of styrene. Equations (5.1) to (5.13) describe the conventional steps included in radical polymerisation, namely initiator decomposition, monomer initiation, monomer propagation, irreversible chain transfers to monomer, solvent initiator, termination by combination and disproportionation. In order to assess the effect of thermal initiation of styrene (possible at high polymerisation temperatures such in some runs performed in this work) the Mayo dimerization of styrene was also included in the kinetic scheme. Equations (5.14) to (5.17) represent the reaction scheme describing RAFT steps involving primary radicals. Finally, Equations (5.18) to (5.25) describe the reaction scheme considering macro-radical intermediate (adduct) and cross-termination in a RAFT polymerisation. In Figure 5.3 is depicted the main chain equilibration step in RAFT polymerisation.

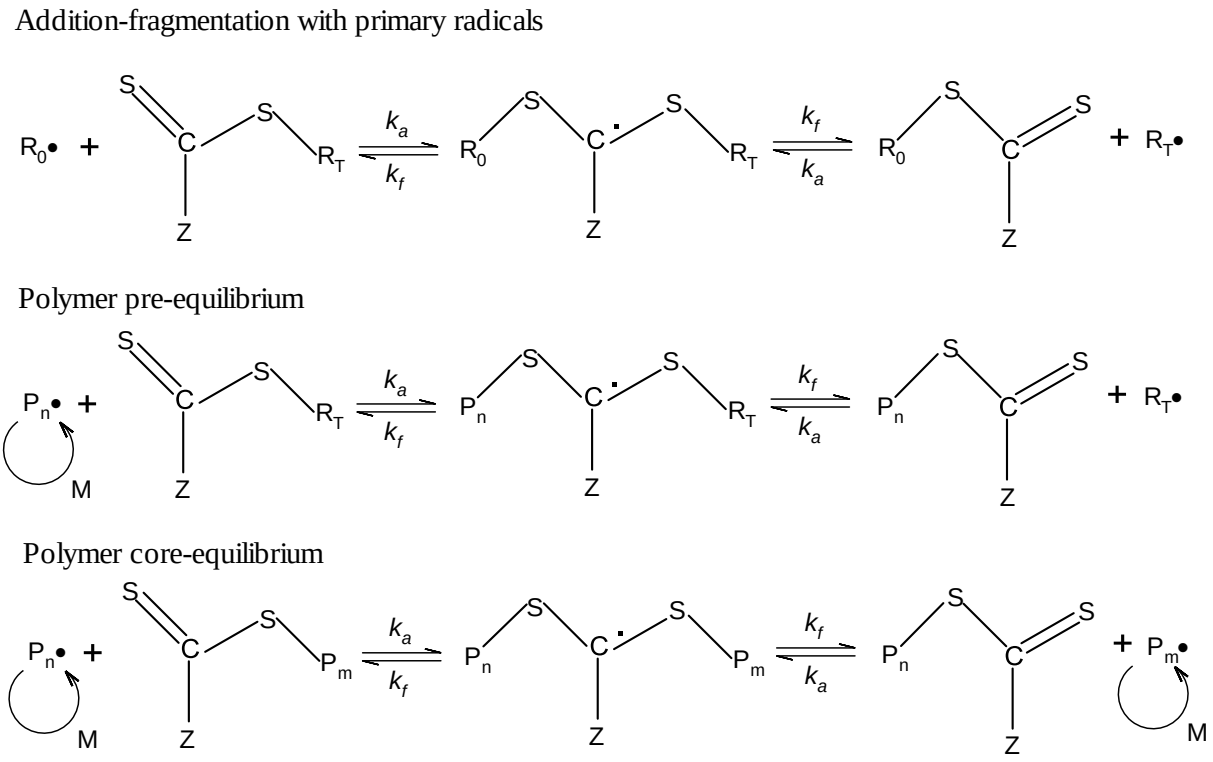

Figure 5.3. Depiction of the main chain equilibration step in RAFT polymerisation.

Initiator Decomposition:

$$I \xrightarrow{k_d} 2fR_0 \tag{5.1}$$

Mayo dimerization of styrene:

$$M + M \underset{k_{dim}^{-1}}{\overset{k_{dim}}{\rightleftharpoons}} MM \tag{5.2}$$

Thermal initiation of styrene:

$$M + MM \xrightarrow{k_{IA}} R_M + R_D \tag{5.3}$$

Monomer initiation by primary radicals of the initiator:

$$R_0 + M \xrightarrow{k_{IR}} P_1 \tag{5.4}$$

Monomer initiation by primary radicals of the monomer:

$$R_M + M \xrightarrow{k_{IM}} P_2 \tag{5.5}$$

Monomer initiation by primary radicals of the dimer:

$$R_D + M \xrightarrow{k_{ID}} P_3 \tag{5.6}$$

Monomer propagation:

$$P_n + M \xrightarrow{k_p} P_{n+1} \tag{5.7}$$

Irreversible chain transfer to agent:

$$P_n + A \xrightarrow{k_{trA}} D_n + R_0 \tag{5.8}$$

Irreversible chain transfer to monomer:

$$P_n + M \xrightarrow{k_{trM}} D_n + R_M \tag{5.9}$$

Irreversible chain transfer to dimer:

$$P_n + MM \xrightarrow{k_{trMM}} D_n + R_D \tag{5.10}$$

Irreversible chain transfer to initiator:

$$P_n + I \xrightarrow{k_{trI}} D_n + R_0 \tag{5.11}$$

Termination by combination:

$$P_n + P_m \xrightarrow{k_{tc}} D_{n+m} \tag{5.12}$$

Termination by disproportionation:

$$P_n + P_m \xrightarrow{k_{td}} D_n + D_m \tag{5.13}$$

RAFT addition and fragmentation of different kinds of primary radicals:

$$R_0 + A \underset{k_f}{\overset{k_a}{\rightleftharpoons}} R_0A \underset{k_a}{\overset{k_f}{\rightleftharpoons}} a + R_A \tag{5.14}$$

$$R_M + A \underset{k_f}{\overset{k_a}{\rightleftharpoons}} R_MA \underset{k_a}{\overset{k_f}{\rightleftharpoons}} AP_1 + R_A \tag{5.15}$$

$$R_D + A \underset{k_f}{\overset{k_a}{\rightleftharpoons}} R_DA \underset{k_a}{\overset{k_f}{\rightleftharpoons}} aP_2 + R_A \tag{5.16}$$

Monomer initiation by primary radicals from RAFT:

$$R_A + M \xrightarrow{k_{IRAFT}} P_1 \tag{5.17}$$

RAFT addition with CTA (pre-equilibrium):

$$P_n + A \underset{k_f}{\overset{k_a}{\rightleftharpoons}} P_nA + R_0 \tag{5.18}$$

RAFT addition and fragmentation:

$$P_n + AP_m \underset{k_f}{\overset{k_a}{\rightleftharpoons}} P_nA^*P_M \underset{k_a}{\overset{k_f}{\rightleftharpoons}} AP_n + P_m \tag{5.19}$$

Cross-termination:

$$P_n + P_rA^*P_m \xrightarrow{k_{tcr}} D_{n+r+m} \tag{5.20}$$

Cross-oligomer termination:

$$P_1 + P_rA^*P_m \xrightarrow{k_{cot}} D_{1+r+m} \tag{5.21}$$

$$P_2 + P_rA^*P_m \xrightarrow{k_{cot}} D_{2+r+m} \tag{5.22}$$

Cross-primary radicals termination:

$$R_0 + P_r A^* P_m \xrightarrow{k_{cot}} D_{r+m} \quad (5.23)$$

$$R_M + P_r A^* P_m \xrightarrow{k_{cot}} D_{1+r+m} \quad (5.24)$$

$$R_D + P_r A^* P_m \xrightarrow{k_{cot}} D_{2+r+m} \quad (5.25)$$

Table 5.3. Set of chemical species considered in the RAFT polymerisation of styrene.

Group description	Alias
Styrene monomer	M
Thermal initiator (AIBN)	I
Dimer from styrene	MM
Solvent	T
Primary radical from initiator	R_0
Primary radical from monomer	R_M
Primary radical from dimer	R_D
Primary radical from RAFT agent	R_A
Active polymer chain with DP= $n \geq 1$	P_n
Dead polymer chain with DP= $n \geq 1$	D_n
RAFT agent	A
Dormant polymer chain with DP= $n \geq 1$	APn
Macro-radical intermediate (adduct)	$P_nA^*P_m$

This kinetic scheme is based on the RAFT modelling work recently published by Saldívar-Guerra (Zapata-González *et al.*, 2011). It is important to stress that modelling of RAFT process was a controversial subject in the last decade, as reported in some important papers (Barner-Kowollik *et al*., 2001 and 2003; Wang and Zhu, 2003; Wang *et al*., 2003; Wulkow *et al*., 2004). Definition of at least the following four fundamental types of chains was considered in most past works: propagating radical chains P_n, adduct radical chains $P_nT^*P_m$, dormant chains TP_n and dead chains D_n (see e.g. Sun *et al*., 2008; Wang and Zhu, 2003; Zhang and Ray, 2001). An additional definition of primary intermediate radicals (formed in the pre-equilibrium) can also be found in these papers (Sun *et al*., 2008; Zhang and Ray, 2001). Works dealing simultaneously with one-, two- and three-arm adducts were also recently published (see e.g. Hernández-Ortiz *et al.*, 2010). Principles here described were also

recently used by Zapata-González *et al.*, (2011) to calculate the full molecular weight distribution in RAFT polymerisation.

Table 5.4. Basic set of rate coefficients considered in the modelling studies of the NMRP copolymerisation of STY/DVB monomers.

Group description [a)]	Rate coefficient expression [b)]
Initiator thermal decomposition	$k_d = 4.31 \times 10^{15} \exp(-131.7 \times 10^3/RT)$ $(s^{-1}), f = 0.6$
Styrene propagation	$k_p = 4.27 \times 10^7 \exp(-32.5 \times 10^3/RT)$
Initiation of styrene by primary radicals	$k_{IR} = k_{ID} = k_{IM} = k_{IT} = k_P$
Chain transfer to monomer	$C_M = \frac{k_{fM}}{k_P} = 0.2128 \exp(-23.5 \times 10^3/RT)$
Chain transfer to solvent	$k_{fT} = 1.8$
Chain transfer to dimer	$k_{fD} = 50$
Mayo dimerization	$k_{dim} = 188.97 \exp(-67.7 \times 10^3/RT)$
Dimer decomposition	$k_{dim}^{-1} = 5.49 \times 10^9 \exp(-106.1 \times 10^3/RT)$ (s^{-1})
Thermal initiation	$k_{IA} = 6.539 \times 10^{12} \exp(-153.1 \times 10^3/RT)$
Radical termination	$k_p/\sqrt{k_t} = 426.4 \exp(-26 \times 10^3/RT)$ $\alpha_{td} = \frac{k_{td}}{k_t} = 0, \alpha_{tc} = \frac{k_{tc}}{k_t} = 1$

[a)] Kinetic parameters expressed in $dm^3 mol^{-1} s^{-1}$, unless otherwise stated. [b)] References of the rate coefficients are the same as in Table 4.4 of Chapter 4.

5.3.2 Results and Discussion

Main experimental results obtained in this chapter for styrene RAFT polymerisation are graphically summarized in Figures (5.4)-(5.12). In those figures, for each run described in Table 5.1, the following information is provided:

- Dynamics of monomer conversion.
- Dynamics of average molecular weights ($\bar{M}_n$ and $\bar{M}_w$) and of molecular weight dispersity (D_M).
- Observed Refractive Index (RI) signal in SEC chromatographic traces correspondent to RAFT polystyrene samples collected at different reaction times. Change of the concentration and molecular weight of the polymer population along the reaction time is thus showed.

- Observed Multi-Angle Laser Light Scattering (MALLS) signal in SEC chromatographic traces correspondent to RAFT polystyrene samples also collected at different reaction times. Reaction time growth of the molecular size of the polymer population can be here observed.
- Comparison of the observed RI and MALLS signals correspondent to samples with t = 12 hr reaction time. With these comparisons, the effect of operation conditions on the molecular architecture of the RAFT produced polystyrene (namely polymer population homogeneity) is highlighted.

Besides insights on the kinetics of monomer consumption and product formation with aqueous RAFT suspension, important features of product molecular structure are also provided by the results presented in Figures (5.4)-(5.12). Note that crucial details of the molecular of the produced RAFT polystyrene are not discernible when only the average properties of the polymer are observed. In fact, the formation of a higher size secondary polymer population (SP) is observed in these SEC traces when DDMAT or CDT are used as RAFT agents but not when TBTGA is considered. This is a relevant result with these commercially available CTAs, confirming the importance of the choice of the RAFT agent to achieve a higher control of the polymer molecular architecture.

Formation of higher sized secondary polymer populations is almost only residually observed when the RI signal is considered but its importance becomes evident with the MALLS signal (see graphics (c), (d) and (e) along Figures (5.4)-(5.12)). Using multiple detection is therefore an important advantage when a rigorous characterization of the molecular architecture of the products is sought. For instance, the estimation of the molecular weight dispersity (D_M) is presented in graphics (b) of Figures (5.4)-(5.12) considering the inclusion of the secondary population and the exclusion of these chains (using only the main RI peak). In spite of some experimental uncertainties (effect of noisy signals with diluted samples, etc.) huge differences in D_M are observed considering the presence/absence of this secondary population when DDMAT or CDT are used as RAFT agents. With TBTGA (see Figure 5.4), in spite of the lower polymerisation rate, a polymer with a reasonable molecular homogeneity is produced (D_M around 1.4). Very low values of D_M (around 1.2) are estimated with DDMAT or CDT when the secondary population is not included but very high dispersity of polymer population ($D_M \sim 2$ or even higher) results when these chains are accounted.

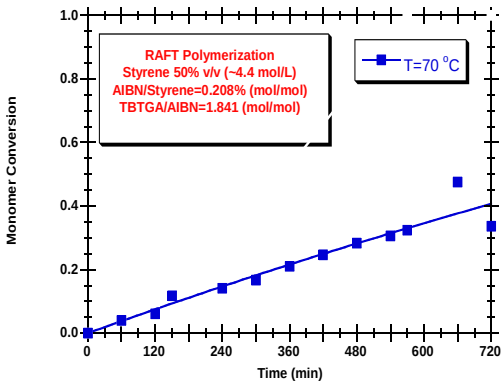

(a)

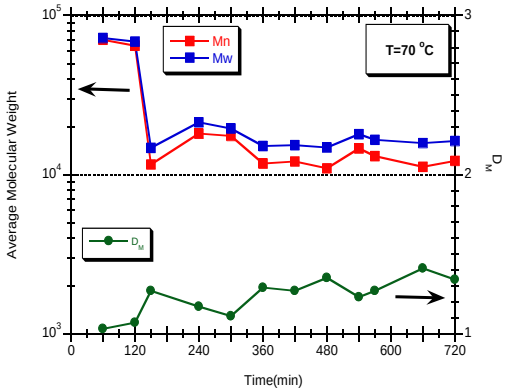

(b)

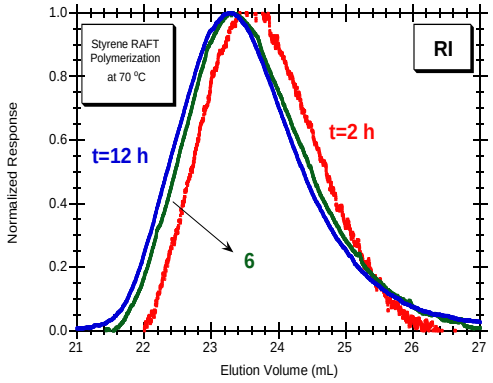

(c)

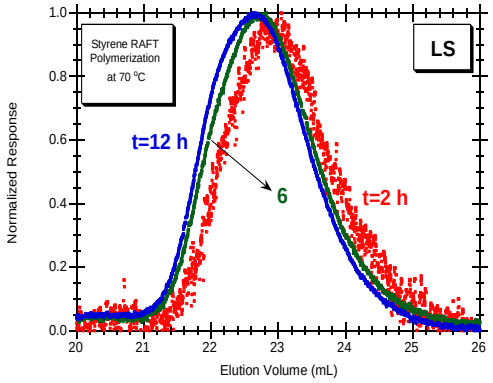

(d)

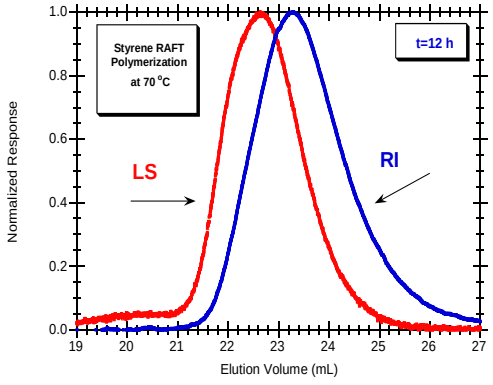

(e)

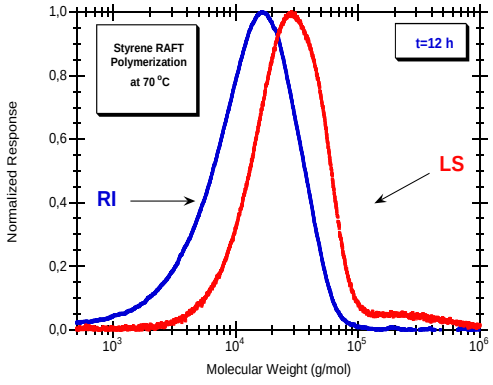

(f)

Figure 5.4. Main results for RAFT polystyrene synthesis in aqueous suspension at 70 °C using TBTGA CTA (run 1 in Table 5.1). (a) Measured reaction time evolution of monomer conversion. (b) Measured reaction time evolution of molecular weight dispersity (D_M) and average molecular weights ($\bar{M}_n$ and $\bar{M}_w$). (c) Normalized RI signal of polystyrene samples with different polymerisation time. (d) Normalized MALLS signal (90° detector) for the same samples described in (c). (e) Comparison of the normalized RI and MALLS signals of a polystyrene sample with polymerisation time t = 12 h. (f) Change of the RI and LS signals along the molecular weight for the same sample described in (e).

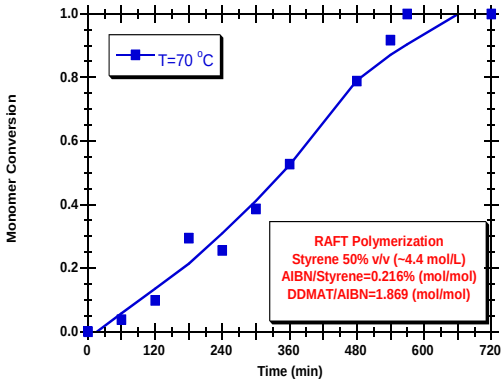

(a)

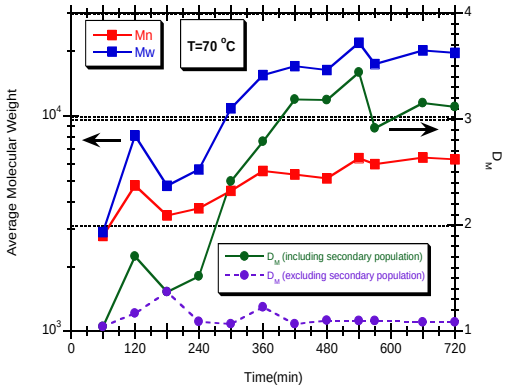

(b)

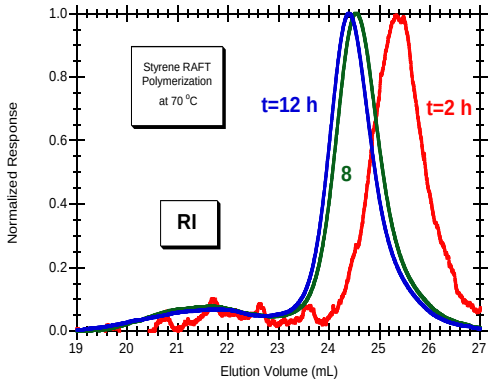

(c)

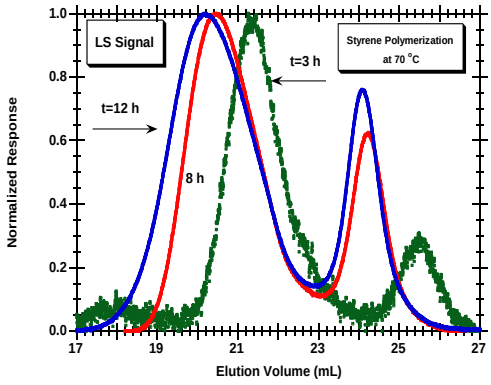

(d)

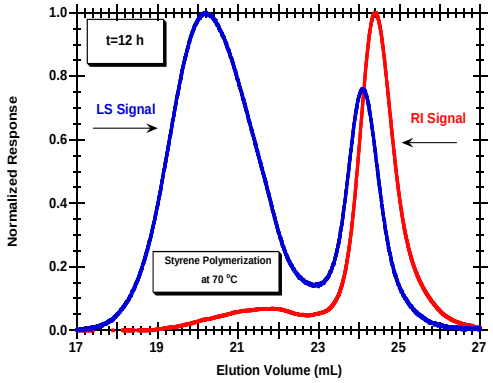

(e)

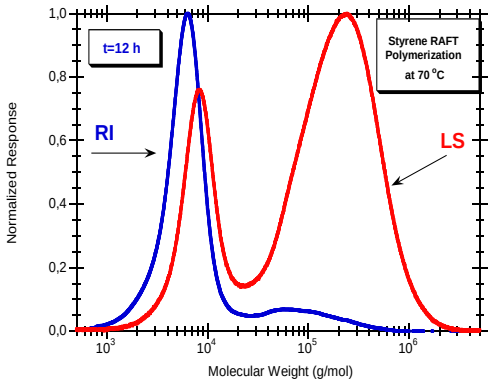

(f)

Figure 5.5. Main results for RAFT polystyrene synthesis in aqueous suspension at 70 °C using DDMAT CTA (run 2 in Table 5.1). (a) Measured reaction time evolution of monomer conversion. (b) Measured reaction time evolution of molecular weight dispersity (D_M) and average molecular weights ($\overline{M}_n$ and $\overline{M}_w$). (c) Normalized RI signal of polystyrene samples with different polymerisation time. (d) Normalized MALLS signal (90° detector) for the same samples described in (c). (e) Comparison of the normalized RI and MALLS signals of a polystyrene sample with polymerisation time t = 12 h. (f) Change of the RI and LS signals along the molecular weight for the same sample described in (e).

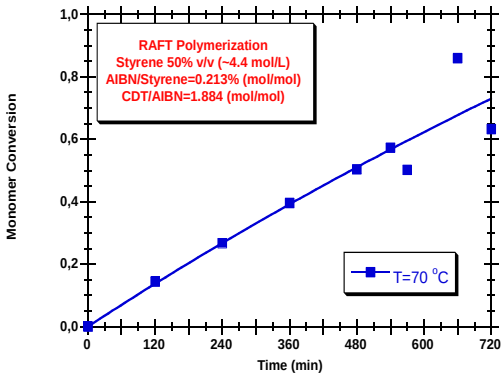

(a)

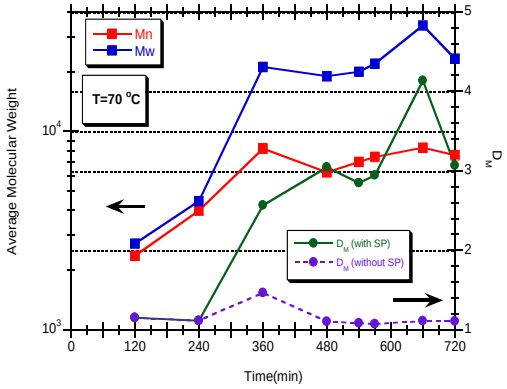

(b)

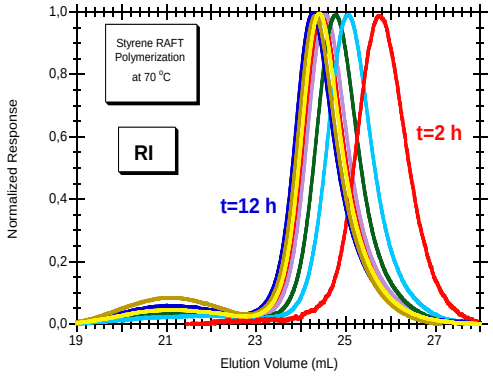

(c)

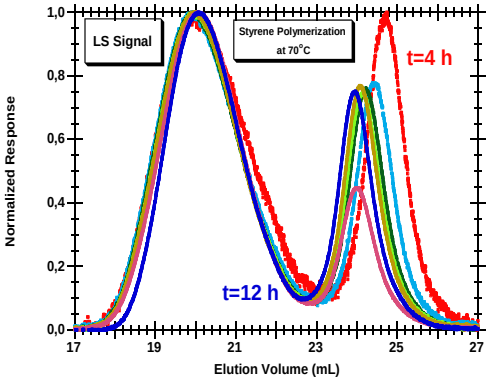

(d)

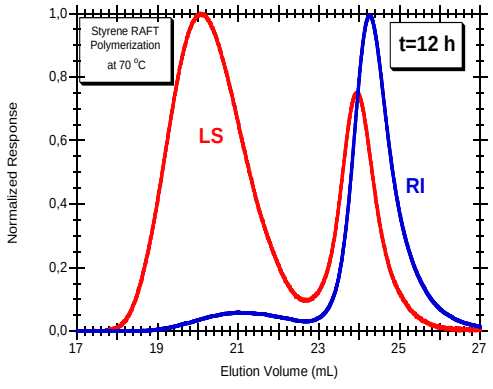

(e)

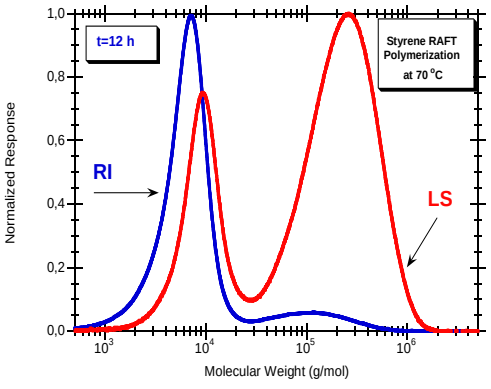

(f)

Figure 5.6. Main results for RAFT polystyrene synthesis in aqueous suspension at 70 °C using CDT CTA (run 3 in Table 5.1). (a) Measured reaction time evolution of monomer conversion. (b) Measured reaction time evolution of molecular weight dispersity (D_M) and average molecular weights ($\bar{M}_n$ and $\bar{M}_w$). (c) Normalized RI signal of polystyrene samples with different polymerisation time. (d) Normalized MALLS signal (90° detector) for the same samples described in (c). (e) Comparison of the normalized RI and MALLS signals of a polystyrene sample with polymerisation time t = 12 h. (f) Change of the RI and LS signals along the molecular weight for the same sample described in (e).

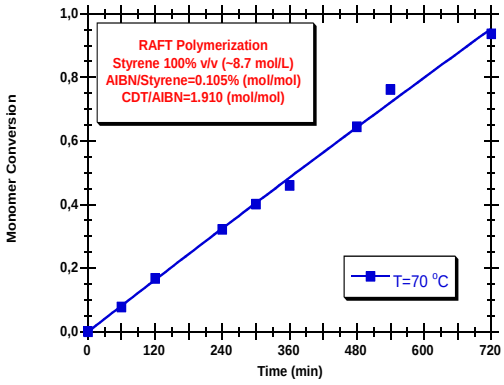

(a)

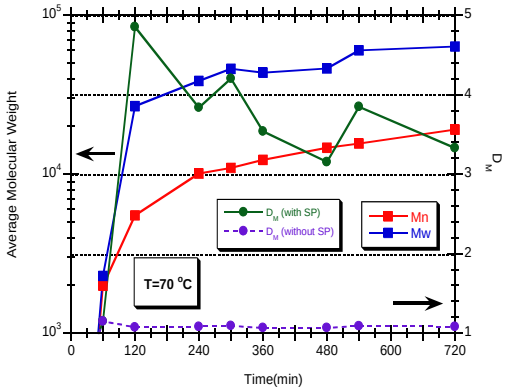

(b)

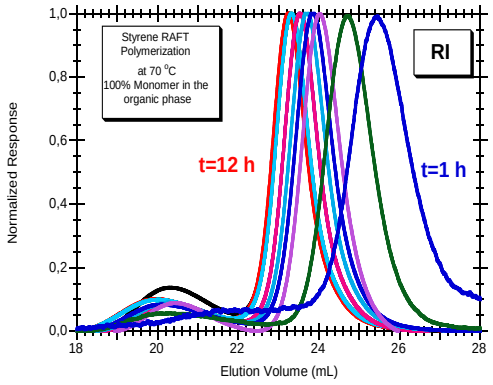

(c)

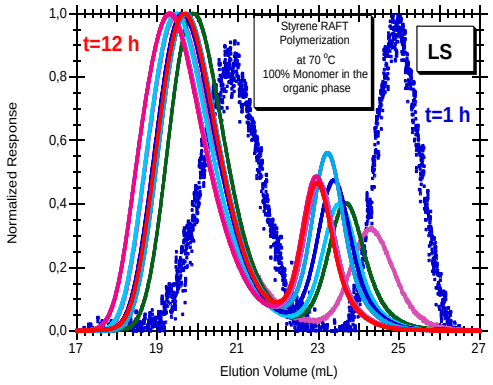

(d)

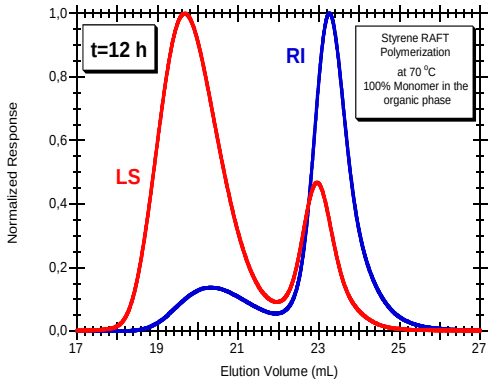

(e)

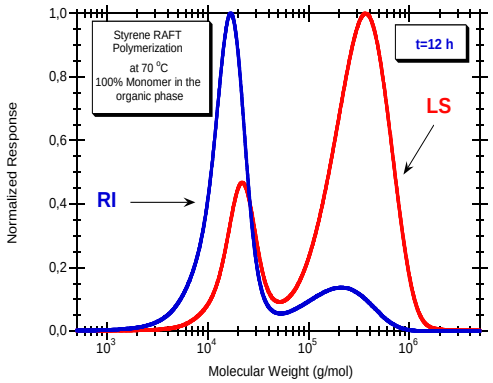

(f)

Figure 5.7. Main results for RAFT polystyrene synthesis in aqueous suspension at 70 °C using CDT CTA (run 4 in Table 5.1). (a) Measured reaction time evolution of monomer conversion. (b) Measured reaction time evolution of molecular weight dispersity (D_M) and average molecular weights ($\bar{M}_n$ and $\bar{M}_w$). (c) Normalized RI signal of polystyrene samples with different polymerisation time. (d) Normalized MALLS signal (90° detector) for the same samples described in (c). (e) Comparison of the normalized RI and MALLS signals of a polystyrene sample with polymerisation time t = 12 h. (f) Change of the RI and LS signals along the molecular weight for the same sample described in (e).

Differences in the control of polymerisation observed with the three commercially available RAFT agents used in the present work are a consequence of their distinct chemical nature, as illustrated in Figure 5.1. TBTGA belongs to the class of the dithiobenzoates (with the free radical leaving group $R_T = -CH_2 - CO - OH$) which present very high transfer constants, are prone to hydrolysis and cause retardation when high concentrations are used (Moad *et al.*, 2005, 2009 and 2012). DDMAT and CDT are trithiocarbonates with high transfer constants, are more hydrolytically stable when compared with dithiobenzoates and cause less retardation (Moad *et al.*, 2005, 2009 and 2012; see also the online section of Sigma Aldrich dedicated to RAFT polymerisation, http://sigmaaldrich.com). The free radical leaving groups of DDMAT and CDT are $R_T = -C(CH_3)_2 - CO - OH$ and $RT = -CH_2 - CN$, respectively, with both bearing the same Z-group ($CH_3(CH_2)_{10}CH_2-$). The Z-group controls the C=S double bond reactivity with concomitant influence on the rate of addition and fragmentation (see Figure 5.3 where the general structure of a RAFT agent, $Z - C(= S) - S - R_T$, is also depicted). Note that the Z-group in TBTGA is the aromatic ring and therefore differences between the addition/fragmentation rates are expected when polymerisation is performed with TBTGA or alternatively with DDMAT/CDT, but not when the latter pair is compared (both RAFT agents with the same Z-group).

Experimental results obtained show that the incidence of the secondary population is dependent on the polymerisation temperature. This can be observed by comparing (e.g.) graphics (d) in Figures 5.5, 5.8, 5.9, 5.10 and 5.12 corresponding all to RAFT polymerisation with DDMAT (maintaining $y_I^{RAFT} \sim 2$) at 70, 90, 110, 130 and 150 °C. A higher impact of these phenomena was found to occur at lower polymerisation temperatures, namely at 70 and 90 °C (see Figures 5.5 and 5.8) and seems to have a lower importance at 110 °C. These results show that this formation process is also reaction-time dependent, enlightening the importance of knowing the detailed kinetics of addition/fragmentation in the formation of polymers with low dispersity using the RAFT technique. Note that this phenomena cannot be eliminated by increasing the initial RAFT concentration (at least maintaining reasonable reaction rates), as it can be observed by comparing Figures 5.10 and 5.11 both corresponding to RAFT polymerisation with DDMAT at 130 °C and considering $y_I^{RAFT} \sim 2$ and $y_I^{RAFT} \sim 4$, respectively.

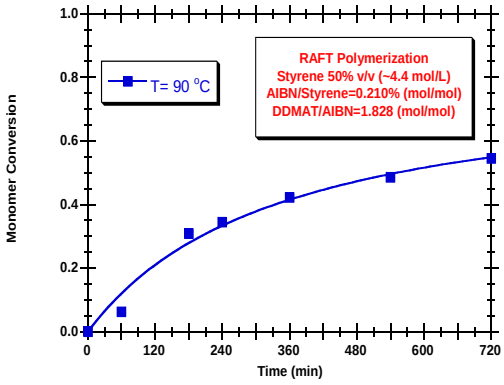

(a)

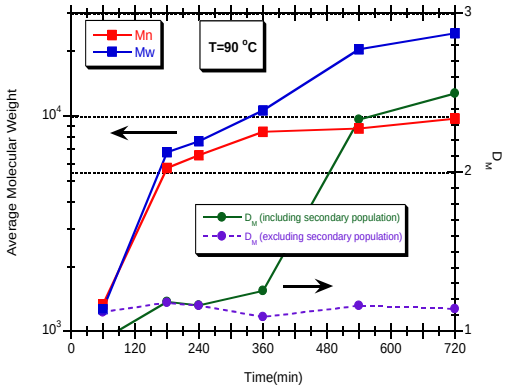

(b)

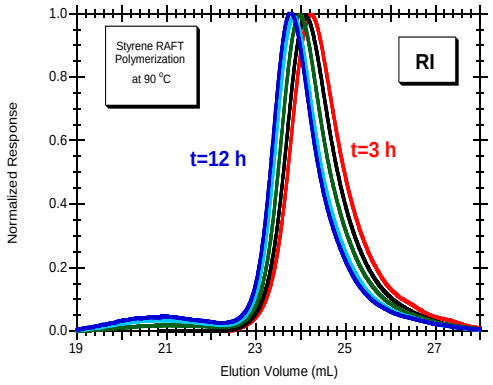

(c)

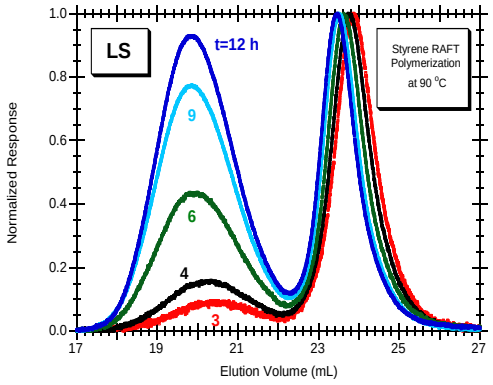

(d)

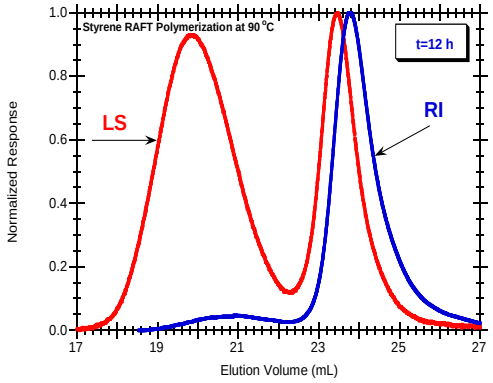

(e)

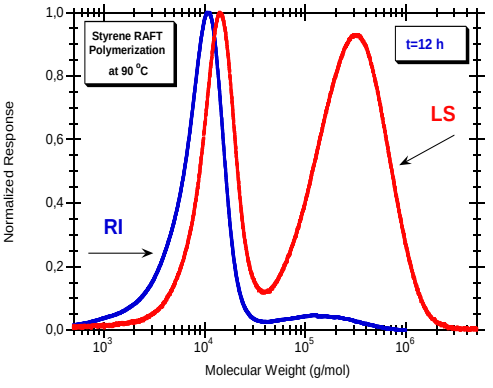

(f)

Figure 5.8. Main results for RAFT polystyrene synthesis in aqueous suspension at 90 °C using DDMAT CTA (run 5 in Table 5.1). (a) Measured reaction time evolution of monomer conversion. (b) Measured reaction time evolution of molecular weight dispersity (D_M) and average molecular weights ($\overline{M}_n$ and $\overline{M}_w$). (c) Normalized RI signal of polystyrene samples with different polymerisation time. (d) Normalized MALLS signal (90° detector) for the same samples described in (c). (e) Comparison of the normalized RI and MALLS signals of a polystyrene sample with polymerisation time t = 12 h. (f) Change of the RI and LS signals along the molecular weight for the same sample described in (e).

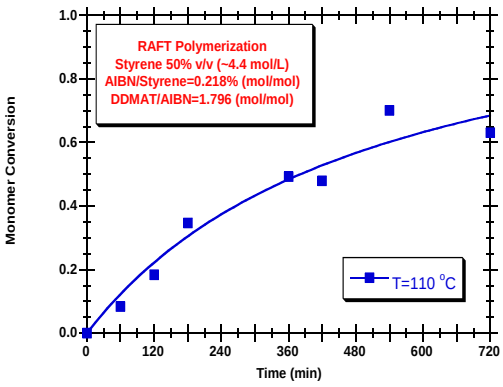

(a)

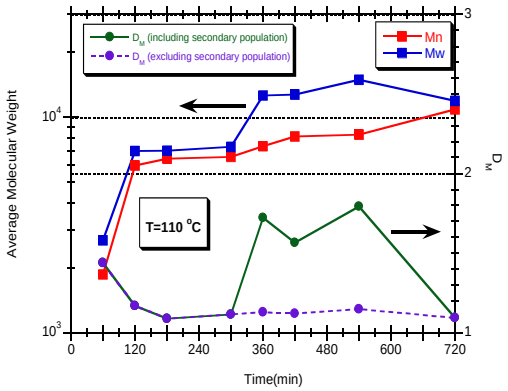

(b)

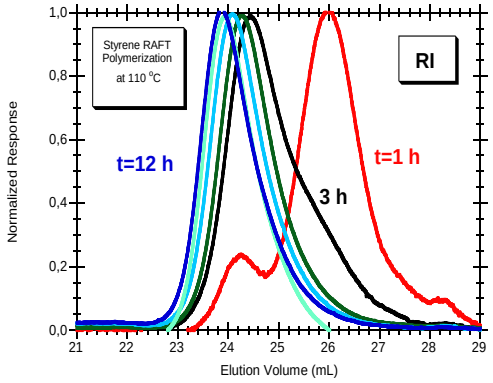

(c)

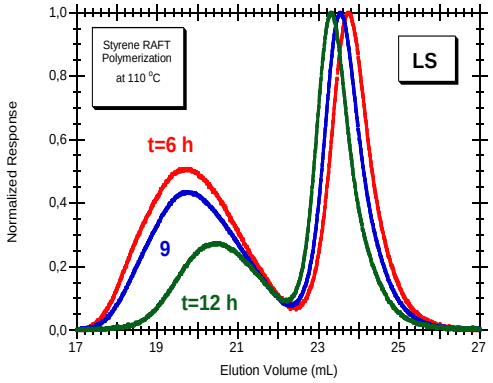

(d)

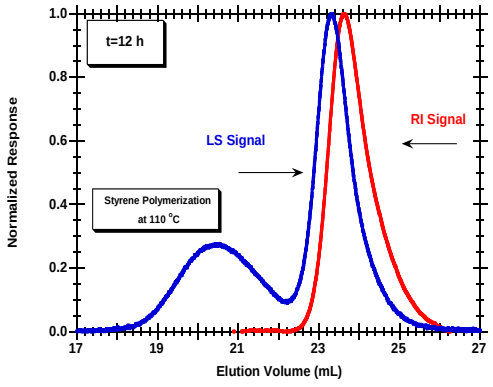

(e)

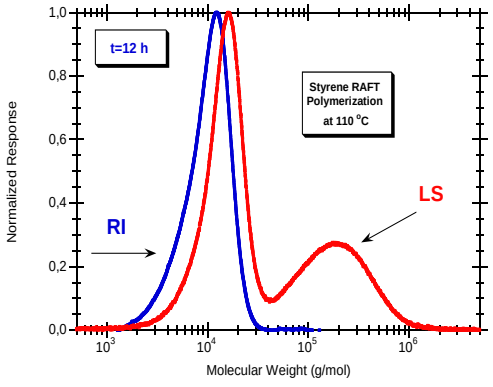

(f)

Figure 5.9. Main results for RAFT polystyrene synthesis in aqueous suspension at 110 °C using DDMAT CTA (run 6 in Table 5.1). (a) Measured reaction time evolution of monomer conversion. (b) Measured reaction time evolution of molecular weight dispersity (D_M) and average molecular weights ($\bar{M}_n$ and $\bar{M}_w$). (c) Normalized RI signal of polystyrene samples with different polymerisation time. (d) Normalized MALLS signal (90° detector) for the same samples described in (c). (e) Comparison of the normalized RI and MALLS signals of a polystyrene sample with polymerisation time t = 12 h. (f) Change of the RI and LS signals along the molecular weight for the same sample described in (e).

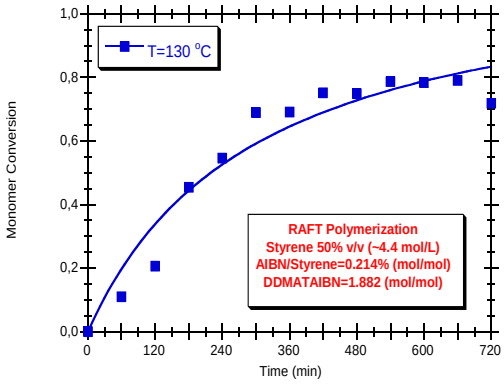

(a)

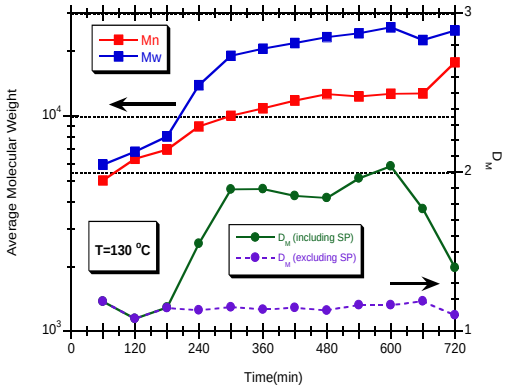

(b)

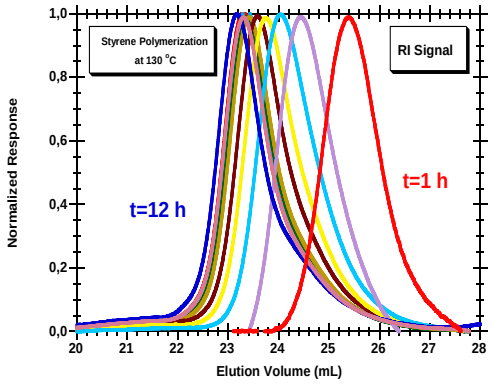

(c)

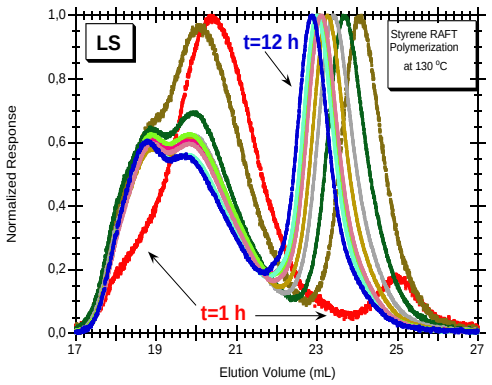

(d)

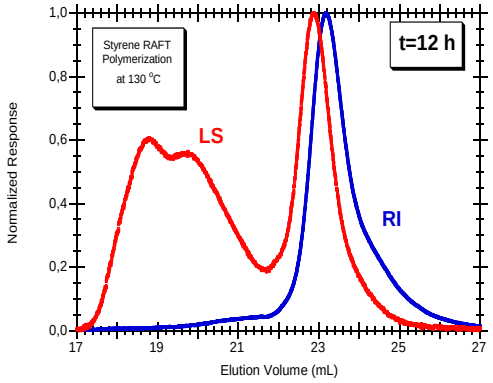

(e)

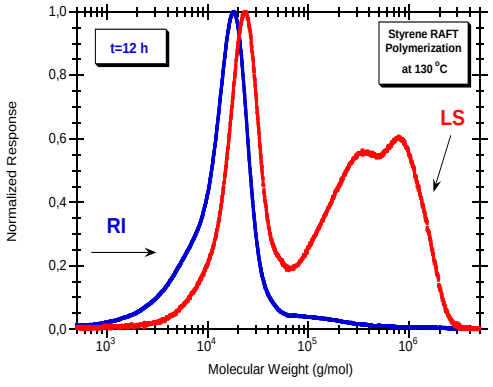

(f)

Figure 5.10. Main results for RAFT polystyrene synthesis in aqueous suspension at 130 °C using DDMAT CTA (run 7 in Table 5.1). (a) Measured reaction time evolution of monomer conversion. (b) Measured reaction time evolution of molecular weight dispersity (D_M) and average molecular weights ($\overline{M}_n$ and $\overline{M}_w$). (c) Normalized RI signal of polystyrene samples with different polymerisation time. (d) Normalized MALLS signal (90° detector) for the same samples described in (c). (e) Comparison of the normalized RI and MALLS signals of a polystyrene sample with polymerisation time t = 12 h. (f) Change of the RI and LS signals along the molecular weight for the same sample described in (e).

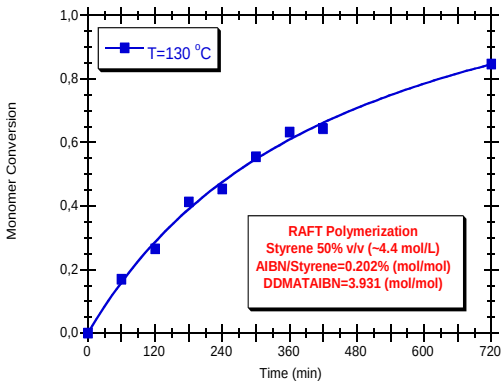

(a)

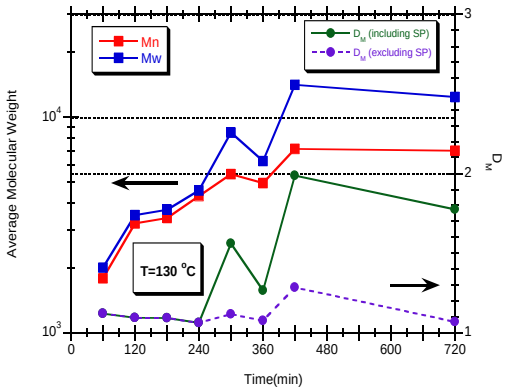

(b)

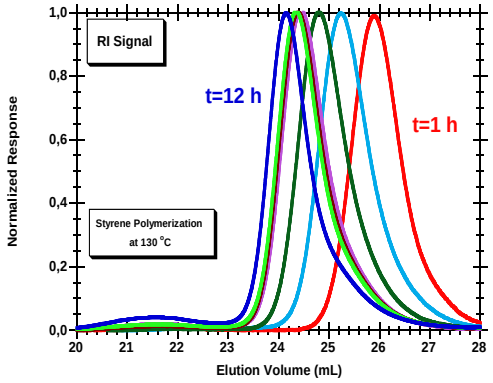

(c)

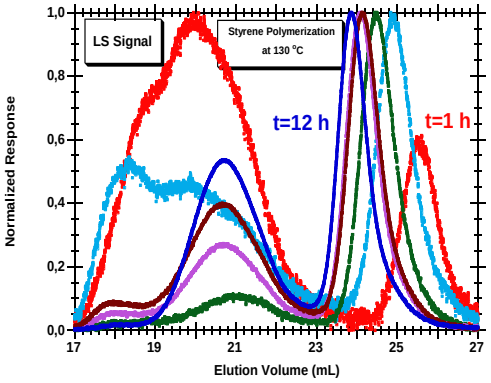

(d)

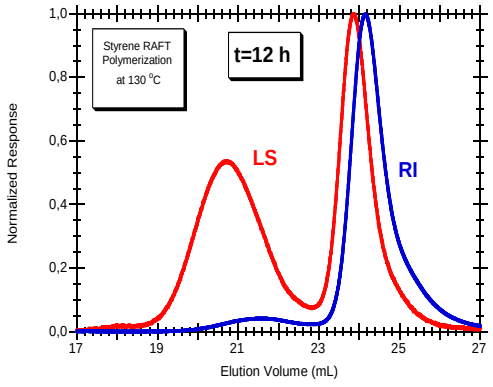

(e)

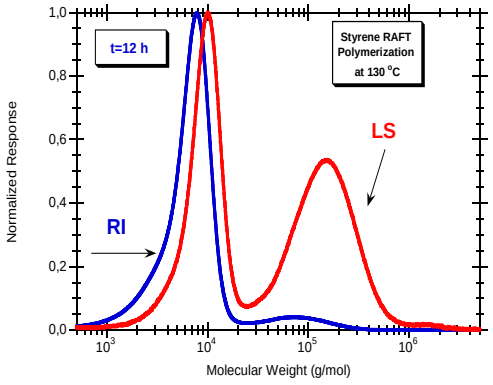

(f)

Figure 5.11. Main results for RAFT polystyrene synthesis in aqueous suspension at 130 °C using DDMAT CTA (run 8 in Table 5.1). (a) Measured reaction time evolution of monomer conversion. (b) Measured reaction time evolution of molecular weight dispersity (D_M) and average molecular weights ($\bar{M}_n$ and $\bar{M}_w$). (c) Normalized RI signal of polystyrene samples with different polymerisation time. (d) Normalized MALLS signal (90° detector) for the same samples described in (c). (e) Comparison of the normalized RI and MALLS signals of a polystyrene sample with polymerisation time t = 12 h. (f) Change of the RI and LS signals along the molecular weight for the same sample described in (e).

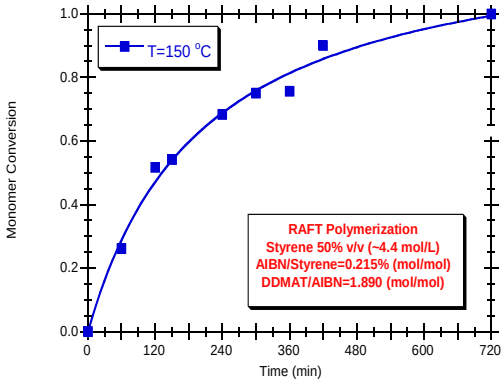

(a)

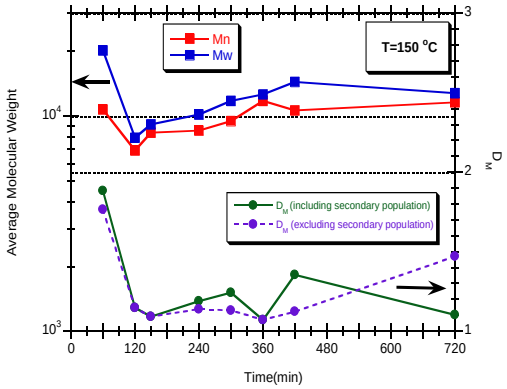

(b)

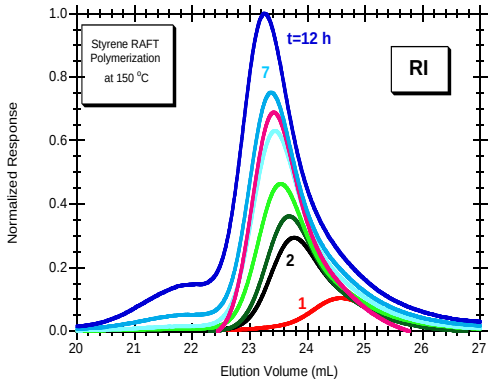

(c)

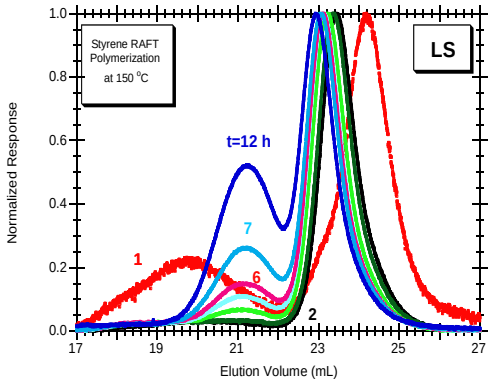

(d)

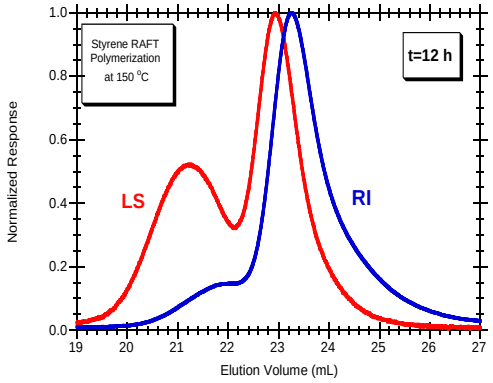

(e)

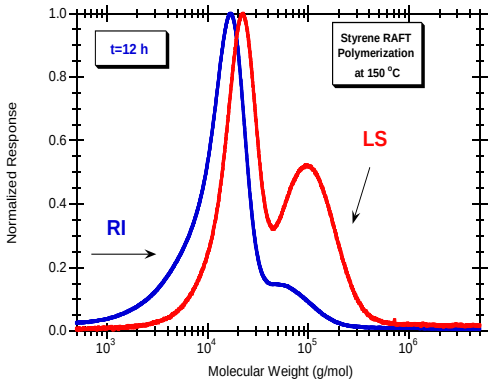

(f)

Figure 5.12. Main results for RAFT polystyrene synthesis in aqueous suspension at 150 °C using DDMAT CTA (run 9 in Table 5.1). (a) Measured reaction time evolution of monomer conversion. (b) Measured reaction time evolution of molecular weight dispersity (D_M) and average molecular weights ($\overline{M}_n$ and $\overline{M}_w$). (c) Normalized RI signal of polystyrene samples with different polymerisation time. (d) Normalized MALLS signal (90° detector) for the same samples described in (c). (e) Comparison of the normalized RI and MALLS signals of a polystyrene sample with polymerisation time t = 12 h. (f) Change of the RI and LS signals along the molecular weight for the same sample described in (e).

Some of these issues are further illustrated in Figures 5.13 and 5.14 where the effect of the polymerisation temperature on the observed RI and MALLS signals of the final samples (t=12 hr) are directly compared. Measured effects of the reaction temperature and of initial mole ratio between RAFT agent and initiator on the dynamics of monomer conversion are presented in Figures 5.15 and 5.16.

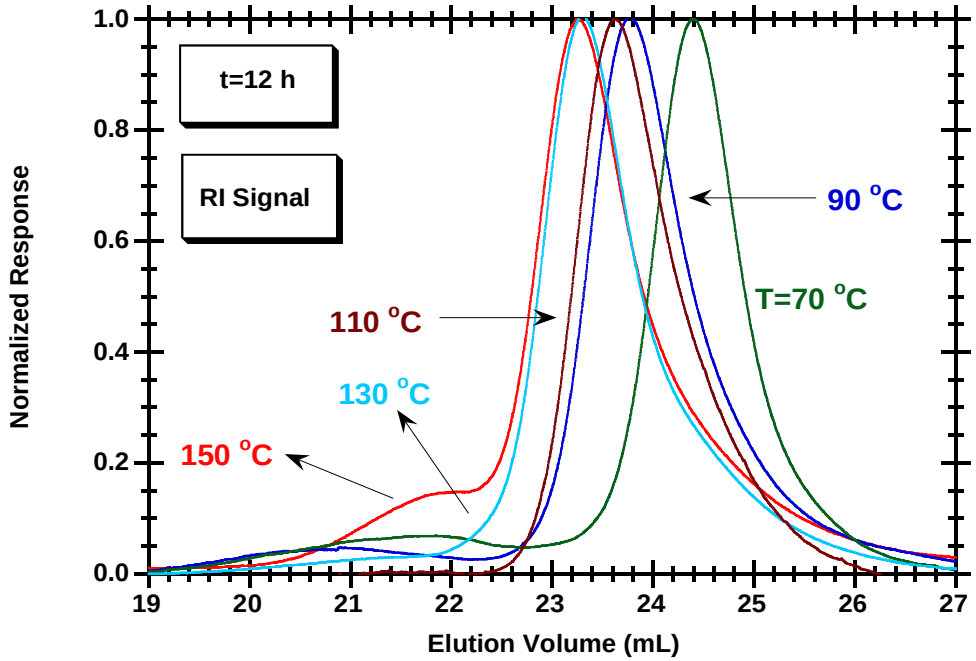

Figure 5.13. Effect of the polymerisation temperature (in the range 70 to 150 °C) on the observed RI signals of the final samples (t=12 hr).

The effect on the kinetics of polymerisation of the change of the RAFT agent is illustrated in Figures (5.17)-(5.20) where three experimental runs at 70 °C using TBTGA, DDMAT and CDT are compared. Lowering of polymerisation rate when using the dithiobenzoate TBTGA instead of trithiocarbonates (DDMAT or CDT) is here clearly observed (Figure 5.17). Different conversion profiles are observed and the retardation effect associated to dithiobenzoates (TBTGA) becomes clear when compared with trithiocarbonates (DDMAT and CDT). Some scattering observed for the measured values of monomer conversion is possibly due to non-ideal sampling of the reactor along polymerisation time due to the special heterogeneity of the suspension (adhesion of organic phase to the reactor walls was evident with some polymerisation runs). This issue is an important shortcoming of the polymerisation

conditions here explored. Observed dynamics of $\bar{M}_n$ and $\bar{M}_w$ for these same three experiments are presented in Figure 5.18 and 5.19.

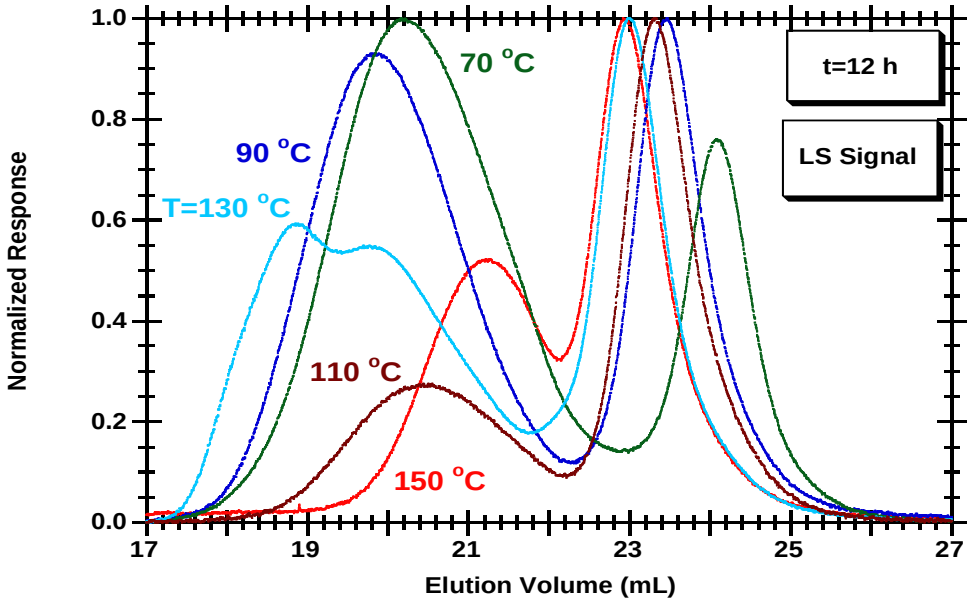

Figure 5.14. Similar comparison described in Figure 5.13 considering the MALLS signal.

In spite of differences in the earlier polymerisation stages (with measurements affected by the noisy signal due to low polymer concentration), similar trends are observed with final average molecular weights in the range 7000 to 11000 for $\bar{M}_n$ and 15000 to 30000 for $\bar{M}_w$. Nevertheless, important differences are observed in the product molecular size homogeneity due to the influence of the secondary population that is formed when DDMAT or CDT are used. In fact, with TBTGA reasonable low values of the molecular weight dispersity (D_M ~ 1.2) are achieved, as can be observed in Figure 5.20. With DDMAT or CDT, very high values of D_M are observed when this high size set of chains is considered in the polymer population although dispersity values close to 1 are estimated in the absence of these secondary chains.

It is also enlightning to compare the synthesis of polystyrenes using different polymerisation techniques, as illustrated in Figures (5.21)-(5.25). Results for styrene polymerisation at 130 °C using FRP, NMRP and RAFT are presented in these Figures, including the dynamics of product formation and some details of the polymers molecular architectures. Similar reaction rates are observed when these FRP and RAFT runs are compared and lower monomer conversions were measured with NMRP in the described conditions. Similar dynamics for $\bar{M}_w$

were measured with RAFT and NMRP (final values in the range of 20000) but nearly five times higher values of $\bar{M}_w$ result with FRP (Figure 5.22).

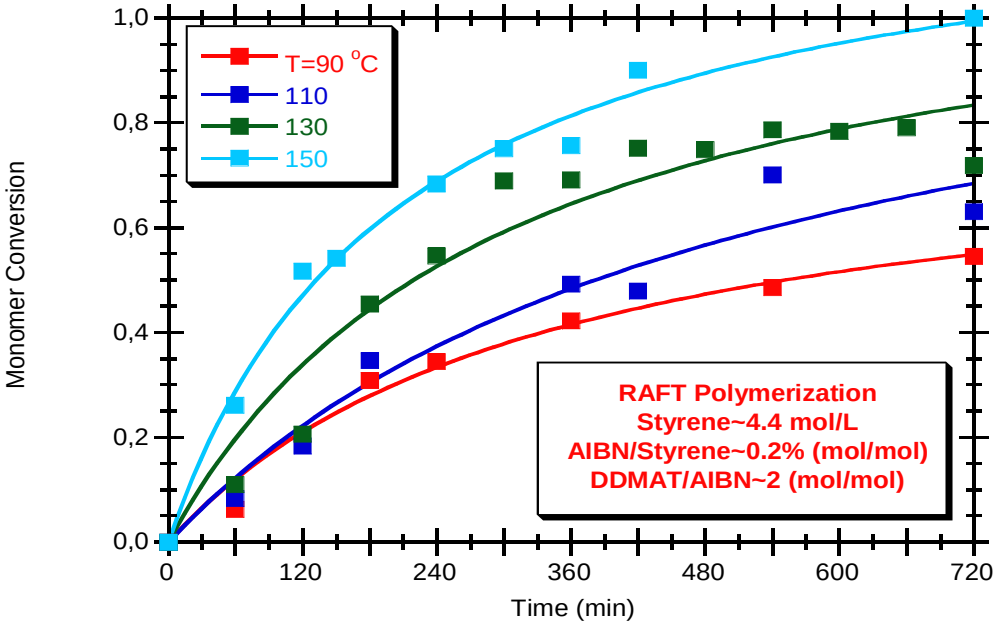

Figure 5.15. Measured dynamics of monomer conversion for RAFT styrene polymerisation in aqueous suspension at different temperatures and using DDMAT as CTA agent.

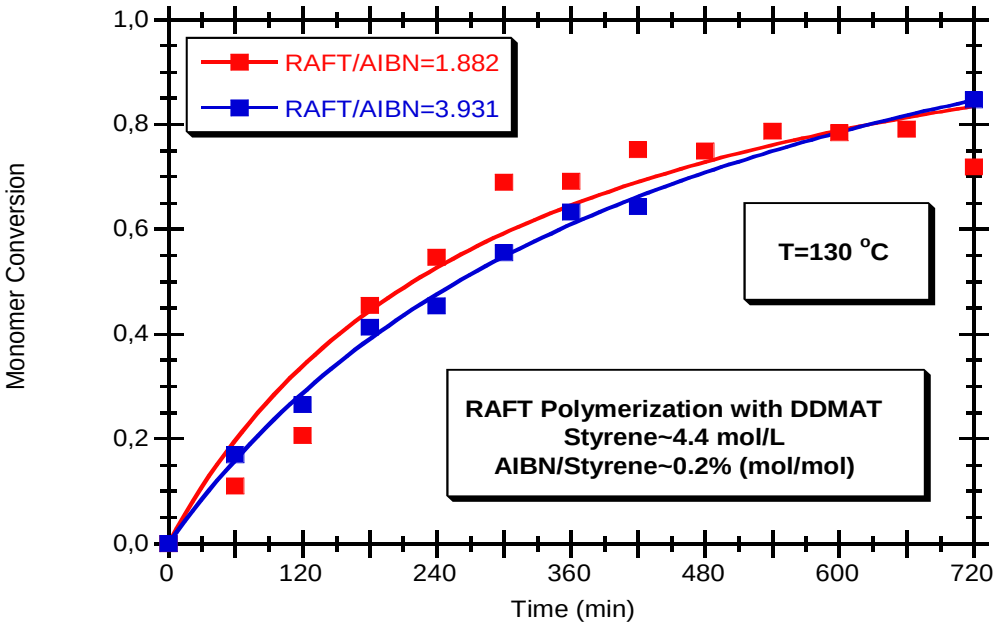

Figure 5.16. Measured dynamics of monomer conversion for RAFT styrene polymerisation in aqueous suspension at 130 °C and using DDMAT as CTA agent.

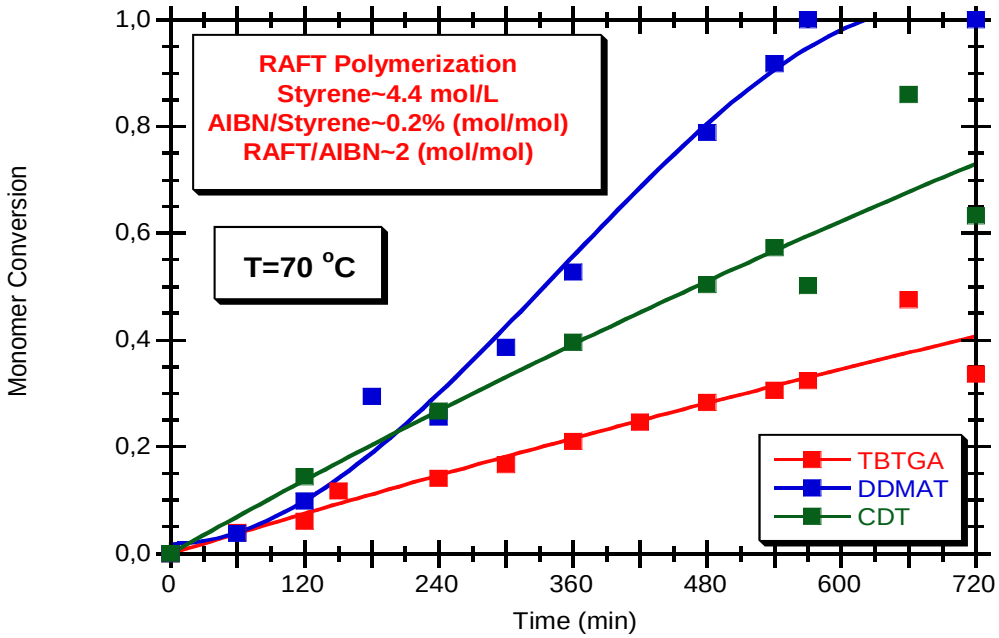

Figure 5.17. Comparison of the observed time evolution of monomer conversion for aqueous suspension of RAFT synthesis of polystyrene at 70 °C using the CTA agents DDMAT, TBTGA and CDT.

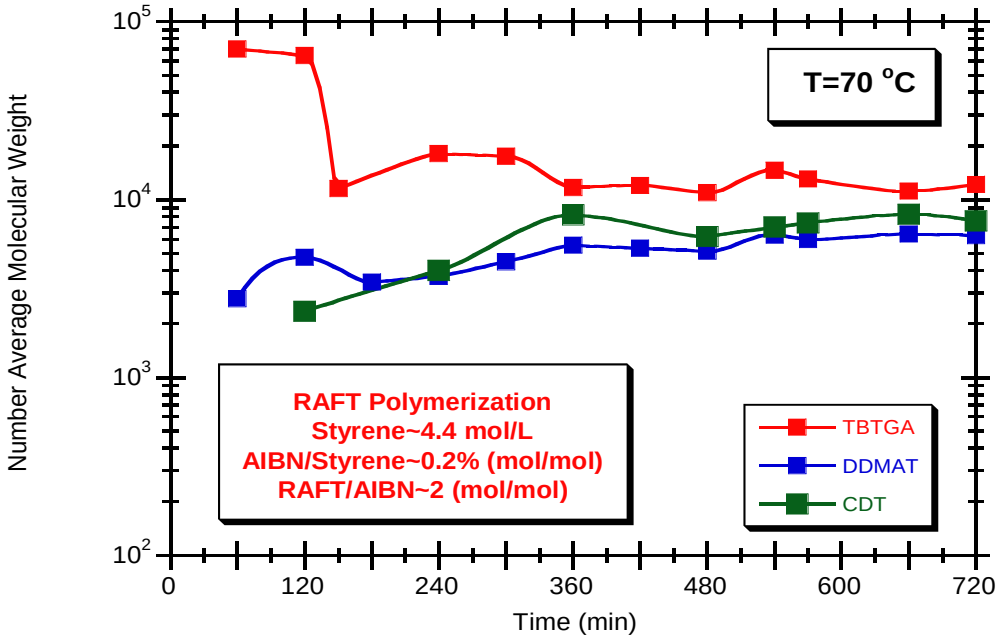

Figure 5.18. Comparison of the observed time evolution of $\bar{M}_n$ for aqueous suspension of RAFT synthesis of polystyrene at 70 °C using the CTA agents DDMAT, TBTGA and CDT.

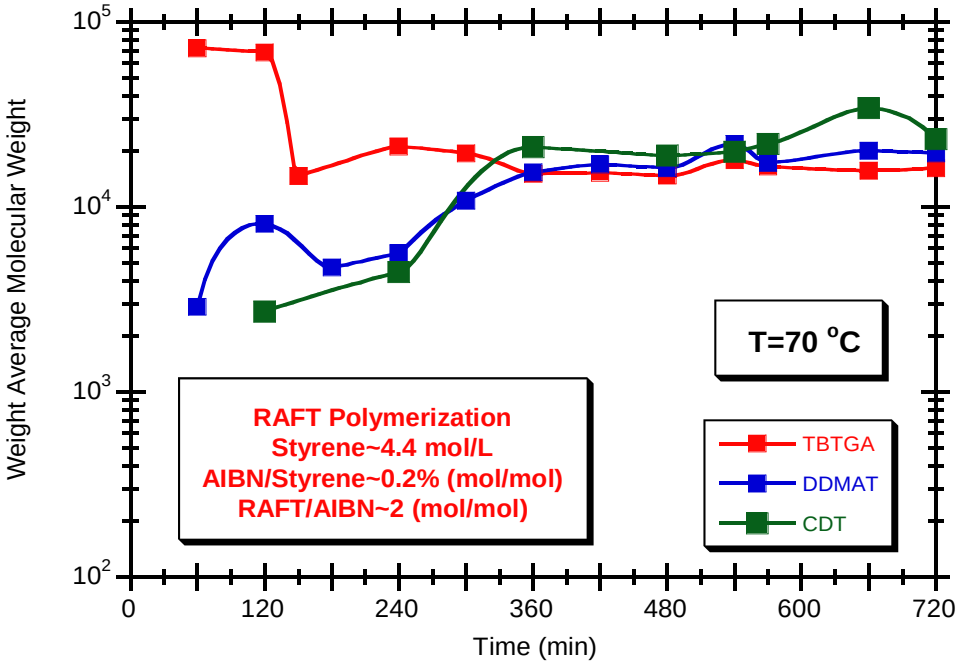

Figure 5.19. Comparison of the observed time evolution of $\bar{M}_w$ for aqueous suspension of RAFT synthesis of polystyrene at 70 °C using the CTA agents DDMAT, TBTGA and CDT.

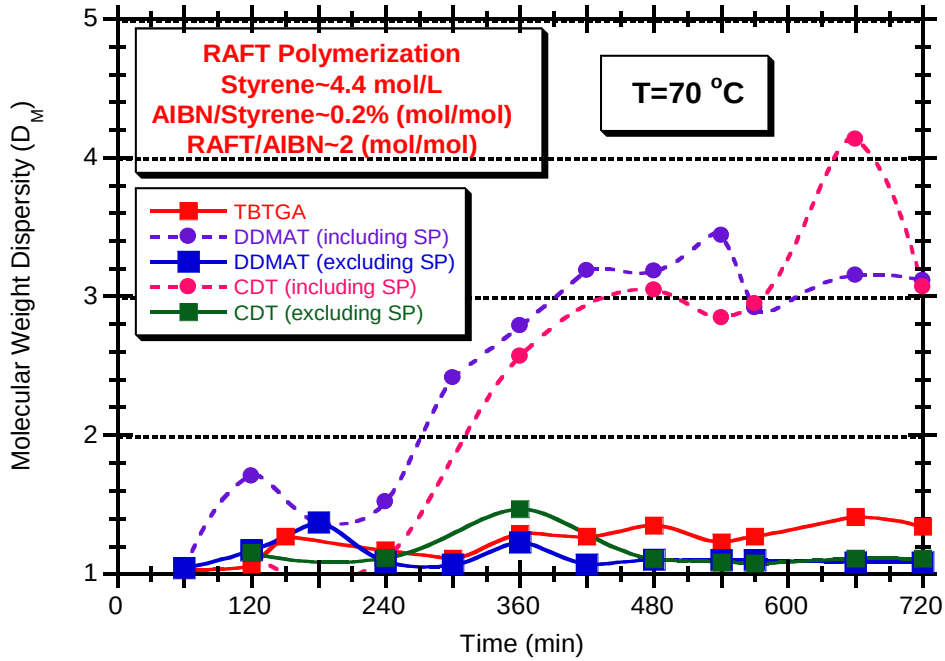

Figure 5.20. Comparison of the observed time evolution of D_M for aqueous suspension of RAFT synthesis of polystyrene at 70 °C using the CTA agents DDMAT, TBTGA and CDT.

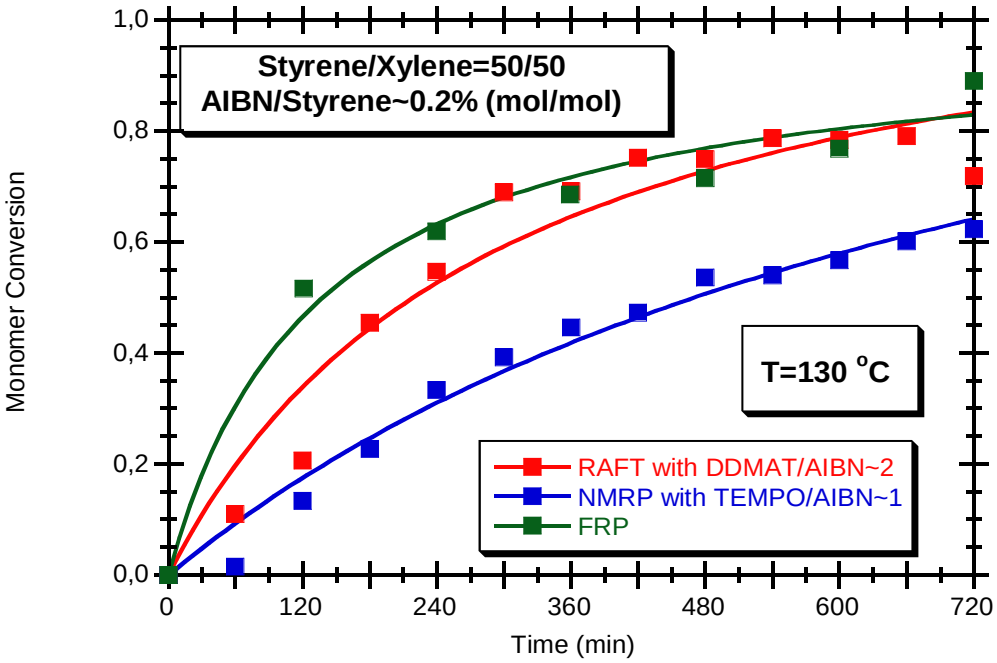

Figure 5.21. Measured dynamics of monomer conversion for polystyrene synthesis in aqueous suspension at 130 °C considering different reaction techniques (FRP, NMRP and RAFT).

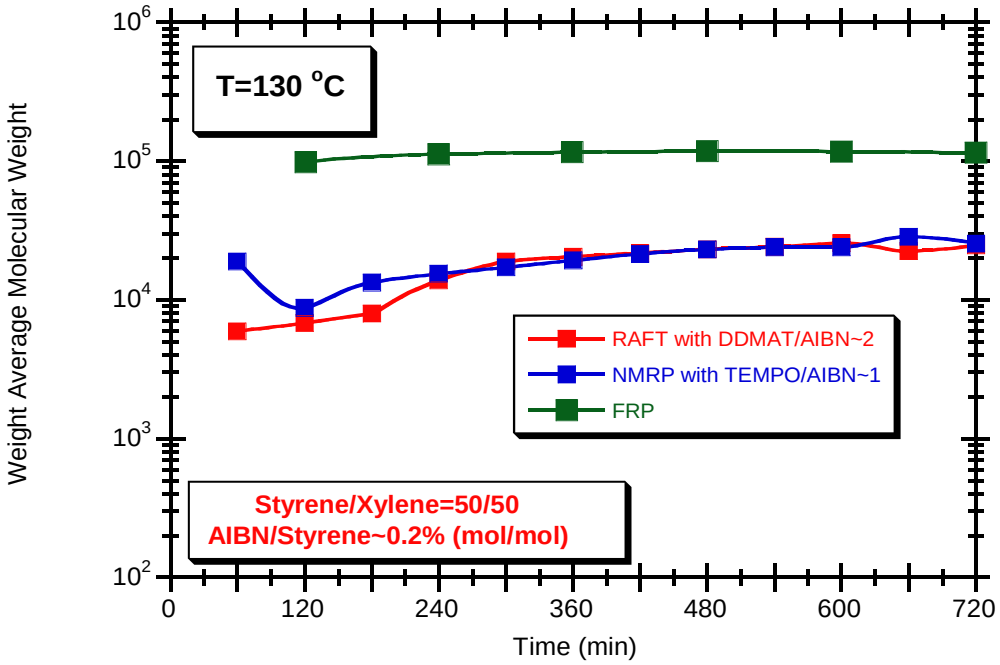

Figure 5.22. Measured dynamics of $\bar{M}_w$ for polystyrene synthesis in aqueous suspension at 130 °C considering different reaction techniques (FRP, NMRP and RAFT).

Molecular size distribution, as seen by SEC, is showed in Figures 5.23 and 5.24 making evident the high size dispersion associated with FRP synthesis. Higher homogeneity of polymer population is observed when NMRP or RAFT are considered but the latter system (is these particular conditions) is affected by the formation of a bimodal size distribution. These issues are reflected in the molecular weight dispersity of the products, as presented in Figure 5.25. Only in the absence of this secondary population similar values of D_M are obtained using NMRP or RAFT.

5.4 RAFT Copolymerisation of Styrene with Divinylbenzene

5.4.1 Results and Discussion

In Table 5.5 are presented some vibrational assignments correspondent to styrene and divinylbenzene monomers (Choi and Kertesz, 1997; Colthup *et al*., 1990; Hecker, 2000). These features can also be observed in Figure 5.26 where the *off-line* IR spectra collected for STY, DVB RAFT polystyrene and RAFT STY/DVB (95/5) are compared. Especially important for the study of the kinetics of crosslinking are the assignments correspondent to C=C bonds that can be identified at around 992, 1019, 1410, 1452 and 1630 cm^{-1}. For this chemical group, strong absorptions and well defined peaks (minimizing the interference with other structures) are observed at 992 and 1630 cm^{-1}. These characteristics frequencies are therefore good candidates to obtain information concerning the monomers carbon-carbon double bonds consumptions and also concerning the presence of pendant double bonds in the polymer/network. In fact, these bands are not present in isolated RAFT polystyrene and very low responses are observed in these regions for isolated RAFT STY/DVB (95/5) networks due to the relative small amount of DVB used (see Figure 5.26). Potentialities of *off-line* FTIR analysis of isolated products are further enhanced in Figures (5.27)-(5.29) where RAFT materials with high pendant double bonds content (e.g. resulting from DVB homopolymerisation) are considered. Clear qualitative information about the presence of the PDBs in the networks can be obtained and the comparison of products with different reaction times and/or resulting from different initial compositions can also be performed.

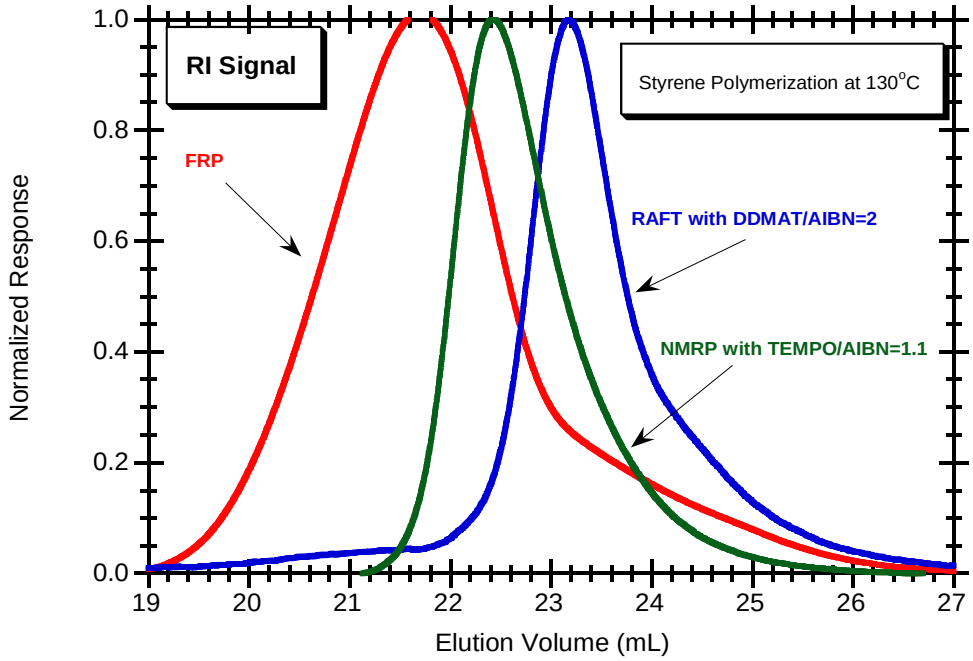

Figure 5.23. Observed RI SEC traces for polystyrene synthesis in aqueous suspension at 130 °C considering different reaction techniques (FRP, NMRP and RAFT).

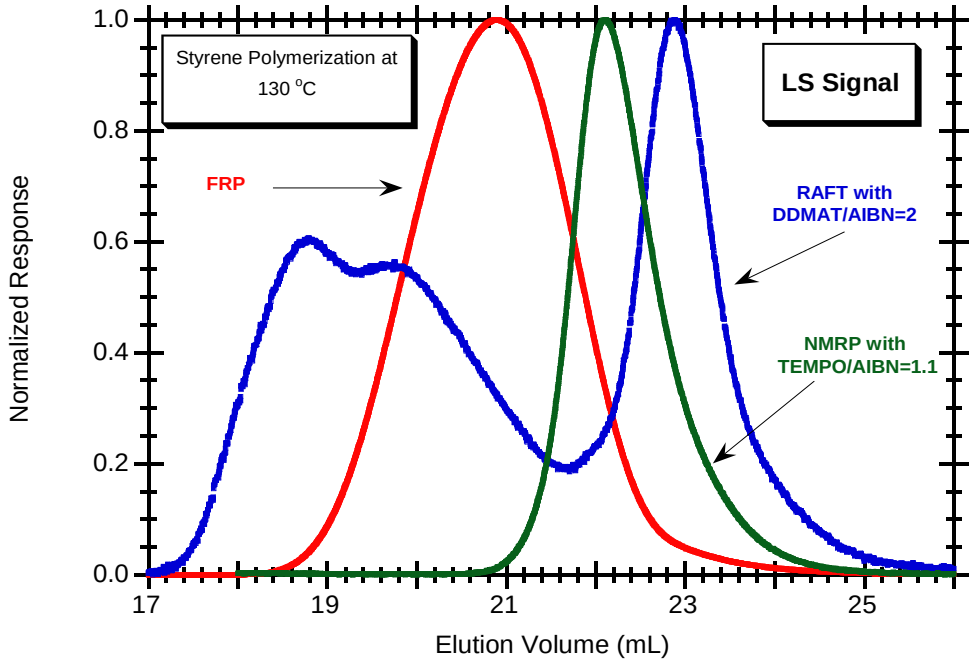

Figure 5.24. Observed MALLS SEC traces for polystyrene synthesis in aqueous suspension at 130 °C considering different reaction techniques (FRP, NMRP and RAFT).

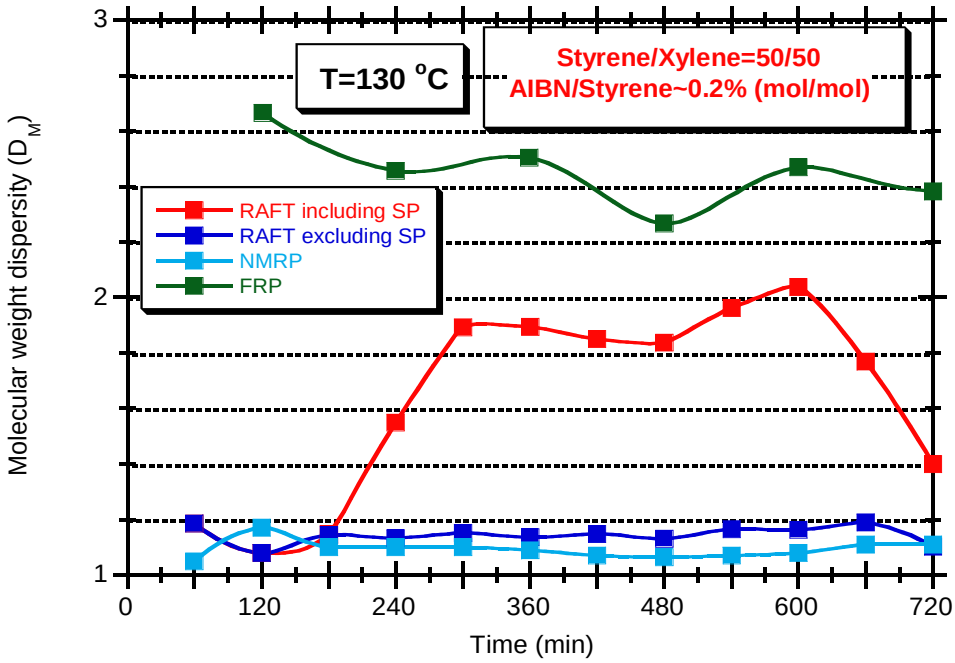

Figure 5.25. Observed D_M for polystyrene synthesis in aqueous suspension at 130 °C considering different reaction techniques (FRP, NMRP and RAFT).

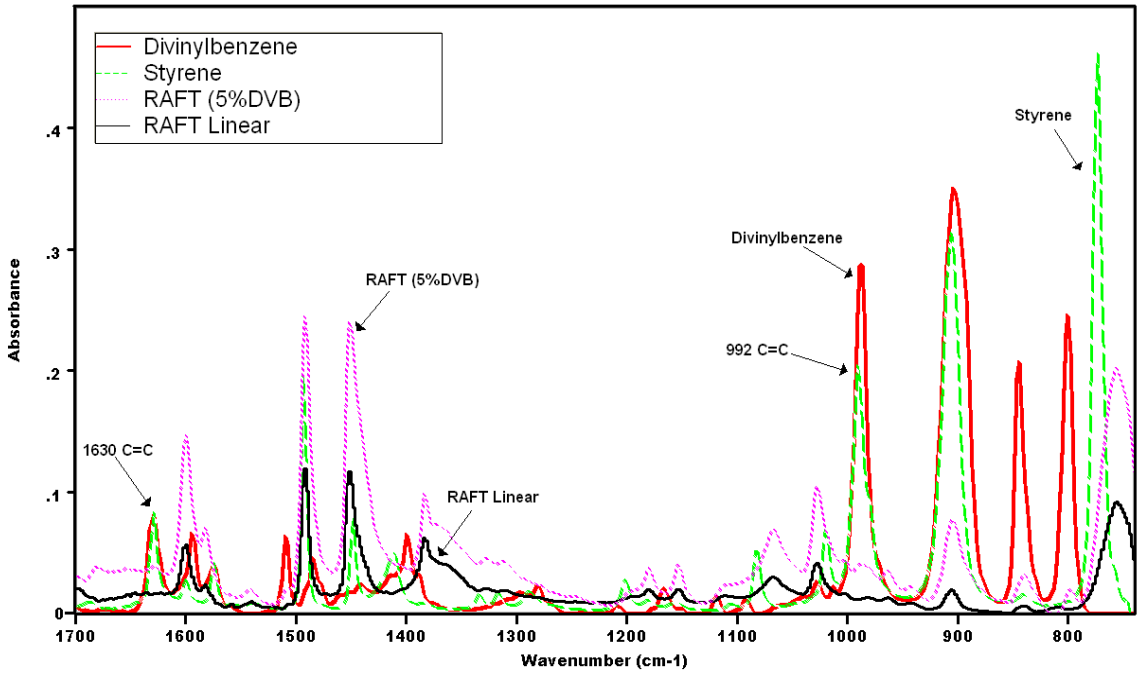

Figure 5.26. Observed *off-line* FTIR spectra for styrene and divinylbenzene monomers and polystyrene (run 7 in Table 5.1) and poly(STY/DVB) with 5 % DVB (run 1 in Table 5.2).

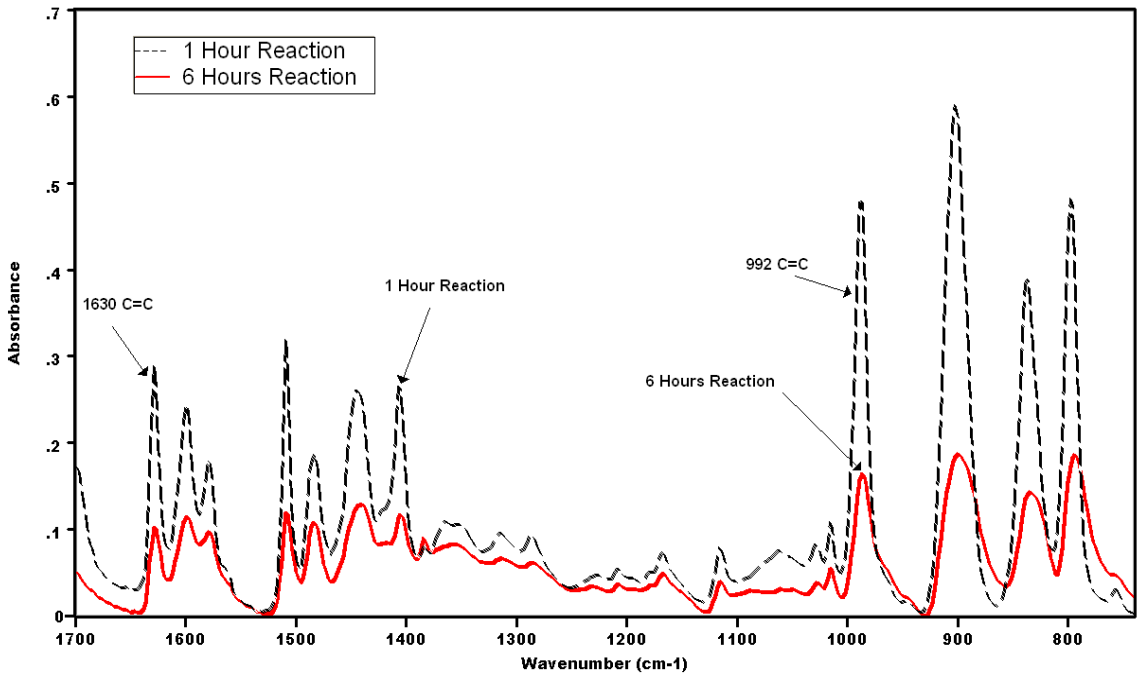

Figure 5.27. Observed *off-line* FTIR spectra for DVB networks correspondent to different polymerisation times for run 2 in Table 5.2.

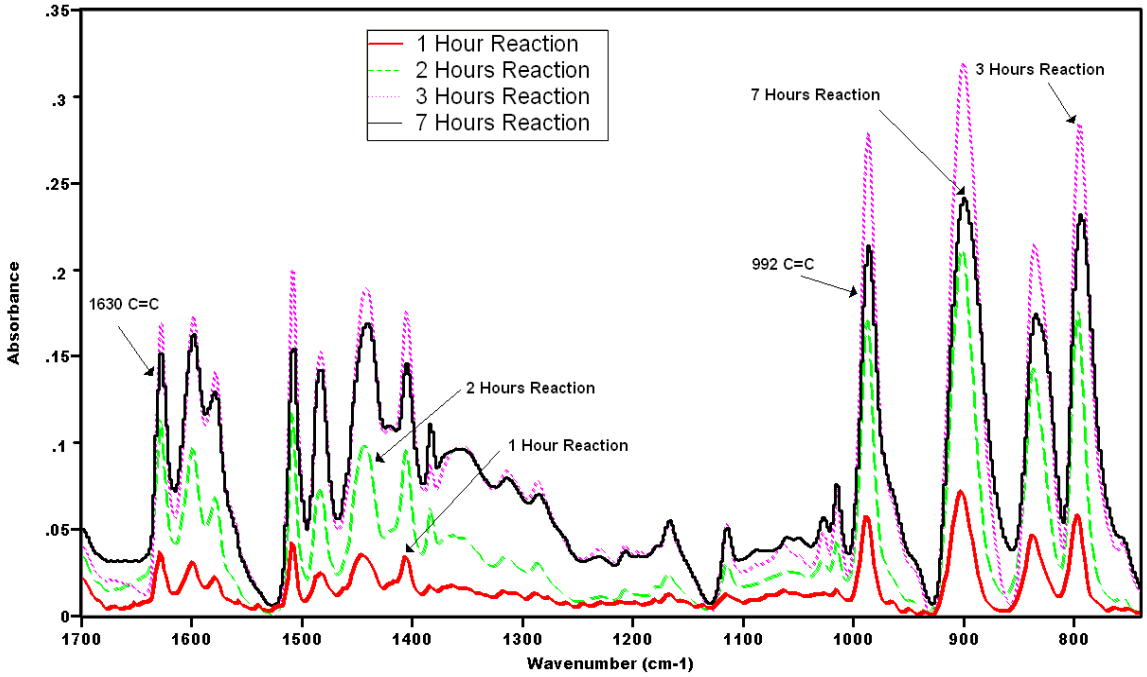

Figure 5.28. Observed *off-line* FTIR spectra for DVB networks correspondent to different polymerisation times for run 3 in Table 5.2.

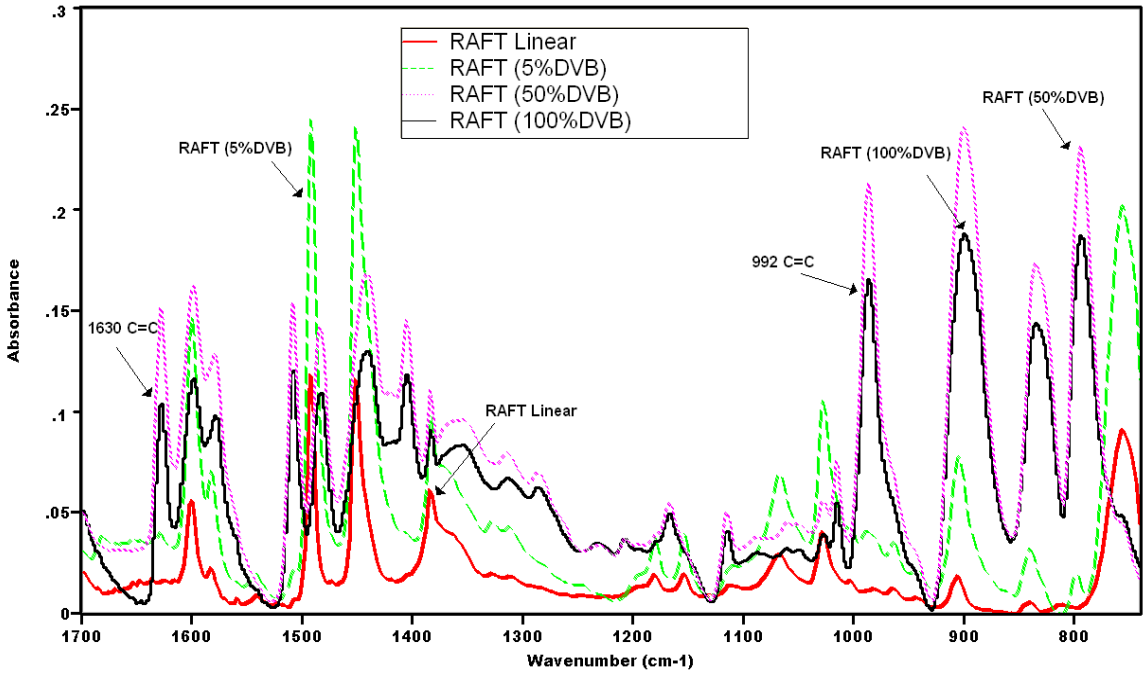

Figure 5.29. Observed *off-line* FTIR spectra for final samples correspondent to runs 1, 2 and 3 in Table 5.2 and for run 7 in Table 5.1.

Table 5.5. Some IR vibrational assignments for styrene and divinylbenzene**.**

Wave number (cm^{-1})	Peak assignment
776	Puckering ring C-H out-of-plane bending
795	*m*-di-substituted ring bending
841	Ring C-H out-of-plane
909	Ring C-H out-of-plane bending and $=CH_2$ wag
992	C=C torsion and $=CH_2$ wag
1019	$=CH_2$ rock and ring C-C stretching
1083	Ring C-C stretching
1202	C-C stretching
1410	*p*-di-substituted phenyl ring stretching and $=CH_2$ scissoring
1452	$=CH_2$ scissoring and ring C-H in-plane-bending
1494	ring C-H in-plane-bending
1510	*p*-di-substituted phenyl ring stretching
1600	C-C stretching
1630	C=C stretching

Attempts to use FTIR-ATR for *in-line* monitoring of aqueous suspension RAFT crosslinking polymerisation are presented in Figures (5.30)-(5.33). In such cases (runs 2 and 3 in Table 5.2), polymerisation conditions were designed in order to try maximize the C=C responses in the IR spectra (only DVB in run 2 and DVB/toluene 50/50 in run 3). Nevertheless, the strong influence of water cannot be eliminated (measurements were performed using water background) and only the lower frequencies regions of the spectra can be considered (see Figures (5.30)-(5.33)). Despite these issues, good IR responses are observed in some useful bands (especially for run 2), namely with the 992 cm^{-1} peak.

These data, collected by *in-line* FTIR-ATR, were used to estimate the double bonds conversion (p) using the 992 cm^{-1} for C=C quantification and, alternatively, the peaks at 909, 841 or 795 cm^{-1} as internal references. Similar results were obtained for run 2 in Table 5.2 considering different references but, for run 3 in Table 5.2, calculations were only possible with 909 cm^{-1} peak as internal reference. Important discrepancies between the estimated double bond conversion using *in-line* FTIR-ATR and gravimetric or SEC measurements are observed. Monomer conversion (p_M) measured by SEC and gravimetry was used to estimate the double bond conversion in the framework of the equal reactivity model: $p_M = p(2 - p)$. Coating of the FTIR-ATR probe, catastrophic coagulation (see e.g. Salehpour and Dubé, 2012 and references therein) are some issues with possible negative impact on the *in-line* FTIR-ATR measurements. On the other hand, the choice of a reference peak with constant intensity along polymerisation is not a straightforward solution because shifts in peaks intensities are possible, as before reported with Raman spectroscopy. Further developments on the *in-line* FTIR-ATR measurements here reported are therefore needed in order to improve the reliability of the results.

Off-line FTIR analysis of isolated products provides important qualitative information concerning the presence of PDBs in the networks, as above described. In principle, quantification of PDBs in these materials is also possible using *off-line* FTIR if an appropriated internal reference in the spectra is found. This possibility was explored in the present work considering the main C=C absorptions at 992 and 1630 cm^{-1} and trying different internal references, namely those correspondent to 841, 909, 1494 and 1600 cm^{-1}. Some results of this analysis are presented in Figures 5.34 and 5.35 considering samples collected at different polymerisation times during runs 2 and 3 in Table 5.2.

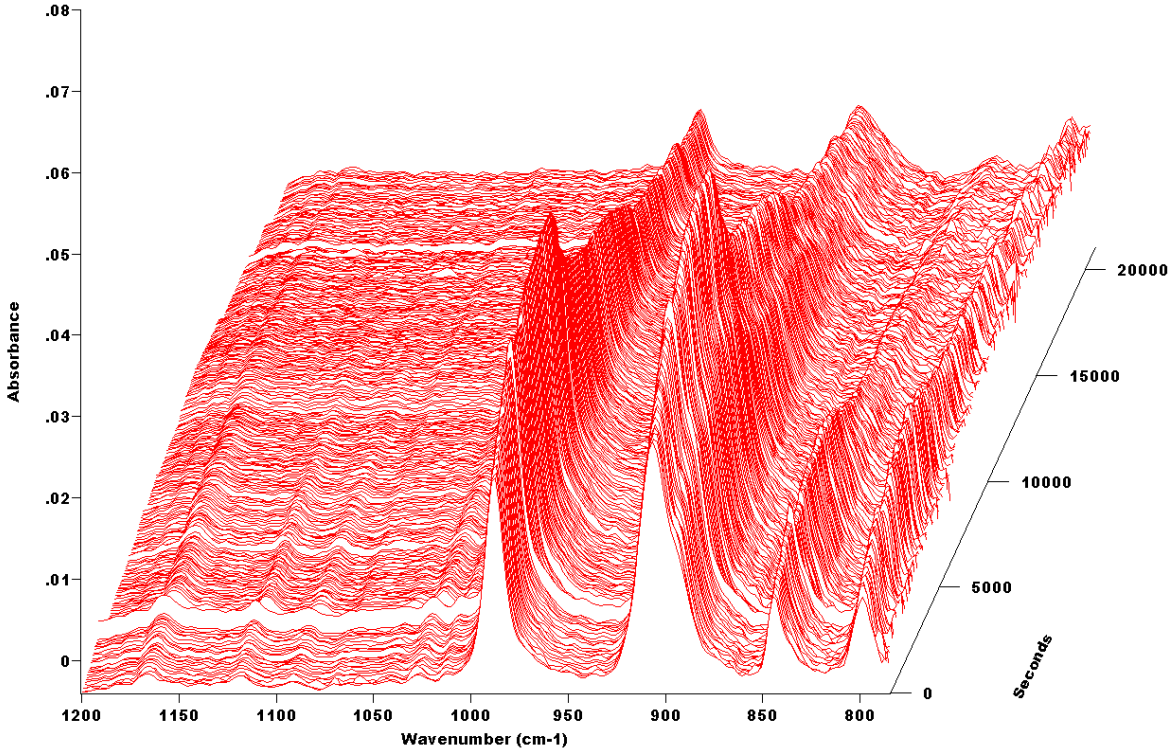

Figure 5.30. FTIR-ATR spectra observed during the *in-line* monitoring for the aqueous suspension RAFT polymerisation of divinylbenzene at 70 °C with 100 % DVB in the organic phase (run 2 in Table 5.2).

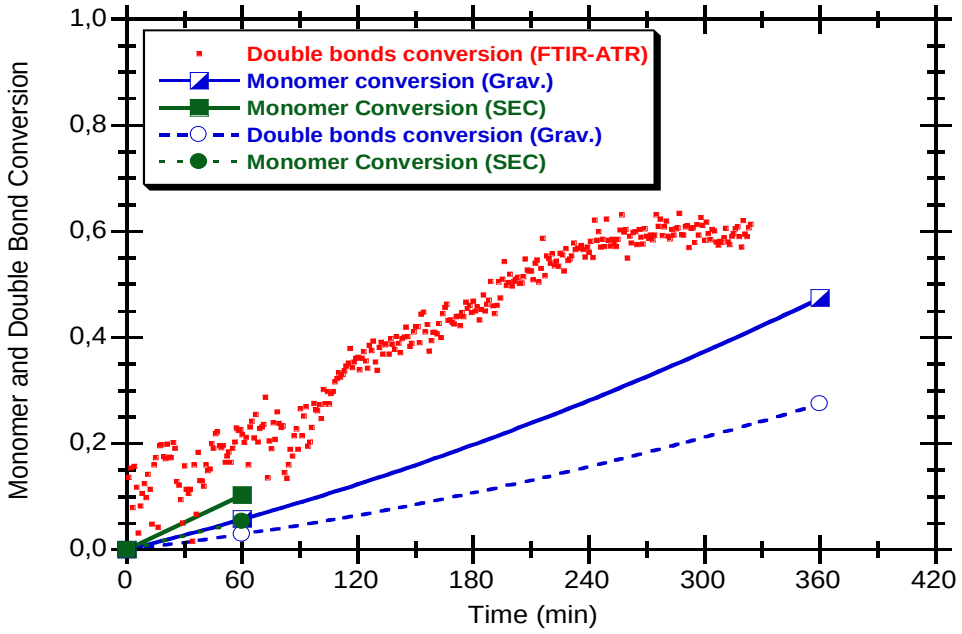

Figure 5.31. Estimated pendant double bond conversion using *in-line* FTIR-ATR monitoring and estimated monomer conversion using SEC for run 2 in Table 5.2.

Consistent profiles for the change of PDBs with reaction time where obtained when the 1630 cm^{-1} peak was considered to monitor this chemical group and 1494 cm^{-1} peak was used as internal reference. In fact, for long enough polymerisation time, the decrease of PDBs concentration with reaction time was before experimentally observed considering alternative measurement techniques (Gonçalves *et al*., 2013a; Hecker, 2000; see Figure 5.41 in this chapter) and also predicted using kinetic modelling (Aguiar, 2013; Aguiar *et al*., 2013) with or without cyclization inclusion. With this analysis was also observed that the 1630 cm^{-1} peak is a better choice to monitor PDBs that the 992 cm^{-1} alternative peak. Better results would be probably obtained if the 1630 cm^{-1} was also considered in the *in-line* FTIR-ATR analysis above described but the presence of water interferes with measurements at this region.

One possibility to perform a quantitative analysis of the *off-line* FTIR data is through the comparison of normalized peak intensities for the isolated polymer/network and the constitutive monomer, as described in Equation (5.26):

$$IPDB = \frac{(I_{1630}/I_{1494})_{Network}}{(I_{1630}/I_{1494})_{DVB}} \tag{5.26}$$

This index of pendant double bonds *(IPDB)* should represent the number of PDBs per aromatic ring in the network, comparatively to the DVB monomer, if the proportion between the IR responses of the chemical groups in the monomer and network is the same. Results for this index with RAFT networks synthesized in this work are presented in Figure 5.36. However, as presented in that Figure, too high values are observed for this index (approaching the unrealistic value $IPDB = 1$ in the early stages of polymerisation) which means that the proportion of the IR responses of these chemical groups is not the same in the polymer and in the monomer. Partially, these inconsistencies can be a consequence of the DVB commercial grade used in this work comprising two isomers (*m*-divinylbenzene and *p*-divinylbenzene) and also ethylvinylbenzene. The use of purified isomers is preferable to perform fundamental studies on this polymerisation system (Hecker, 2000). This approach was not tested in this chapter and the practical usefulness of the measurements performed was explored through the calibration between normalized FTIR 1630 cm^{-1} peak intensity (I_{1630}/I_{1494}) and PDBs concentrations measured by ICl titration.

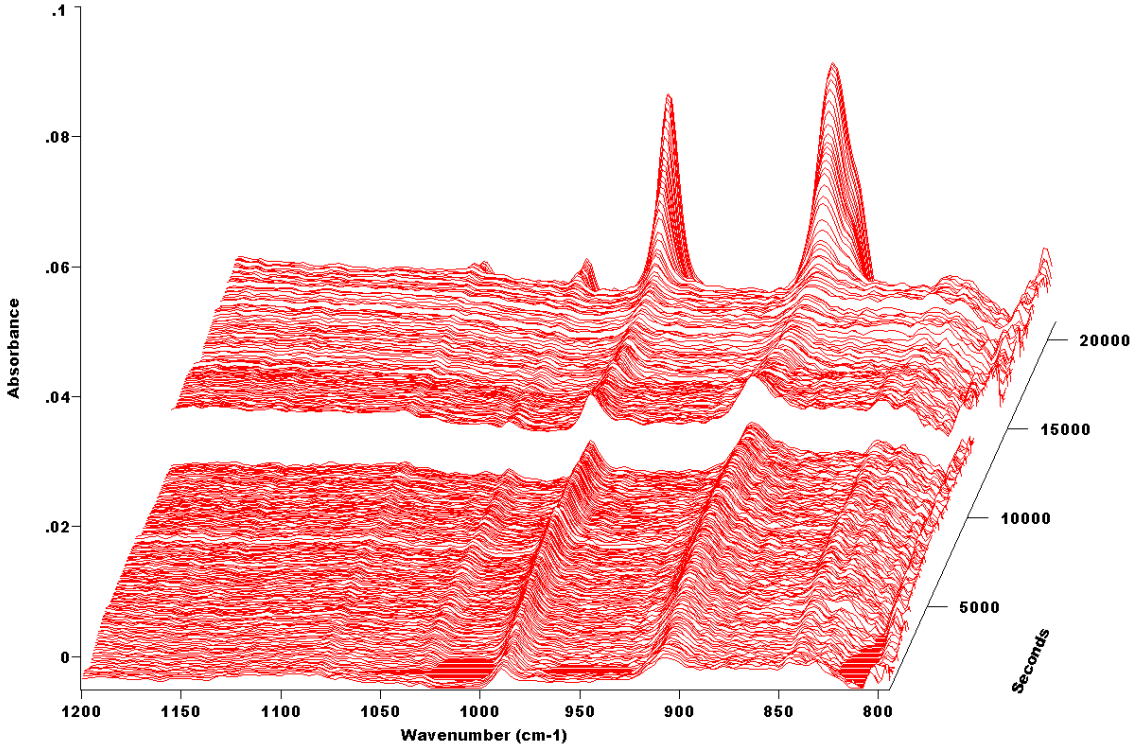

Figure 5.32. FTIR-ATR spectra observed during the *in-line* monitoring for the aqueous suspension RAFT polymerisation of divinylbenzene at 70 °C with 50 % DVB in the organic phase (run 3 in Table 5.2).

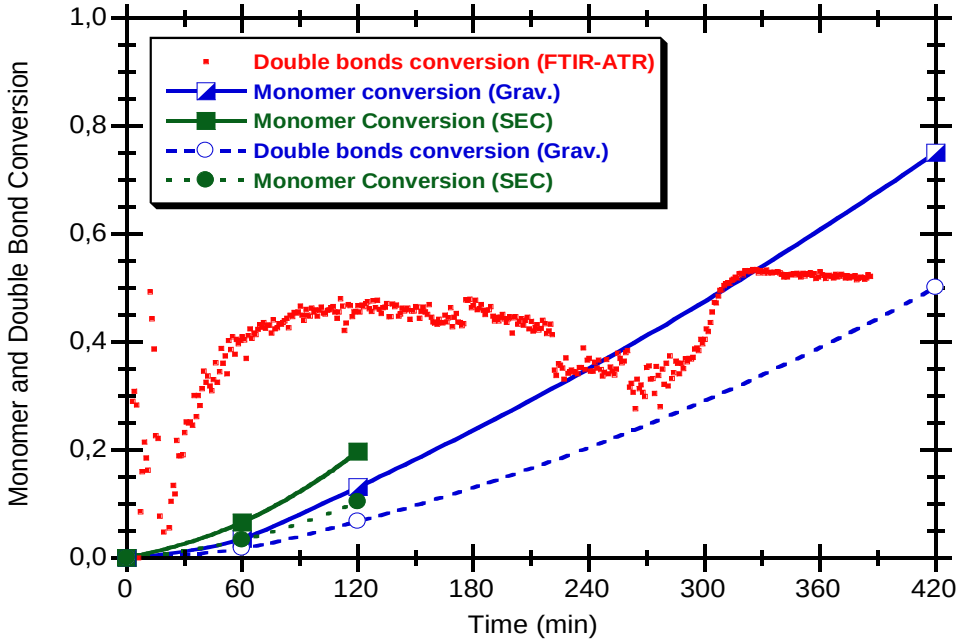

Figure 5.33. Estimated pendant double bond conversion using *in-line* FTIR-ATR monitoring and estimated monomer conversion using SEC for run 3 in Table 5.2.

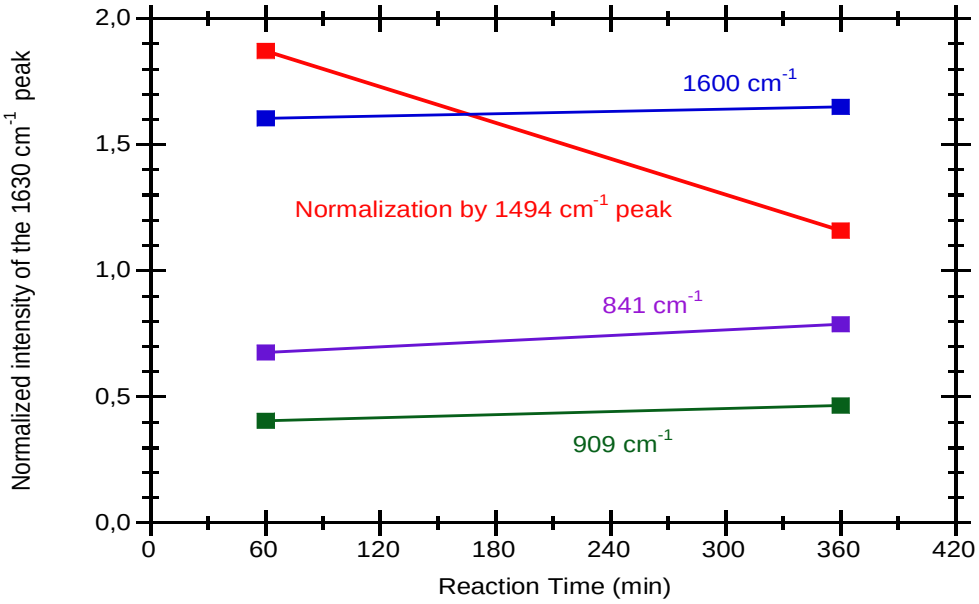

Figure 5.34. Normalized intensity of the FTIR 1630 cm^{-1} peak correspondent to C=C bonds considering different internal references (842, 909, 1494 and 1600 cm^{-1}). The values presented are correspondent to *off-line* FTIR analysis of samples collected at different reaction times for run 2 in Table 5.2.

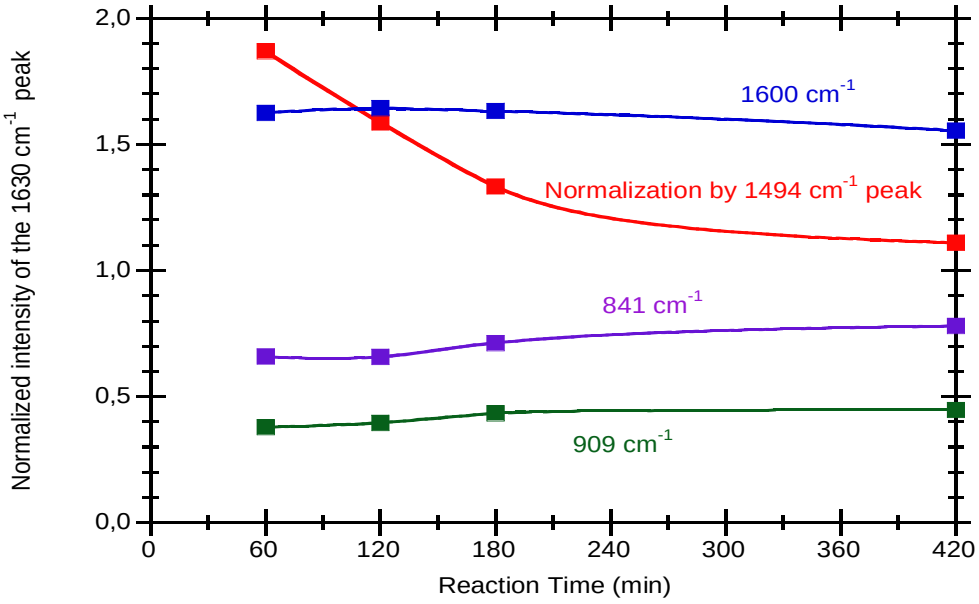

Figure 5.35. Normalized intensity of the FTIR 1630 cm^{-1} peak correspondent to C=C bonds considering different internal references (842, 909, 1494 and 1600 cm^{-1}). The values presented are correspondent to *off-line* FTIR analysis of samples collected at different reaction times for run 3 in Table 5.2.

To obtain this calibration, the final samples correspondent to runs 1, 2 and 3 in Table 5.2 were considered. Measurements using both methods (FTIR and ICl titration) were performed for these networks. The following relation between the normalized FTIR 1630 cm^{-1} peak intensity (I_{1630}/I_{1494}) and the concentration of PDBs in the network (expressed in mol/g of polymer) was thus estimated:

$$(I_{1630}/I_{1494}) = 335 \times [PDB] \tag{5.27}$$

This calibration was used to estimate the PDB concentration for networks with a single (and simpler) FTIR measurement. These results are presented in Figure 5.37. Dynamics of PDBs concentration for runs 2 and 3 in Table 5.2 were obtained and compared with the reaction time evolution of the same variable for run 1 which was fully measured using ICl titration. Note that a much smaller amount of DVB was used in run 1 and, under these circumstances, chemical titration is preferable to FTIR spectroscopy due to the low response of PDBs observed (when compared with that correspondent to other groups).

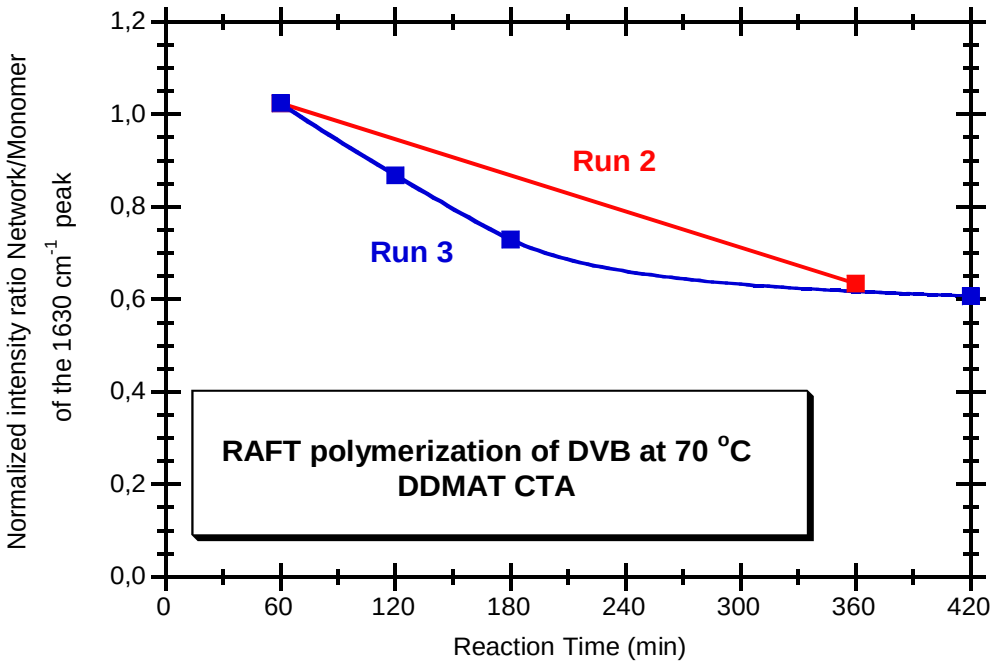

Figure 5.36. Observed ratios between network and DVB considering the normalized FTIR 1630 cm^{-1} peak (using the 1494 cm^{-1} as internal reference). Measurements are correspondent to samples with different polymerisation times in runs 2 and 3 in Table 5.2. (see Eq. (5.26)).

Results presented in Figure 5.37 show the (small) effect of intramolecular cyclization that is probably caused when monomer is diluted from bulk to a 50 % monomer/solvent solution (see comparison between runs 2 and 3 in Table 5.2). Strategy here presented should be extended to more diluted polymerisation systems in order to assess the possible effect of cyclization on network formation, even with RAFT polymerisation. Comparison of the incidence of these intramolecular mechanisms in FRP, NMRP (Gonçalves *et al*., 2013a; Aguiar, 2013; Aguiar *et al*., 2013a and 2013b) and RAFT of STY/DVB is an expected result of this research line. Results here presented (and expected extensions) can be used to develop kinetic modelling studies including intramolecular cyclizations with RAFT STY/DVB polymerisation, as recently performed with NMRP of the same chemical system (Aguiar, 2013; Aguiar *et al*., 2013a and 2013b). SEC/RI/MALLS proved to be a valuable technique to obtain insights on the RAFT crosslinking polymerisation. Figure 5.38 shows measured dynamics of $\bar{M}_n$, $\bar{M}_w$ and $\bar{M}_z$ for STY/DVB (95/5) RAFT copolymerisations at 130 °C (run 1 in Table 5.2). Gelation at around 360 min identified with these conditions. Dissimilitudes between linear (STY) and non-linear (STY/DVB) RAFT polymerisation are highlighted in Figure 5.39 where the measured dynamics of $\bar{M}_w$ for run 7 in Table 5.1 and run 1 in Table 5.2 are compared.

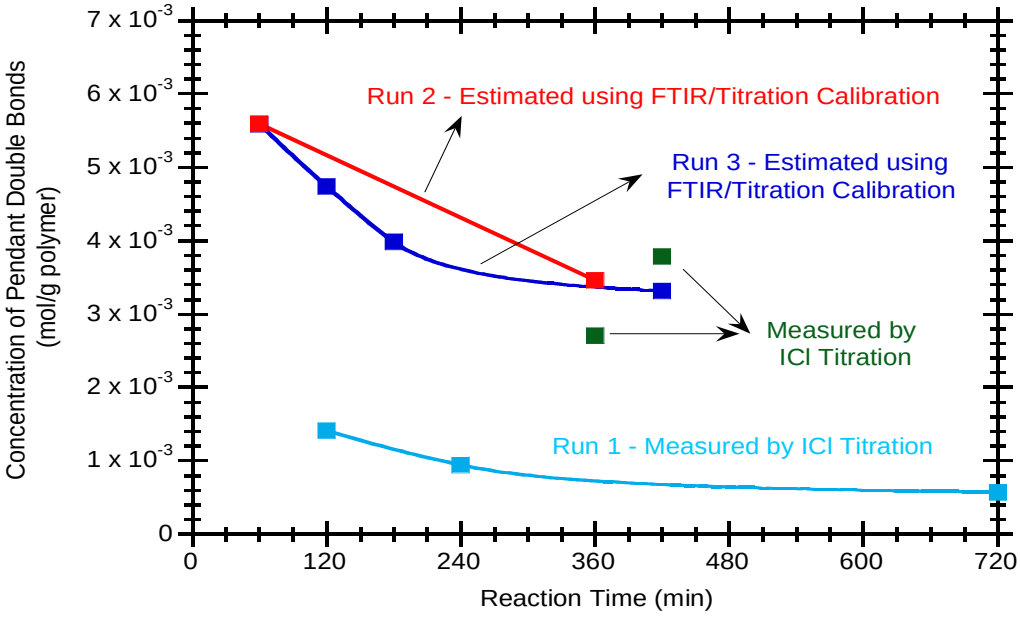

Figure 5.37. Dynamics of the PDB concentration (mol/g polymer) measured by ICL titration (run 1 in Table 5.2) and considering also the calibration between the normalized FTIR 1630 cm^{-1} peak intensity (I_{1630}/I_{1494}) and PDB concentration.

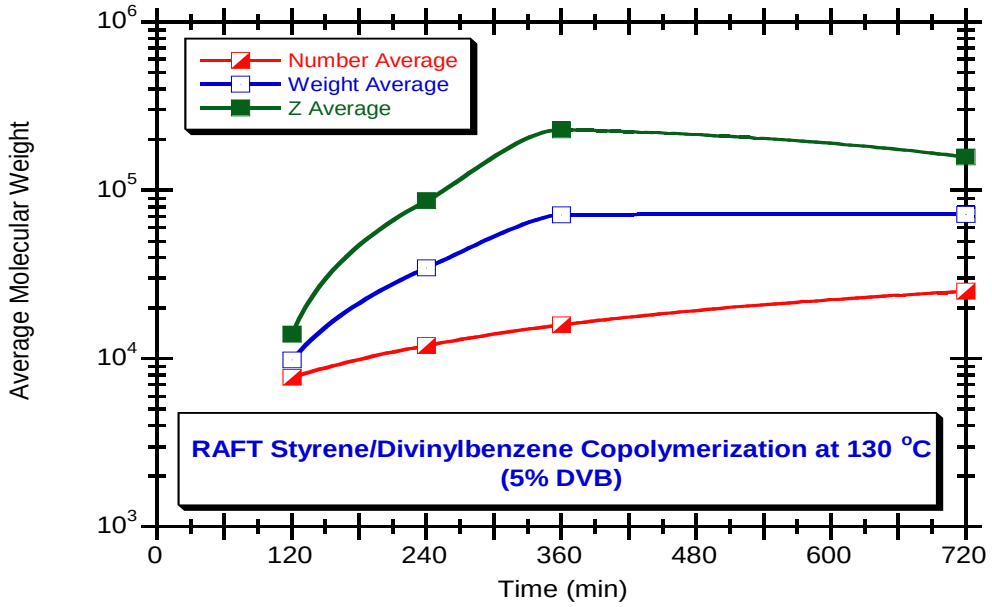

Figure 5.38. Measured dynamics of $\bar{M}_n$, $\bar{M}_w$ and $\bar{M}_z$ in aqueous suspension RAFT copolymerisation of STY/DVB (run 1 in Table 5.2)

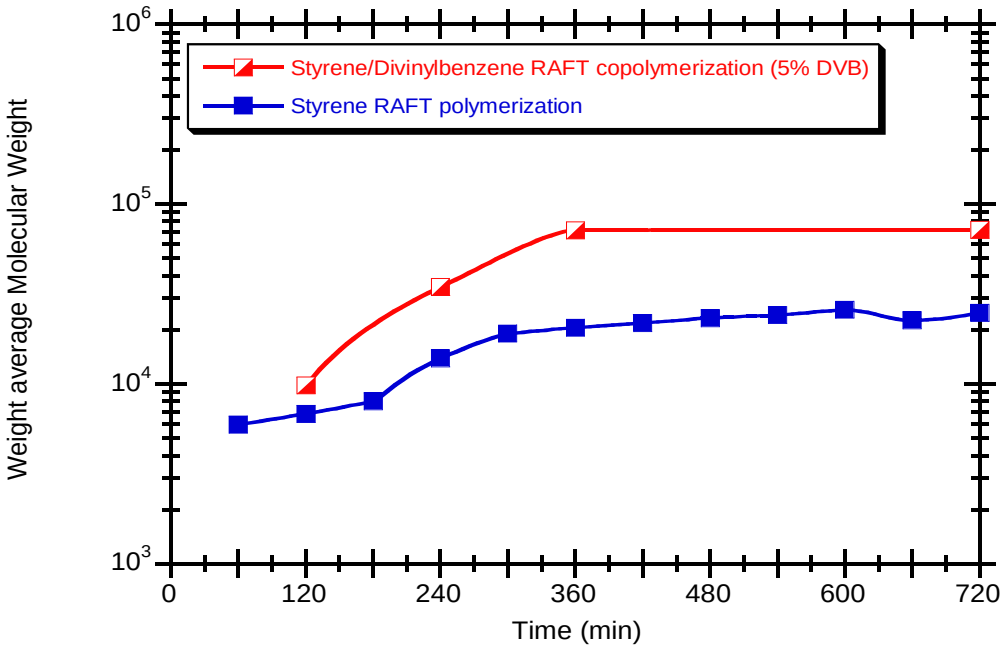

Figure 5.39. Comparison of the observed dynamics of $\bar{M}_w$ in aqueous RAFT suspension polymerisation of styrene (run 7 in Table 5.1) and RAFT copolymerisation of STY/DVB (run 1 in Table 5.2).

SEC estimated monomer conversion for these same two runs is showed in Figure 5.40 and similar kinetics for the linear and non-linear cases is observed under these circumstances. Measured time evolution of PDBs concentration for STY/DVB (95/5) RAFT copolymerisation (run 1 in Table 5.2) is showed in Figure 5.41. These concentrations were measured through the ICl titration method above described (Gonçalves *et al*., 2013a).

The impact of some operation conditions on the dynamics of STY/DVB RAFT products formation was studied through the change of particular parameters, such as the kind of RAFT CTA considered. The effect of the initial organic phase composition (e.g. STY, DVB, and diluent amounts) on the dynamics of global monomer conversion was briefly assessed through comparisons of runs 2 in Table 5.1 and runs 2 and 3 in Table 5.2 (see Figure 5.42) where the same reaction temperature and RAFT CTA were considered (70 °C and DDMAT). Similar dynamics of monomer conversions where measured within the ascribed RAFT polymerisation conditions.

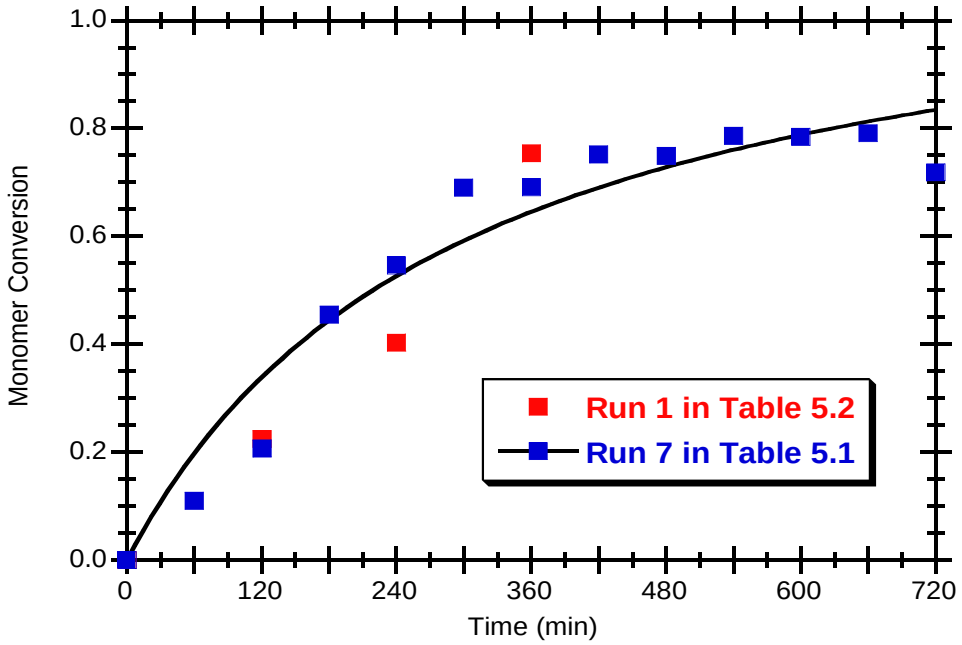

Figure 5.40. Measured dynamics of monomer conversion in aqueous suspension RAFT polymerisation of styrene (run in Table 5.1) and RAFT copolymerisation of STY/DVB (run 1 in Table 5.2).

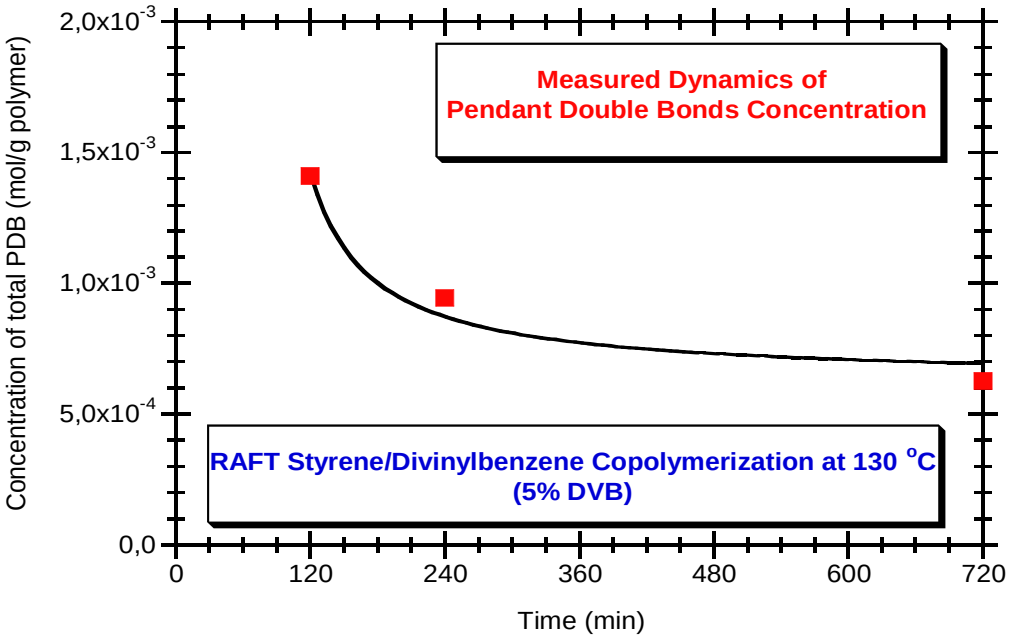

Figure 5.41. Measured dynamics of PDB concentration in RAFT copolymerisation of STY/DVB (run 1 in Table 5.2).

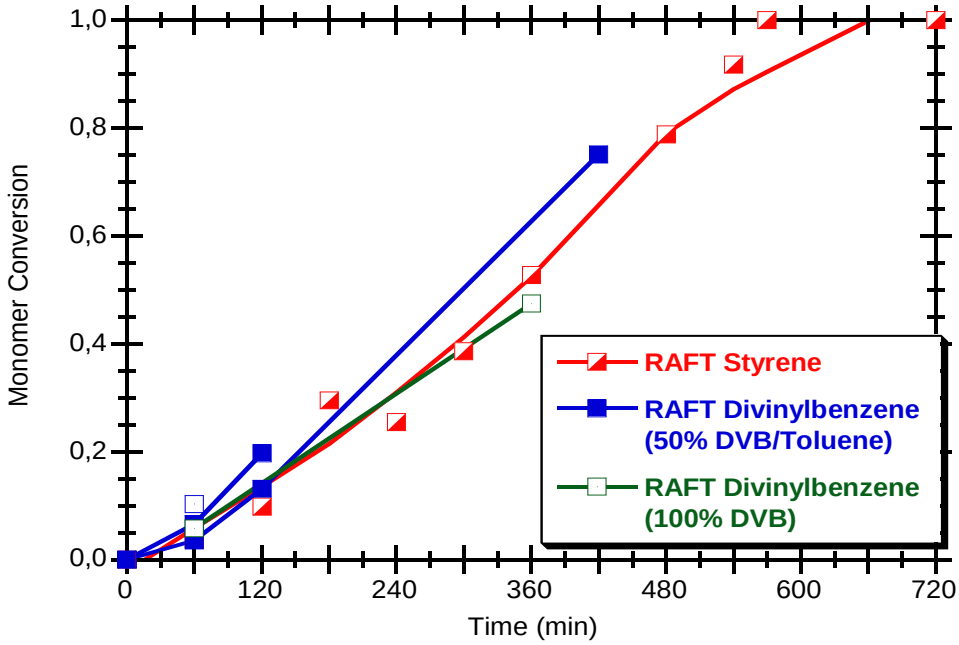

Figure 5.42. Comparison of the measured dynamics of monomer conversion in aqueous suspension RAFT polymerisation of styrene (run 2 in Table 5.1) and DVB (runs 2 and 3 in Table 5.2) at 70 °C.

Key features of the RAFT crosslinking mechanism become evident when the SEC traces of products with different polymerisation times are compared. Observation of these SEC traces for linear (STY) and non-linear (STY/DVB) runs highlights central issues of network formation. In Figure 5.43 are showed the SEC RI signals of polystyrene samples correspondent to different polymerisation times. Besides the growth of with reaction time of the main polymer population, a secondary polymer population with higher size and low concentration can be identified in these chromatograms. This feature is enhanced in Figure 5.44 where the LS and RI signals of the final sample correspondent to the same run (run 3 in Table 5.1) are compared. The huge molecular size of the secondary population becomes evident through the respective LS signal. This means that, even in the linear case, non-ideal mechanisms can be involved in RAFT polymerisation leading to an increase of the products dispersity. Slow fragmentation mechanisms in RAFT leading to bimodal distributions formation are a possible justification for these observations (Zapata-González *et al.*, 2011). Differences/similarities between STY and DVB RAFT polymerisations are illustrated in Figure 5.45 where the observed time evolution of $\bar{M}_w$ for runs 2 in Table 5.1 and runs 2 and 3 in Table 5.2 are compared.

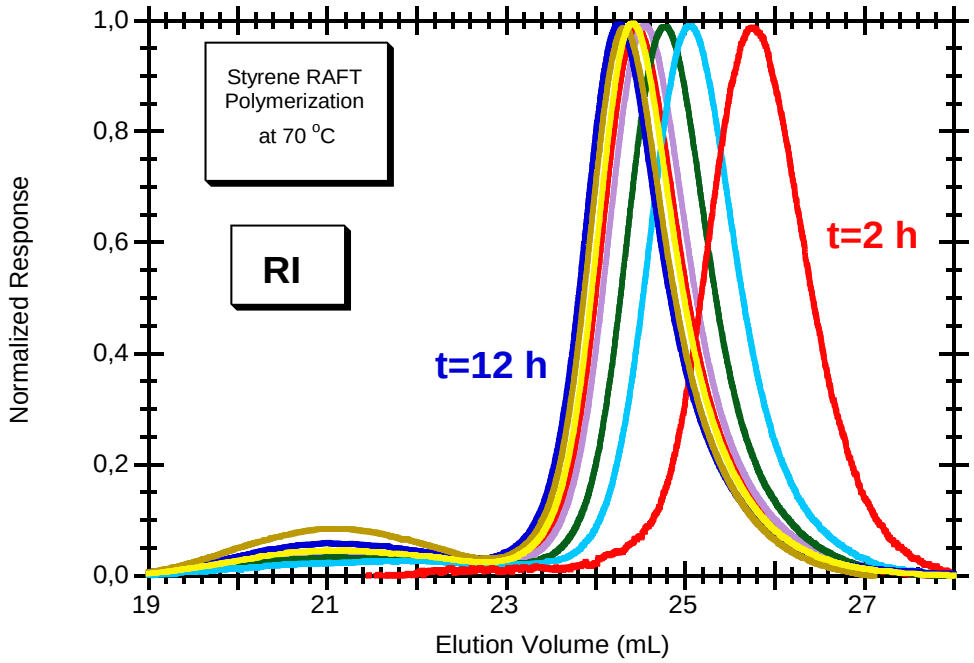

Figure 5.43. Normalized RI signal of polystyrene samples (run 3 in Table 5.1) with different polymerisation times.

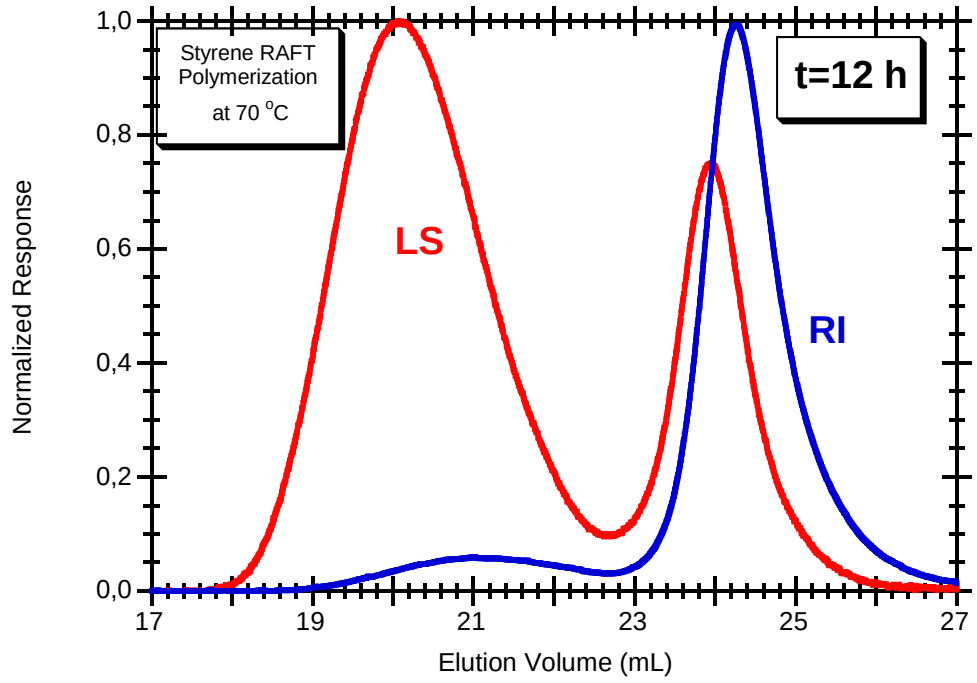

Figure 5.44. Comparison of the normalized RI and MALLS signals of a polystyrene sample (run 3 in Table 5.1) with polymerisation time t= 12 h.

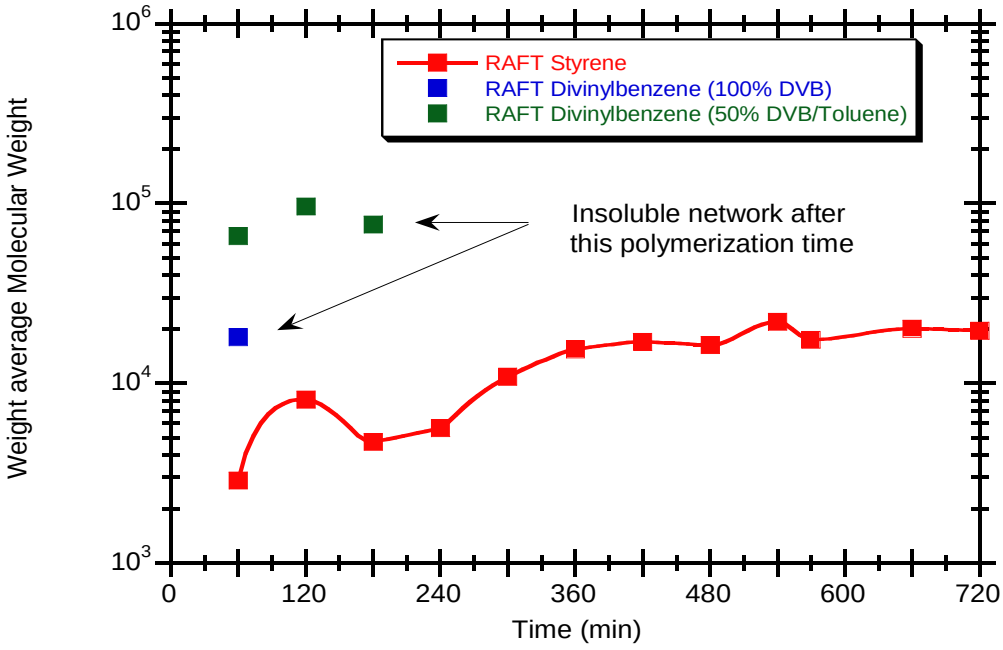

Figure 5.45. Measured dynamics of $\bar{M}_w$ for RAFT styrene polymerisation (run 2 in Table 5.1) and RAFT DVB (runs 2 and 3 in Table 5.2).

For the DVB RAFT polymerisation runs (2 and 3), the values presented are correspondent to the soluble phase which, in contrast to pure STY polymerisation, vanishes after some polymerisation time. Coexistence of sol and gel is observed when STY/DVB RAFT polymerisation is promoted, even with low amount of DVB (e.g. run 1 in Table 5.2). In spite of these important differences, some similarities in the SEC traces of RAFT polystyrene and soluble RAFT poly (STY/DVB) can be identified, as shown in Figure 5.46. RI signal shows a bimodal population for poly(STY/DVB) and the very high molecular size of the secondary (crosslinked) set of chains is highlighted by the correspondent LS signal. Molecular size of the secondary population developed with S RAFT polymerisation (as above discussed) is located in a region close to that observed with non-linear RAFT polymerisation but the correspondent concentration is significantly lower comparatively to the latter.

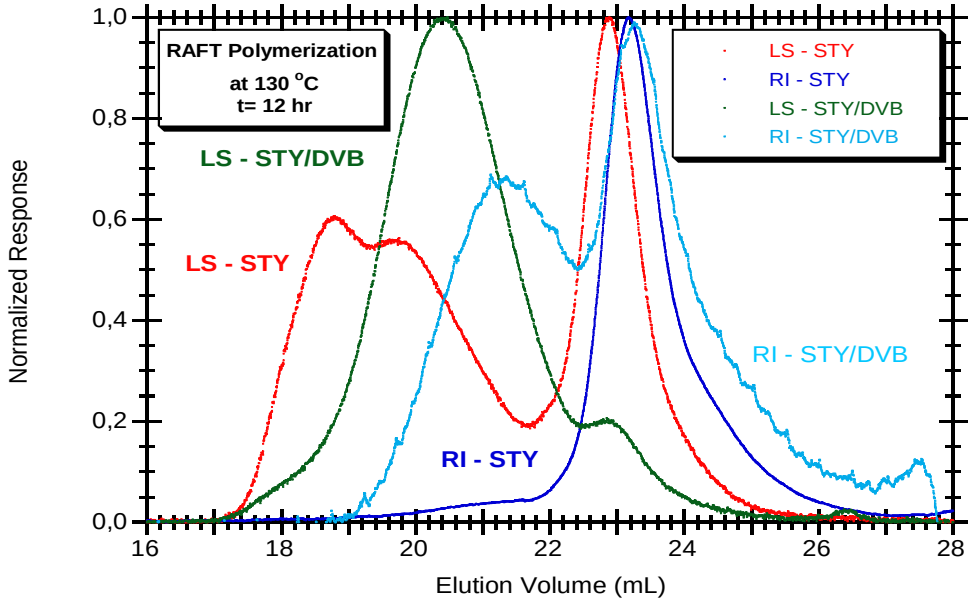

Figure 5.46. Normalized RI and LS signals observed for polystyrene (run 7 in Table 5.1) and soluble poly (STY/DVB) network (run 1 in Table 5.2) synthesized RAFT polymerisation at 130 °C.

Comparisons for the molecular architecture of the different RAFT products synthesized in this work are also illustrated in Figures 5.47 and 5.48. SEC observed structural dissimilitudes of RAFT poly(STY) and soluble poly(DVB)s are showed in Figure 5.47. Even analysing only the soluble phase, the highly crosslinked nature of the latter systems show a clear contrast with the linear case (see also Figure 5.46 for comparison with poly(STY/DVB) with low amount of DVB). Figure 5.48 compares the SEC traces of poly(DVB) samples, prepared with 50 % of toluene, and collected at different reaction times. Dynamics of two different sub-

populations can be observed and differences between samples correspondent to 2 and 3 hours of reaction time are a consequence of gelation.

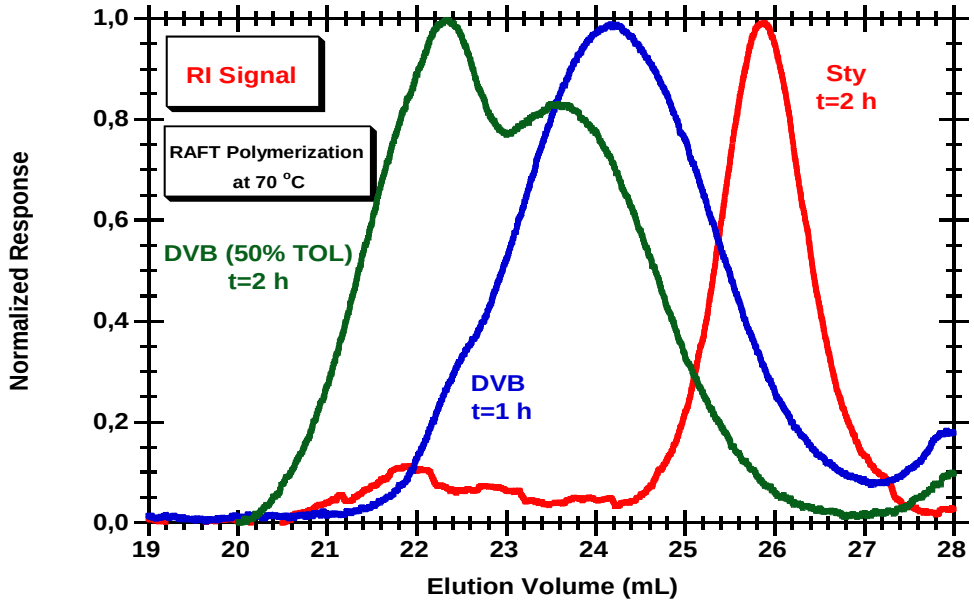

Figure 5.47. Comparison of the observed RI signal for RAFT synthesized polystyrene (run 2 in Table 5.1) and soluble poly(DVB) (runs 2 and 3 in Table 5.2).

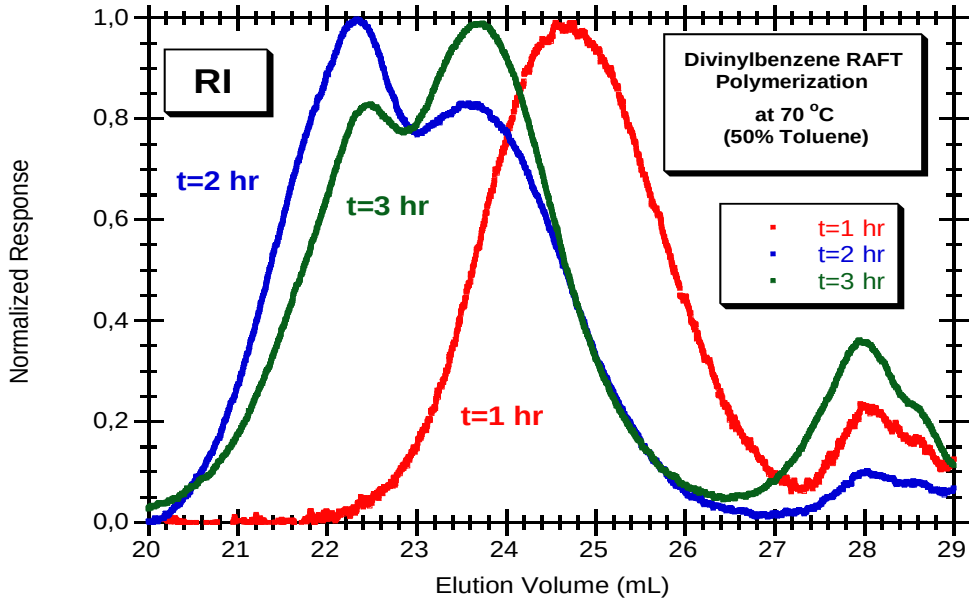

Figure 5.48. Observed RI signal for RAFT synthesized soluble poly(DVB) samples. Different stages of the crosslinking process (reaction times 1, 2 and 3 hr) are compared.

Results present in Figures 5.47 and 5.48 also show structural differences between RAFT poly(DVB) products synthesized using different dilutions (bulk and 50 % toluene), evidencing the possible effect of cyclization due to intramolecular propagation. In Figure 5.49(a)-(d) are shown examples of dried products obtained analysed by SEM. It was possible to observe the influence of synthesis conditions on the morphology of the produced materials.

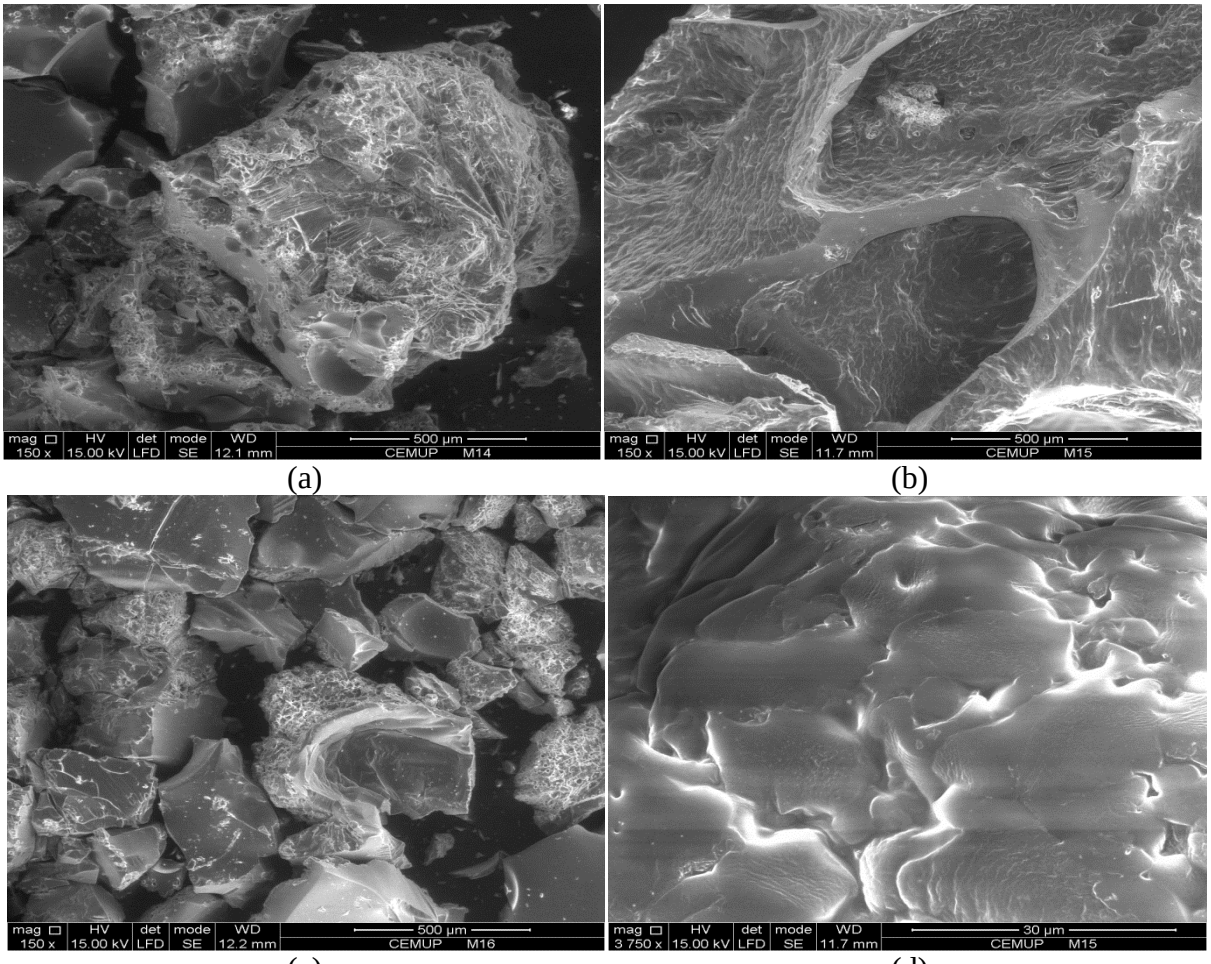

Figure 5.49. SEM micrographs of different polystyrene samples synthesized by RAFT.

5.5 Conclusions

Aqueous suspension RAFT polymerisations of styrene and styrene/divinylbenzene were experimentally studied using three different commercially available RAFT agents. An experimental program was performed changing (besides the chemical nature of the RAFT agent), the amount of DVB in the initial monomer mixture (0 to 100 %), the polymerisation temperature (in the range 70 to 150 °C), dilution in the organic phase and the initial composition (monomer, initiator and RAFT agent initial concentrations in the organic phase). A strong influence of the operation conditions on the kinetics of polymerisation and polymer

molecular architecture was observed. Product analysis by SEC with RI and also MALLS detection provided important information concerning the influence of the synthesis conditions on the polymer population homogeneity. Some polymerisation runs were designed in order to promote gel formation and the dynamics of network formation was thus assessed in a single pot reaction.

The incidence of the secondary population is dependent on the polymerisation temperature and is also a reaction-time dependent process. A higher importance of this phenomenon was found to occur at lower polymerisation temperatures (e.g. 70 °C). These observations enlighten the importance of the kinetics of addition/fragmentation in the formation of polymers with low dispersity using the RAFT technique. These effects are more pronounced when trithiocarbonates (DDMAT or CDT) are used. They could be related with slow fragmentation mechanisms leading to bimodal distributions (Zapata-González *et al*., 2011) but later fundamental results of RAFT mechanism (see below) rule out that explanation. The inspection of the molecular architecture of the soluble part provided by SEC shows that the RAFT crosslinking process, in a single pot reaction, also has a random nature and (as also showed with NMRP (Gonçalves *et al*., 2013a)) only a limited control on the network structure is possible by replacing FRP with RAFT. The effect of dilution on gelation was also detected, providing an evidence for the occurrence of intramolecular reactions (cyclization) which again cannot be totally suppressed using RAFT. Production, without gelation, of high functionalized materials based of vinyl/divinyl copolymerisation is possibly the major advantage of the CRP techniques (comparatively to FRP) in this context. The combination of CRP techniques with a multi-step polymerisation (e.g. synthesis of functionalized primary polymer chains followed by crosslinking) seems to be a more effective strategy to obtain networks with controlled molecular architecture.

Recent developments on pulsed-laser – assisted techniques, namely Single – Pulse/Pulsed – Laser – Polymerisation/Time-Resolved Electron Paramagnetic Resonance (SP-PLP-EPR) (Barth and Buback, 2010) should also be considered in the discussion of the RAFT results obtained in this research. Indeed, using this technique it is possible the experimental study of polymerisation systems with more than one kind of radicals as for instance acrylates with secondary radicals or tertiary midchain radicals (appearing due to backbiting of secondary radicals). Moreover, this technique can be used to enlighten the problem concerning the different types of radicals involved in RAFT polymerisation and associated kinetic mechanisms. In fact, using this technique, rate coefficients of addition and fragmentation (and

the correspondent equilibrium constants) were directly measured for butyl acrylate RAFT polymerisation using a trithiocarbonate (Meiser *et al.*, 2013). Other issues of RAFT polymerisation were also very recently addressed by the same research group when studying the kinetics of dithiobenzoate-mediated methyl methacrylate polymerisation (Sidoruk *et al.*, 2013). In this latter paper, different explanations for retardation with thiobenzoates were analysed, namely the following four mechanisms debated by scientific community: slow fragmentation of the RAFT intermediate radical, intermediate radical termination, intermediate radical termination followed by "missing step" and cross-termination restricted to small radicals. It was found that the concentration of the intermediate radicals is reduced compared with retarded systems and that cross-termination occurs to a weaker extent in the framework of the chemical system studied. Significant amounts of "missing step" products were also observed (Sidoruk *et al.*, 2013). It was also concluded that slow addition and "missing step" reactions contribute to the absence of rate retardation in dithiobenzoate mediated MMA polymerisation (Sidoruk *et al.*, 2013). Thus, experimental results of Buback group seem to show that the effect of slow fragmentation mechanisms should be discarded in RAFT polymerisation. Eventually, the secondary peak observed in the RAFT experiments performed in this work should be a consequence of the formation of 3-arm bridges during the polymerisation process, leading to the formation of high molecular sized polymer species. New theoretical developments allowing the modeling of such complex mechanism should be sought in order to validate this hypothesis.

Isolated products were characterized using FTIR and information concerning the presence of double bonds in the networks was obtained (important issue when materials functionalization is sought). PDBs in the networks were also quantified through chemical titration with ICl. This latter method is a complement of FTIR analysis when the concentration of these functional groups is low (e.g. due to small amount of DVB in the initial mixture). *In-line* FTIR-ATR was also tried in order to obtain real-time information concerning these RAFT polymerisations. Nevertheless, these measurements are probably affected by probe coating/catastrophic coagulation (Salehpour and Dubé, 2012) and further developments are needed in order to increase the reliability of this approach.

Additional knowledge aiding in the specification of operation conditions leading to tailored polymers based on the RAFT process was thus obtained considering the aqueous suspension styrene polymerisation as a model system. Studies here presented should also be useful to design similar processes with different classes of vinyl monomers. The assessment of the

RAFT process in the framework of the production networks or gels with controlled molecular architecture is another possible extension of this work. In this context, the operation with aqueous suspension is specially appropriated because allows the study of the vinyl/multivinyl crosslinking process, even after gelation, using a single pot reaction.

CHAPTER 6

INVERSE-SUSPENSION FREE-RADICAL POLYMERISATION LEADING TO HYDROGELS FORMATION

Abstract. Experimental studies concerning the synthesis process of hydrogels through the copolymerisation of acrylic acid (AA), acrylamide (AAM), *n*-isopropylacrylamide (NIPA) and methacrylic acid (MAA) with different kinds of crosslinking agents, namely bifunctional (N,N´-methylene bisacrylamide (MBAm) and 1,6-hexanediol diacrylate (HDDA)) trifunctional (trimethylolpropane triacrylate (TMPTA)) and tetrafunctional (tetraallyloxyethane (TAO)) were performed. Hydrogels synthesis was made mainly through inverse-suspension (solution polymerisation also performed) in batch reactor mode. The following variables were changed along the experimental program:

- Parameters changed:
  - Water soluble monomer leading to different hydrogels (superabsorbent, temperature and/or pH sensitive).
  - Monomer dilution, amount and kind (bi-, tri- and tetra-functional) of crosslinker.
  - Initiation system by redox initiation (APS/TEMED) and thermal initiation (V50).
- Products characterization:
  - Dynamics of conversion using gravimetry and size exclusion chromatography (SEC) with refractive index (RI) detection using water as eluent.
  - Dynamics of weigh fraction of gel.
  - The molecular architecture of the products through the determination of average molecular weights, *z*-average radius of gyration and absolute molecular weight distribution using the aqueous SEC/RI/MALLS system.
  - *In-line* FTIR-ATR for estimation some kinetic parameters.
  - The morphology of the produced hydrogels beads using SEM.
  - Swelling ratio changes on hydrogels with pH and/or temperature.

As a complement to this experimental data a general kinetic approach is exploited to describe the formation of these hydrogels.

This chapter is based on the following publications:

M.A.D. Gonçalves, V.D. Pinto, R.C.S. Dias, M.R.P.F.N. Costa, *Macromol. Symp*. 306-307 (2011) 107-125.

M.A.D. Gonçalves, V.D. Pinto, R.C.S. Dias, M.R.P.F.N. Costa, *J. Nanostrc. Polym. Nanocomp*. 9 (2013) 40-45.

6.1 Introduction

Hydrogels are three dimensional networks of hydrophilic polymers holding a large amount of water while maintaining the solid state. Hydrogels can swell significantly in the presence of an aqueous solution and can also deswell upon certain stimulations. Thus, hydrophilic gels are able to retain, at a high absorption rate, huge amounts of water (up to 1000 g/g relatively to the dry weight). Thanks to these unique properties, superabsorbent polymers (SAP) have many important applications in hygienic/sanitary industries, agriculture, environment, separation process and other chemical engineering operations. According to the provenience of the materials used in the synthesis, SAPs can be divided in two groups: synthetic SAP that are obtained through the copolymerisation of petrochemical-based monomers and those SAP obtained from the grafting of natural polymers such as polysaccharides (e.g., starch) or polypeptides (Buchholz and Graham, 1997; Buchholz and Peppas, 1994; Zohuriaan-Mehr and Kabiri, 2008).

Synthetic SAPs are mainly obtained through the polymerisation of acrylic acid (AA) with different kinds of crosslinkers such as N,N′-methylenebisacrylamide (MBAm), trimethylolpropane triacrylate (TMPTA) or tetraallyloxyethane (TAO). Water-phase polymerisations are generally carried out and therefore the low solubility of some crosslinkers in aqueous medium should be accounted for (Arriola *et al.*, 1997). This problem can be overcome by using an organic solvent and conventional crosslinkers (e.g. divinylbenzene or ethylene glycol dimethacrylate) at the expenses of introducing in the products chemicals hindering the direct use of the materials for some applications. In practice, SAPs are produced using the aforementioned kinds of crosslinkers at levels in the range 0.01 to 2 wt % (considering TMPTA as a model crosslinker) in order to obtain materials with a high swelling ratio (which is attained at a low crosslinker content) and a low soluble fraction (which is more easily fulfilled using a higher crosslinker content). The mole fraction of crosslinker (y_C) used in the production of such materials can therefore be as lower as 0.0025 % to 0.5 %.

Thermal, redox or even photo initiation are used to carry out the free radical copolymerisation of acrylic acid aqueous solutions in the presence of crosslinkers. Aqueous solutions of AA salts (obtained through the neutralization of AA with a base such as NaOH) are also usually considered in SAP production. Reaction temperatures in the range 40 to 70 °C are often considered in these synthesis processes. Note that in several kinetic studies concerning the polymerisation of acrylic and methacrylic acid (namely using PLP), much lower temperature

ranges have been considered (e.g. 2 °C to ambient temperature). Nevertheless, in order to assure high reaction rates (and almost complete monomer conversion) in industrial processes, higher temperatures must be used. Other parameters such as the degree of neutralization and monomer concentration have a strong impact on the polymerisation of these ionic monomers (Anseth *et al.*, 1996; Beuermann *et al*., 2006, 2007a, 2007b, 2007c and 2008; Buback and Junkers, 2006; Buback *et al.*, 2008b; Cutié *et al*., 1997a and 1997b; Henton *et al*., 1997; Kabanov *et al*., 1973 and 1975; Kuchta *et al*., 2000; Kurland, 1980; Lacík *et al*., 2001, 2003, 2004 and 2009; Li and Schork, 2006; Renard and McKenna, 2000).

Lack of reaction control often associated with aqueous solution production of SAPs (fast exothermic reaction and high viscosity with a concomitant temperature raise) can be overcome using inverse suspension polymerisation which also allows the direct synthesis of powder products or microspheres (Bahaj *et al.*, 2010; Bajpai *et al.*, 2007; Bodugöz and Güven, 2002; Chen *et al*., 2004; Kiatkamjornwong and Phunchareon, 1999; Omidian *et al*., 2003; Wang *et al*., 1997). Porous hydrogels composites with improved properties can also be synthesized changing the conventional procedure through the introduction of inorganic fillers and a porogen (Kabiri *et al*., 2004).

Smart hydrogels are water compatible polymer networks undergoing fast and reversible changes in their hydrophilic/hydrophobic microstructure. These hydrogels are also capable of responding to changes in parameters such as temperature, pH, electric or magnetic fields and are often designated as ‘stimuli-responsive’ polymers or ‘smart’ polymers. Changes at microscopic level become macroscopically apparent and include a huge shrinking/swelling of the network. In Figure 6.1 is depicted a model of a stimuli-responsive drug-delivery system.

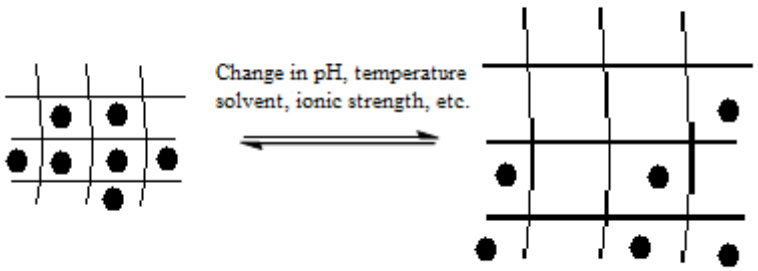

Figure 6.1. A model depicting a stimuli-responsive drug-delivery system (adapted from Bajpai *et al.*, 2010).

These reversibility transitions are driven by neutralization of charged groups due to pH shift, changes in efficiency of hydrogen bonding or in ionic strength (Galaev and Mattiasson, 2008). Owing to these unique features, hydrogels have found many applications as biomaterials for drug and protein delivery, tissue engineering, nanotechnology and microfabrication techniques. pH sensitive hydrogels are polyelectrolytes containing ionisable groups (pendant acidic or basic groups) which are able to release or accept protons. These mechanisms can be stimulated by changes in the environmental pH where the polymer network is located. Hydrogels containing weakly acid groups swell when the pH is increased and, conversely, those containing weakly basic groups collapse by increasing the pH. These phase transitions (swelling/deswelling) can be explored to synthesize useful materials for drug delivery systems (Bajpai *et al*., 2010). Nevertheless, the performance of these smart hydrogels (e.g. swelling kinetics) is strongly dependent on the molecular architecture of the networks (e.g. composition or crosslinking density) and on the synthesis conditions used in their production. Temperature of preparation, polymerisation medium (e.g. solution, suspension or emulsion) and/or the presence of a porogen leading to porous hydrogel are some parameters with influence in the end-use properties of such advanced materials (Gemeinhart *et al*., 2000). The size and shape of the synthesized gel particles, conditioning the water diffusion process, also have a strong impact on the response time of pH sensitive hydrogels.

Ionic hydrogels, known as polyelectrolytes, are prepared through the polymerisation of cationic or anionic monomers. A combination of positive and negative charges leads to amphoteric macromolecules (Sen and Guven, 1999; Sutani *et al*., 2002). Anionic hydrogels networks are known as acid homopolymers charged negatively or copolymers of anionic monomer. Anionic hydrogels are known to exhibit a marked increase in the swelling ratio with increase in the environmental pH (Ende *et al*., 1995; Lee and Chiu, 2002). Some anionic hydrogels are presented in Figure 6.2. As cationic hydrogel networks are commonly referred the homopolymers of positively charged basic, cationic monomers, copolymers of cationic and natural monomers. Some cationic hydrogels as PDMAEMA and Poly(vinyl pyridine) are shown in Figure 6.3 as example.

As schematized in Figures 6.4 and 6.5, the response to pH of cationic pendent groups is contrary to that of anionic pendant groups. The cationic hydrogel remain collapsed in the basic environment and swollen in the acid environment due to electrostatic repulsion between the positively charged groups (Ende *et al*., 1995; Lee and Chiu, 2002). For the anionic

hydrogel the opposite situation takes place. In Figure 6.6 is represented the behaviour of a cationic and an anionic hydrogel in acid and basic medium.

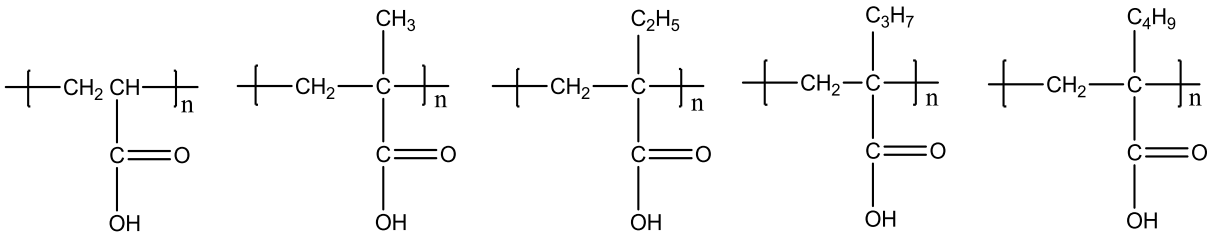

Figure 6.2. Structural representation of some anionic hydrogels.

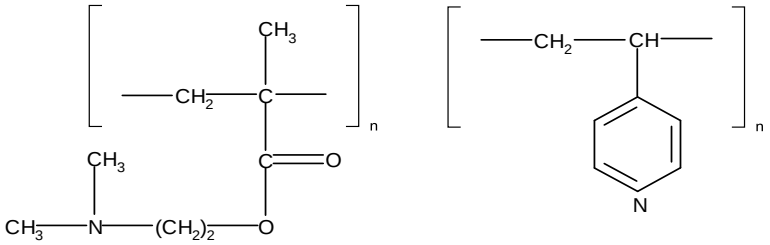

Figure 6.3. Structural representation of some cationic hydrogels.

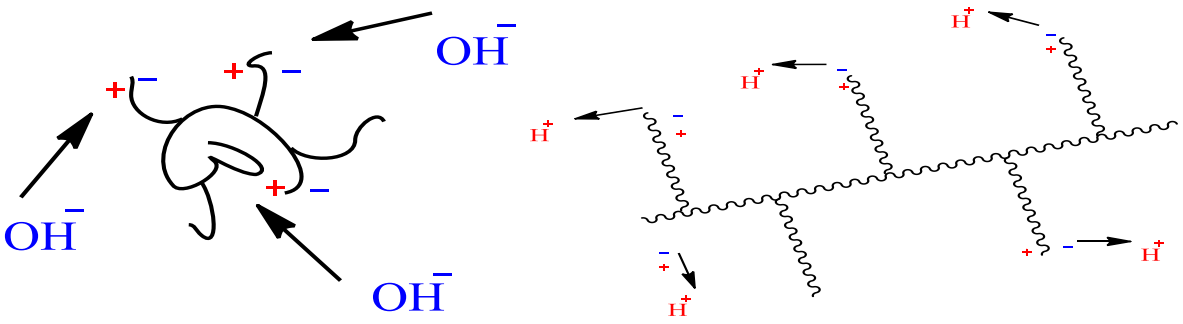

(a) (b)

Figure 6.4. (a) Schematic of the response of a cationic hydrogel in basic medium. (b) Schematic of the response of a cationic hydrogel in acid medium.

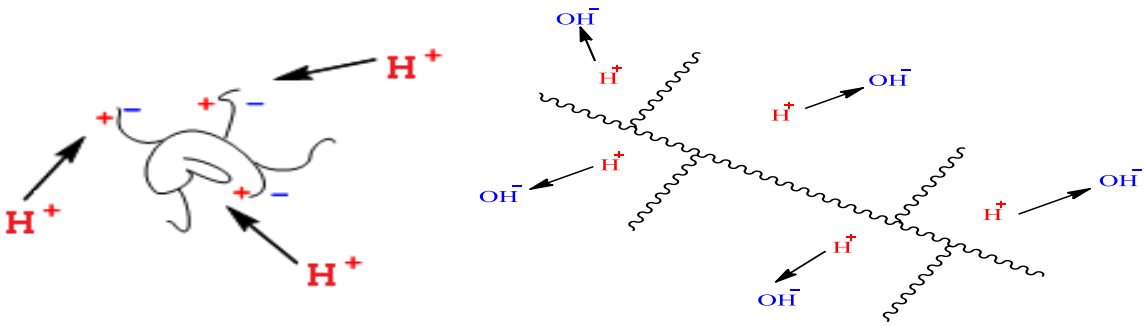

(a) (b)

Figure 6.5. (a)Schematic of the response of an anionic hydrogel in acid medium. (b) Schematic of the response of an anionic hydrogel in basic medium.

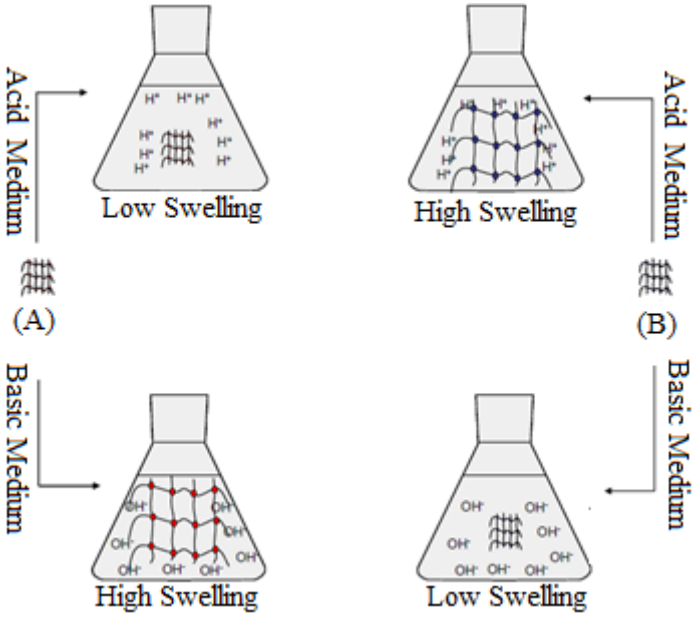

Figure 6.6. Schematic of a pH-sensitive hydrogel in acidic and basic medium. (A) Anionic (B) cationic.

Amphoteric hydrogels networks are macromolecules that have positive and negative charges in the entire polymer network. The presence of ionic species along the polymeric chain has distinct effects on the properties of the amphoteric hydrogels as they are in solution or in solid state. In Figure 6.7 is a schematic representation of an amphoteric hydrogel. Neutral or non-ionic hydrogels are homopolymeric or copolymeric networks which do not have any charged group in their structure. Neutral hydrogels swell to equilibrium when the osmotic pressure of the solvent is balanced with the sub-chain stretching energy (Bajpai *et al.*, 2010). The swelling and collapse of neutral hydrogel networks occur as a result of a change in the environmental temperature (Ostroha *et al.*, 2004). Some neutral hydrogels networks are shown in Figure 6.8.

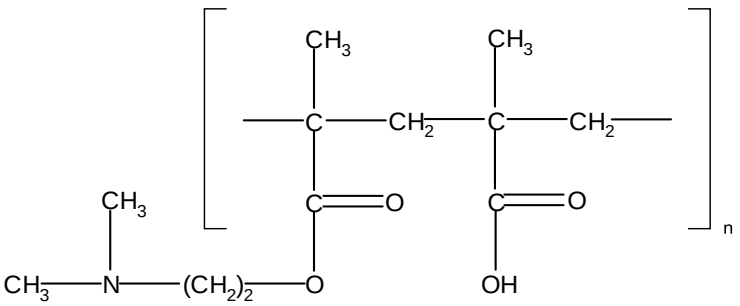

Figure 6.7 Schematic representation of a polyamphoteric hydrogel of MAA/DMAEMA.

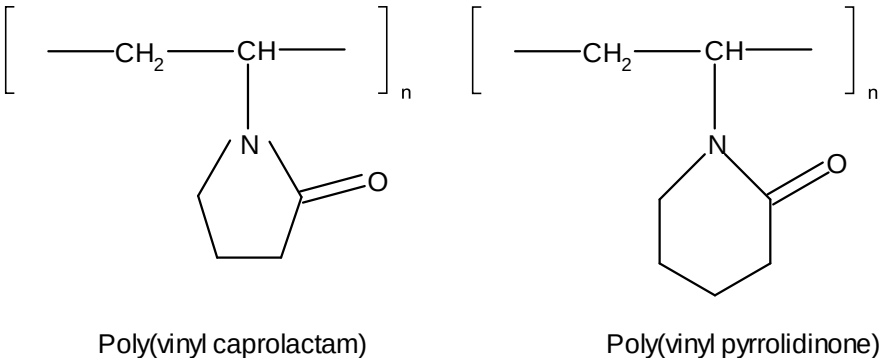

Figure 6.8 . Schematic representation of some neutral hydrogels.

Temperature-sensitive hydrogels have the capability of collapsing and swelling with temperature shifts in the surrounding medium. they can be classified as negative and positive thermosensitive hydrogels as well as thermally reversible gels (Peppas *et al*., 2000; Qiu and Park, 2001). This class is probably the most commonly studied of environmental-sensitive polymer systems in drug-delivery research. Thermoresponsive hydrogels may be prepared by crosslinking polymers which exhibit a lower critical solubility temperature (LCST) (Wu *et al*., 2003). The common characteristic of temperature-sensitive polymers is the presence of hydrophobic groups, such as methyl, ethyl and propyl (Qiu and Park, 2001). Some structures of these polymers are shown in Figure 6.9.

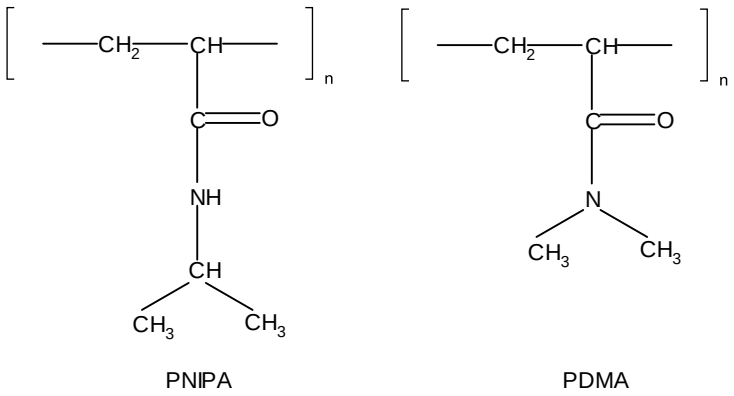

Figure 6.9. Structures of some temperature-sensitive polymers.

Negative temperature-sensitive hydrogels have a LCST and collapse when heated above it. These hydrogels show an *on-off* drug release (Soppimath *et al*., 2002) with *on* at a low temperature and *off* at high temperature allowing pulsatile drug release. In Figure 6.10 is represented the response of a negative temperature-sensitive hydrogel when heated/cooled. Positive temperature-sensitive hydrogels have an upper critical temperature (UCST). These hydrogels collapse upon cooling below the UCST. Poly(acrylic acid) and poly(acrylamide) have a positive temperature dependence of swelling (Qiu and Park, 2001). There are several

studies with the goal of synthesizing hydrogels with double sensitivity. This is accomplished with the copolymerisation of a temperature-sensitive monomer, usually NIPA, with a pH-sensitive monomer such AA or MAA (Brazel and Peppas, 1995; Chen and Hoffman, 1995; Feil *et al*., 1992; Liang *et al*., 2004; Vakkalanka *et al*., 1996; Yong-Hee *et al.*, 1994). These new classes of polymers are able to react to environmental changes and have found utility in intracellular drug delivery in which subtle pH differences across the endosomal membrane trigger the delivery of protein or DNA (Bajpai *et al*., 2010).

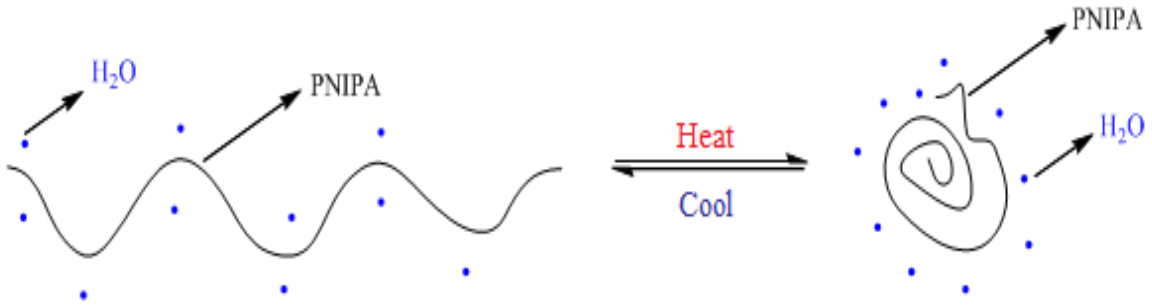

Figure 6.10. Illustration of the physical response of a negative temperature-sensitive hydrogel when submitted to heat or cool processes.

This chapter reports the synthesis/characterization of different classes of hydrogels and also the kinetics of their formation process. Time-evolution, in a batch reactor, of key properties, namely monomer conversion, weight fraction of gel, molecular weights and average radius of gyration of the soluble phase are assessed. The performance of the resulting hydrogels was also assessed (e.g. swelling ratio in different environmental conditions) in order to relate the synthesis conditions with the end-use properties of such materials. A general kinetic approach is used to predict the dynamics of hydrogel formation. Comparison between experimental measurements and these predictions allow the validation of a computational tool useful in the design of processes for production of tailored hydrogels.

6.2 Experimental Part

6.2.1 Materials

N-isopropylacrylamide (NIPA) of 99 % purity, N,N-dimethylacrylamide (DMA) of 99 % purity stabilized with 500 ppm monomethyl ether hydroquinone (MEHQ), acrylic acid (AA) of 99 % purity stabilized with 180-200 ppm MEHQ, methacrylic acid (MAA) of 99 % purity stabilized with 250 ppm MEHQ, methylene bisacrylamide (MBAm) of 99 % purity, 1,6-

hexanediol diacrylate (HDDA) of 80 % purity stabilized with 100 ppm MEHQ, trimethylpropane triacrylate (TMPTA) stabilized with 100 ppm methylethylhydroquinone, tetraallyoxyethane (TAO), hydroquinone of 99 % purity, cyclohexane of 99 % purity, 2,2-azobis(2-methylpropionamidine) dihydrochloride (V50) of 98 % purity, and the redox system ammonium persulfate (APS) of 98 % purity, tetramethylethylenediamine (TEMED) of 99 % purity, thioglycolic acid (CTA) with 99 % purity. All of them were purchased from Sigma-Aldrich. Acrylamide (AAM) with 98 % purity and ethyl cellulose (stabilizer) were purchased from Fluka. Span 60 and Span 80 (stabilizers) were purchased from Panreac. A current grade of liquid paraffin, toluene and sodium hydroxide (NaOH) were used when needed. All the products were used as received.

6.2.2 Polymerisation Set-up

The aqueous solution homopolymerisation of acrylic acid was performed in batch reactor in order to have some insight concerning the kinetics of polymerisation of this monomer in conditions similar to those used to synthesize SAP materials. These polymerisations were *in-line* monitored using a FTIR-ATR probe which allows the measurement of monomer conversion. The same experimental set-up, a reactor with maximum capacity of 2.5 L for which a detailed description has been presented in section chapter 2 was used to synthesize SAP materials based on acrylic acid/trimethylolpropane triacrylate copolymerisation. In order to extend the process to the post-gelation period, maintaining good agitation and heat dissipation conditions, these experiments were performed in inverse suspension. This technique is especially useful for gel production at isothermal conditions since keeping a good stirring of the reaction vessel is a key feature. In the continuous phase, toluene and/or cyclohexane were used as organic diluents and Span 60 and/or ethylcellulose as oil-suspending agents. The ratio oil-phase/water-phase in the reactor was 5/1 and the agitation speed of 400 rpm. Volume fraction of acrylic acid in the aqueous phase was $V_{AA} = 15$ %. A similar feed composition was used in the solution homopolymerisation of acrylic acid. Polymerisations of smart hydrogels were performed in a batch reactor using also the inverse suspension process. Reactions were performed at low scale in a 200 mL reaction vessel and at higher scale in a 2.5 L reaction device (description in chapter 2). Stable suspensions were produced with a volumetric ratio aqueous/organic phases=0.2, 1 % (w/w) of surfactant in the continuous phase and agitation speed at 300 rpm. Argon sweeping was used to prevent inhibition of the polymerisation by oxygen. NIPA, DMA, AAM, AA and MAA were chose as

the main water soluble monomers. MBAm, TMPTA and HDDA were selected as crosslinkers. The influence of the kind of crosslinker (e.g. bifunctional/trifunctional) on the gelation process could therefore be observed. The pair APS/TEMED was used for redox initiation at low polymerisation temperature (e.g. 20 °C) whereas V50 was selected as a thermal initiator (polymerisations at 50 °C). Cyclohexane was chosen for the continuous phase in the inverse suspension polymerisations with Span 80 as stabilizer. Partial neutralization of AA/MAA was carried out using sodium hydroxide. Thioglycolic acid was chosen as a chain transfer agent (CTA). A few solution polymerisations were *in-line* monitored using an immersion probe exploiting FTIR-ATR detection.

6.2.3 Product Analysis by SEC/RI/MALLS

At prescribed polymerisation times, reaction samples were collected from the reactor, quenched at low temperature in a solution containing hydroquinone to stop the reactions, and afterward prepared for injection of the soluble polymer in the SEC/RI/MALLS system. Dynamics of monomer depletion, weight fraction of gel, molecular weights and average radius of gyration were thus measured. The same equipment and procedures as in the previous chapters were used changing the eluent for water (with 200 ppm of sodium azide and 0.1 M of Na_2HPO_4 with pH=9) at T = 50 °C, flow rate of 0.5 ml/min and changing the size exclusion chromatography system. For this analysis a train of 3 SEC aqueous columns (Viskotek A2000 + Viskotek A3000 + Viskotek A6000) were considered to fractionate the polymers by size (different configurations were also used in order to not exceed the recommended maximum column pressures).

Polymerisation samples collected from the inverse suspension reaction set-up at different polymerisation time were treated as above described and the products were characterized by SEC/RI/MALLS. Important features of the crosslinking process can be obtained by such analysis, as depicted in Figures 6.11-6.16. Measurements of the following properties were thus carried out:

- Monomer conversions of the main water soluble vinyl monomers. Low crosslinker concentrations were used in this experimental program and the dynamics of their consumption could not be estimated.
- Molecular weight distributions (and their averages) before and after gelation (soluble phase).
- *z*-average radius of gyration before and after gelation (soluble phase).

- Weight fraction of gel (w_g).

In Figure 6.11 is shown the chromatographic traces (RI signal) of an AA/TMPTA sample where the soluble polymer and monomer traces were used to quantify the dynamics of gel formation. Figures 6.12 and 6.13 shows the chromatographic traces (RI and MALLS signals, respectively) for an AA/MBAm sample collected at different reaction times (10, 120 and 240 min) allowing the characterization before and after gelation of the molecular architecture the soluble phase during hydrogels synthesis.

Simultaneous detection of RI and MALLS allowed the measurement of MWD (and related averages) and *z*-average radius of gyration of the extractable material as presented in Figure 6.14. For this particular sample (acrylamide based) $\bar{M}_w = 1.4 \times 10^6$ and $\bar{R}_g$ =176 nm were measured. In Figure 6.15 are shown the chromatographic traces (RI signal) of two monomers (AA and AAM) present in the samples collected from the inverse suspension polymerisation at different reaction times (0, 20, 40, 60, 120, 180 and 240 min). Dynamics of monomer consumptions of monomers were thus estimated using their peak areas. The effect of synthesis conditions on the kinetics of the polymerisation and the estimation of rate parameters was thereafter performed, as depicted in Figure 6.16, using the superabsorbent synthesis (AA/MBAm based) as a case study.

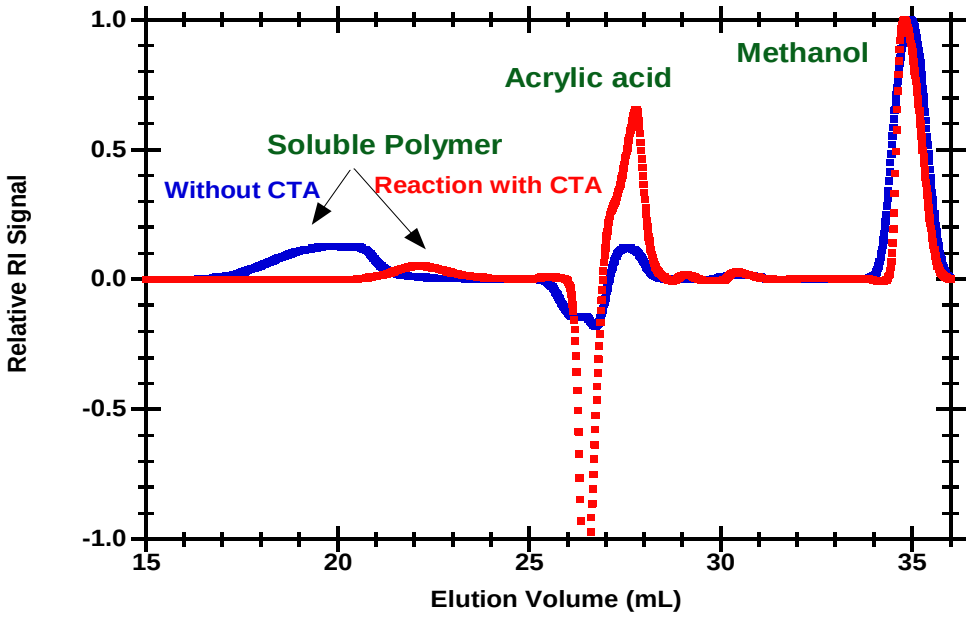

Figure 6.11. Chromatographic traces (RI signal) observed for AA/TMPTA samples synthesized through the inverse suspension process.

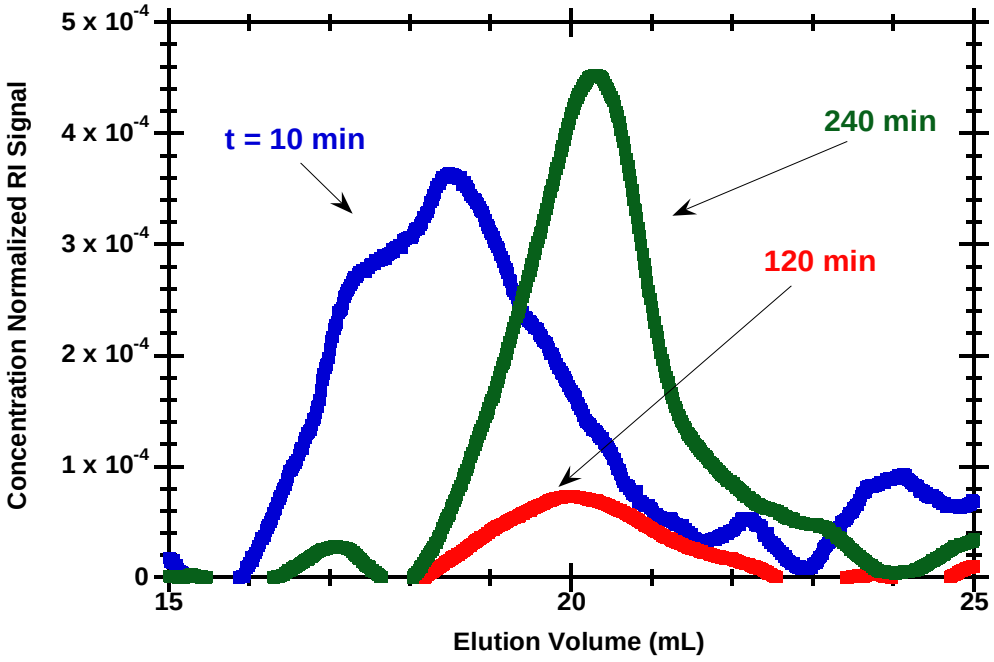

Figure 6.12. Chromatographic traces (RI signal) of the soluble polymer of the samples of AA/MBAm hydrogel collected at different reaction times.

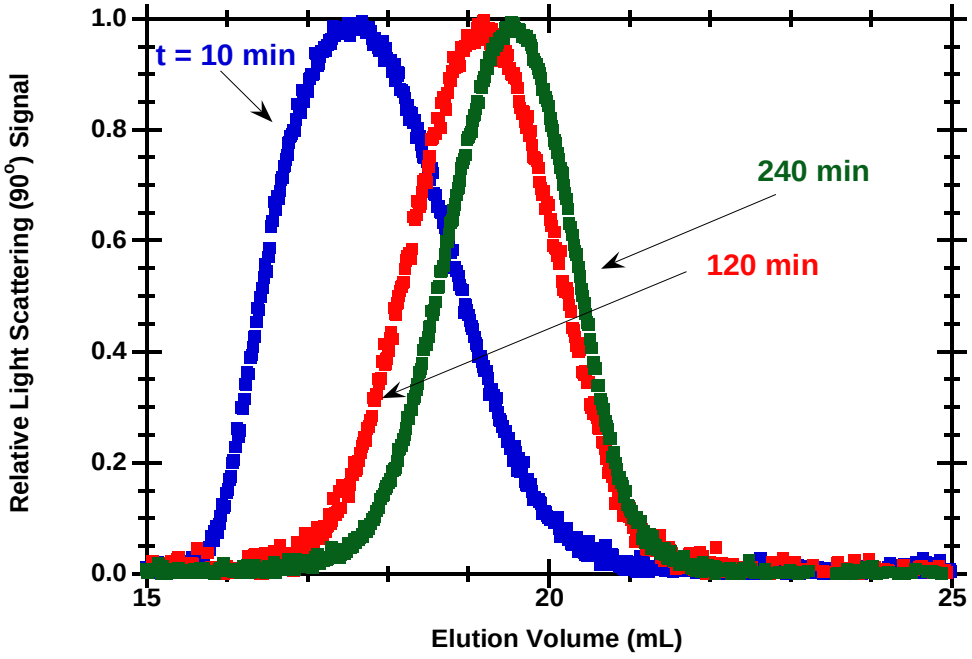

Figure 6.13. MALLS chromatographic traces (only the 90° signal is shown) of the soluble polymer samples of AA/MBAm hydrogel collected at different reaction times.

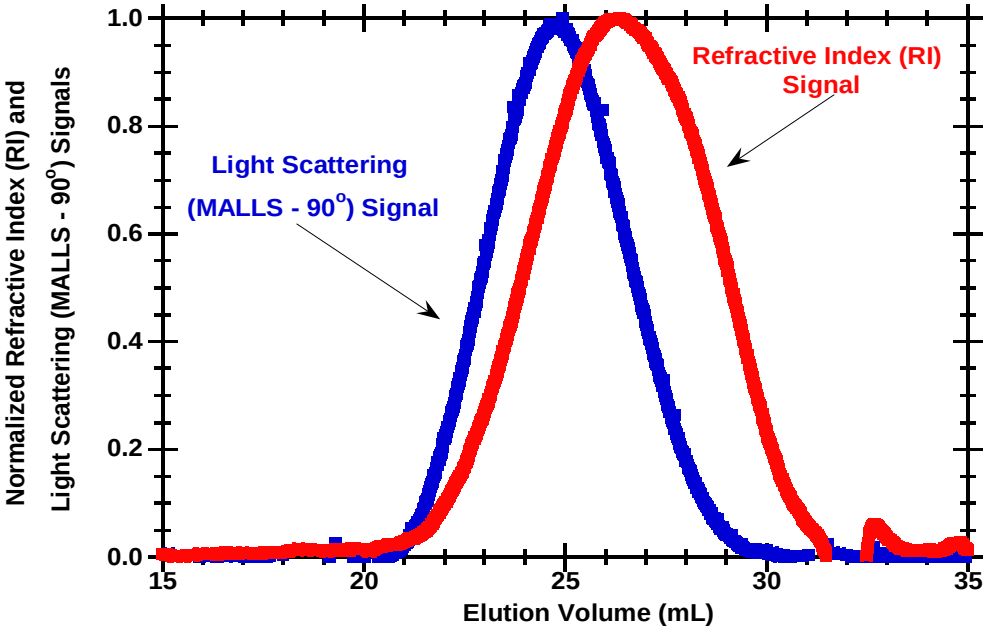

Figure 6.14. Comparison of RI and LS signals observed in the SEC/RI/MALLS analysis of the soluble fraction of hydrogels or their linear counterparts. In this particularly case is an acrylamide based sample.

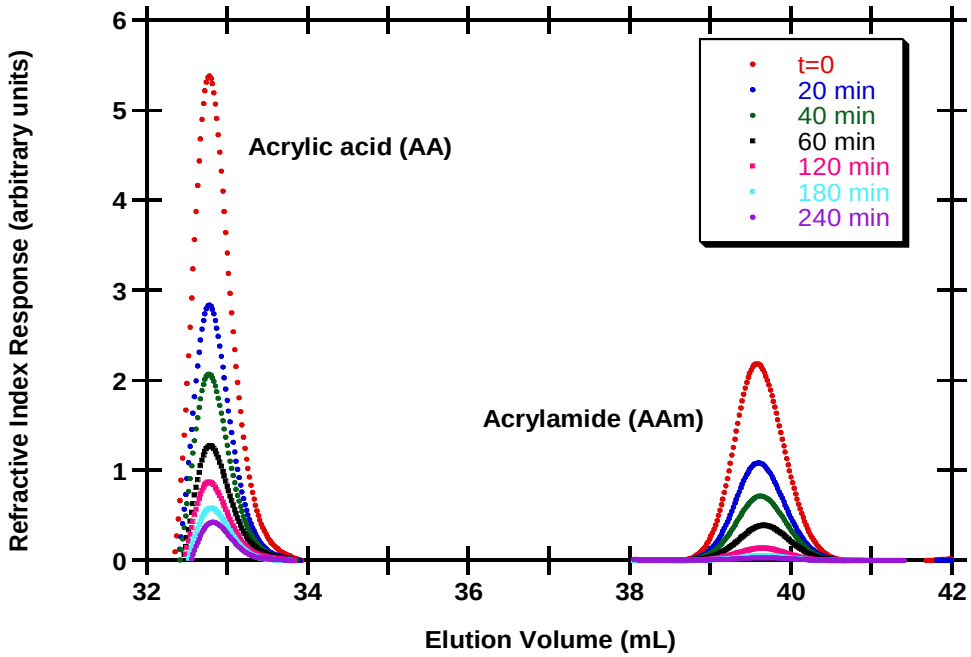

Figure 6.15. Chromatographic traces of two monomers (AA and AAM) present in inverse suspension polymerisation samples collected at different reactions times.

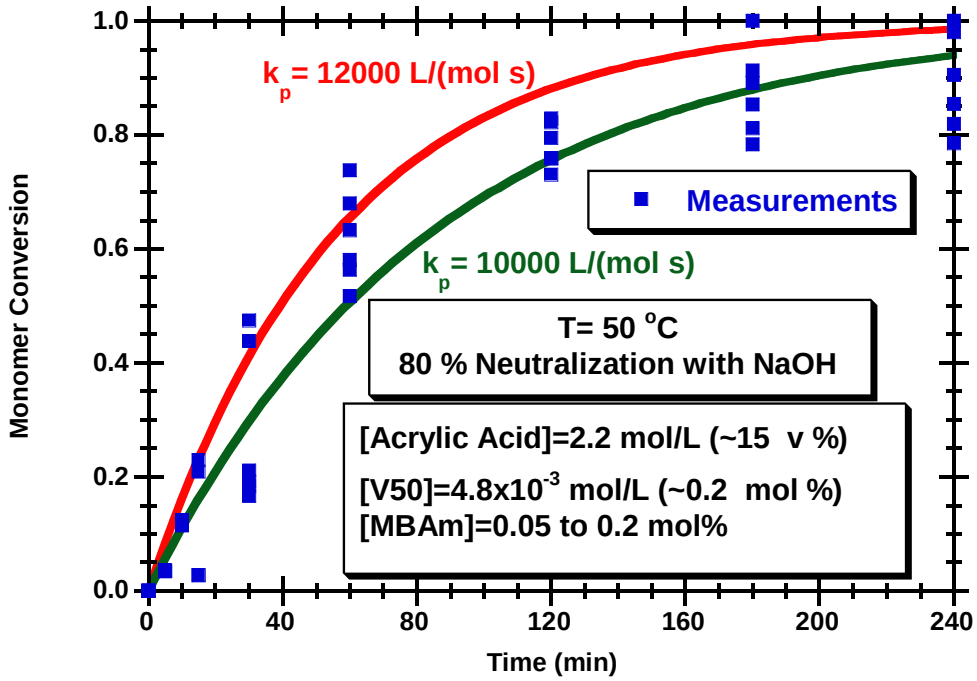

Figure 6.16. Comparison of observed and predicted reaction time evolution of monomer conversion during inverse suspension synthesis of hydrogels.

6.3 Kinetic Studies

6.3.1 Kinetic Modelling Considering Copolymerisation

A very simple kinetic scheme describing the copolymerisation of acrylic acid (or other acrylic monomer) with a multifunctional crosslinker (CL) is presented in Table 6.1. A generic crosslinker with functionality α (number of active double bonds) is here considered. N,N′-methylenebisacrylamide (MBAm), with $\alpha = 2$, and trimethylolpropane triacrylate (TMPTA), with $\alpha = 3$, tetraallyloxyethane ($\alpha = 4$) are examples of such crosslinkers which are industrially used in the preparation of acrylic SAPs. A linear copolymerisation results if a chemical system including a second monomer with a single active double bond ($\alpha = 1$) is considered.

In Table 6.1, $P_{k,m,n}$ represent the ensemble of polymer molecules bearing *k* radicals, *m* pendent double bonds and *n* repeating units. As shown in previous chapters, this kinetic approach was conceived in order to deal with much more detailed descriptions of non-linear polymerisation systems. Consideration of different kinds of polymer radicals (different reactivities), different kinds of pendant double bonds (generically macromonomers with different reactivities) and discrimination of different structural repeating units (e.g. moieties derived from vinyl and

multivinyl monomers) are some examples of peculiarities that can be accommodated by this method. The automation of the simulation tool developed allows the analysis of these more complex systems without rewriting all the involved equations. This feature will be explored below in the present work when discussing, for instance, the influence of the reactivity of the two PDBs of TMPTA on the dynamics of gelation.

In the kinetic scheme above presented, I represent the thermal initiator (e.g. V50) decomposing into a pair of primary radicals R_0 with an associated efficiency *f*. Three different initiation steps arising from the reaction of primary radicals with acrylic acid, crosslinker and PDBs are considered and similarly three different propagation mechanisms related to the reaction of polymer radicals with these same species are also considered. Termination by combination (dominant in acrylates) and termination by disproportionation are also included in the kinetic scheme. Due to their relative low impact on the dynamics of gelation (e.g. comparatively to polymerisation of PDBs) and also for the sake of simplicity, chain transfer reactions (e.g. to solvent or monomer) are not included in this analysis. Kinetic parameters (rate coefficients) involved in mechanisms described in Table 6.1 play an important role when predictions of the dynamics of polymerisation are desired. Estimates for these kinetic parameters, are below discussed.

Table 6.1. Kinetic scheme describing the polymerisation of acrylic acid (AA) with a multifunctional crosslinker.

Kinetic Step	Chemical Equation
Initiator Thermal Decomposition	$I \xrightarrow{k_d} 2fR_0$
Acrylic Acid initiation	$R_0 + AA \xrightarrow{k_{I_1}} P_{1,0,1}$
Crosslinker initiation	$R_0 + CL \xrightarrow{k_{I2}} P_{1,\alpha-1,1}$
Pendent Double Bonds (PDB) initiation	$R_0 + P_{k,m,n} \xrightarrow{k_{I3}} P_{k+1,m-1,n}$
Acrylic acid propagation	$P_{k,m,n} + AA \xrightarrow{k_{p1}} P_{k,m,n+1}$
Crosslinker propagation	$P_{k,m,n} + CL \xrightarrow{k_{p2}} P_{k,m+\alpha-1,n+1}$
PDB propagation (crosslinking)	$P_{k,m,n} + P_{k',m',n'} \xrightarrow{k_{p3}} P_{k+k',m+m'-1,n+n'}$
Termination by combination	$P_{k,m,n} + P_{k',m',n'} \xrightarrow{k_{tc}} P_{k+k'-2,m+m',n+n'}$
Termination by disproportionation	$P_{k,m,n} + P_{k',m',n'} \xrightarrow{k_{td}} P_{k-1,m,n} + P_{k'-1,m,n}$

6.3.2 Kinetic Modelling Considering Terpolymerisation

A general kinetic approach based on population balances of generating functions (Costa and Dias, 1994 and 2005; Dias and Costa, 2010) allows the description of gel formation based on the underlying reaction steps. Kinetic schemes with flexible degree of complexity can be considered in the framework of the present chapter, including not only crosslinking mechanisms but also transfers to polymer if needed. Predictions of key properties of non-linear polymers are thus possible before and after gelation. The application of this method to the study of the dynamics of superabsorbent hydrogels formation was discussed above (Gonçalves *et al*., 2011b), including also the comparison of this theory with alternatively approaches, namely the theory of branching processes (TBP). Free-radical crosslinking polymerisations are kinetically controlled and therefore, other equilibrium gelation theories, such as TBP, cannot be straightforwardly applied to these systems. Important features of TBP in the description of non-linear polymerisation (e.g. calculation of elastic properties of polymer network) are presented by Dušek *et al*., 2005 and references therein.

The ability of the above mentioned general kinetic approach to deal with the dynamics of hydrogel formation will be here illustrated using a terpolymerisation crosslinking system as case study (e.g. AA/AAM/MBAm). A simple description of polymer molecules is obtained by counting the number of acrylic acid units incorporated in the polymer (x), the number of polymerized acrylamide units (y), the number of polymerized MBAm units (z), the number of radicals belonging to the polymer molecule (k) and the number of pendant double bonds (m). A five dimensional distribution, ($P_{k,m}^{x,y,z}$) is therefore used to describe polymer structure. An even simple analysis is possible if only the global degree of polymerisation is sought. In these circumstances, the counting of the three kinds of structural units present in polymer molecules can be lumped into a single variable and a three dimensional distribution can be used (its variables are the degree of polymerisation, the number of radicals and the number of pendant double bonds). The flexibility of this general kinetic approach to accommodate models with different degrees of complexity has been discussed in previous publications of this research group (Costa and Dias, 1994 and 2005; Dias and Costa, 2010).

An illustration of the kinetics schemes considered in the modelling studies is provided in Table 6.2, encompassing the following generic steps of radical polymerisation: initiator decomposition, monomer initiation, propagation, chain transfer, termination and inhibition.

Table 6.2. Kinetic schemes considered in the modelling studies with the generic steps of radical polymerisation.

Kinetic Step	Chemical Equation
Initiator Decomposition	$I \xrightarrow{k_d} 2fR_0$
Acrylic Acid (M_1) initiation	$R_0 + M_1 \xrightarrow{k_{I1}} P_{1,0}^{1,0,0}$
Acrylamide (M_2) initiation	$R_0 + M_2 \xrightarrow{k_{I2}} P_{1,0}^{0,1,0}$
MBAm (M_3) initiation	$R_0 + M_3 \xrightarrow{k_{I2}} P_{1,1}^{0,0,1}$
Pendent Double Bonds (PDB) initiation	$R_0 + P_{k,m}^{x,y,z} \xrightarrow{k_{I4}} P_{k+1,m-1}^{x,y,z}$
Acrylic acid propagation	$P_{k,m}^{x,y,z} + M_1 \xrightarrow{k_{p1}} P_{k,m}^{x+1,y,z}$
Acrylamide Propagation	$P_{k,m}^{x,y,z} + M_2 \xrightarrow{k_{p2}} P_{k,m}^{x,y+1,z}$
MBAm propagation	$P_{k,m}^{x,y,z} + M_3 \xrightarrow{k_{p3}} P_{k,m+1}^{x,y,z+1}$
Pendant double bond propagation	$P_{k,m}^{x,y,z} + P_{k',m'}^{x',y',z'} \xrightarrow{k_{p4}} P_{k+k',m+m'}^{x+x',y+y',z+z'}$
Chain transfer to acrylic acid	$P_{k,m}^{x,y,z} + M_1 \xrightarrow{k_{M1}} P_{k-1,m}^{x,y,z} + R_0$
Chain transfer to acrylamide	$P_{k,m}^{x,y,z} + M_2 \xrightarrow{k_{M2}} P_{k-1,m}^{x,y,z} + R_0$
Chain transfer to agent	$P_{k,m}^{x,y,z} + S \xrightarrow{k_S} P_{k-1,m}^{x,y,z} + R_0$
Termination by combination	$P_{k,m}^{x,y,z} + P_{k',m'}^{x',y',z'} \xrightarrow{k_{tc}} P_{k+k'-2,m+m'}^{x+x',y+y',z+z'}$
Termination by disproportionation	$P_{k,m}^{x,y,z} + P_{k',m'}^{x',y',z'} \xrightarrow{k_{tc}} P_{k-1,m}^{x,y,z} + P_{k'-1,m'}^{x',y'z'}$
Inhibition	$R_0 + Z \xrightarrow{k_Z}$ Inactive Products
	$P_{k,m}^{x,y,z} + Z \xrightarrow{k_{tc}} P_{k-1,m}^{x,y,z}$

6.3.3 Kinetic Parameters

Despite the technical importance of poly(acrylic acid) and poly(methacrylic acid), scarce information concerning the kinetics of polymerisation of these monomers in aqueous phase could be found in the literature up to about one decade ago. In the last years, this challenging problem was studied by a few research groups aiming at measuring propagation and termination rate coefficients of these monomers, especially in aqueous phase and considering different synthesis conditions (showing the effect of temperature, concentration, pH, ionic strength, etc.). A short review concerning this issue is presented in Tables 6.3-6.6 where the

correspondent bibliographic sources and main remarks concerning the measurements are also described.

Among other important issues, PLP-SEC measurements for water soluble monomers are difficult because SEC analysis cannot be carried out using THF as eluent and this well established technique is not directly feasible. This issue can be partially circumvented by performing a prior modification of poly(acrylic acid) generating the related methyl ester which can be afterwards analysed using the conventional PLP-SEC with THF as eluent.

Table 6.3. Some values of the propagation rate constant (k_p) of acrylic acid (AA) in water.

k_p(L mol^{-1}s^{-1})	T (°C)	pH	[M]	Remarks
~500 to ~2000 [a)]	Room	2.2-2.9	30 %wt AA	Minimum at pH ~6.5 k_p ↓ with ↑ conversion k_p ↓ with ↑ ionic strength
~30000 to ~60000 [b)]	20	N.N.	0.83-0.90 mol/L	k_p ↓ with ↑ [M]
~40000 to ~70000 [b)]	25	N:N.	0.90-1.37 mol/L	
$\ln k_p = 16.30 \pm 0.29 - \frac{1437 \pm 83}{T(K)}$ ($k_p = 88926$ @20 °C) [c)]	2.3-25	N.N.	30 %wt AA	
$\ln k_p = 16.00 \pm 0.39 - \frac{1468 \pm 112}{T(K)}$ ($k_p = 59264$ @20 °C) [c)]	2.3-28.5	N.N	40 %wt AA	k_p ↓ with ↑ [M]
$\ln k_p = 20.40 \pm 0.60 - \frac{2523 \pm 171}{T(K)}$ ($k_p = 131804$ @20 °C) [d)]	2.5-19.5	N.N	1 %wt AA	2%, 5% AA also included
$\ln k_p = 20.00 \pm 0.64 - \frac{2343 \pm 179}{T(K)}$ ($k_p = 163311$ @20 °C) [d)]	2.8-24.7	N.N.	3 %wt AA	Maximum k_p at ~3% AA
$\ln k_p = 18.00 \pm 0.74 - \frac{1848 \pm 209}{T(K)}$ ($k_p = 119711$ @20 °C) [d)]	2.1-20.1	N.N.	10 %wt AA	Solvent equality effects; Association of AA with polymer/radicals
112000 [e)]	6	10 %N.	0.69 mol/L	[M] corresponds to ~5%wt AA. A model for the dependence of k_p with neutralization is presented.
82200 [e)]	6	50 %N.	0.69 mol/L	
16700 [e)]	6	95 %N.	0.69 mol/L	
59900 [e)]	6	110%N.	0.69 mol/L	

Table 6.3. Continuation.

k_p(L mol^{-1}s^{-1})	T (°C)	pH	[M]	Remarks
38667 [f)]	55	65 %N.	33% solids (AA) (~25 %wt AA)	Estimated from experimental data in [g)]
650 [h)]	23	7.9	1.2 mol/L AA	
6600 [h)]	23	11	1.2 mol/L AA	
2500 [h)]	23	13.6	1.2 mol/L AA	
5000 [i)]	50	N:N.	bulk	

Without estimation of k_p, important kinetic data concerning the aqueous polymerisation of AA or AA/TMPTA is presented (Arriola *et al*., 1997; Cutié *et al*., 1997a and 1997b; Henton *et al*., 1997). The effect of neutralization of AA and solids content (dilution related) was extensively studied in these works in the temperature range 55 to 85 °C. R= 8.314 J mol^{-1}K^{-1}. [a)] Anseth *et al*., 1996; [b)] Kuchta *et al*., 2000; [c)] Lacík *et al*., 2001; [d)] Lacík *et al*., 2003; [e)] Lacík *et al*., 2004; [f)] Li and Schork, 2006; [g)] Cutié *et al*., 1997a; [h)] Kabanov *et al*., 1973 and 1975; [i)] Kurland, 1980.

A similar procedure can be used with poly(methacrylic acid). Nevertheless, polymer modification can introduce non negligible errors in molecular weight measurements and so to rate coefficient estimates. A detailed discussion concerning this issue and other important features associated with measurements of rate coefficients of water soluble monomers can be found in the references presented in Tables 6.3-6.6.

To sum up, propagation and termination rate coefficients, besides temperature, also depend (at least) on:

- Monomer/solvent concentration ratio with non-ionic systems. A decrease of about one order of magnitude in k_p was observed upon increasing monomer concentration.
- Degree of ionization. At low monomer concentration, a decrease in k_p of about one order of magnitude was measured when the degree of ionization was changed from 0 to 100 %.
- Opposite variations were observed when the two effects (monomer concentration and ionization) are present: a weaker drop of k_p with monomer concentration was found when the monomer is partially ionized. For a fully ionized monomer, k_p increases when monomer concentration is also increased.
- Occurrence of Trommsdorff effect is another issue complicating the kinetics of these polymerisation systems.

It is therefore difficult to establish a fully reliable set of kinetic parameters valid for the different conditions to be considered in the synthesis of water soluble homopolymers based on acrylic or methacrylic acids or related superabsorbent hydrogels. The aim of the present work is the development of a simple kinetic model being able to capture the essential features of SAP production considering particular operation conditions with an associated set of kinetic parameters. Conversely this method can be used to predict the influence of the change of operating conditions (change in temperature, pH, and so on, and the concomitant change in the kinetic parameters) on the dynamics of gelation. These aspects are illustrated in the next section where simulations performed with different sets of kinetic parameters are presented.

Table 6.4. Some reported values of the propagation rate constant (k_p) of methacrylic acid (MMA) in water.

k_p(L mol^{-1}s^{-1})	T (°C)	pH	[M]	Remarks
$\ln k_p = 14.36 \pm 0.47 - \frac{1839 \pm 145}{T(K)}$ ($k_p = 3241$@20 °C) [a)]	18-89	N.N.	15 %wt MAA	$k_p \downarrow$ with $\uparrow$ [M]
$\ln k_p = \ln 4.62 \times 10^6 - \frac{16.5 \pm 0.5}{10^{-3} RT(K)}$ ($k_p = 5284$ @20 °C) [b)]	20-80	N.N.	5 %wt MAA	15%, 30%, 60% MAA also included $k_p \downarrow$ with $\uparrow$ [M]
$\ln k_p = \ln 0.63 \times 10^6 - \frac{15.3 \pm 1.1}{10^{-3} RT(K)}$ ($k_p = 1179$ @20 °C) [b)]	23-80	N.N.	45 %wt MAA	Intermolecular interactions Between H_2O, MAA and transition state structures
$\ln k_p = \ln 0.38 \times 10^6 - \frac{16.1 \pm 1.6}{10^{-3} RT(K)}$ ($k_p = 512$ @20 °C) [b)]	25-60	N.N.	100 %wt MAA	
$\ln k_p = 14.30 \pm 0.2 - \frac{1801 \pm 43}{T(K)}$ ($k_p = 3475$@20 °C) [c)]	18-89	N.N.	15 %wt MAA	IUPAC benchmark
7700 [d)]	50	N.N.	10 % MAA	
4900 [d)]	50	N.N.	20 % MAA	$k_p \downarrow$ with $\uparrow$ [M]
3300 [d)]	50	N.N.	30 % MAA	$k_p \downarrow$ with $\uparrow$ conversion
6602 [e)]	60	70 % N.	5 % MAA	Other measurements were performed. Variation of k_p with T, [M] and N. Is available
4229 [e)]	60	70 % N.	20 % MAA	
2702 [e)]	60	70 % N.	40 % MAA	
2477 [e)]	80	100%N.	40 % MAA	

Increase of k_p with increasing MAA concentration for fully monomer ionization and T =40 °C is reported in Beuermann *et al*., 2007a. Ionic and hydrogen-bonded intermolecular interactions between the activated state and the molecular environment can be at the source of the variation of k_p with monomer concentration and degree of ionization. Increase of k_p with conversion was observed in Beuermann *et al*., 2007b. R=8.314 J mol^{-1}k^{-1}. [a)] Kuchta *et al*., 2000; [b)] Beuermann *et al*., 2006; [c)] Beuermann *et al*., 2007c; [d)] Buback *et al*., 2008b; [e)] Lacík *et al*., 2009;

Table 6.5. Some reported values of the termination rate constant (k_t) of acrylic acid (AA) in water.

k_t(L mol^{-1}s^{-1})	T (°C)	pH	[M]	Remarks
$\sim 3 \times 10^3$ to $\sim 5 \times 10^4$ [a)]	Room	2.2-9.9	30 %wt AA	Minimum at pH~6.5
Very low values ($k_t = 0.1$ to 1) at high conversion (~0.9) and pH=6.5				$k_t \downarrow$ with conversion $k_t \downarrow$ with ionic strength
$k_p/\sqrt{k_t} = 25$ to 40 [b)]	70	75 %N.		Inverse suspension
3×10^8 [c)]	55	65 %N.	33 % solids (AA) (~25 %wt AA)	Estimated from experimental data in[d)]

[a)] Anseth *et al.*, 1996; [b)] Renard and McKenna, 2000; [c)] Li and Shork, 2006; [d)] Cutié *et al.*, 1997a;

Table 6.6. Some reported values of the termination rate constant (k_t) of methacrylic acid (MAA) in water.

k_t(L mol^{-1}s^{-1})	T (°C)	pH	[M]	Remarks
Decrease from $\sim 10^7$ to 1.8×10^5 [a)]	50	N.N.	30%wt MAA	$k_t \downarrow$ with conversion P= 200 bar
Decrease from $\sim 6 \times 10^6$ to 10^5 [a)]	50	N.N.	60 %wt MAA	$k_t \downarrow$ with conversion P= 200 bar
$k_t = \frac{1}{\frac{1}{k_{t,SD}} + \frac{\exp(C_\eta W_{MAA}^0 p)}{k_{t,TD}} + C_{RD}(1-p)k_p}$ [a)] $k_{t,SD} = 7.9 \times 10^6$, $k_{t,TD} = 10^9$ $C_\eta = 39$, $C_{RD} = 77.5$ [a)]		N.N.	W_{MAA}^0	Change of k_t with conversion (p) for different initial fraction of MAA (W_{MAA}^0) weight
$k_{t,SD} = 3.53 \times 10^7 \pm 8.47 \times 10^6$ [b)] $k_{t,TD} = 2.79 \times 10^8 \pm 4.52 \times 10^8$ [b)] $C_\eta = 10.9 \pm 4.72$ [b)] $C_{RD} = 517 \pm 212$ [b)]	50	N.N.		Same expression for change of k_t with p used in [a)] was considered

[a)] Beuermann *et al.*, 2008; **[b)]** Buback *et al.*, 2008b;

6.4 Results and Discussion

6.4.1 Simulation Results Using the Proposed Kinetic Approach

Figure 6.17 depicts the predicted dynamics of the weight fraction of gel (w_g) and monomer conversion (p) during a batch SAP production. Simulations were carried out considering the synthesis with a trifunctional crosslinker (TMPTA used as case study) at an initial mole fraction in the monomer mixture $y_C = 0.0025$ % (around the lower limit used in practice (Arriola *et al.*, 2007)). In these simulations three different values of the rate coefficient for the homopropagation of acrylic acid (k_{p1}) were considered, in a range that is plausible for this

monomer in these particular conditions (see Table 6.3 and Li and Schork, 2006). An initial mole ratio between initiator and monomer $y_I = 0.3\ \%$ and a rate coefficient for initiator unimolecular decomposition $k_d = 8.4 \times 10^{-6} s^{-1}$ valid for V50 (2,2′-Azobis(2-methylpropionamidine)dihydrochloride) at $T = 50$ °C have been assumed. Initial volumetric fraction of acrylic acid in the aqueous phase was set as $V_{AA} = 15\ \%$. The reactivity ratio for acrylic acid/TMPTA was considered to be $r_1 = k_{p1}/k_{p2} = 0.77$ as previously measured for this chemical system in similar conditions (Arriola *et al*., 2007). Note that, for the sake of simplicity, polymer radicals derived from the two monomers were not distinguished in the present analysis and by consequence $r_2 = k_{p2}/k_{p1} = 1/r_1$ corresponds to an ideal copolymerisation (note that the reactivity ratio for TMPTA is very difficult to measure (Arriola *et al*., 2007)). The reactivity of pendant double bonds is another parameter of a very difficult experimental estimation (Arriola, *et al*., 2007).

In simulations presented in Figure 6.17 the value $r^* = k_{p3}/k_{p1} = 1$ was chosen, which corresponds to an equal reactivity of PDB and acrylic acid (under these conditions, reactivity of PDBs is higher than individual double bonds of TMPTA: $r_{PDB} = k_{p3}/(k_{p2}/3) = 2.31$. To the termination rate coefficient was assigned the value $k_t = 5 \times 10^7 \mathrm{Lmol^{-1}s^{-1}}$ which is also in the range of the values considered in other works concerning also the kinetics of acrylic acid polymerisation (Li and Schork, 2006). Equality between initiation and propagation rate coefficients ($k_{pj} = k_{Ij}$) was also considered along this work. Results presented in Figure 6.17 show the important impact of the rate coefficient of acrylic acid (i.e. temperature, pH, concentration, ionic strength) in gel formation during superabsorbent hydrogels production. With higher values of k_{p1}, the primary chain length increases with concomitant higher gel formation. Figure 6.18 shows the predicted dynamics of the weight average molecular weight ($\bar{M}_w$) for the the same systems described in Figure 6.17.

The ability of the present method to predict polymer properties before and after gelation becomes here evident. Besides MWD and its averages, *z*-average radius of gyration (Θ state) and sequences distributions can also be computed before and after gelation as before shown (Costa and Dias, 1994, 2003, 2005, 2006 and 2007; Dias and Costa, 2003, 2005a, 2005b, 2006, 2007 and 2010; Gonçalves *et al*., 2007, 2010a, 2010b, 2010c, 2010d and 2011a; Trigo *et al*., 2008). The effect of the reactivity of pendant double bonds on the predicted dynamics of the weight fraction of gel (w_g) and monomer conversion (p) for batch SAP production using a trifunctional crosslinker is presented in Figure 6.19. The following parameters

(according to the above discussion) were now fixed: $y_C = 0.0025$ %, $y_I = 0.3$ %, $k_d = 8.4 \times 10^{-6} s^{-1}$, $V_{AA} = 15$ %, $r_1 = 0.77$, $r_2 = 1/r_1$, $k_{p1} = 20000$ L mol^{-1} s^{-1}, $k_t = 5 \times 10^7$ L mol^{-1}s^{-1}.

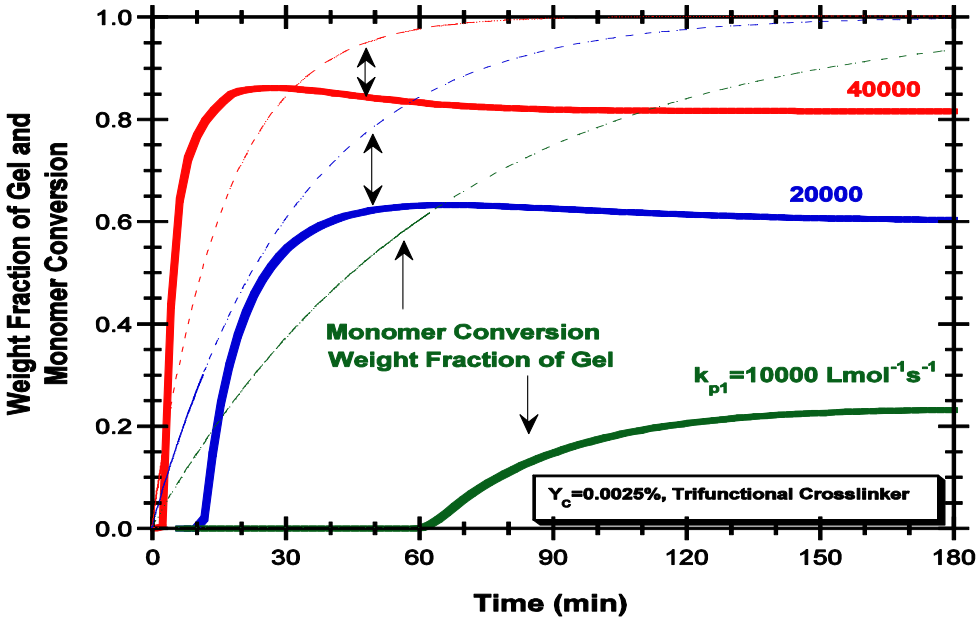

Figure 6.17. Predicted dynamics of the weight fraction of gel and monomer conversion in batch SAP production using a trifunctional crosslinker with $y_C = 0.0025$ %.

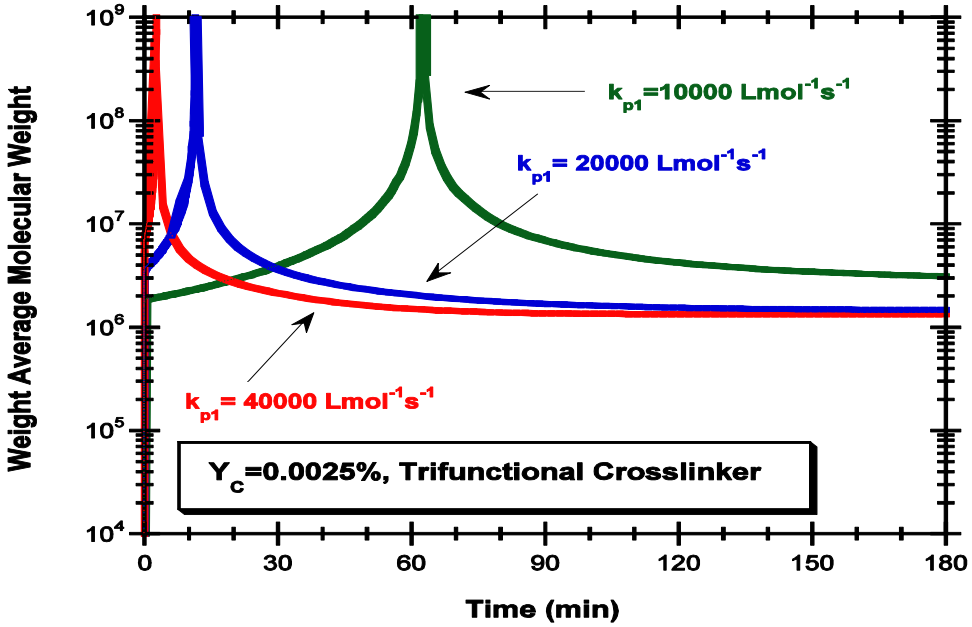

Figure 6.18. Predicted dynamics of the weight average molecular weight in batch SAP production using a trifunctional crosslinker with $y_C = 0.0025$ %.

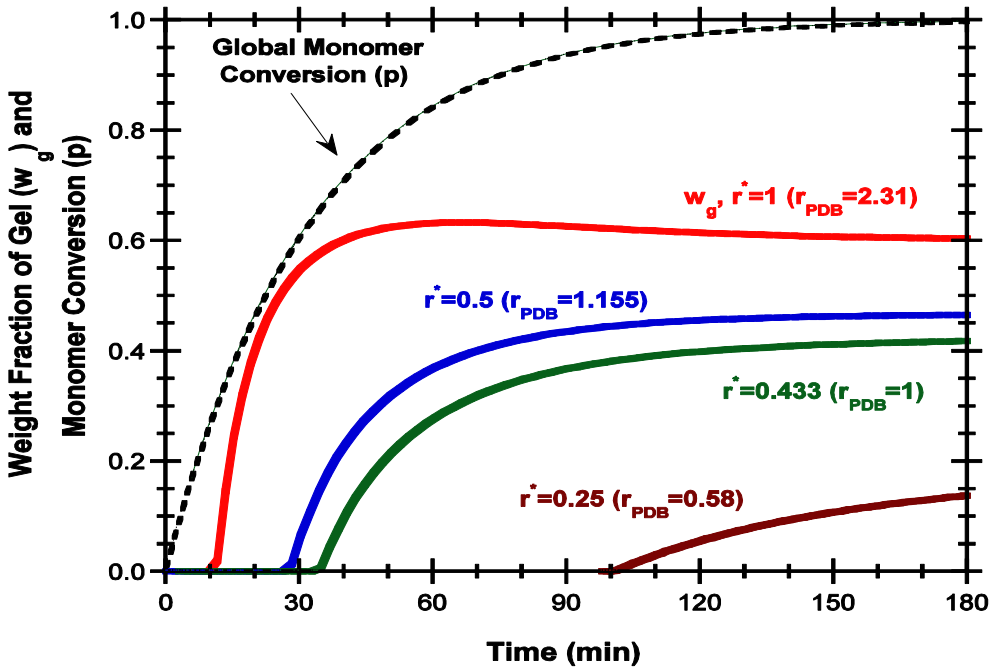

Figure 6.19. Prediction dynamics of the weight fraction of gel and monomer conversion in batch SAP production using a trifunctional crosslinker with $y_C = 0.0025$ %.

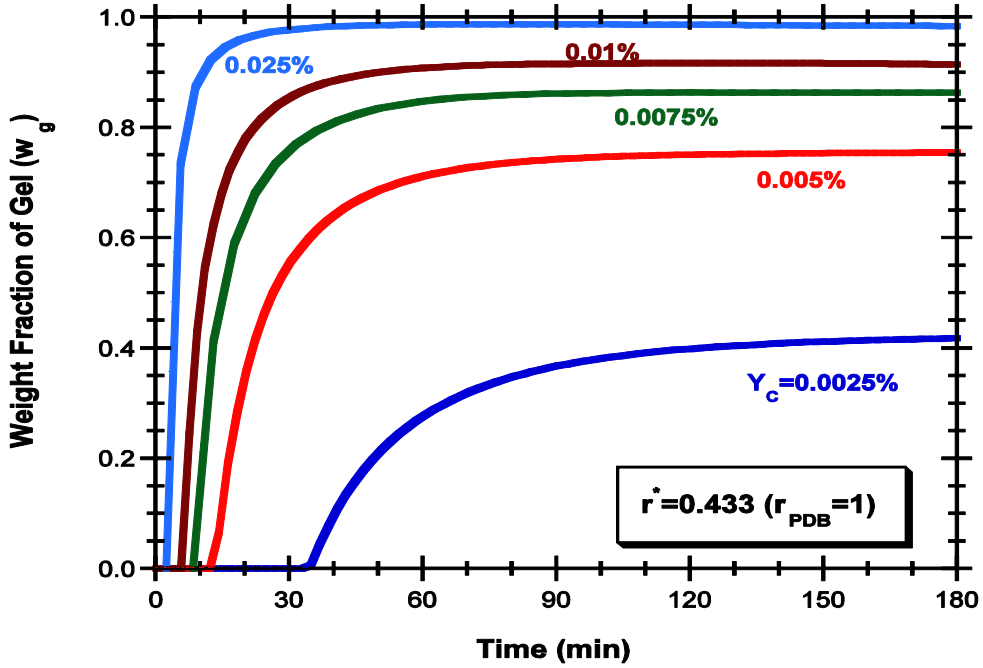

Figure 6.20. Predicted dynamics of the weight fraction of gel in batch SAP production considering different initial mole fraction of trifunctional crosslinker (y_C).

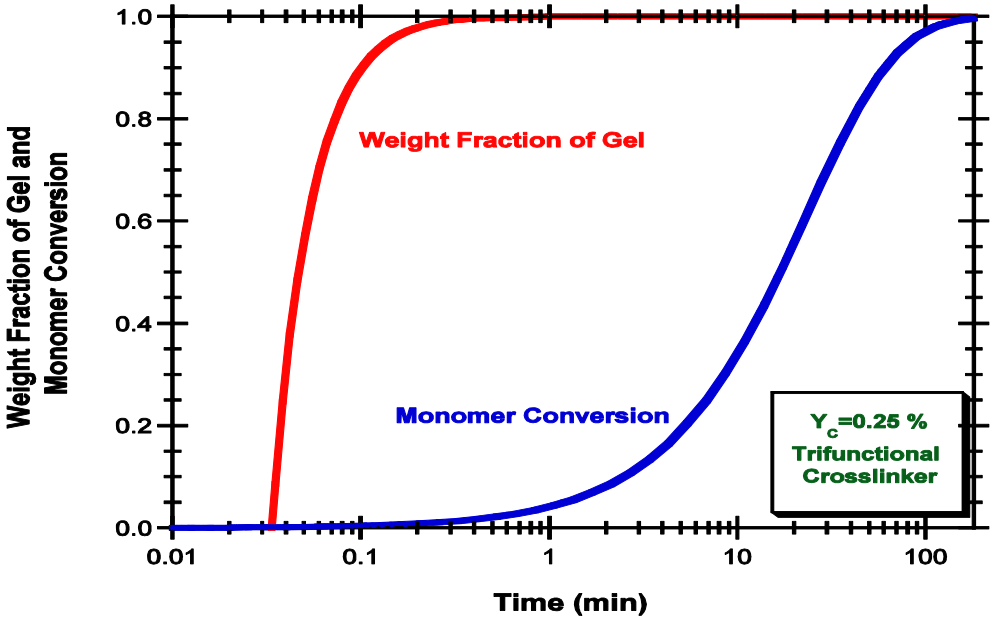

Figure 6.21. Predicted time evolution of monomer conversion and weight gel fraction during acrylic acid/triacrylate copolymerisation with $y_C = 0.25$ %. Other parameters considered in the simulations: $y_I = 0.3$ %, $k_d = 8.4 \times 10^{-6} \mathrm{s}^{-1}$ (T=50 °C for V50), $V_{AA} = 15$ %, $r_1 = 1/3$, $r_2 = 3$, $k_{p1} = 30000$ L mol^{-1} s^{-1}, $k_t = 5 \times 10^7$ L mol^{-1}s^{-1}, $r^* = 1$ ($r_{PDB} = 1$).

Under these conditions, the reactivity of pendant double bonds (quantified by the parameter r* or equivalently by r_{PDB}) has a huge effect on the dynamics of gel formation. As expected, low gel content is predicted if the reactivity of PDBs is much lower than for the initial double bonds of the crosslinker (e.g. $r_{PDB} = 0.58$) and increases with the value of this parameter. Due to the low content of crosslinker in the polymerisation system, the overall monomer conversion is almost insensitive to this parameter. Simulations like those presented in Figure 6.19 can be used to estimate the reactivity of PDBs using experimental measurements of the dynamics of gel formation.

The effect of the initial mole fraction of crosslinker on the dynamics of the weight fraction of gel is illustrated in Figure 6.20. This parameter can be readily used to manipulate the properties of the final products, as depicted in that Figure. Simulations for y_C ranging from the lower limit used in practice (around 0.0025 %) to ten times this value show the change of w_g from around 0.4 to 1. Remaining parameters fixed in these simulations are: $y_I = 0.3$ %, $k_d = 8.4 \times 10^{-6} \mathrm{s}^{-1}$ (T=50 °C for V50), $V_{AA} = 15$ %, $r_1 = 0.77$, $r_2 = 1/r_1$, $k_{p1} = 20000$ L mol^{-1} s^{-1}, $k_t = 5 \times 10^7$ L mol^{-1}s^{-1}, $r^* = 0.433$ ($r_{PDB} = 1$). Operation with the higher limit of y_C (around 0.25 %) is illustrated in Figure 6.21. Under these conditions gelation is

predicted to occur within some hundredths of seconds and the weight fraction of gel in the polymer rises very fast to around 1. However, in practice, polymerisation must be prolonged in order to reach high monomer conversion.

The ability to numerical calculate the characteristics equations presented in Gonçalves *et al*., 2011b is a crucial step for the prediction of gel properties using generating functions of population balance equations, as proposed by Dias and Costa in the same paper (Gonçalves *et al*., 2011b). Development of very sharp numerical boundary layers is a special feature of these problems making very difficult the treatment of the associated two point boundary value problems (TPBVP), as discussed before (Costa and Dias, 2003 and 2005; Dias and Costa, 2003 and 2005b). These aspects are illustrated for the present chemical systems in Figure 6.22 and Figure 6.23. Note that the solution of this kind of problems in the context of this theory plays a role equivalent to the calculation of the extinction probabilities in the framework of the Theory of the Branching Processes presented in Gonçalves *et al*., 2011b.

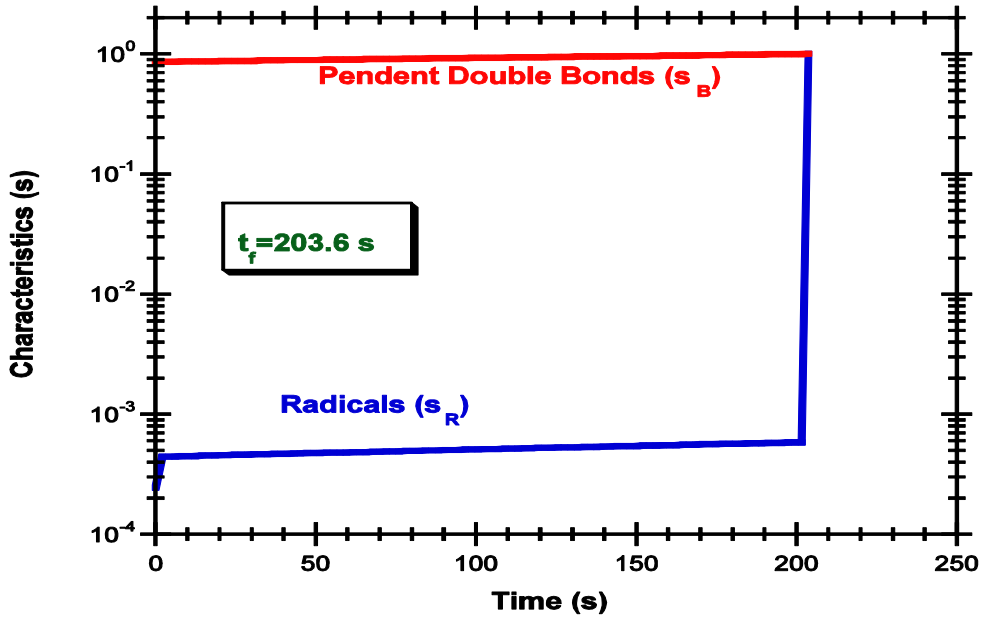

Figure 6.22. Numerical solution of the characteristics (vector s) correspondent to the SAP synthesis using the conditions described for Figure 6.21. For illustration purposes the chosen polymerisation time was $t = 203.6$ s.

Another possible way to manipulate the dynamics of gelation is the choice of the functionality of the crosslinker, as depicted in Figure 6.24. Three different synthesis processes, correspondent to the use of crosslinkers with different functionalities (2, 3 and 4) by

considering N,N′-methylenebisacrylamide (α = 2), trimethylolpropane triacrylate (α = 3) and tetraallyloxyethane (α = 4) as case studies, were simulated with the following parameters: $y_C = 0.005$ %, $y_I = 0.3$ %, $k_d = 8.4 \times 10^{-6}\text{s}^{-1}$ (T=50 °C for V50), $V_{AA} = 15$ %, $k_{p1} = 20000$ Lmol^{-1}s^{-1}, $r_1 = 0.77$, $r_2 = 1/r_1$, $r^* = r_2/\alpha$ ($r_{PDB} = 1$), $k_t = 5 \times 10^7$ Lmol^{-1}s^{-1}. As expected, in the same conditions, the use of a crosslinker with higher functionally generates a higher amount of gel at a much higher pace. Substitution effects changing the reactivities of the different pendant double bonds of the crosslinker and possible low solubility of the crosslinker in the aqueous phase are some issues complicating the simple analysis here performed.

A numerical algorithm to obtain the solutions of the expressions presented by Dias and Costa (Gonçalves *et al.*, 2011b) was implemented in order to be able to compare the predictions of TBP with those of the kinetic modelling developed in this chapter, as shown in Figure 6.25. Besides the initial mole fraction of double bonds belonging to the crosslinker (which is related with y_C by $y_D = 2y_C/(1 + y_C)$), parameters needed in TBP simulations are the fraction of termination by coupling (fixed in $\alpha_{tc} = 1$ as in kinetic simulations) and the probability of propagation, γ. Calculations have shown that, besides y_C, the parameter γ also has a strong effect on the gelation process.

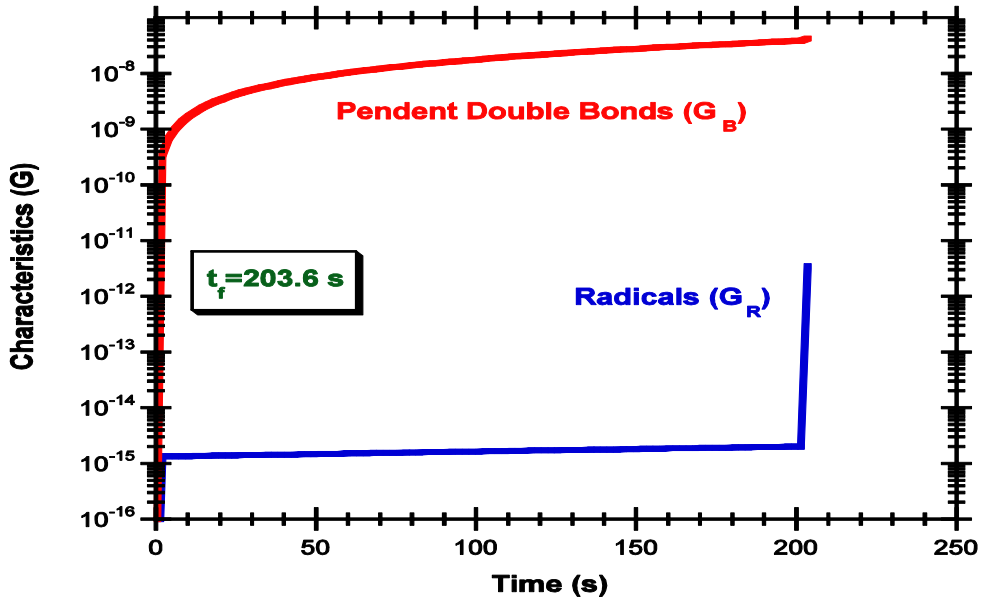

Figure 6.23. Numerical solution of the characteristics (vector G) correspondent to the SAP synthesis using the conditions described for Figure 6.21. For illustration purposes the chosen polymerisation time was t = 203.6 s.

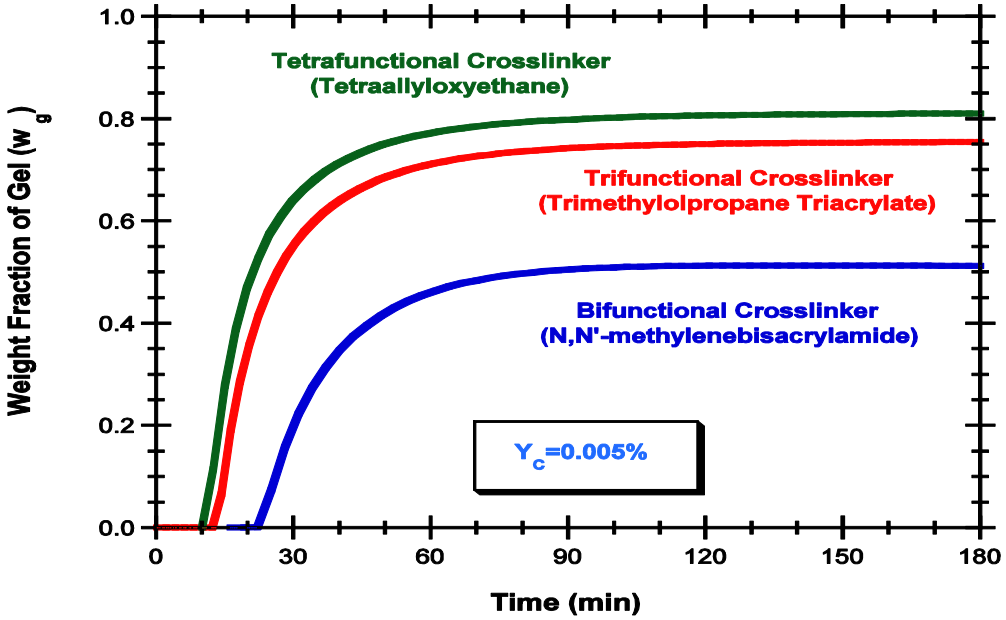

Figure 6.24. Predicted dynamics of the weight fraction of gel (w_g) in batch SAP production considering three different synthesis processes correspondent to the use of three crosslinkers with different functionalities (bi-, tri- and tetra-functional, considering N,N′-methylenebisacrylamide ($\alpha = 2$), trimethylolpropane triacrylate ($\alpha = 3$) and tetraallyloxyethane ($\alpha = 4$) as case studies).

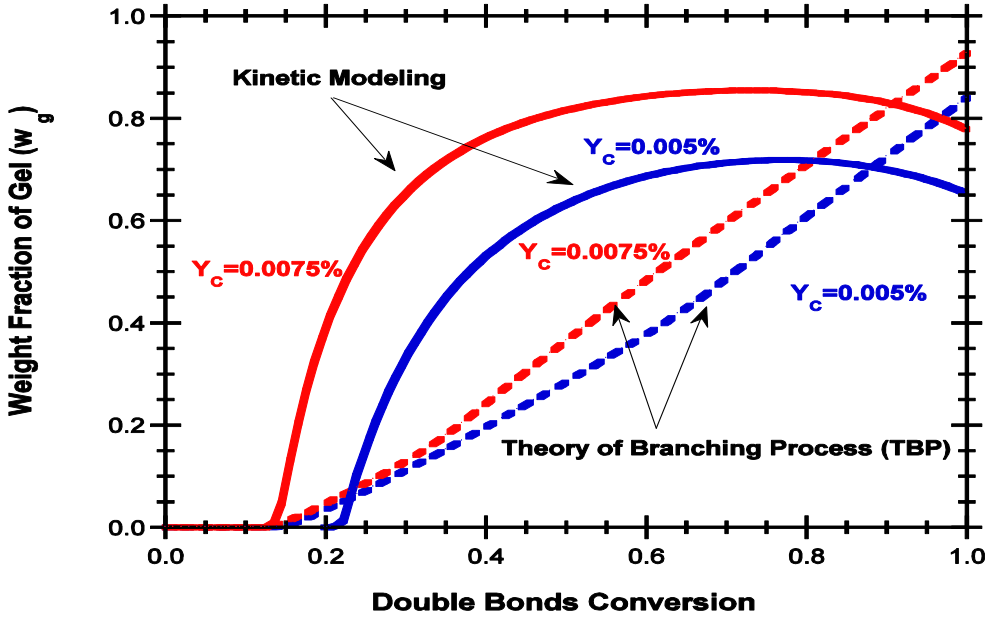

Figure 6.25. Comparison between the predictions of the Theory of Branching Process (TBP) and the proposed kinetic approach for the weight fraction of gel in the copolymerisation of a vinyl monomer with a bifunctional crosslinker (two initial compositions were considered using AA + MBAm as case study).

The simulation results with TBP presented in that same Figure 6.25 were performed with $\alpha_{tc} = 1$ and $\gamma = 0.9999$, which is an average value correspondent to kinetic calculations. Note that this parameter is not strictly constant during the polymerisation. The rest of parameters considered in the simulations with the kinetic approach were: $y_I = 0.3$ %, $k_d = 8.4 \times 10^{-6} \mathrm{s}^{-1}$ (T=50 °C for V50), $V_{AA} = 15$ %, $k_{p1} = 20000$ $\mathrm{Lmol^{-1}s^{-1}}$, $r_1 = 0.5$, $r_2 = 1/r_1 = 2$, $r^* = r_2/2 = 1$ ($r_{PDB} = 1$), $k_t = 5 \times 10^7 \mathrm{Lmol^{-1}s^{-1}}$ (with $\alpha_{tc} = 1$).

The huge differences between predictions presented in Figure 6.25 illustrate the dissimilitudes between the two approaches. As the present processes are kinetic controlled, the direct application of the classical TBP seems to be incorrect and more elaborated models based on this theory must be developed in order to be valid (Dotson, 1992).

6.4.2 Experimental Results Obtained with *in-line* FTIR-ATR Method

A few kinetic parameters (e.g. vinyl monomer propagation) needed for using the above described kinetic approach were estimated using *in-line* FTIR-ATR monitoring of solution aqueous polymerisation, as illustrated with some examples in Figures 6.26-6.29. These results were obtained using the FTIR-ATR procedures detailed in previous chapters and in appendix A). In Figures 6.26 and 6.27 fast exothermic reactions and high viscosity polymerisation media are observed even when operating at a high dilution. Good stirring and efficient heat dissipation becomes difficult and the development of transient temperature histories are possible.

These issues can be circumvented using inverse suspension polymerisation. Besides nearly isothermal temperature histories along the polymerisation, good stirring is kept even after gelation. The dynamics of crosslinking can thus be analysed in a single pot reaction and easily handled hydrogel beads are produced at the end. Figures 6.28 and 6.29 shows the *in-line* FTIR-ATR estimated monomer conversion for aqueous solution polymerisations of AA and AAM, respectively. Figure 6.28 shows an inhibition time of around 20 min followed by a fast exothermic reaction. Difficulties in heat dissipation and high viscosity of the medium affect the quality of these measurements. The 1420 $\mathrm{cm^{-1}}$ peak arising from CH_2 deformation was used to estimate monomer conversion. The same peak was used to estimate the monomer conversion for acrylamide monomer in Figure 6.29.

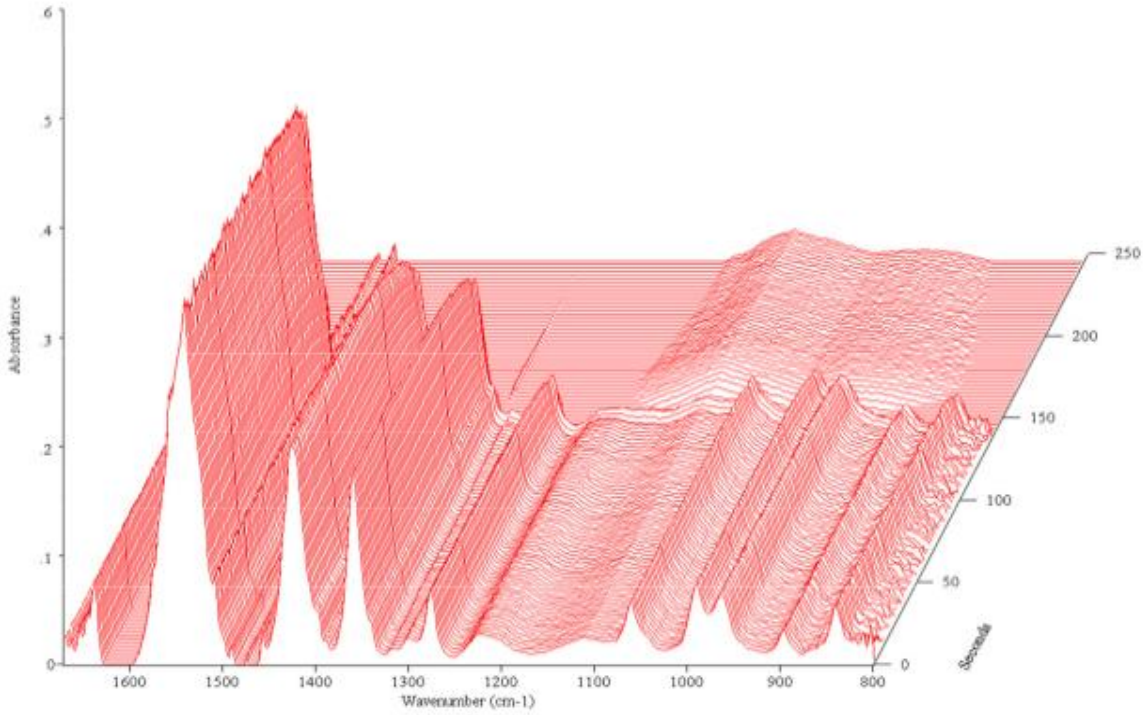

Figure 6.26. FTIR-ATR spectra observed during *in-line* monitoring of aqueous solution polymerisation of AA with 40 % concentration (v/v), 80 % neutralization, *T*=50 °C, initiation by V50 (mole ratio initiator/monomer= 0.2 %).

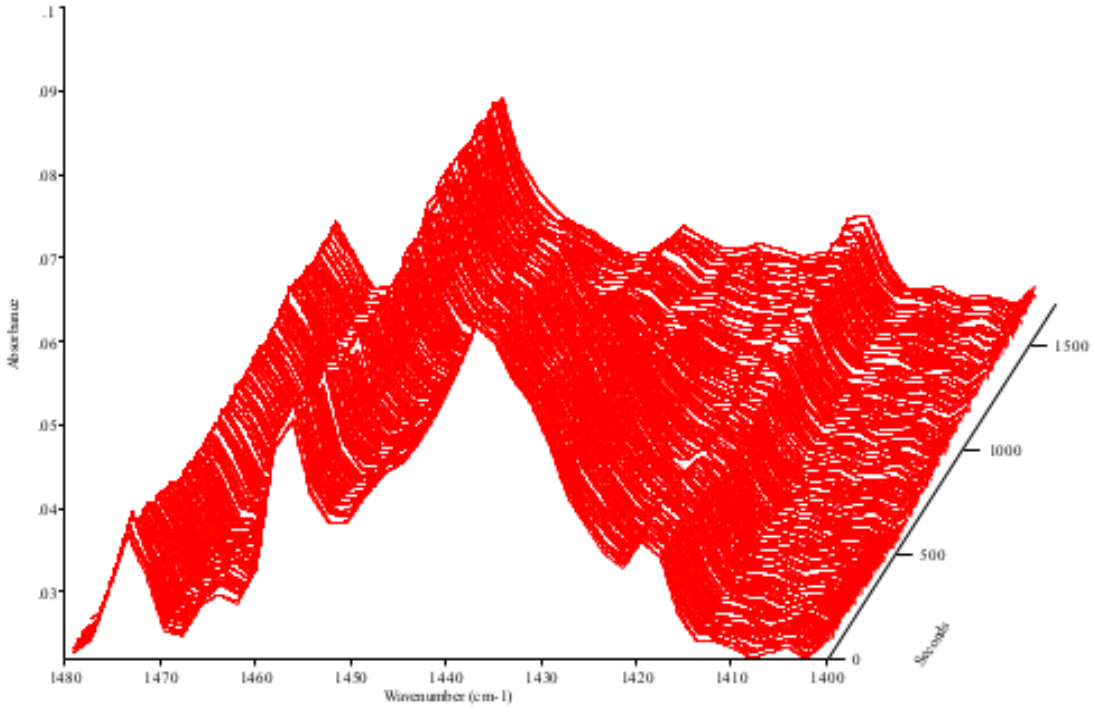

Figure 6.27. FTIR-ATR spectra observed during *in-line* monitoring of aqueous solution polymerisation of AAM polymerisation at 9 % (w/w), *T*= 20 °C, initiation by APS/TEMED (mole ratio initiator/monomer = 0.2 %).

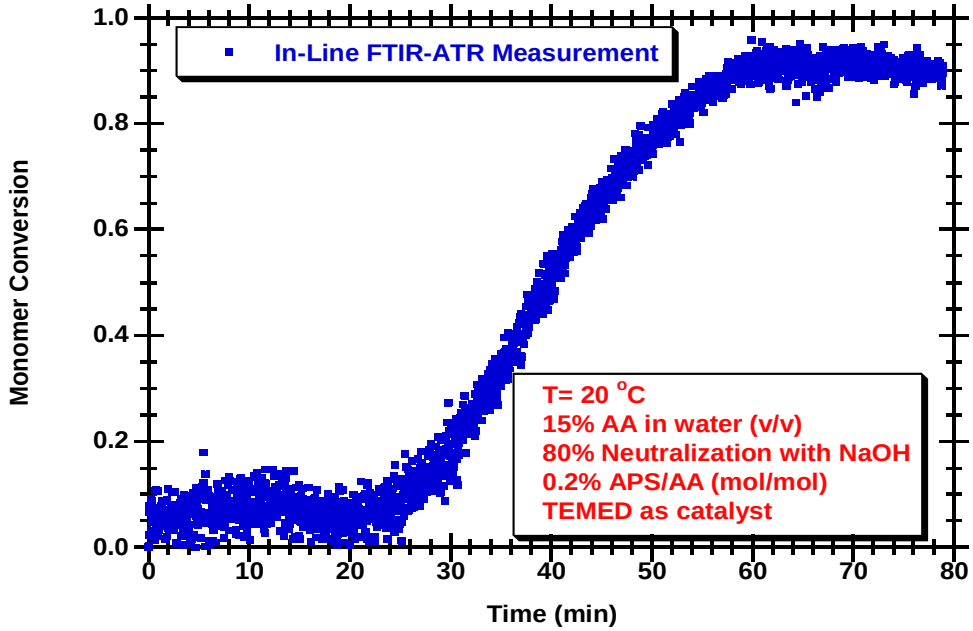

Figure 6.28. *In-line* FTIR-ATR estimated monomer conversion for aqueous monomer solution polymerisation of AA at 15 % concentration (v/v), 80% neutralization, *T*= 20 °C, initiation by 0.2 % APS/TEMED.

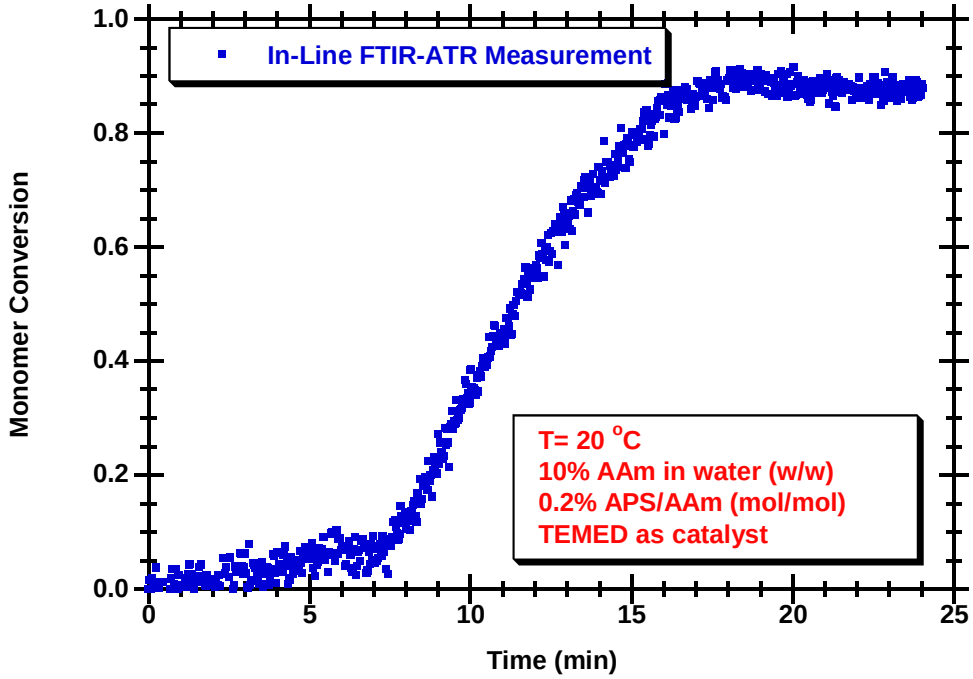

Figure 6.29. *In-line* FTIR-ATR estimated monomer conversion for aqueous monomer solution polymerisation of AAM at 9 % concentration (w/w), *T*=20 °C, initiation by 0.2 % APS/TEMED.

In Figure 6.30 are compared the experimental results of representative experiments performed in this context with predictions obtained using the kinetic model developed in this work. Only a noisy trend of the monomer conversion could be obtained with the *in-line* FTIR-ATR monitoring technique. This noise is probably due to the effect of the reactor agitation which causes the misalignment of the FTIR-ATR apparatus. Nevertheless, the experimental trend for monomer conversion presented in Figure 6.30 seems to confirm the reasonableness of the kinetics used.

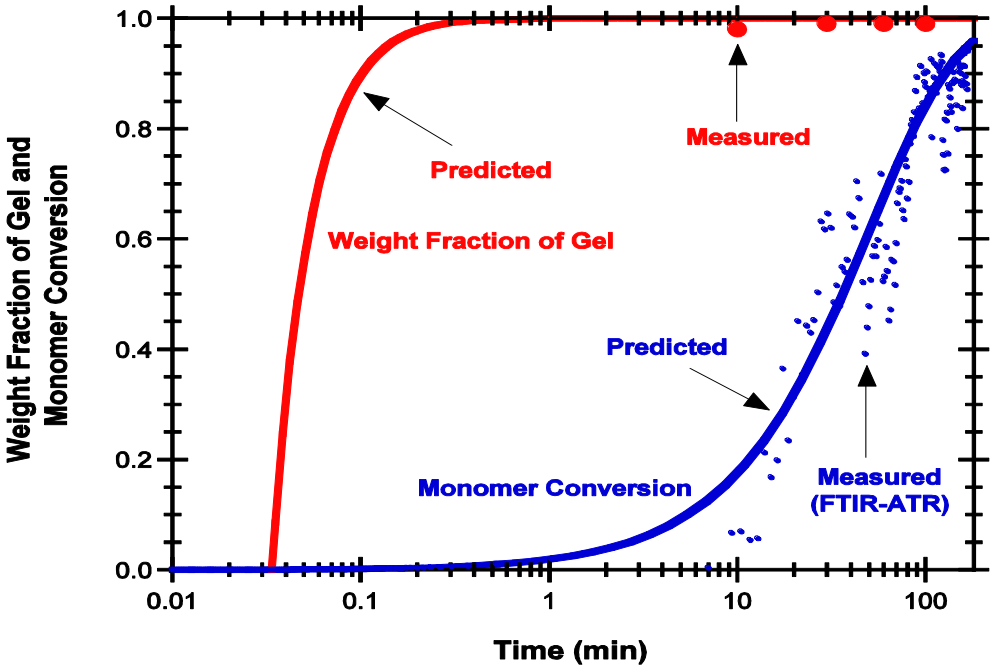

Figure 6.30. Comparison between experimentally observed and predicted dynamics of monomer conversion and weight fraction of gel during the homopolymerisation of AA and its crosslinking with TMPTA at T = 50 °C. Homopolymerisation of AA was performed in water solution with $V_{AA} = 15$ % and $y_I = 0.1$ %. Crosslinking copolymerisation was performed in inverse suspension considering similar composition of the aqueous phase and $y_C = 0.25$ %.

Dynamics of the weight fraction of gel was also experimentally measured by collecting from the reactor samples at different polymerisation time. Insoluble (gel) mass fraction in these samples was later measured and, in all samples, a fraction of gel close to 1 was observed, as presented in Figure 6.30. In the synthesis of SAP materials performed in this work, the initial mole fraction of crosslinker (TMPTA) used is close to the upper limit considered for practical applications ($y_C = 0.25$ %). In these conditions a very fast gelation with gel weight fraction w_g close to 1 after around one minute of polymerisation is predicted by the kinetic model and this

behaviour was experimentally confirmed. Main features of this polymerisation system could therefore be captured by the simple kinetic model here considered. Other parameters considered in the simulations: $k_d = 8.4 \times 10^{-6}\text{s}^{-1}$ (T=50 °C for V50), $k_{p1} = 30000$ Lmol^{-1}s^{-1}, $r_1 = 0.77$, $r_2 = 1/r_1$, $r^* = 0.433$ ($r_{PDB} = 1$), $k_t = 5 \times 10^7$Lmol^{-1}s^{-1}.

A comparison between the predictions of the above described kinetic models and experimental measurements are depicted in Figures 6.31 and 6.32. Good agreement between predictions/measurements could only be obtained if a very low reactivity of the pendant double bonds of the crosslinker is considered. In Figure 6.31 a good agreement between predicted and measured molecular weights is observed if a low reactivity of PDB is considered ($r_{PDB} = k_{p4}/k_{p1} = 0.1$). In Figure 6.32 it was not possible to have a good description of the dynamics of weight fraction of gel for the same parameters. These discrepancies are likely to arise from the heterogeneity of network formation process, highlighting the effects of intramolecular cyclization, phase separation during the formation of the hydrogel or excluded volume effects, as previously pointed out (Dušek, 1996).

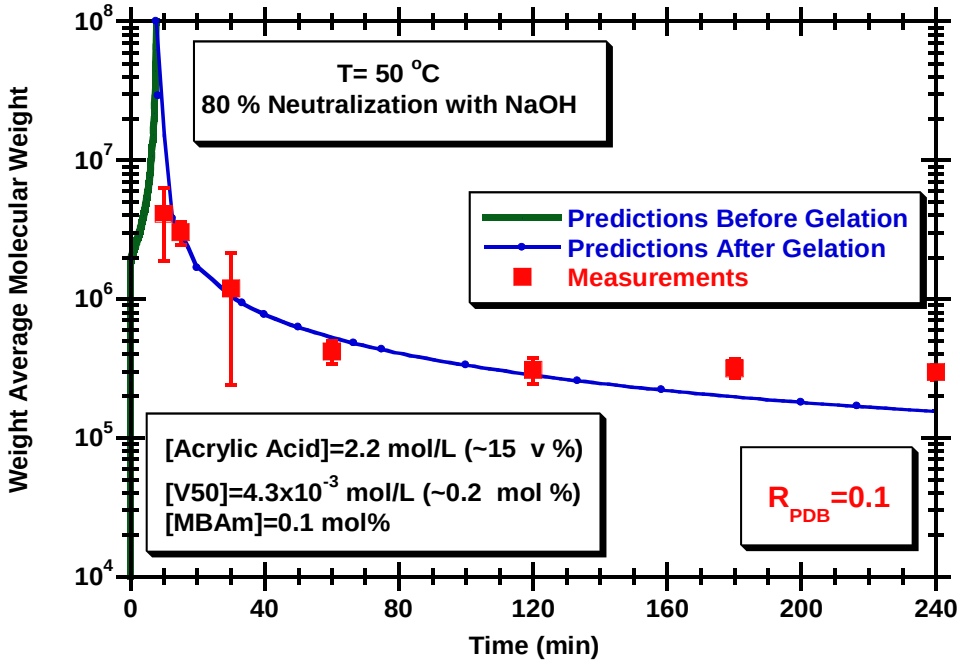

Figure 6.31. Predicted and measured time evolution of the molecular weight of the soluble phase during inverse suspension hydrogels formation. Synthesis of AA/MBAm superabsorbent hydrogel was here considered for illustration purposes.

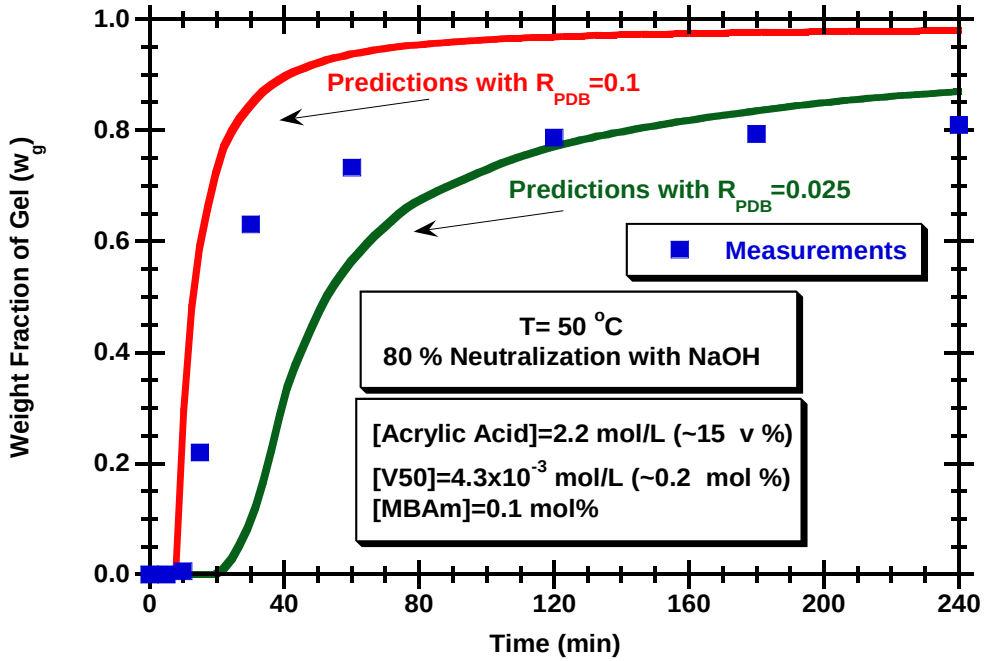

Figure 6.32. Predicted and measured time evolution of the weight fraction of gel for the same system described in Figure 6.31.

6.4.3 Characterization of the Obtained Hydrogels

The kinetics of polymerisation has a huge impact on the dynamics of gel formation. Moreover with the same chemical system (e.g. polymerisation involving AA or MAA), besides temperature or initial concentrations (monomers, initiators, etc.), the pH of the reaction media has an enormous influence on the dynamics of crosslinking process (Gonçalves *et al.*, 2011b). Measurement of kinetics of polymerisation at different operation conditions is thereafter a key issue in the study of hydrogel synthesis. The typical synthesis conditions of FRP of these hydrogels are in Table 7.1 of chapter 7.

A relation between the synthesis conditions and hydrogel performances can be assessed as depicted in Figures 6.33-6.36. Different pH-sensitive (Figures 6.33 and 6.35), temperature-sensitive (Figure 6.34) and superabsorbent hydrogels (6.36) were tested. Monomer chemical structures, initial proportion between monomers, initial amount of crosslinker, degree of neutralization (e.g. with AA/MAA) and polymerisation temperature are some parameters which were identified to have an important influence on the materials swelling ratio. Thus in Figure 6.33 is shown the usefulness of hydrogels as pH sensitive materials (e.g. drug delivery applications). The initial composition of the polymerisation system has an impact on the

performance of the stimuli-responsive gel beads. Figure 6.34 highlight the high response to temperature of PNIPA hydrogel in comparison with a non-temperature-responsive hydrogel (PDMA). In figure 6.35 can be observed the stimulation by the pH of the environmental media, namely when comparing acidic media with basic media. A swelling increase by around 8 times triggered by pH change from 1.2 to 7.5 was measured for this hydrogel. Equilibrium swelling ratio of around 900 can be reached with these particular synthesis conditions as presented in Figure 6.36.

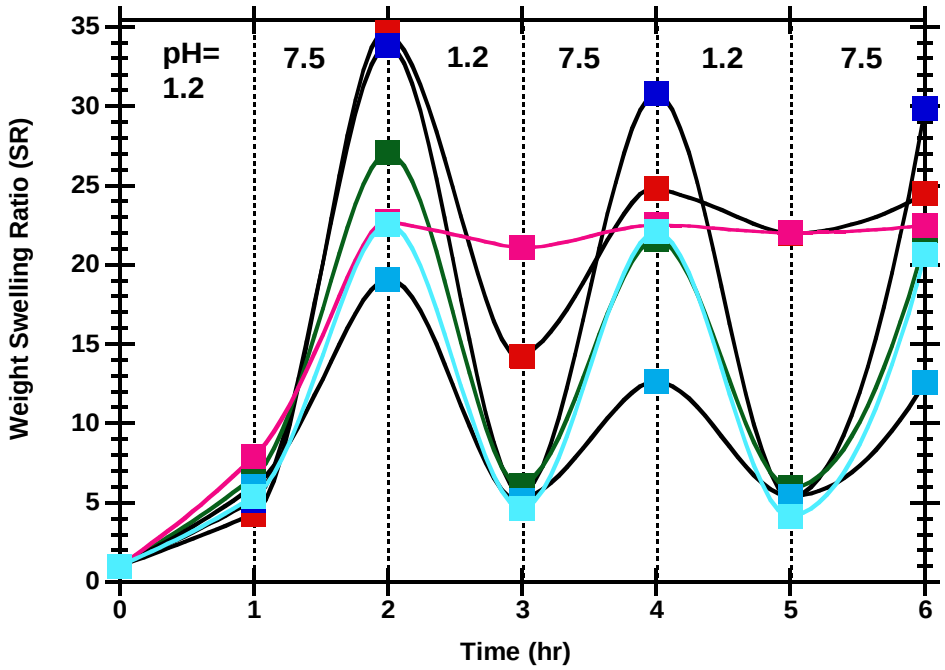

Figure 6.33. Repeated swelling (pH=7.5 and collapsing pH=1.2) of inverse suspension synthesized AA/AAM/MBAm hydrogels.

Actually the issue of network heterogeneity is important in different chemical systems and several different experimental techniques have been used to try to elucidate this phenomenon (Dušek, 1996; Duchet and Pascault, 2003). Analysis by SEM is a useful technique here illustrated in Figure 6.37. Despite the care to avoid artefacts from interaction with electron beam (Dušek, 1996; Duchet and Pascault, 2003), formation of particle populations with very different sizes are discernible (at micro- and nano-scales), leading to believe into the heterogeneity of the formation process of the hydrogels here studied.

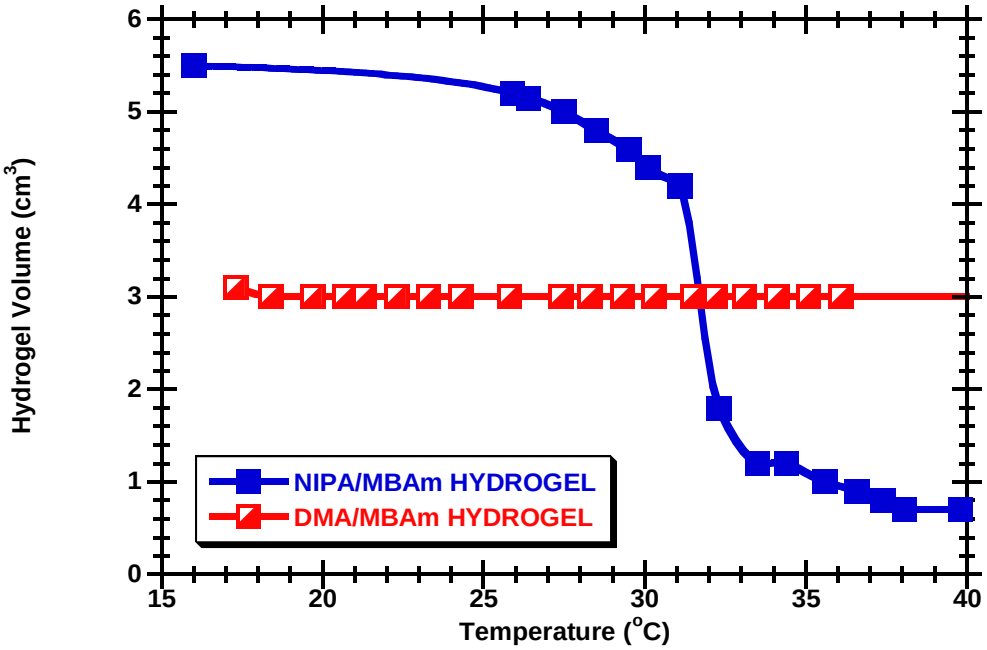

Figure 6.34. Observed volume change of NIPA/MBAm and DMA/MBAm inverse suspension synthesized hydrogels stimulated by temperature.

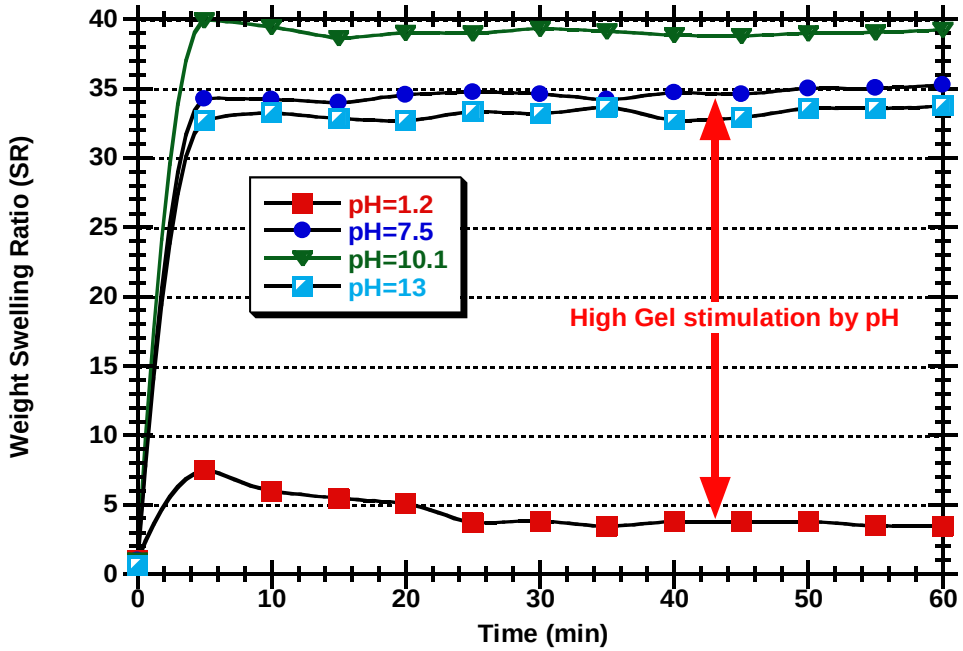

Figure 6.35. Measured dynamics of swelling of an inverse suspension synthesized pH-responsive hydrogel (AA/AAM/MBAm) in buffer solutions of different values of pH.

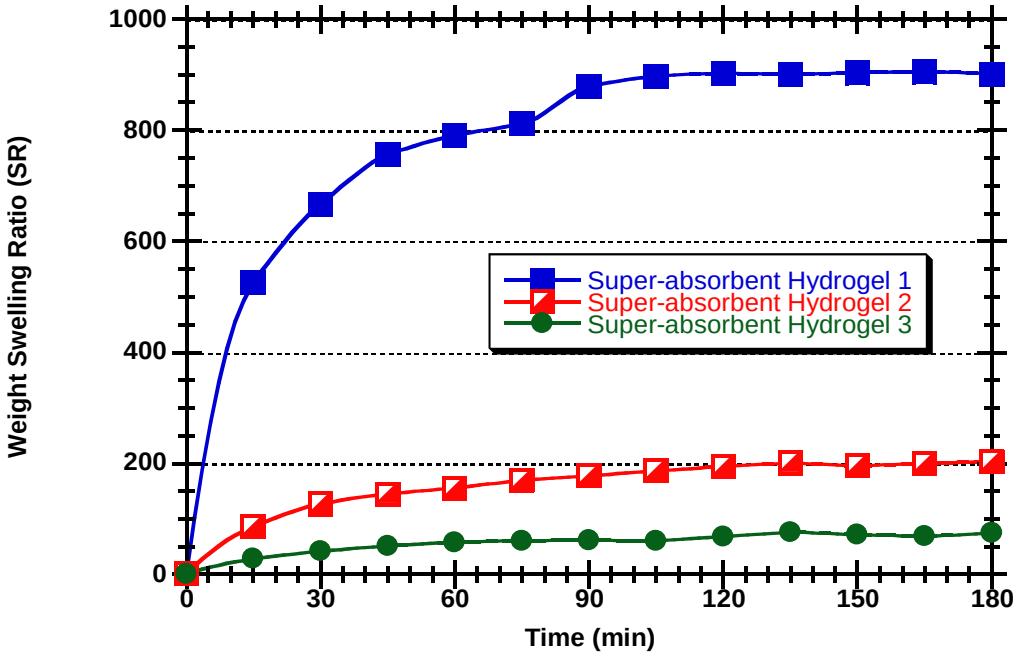

Figure 6.36. Examples of the measured swelling kinetics of different superabsorbent hydrogels showing the effect of synthesis conditions on the materials performance.

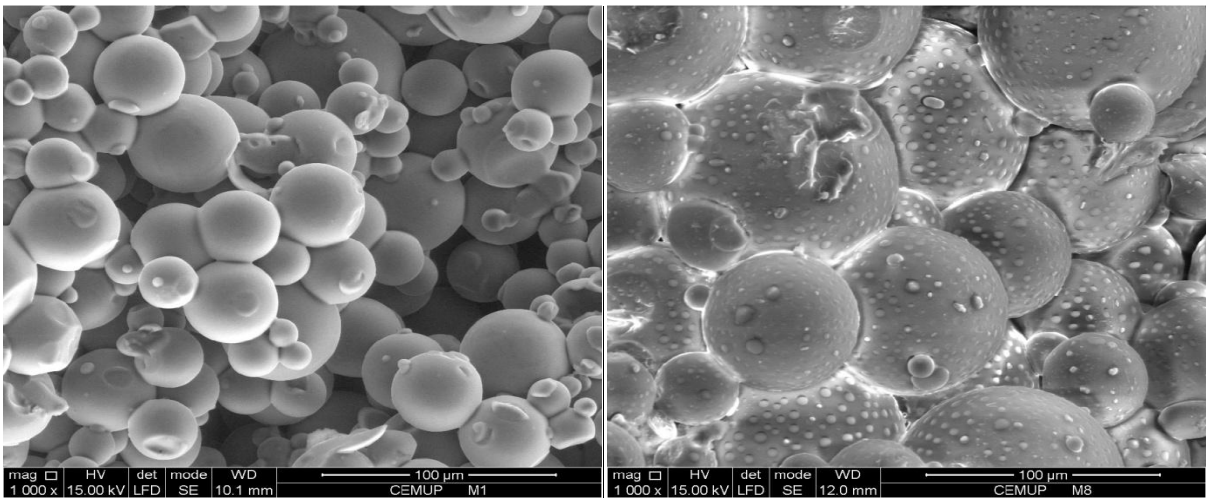

(a) (b)

Figure 6.37. Gel micrographs of inverse suspension synthesized hydrogel beads. (a) AA/MBAm hydrogel. (b) DMA/MBAm hydrogel.

6.5 Conclusions

Comparison between predictions of the proposed kinetic method and measurements performed in the acrylic acid/trimethylolpropane triacrylate copolymerisation show that this simple model is able to capture the main features of this polymerisation system. The

dynamics of hydrogel formation by terpolymerisation of (AA/AAM, MBAm) was investigated through their production in a batch reactor operating with inverse-suspension. A general kinetic approach was applied to the modelling studies concerning the synthesis of these materials. Comparison of experimental data with predictions of the developed kinetic models put into evidence the likely heterogeneity of the network formation process (e.g. loop formation reactions and phase segregation). Additional experimental work with a much lower initial mole fraction of crosslinker (and also different kinds of crosslinkers) should be performed in order to confirm the good foundations of this theory. Estimates of the reactivity of pendant double bonds of the crosslinkers can also eventually be obtained by comparison of these new experimental results with model predictions.

CHAPTER 7

INVERSE-SUSPENSION REVERSIBLE ADDITION-FRAGMENTATION RADICAL POLYMERISATION LEADING TO HYDROGELS FORMATION

Abstract. Temperature and pH stimuli–responsive hydrogel particles were synthesized using inverse-suspension polymerisation (with a few runs also carried out with solution polymerisation) in a batch stirred reactor. Different water soluble co-monomers were present in the initial mixture (e.g. N-isopropylacrylamide and acrylic acid) as well as crosslinkers with different functionalities. Commercially available RAFT agents 4-cyano-4-phenyl carbonothioylthio-pentanoic acid (CPA), 2-(dodecylthiocarbonothioylthio)-2-methylpropionic acid (DDMAT) and cyanomethyl dodecyl trithiocarbonate (CDT) were alternatively used. Thus along the experimental program were changed/assessed the following variables:

- Parameters changed:
    - Kind and/or monomers concentrations.
    - Kind and/or crosslinker concentrations.
    - Kind and/or RAFT agents concentrations.
    - Kind of solvent and monomer dilution (aqueous system/organic solvent).
    - Initiation system.
    - Degree of neutralization.
- Products characterization:
    - SEC with a tetra-detector array (RI+UV+IVDP+LS) running with aqueous eluent allowing the determination of average molecular weights, conversion, *z*-average radius of gyration and viscosity.
    - *In-line* FTIR-ATR for estimation some kinetic parameters.
    - Swelling ratio changes of hydrogels with pH and/or temperature.
    - Drug delivery testing of hydrogels triggered by environmental changes.

This chapter is based on the following publication:

M.A.D. Gonçalves, V.D. Pinto, R.A.S. Costa, R.C.S. Dias, J.C. Hernández-Ortiz, M.R.P.F.N. Costa, *Macromol. Symp*. 333 (2013) 41-54.

7.1 Introduction

Hydrogels have been extensively studied in the last decades due to their potential new application in biotechnology and biomedicine (Bajpai *et al*., 2010; Galaev and Matiasson, 2008). Researches on this field are specially focused on the so called smart hydrogels (or stimuli responsive hydrogels) with properties sensitive to changes triggered by the environmental conditions. Generally speaking, formation of soluble networks and gels has been experimentally and theoretically studied since the beginning of polymer science. With systems involving vinyl/divinyl monomers, classical free radical polymerisation (FRP) mechanisms were mainly considered in these studies. A new importance was given to this subject with the advent of controlled radical polymerisation (CRP). New studies in this research area were driven by the possibility of improvement of networks and gels properties as a result of higher structural homogeneity. In fact, in the last years, the three main techniques, ATRP (Gao *et al*., 2007 and 2008; Gonçalves *et al.*, 2010a, 2010b, 2010c and 2010d; Yu *et al*., 2007), NMRP (Abrol *et al*., 1997; Gonçalves *et al*., 2010c, 2010d and 2013a; Hernández-Ortiz *et al*., 2012; Ide and Fukuda, 1997; Tuinman *et al*., 2006; Zetterlund *et al*., 2005) and RAFT (Yu *et al*., 2008 and 2009), were exploited aiming the production of advanced polymer networks belonging to different classes (organic or water compatible materials).

RAFT polymerisation can be used in a broad range of operation conditions and with different monomer classes, including water compatible monomers, these advantages are explored in this work by considering the inverse-suspension synthesis of different classes of stimuli-responsive hydrogels particles and using three different commercially available RAFT agents. FRP analysis of the same materials was also performed in order to highlight the differences between the two processes (namely in the observed kinetics of polymerisation). The use of different polymer characterization methods (such as SEC with tetra-detection and *in-line* FTIR monitoring) to study the formation of such networks is illustrated. The usefulness of such techniques to describe the crosslinking process is discussed. Final applications of the produced materials are also tested through drug delivery studies. Experimental results here reported aims to contribute to the sought linking between the production conditions of advanced materials and their structure/properties. Development of tools helping in the synthesis of tailored materials is the ultimate goal of this chapter.

7.2 Experimental Part

7.2.1 Materials

N-isopropylacrylamide (NIPA) of 99 % purity, N,N-dimethylacrylamide (DMA) of 99 % purity stabilized with 500 ppm monomethyl ether hydroquinone (MEHQ), 2-(dimethylamino)ethyl methacrylate (DMAEMA) of 98 % purity stabilized with 700-1000 ppm MEHQ, acrylic acid (AA) of 99 % purity stabilized with 180-200 ppm MEHQ, methacrylic acid (MAA) of 99 % purity stabilized with 250 ppm MEHQ, N,N'-methylenebisacrylamide (MBAm) of 99 % purity, ethylene glycol dimethacrylate (EGDMA) of 98 % purity stabilized with 90-110 ppm MEHQ, trimethylolpropane triacrylate (TMPTA) stabilized with 100 ppm methylethylhydroquinone, 1,1,2,2-tetraallyloxyethane (TAO), AIBN of 98 % purity, 2,2'-azobis(2-methylproprionamidine) dihydrochloride (V50) of 98 % purity, ammonium persulfate (APS) of 98 % purity and N,N,N',N'-tetramethylethylenediamine (TEMED) of 99 % purity were purchased from Sigma-Aldrich and used as received. The commercially available RAFT agents 2-(dodecylthiocarbonothioylthio)-2-methylpropionic acid (DDMAT) of 98 % purity, 4-cyano-4-(phenylcarbonothioylthio) pentanoic acid (CPA) (chemical structure in Figure 7.1) of 97 % purity and cyanomethyl dodecyl trithiocarbonate (CDT) of 98 % purity were also purchased from Sigma Aldrich and used as received. Dimethylformamide (DMF) of 99.5 % purity (Fisher Scientific), tetrahydrofuran (THF) of 99 % purity (Fisher Scientific) and cyclohexane of 99 % purity (Sigma Aldrich) were also used as received. A current grade of liquid paraffin was used when needed. Caffeine of 98.5 % purity, ibuprofen of 99 % purity, 5-fluorouracil (5Fu) of 98.5 % purity and isonicotinic acid hydrazide (isoniazid) of 99 % purity were purchased from Acros Organics and used as model chemicals in the drug release tests performed. Ibuprofen was also transformed in its sodium salt in order to increase the solubility of the drug in the aqueous solutions considered.

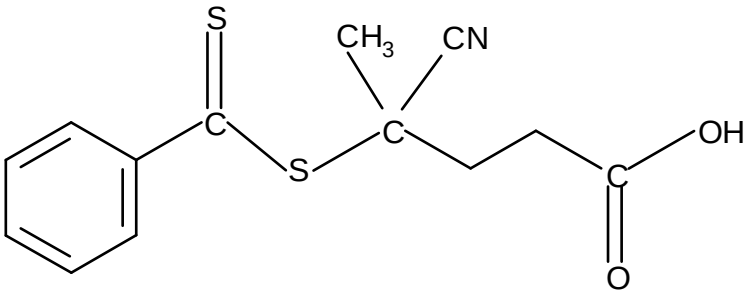

Figure 7.1. Chemical structure of CPA RAFT agent. In chapter 5 were presented the chemical structures of DDMAT and CDT.

7.2.2 Polymerisation Set-up

Hydrogels were synthesized in batch reactor using the inverse suspension process. Polymerisations were performed at 200 mL total volume scale with stable suspension formation using volumetric ratio aqueous/organic phases =1/5, 1 % (w/w) of surfactant (span 80) in the continuous phase and agitation speed at 300 rpm. Gel production at isothermal conditions and keeping a good stirring of the reaction vessel was possible using these conditions. When applicable, reactants were previously bubbled with argon that was also sweep in the reaction medium during the polymerisations in order to prevent inhibition by oxygen. At prescribed polymerisation times, reaction samples were collected from the reactor, quenched at low temperature in a solution containing hydroquinone to stop the reaction, and afterwards prepared for injection of the soluble polymer in the SEC system (Gonçalves *et al.*, 2013b). Morphology of the final gel beads, after products purification, was also characterized by SEM. Micro appearance of the produced materials is illustrated in Figure 7.2(a)-(d). In some cases, formation of fused material was observed due to post-treatment of the products like precipitation and drying.

Tables 7.1-7.3 describe the details of a set of experiments performed in this research. Different polymerisations were performed combining different water compatible vinyl monomers and crosslinkers. Initiation system was also changed along the experimental program. Conventional (FRP) and RAFT mechanism were used.

Table 7.1. A set of polymerisation runs performed in the inverse suspension FRP synthesis of pH/temperature responsive hydrogels. Water was used as solvent in the dispersed phase and cyclohexane was considered as continuous medium. Polymerisations at 20 °C.

Run	M_1	M_2	CL	I	$y_{M_1}(\%)$	$y_C(\%)$	$y_I(\%)$	$y_m(\%)$
1	NIPA		MBAm	APS	100	1	0.25	10
2	NIPA	AA	MBAm	APS	50	1	0.25	14.5
3	NIPA	MAA	MBAm	APS	67	1	0.25	13.8
4	NIPA	AA	MBAm	APS	88	1	0.26	11.1
5	NIPA		TAO	APS	100	1	0.25	10
6	NIPA		TMPTA	APS	100	1	0.25	10
7	NIPA		MBAm	APS	100	2	0.25	10

Table 7.2. A set of polymerisation runs performed in the inverse-suspension RAFT synthesis of water compatible polymers and hydrogels. DMF was used as solvent in the dispersed phase and liquid paraffin was considered as continuous medium. Polymerisations at 70 °C. DDMAT was used as RAFT agent.

Run	M_1	M_2	CL	I	$y_{M_1}(\%)$	$y_C(\%)$	$y_I(\%)$	$y_m(\%)$	y_I^{RAFT}
1	NIPA			AIBN	100	0	0.24	25.6	4.18
2	AA			AIBN	100	0	0.23	17.9	4.42
3	DMA			AIBN	100	0	0.06	33.2	5.03
4	MAA			AIBN	100	0	0.05	33.6	5.00
5	AA			AIBN	100	0	0.03	40.4	8.69
6	AA		MBAm	AIBN	100	1	0.04	40.3	8.64
7	NIPA		MBAm	AIBN	100	1	0.04	30.0	8.96
8	NIPA	AA	MBAm	AIBN	90	1	0.04	31.0	9.00

Table 7.3. A set of polymerisation runs performed in the synthesis of water compatible polymers and hydrogels considering liquid paraffin as continuous medium. EGDMA was used as crosslinker in runs 1-3 and MBAm in runs 4-5. Polymerisations at 60 °C with exception of run 4 (50 °C). Water was used as solvent in runs 2 and 4 and DMF in run 5. RAFT agents used: CPA in runs 3-4 and CDT in run 5.

Run	M_1	M_2	I	$y_{M_1}(\%)$	$y_C(\%)$	$y_I(\%)$	$y_m(\%)$	y_I^{RAFT}
1	DMAEMA		AIBN	100	4.55	0.5	100	0
2	DMAEMA		V50	100	4.88	0.3	73	0
3	DMAEMA		AIBN	100	4.76	0.5	100	1.98
4	DMAEMA	MAA	V50	35	2	0.14	50	1.94
5	NIPA	AA	AIBN	88	1	0.36	22	1.99

Slightly different reaction conditions were used in the experimental runs 1 and 3 in table 7.3, aiming at the improvement of the *in-line* FTIR-ATR measurements. Liquid paraffin was used to minimize the IR absorption of the continuous medium and solvent (e.g. water or DMF) was not used in the polymerisation phase to eliminate the usual strong influence of these compounds on the IR spectra of monomers and produced polymers. Liquid paraffin was also considered in order to promote a low thermodynamic affinity with monomers and produced gels. Precipitation of the products in the particulate form along the polymerisation was thus observed and good stirring conditions, as well as, good heat dissipation could be maintained during the reactions. After purification, powder gels were obtained as final products. Effect of other synthesis conditions on the crosslinking process, such as, presence of solvent and the

nature of monomers and RAFT agents, was also assessed in this set of polymerisations as reported with the remaining experimental runs of table 7.3.

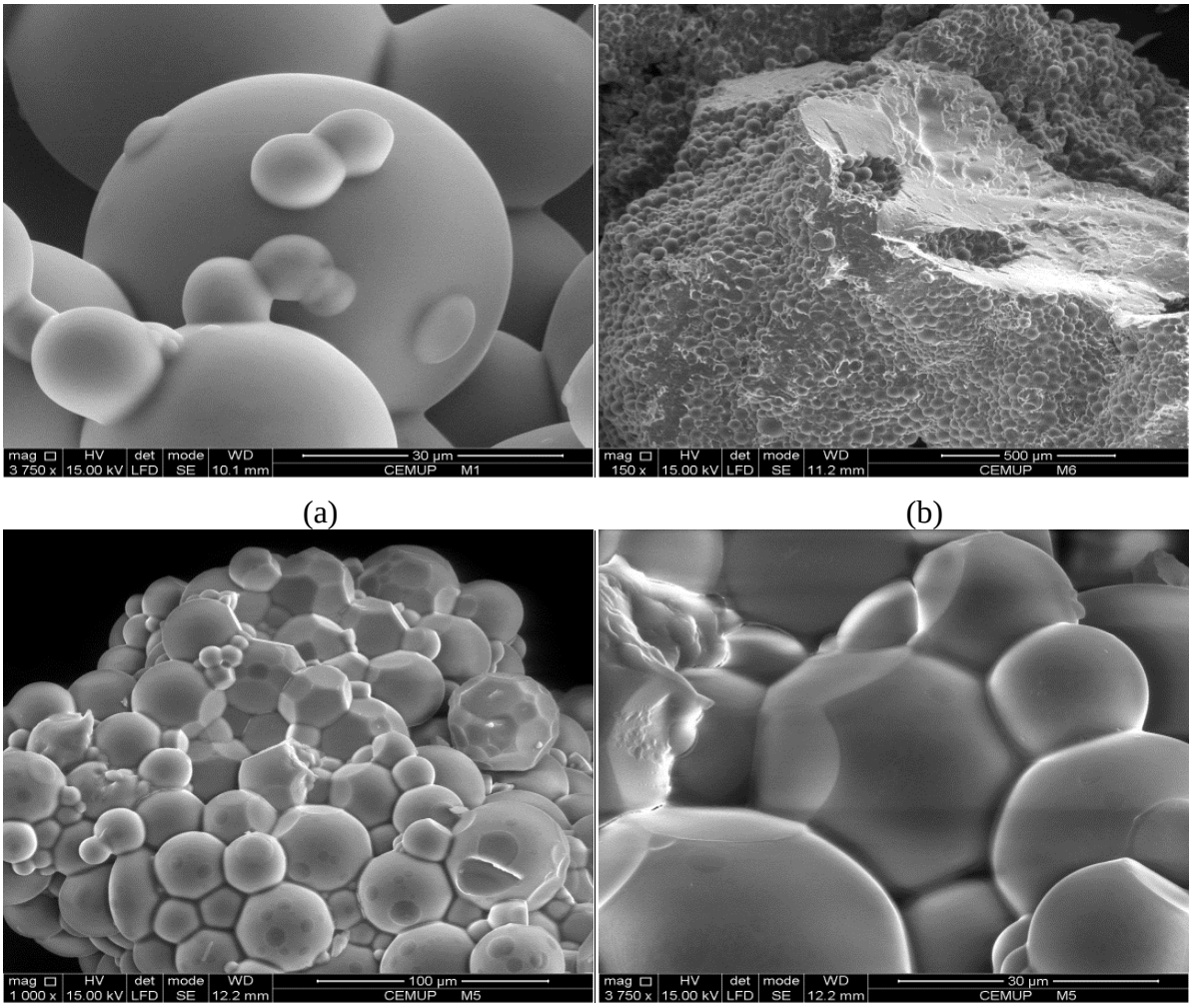

Figure 7.2. SEM micrographs of some hydrogel beads synthesized using the inverse-suspension technique. (a) AA/MBAm hydrogel. (b) NIPA/MBAm hydrogel. (c) and (d) NIPA/AA/MBAm hydrogel. In some cases, formation of fused material was observed due to the post-treatment of the products (precipitation/drying).

7.2.3 Product Analysis by SEC with a Tetra Detector Array

The SEC apparatus used is composed of a Viskotek GPCmax VE 2001 integrated solvent and sample delivery module which includes a tetra detector array with refractive index (RI), light scattering (LS), viscosity (IVDP) and ultraviolet (UV) detection. Analysis were performed directly in aqueous eluents (pH of the eluent was changed according the polymer analysed) and using typically a flow-rate of 0.5 mL/min. Temperature of the analysis (in the range of 30 to 50 °C) was also changed according the different conformations of the polymers in aqueous solutions (e.g. collapsing of NIPA based materials at around 37 °C). A train of 3 SEC

columns (Viskotek A2000 + Viskotek A3000 + Viskotek A6000) was considered to fractionate the polymers by size (different configurations were also used in order to not exceed the recommended maximum column pressures). Simultaneous measurement of RI, LS and intrinsic viscosity signals yield absolute molecular weight, branching factors, hydrodynamic radius and radius of gyration of the soluble phase. Monomer conversion was also estimated through the measurement of the monomers peak areas in these chromatograms. Typical results concerning the analysis of water soluble polymers with this apparatus are illustrated in Figures 7.3 and 7.4. Simultaneous detection of three signals (RI, LS and IVDP) allows the detailed characterization of the molecular architecture of the soluble phase and the observation of the influence of the production conditions (e.g. comparison FRP/RAFT synthesis) on the dynamics of crosslinking. Light scattering measurements proved to be especially important because they show the possibility of occurrence of non-ideal RAFT polymerisation, as below described. In this chapter, UV detection was used to carry out drug release studies with the synthesized hydrogels, as also below described.

7.2.4 *In-line* FTIR-ATR Measurements

An attenuated total reflection (ATR) immersion probe, coupled to a Fourier Transform Infra-Red spectrophotometer (which technical features were described in Gonçalves *et al*., 2010b) was used to perform the *in-line* monitoring of polymerisation runs, aiming the measurement of the building process of the networks. Typical results obtained with the *in-line* FTIR-ATR monitoring of hydrogel formation are illustrated in Figures 7.5 and 7.6. These runs were designed in order to have optimum conditions for FTIR measurements (minimizing possible interferences with monomer/polymer spectra) but limited information concerning the crosslinking process was obtained.

Figure 7.5 shows *in-line* FTIR-ATR spectra observed during DMAEMA/EGDMA FRP polymerisation (run 1 in Table 7.3). Absorption peak at around 935 cm^{-1} was considered to estimate the double bonds conversion, using also the peak at around 1720 cm^{-1} as internal reference. In Figure 7.6 is shown the FTIR-ATR estimated dynamics of monomer conversion for DMAEMA/EGDMA polymerisation (run 1 in Table 7.3). Similar measurements were performed with runs 2 and 3 in Table 7.3 but even lower monomer conversions were observed in these experiments (almost negligible after 8 hours of polymerisation in run 3). Coating of the probe at relative low conversion (around 40 % as recently reported in other studies (Salehpour and Dubé, 2012)) is a possible shortcoming of these *in-line* measurements. *Off-line* FTIR analysis of previously

isolated networks samples collected at different polymerisation times seems to lead to a better description of the crosslinking process, namely concerning the pendant double bonds reactivity (Hecker, 2000). Crosslinker amount used in hydrogels preparation is very low (a few percent) and even with *off-line* FTIR monitoring the study of the crosslinking process is a difficult task. ^{13}C labelling of the crosslinker (as before performed with trimethylolpropane triacrylate (TMPTA) in the framework of network in superabsorbent gels (Arriola *et al.*, 1997)) should be a better option in this context.

7.2.5 Swelling Ratio Sensitivity Measurements

Synthesized hydrogel particles, after isolation, were tested in order to assess their sensitivity to stimulations triggered by changes in the surrounding media. In particular, was measured the variation of the hydrogels weight swelling ratio, in water solutions, at different temperatures and/or pH values. Stimulation of the networks by changes in these parameters was thus observed. Typical results obtained are presented in Figure 7.7 where sensitivity of NIPA/MBAm hydrogels to temperature changes is used as illustration example.

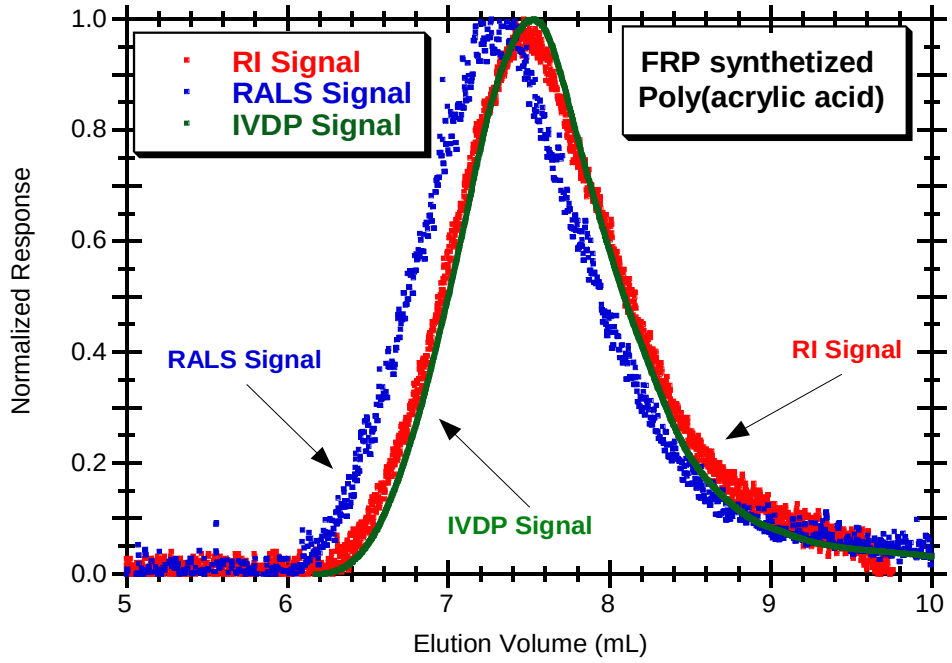

Figure 7.3. Refractive index (RI), right angle light scattering (RALS) and intrinsic viscosity-differential pressure (IVDP) signals simultaneously observed in the SEC analysis of a water soluble PAA sample.

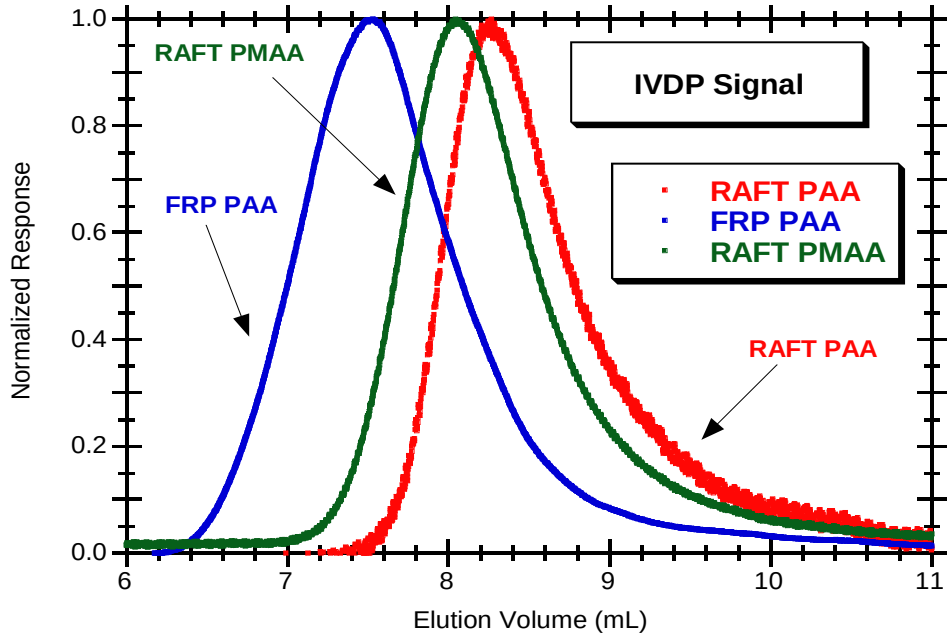

Figure 7.4. IVDP signals observed in the SEC analysis of different water soluble polymers synthesized, highlighting the influence of operation conditions (FRP/RAFT) on the products molecular structure and properties.

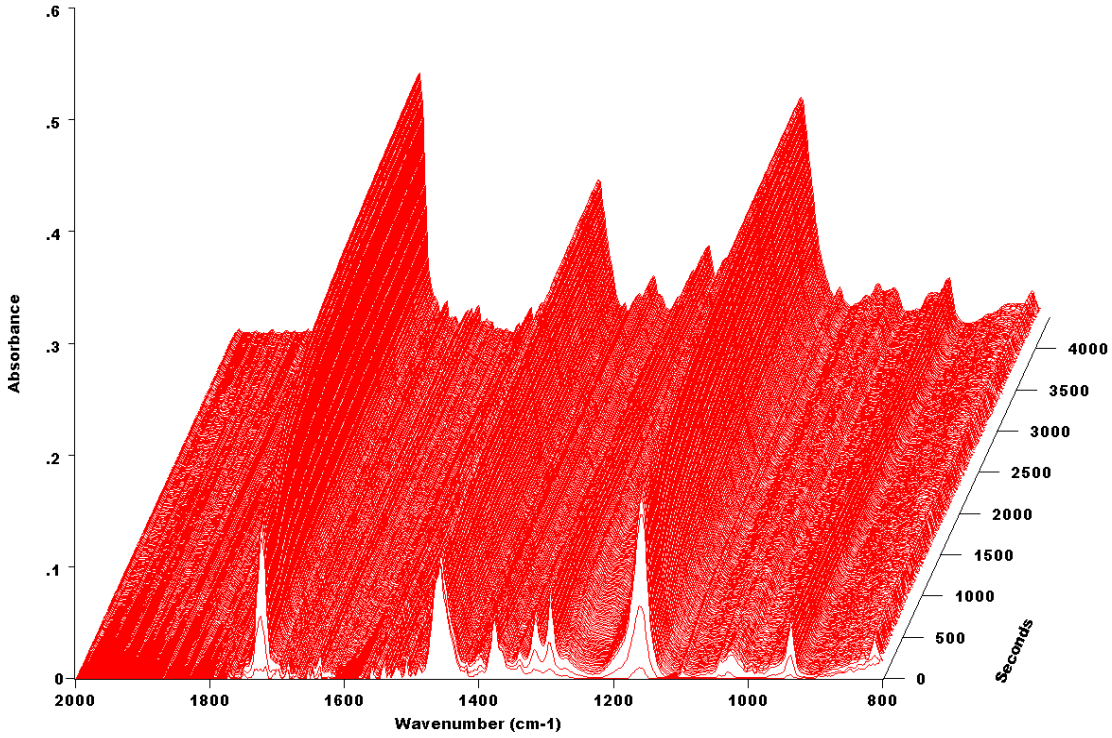

Figure 7.5. *In-line* FTIR-ATR spectra observed during DMAEMA/EGDMA FRP polymerisation (run 1 in Table 7.3). Absorption peak at around 935 cm^{-1} was considered to estimate the double bonds conversion, using also the peak at 1720 cm^{-1} as internal reference.

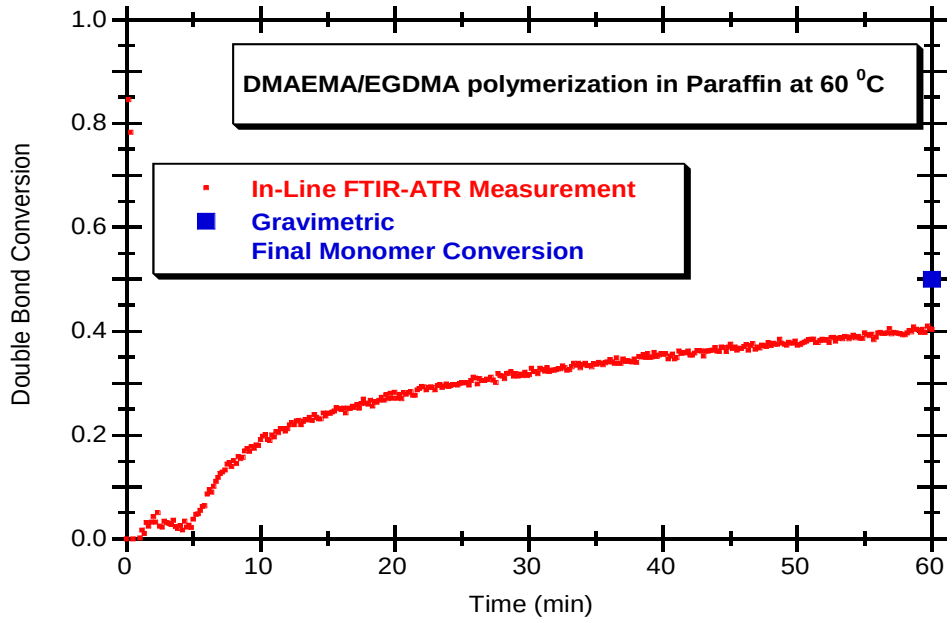

Figure 7.6. FTIR-ATR estimated dynamics of monomer conversion for DMAEMA/EGDMA polymerisation (run 1 in Table 7.3). Similar measurements were performed with runs 2 and 3 in Table 7.3 but even lower monomer conversions were obtained in these experiments (almost negligible after 8 hours of polymerisation in run 3).

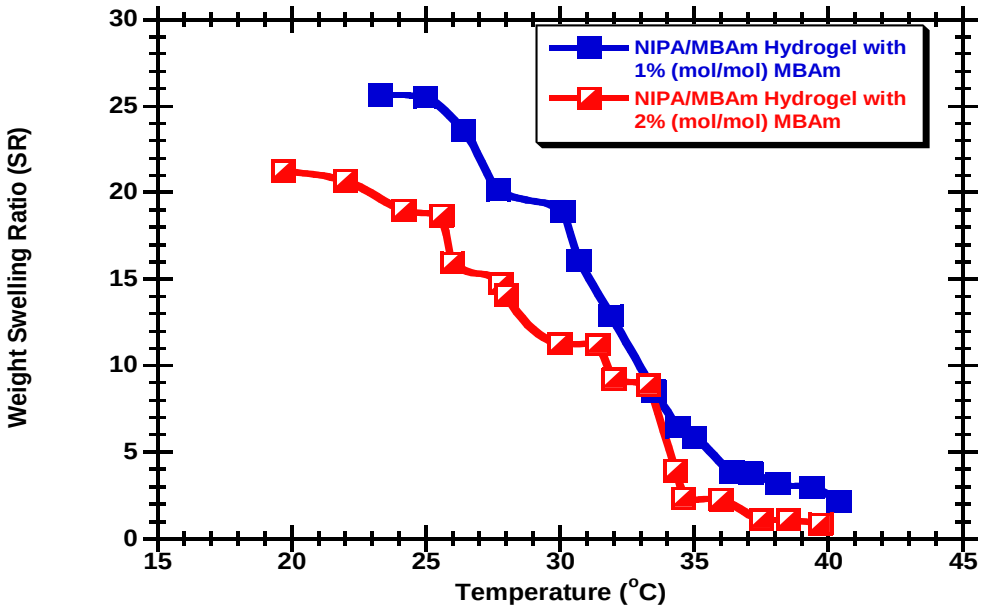

Figure 7.7. Measured equilibrium swelling ratio of NIPA/MBAm hydrogels in aqueous solutions at different temperatures illustrating networks sensitivity to changes in this parameter.

7.2.6. Drug Release Testing

The performance of the produced hydrogels was also assessed by considering drug delivery applications. Different model drugs (caffeine, 5-fluorouracil, isoniazid and ibuprofen) were considered in these studies which were carried out pouring pre-incubated network particles in aqueous solutions at different conditions (changing pH/temperature). Drug release was measured by UV detection in aqueous samples collected at different elapsed times. Typical results are presented in Figure 7.8 using the caffeine release from a NIPA/MAA/MBAm hydrogel at different pH/temperature conditions as illustration example. Two different surrounding water solutions were considered: pH=1/*T*=37 °C (collapsed particles) and pH=7/*T*=22 °C (swollen particles). Hydrogel beads were pre-loaded with caffeine during 48 hr in a 2.25 mg/ml drug water solution. In spite of the complexities associated with the mathematical modelling for drug delivery (Bajpai *et al*., 2010; Galaev and Matiasson, 2008), a good agreement is observed by fitting the experimental data to exponential rise laws (the effect of different stimulations on the drug release profiles observed is also here highlighted).

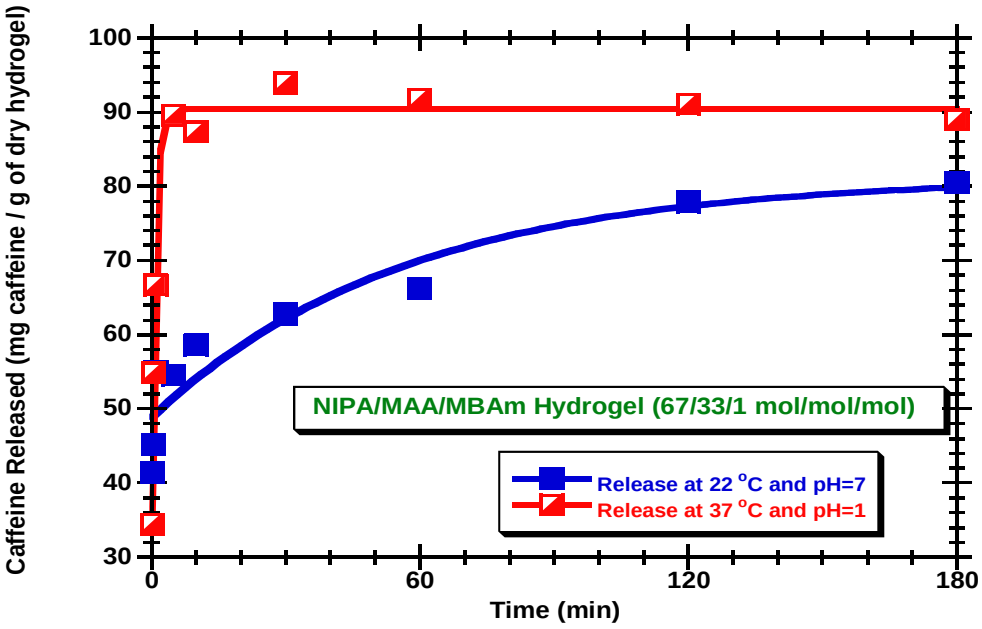

Figure 7.8. Dynamics of caffeine release from a pH/temperature sensitive synthesized hydrogel (NIPA/AA/MBAm) measured by UV detection at 270 nm. Two different surrounding water solutions were considered: pH=1/*T*=37 °C (collapsed particles). And pH=7/*T*= 22 °C (swollen particles). Drug loading was performed by swelling the hydrogel beads in caffeine aqueous solution during 48 hours.

Applications of the different classes of "smart" hydrogels here studied are further depicted in Figures 7.9-7.14. In Figure 7.9 is presented the measured equilibrium weight swelling ratio of anionic (AA based) and cationic (DMAEMA based) hydrogels in aqueous solutions at different pH values. These results illustrate the networks sensitivity to changes of this parameter. Note that an inverse effect of the pH on the swelling ratio of these hydrogels can be explored to trigger different macroscopic effects, as for instance the transition between shrunk to swollen networks by changing the pH from 1 to 8 (e.g. resembling the stomach/intestine pH change in human body) with AA hydrogels and the opposite with DMAEMA hydrogels. In Figure 7.10 is showed the comparison for the change of the equilibrium weight swelling ratio with pH considering FRP and RAFT synthesized AA hydrogels. These results illustrate the high effect of the synthesis technique used on the swelling properties of the hydrogels. In fact, the primary chain length of the networks is strongly affected when FRP is replaced by RAFT. This effect can eventually be used to tune the swelling properties of the hydrogels (e.g. designing the initial ratios between monomers/RAFT agent/initiator). It is worth to note that measurements presented in Figures 7.9 and 7.10 were obtained using buffer aqueous solutions at different pH values.

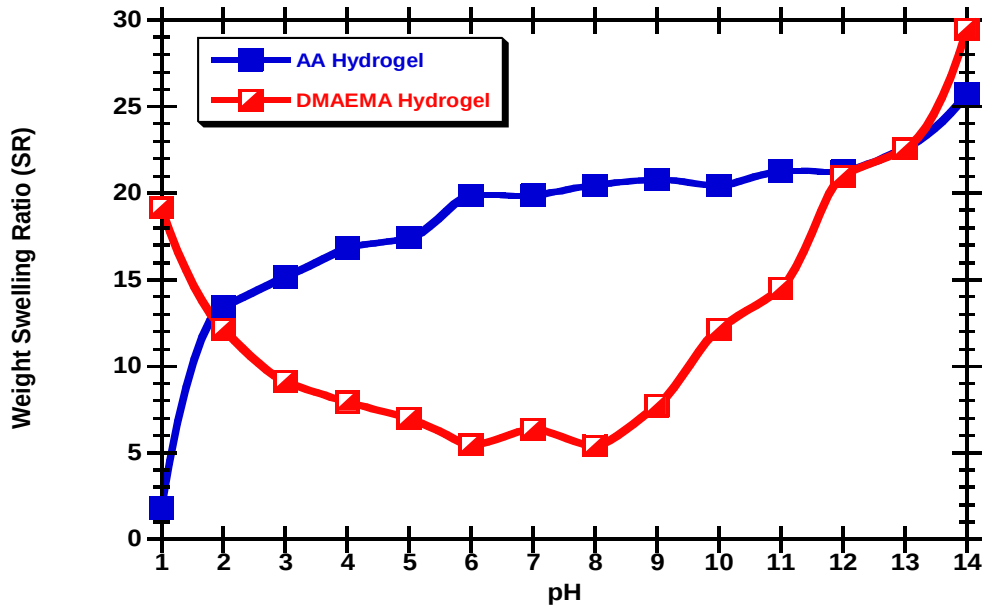

Figure 7.9. Measured equilibrium weight swelling ration of anionic (AA based) and cationic (DMAEMA based) hydrogels in aqueous solutions at different pH values illustrating networks sensitivity to changes in this parameter. Inverse effect of the pH on the swelling ratio of these hydrogels can be exploited to trigger different macroscopic effects (e.g. shrunk to swollen networks by changing the pH from 1 to 8 with AA hydrogels and the opposite with DMAEMA hydrogels).

These buffer solutions were prepared using the proper amounts of HCl, NaOH, KCl, KHP (potassium hydrogen phthalate - $C_8H_5KO_4$), KH_2PO_4 (potassium dihydrogen phosphate), $Na_2B_4O_710H_2O$ (borax) and Na_2HPO_4 (disodium hydrogen phosphate). Nevertheless, the swelling ratio of hydrogels is also strongly dependent on the ionic strength and size of the ions and counter-ions present in the used aqueous solutions. Accordingly, a different dependence of the hydrogels swelling ratio on pH changes can be observed if other aqueous solutions at the same pH values are considered (e.g. changing the used salts and/or using just HCl and NaOH to prepare the aqueous solutions with the desired pH values).

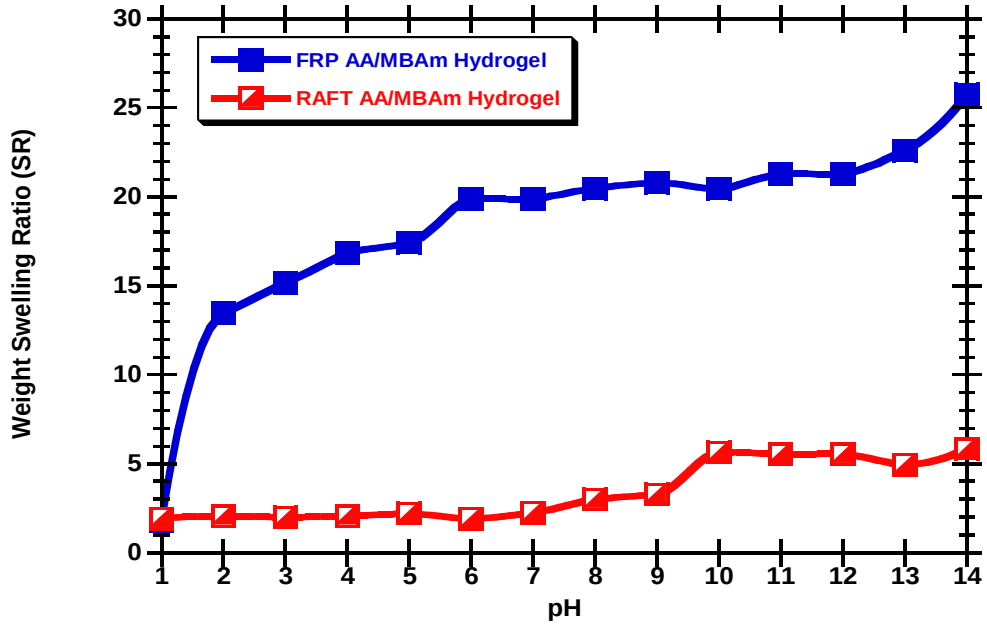

Figure 7.10. Comparison of the change of the equilibrium weight swelling ratio with pH for FRP and RAFT synthesized AA hydrogels. High effect of the synthesis technique used on this parameter is observed. The primary chain length of the networks is strongly affected when FRP is replaced by RAFT and this effect can eventually be used to tune the swelling properties of the hydrogels. Note that results presented in Figures 7.9 and 7.10 were obtained using buffer aqueous solutions at different pH values. The swelling ratio of hydrogels is also strongly dependent on the ionic strength and size of the ions/counter-ions present in the solutions. A different dependence of SR can be observed if other aqueous solutions at the same pH values are considered (e.g. changing the used salts).

Measured dynamics of release of different drugs from cationic and anionic hydrogels is illustrated in Figures 7.11-7.14. In Figure 7.11 and 7.12 is showed the dynamics of release of 5-fluorouracil from DMAEMA based (cationic) and AA based (anionic) hydrogels, respectively. In both cases, the release of the drug was measured in acidic (pH=1) and alkaline (pH=10) aqueous solutions. In spite of the differences between the two hydrogels,

slightly higher steady state release of the drug was always observed with the alkaline environment.

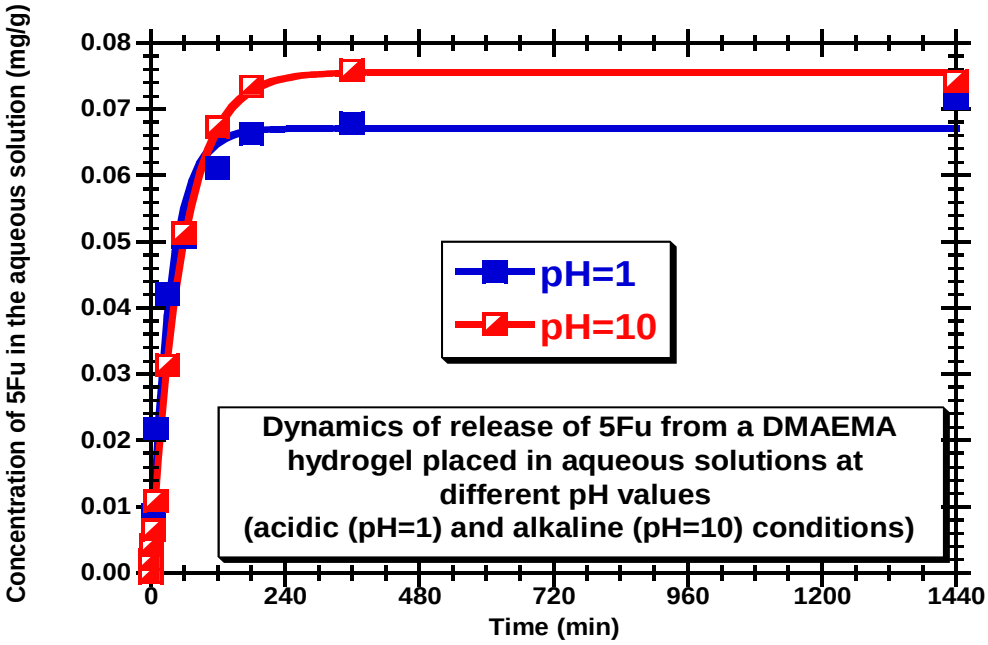

Figure 7.11. Dynamics of release of 5-fluoruracil from a pH sensitive hydrogel (cationic hydrogel based on DMAEMA) measured by UV detection at 270 nm.

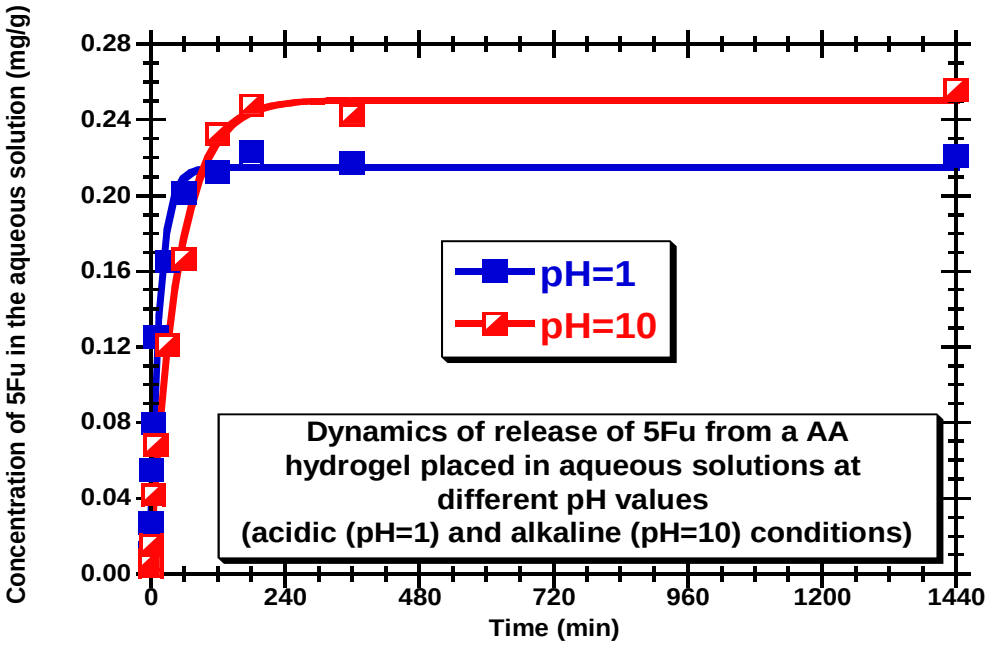

Figure 7.12. Dynamics of release of 5-fluoruracil from a pH sensitive hydrogel (anionic hydrogel based on AA) measured by UV detection at 270 nm.

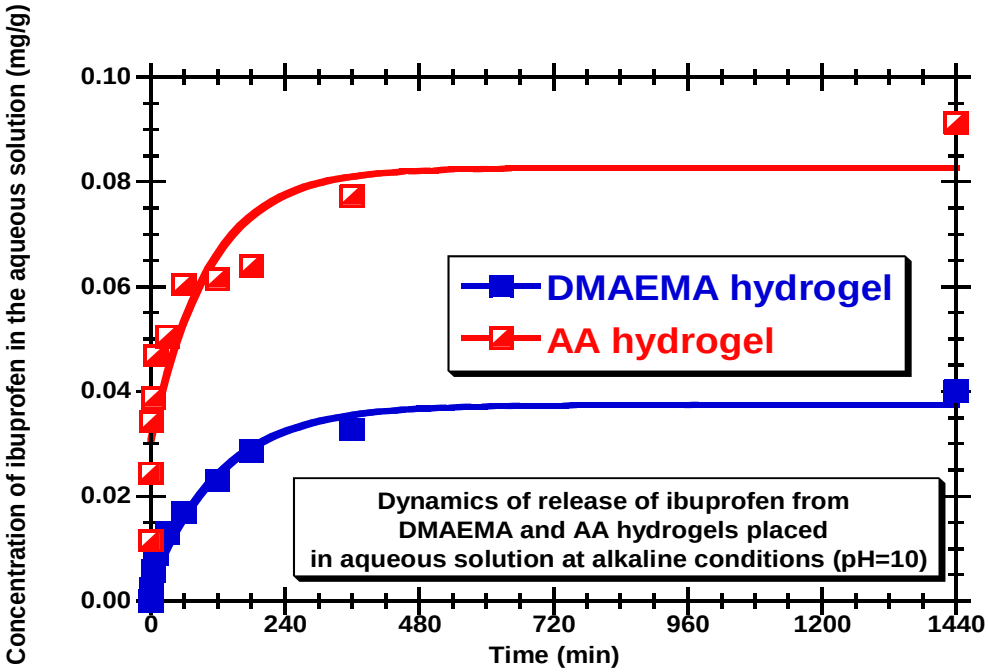

Figure 7.13. Comparison of the dynamics release of ibuprofen from cationic (DMAEMA based) and anionic (AA based) hydrogels, both placed in aqueous solution at pH=10 (release measured by UV detection at 223 nm).

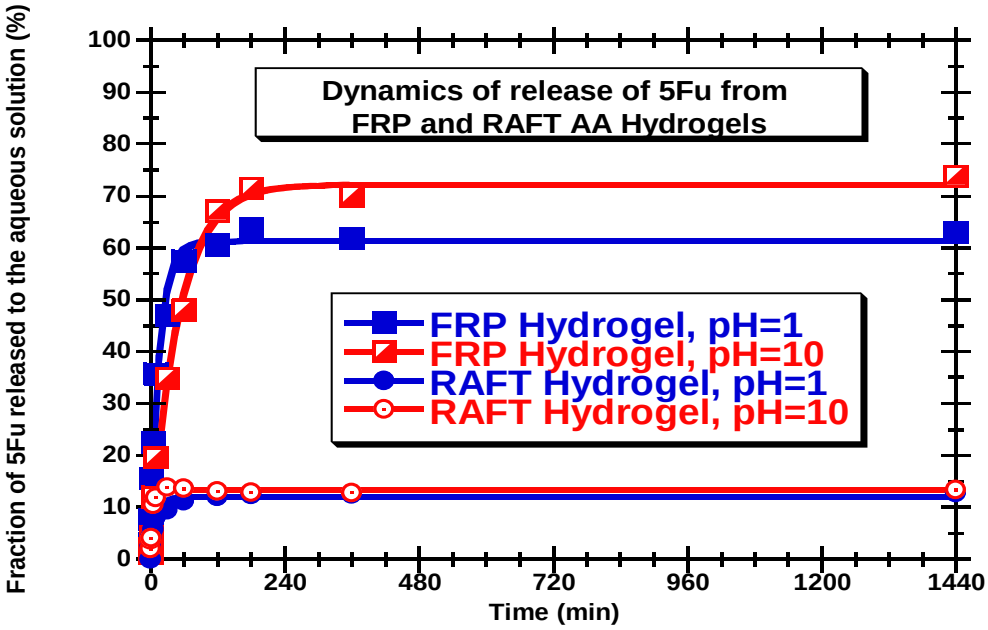

Figure 7.14. Dynamics of release of 5-fluorouracil from FRP and RAFT synthesized pH sensitive hydrogels illustrating the effect of the molecular architecture of the networks on their performance. Amount of drug released is here expressed as the fraction of drug loaded in the hydrogel that is transferred to the aqueous solution (release measured by UV detection at 270 nm).

Note that some other complex effects such as hydrogel/drug interaction (Bajpai *et al*., 2010; Galaev and Matiasson, 2008) (e.g. see discussions about diffusion and chemically controlled delivery systems in chapter 11 of Galaev and Mattiasson, 2008) should be taken into account when drug release studies are performed, as for instance formation of complexes between drugs and polymer networks. These issues also have a strong effect on the amount of a specific drug that is possible to load in a hydrogel. The effect of the combination between specific drugs and hydrogels is illustrated in Figure 7.13 where the dynamics of release of ibuprofen from DMAEMA and AA polymer networks, both placed in aqueous solution at pH=10 (release measured by UV detection at 223 nm), is showed. Comparison of the dynamics of release of 5-fluorouracil from FRP and RAFT synthesized pH sensitive hydrogels is illustrated in Figure 7.14. The amount of drug released in this case is expressed as the fraction of drug loaded in the hydrogel that is transferred to the aqueous solution (release measured by UV detection at 270 nm). Note that much lower release fractions were observed (both at pH=1 and 10) when RAFT hydrogels were considered. In all cases presented in Figures 7.11-7.14, drugs loadings were performed by swelling the hydrogels in 5-fluorouracil or ibuprofen aqueous solutions during 48 hr. These results should be a consequence of the different molecular architectures associated with FRP and RAFT networks (affecting namely their swelling ratio, as showed in Figure 7.10) and highlight the relation between structure and end use properties of these materials.

7.3 Results and Discussion

Reversible addition-fragmentation chain transfer polymerisation is probably the most versatile CRP technique allowing the polymerisation of different classes of monomers. Nevertheless, the degree of control of polymerisation that is attained with RAFT is strongly dependent on the reaction conditions used. Specific combination between monomer, RAFT agent, initiator and solvent used in the polymerisation is a central issue to obtain tailored products with RAFT polymerisation.

Temperature and initial proportions monomer/RAFT agent/initiator/solvent also have a huge effect on the kinetics of formation and on the control of the molar masses of RAFT polymers. Some other issues arise when RAFT is directly performed in water, namely the low solubility of most RAFT agents in pure water (forcing the use organic co-solvents) and their potential hydrolysis (pH dependent) with loss of control on the polymerisation process (see Chaduc *et al*., 2012a and references therein). When aqueous dispersed systems are considered (e.g. the

industrially important emulsion/miniemulsion/suspension processes and their inverse counterparts) some other aspects like the transport of reactants (monomers, initiators, RAFT agents) between organic and aqueous phases become also of crucial importance. In this context, the RAFT inverse miniemulsion of acrylamide and acrylic acid were recently reported (Ouyang *et al*., 2011; Qi *et al*., 2007) and the effect of pH on the hydrolysis of the RAFT agent and polymerisation in the continuous phase (eventually in the absence of RAFT agent) were identified as phenomena potentially involved in some loss of control observed with particular conditions. A secondary peak was observed in the RI curve (see discussion below in the context of the results here presented) which was attributed to different polymer populations formed in both phases (aqueous and organic). These aspects get an additional importance in the framework of RAFT dispersed systems that has been very recently explored to produce amphiphilic copolymers and nanoparticles/nano-objects with different morphologies like spheres, fibres and vesicles (Chaduc *et al*., 2012b; Zhang *et al*., 2011, 2012a and 2012b). Below are discussed some of the findings involving probably related mechanisms that are present in the RAFT inverse suspension formation of hydrogels or their linear counterparts.

Very fast reactions are generally involved in the FRP synthesis of hydrogels, as before showed with different classes of monomers (Gonçalves *et al*., 2011b and 2013b). Fast gelation is observed with a few percent of crosslinker agent and parameters such as polymerisation temperature, monomer concentration and neutralization have a very strong influence on the dynamics of gelation (see results presented in Gonçalves *et al*., 2011b and 2013b). Similar behaviour was observed in the FRP polymerisation runs detailed in Table 7.1, even considering a low polymerisation temperature (T=20 °C).

It is known that more amenable kinetics of polymerisation can be achieved on replacing FRP by RAFT polymerisation. Design of operation conditions, namely the initial proportions between initiator/RAFT agent/monomer, can be used to manipulate reaction rates and also to design the degree of polymerisation. With network formation, these parameters can be used to try the manipulation of the primary chain length (thus affecting gelation) and the minimization of intramolecular reactions (cyclizations) leading to the decrease of crosslinking efficiency.

If a direct aqueous polymerisation is intended, as in many cases involving hydrogels, a major problem to be faced with RAFT polymerisation is the low water solubility of usual RAFT agents. This issue applies to DDMAT and therefore the aqueous RAFT polymerisation is not

possible in practice. This problem can be circumvented by using a different solvent, such as DMF, as described in Table 7.2. Under these conditions reasonable reaction rates were observed with RAFT polymerisation at T=70 °C considering relatively high initial mole ratios RAFT agent/initiator (see Table 7.2). Kinetics of these RAFT polymerisations is illustrated in Figures 7.15-7.20 considering different water compatible monomers. In these Figures are showed the dynamics of monomer conversion concerning the inverse-suspension RAFT synthesis of water compatible polymers and hydrogels in Table 7.2. Runs 1, 2, 3, 4, 5 and 6 are depicted in Figures 7.15, 7.16, 7.17, 7.18, 7.19 and 7.20, respectively.

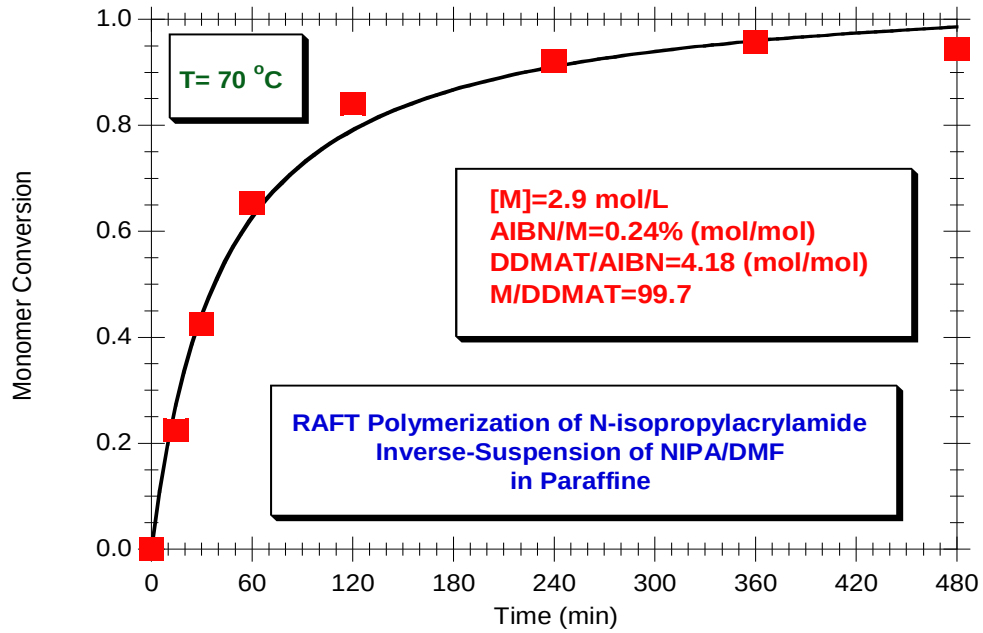

Figure 7.15. Observed dynamics of monomer conversion (run 1 in Table 7.2) concerning the inverse-suspension of NIPA RAFT polymerisation with $y_I^{RAFT} = 4.18$.

When RAFT network formation was sought using similar conditions (runs 6 to 8 in Table 7.2), lower gel fractions were observed in the products indicating a different crosslinking process when compared with FRP (theoretical and experimental kinetic studies on hydrogel formation by FRP where reported (Gonçalves *et al.*, 2011b and 2013b). Presence of such soluble phase is highlighted in Figure 7.21 where the SEC traces of the final sample correspondent to run 6 in Table 7.2 are used to illustrate this issue. Note that besides the RI signal of the polymer (indicating the presence of soluble material), the LS signal is also presented and the coexistence of secondary population with low concentration but very high size can be observed.

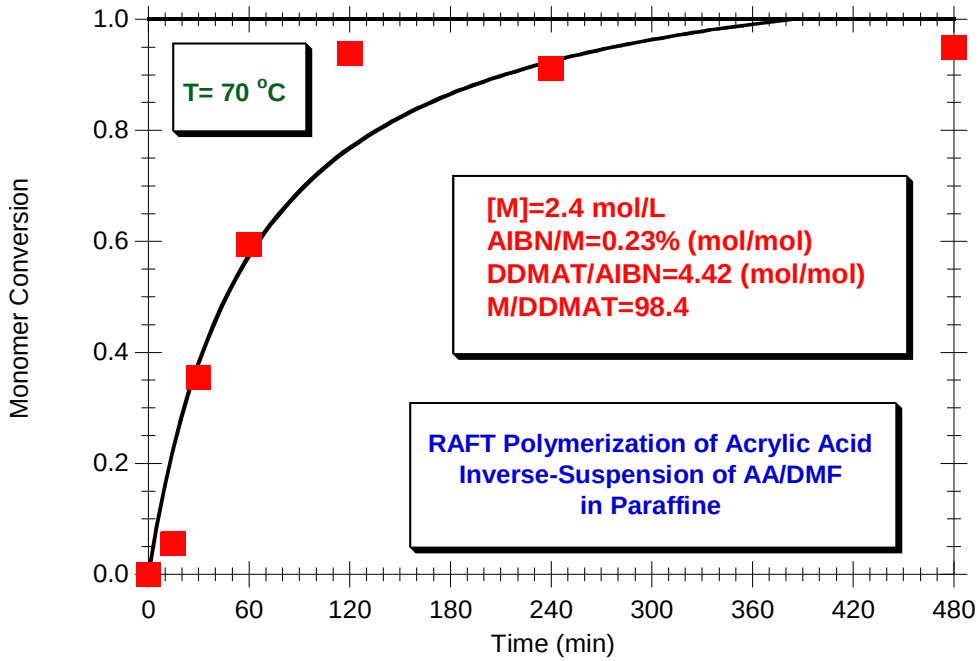

Figure 7.16. Observed dynamics of monomer conversion (run 2 in Table 7.2) concerning the inverse-suspension of AA RAFT polymerisation with $y_I^{RAFT} = 4.42$.

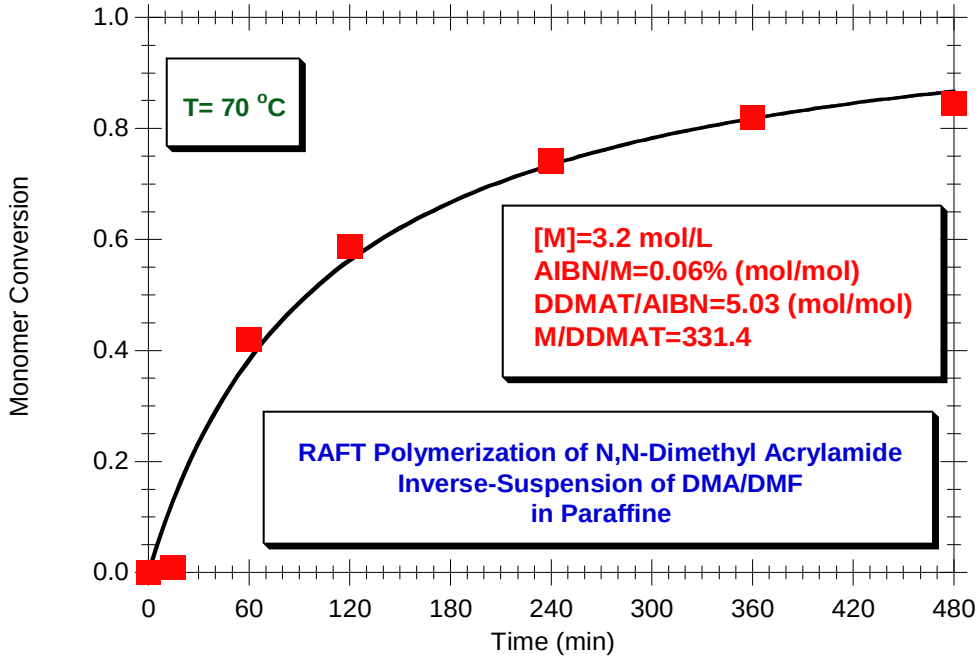

Figure 7.17. Observed dynamics of monomer conversion (run 3 in Table 7.2) concerning the inverse-suspension of DMA RAFT polymerisation with $y_I^{RAFT} = 5.03$.

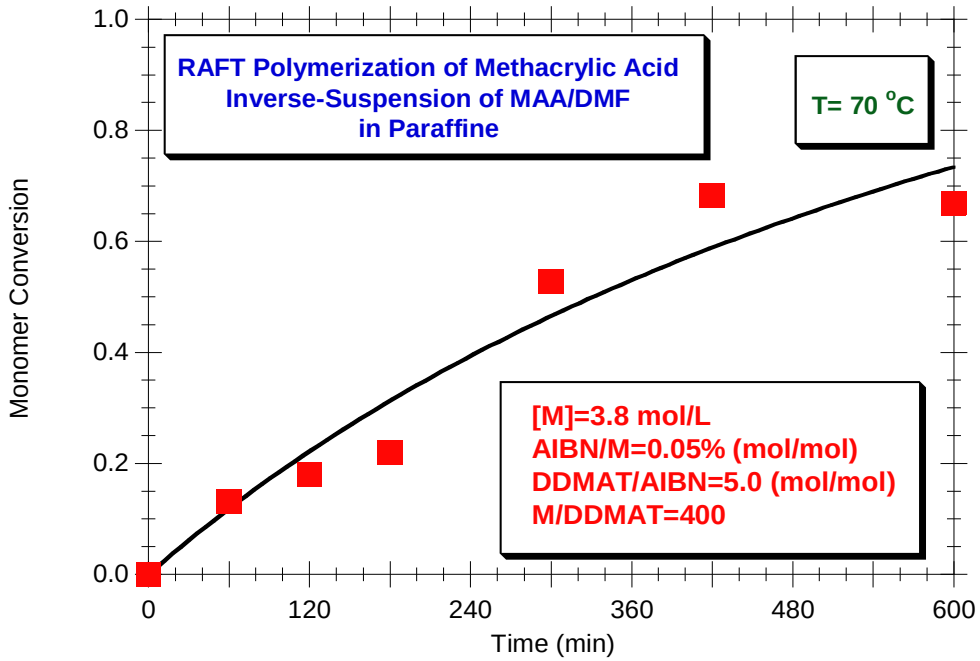

Figure 7.18. Observed dynamics of monomer conversion (run 4 in Table 7.2) concerning the inverse-suspension of MAA RAFT polymerisation with $y_I^{RAFT} = 5.00$.

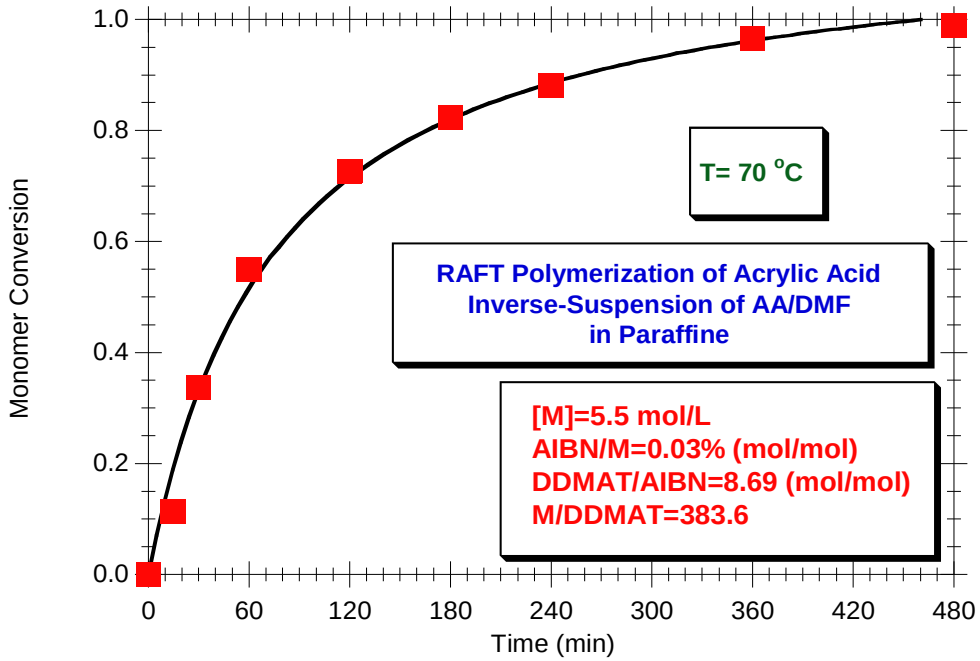

Figure 7.19. Observed dynamics of monomer conversion (run 5 in Table 7.2) concerning the inverse-suspension of AA RAFT polymerisation with $y_I^{RAFT} = 8.69$.

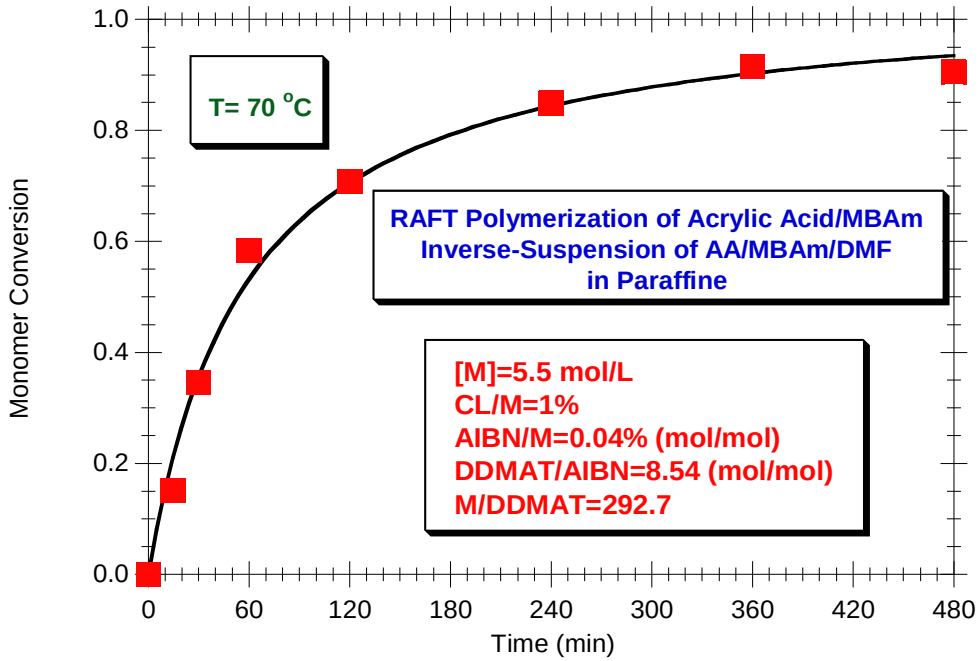

Figure 7.20. Observed dynamics of monomer conversion (run 6 in Table 7.2) concerning the inverse-suspension of AA/MBAm RAFT polymerisation with $y_I^{RAFT} = 8.54$.

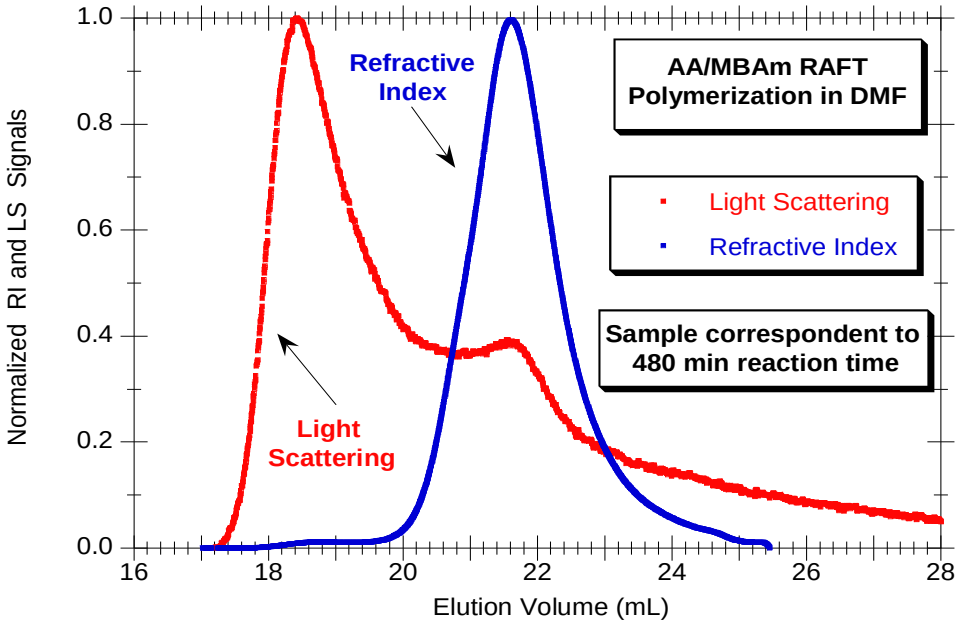

Figure 7.21. SEC chromatographic traces showing the presence of soluble material in AA/MBAm RAFT polymerisation in DMF (run 6 in Table 7.2) and the formation of a secondary population with high molecular size and very low concentration.

This secondary population was also observed in linear RAFT polymerisations, as below discussed, and is a possible consequence of non-ideal steps involved in the RAFT mechanism. Lower amounts of gel observed in these runs can result of the low primary chain length imposed by the RAFT process (mole ratio monomer/RAFT agent around 290). Dynamics of gel formation in RAFT hydrogel synthesis is also illustrated in Figure 7.22 considering different operation conditions, namely a lower mole ratio y_I^{RAFT} (see run 4 in Table 7.3), here with measurement of high final gel content. Mathematical modelling of RAFT non-linear polymerisation can be especially useful to aid with the interpretation of such results and to elucidate the mechanistic differences between RAFT and FRP crosslinking processes (Gonçalves *et al*., 2013c; Wang *et al*., 2012).

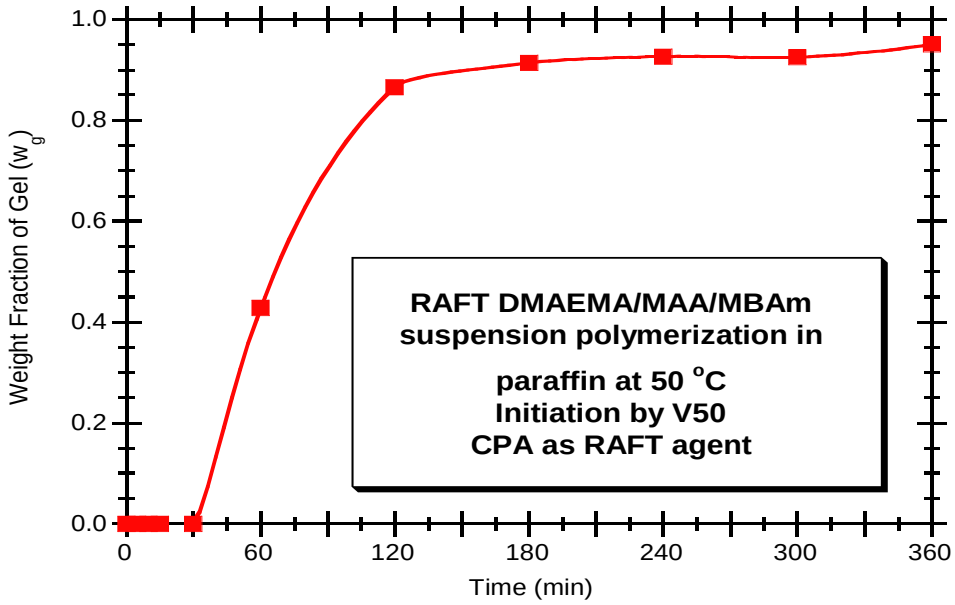

Figure 7.22. Dynamics of gel formation during the RAFT synthesis of stimuli-responsive hydrogels. DMAEMA/MAA/MBAm RAFT polymerisation at 50 °C using CPA agent (run 4 in Table 7.3) is here considered for illustration purposes.

The importance of multiple detection in the SEC analysis of the RAFT products is also highlighted in Figures 7.23 and 7.24. Formation of a secondary population at a very low concentration (almost negligible with RI or viscosity detection) but with very high molecular size (strong LS signal) was observed even with mono-vinyl monomer RAFT polymerisation, as illustrated in Figure 7.23. The dynamics of growth of such population is showed in Figure 7.24. A possible justification for this phenomenon can be found in the framework of the RAFT slow fragmentation model leading to bimodal distributions formation. High concentration of intermediate radicals and the longer polymer chains associated to such

species could be at the source of such non-ideal behaviour, as recently showed using mathematical modelling (Zapata-González *et al.*, 2011), an explanation practically ruled out more recently on account of more fundamental studies.

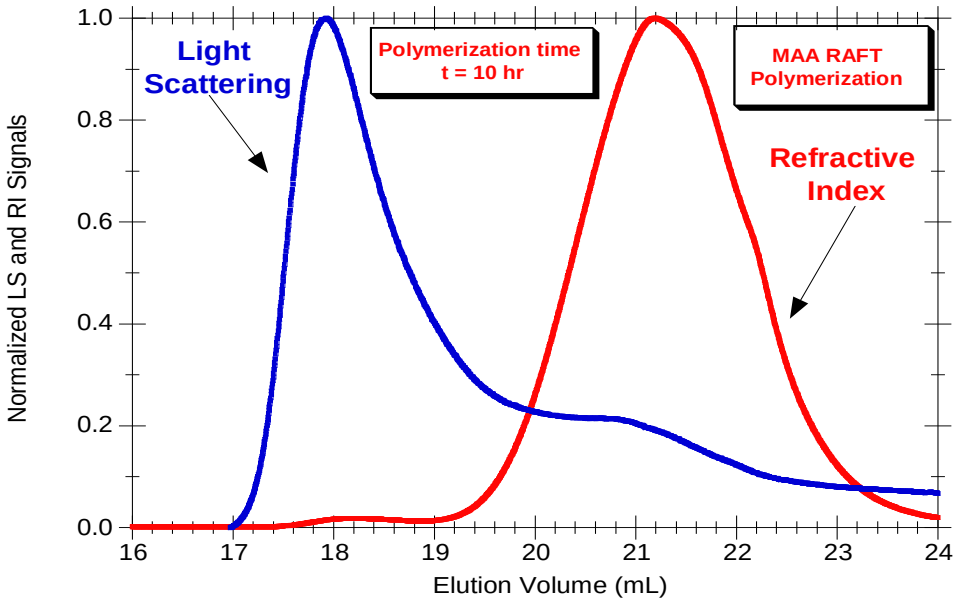

Figure 7.23. SEC chromatographic traces showing the formation of a secondary population with high molecular size and very low concentration in RAFT polymerisation (run 4 in Table 7.2).

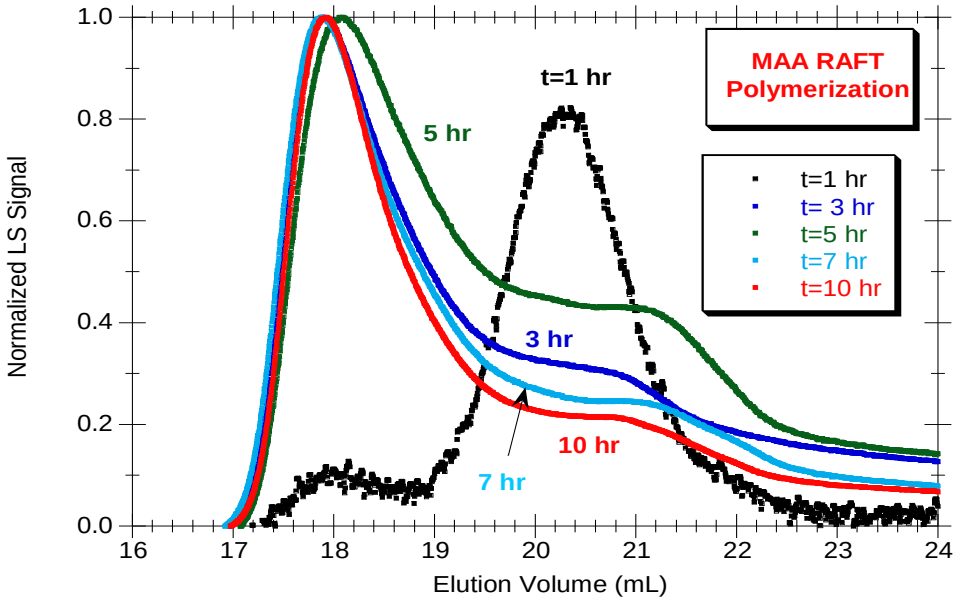

Figure 7.24. Dynamics of formation of the secondary population observed by light scattering in the same run of Figure 7.23.

Hydrolysis of the RAFT agent and/or polymerisation both in aqueous and organic phases (with formation of controlled and non-controlled polymer populations) should be the key mechanisms, also with a potential effect on the loss of control in these polymerisation systems, as discussed above. Additional theoretical/experimental studies should help in the interpretation of the experimental observations here presented.

7.4 Conclusions

A comprehensive experimental program concerning the synthesis, characterization and testing (e.g. for drug delivery applications) of smart hydrogels was performed. Combining different aqueous compatible monomers, pH and temperature sensitive materials were obtained. Anionic, cationic and amphoteric network gel beads were produced using the inverse-suspension technique. The kinetics of their building process was studied by SEC with a tetra detection array and also using *in-line* FTIR-ATR.

Only limited information on the crosslinking process was possible to obtain with *in-line* FTIR-ATR monitoring, even using optimized conditions for IR measurements (bulk monomer polymerisation in a dispersed media with low IR absorbance). The Possibility of probe coating during the synthesis process and the low crosslinker content associated to hydrogels production are factors affecting negatively the use of such technique in this context. Use of *off-line* FTIR analysis of isolated polymers (Gonçalves *et al.*, 2013c; Hecker, 2000), chemical analysis of pendant double bonds (Gonçalves *et al*., 2013a; Hecker, 2000) or ^{13}C labelling of the crosslinker (Arriola *et al*., 1997) should provide improved information concerning the crosslinking process.

Additional work in this research should hopefully also elucidate if really important gains in the sensitivity of these hydrogels can be achieved through replacement of FRP by RAFT polymerisation. Complementation of the experimental work here reported with new theoretical developments on the kinetic description of gels formation by the RAFT process (Gonçalves *et al.*, 2013c) should also be explored, in this way, it is expected to improve simulation tools with the purpose of helping the specification of synthesis conditions leading to tailored advanced materials.

Several issues concerning RAFT polymerisation were discussed in the conclusions of chapter 5 and are equally applied when using aqueous polymerisation systems.

CHAPTER 8

CONCLUSIONS AND SUGGESTIONS FOR FUTURE WORK

This work has carried out a study on the synthesis and characterization of hyperbranched polymers, gels and hydrogels arising from the radical polymerisation of multivinyl monomers. The experimental program has considered the following aspects:

- Radical polymerisation techniques used:
    - Free radical polymerisation (FRP).
    - Atom transfer radical polymerisation (ATRP).
    - Nitroxide mediated radical polymerisation (NMRP).
    - Reversible addition-fragmentation radical polymerisation (RAFT).
- Different kinds of monomer/products families:
    - For organic system:
        - Styrenics.
        - Acrylates.
        - Methacrylates.
    - For aqueous system:
        - Acrylic and methacrylic acids copolymers.
        - Acrylamides.
- Reaction systems:
    - Solution/bulk.
    - Suspension.
    - Inverse-suspension.
- Polymerisation reactors:
    - Batch (atmospheric and pressurized).
    - Semi-batch.
- Tested parameters in the polymerisations:
    - Temperature.
    - Monomers concentration.
    - Crosslinker concentration and functionalization.
    - Initiation system (thermal decomposition and redox).
    - Concentration/kind of polymerisation controlling agents.
- Products characterization:
    - Molecular architecture of the products by:
        - GPC/RI/MALLS.

    - GPC/RI/MALLS/IVDP/UV.
  - Gravimetric analysis (conversion and gel fraction).
  - Titrimetric analysis of pendant double bonds.
  - *In-line* and *off-line* FTIR-ATR.
- Products tested in terms of:
  - Swelling ratio.
  - Controlled drug release.

These experimental results were used to test simulation tools to predict:

- Gelation and relative amount of gel.
- Molecular masses before and after gelation.
- Radius of gyration before and after gelation.
- In the absence/presence of intramolecular cyclizations.

The obtained products were characterized through size exclusion chromatography systems. Comprising RI and MALLS detectors only (non-aqueous polymers) and with a tetra-detector array for hydrophilic polymers. With these systems it was possible to obtain detailed information about the molecular architecture of the synthesized materials. Namely, the number, weight and *z* average molecular weights ($\overline{M}_n$, $\overline{M}_w$, $\overline{M}_z$) as well as the average radius of gyration ($\bar{R}_g$) of the products were measured. Besides these average values, molecular weights distributions and the variation of absolute molecular weight and radius of gyration with the elution volume were also measured. A differential refractometer was used to measure the required refractive index increment (*dn/dc*) of polymers, monomers and solvents. The gravimetric method was used to determine the monomer conversion and the gel fraction.

The use of *in-line* FTIR-ATR has also allowed the determination of the monomer conversion (with some limitations) and has confirmed the formation of different kinds of polymer populations. In batch mode, FTIR allowed qualitative information of pendant double bonds. The concentration of pendant double bonds was also measured by the iodine chloride addition method. The morphology of the gel beads was observed by scanning electron microscopy.

The networks structure has a strong influence on the final product properties. The materials obtained by conventional radical polymerisation (FRP) have high molecular weight dispersion indices leading to a network with a broad distribution of molecular weights of its internal chains.

Important improvements were made by changing the feed policy of the reactants, using semi-batch reactors and chain transfer agents (Gonçalves *et al.*, 2007). Controlled radical polymerisation techniques (ATRP, NMRP and RAFT) lead to a higher homogeneity of the networks, decreasing the effect of intramolecular cyclizations and permitting the increase of the amount of effective crosslinks. However, as assessed in this work, the actual networks are far from ideality, and further studies must still be performed to better understand their structure from a quantitative point of view.

The use of water compatible monomers to produce superabsorbent polymers and smart hydrogels is known to be useful for applications in biomedical, pharmaceutical and environmental industries. It was shown that hydrogel networks are potentially useful in controlled drug delivery by taking advantage of the unique properties of the produced polymers. Such "smart" hydrogels can respond to stimulation on pH, temperature, ionic strength, among others leading to changes of retention of the active encapsulated species.

For the conventional radical polymerisation (FRP) presented in chapter 2 it was shown that the experimental results here presented concerning the semi-batch solution polymerisation of styrene and divinylbenzene showed the possibility of control gelation through the design of appropriated feeding policies (Gonçalves *et al.*, 2007). Nevertheless, some shortcomings of this approach should be here pointed out. Lack of reproducibility of the polymerisations was found during this research. This problem is likely a consequence of non-constant feeding rates due to the peristaltic pumps used. Note that even a small error in the feeding flow rates has a high effect on crosslinking process, especially when divinyl monomer is to be feed to the polymerisation mixture. In principle, this shortcoming can be avoided using higher precision pumps (e.g. syringe pumps/GPC pumps).

Semi-batch STY/DVB as here studied cannot also be extended to the production of polymer particles in a process similar to suspension polymerisation (a process later on explored in this research). Emulsion semi-batch polymerisation of vinyl/multivinyl monomers is an alternative to the production of these kinds of particles but much more complex mechanistic issues are expected in the framework of such heterogeneous processes. Inter-phase transport of both monomers (vinyl/multivinyl) and radical compartmentalization are some phenomena leading to the need of development of a much more complex analysis when emulsion semi-batch crosslinking polymerisation is to be considered.

A detailed kinetic model taking into account some complexities of these polymerisation systems has been developed in the absence of intramolecular reactions. The modelling studies can be used to design new feed policies with impact on the properties of the synthesized materials. For the copolymerisation of MMA with EGDMA in toluene at 60 °C using batch operation a general kinetic approach was applied. The decrease of the reactivity of pendant double bonds measured in this work is consistent with earlier studies with the same chemical system (Landin *et al*., 1988; Li *et al.*, 1989a and 1989b). For experiments at low monomer conversion (less to 0.5) a good agreement between predictions and experimental measurements is observed. Predicted weight average molecular weights and *z*-average radius of gyration are too low at higher monomer conversions with nonlinear systems (Trigo *et al.*, 2008).

In chapter 2 the suspension copolymerisation of styrene/divinylbenzene with gel formation was also described. It was shown that the main features of this crosslinking process can be captured by the kinetic model developed using as a single fitting parameter the relative reactivity of the pendant double bonds. Under these circumstances, with the same set of kinetic parameters, it is possible obtain good predictions of the dynamics of $\overline{M}_w$ before and also after gelation, which is a major contribution of this work for the polymer reaction engineering of such processes. Nevertheless, the unrealistic low values of reactivity estimated (around 6 % of styrene reactivity) should be mostly a consequence of neglecting intramolecular cyclizations in the model used (Gonçalves *et al*., 2011a).

Important differences were observed in the molecular architecture of non-linear products synthesized either by FRP or by ATRP as shown in chapter 3. Improved microgel homogeneity can be obtained by ATRP of acrylate/diacrylate monomers. Comparatively to FRP, ATRP also allows the operation with higher crosslinker mole fraction without gel formation. These results can be especially useful to obtain hyperbranched polymers at higher conversions than with FRP. The effect of cyclizations on the molecular architecture of these products was also detected: ATRP allows the production of more homogeneous hyperbranched polyacrylates (less intramolecular cyclizations) than FRP but, even with ATRP, this mechanism becomes increasingly important with higher dilution (Gonçalves *et al.*, 2010a, 2010b, 2010c and 2010d). It was also shown that, besides molecular weights, the *z*-average radius of gyration can also be predicted with reliability in the framework of the present kinetic approach. The good foundations of this simulation tool make it useful to design hyperbranched polymers with tailored properties.

It was shown in chapter 4 that an unified theoretical kinetic approach is capable of dealing with NMRP and captures the most important aspects of this system. The sensitivity analysis studies performed show that the reactivity of pendant double bonds is the controlling factor for the formation of non-linear structures. This single parameter was used in the fitting studies. For the NMRP of STY/DVB in solution polymerisation system, reduced reactivities of PDB were estimated in comparison to the vinyl monomers. This technique showed that, when compared with FRP, NMRP allows only limited control over the crosslinking process. NMRP non-linear polymerisation proceeds in a similar way to a random FRP process and, therefore, a polymer population with a very broad distribution of sizes is formed (Gonçalves *et al.*, 2010c and 2010d). Moreover, the occurrence of intramolecular cyclizations was detected by SEC/RI/MALLS of NMRP STY/DVB products by comparing experiments at different monomer dilutions. Therefore, such reactions cannot be completely avoided by using NMRP, especially at a low starting monomer concentration.

The incidence of intramolecular cyclization reactions with NMRP of STY/DVB was also detected through the quantification of PDBs polymer concentration, which was measured using chemical analysis.

Hence this work has confirmed that the NMRP technique allows the synthesis of hyperbranched polymers with improved homogeneity, owing to less intramolecular cyclizations as compared to conventional radical polymerisations. Moreover, it was also shown that NMRP allows operation with higher divinyl monomer content without gelation, which is an important issue in the production of hyperbranched polymers.

Polymerisations runs were extended past the gel point also as discussed in chapter 4 (in aqueous suspension system) and so the dynamics of gel formation could be studied. The impact of certain operation parameters on the crosslinking process was assessed: the initial amount of crosslinker (DVB) content was changed between 0 and 100 %, initial monomer dilution, global monomer concentration in the organic phase was changed between 20 and 100 % v/v, polymerisation temperature, experiments at 90 and 130 °C were carried out. Previous results for STY/DVB gel formation at 60 °C were also considered for comparison purposes and polymerisation mechanism: different runs comparing FRP with NMRP were carried out through the change of the initial ratios of initiator/monomer and mediator/initiator (Gonçalves *et al.*, 2013a).

Results obtained in the chapter 4 are especially useful in the study of the effect of intramolecular cyclization reactions on the crosslinking process. Experimental data obtained (Gonçalves *et al*., 2013a) were explored to develop mathematical models including the effect of primary cyclization based on the development of balance of sequences connecting radical centers and pendant double bonds present in the same polymer chain (Aguiar *et al*., 2013a). The rate constant for cyclization was considered a function of the sequence length. Studies included the pre- and post-gelation periods and comparisons between experimental measurements and model predictions for pendant double bond concentration, average molecular weights and weight fraction of gel were thus performed (Aguiar *et al*., 2013b). It was possible the estimation of the rate constant of cyclization for the smallest ring (3 monomeric units). A value in the order of 500 s^{-1} was estimated for this parameter at 90 °C rather high when compared with the intermolecular propagation (as k_p[M+PDB] lies between 1000 and 10000 s^{-1}). Jacobsen-Stockmayer theory predicts that pairs of radical site + PDB in the same molecule with longer distances between them show a decreasing rate of cyclization, but their impact stays strong even at bulk conditions and is a major factor in all multivinyl radical polymerisations. Influence of key polymerisation parameters (e.g. crosslinker content, monomer dilution, reaction temperature) on cyclization was also identified through the comparison of experimental data with different kinds of mathematical models (Gonçalves *et al*., 2013a; Aguiar *et al.*, 2013a and 2013b). In these studies a much higher relative crosslinking reactivity was observed at 130 °C as compared to 90 °C, likely as an effect of the chain mobility (Aguiar *et al*., 2013b). Despite the efforts here reported for the clarification of these kinds of crosslinking processes, this is an open issue in the scientific community, as testified by other very recent publications on this field (Scott *et al*., 2014; Nikitin *et al*., 2013; Hamzehlou *et al*., 2013). The impact of the use of different kinds of polymerisation mechanisms (e.g. FRP/NMRP) on crosslinking (trying to avoid/decrease cyclizations) and development of mechanistic models able to describe such complex polymerisations are some research lines also explored in these publications which will be probably enhanced in future works.

Experimental work of chapter 5 has been focused in RAFT polymerisation with the trithiocarbonates DDMAT and CDT lead to the formation of a secondary polymer population with low concentration but high molecular size. This secondary population is only residually discernible when the RI signal is observed but becomes evident when the MALLS signal is inspected. Formation of this side population is not observed when RAFT agent dithiobenzoate

TBTGA is used, confirming the influence of the chemical structure of the RAFT agent on the degree of control of the polymerisation that is achieved in RAFT processes (Gonçalves *et al.*, 2013c).

Recent developments on pulsed-laser assisted techniques, namely Single–Pulse/Pulsed–Laser–Polymerisation/Time-Resolved Electron-Paramagnetic-Resonance (SP-PLP-EPR) (Barth and Buback, 2010) should also be considered in the discussion of the RAFT results obtained in chapters 5 and 7. In fact, using this technique it is possible the experimental study of polymerisation systems with more than one kind of radicals as for instance acrylates with secondary radicals or tertiary midchain radicals (appearing due to backbiting of secondary radicals). Moreover, this technique can be used to enlighten the problem concerning the different types of radicals involved in RAFT polymerisation and associated kinetic mechanisms. In fact, using this technique, rate coefficients of addition and fragmentation (and the correspondent equilibrium constants) were directly measured for butyl acrylate RAFT polymerisation using a trithiocarbonate (Meiser *et al*., 2013).

Other issues of RAFT polymerisation were also very recently addressed by the same research group when studying the kinetics of dithiobenzoate-mediated methyl methacrylate polymerisation (Sidoruk *et al.*, 2013). In this latter paper, different explanations for retardation with thiobenzoates were analysed, namely the following four mechanisms debated by scientific community:

- Slow fragmentation of the RAFT intermediate radical.
- Intermediate radical termination.
- Intermediate radical termination followed by "missing step"
- Cross-termination restricted to small radicals.

It was found that the concentration of the intermediate radicals is reduced compared with retarded systems and that cross-termination occurs to a weaker extent in the framework of the chemical system studied. Significant amounts of "missing step" products were also observed (Sidoruk *et al.*, 2013). It was also concluded that slow addition and "missing step" reactions contribute to the absence of rate retardation in dithiobenzoate mediated MMA polymerisation (Sidoruk *et al.*, 2013). Thus, experimental results of Buback group seem to show that the effect of slow fragmentation mechanisms should be small in RAFT polymerisation. Possibly, the secondary peak observed in the RAFT experiments performed in this work should be a consequence of the formation of 3-arm bridges during the polymerisation process, leading to

the formation of high size polymer species. New theoretical developments allowing the modeling of such complex mechanism should be sought in order to validate this hypothesis.

In chapter 6 it is shown that the impact of intramolecular cyclizations in superabsorbent hydrogels production should be weak (in contrast to styrene/divinylbenzene copolymers and similar) due to the very low content of crosslinker used and to the high values of the primary chain lengths involved. Polymerisation temperature, degree of neutralization of monomers (when AA or MAA are used), initial amount of crosslinker and other features of initial composition of the polymerisation system (e.g. ratios between main vinyl monomers) are some operation parameters with a strong effect on end-use properties of the synthesized hydrogels (Gonçalves *et al.*, 2011b and 2013b). Gelation kinetics in aqueous systems is faster when compared with organic systems. The produced materials were characterized in terms of swelling ratio and their environmental response to temperature and/or pH changes. These studies here presented are hopefully improvements for the development of tools concerning the design of production processes of tailored hydrogels.

In chapter 7 a comparison between the synthesis processes of these kinds of networks using FRP and RAFT polymerisation (considering three different commercially available RAFT agents) was experimentally performed. Important dissimilitudes in the dynamics of gel formation were identified when FRP mechanism is replaced by the RAFT polymerisation. Some peculiarities of the RAFT synthesis were studied (e.g. solubility of the used RAFT agents in water and monomers considered, effect of initial composition/kinetics on gelation) in order to find proper conditions to produce the sought hydrogels using this CRP technique. The use of multiple detection (especially including light scattering) in SEC analysis proved to be very important in order to obtain a rigorous characterization of products molecular architecture. In fact, the formation of an unexpected higher size secondary polymer population was detected by light scattering when RAFT polymerisation is used, even with mono-vinyl monomers (Gonçalves *et al.*, 2013d). It would seem that these results could be be explained in the framework of recent theoretical findings describing the RAFT slow fragmentation model leading to bimodal distributions formation (Zapata-González *et al.*, 2011), but this is in contradiction with other experimental evidence as above discussed. Therefore, other mechanisms causing loss of control such as hydrolysis of the RAFT agent and/or simultaneous polymerisation in aqueous and organic phases should also be considered in further developments on this research line.

Future Work

Experimental results here presented concerning the formation of hyperbranched polymers and gels/hydrogels can be used in future works as a contribution in the design of conditions allowing the synthesis of advanced materials with tailored properties. Nowadays, special applications of these kinds of materials are being found in biomedicine, pharmaceutics, separation processes or environmental industries. Research here presented can be directly applicable to the preparation of Molecular Imprinted Polymers (MIPs), Interpenetrating Polymer Networks (IPN) or generic gels/hydrogels for biomolecules immobilization (e.g. proteins). The synthesis of polymer nanoparticles with tailored sorption affinity for small molecules and oligomers is thus a possible extension of the ideas here explored. In fact, should be possible (for instance) the production of polymer particles suspended in a hydrophobic non-solvent with sizes in the nanometric scale and using RAFT polymerisation of water compatible monomers (e.g.) including a crosslinker. Highly branched structures with a broad length distribution of internal loops are thus expected. In this context, the operation in a tubular microfluidic reactor should be especially interesting because the upper size limit arising from the droplets will prevent it from becoming a gel (if desired). Exploitation of two steps crosslinking processes (e.g. linear chains formatted by RAFT submitted to a post-condensation of backbone functional groups) should also allow an upper control of the molecular architectures of these kinds of products.

In these new researches, the chosen co-monomers, solvents, the selected initiating system and the reaction conditions should lead to a variety of micro-gel architectures with widely different thermodynamic affinities to the selected species. Moreover, different extents of crosslinking lead to a spectrum of swelling capabilities. Additional steric effects are also expected to arise from the presence of loops, and even molecular imprinting can be obtained with appropriate auxiliary diluents. In the framework of these studies, theoretical tools allowing the prediction of the structure of the polymer particles (at a detailed enough extent) will also play a central role. For instance, use of advanced thermodynamic modeling, including molecular dynamics, should contribute to the prediction of the equilibrium and dynamic sorption properties, namely the diffusion profile and swelling behaviour of particles. Hopefully, these predictions should be experimentally validated through the study the effect of several operation conditions on the particle swelling and by testing chromatography columns using beds of microparticles coated by the produced materials. The ultimate goal should be the development of an expert system for the molecular design of materials capable

of specific sorption and reversible release of given substrates, with intended applications mostly in biomedicine and pharmacy, but also for industrial separation processes.

REFERENCES

Abrol, S., Kambouris, P.A., Looney, M.G., Solomon, D.H., 1997. Studies on microgels .3. Synthesis using living free radical polymerization . *Macromol. Rapid Comm*. 18, 755-760.

Abrol, S., Caulfield, M.J., Qiao, G.G., Solomon, D.H., 2001. Studies on microgels .5. Synthesis of microgels via living free radical polymerization. *Polymer* 42, 5987-5991.

Achilleos, M., Krasia-Christoforou, T., Patrickios, C.S., 2007. Amphiphilic model co-networks based on combinations of methacrylate, acrylate, and styrenic units: synthesis by RAFT radical polymerization and characterization of the swelling behaviour. *Macromolecules* 40, 5575-5581.

Aguiar, L.G., 2013. Synthesis of styrene-divinylbenzene copolymers using free radical and nitroxide mediated polymerization: experiments and mathematical modeling. PhD thesis (in Portuguese), *University of São Paulo,* Brazil.

Aguiar, L.G., Gonçalves, M.A.D., Pinto, V.D., Dias, R.C.S., Costa, M.R.P.F.N., Giudici, R., 2013a. Development of cyclic propagation kinetics for modeling the nitroxide-mediated radical copolymerization of styrene-divinylbenzene. *Macromol. React. Eng.* DOI: 10.1002/mren201300105.

Aguiar, L.G., Gonçalves, M.A.D., Pinto, V.D., Dias, R.C.S., Costa, M.R.P.F.N., Giudici, R., 2013b. Mathematical modeling of NMRP of styrene-divinylbenzene over the pre- and post-gelation periods including cyclization. *Macromol. React. Eng.* DOI: 10.1002/mren.201300171.

Ahmad, N.M., Heatley, F., Lovell, P.A., 1998. Chain transfer to polymer in free-radical solution polymerization of n-butyl acrylate studied by NMR spectroscopy. *Macromolecules* 31, 2822-2827.

Ameduri, B., Boutevin, B., 1999. Use of telechelic fluorinated diiodides to obtain well defined fluoropolymers. *Journal of Fluorine Chemistry* 100, 97-116.

Alam, M.N., Zetterlund, P.B., Okubo, M., 2006. Network formation in nitroxide-mediated radical copolymerization of styrene and divinylbenzene in miniemulsion. *Macromol. Chem. Physic*. 207, 1732-1741.

Anseth, K.S., Scott, R.A., Peppas, N.A., 1996. Effects of ionization on the reaction behavior and kinetics of acrylic acid polymerizations. *Macromolecules* 29, 8308-8312.

Arriola, D.J., Cutié, S.S., Henton, D.E., Powell, C., Smith, P.B., 1997. Crosslinker reactivity and the structure of superabsorbent gels. *J. Appl. Polym. Sci*. 63, 439-451.

Arzamendi, G., Forcada, J., Asúa, J.M., 1994. Kinetics of long chain branching in emulsion polymerisation. *Macromolecules* 27. 6068-6079.

Asúa, J.M., Beuermann, S., Buback, M., Castignolles, B., Charleaux, B., Gilbert, R.G., Hutchinson, R.A., Leiza, J.R., Nikitin, A.N., Vairon, J.P., van Herk, A.M., 2004. Critically evaluated rate coefficients for free-radical polymerization, 5-Propagation rate coefficient for butyl acrylate. *Macromol. Chem. Physic.* 205, 2151-2160.

Bahaj, H., Benaddi, R., Bakass, M., Bayane, C., 2010. Swelling of superabsorbent polymers in an aqueous medium. *J. Appl. Polym. Sci.* 115, 2479-2484.

Bajpai, S.K., Bajpai, M., Sharma, L., 2007. Inverse suspension polymerization of poly(methacrylic acid-co-partially neutralized acrylic acid) superabsorbent hydrogels: synthesis and water uptake behaviour. *Designed Monomer and Polymers* 10, 181-.

Bajpai, A., Shukla, S., Saini R., Tiwari, A., 2010. Stimuli Responsive Drug Delivery Systems: From Introduction to Application 1st ed.: Smithers Rapra, ISBN-13: 978-1847354167.

Bannister, I., Billingham, N.C., Armes, S.P., Rannard, S.P., Findlay, P., 2006. Development of branching in living radical copolymerization of vinyl and divinyl monomers. *Macromolecules* 39, 7483-7492

Barner-Kowollik, C., Quinn, J.F., Morsley,, D.R., Davis, T.P., 2001. Modeling the reversible addition-fragmentation chain transfer process in cumyl dithiobenzoate-mediated styrene homopolymerizations: Assessing rate coefficients for the addition-fragmentation equilibrium. *J. Polym. Sci. Pol. Chem.*39, 1353-1365.

Barner-Kowollik, C., Coote, M.L., Davis, T.P., Radom, L., Vana, P., 2003. The reversible addition-fragmentation chain transfer process and the strength and limitations of modeling: Comment on "the magnitude of the fragmentation coefficient". *J. Polym. Sci. Pol. Chem.*41, 2828-2832.

Barner-Kowollik, C., Günzler, F., Junkers, T., 2008. Pushing the limit: pulsed laser polymerization of n-Butyl acrylate at 500 Hz. *Macromolecules* 41, 8971-8973.

Barson, C.A., Bevington, J.C., 1997. Further studies of end groups derived from benzoyl peroxide. *J. Polym. Sci. Pol. Chem*. 35, 2955-2960

Barth, J., Buback, M., 2010. SP-PLP-EPR—A novel method for detailed studies into the termination kinetics of radical polymerization. *Macromol. React. Eng.* 4, 288-301.

Bayramoglu, G., Senkal, F.B., Celik, G., Arica, M.Y., 2007. Preparation and characterization of sulphonyl-hydrazine attached poly (styrene-divinylbenzene) beads for separation of albumin. *Colloids and Surfaces A* 294, 56-63.

Beckwith, A.L, Bowry, V.W., Ingold, K.H., 1992. Kinetics of nitroxide radical trapping .1. Solvent effects. *J. Am. Chem. Soc.* 114, 4983-4992.

Belincanta-Ximenes. J., Mesa. P.V.R., Lona. L.M.F., Vivaldo-Lima. E., McManus. N.T., Penlidis. A., 2007. Simulation of styrene polymerization by monomolecular and bimolecular nitroxide-mediated radicals processes over a range of reaction conditions. *Macromol. Theor. Simul*. 16, 194-208.

Beuermann, S., Buback, M., Davis, T.P., Gilbert, R.G., Hutchinson, R.A., Olaj, O.F., Russel, G.T., Schweer, J., van Herk, A.M., 1997. Critically evaluated rate coefficients for free-radical polymerization .2. Propagation rate coefficients for methyl methacrylate. *Macromol. Chem. Physic*. 198, 1545-1560.

Beuermann, S., Buback, M., 2002. Rate coefficients of free-radical polymerization deduced from pulsed laser experiments. *Prog. Polym. Sci.* 27, 191-254.

Beuermann, S., Buback, M., Hesse, P., Lacík, I., 2006. Free-radical propagation rate coefficient of non-ionized methacrylic acid in aqueous solution from low monomer concentrations to bulk polymerisation. *Macromolecules* 39, 184-193.

Beuermann, S., Buback, M., Hesse, P., Kukučková, S., Lacík, I., 2007a. Propagation kinetics of free-radical methacrylic acid polymerisation in aqueous solution. The effect of concentration and degree of ionization. *Macromol. Symp*. 248, 23-32.

Beuermann, S., Buback, M., Hesse, P., Kukučková, S., Lacík, I., 2007b. Propagation rate coefficient of non-ionized methacrylic acid radical polymerisation in aqueous solution. The effect of monomer conversion. *Macromol. Symp*. 248, 41-49

Beuermann, S., Buback, M., Hesse, P., Gilbert, R.G., Kuchta, F-D., Lacík, I., van Herk, A.M., 2007c. Critically evaluated rate coefficients for free-radical polymerisation. Part 6: Propagation rate coefficient of methacrylic acid in aqueous solution. *Pure and Applied Chemistry* 79, 1463-1469.

Beuermann, S., Buback, M., Hesse, P., Hutchinson, R.A., Kukučková, S., Lacík, I., 2008. Termination kinetics of the free-radical polymerisation of non-ionized methacrylic acid in aqueous solution. *Macromolecules* 41, 3513-3520.

Bevington, J.C., 1955. The sensitized polymerization of styrene- the rate and efficiency of initiation. *Transactions Faraday Society* 51, 1392-1397.

Biasutti, J.D., Davis, T.P., Lucien, F.P., Heuts, J.P.A., 2005. Reversible addition-fragmentation chain transfer polymerization of methyl methacrylate in suspension. *J. Polym. Sci. Pol. Chem*. 43, 2001-2012.

Bodugöz, H., Güven, O., 2002. The synthesis of nonporous poly(isobutyl methacrylate) microspheres by suspension polymerization technique and investigation of their swelling properties. *J. Appl. Polym. Sci.* 83, 349-356.

Boschmann, D., Vana, P., 2007. Z-RAFT star polymerizations of acrylates: Star coupling via intermolecular chain transfer to polymer. *Macromolecules* 40, 2683-2693.

Brandrup, J., Immergut, E.H., Grulke, E.A., Abe, A., Bloch, D.R., 1999. Polymer Handbook, 4th edition. John Wiley & Sons.

Braunecker, W. A., Matyjaszewski, K., 2007. Controlled/Living radical polymerization: Features, developments, and perspectives. *Prog. Polym. Sci*. 32, 93-146.

Brazel, C.S., Peppas, N.A., 1995. Synthesis and characterization of thermomechanically and chemomechanically responsive poly(N-isopropylacrylamide-co-methacrylic acid) hydrogels. *Macromolecules* 28, 8016-8020.

Britton, D., Heatley, F., Lovell, P.A., 1998. Chain transfer to polymer in free-radical bulk and emulsion polymerisation of vinyl acetate studied by NMR spectroscopy. *Macromolecules* 31, 2828-2837.

Buback, M., Gilbert, R.G., Hutchinson, R.A., Klumperman, B., Kuchta, F.D., Manders, B.G., O'Driscoll, K.F., Russel, G.T., Schweer, J., 1995. Critically Evaluated Rate Coefficients for Free-Radical Polymerization .1. Propagation Rate Coefficient for Styrene. *Macromol. Chem. Physic.* 196, 3267-3280.

Buback, M., Junkers, T., 2006. Termination kinetics of tert-butyl methacrylate and of n-butyl methacrylate free-radical bulk homopolymerizations. *Macromol. Chem. Physic.* 207, 1640-1650.

Buback, M., Hesse, P., Junkers, T., Sergeeva, T., Theis, T., 2008a. PLP labelling in ESR spectroscopy analysis of secondary and tertiary acrylate propagating radicals. *Macromolecules* 41, 288-291.

Buback, M., Hesse, P., Hutchinson, R.A., Kasák, P., Lacík, I., Stach, M., Utz, I., 2008b. Kinetics and modeling of free-radical batch polymerization of nonionized methacrylic acid in aqueous solution. *Ind. Eng. Chem. Res*. 47, 8197-8204.

Buchholz, F.L., Graham, A.T. (Eds.), 1997. Modern superabsorbent polymer technology. New York: Wiley.VCH, ISBN 978-0-471-19411-8.

Buchholz, F.L., Peppas, N.A., 1994. Superabsorbent Polymers: Science and Technology. ACS symposium Series, Washington.

Búrdalo. J., Medrano. R., Saiz. E., Tarazona. M.P., 2000. A simple method to determine unperturbed dimensions of polymers using size exclusion chromatography and multi angle light scattering. *Polymer* 41. 1615-1620.

Butté, A., Storti, G., Morbidelli, M., 2000. Miniemulsion living free radical polymerization of styrene. *Macromolecules* 33, 3485-3487.

Butté, A., Storti, G., Morbidelli, M., 2001. Miniemulsion living free radical polymerization by RAFT. *Macromolecules* 34, 5885-5896.

Carothers, W.H., 1936. Polymers and polyfunctionality. *Transactions Faraday Society* 32, 39-49.

Chaduc, I., Lansalot, M., D'Agosto, F., Charleux, B., 2012a. RAFT polymerisation of methacrylic acid in water. *Macromolecules* 45, 1241-1247.

Chaduc, I., Girod, M., Antoine, R., Charleux, B., D'Agosto, F., Lansalot, M., 2012b. Batch emulsion polymerisation mediated by poly(methacrylic acid) macro RAFT agents: One-pot synthesis of self-stabilized particles. *Macromolecules* 45, 5881-5893.

Chatzi, E.G., Kammona, O., Kiparissides, C., 1997. Use of midrange infrared optical-fiber probe for the on-line monitoring of 2-ethylhexyl acrylate/styrene emulsion copolymerization. *J. Appl. Polym. Sci.* 63,799-809.

Chen, G.H., Hoffman, A.S., 1995. Graft-copolymers that exhibit temperature-induced phase-transitions over a wide-range of pH. *Nature* 373, 49-52.

Chen, X., Shan, G., Huang, J., Huang, Z., Weng, Z., 2004. Synthesis and properties of acrylic-based superabsorbent. *J. Appl. Polym. Sci.* 92, 619-624.

Cheyney, L.V.E., Kelley, E.J., 1942. Unsaturation of synthetic rubberlike materials. *Ind. Eng. Chem*. 34, 1323-1326.

Choi, C.H., Kertesz, M., 1997. Conformational information from vibrational spectra of styrene, trans-stilbene, and cis-stilbene. *J. Phys. Chem. A* 101, 3823-3831.

Coelho, J.F.J, Silva, A.M.F.P, Popov, A.V., Persec V., Abreu, M.V., Gonçalves, P.M.F.O., Gil, M.H., 2006a. Syntehsis of poly(vinyl chloride)-b-poly(n-butyl acrylate)-b-poly(vinyl chloride) by the competitive single-electron-transfer/degenerative-chain-transfer-mediated living radical polymerisation in water. *J. Polym. Sci. Pol. Chem*. 44, 3001-3008.

Coelho, J.F.J, Carreira, M., Popov, A.V., Gonçalves, P.M.F.O., Gil, M.H., 2006b. termal and mechanical characterization of poly(vinyl chloride)-b-poly(n-butyl acrylate)-b-poly(vinyl chloride) by single electron transfer-degenerative chain transfer mediated living radical polymerisation in water. *Eur. Polym. J*. 42, 2313-2319.

Coelho, J.F.J, Carreira, M., Gonçalves, P.M.F.O., Popov, A.V., Gil, M.H., 2006c. Processability and characterization of poly(vinyl chloride)-b-poly(n-butyl acrylate)-b-poly(vinyl chloride) prepared by living radical polymerisation of vinyl chloride. Comparison with a flexible commercial resin formulation prepared with PVC and dioctyl phthalate. *Journal of. Vinyl & Additive Technology* 12, 159-165.

Coelho, J.F.J, Carvalho, E.Y., Marques, D.S., Popov, A.V., Persec., V., Gil, M.H, 2008. Influence of the isomeric structures of butyl acrylate on its single-electron transfer-degenerative chain transfer living radical polymerisation in water catalyzed by $Na_2S_2O_4$. *J. Polym. Sci. Pol. Chem.* 46, 6542-6551.

Coelho, J.F.J, Gois, J.R., Fonseca, A.C., Carvalho, R.A., Popov, A.V., Persec., V., Gil, M.H., 2009. Synthesis of poly(2-methoxyethyl acrylate) by single electron transfer-degenerative chain transfer living radical polymerisation catalyzed by $Na_2S_2O_4$ in water. *J. Polym. Sci. Pol. Chem*. 47, 4454-4463.

Coelho, J.F.J, Fonseca, A.C., Gois, J.R., Gonçalves, P.M.F.O., Popov, A.V., Gil, M.H., 2011a. Scaling-up of poly(vinyl chloride) prepared by single electron transfer degenerative chain transfer mediated living radical polymerisation in water media: Low molecular weight. Kinetic analysis. *Chem. Eng. J.* 169, 399-413.

Coelho, J.F.J, Fonseca, A.C., Gonçalves, P.M.F.O., Popov, A.V., Gil, M.H., 2011b. Particle features and morphology of poly(vinyl chloride) prepared by living radical polymerisation in aqueous media. Insight about particle formation mechanism. *Polymer* 52, 2998-3010.

Colthup, N.B., Daly, L.H., Wiberley, S.E., 1990. Introduction to infrared and raman spectroscopy, third ed., Academic Press, Boston.

Cooper, A.I., Hems, W.P., Holmes, A.B., 1998. Synthesis of cross-linked polymer microspheres in supercritical carbon dioxide. *Macromol. Rapid Comm*. 19, 353-357.

Cooper, A.I., Hems, W.P., Holmes, A.B., 1999. Synthesis of highly cross-linked polymers in supercritical carbon dioxide by heterogeneous polymerization. *Macromolecules* 32, 2156-2166.

Costa, M.R.P.F.N., Dias, R.C.S., 1994. A general kinetic analysis of non-linear irreversible copolymerizations. *Chem. Eng. Sci.* 49, 491-516.

Costa, M.R.P.F.N., Dias, R.C.S., 2003. Prediction of Sol Fraction and Average Molecular Weights after Gelation for Non-Linear Free Radical Polymerizations Using a Kinetic Approach. *Macromol. Theor. Simul.* 12, 560-572.

Costa, M.R.P.F.N., Dias, R.C.S., 2005. An improved General Kinetic Analysis of Non-Linear Irreversible Polymerizations. *Chem. Eng. Sci.* 60, 423-446.

Costa, M.R.P.F.N., Dias, R.C.S., 2006. Kinetic modeling of non-linear polymerization. *Macromol. Symp*. 242, 72-82.

Costa, M.R.P.F.N., Dias, R.C.S., 2007. Prediction of Mean-Square Radius of Gyration of Tree-Like Polymers by a General Kinetic Approach. *Polymer* 48, 1785-1801.

Coutinho, F.M.B., Rabelo, D., 1992. Scanning electron-microscopy study of styrene divinylbenzene copolymers. *Eur. Polym. J*. 28, 1553-1557.

Crompton, T.R., Reid, V.W., 1963. Unsaturation in high impact polystyrene: analytical studies. *J. Polym. Sci. Part A* 1, 347-355.

Cunningham, M., 2008. Controlled/living radical polymerization in aqueous dispersed systems. *Prog. Polym. Sci*. 33, 365-398.

Cutié, S.S., Henton, D.E., Powell, C., Reim, R.E., Smith, P.B., Staples, T.L., 1997a. The effects of MEHQ on the polymerization of acrylic acid in the preparation of superabsorbent gels. *J. Appl. Polym. Sci*. 64, 577-589.

Cutié, S.S., Smith, P.B., Henton, D.E., Staples, T.L., Powell, C., 1997b. Acrylic acid polymerisation kinetics. *J. Appl. Polym. Sci*. *Pol. Phys* 35, 2029-2047.

Destarac, M., 2010. Controlled radical polymerization: industrial stakes, obstacles and achievements. *Macromolecules* 4, 165-179.

Dias, R.C.S., Costa, M.R.P.F.N., 2003. A New Look at Kinetic Modeling of Nonlinear Free Radical Polymerizations with Terminal Branching and Chain Transfer to Polymer. *Macromolecules* 36, 8853-8863.

Dias, R.C.S., Costa, M.R.P.F.N., 2005a. Semibatch operation and primary cyclization effects in homogeneous free-radical crosslinking copolymerizations. *Polymer* 46, 6163-6173.

Dias, R.C.S., Costa, M.R.P.F.N., 2005b. Transient Behavior and Gelation of Free Radical Polymerizations in Continuous Stirred Tank Reactors. *Macromol Theor. Simul.* 14, 243-255.

Dias, R.C.S., Costa, M.R.P.F.N., 2006. A general kinetic method to predict sequence length distributions for non-linear irreversible multicomponent polymerizations. *Polymer* 47, 6895-6913.

Dias, R.C.S., Costa, M.R.P.F.N., 2007. Branching and crosslinking in coordination terpolymerization. *Macromol. React. Eng.* 1, 440-467.

Dias, R.C.S., Costa, M.R.P.F.N., 2010. Calculation of CLD using population balance equations of generating functions: Linear and non-linear ideal controlled radical polymerization. *Macromol. Theor. Simul.* 19, 323-341.

Dobkowski, Z., 1985. Characterization of branched polydispersed polymers- Influence of solvents on the branching parameters. *J. Appl. Polym. Sci.* 30, 355-362.

Dotson, N.A., 1992. Correlations in non-linear free-radical polymerizations: substitution effect. *Macromolecules* 25, 308-321.

Duchet, J., Pascault, J.P., 2003. Do epoxy-amine networks become inhomogeneous at the nanometric scale? *J. Polym. Sci. Pol. Phys*. 41, 2422-2432.

Dušek, K., 1996. Are cured thermoset resins inhomogeneous? *Die Angewandte Makromoleculare Chemie* 240, 1-15.

Dušek, K., Dŭsková-Smrčcková, M., Huybrechts, J., 2005. Control of performance of nanostructured polymer network precursors by differences in reactivity of functional groups. *Journal of Nanostructured Polymer and Nanocomposites* 1, 45-53.

Dušek, K., 2007. My fifty years with polymer gels and networks and beyond. *Polym. Bull*. 58, 321-338.

Ende, M.T., Hariharan, D., Peppas, N.A., 1995. Factors influencing drug and protein transport and release from ionic hydrogels. *Reactive Polymers* 25, 127-137.

Feil, H., Bae, Y.H., Feijen, J., Kim, S.W., 1992. Mutual influence of pH and temperature on the swelling of ionisable and thermosensitive hydrogels. *Macromolecules* 25, 5528-5530.

Fernández-Garcia, M., Martinez, J.J., Madruga, E.L., 1998. Solvent effects on the free-radical polymerization of methyl methacrylate. *Polymer* 39, 991-995.

Fernández-García, M., Fernández-Sanz, M., Madruga, E.L., 2004. Free-radical copolymerization of styrene with butyl acrylate. II. Elemental kinetic copolymerization step predictions from homopolymerization data. *J. Polym. Sci. Pol. Chem.* 42, 130-136.

Fischer, H., Radom, L., 2001. Factors controlling the addition carbon-centered radicals to alkenes – an experimental and theoretical perspective. *Angew. Chem., Int.Ed.Engl*. 40, 1340-1371.

Fixman, M., 1955. Excluded volume in polymer chains. *Journal of Chemical Physics* 23, 1656-1659.

Flory, P.J., 1941a. Molecular size distribution in three dimensional polymers. I. Gelation. *J. Am. Chem. Soc.* 63, 3083-3090.

Flory, P.J., 1941b. Molecular size distribution in three dimensional polymers. II. Trifunctional branching units. *J. Am. Chem. Soc.* 63, 3091-3096.

Flory, P.J., 1941c. Molecular size distribution in three dimensional polymers. III. Tetrafunctional branching units. *J. Am. Chem. Soc.* 63, 3096-3100.

Fu, I., Cunningham, M.F., Hutchinson, R.A., 2007a. Modeling of nitroxide-mediated semi-batch radical polymerization. *Macromol. React. Eng.* 1, 243-252.

Fu, I., Mirzaei A., Cunningham, M.F., Hutchinson, R.A., 2007b. Atom-transfer radical batch and semi-batch polymerization of styrene. *Macromol. React. Eng.* 1, 425-439.

Fukuda, T., Terauchi, T., Goto, A., Ohno, K., Tsujii, Y., Miyamoto, T., Kobatake, S., Yamada, B., 1996. Mechanisms and kinetics of nitroxide-controlled free-radical polymerization. *Macromolecules* 29, 6393-6398.

Gaborieau, M., Gilbert, R.G., Gray-Weale, A., Hernandez, J.M., Castignolles, P., 2007. Theory of multiple-detection size-exclusion chromatography of complex branched polymers. *Macromol. Theor. Simul*. 16, 13-28.

Galaev, I., Mattiasson, B., 2008. Smart polymers: Applications in biotechnology and biomedicine, second ed. CRC Press, Boca Raton.

Gao, C., Yan, D. 2004. Hyperbranched polymers: from synthesis to applications. *Prog. Polym. Sci.*, 29, 183-275.

Gao, H., Min, K., Matyjazewski, K., 2007. Determination of gel point during atom transfer radical copolymerization with cross-linker. *Macromolecules* 40, 7763-7770.

Gao, H., Li, W., Matyjazewski, K., 2008. Synthesis of polyacrylate network by ATRP: Parameters influencing experimental gel points. *Macromolecules* 41, 2335-2340.

Gao, H., Polanowski, P., Matyjazewski, K., 2009. Gelation in living copolymerization of monomer and divinyl cross-linker: comparison of ATRP experiments with Monte-Carlo simulations. *Macromolecules* 42, 5925-5932.

García-Morán, P.R., Jaramillo-Soto, G., Albores-Velasco, M.E., Vivaldo-Lima, E., 2009. An experimental study on the free-radical copolymerization kinetics with crosslinking of styrene and divinylbenzene in supercritical carbon dioxide. *Macromol. React. Eng.* 3, 58-70.

Gaynor, S.G., Wang, J.S., Matyjaszewski, K., 1995. Controlled radical polymerization by degenerative transfer – effect of the structure of the transfer agent. *Macromolecules* 28, 8051-8056.

Gemeinhart, R.A., Chen, J., Park, H., Park, K., 2000. pH-sensitivity of fast responsive superporous hydrogels. *Journal of Biomaterials Science, Pol. Ed.* 11, 1371-1380.

Georges, M.K., Veregin, R.P.N., Kazmaier, P.M., Hamer, G.K., 1993. Narrow molecular-weight resins by a free-radical polymerization process. *Macromolecules* 26, 2987-2988.

Gonçalves, M.A.D., Dias, R.C.S., Costa, M.R.P.F.N., 2007. Time Programmed Feed of Semi-Batch Reactors with Non-Linear Radical Copolymerizations: An Experimental Study of the System Styrene + Divinylbenzene Using SEC/MALLS. *Macromol. Symp.* 259, 124-134.

Gonçalves, M.A.D., Dias, R.C.S., Costa, M.R.P.F.N., 2010a. Prediction and experimental characterization of the molecular architecture of FRP and ATRP synthesized polyacrylate networks. *Macromol. Symp.* 289, 1-17.

Gonçalves, M.A.D., Pinto, V.D., Dias, R.C.S., Costa, M.R.P.F.N., 2010b. FTIR-ATR monitoring and SEC/RI/MALLS characterization of ATRP synthesized hyperbranched polyacrylates. *Macromol. Symp.* 296, 210-228.

Gonçalves, M.A.D., Dias, R.C.S., Costa, M.R.P.F.N., 2010c. Kinetic modeling of hyperbranched polymer synthesis through atom-transfer and nitroxide-mediated radical polymerization of vinyl/divinyl monomers. *Chem. Eng. Technol*. 33, 1797-1813.

Gonçalves, M.A.D., Trigo, I.M.R., Dias, R.C.S., Costa, M.R.P.F.N., 2010d. Kinetic modeling of the molecular architecture of crosslinked copolymers synthesized by controlled radical polymerization techniques. *Macromol. Symp.* 291-292, 239-250.

Gonçalves, M.A.D., Pinto, V.D., Dias, R.C.S., Costa, M.R.P.F.N., 2011a. Kinetic modeling of the suspension copolymerisation of styrene/divinylbenzene with gel formation. *Macromol. Symp*. 302, 179-190.

Gonçalves, M.A.D., Pinto, V.D., Dias, R.C.S., Costa, M.R.P.F.N., 2011b. Modeling studies on the synthesis of superabsorbent hydrogels using population mass balance equations. *Macromol. Symp*. 306-307, 107-125.

Gonçalves, M.A.D., Pinto, V.D., Dias, R.C.S., Costa, M.R.P.F.N., Aguiar, L.G., Giudici, R., 2013a. Gel formation in aqueous suspension nitroxide-mediated radical co-polymerization of styrene/divinylbenzene. *Macromol. React. Eng.* 7, 155-175.

Gonçalves, M.A.D., Pinto, V.D., Dias, R.C.S., Costa, M.R.P.F.N., 2013b. Polymer reaction engineering studies on smart hydrogels formation. *Journal of Nanostructured Polymer and Nanocomposites* 9, 40-45.

Gonçalves, M.A.D., Pinto, V.D., Dias, R.C.S., Costa, M.R.P.F.N., Hernández-Ortiz, J.C., 2013c. Dynamics of network formation in aqueous suspension RAFT styrene/divinylbenzene copolymerisation. *Macromol. Symp.* 333, 273-285.

Gonçalves, M.A.D., Pinto, V.D., Costa, R., Dias, R.C.S., Hernández-Ortiz, J.C., Costa, M.R.P.F.N., 2013d. Stimuli-responsive hydrogels synthesis using free-radical and RAFT polymerisation. *Macromol. Symp.* 333, 41-54.

González, I., Leiza, J.R., Asúa. J.M., 2006. Exploring the limits of branching and gel content in the emulsion polymerization of nBa. *Macromolecules* 39, 5015-5020.

González, I., Asúa. J.M., Leiza, J.R., 2007. The role of methyl methacrylate on branching and gel formation in the emulsion copolymerization of BA/MMA. *Polymer* 48, 2542-2547.

Goto, A., Ohno, K., Fukuda, T., 1998. Mechanism and kinetics of iodide-mediated polymerization of styrene. *Macromolecules* 31, 2809-2814.

Goto, A., Fukuda, T., 2004. Kinetics of living radical polymerization. *Prog. Polym. Sci*. 29, 329-385.

Greszta, G., Matyjaszewski, K., 1996. Mechanisms of controlled/"living" radical polymerisation of styrene in the presence of nitroxyl radicals. Kinetics and simulations. *Macromolecules* 29, 7661-7670.

Gretton-Watson, S.P., Alpay, E., Steinke, J.H.G., Higgins, J.S., 2006. Multi-functional monomer derived hyperbranched poly(methyl methacrylate): Kinetic modelling and experimental validation. *Chem. Eng. Sci.* 61, 1421-1433.

Hamzehlou, S., Reyes, Y., Leiza, J.R., 2013. A new insight into the formation of polymer networks: A kinetic Monte Carlo simulation of the cross-linking polymerization of S/DVB. *Macromolecules* 46, 9064-9073.

Hecker, M., 2000. Experimentelle Untersuchungen und Monte-Carlo-Simulation netzwerkbildender Copolymerisationen. Fortschritte der Polymerisationstechnik II (H.U. Moritz ed.), ISBN 3-89685-353-8, *Wissenschaft & Technik Verlag*, Berlin.

Henton, D.E., Powell, C., Reim, R.E., 1997. The decomposition of sodium persulfate in the presence of acrylic acid. *J. Appl. Polym. Sci*. 64, 591-600.

Hernández-Ortiz, J.C., Vivaldo-Lima, E., Lona, L.M.F., McManus, N.T., Penlidis, A., 2009. Modeling of the nitroxide-mediated radical copolymerization of styrene and divinylbenzene. *Macromol. React. Eng.* 3, 288-311.

Hernández-Ortiz, J.C., Jaramillo-Soto, G., Palacios-Alquisira, J., Vivaldo-Lima, E., 2010. Modeling of polymerization kinetics and molecular weight development in the microwave-activated RAFT polymerization of styrene. *Macromol. React. Eng.*4, 210-221.

Hernández-Ortiz, J.C., Vivaldo-Lima, E., Penlidis, A., 2012. Modeling of network formation in nitroxide-mediated radical copolymerisation of vinyl/divinyl monomers using a multifunctional polymer molecule approach. *Macromol. Theor. Simul.* 21, 302-321.

Heuts, J.P.A., Russel, G.T., Smith, G.B., van Herk, A.M., 2007. The importance of chain-length dependent kinetics in free-radical polymerization: a preliminary guide. *Macromol. Symp.* 248, 12-22.

Hirao, A., Tanaka, S., Goseki, R., Ishizone, T., 2011. Living Anionic Polymerization of 1,4-Divinylbenzene. *Macromolecules* 44, 4579-4582.

Hornung, C.H., Almar, P., Saubern, S., Chiefari, J., 2012. A continuous flow process for the radical induced end group removal of RAFT polymers. *Macromol. React. Eng*. 6, 246-251.

Hua, H., Dubé, M.A., 2001. Terpolymerization monitoring with ATR-FTIR spectroscopy. *J. Appl. Polym. Sci*. 39, 1860-1876.

Hua, H., Dubé, M.A., 2002. In-line monitoring of emulsion homo- and copolymerizations using ATR-FTIR. *Polym. React. Eng.* 10, 21-40.

Hua, H., Rivard, T., Dubé, M.A., 2004. Off-line monitoring of styrene/butyl acrylate copolymerizations in toluene using ATR-FTIR spectroscopy. *Polymer* 45, 345-354.

Hui, A.W., Hamielec, A.E., 1976. Thermal polymerization of styrene at high conversions and temperatures- an experimental study. *J. Appl. Polym. Sci.* 16, 749-&.

Hutchinson, R.A., 2005. Free Radical Polymerization: Homogeneous. Handbook of Polymer Reaction Engineering. Wiley, VCH.

Hutchinson, R.A., Penlidis, A., 2007. Free Radical Polymerization: Homogeneous systems. Handbook of Polymer Reaction Engineering. Blackwell Publishing.

Ide, N., Fukuda, T., 1997. Nitroxide-controlled free-radical copolymerization of vinyl and divinyl monomers. Evaluation of pendant-vinyl reactivity. *Macromolecules* 30, 4268-4271.

Ide, N., Fukuda, T., 1999. Nitroxide-controlled free-radical copolymerization of vinyl and divinyl monomers. 2. Gelation. *Macromolecules* 32, 95-99.

Ioan, S., Bercea, M., Ioan. C., Simionescu, B.C., 1995. Solution properties of ultrahigh molecular-weight polymers .20. Polymer-chain dimensions of Poly(methyl methacrylate). *Eur. Polym. J.* 31, 85- 89.

Iovu, M.C., Matyjaszewski, K., 2003. Controlled/living radical polymerization of vinyl acetate by degenerative transfer with alkyl iodides. *Macromolecules* 36, 9346-9354.

Jackson, C., Chen, Y.J., Mays, J.W., 1996. Dilute solution properties of randomly branched poly(methyl methacrylate). *J. Appl. Polym. Sci* 59, 179-188.

Jaramillo-Soto, G., Vivaldo-Lima, E., 2012. RAFT copolymerization of styrene/divinylbenzene in supercritical carbon dioxide. *Australian Journal of Chemistry* 65, 1177-1185.

Jenkins, A.D., Jones, R.G., Moad, G., 2010. Terminology for reversible-deactivation radical polymerisation previously called “controlled” radical or “living” radical polymerisation (IUPAC Recommendations 2010). *Pure and Applied Chemistry* 82, 482-491.

Jovanović, R., Dubé, M.A., 2001. Off-line monitoring of butyl acrylate and vinyl acetate homopolymerization and copolymerization in toluene. *J. Appl. Polym. Sci* 82, 2958-2977.

Jovanović, R., Dubé, M.A., 2003. In-line monitoring of butyl acrylate/vinyl acetate emulsion copolymerization using ATR-FTIR spectroscopy. *Polym. React. Eng.* 11, 233-257.

Kabanov, V.A., Topchiev, D.A., Karaputadze, T.M., 1973. Some features of radical polymerization of acrylic and methacrylic acid salts in aqueous-solutions. *J. Polym. Sci.: Pol. Sym.* 42, 173-183.

Kabanov, V.A., Topchiev, D.A., Karaputadze, T.M., 1975. Kinetics and mechanism of radical polymerization of weak unsaturated acids in aqueous solutions. *Eur. Polym. J.* 11, 153-159.

Kabiri, K., Zohuriaan-Mehr, M.J., 2004. Porous superabsorbent hydrogel composites: Synthesis, morphology and swelling rate. *Macromolecular Materials and Engineering* 289, 653-661.

Kamigaito, M., Ando, T., Sawamoto, M., 2001. Metal-catalyzed living radical polymerization. *Chemical Reviews* 101, 3689-3745.

Kamigaito, M., Ando, T., Sawamoto, M., 2004. Metal-catalyzed living radical polymerization: discovery and developments. *Chemical Record* 4, 159-175.

Karyappa, R.B., Natarajan, U., 2008. Monte-Carlo simulations of chain dimensions conformational properties of various poly(n-alkyl methacrylates) in solution. *J. Macromol. Sci. B* 47, 1075-1086.

Kato, M., Kamigaito, M., Sawamoto, M., Higashimura, T., 1995. Polymerization of methyl methacrylate with the carbon-tetrachloride dichlorotris(triphenylphosphine) ruthenium(II) methylaluminum bis(2,6-di-tert-butylphenoxide) initiating system- possibility of living radical polymerization. *Macromolecules* 28, 1721-1723.

Kemp, A.R., Peters, H., 1943. Unsaturation of butadiene and related polymers – As determined by iodine chloride addition. *Ind. Eng. Chem.*15, 453-459.

Kiatkamjornwong, S., Phunchareon, P., 1999. Influence of reaction parameters on water absorption of neutralized poly(acrylic acid-co-acrylamide) synthesized by inverse suspension polymerization. *J. Appl. Polym. Sci.* 72, 1349-1366.

Kiatkamjornwong, S., Chientachakul, P., Prasassarakich, P., Damronglerd, S., 2001. Kinetic studies on styrene/divinylbenzene copolymerization by suspension technique. *J. Appl. Polym. Sci*. 82, 1521-1540.

Knothe, G., 2002. Structure indices in FA chemistry. How relevant is the iodine value? *Journal of the American Oil Chemists Society* 79, 847-854.

Krasia, T.C., Patrickios, C.S., 2006. Amphiphilic polymethacrylate model co-networks: synthesis by RAFT radical polymerization and characterization of the swelling behaviour. *Macromolecules* 39, 2467-2473.

Krstina, J., Moad, G., Rizzardo, E., Winzor, C.L., Berge, C.T., Fryd, M., 1995. Narrow polydispersity block-copolymers by free-radical polymerization in the presence of macromonomers. *Macromolecules* 28, 5381-5385.

Kuchta, F-D., van Herk., A.M., German, A.L., 2000. Propagation kinetics of acrylic and methacrylic acid in water and organic solvents studied by pulsed-laser polymerization. *Macromolecules* 33, 3641-3649.

Kurata, M., Stockmayer, W.H., Roig, A., 1960. Excluded volume effect of linear polymer molecules. J. *Chem. Phys.* 33, 151-155.

Kurland, J.J., 1980. Quantitative aspects of synergistic inhibition of oxygen and para-methoxyphenol in acrylic-acid polymerization. *J. Polym. Sci*. 18, 1139-1145.

Lacík, I., Buback, M., Beuermann, S., 2001. Aqueous phase size-exclusion-chromatography used for PLP-SEC studies into free-radical propagation rate of acrylic acid in aqueous solution. *Macromolecules* 34, 6224-6228.

Lacík, I., Buback, M., Beuermann, S., 2003. PLP-SEC study into the free-radical propagation rate of nonionized acrylic acid in aqueous solution. *Macromolecules.* 36, 9335-9363.

Lacík, I., Buback, M., Beuermann, S., 2004. PLP-SEC study into the free-radical propagation rate coefficients of partially and fully ionized acrylic acid in aqueous solution. *Macromol. Chem. Physic.* 205, 1080-1087.

Lacík, I., Učňová, L., Kukučková, S., Buback, M., Hesse, P., Beuermann, S., 2009. Propagation rate coefficient of free radical polymerisation of partially and fully ionized methacrylic acid in aqueous solution. *Macromolecules* 42, 7753-7761.

Landin, D.T., Macosko, C.W., 1988. Cyclization and reduced reactivity of pendant vinyls during the copolymerization of methyl-methacrylate and ethylene-glycol dimethacrylate. *Macromolecules* 21, 846-851.

Lee, T.S., Kolthoff, I.M., Mairs, M.A., 1948. Determination of unsaturation of synthetic and natural rubbers by means of iodine monochloride. *J. Polym. Sci.* 3, 66-84.

Lee, T.S., Kolthoff, I.M., Johnson, E., 1950. Determination of unsaturation of butyl rubbers and certain branched olefins – iodine monochloride method. *Analytical Chemistry* 22, 995-1001.

Lee, W-F., Chiu, R-J., 2002. Investigation of charge effects on drug release behaviour for ionic thermosensitive hydrogels. *Materials Science and Engineering C* 20, 161-166.

Li, R., Schork, F.J., 2006. Modeling of the inhibition mechanism of acrylic acid polymerization. *Ind. Eng. Chem. Res.* 45, 3001-3008.

Li, W.H., Hamielec, A.E., Crowe, C.M., 1989a. Kinetics of free-radical copolymerization of methyl-methacrylate and ethylene-glycol dimethacrylate .1. Experimental Investigation. *Polymer* 30, 1513-1517.

Li, W.H., Hamielec, A.E., Crowe, C.M., 1989b. Kinetics of free-radical copolymerization of methyl-methacrylate and ethylene-glycol Dimethacrylate .2. Analysis of gelation and the pre-gel region. *Polymer* 30, 1518-1523.

Liang, H.F., Hong, M.H., Ho, R.M., Chung, C.K., Lin, Y.H., Chen, C.H., Sung, H.W., 2004. Novel method using a temperature-sensitive polymer (methylcellulose) to thermally gel aqueous alginate as a pH-sensitive hydrogel. *Biomacromolecules* 5, 1917-1925.

Liu, Y., Tu. W., Cao, D., 2010. Synthesis of gold nanoparticles coated with polystyrene-block-poly(N-isopropylacrylamide) and their thermoresponsive ultraviolet visible absorbance. *Ind. Eng. Chem. Res*. 49, 2707-2715.

Lu, F., Luo, Y., Li, B., 2010. pH effects on the synthesis of nanocapsules via interfacial miniemulsion polymerization mediated by amphiphilic RAFT agent with R group of poly(methyl acrylic acid-*ran*-styrene). *Ind. Eng. Chem. Res.* 49, 2206-2212.

Ma, G.-H, Nagai, M., Omi, S., 2001. Study on preparation of monodispersed poly(styrene-co-N-dimethylaminoethyl methacrylate) composite microspheres by SPG (Shirasu porous glass) emulsification technique. *J. Appl. Polym. Sci.* 79, 2408-2424.

Ma, G.-H, Chen, A.-Y., Su, Z., Omi, S., 2003. Preparation of uniform hollow polystyrene particles with large voids by a glass-membrane emulsification technique and a subsequent suspension polymerization. *J. Appl. Polym. Sci.* 87, 244-251.

Maeder, S., Gilbert, R.G., 1998. Measurement of transfer constant for butyl acrylate free-radical polymerization. *Macromolecules* 31, 4410-4418.

Matheson, M.S., Auer, E.E., Bevilacqua, E.B., Hart, E.J., 1949. Rate constants in free radical polymerization .1. Methyl methacrylate. *J. Am. Chem. Soc.* 71, 497- 504.

Matsumoto, A., 1995. Free-radical crosslinking polymerization and copolymerization of multivinyl compounds. *Adv. Polym. Sci.* 123, 41-80.

Matyjaszewski, K., Paik, H.J., Zhou, P., Diamantini, S.J., 2001. Determination of activation deactivation rate constants of model compounds in atom transfer radical polymerization. *Macromolecules* 34. 5125-5131.

Matyjaszewski, K., Xia, J.H., 2001. Atom transfer radical polymerization. *Chemical Reviews* 101, 2921-2990.

Matyjaszewski, K., Xia, J.H., 2002. Handbook of radical polymerization. Davis, T.P., Matyjaszewski, K., edition. John Wiley and Sons, Hoboken.

McKenna, T.F., Villanueva, A., Santos, A.M., 1999. Effect of solvent on the rate constants in solution polymerisation. Part I. Butyl acrylate. *J. Polym. Sci. Pol. Chem.* 37, 571-588.

McNaughton, A.D., Wilkinson, A., 2012. IUPAC. Compendium of Chemical Technology http//goldbook.iupac.org/PDF/goldbook.pdf.

Meiser, W., Buback, M., Sidoruk, A., 2013. EPR Investigations into the Kinetics of Trithiocarbonate-Mediated RAFT-Polymerization of Butyl Acrylate. *Macromol. Chem. Physic.* 214, 2108-2114.

Moad, G., Solomon, D.H, Johns, S.R., Willing, R.J., 1982. Structure of benzoyl peroxide initiated polystyrene – Determination of the initiator-derived functionality by C-13 NMR. *Macromolecules* 15, 1188-1191.

Moad, G., Rizzardo, E., Tang, S.H., 2005. Living radical polymerization by the RAFT process. *Australian Journal of Chemistry* 58, 379-410.

Moad, G., Solomon, D.H., 2006. The Chemistry of Radical Polymerization, 2nd edition. Elsevier, Oxford.

Moad, G., Rizzardo, E., Tang, S.H., 2009. Living radical polymerization by the RAFT process – a third update. *Australian Journal of Chemistry* 62, 1402-1472.

Moad, G., Rizzardo, E., Tang, S.H., 2012. Living radical polymerization by the RAFT process – a second update. *Australian Journal of Chemistry* 65, 985-1076.

Nikitin, A.N., Hutchinson, R.A., 2005. The effect of intramolecular transfer to polymer on stationary free radical polymerization of alkyl acrylates. *Macromolecules* 38, 1581-1590.

Nikitin, A.N., Hutchinson, R.A., 2006. The effect of intramolecular transfer to polymer on stationary free radical polymerization of alkyl acrylates, 2- Improved consideration of termination. *Macromol. Theor. Simul.* 15, 128-136.

Nikitin, A.N., Hutchinson, R.A., Buback, M., Hesse, P., 2007. Determination of intramolecular chain transfer and midchain radical propagation rate coefficients for butyl acrylate by pulsed laser polymerization. *Macromolecules* 40, 8631-8641.

Nikitin, A.N., Hutchinson, R.A., Kalfas, G.A., Richards, J.R., Bruni, C., 2009. The effect of intramolecular transfer to polymer on stationary free-radical polymerization of alkyl acrylates, 3- Consideration of solution polymerization up to high conversions. *Macromol. Theor. Simul.* 18, 247-258.

Nikitin, A.N., Wulkow, M., Schütte, C., 2013. Modeling of free radical styrene/divinylbenzene copolymerization with the numerical fractionation technique. *Macromol. Theor. Simul*. 22, 475-489.

Nogueira, T.R., Lona, L.M.F., McManus, N.T., Vivaldo-Lima, E., Penlidis, A., 2010. Nitroxide-mediated radical copolymerization of styrene and divinylbenzene: increased polymerization rate by using TBEC as initiator. *Journal of Materials Science* 45, 1878-1884.

Nyhus, A.K., Hagen, S., Berge, A., 1999. A Kinetic Study of the Polymerization of Pure *meta*- Divinylbenzene and *para*- Divinylbenzene. *J. Polym. Sci. Pol. Chem.* 37, 3345-3359.

O'Brien, N., McKee, A., Sherrington, D.C., Slark, A.T., Titterton, A., 2000. Facile, versatile and cost effective route to branched vinyl polymers. *Polymer* 41, 6027-6031.

Odian, G., 2004. Principles of Polymerization, 4th ed. New York: Wiley-Interscience, ISBN. 978-0-471-27400.

Ohno, K., Goto, A., Fukuda, T., Xia, J., Matyjaszewski, K., 1998. Kinetic study on the activation process in an atom transfer radical polymerization. *Macromolecules* 31, 2699-2701.

Okay, O., Kaya, D., Pekcan, O., 1999. Free-radical crosslinking copolymerization of styrene and divinylbenzene: real time monitoring of the gel effect using fluorescence probe. *Polymer* 40, 6179-6187.

Okay, O., 2000. Macroporous Copolymer Networks. *Prog. Polym. Sci.* 25, 711-779.

Omidian, H., Zohuriaan-Mehr, M.J., Bouhendi, H., 2003. Polymerization of sodium acrylate in inverse-suspension stabilized by sorbitan fatty esters. *Eur. Polym. J.* 39, 1013-1018.

Ostroha, J., Pong, M., Lowman, A., Dan, N., 2004. Controlling the collapse/swelling transition in charged hydrogels. *Biomaterials* 25-, 4345-4353.

Ouyang, L., Wang, L., Schork, F.J., 2011. RAFT inverse miniemulsion polymerization of acrylic acid and sodium acrylate. *Macromol. React. Eng*. 5, 163-169.

Ouzineb, K., Hua, H., Jovanović, R., Dubé, M.A., McKenna, T. F., 2003. Monomer compartmentalisation in miniemulsion polymerization studied by infrared spectroscopy. *Comptes Rendus Chemie* 6, 1343-1349.

Pascual, S., Coutin, B., Tardi, M., Polton, A., Vairon, J.P., 1999. Homogeneous atom transfer radical polymerization of styrene initiated by 1-chloro-I-phenylethane copper (I) chloride bipyridine in the presence of dimethylformamide. *Macromolecules* 32, 1432-1437.

Penzel, E., Goetz, N., 1990a. Solution properties of polyacrylic esters. 1. Light-scattering and viscosity measurements in tetrahydrofuran. *Angew. Makromol. Chem.* 178, 191-200.

Penzel, E., Goetz, N., 1990b. Solution properties of polyacrylic esters. 2. Evaluation of unperturbed dimensions. *Angew. Makromol. Chem.* 178, 201-208.

Peppas, N.A., Bures, P., Leobandung, W., Ichikawa, H., 2000. Hydrogels in pharmaceutical formulations. *European Journal of Pharmaceutics & Biopharmaceutics* 50, 27-46.

Percec, V., Barboiu, B., 1995. Living radical polymerization of styrene initiated by arene sulfonyl chlorides and Cu-I(BPY)(N)Cl. *Macromolecules* 28, 7970-7972.

Percec, V., Popov, A.V., Ramirez-Castillo, E., Monteiro, M., Barboiu, B., Weichold, O., Ansadei, A.D., Mitchell, C.M., 2002. Aqueous room temperature metal-catalyzed living radical polymerization of vinyl chloride. *J. Am. Chem. Soc.* 124, 4940-4941.

Percec, V., Popov, A.V., Ramirez-Castillo, E., Weichold, O., 2003. Living radical polymerization of vinyl chloride initiated with iodoform and catalyzed by nascent Cu-0/tris(2-aminoethyl)amine or polyethylamine in water at 25 degrees C proceeds by a new competing pathways mechanism. *J. Polym. Sci. Pol. Chem.* 41, 3283-3299.

Percec, V., Popov, A.V., Ramirez-Castillo, E., Coelho, J.F.J., Hinojosa-Falcon, L.A., 2004ª. Non-transition metal-catalyzed living radical polymerization of vinyl chloride initiated with iodoform in water at 25 degrees C. *J. Polym. Sci. Pol. Chem.* 42, 6267-6282.

Percec, V., Popov, A.V., Ramirez-Castillo, E., Weichold, O., 2004b. Acceleration of the single electron transfer-degenerative chain transfer mediated living radical polymerization (SET-DTLRP) of vinyl chloride in water at 25 degrees C. *J. Polym. Sci. Pol. Chem.* 42, 6364-6374.

Percec, V., Popov, A.V., Ramirez-Castillo, E., Coelho, J.F.J., 2005. Single electron transfer-degenerative chain transfer mediated living radical polymerization (SET-DTLRP) of vinyl chloride initiated with methylene iodide and catalyzed by sodium dithionite. *J. Polym. Sci. Pol. Chem.* 43, 773-778.

Peters, E.C., Svec, F., Frechét, J.N.J., Viklund, C., Irgum, K., 1999. Control of porous properties and surface chemistry in "molded" porous polymer monoliths prepared by polymerization in the presence of TEMPO. *Macromolecules* 32, 6377-6379.

Pinto, M.A., Li, R., Immanuel, C.D., Lovell, P.A., Shorck, J.F., 2008. Effects of reversible addition fragmentation transfer (RAFT) on branching in vinyl acetate bulk polymerisation. *Ind. Eng. Chem. Res.* 47, 509-523.

Plessis, C., Arzamendi, G., Leiza, J.R., Schoonbrood, H.A.S., Charmot, D., Asúa, J.M., 2000a. Seeded semi-batch emulsion polymerisation of n-butyl acrylate. Kinetics and structural properties. *Macromolecules* 33, 5041-5047

Plessis, C., Arzamendi, G., Leiza, J.R., Schoonbrood, H.A.S., Charmot, D., Asúa, J.M., 2000b. A decrease in effective acrylate propagation rate constants caused by intramolecular chain transfer. *Macromoleucles* 33, 4-7.

Plessis, C., Arzamendi, G., Leiza, J.R., Schoonbrood, H.A.S., Charmot, D., Asúa, J.M., 2001. Modeling of seeded semi-batch emulsion polymerisation of n-Ba. *Ind. Eng. Chem. Res.* 40, 3883-3894.

Poly, J., Wilson, D.J., Destarac, M., Taton, D., 2008. Synthesis of poly(vinyl acetate) nanogels by xanthate-mediated radical crosslinking copolymerization. *Macromol. Rapid Comm.* 29, 1965-1972.

Qi, G., Jones, C.W., Schork, J.F., 2007. RAFT inverse miniemulsion polymerization of acrylamide. *Macromol. Rapid Comm.* 28, 1010-1016.

Qiu, Y., Park, K., 2001. Environmental-sensitive hydrogels for drug delivery. *Advanced Drug Delivered Reviews* 53, 321-339.

Quintero-Ortega, I.A., García-Morán, P.R., Jaramillo-Soto, G., Vivaldo-Lima, E., Luna-Barcenas, G., 2009. Evaluation of the performance of a kinetic model for free-radical copolymerization of vinyl/divinyl monomers in supercritical carbon dioxide. *Macromol. Symp.* 283-284, 103-109.

Renard, B., McKenna, T.F., 2000. Kinetics of polymerization of partially neutralised acrylic acid in inverse suspensions. *Macromol. Symp.* 150, 251-257.

Rivera, M.R., Rodríguez-Hernández, A.A., Hernández, N., Castillo. P., Saldívar. E., Ríos, L., 2005. Controlled/living free radical copolymerization of styrene and butyl acrylate in bulk and emulsion with industrial monomers. Influence of monomer addition on polymer properties. *Ind. Eng. Chem. Res.* 44, 2792-2801.

Roa-Luna, M., Jaramillo-Soto, G., Castañeda-Flores, P.V., Vivaldo-Lima, E., 2010. Copolymerization kinetics of styrene and divinylbenzene on the presence of s-thiobenzoyl thioglycolic acid as RAFT agent. *Chem. Eng. Technol*. 33, 1893-1899.

Roberge, S., Dubé, M.A., 2007. Inline monitoring of styrene/butyl acrylate miniemulsion polymerization using ATR-FTIR spectroscopy. *J. Appl. Polym. Sci.* 103, 46-52.

Rolland-Sabaté, A., Mendez-Montealvo, M.G., Colonna, P., Planchot, V., 2008. Online determination of chemistry properties and observation of deviations from power low behavior. *Biomacromolecules* 9, 1719-1730.

Russum, J.P., Jones, C.W., Schork, J.F., 2005. Continuous living polymerization in miniemulsion using reversible addition fragmentation chain transfer (RAFT) in a tubular reactor. *Ind. Eng. Chem. Res.* 44, 2484-2493.

Russum, J.P., Jones, C.W., Schork, J.F., 2006. Impact of flow regime on polydispersity in tubular RAFT miniemulsion polymerization. *AIChE J*. 52, 1566-1576.

Saka, Y., Zetterlund, P.B., Okubo, M., 2007. Gel formation and primary chain lengths in nitroxide-mediated radical copolymerization of styrene and divinylbenzene in miniemulsion. *Polymer 48*, 1229-1236.

Saldívar-Guerra, E., Bonilla-Cruz, J., Hernández-Mireles, B., Ramírez-Manzanarez, G., 2009. Progress in controlled grafting-form by nitroxide chemistry. *Macromol. Symp.* 283-284, 110-119.

Salehpour, S., Dubé, M., 2012. Reaction monitoring of glycerol step-growth polymerization using ATR-FTIR spectroscopy. *Macromol. React. Eng*. 6, 85-92.

Saunders, G., Cormack, P.A.G., Graham, S., Sherrington, D.C., 2005. Use of Rapid Triple Detection Size Exclusion Chromatography To Evaluate the Evolution of Molar Mass and Branching Architecture during Free Radical Branching Copolymerization of Methyl Methacrylate and Ethylene Glycol Dimethacrylate. *Macromolecules* 38, 6418-6422.

Scott, A.J., Nabifar A., Hernández-Ortiz, J.C., McManus, N.T., Vivaldo-Lima, E., Penlidis, A., 2014. Crosslinking nitroxide-mediated radical copolymerization of styrene with divinylbenzene. *Eur. Polym. J.* 51, 87-11.

Sen, M., Guven, O., 1999. Radiation synthesis of poly(N-vinyl 2-pyrrolidone/itaconic acid) hydrogels and their controlled released behaviours. *Radiation Physics & Chemistry* 55, 113-120.

Shim, S.E., Yang, S., Jin, M.J., Chang, Y.H., Choe, S., 2004. Effect of the polymerization parameters on the morphology and spherical particle size of poly(styrene-co-divinylbenzene) prepared by precipitation polymerization. *Colloid Polymer Science* 283, 41-48.

Shipp, D.A., Matyjaszewski, K., 2000. Kinetic analysis of controlled/"living" radical polymerizations by simulations. 2. Apparent external orders of reactants in atom transfer radical polymerization. *Macromolecules* 33, 1553-1559.

Sidoruk, A., Buback, M., Meiser, W., 2013. Kinetics of Dithiobenzoate-Mediated Methyl Methacrylate Polymerization. *Macromol. Chem. Physic*. 214, 1738-1748.

Sigma Aldrich co, http://sigmaaldrich.com (accessed May 2012).

Smith, G.B., Russell, G.T., 2007. The cutthroat competition between termination and transfer to shape the kinetics of radical polymerization. *Macromol. Symp*. 248, 1-11.

Smulders, W.W., Jones, C.W., Schork, J.F., 2005. Continuous RAFT miniemulsion polymerization of styrene in a train of CSTRs. *AIChE J.* 51, 1009-1021.

Solomon, D.H., Rizzardo, E., Cacioli, P., 1986. US Patent 4 581 429.

Soppimath, K.S., Aminabhavi, T.M., Dave, A.M., Kumbar, S.G., Rudzinski, W.E., 2002. Stimulus-responsive "smart" hydrogels as novel drug delivery systems. *Drug Development & Industrial Pharmacy.* 28, 957-974.

Staudinger, H., Husemann, H., 1935. Über hochpolymere Verbindungen, 116. Mitteil.: Über das begrenzt quellbare Poly-styrol. *Berichte* 68, 1618-1634.

Staudinger, H., Heuer, W., Husemann, H., Rabinovitch, I.J., 1936. The insoluble polystyrene. *Transactions Faraday Society* 32, 323-332.

Steinhauser, M.O., 2005. A molecular dynamic study on universal properties of polymer chains in different solvent qualities. Part I. A review of linear chain properties. *J. Chem. Physic*. 122, 094901.

Stockmayer, W.H., 1943. Theory of molecular size distribution and gel formation in branched-chain polymers. *J. Polym. Sci*. 11, 45-55.

Stockmayer, W.H., 1944. Theory of molecular size distribution and gel formation in branched polymers II General cross linking. *J. Polym. Sci*. 12, 125-131.

Stockmayer, W.H., Fixman, M., 1963. On the estimation of unperturbed dimensions from intrinsic viscosities. *J. Chem. Phys.* 1, 137-141.

Storey, R.F., Donnalley, A.B., Maggio, T.L., 1998. Real-time monitoring of carbocationic polymerization of isobutylene using in situ FTIR-ATR spectroscopy with conduit and diamond-composite sensor technology. *Macromolecules* 31, 1523-1526.

Sun, X., Luo, Y., Wang, R., Li, B-G., Zhu, S., 2008. Semibatch RAFT polymerization for producing ST/BA copolymers with controlled gradient composition profiles. *AIChE J*. 54, 1073-1087.

Sutani, K., Kaetsu, I. Ushida, K., Matsubara, Y., 2002. Stimulus responsive drug release from polymer gel. Controlled release of ionic drug from polyampholite gel. *Radiation Physics & Chemistry* 64, 331-336.

Szwarc, M., 1956. Living polymers. *Nature* 178, 1168-1169.

Tanaka, T., Suzuki, T., Saka, Y., Zetterlund, P.B., Okubo, M., 2007. Mechanical properties of cross-linked polymer particles prepared by nitroxide-mediated radical polymerization in aqueous micro-suspension. *Polymer* 48, 3836-3843.

Tang, W., Tsarevsky, N.V., Matyjaszewski, K., 2006. Determination of equilibrium constants for atom transfer radical polymerization. *J. Am. Chem. Soc.* 128, 1598-1604.

Tang, W., Matyjaszewski, K., 2007. Effects of initiator structure on activation rate constants in ATRP. *Macromolecules* 40, 1858-1863.

Tang, W., Kwak, Y., Braunecker, W., Tsarevski, N.V., Coote, M.L., Matyjaszewski, K., 2008. Understanding atom transfer radical polymerization: Effect of ligand and initiator structures on the equilibrium constants. *J. Am. Chem. Soc*. 130, 10702-10713.

Tarazona, M.P., Saiz, E., 2003. Combination of SEC-MALS experimental procedures and theoretical analysis for studying the solution properties of macromolecules. *Journal Biochemical Biophysical Methods* 56, 95-116.

Tatemoto, M., 1992. Development of iodine transfer polymerization and its applications to telechelically reactive polymers. *Kobunshi Ronbunshu* 49, 765-783.

Terao, K., Mays, J.W., 2004. On line measurement of molecular weight and radius of gyration of polystyrene in a good solvent and in a theta solvent measured with a two-angle light scattering detector. *Eur. Polym. J.* 40, 1623-1627.

Tobita, H., Hamielec, A.E., 1989. Modeling of network formation in free-radical polymerization. *Macromolecules* 22, 3098-3105

Trigo, I.M.R., Gonçalves, M.A.D., Dias, R.C.S., Costa, M.R.P.F.N., 2008. Molecular Architecture of Non-Linear Polymers: Kinetic Modeling and Experimental Characterization of the System Methyl Methacrylate + Ethylene Glycol Dimethacrylate. *Macromol. Symp.* 271, 107-119.

Tuinman, E., McManus, N.T., Roa-Luna, M., Vivaldo-Lima, E., Lona, L.M.F., Penlidis, A., 2006. Controlled free-radical copolymerization kinetics of styrene and divinylbenzene by bimolecular NMRP using TEMPO and dibenzoyl peroxide. *J. Macromol. Sci.* 43, 995-1011.

Vakkalanka, S.K., Brazel, C.S., Peppas, N.A., 1996. Temperature- and pH-sensitive terpolymers for modulated delivery of streptokinase. *Journal of Biomedical Science Pol. Ed.* 8, 119-129.

Viklund C., Nordstöm, A., Irgum, K., Svec, F., Frechét, J.M.J., 2001. Preparation of porous poly(styrene-co-divinylbenzene) monoliths with controlled pore size distributions initiated by stable free radicals and their pore surface functionalization by grafting. *Macromolecules.* 34, 4361-4369.

Wang, A.R., Zhu, S., 2003. Modeling the reversible addition-fragmentation transfer polymerization process. *J. Polym. Sci. Pol. Chem.* 41, 1553-1566.

Wang, A.R., Zhu, S., Kwak, Y., Goto, A., Fukuda, T., Monteiro, M.S., 2003. A difference of six orders magnitude: A reply to "the magnitude of the fragmentation rate coefficient". *J. Polym. Sci. Pol. Chem.* 41, 2833-2839.

Wang, D., Li, X., Wang, W-J., Gong, X., Li, B-J., Zhu, S., 2012. Kinetics and modeling of semi-batch RAFT copolymerisation with hyperbranching. *Macromolecules* 45, 28-38.

Wang, D., Wang, W-J., Li, B-J., Zhu, S., 2013. Semi-batch RAFT polymerization for branched polyacrylamide production: effect of divinyl monomer feeding policies. *AIChE J.* 59, 1322-1333.

Wang, G., Li, M., Chen, X., 1997. Inverse suspension polymerization of sodium acrylate. *J. Appl. Polym. Sci.* 65, 789-794.

Wang, J.S., Matyjaszewski, K., 1995. Controlled living radical polymerization- halogen atom-transfer radical polymerization promoted by a Cu(I)Cu(II) redox process. *Macromolecules* 28, 7901-7910.

Wang, W., Hutchinson, R.A., 2008. Recent advances in the study of high-temperature free radical acrylic solution copolymerization. *Macromol. React. Eng*. 2, 199-214.

Wieczorek, P.P., Ilavský, M., Kolarz, B.N., Dušek, K., 1982. Mechanical-Behavior and structure of single beads of homogenous and macroporous styrene-divinylbenzene copolymers. *J. Appl. Polym. Sci.* 27, 277-288.

Willemse, R.X.E., van Herk, A.M., Panchenko, E., Junkers, T., Buback, M., 2005. PLP-ESR monitoring of midchain radicals in n-butyl acrylate polymerization. *Macromolecules* 38, 5098-5103.

Wojaczyańska , M., Kolarz, B.N., 1995. Structure of some styrene-divinylbenzene copolymers. *J. Appl. Polym. Sci*. 56, 433-439.

Wu, X.Y., Zhang, Q., Arshady, R., 2003. Introduction to polymeric biomaterials. Ed. R. Arshady, the PBM series nº1, Citrus Books, London, United Kingdom.

Wulkow, M., Busch, M., Davis, T.P., Barner-Kowollik, C., 2004. Implementing the reversible addition-fragmentation chain transfer process in PREDICI. *J. Polym. Sci. Polym. Chem*. 42, 1441-1448.

Xia, J., Matyjaszewski, K., 1997. Controlled/"living" radical polymerization. Atom transfer radical polymerization using multidentate amine ligands. *Macromolecules* 30, 7697-7700.

Xu, Z., Hadjichristidis, N., Fetters, L.J., Mays, J.W., 1995. Structure chain-flexibility relationships of polymers. *Adv. Polymer Sci.* 120, 1-50.

Ye, C., Luo, Y., Liu, X., 2011. Synthesis of non-collapsed hollow polymeric nanoparticles with shell thickness o the order of polymer gyration radius. *Polymer* 52, 683-693.

Yong-Hee, K., Bae, Y.H., Kim, S.W., 1994. pH/temperature-sensitive polymers for macromolecular drug loading and release. *Journal of Controlled Release* 28, 143-152.

Yoon, D.Y., Suter, U.W., Sundararajan, P.R., Flory, P.J., 1975. Conformational characteristics of poly(methyl acrylate). *Macromolecules* 8, 784-789.

Yu, Q., Zhou, M., Ding, Y., Jiang, B., Zhu, S., 2007. Development of networks in atom transfer radical polymerization of dimethacrylates. *Polymer* 48, 7058-7064.

Yu, Q., Zhu, Y., Ding, Y., Zhu, S., 2008. Reaction behavior and network development in RAFT radical polymerization of dimethacrylates. *Macromol. Chem. Physic*. 209, 551-556.

Yu, Q., Xu, S., Zhang, H., Ding, Y., Zhu, S., 2009. Comparison of reaction kinetics and gelation beahviours in atom transfer, reversible addition fragmentation chain transfer and conventional free radical copolymerisation of oligo(ethylene glycol) methyl ether methacrylate and oligo(ethylene glycol) dimethacrylate. *Polymer* 50, 3488-3494.

Yuyama, H., Hashimoto, T., Ma, G.-H., Nagai, M., Omi, S., 2008. Mechanism of suspension polymerization of uniform monomer droplets prepared by class membrane (Shirasu Porous Glass) emulsification technique. *J. Appl. Polym. Sci.* 78, 1025.

Zapata-González, I., Sladívar-Guerra, E., Ortiz-Cisneros, J., 2011. Full molecular weight distribution in RAFT polymerization. New mechanistic insight by direct integration of the equations. *Macromol. Theor. Simul*. 20, 370-388.

Zetterlund, P.B., Alam, M.N., Minami, H., Okubo, M., 2005. Nitroxide-mediated controlled/living free radical copolymerization of styrene and divinylbenzene in aqueous miniemulsion. *Macromol. Rapid Comm.* 26, 955-960.

Zetterlund, P.B., Kagawa, Y., Okubo, M., 2008. Controlled/living radical polymerization in dispersed systems. *Chemical Reviwes* 108, 3747-3794.

Zhang, M., Ray, W.H., 2001. Modeling of "living" free-radical polymerization with RAFT chemistry. *Ind. Eng. Chem. Res.* 40, 4336-4352.

Zhang, M., Ray, W.H., 2002. Modeling of "living" free-radical polymerization processes. I. Batch, semibatch, and continuous tank reactors. *J. Appl. Polym. Sci*. 86, 1630-1662.

Zhang, W., Charleux, B., Cassagnau, P., 2012a. Viscoelastic properties of water suspension of polymer nanofibers synthesized via RAFT-mediated emulsion polymerization. *Macromolecules* 45, 5273-5280.

Zhang, W., D'Agosto, F., Boyron, O., Rieger, J., Charleux, B., 2012b. Toward a better understanding of the parameters that lead to the formation of nonspherical polystyrene particles via RAFT-mediated one-pot aqueous emulsion polymerization. *Macromolecules* 45, 4075-4084.

Zhang, W., D'Agosto, F., Dugas, P., Rieger, J., Charleux, B., 2013. RAFT-mediated one-pot aqueous emulsion polymerization of methyl methacrylate in presence of poly(methacrylic acid-co-poly(ethylene oxide) methacrylate) trithiocarbonate macromolecular chain transfer agent. *Polymer* 54 2011-2019.

Zioga, A., Ekizoglou, N., Siakali-Kioulafa, E., Hadjichristidis, N., 1997. Characteristic ratio of poly(tetrahydrofurfuryl acrylate) and poly(2-ethylbutyl acrylate). *J. Polym. Sci. Pol. Phys.* 35, 1589-1592.

Zohuriaan-Mehr, M.J., Kabiri, K., 2008. Superabsorbent polymer materials: A review. *Iranian Polymer Journal* 17, 451-477.

List of Publications

Aguiar LG, Gonçalves MAD, Pinto VD, Dias RCS, Costa MRPFN, Giudici R, Mathematical modeling of NMRP of styrene-divinylbenzene over the pre- and post gelation periods including cyclization Macromolecular Reaction Engineering, In Press, DOI: 10.1002/mren.201300171, 2013.

Aguiar LG, Gonçalves MAD, Pinto VD, Dias RCS, Costa MRPFN, Giudici R, Development of cyclic propagation kinetics for modeling the nitroxide-mediated radical copolymerization of styrene-divinylbenzene Macromolecular Reaction Engineering, In Press, DOI: 10.1002/mren.201300105, 2013

Gonçalves, MAD, Pinto, VD, Dias RCS, Hernández-Ortiz J, Costa, MRPFN, Dynamics of network formation in aqueous suspension RAFT styrene/divinylbenzene copolymerization. Macromolecular Symposia, 333, 273-285, 2013.

Gonçalves, MAD, Pinto, VD, Dias RCS, Hernández-Ortiz J, Costa, MRPFN, Stimuli-responsive hydrogels synthesis using free-radical and RAFT copolymerization, Macromolecular Symposia 333, 41-54, 2013.

Gonçalves, MAD, Pinto, VD, RCS, Costa, MRPFN, Aguiar, LG, Giudici, R, Gel formation in aqueous suspension nitroxide-mediated radical co-polymerisation of styrene/divinylbenzene, Macromolecular Reaction Engineering, 7, 155-175, 2013. (Cover Paper).

Gonçalves, MAD, Pinto, VD, Dias, RCS, Costa, MRPFN, Polymer reaction engineering studies on smart hydrogels formation, Journal of Nanostructured Polymers and Nanocomposities, 9, 40-45, 2013.

Gonçalves, MAD, Pinto, VD, RCS, Costa, MRPFN, Modeling Studies on the Synthesis of Superabsorbent Hydrogels using Population Balance Equations. Macromolecular Symposia, 306-307, 107-125, 2011.

Gonçalves, MAD, Pinto, VD, Dias, RCS, Costa, MRPFN, Kinetic Modeling of the Suspension Copolymerization of Styrene/Divinylbenzene with Gel Formation, Macromolecular Symposia, 302, 179-190, 2011.

Gonçalves, MAD, Dias, RCS, Costa, MRPFN, Kinetic Modeling of Hyperbranched Polymer Synthesis through Atom-Transfer and Nitroxide-Mediated Radical Polymerization of Vinyl/Divinyl Monomers. Chemical Engineering Technology, 33, 1797-1813, 2010

Gonçalves, MAD, Pinto, VD, Dias, RCS, Costa, MRPFN, FTIR-ATR Monitoring and SEC/RI/MALLS Characterization of ATRP Synthesized Hyperbranched Polyacrylates, Macromolecular Symposia, 296, 210-228, 2010

Gonçalves, MAD, Trigo, IMR, Dias, RCS, Costa, MRPFN, Kinetic Modeling of the Molecular Architecture of Cross-Linked Copolymers Synthesized by Controlled Radical Polymerization Techniques, Macromolecular Symposia, 291-292, 239-250, 2010.

Gonçalves, MAD, Dias, RCS, Costa, MRPFN, Prediction and Experimental Characterization of the Molecular Architecture of FRP and ATRP Synthesized Polyacryllate Networks, Macromolecular Symposia, 289, 1-17, 2010

Trigo, IMR, Gonçalves, MAD, Dias, RCS, Costa, MRPFN, Molecular Architecture of Non-Linear Polymers: Kinetic Modeling and Experimental Characterization of the System Methyl Methacrylate + Ethylene Glycol Dimethacrylate, Macromolecular Symposia, 271, 107-119, 2008.

Gonçalves, MAD, Dias, RCS, Costa, MRPFN, Time programmed feed of semi-batch reactors with non-linear radical copolymerisations: an experimental study of the system styrene + divinylbenzene using SEC/MALLS, Macromolecular Symposia, 259, 124-134, 2007.

APPENDICES

Appendix A

Sampling Procedures

With solution polymerisations experiments, samples were withdrawn directly from the reactor, stored in two vials and weighed. Then a fraction was diluted in a solvent and analysed in the respective SEC system (aqueous or organic) 24 hours later. The other fraction was precipitated into non-solvent of the polymer (such as methanol or acetone) and used for gravimetric measurements.

With suspension polymerisations experiments, reaction samples, including continuous and dispersed phases, were collected into previous cooled 20 mL glass vials and immediately poured in a refrigerator at -14 °C for at least 1 hour in order to stop the reaction. After decanting, most of the dispersed phase was diluted in a large amount of a non-solvent in order to precipitate the polymer (soluble and insoluble fractions). For samples collected before gelation, a small amount of organic phase was directly diluted in a solvent and analysed by SEC/RI/MALLS. With samples containing gel, the soluble fraction analysed by SEC/RI/MALLS was obtained after the immersion of the global material in a solvent during one day. In Figure A.1 is shown a schematic of a typical procedure after sampling, including the steps for determination of monomer conversion, PDB concentration, gel fraction, average molecular weight and *z*-average radius of gyration.

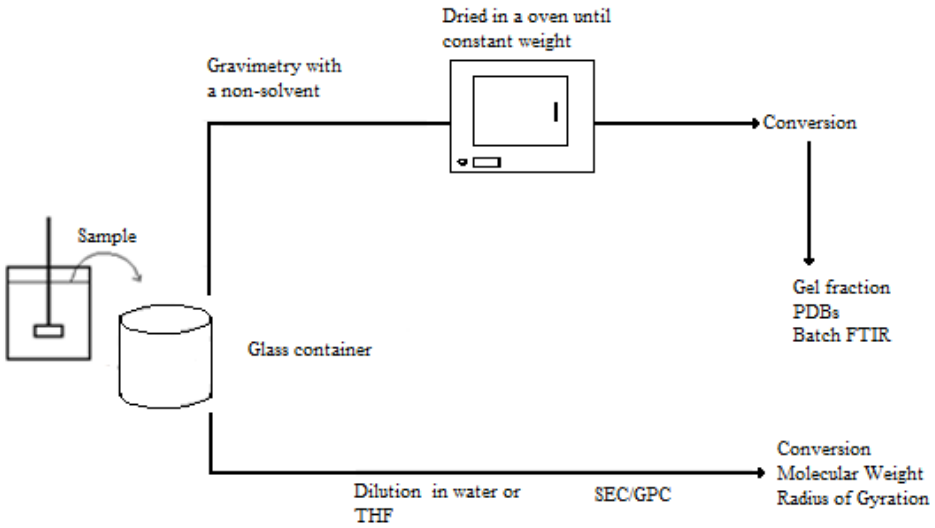

Figure A.1. General scheme of the characterization procedure in all the copolymerisation reactions (depending on the system this scheme may be adapted).

SEC Procedures

SEC is a high performance liquid chromatography technique for the separation of components based on their molecular size in solution. It is widely used as a means of establishing the molecular weight distribution and molecular size of polymers, but can be also employed for the separation of discrete components.

Its core is a flow system implementing the principle of separation and analysis are based on the properties of the polymer molecules in solution. A high pressure pump transports an organic or aqueous solvent (eluent) from a reservoir to a set of columns and detectors at a constant flow rate. A small portion of diluted polymer (around 1 g/L w/w) in that eluent is injected in the system and is incorporated into the flow. The columns are packed with a porous material with a distribution of pore sizes. When a polymer with different sizes of molecules (polydispersed) flows through the column(s), separation occurs based on its hydrodynamic size. It means that polymer molecules split between the pores confinements (stationary phase) and the interstitial space between the particles (the mobile phase). Smaller polymer molecules are able to penetrate in the pore and are transferred to the stationary phase, while the larger ones stay mostly in the mobile phase. Hence, it will take a longer time to the smaller sized molecules to leave the column. Figure A.2 depicts the separation process inside the column.

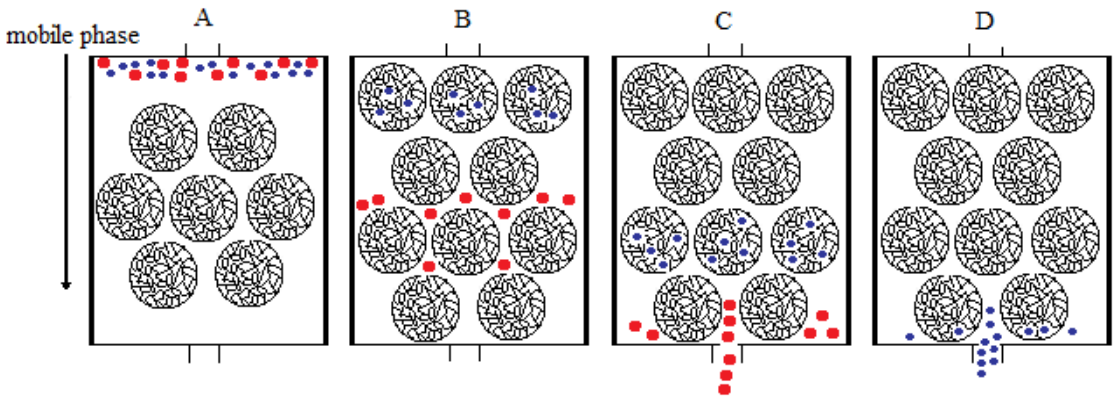

Figure A.2. Schematic of a separation process of a polymer sample based on the molecules size (hydrodynamic volume). Note that A represents the injection step, B the separation, C the elution of large molecules and D the elution of small molecules.

In this work two different systems were used: a SEC/RI/MALLS and a SEC system with a tetra detector array. The SEC/RI/MALLS system consists of a Polymer Laboratories PL-GPC-50 integrated SEC system with differential refractometer (RI), attached to a Multi Angle Laser Light Scattering (MALLS) detector. These systems were used both with organic and

aqueous media. Typically, the organic system used tetrahydrofuran as eluent at 1 ml/min flow rate and with T= 30 °C. With aqueous systems the eluent used was deionised water containing 0.1 M of Na_2HPO_4 and 200 ppm of NaN_3 (pH=9). This system was operated mostly at 0.5 ml/min flow rate at T=50 °C. The SEC organic columns used were a train of three GPC columns PL gel (300 × 7.5 mm) with nominal particle size of 10 μm and pore type MIXED B-LS. In Figure A.3 are shown the instruments that allow the SEC/RI/MALLS measurements.

The differential refractometer used is a WellChrom K-2301 RI detector. The built-in measurement cell of the RI detector operates with a measuring angle of 45° with measurements performed at a wavelength 950 ± 30 nm. The measurement makes use of a light beam emitted from a LED that crosses the sample and the reference cell of the RI detector twice. When both cells contain pure solvent, the system is calibrated to zero by means of a parallel zero-plate which positions the beam on the two detectors diodes in such a manner that the measured light intensities of both diodes are virtually identical. When the sample cell contains a solution with different refractive index with respect to the solvent the light beam is geometrically deflected in an amount depending on the relative change of the refractive index. This results in a change of the light intensity, proportional both to concentration and refractive index difference with respect to the reference of the sample solution. From these intensity changes the signal value is calculated and indicated on the output display.

Light scattering is a non-invasive technique for characterizing macromolecules and a wide range of particles in solution. In contrast to most methods of characterization, it does not require calibration standards. In this sense it is an absolute technique. It can be applied in either batch or chromatographic mode. Light scattering provides the weight averaged molar mass for all molecules in solution (provided their refractive index increment with respect to that solvent stays the same). It is often more useful to use the chromatographic mode, though each technique has its advantages. The multi-angle laser light scattering detector used in the present work is a laser photometer DAWN8+ HELEOS 658 nm with 8 different angles provided by Wyatt Technology Corporation. Figure A.4 shows a schematic of MALLS measurement, in that case with 18-angle. The photometer was calibrated with toluene, and the normalization of its detectors in THF was performed with low molecular weight standard samples of polystyrene. The same PS standard was used to determine the inter-detector volumes (between RI and MALLS detectors).

Figure A.3. Photographic record of the Polymer Laboratories PL-GPC-50 containing the SEC system coupled with RI and MALLS detectors.

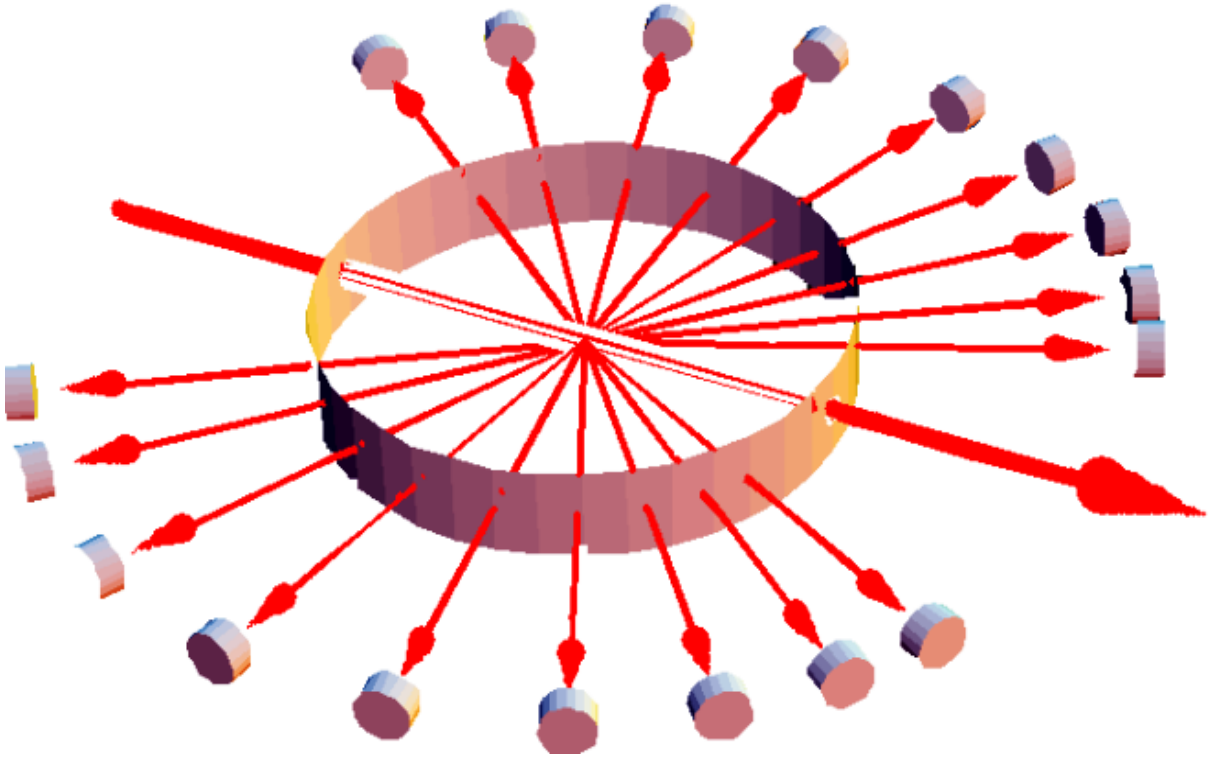

Figure A.4. A view of the MALLS measurement with 18-angle detector. The incident laser beam is polarized vertically with respect to the scattering plane shown (Wyatt, 1997).

The SEC system with a tetra-detector array (Figure A.5) was only used in aqueous media. It is composed of a Viscotek GPCmax VE 2001 integrated and sample delivery module coupled with a tetra-detector array including refractive index (cell volume of 12 µL, a light scattering detector, with two angles (90° and 7°) of wavelength 670 nm and cell volume of 10 µL, a Smartline ultraviolet detector 2550 from Knauer with a deuterium source allowing

wavelength range of 190-990 nm and a viscometer detector based on measuring the differential pressure created by the movement of a sample solution through a series of four capillary tubes (Figure A.6). Since capillaries R_1-R_4 have equal flow resistances, when pure solvent of viscosity η_0 is flowing in all four capillaries, the differential pressure $DP=P_2(+) - P_2(-)$ will be zero, or have some baseline value close to zero. Then as the polymer solution elutes through the bridge, the viscosity in capillaries R_1, R_2 and R_3 will increase to η, while the pure solvent remains flowing through capillary R_4 due to delay volume column. Therefore the *DP* is no longer zero, but increases in approximate proportion to the specific viscosity of the solution. The exact equation is shown below:

$$\eta_{SP} = \frac{4DP}{IP-2DP} \quad \text{(A.1)}$$

Being *DP* the pressure across middle of bridge, IP the inlet pressure through the bridge top to bottom and η_{SP} the specific viscosity of the solution given by $\eta_{SP} = \frac{\eta-\eta_0}{\eta_0}$.

Analyses were performed directly in a water eluent, pH was changed accordingly to the polymer analysed, and using typically a flow rate of 0.5 ml/min. The temperature of the analysis was in the range of 30 to 50 °C and was also change considering the different polymers analysed (PNIPA collapses at around 37 °C). For the aqueous analyses the SEC system used was a train of three columns Viscotek (A2000, A3000 and A6000).

Figure A.5. Photographic record of SEC system with the tetra-detector array (RI-LS-IVDP-UV).

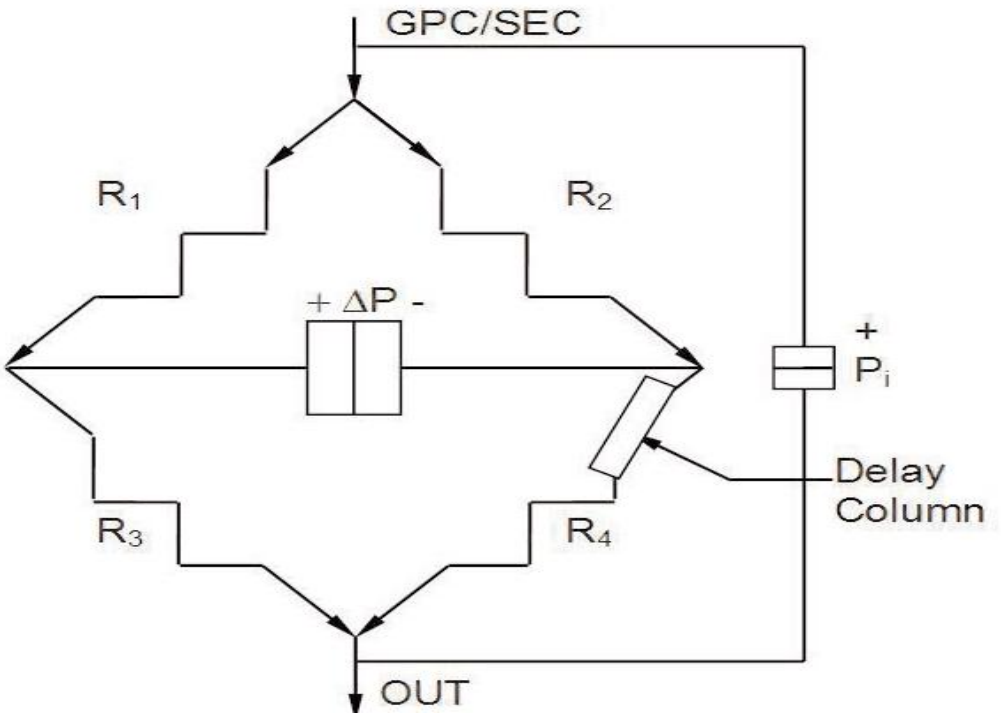

Figure A.6. Schematic of the *on-line* GPC viscometer with a series of four capillary bridges.

FTIR-ATR Immersion Probe Procedures

This approach allows the *in-line* monitoring of the reaction mixture and therefore following monomer conversion at real time. *In-line* FTIR-ATR simultaneous monitoring of vinyl and divinyl monomers can be used to perform real-time specification of feed policies. The use in kinetic studies (e.g. quantification of copolymer reactivity ratios) is another important application of this technique. The system set-up of an *in-line* FTIR-ATR that is used to follow polymerization reactions in this research work is presented in Figure A.7.

Figure A.7. Photographic record of the *in-line* FTIR/ATR system set-up used in this work.

In the polymerizations performed in this research work it is used an ATR immersion probe coupled to a FTIR spectrometer. The following instruments are used: different Axiom analytical immersion probe, model DRR 207 with two different elements, ZnSe element, spectral cut-off 600 cm^{-1}, maximum pressure of 60 bar and temperature operation of 280 ºC and AMTIR element with spectral cut-off at 850 cm^{-1}, maximum pressure and temperature operation 20 bar and 280 °C, respectively. This probe is coupled with an ABB Bomem Fourier Transform Infra-Red spectrometer, model FTLA 2000-104 by a three arms light guide and ABB Bomem, Mercury Cadmium Telluride (MCT) detector (model D10B), cooled with liquid nitrogen, equips the spectrometer in order to increase the sensitivity of the analysis. The spectra are taken in the mid infrared region from the range of 600 to 4000 cm^{-1} with resolution of 4 cm^{-1} using 128 interferograms. These spectra were used to calculate monomer conversion and copolymer composition.

The basic instrument design is quite simple. The IR radiation from a broadband source is first directed into an interferometer, where it is divided and then recombined after the split beams travel different optical paths to generate constructive and destructive interference. Next, the resulting beam passes through the sample compartment and reaches the detector. Unlike double beam spectrometers, single beam FTIR does not obtain transmittance or absorbance IR spectra in real-time. A typical procedure of the FTIR operation is described as follows: a background spectrum is first obtained by collecting an interferogram as raw data, followed by processing the data by Fourier transform conversion; this is a response curve of the spectrometer and takes account of the combined performance of source, interferometer and detector. The background spectrum also includes the contribution from any ambient present in the optical bench, namely water vapour and carbon dioxide. To reduce the strong background absorption from these two molecules in the atmosphere, the optical bench is usually purged with an inert gas (e.g. argon). Spectrometer alignment, which includes optimization of the beam splitter angle, is recommended as part of a periodic maintenance or when a sample accessory is changed.

Conversion Determination

- **By Gravimetric Measurements**

For determining the monomer conversion the gravimetric technique was used. The samples were withdrawn from the reactor at different reaction times. A flask with approximately 20 ml

of a non-solvent capable of precipitating the polymer was used (e.g. methanol, acetone and water). This flask was previously cooled in the refrigerator (to stop the reaction) and was weighed before the addition of the sample (this value is variable), and then weighed again. Afterwards the sample was filtered and dried under vacuum in an oven (40 to 70 °C, depending on the solvent) during 24 hours. At last, the dried polymer was weighed and the conversion is determined. In Figure A.8 shows the process to obtain the experimental value of monomer conversion by gravimetry.

The experimental conversion by gravimetry is obtained through the following expression (Eq. A.2:

$$p = \frac{m_S}{(m_{pol} \times w_0)} \tag{A.2}$$

In the above relation, p is the conversion, m_S the mass of the sample collected, m_{pol} is the mass of polymer and w_0 is the mass fraction of monomer in the dispersed phase at the beginning of the reaction.

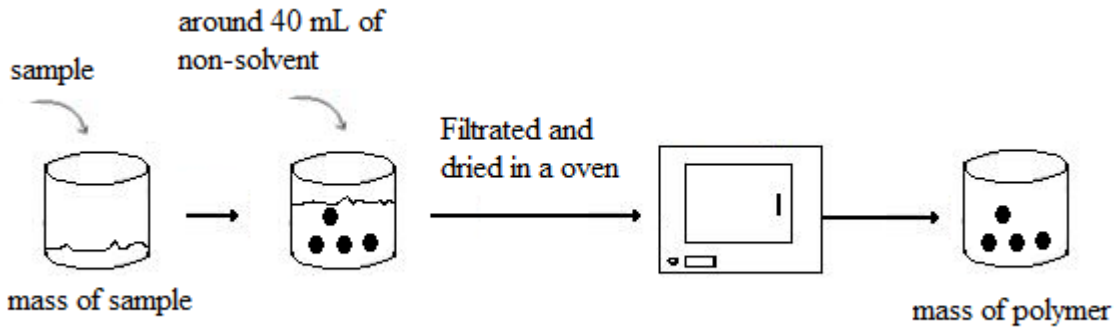

Figure A.8. Schematic of the gravimetric technique used to obtain the monomer conversion in this work.

- **By SEC Using the RI Detector Peak**

The conversion is obtained by comparing the peak areas from the monomer and the polymer. For an accurate measure it is necessary to know the *dn/dc* of the monomers, polymers and solvents (in case they present the same elution volume as the monomer).

- **By *in-line* FTIT-ATR**

Some of the monomer conversions were determined using FTIR-ATR spectra. This measure was made using the selected peak height (usually a double bond that is consumed) at different

reaction time. Another peak height is used as an internal reference (a peak remaining constant during the reaction). Thus, the conversion is given by the following equation (Eq. A.3):

$$p = \frac{\frac{H_{pc}}{H_{pt}}}{\left(\frac{H_{pc}}{H_{pt}}\right)_0} \tag{A.3}$$

Where p is the monomer conversion, H_{pc} the peak height of the C=C consumption over reaction time, H_{pt} the peak height of the internal reference over reaction time and $\left(\frac{H_{pc}}{H_{pt}}\right)_0$ is the initial constant ratio between the two height peaks.

Gel Fraction and Swelling Ratio

The products of a copolymerisation reaction with formation of tridimensional networks consist of fractions of soluble and insoluble polymer. One of the steps of the gel characterization consists of obtaining the gel fraction as a function of reaction time. Thus, it is necessary to extract the soluble fraction which is trapped by the polymer network. When a linear polymer is immersed in a solvent, the chains are dispersed and form a solution.

The procedure for measure the gel fraction is analogous to the gravimetric one. The dried polymer obtained by gravimetry is weighed and placed into a flask with 20 ml of solvent during 24 hours to reach equilibrium. Then the polymer sample is filtered and dried under vacuum at temperature high enough (depending on the solvent boiling point) during 24 hours. After that the sample is weighed again and gel fraction is determined by Eq. A.4:

$$w_g = \frac{m_{pol}}{m_{gel}} \tag{A.4}$$

Being w_g the gel fraction, m_{pol} the mass of polymer (soluble and gel) and m_{gel} the mass of gel.

After the extraction of the soluble fraction, the characterization of gel proceeds with the measure of its swelling ratio capacity. This is started with the contact of the polymeric network (gel only) with a solvent. The network will grow through the absorption of solvent. As the swelling proceeds, the polymer concentration decreases and its elastic energy increases due to the chain stretching. In the presence of an excess of solvent, the gel will continue to swell until the elastic forces of the chains achieve the equilibrium. The swelling ratio (SRa) value is obtained by comparing the weight of the gel before contact with the solvent (m_{gel})

with the weight of the gel when the equilibrium is reached (m_{equi}) by the following relation in Eq. A.5:

$$SRa = \frac{m_{equi}}{m_{gel}} \quad \text{(A.5)}$$

Determination of Pendant Double Bonds by the Iodine Chloride Addition Method

The quantification of pendant double bonds in the polymer networks was carried out by a chemical analysis (Hecker, 2000). Approximately 0.5 g of dried polymer was placed in contact with 20 ml of carbon tetrachloride during 15 hours for samples collected before gel point and 90 hours for samples containing gel, to promote the swelling. After this period, 25 ml of Wijs reactant (iodine-monochloride) were added to the mixture and maintained in the dark for 30 hours (before gel) and 72 hours (after gel). Thus, it was promoted the reaction between the iodine monochloride (ICl) and the pendant double bonds C=C presents in the structure of the polymer. At the end of this stage, 20 ml of potassium iodide (KI) and 150 ml of deionised water were added to the mixture. At this stage, KCl and I_2 are formed due to the reaction of free ICl and KI present in excess. The resulting solution is immediately titrated with a sodium thiosulfate solution at 0.1 N until the almost disappearance of the yellow dark colour is observed. After that, 2 ml of starch solution at 1 % was added to the mixture (soluble starch aids in being able to see the free iodine and getting a repeatable end point) and the titration was continued until the new blue colour totally disappears. The comparison between the titration volumes obtained for the blank (without polymer sample) and the samples allows the determination of pendant double bonds presents in the material. The PDBs concentration is determined by the Eq. A.6:

$$C_{DB} = \frac{(V_{titB} - V_{titS})0.5C_{tit}}{m_{pol}} \quad \text{(A.6)}$$

Where C_{DB} is the concentration for pendant double bonds (mmol/g of polymer), V_{titB} is the volume of titrant spend with the blank sample (mL), V_{titS} the volume of titrant spend in polymer sample (mL), C_{tit} concentration of titulant (mol/L) and m_{pol} is the mass of polymer sample. In Figure A.9 is a scheme of this procedure.

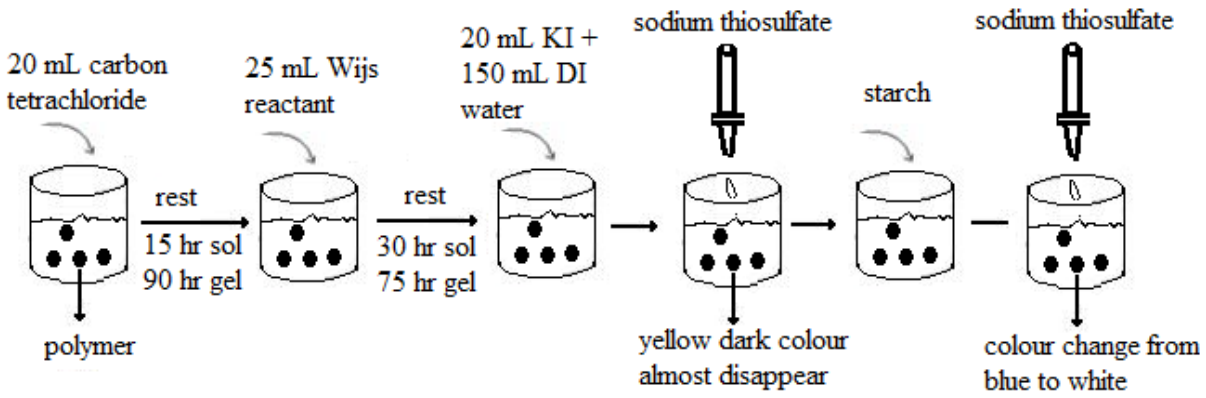

Figure A.9. Experimental procedure for determination of pendant double bonds by iodine method.

FTIR Polymer Samples in Batch Procedure

These spectra are obtained using the dried polymer obtained by gravimetry. The polymer sample and the KBr die powder must be completely out of moisture, so the samples are placed in an oven at 60 °C 24 hours prior to the analysis. If the sample or the KBr die has any humidity the disc will not be formed and the procedure must be repeated. The KBr pellets are prepared at a concentration of approximately 1 % (w/w). Thus, the required amounts of KBr and polymer are mixed and compacted using a mortar. Then the mixed powder is placed into a cylinder and compressed using two polished discs. In order that the mixture is able to form a compact disc a vacuum pump with pressure of less tang 2 cm Hg and a hydraulic press with a maximum load between 6 and 8 tons are used. This assembly is kept this way for at least 3 minutes. After releasing the vacuum and the load, the compacted pellet is removed with extra care (preventing damaging or breaking) and mounted into a disc holder designed to fit in the FTIR instrument. The FTIR apparatus is a BOMEM model MB 104 and the spectra were recorded at a resolution of 4 cm^{-1} between 650 and 4000 cm^{-1} and 48 scans.

Procedure for *dn/dc* Measurements

For the measurement of the refractive index increment (*dn/dc*) of a substance (monomer, solvent or polymer) in a determined eluent (organic or aqueous, depending on the system used) an Optilab DSP Interferometric Refractometer from Wyatt Technology was used.

- Sample preparation

  For an accurate measurement it is best to prepare the sample on the same day at which the measurement is to be made. The same solvent for the sample preparation to flush the cell instrument must be used. The refractometer is very sensitive so these steps are

necessary to make an accurate measurement. The ideal range of concentrations to be injected is between 0.5 and 3.0 mg/mL, but these values can be changed if the substance has a higher or lower response with that eluent. Also, if the substance has a negative response it is necessary to restart the measurement introducing that variable in the instrument.

- Collecting Data

  The sample and the reference cell must be flushed with the eluent for some time (at least 2 hours) before making measurements. Then one must wait for baseline stability before closing the reference cell. Wait for a few minutes to see if the baseline is stable and if so zeroed the instrument and start the measurement. The ASTRA software is then run and the analysis with the lowest concentration should begin and wait for the signal to stabilize (a few minutes) before injecting the other samples. Each sample will yield a plateau on the screen (Figure A.10). When the last sample is finished, the eluent must be injected again and one should check the absence of baseline drifts. Every sample concentration has a correspondent signal (mV) and so it is possible to obtain a linear regression and using the calibration constant of the instrument to calculate the respective *dn/dc*. This calculation is easily done using the ASTRA software. The user must introduce all the concentrations and the program will generate the result.

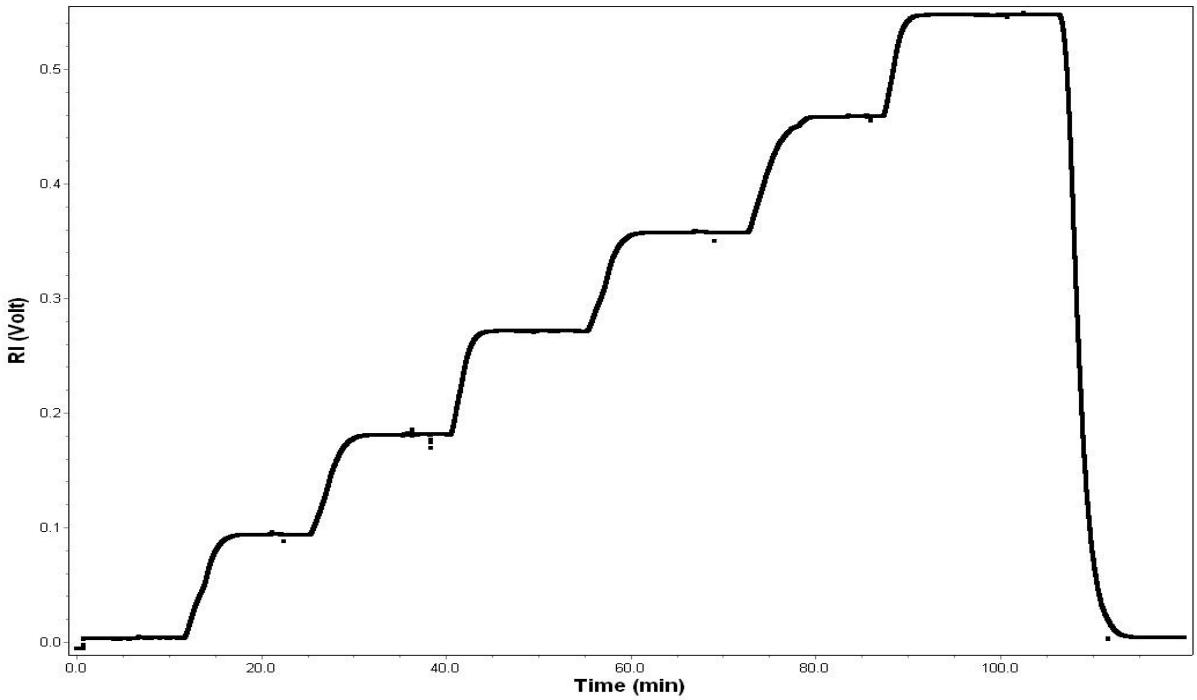

Figure A.10. Diagram RI *versus* time used in the determination of the *dn/dc* of a polystyrene sample.